The glacial and periglacial history of a Middle Pleistocene ice-margin of the British Ice Sheet (BIS) in north Buckinghamshire, England and its influence on geotechnical variability

Simon James Price MSc FGS CGeol EurGeol

Department of Geography, University of Cambridge

Clare Hall College

This dissertation is submitted for the degree of Doctor of Philosophy

September 2018

Supervisors: Professor Philip Gibbard (University of Cambridge)

Professor Malcolm Bolton (University of Cambridge)

Tom Berry (formerly of Arup, now of Jacobs)

Professor Christine Lane (supervised 2017-2018, University of Cambridge)

UNIVERSITY OF CAMBRIDGE

This dissertation is the result of my own work and includes nothing which is the outcome of work done in collaboration except as declared in the Preface and specified in the text. It is not substantially the same as any that I have submitted, or, is being concurrently submitted for a degree or diploma or other qualification at the University of Cambridge or any other University or similar institution except as declared in the Preface and specified in the text. I further state that no substantial part of my dissertation has already been submitted, or, is being concurrently submitted for any such degree, diploma or other qualification at the University of Cambridge or any other University or similar institution except as declared in the Preface and specified in the text. It does not exceed the prescribed word limit for the relevant Degree Committee.

The glacial and periglacial history of a Middle Pleistocene ice-margin of the British Ice Sheet (BIS) in north Buckinghamshire, England and its influence on geotechnical variability

Simon James Price

Resilience is an important factor in the design and operation of new and existing linear infrastructure. Temporal and spatial variability in Quaternary, cold-climate processes, including deposition and weathering of glacigenic sediments and bedrock, subglacial drainage and permafrost development, has resulted in abrupt lateral and vertical anisotropy in the natural geotechnical state of the ground. The ability to anticipate vertical and lateral changes in the physical properties and structure of the shallow subsurface remains a major challenge for geotechnical design.

This research uses a combination of field and laboratory techniques to investigate the Middle Pleistocene history of part of north Buckinghamshire and its potential influence on geotechnical variability of till and Oxford Clay mudrocks. The project area was chosen because of its position relative to the proposed route of Great Britain's second highspeed railway (HS2) and its coincidence with a major Quaternary domain divide between lowland glaciated and non-glaciated, landscape assemblages.

A regional database of geotechnical properties and behaviour was constructed. The database was used to describe variability in geotechnical property and behaviour parameters, against which the results of the laboratory investigations were compared. Geotechnical laboratory analyses included single- and multi-stage triaxial tests to determine undrained shear strength parameters, stress paths and strength envelopes. Small-strain stiffness was analysed using Hall effect sensors in triaxial compression. Compressibility behaviour was examined using 1D consolidation tests. This was supplemented by index testing, clay mineralogy analysis, geological field logging and numerical dating of glacigenic sediments using optically stimulated luminescence (OSL) techniques. The results of the laboratory investigation, and database parameters, were interpreted against a national framework of spatial Quaternary Domains which relate similar geological and geomorphological landscape assemblages to their interpreted Quaternary history.

The research has demonstrated that there were at least two advances of glacier ice into the area, separated by the development of a large, proglacial ice-dammed lake. OSL dating has determined minimum ages of glacigenic sediment deposition between 145±10 ka and 205 ±13 ka. This implies that the glacial events are at least late Wolstonian in age but the OSL ages do not unequivocally discriminate between Middle Pleistocene glacial events. Direct field

evidence for periglaciation occurs in the form of involutions in limestone bedrock and river terrace gravels, sub-horizontal shears in till and Oxford Clay bedrock and frost-cracking within till-derived chalk clasts and micritic limestone bedrock.

There are no appreciable differences in the undrained behaviour of the Oxford Clay related to lithology or clay mineralogy. Geotechnical analyses suggest that the Oxford Clay is weaker and more compressible in areas that have not been previously glaciated, compared to those that have. Variability in undrained shear strength and secant shear modulus, G, is seen to be dependent on depth below ground level, regardless of Quaternary Domain. Variability in compressibility and secant effective strength parameters of the Oxford Clay are interpreted to be a function of proximity to a former Middle Pleistocene margin of the British Ice Sheet (BIS). Subglacial and periglacial shearing are interpreted to result in an increase in initial void ratio, increase in compressibility with a corresponding reduction in the secant angle of shearing resistance.

Chalk-rich tills are stiff, have low compressibility and have mobilised shear strengths up to 477 kPa. The strength and compressibility variability in the ground between Quaternary Domains and between Oxford Clay and till exposed at the ground surface, has important implications for the design of railway infrastructure which requires geological subgrade stiffness and strength for its long-term performance.

‘Soils are made by nature and not by man, and the products of nature are always complex……As soon as we pass from steel and concrete to earth, the omnipotence of theory ceases to exist’

Karl Terzaghi, 1936

Proceedings of the first International Conference on Soil mechanics and Foundation Engineering, Cambridge, Massachusetts, USA

Preface

Declaration

This dissertation is the result of my own work and includes nothing which is the outcome of work done in collaboration except as declared in the Preface and specified in the text.

It is not substantially the same as any that I have submitted, or, is being concurrently submitted for a degree or diploma or other qualification at the University of Cambridge or any other University or similar institution except as declared in the Preface and specified in the text. I further state that no substantial part of my dissertation has already been submitted, or, is being concurrently submitted for any such degree, diploma or other qualification at the University of Cambridge or any other University or similar institution except as declared in the Preface and specified in the text.

It does not exceed the prescribed 80 000-word limit set by the Degree Committee for Earth Sciences and Geography. The word limit excludes the table of contents, photographs, diagrams, figure captions, appendices, bibliography and acknowledgements.

Acknowledgements

In addition to my supervisory group, from whom I've learned so much in crossing the disciplines of Quaternary geology and soil mechanics, there are people and organisations that I would like to thank. Without them, I couldn't have done this research.

I am very grateful to my friends at the British Geological Survey for supporting my leave of absence to study and for granting permission to access their geotechnical laboratory facilities, data and information and expertise. I would really like to thank Helen Reeves, Jon Lee, Pete Hobbs, Matt Kirkham, Dave Entwisle and Sue Self.

I thank Network Rail and Highways England for their support for the project and their help in facilitating access to sites, data and information, including that for East West Rail. Luke Swain and David Hutchinson (Network Rail) and David Patterson (Highways England) are thanked as are the field staff at Bam Ritchies who conducted the ground investigations for East West Rail. The laboratory staff at PSL Laboratories in Doncaster are thanked for facilitating my lab visits during collection of some of the samples I used for this research. James at Oakley Soils is thanked for apparently being one of the only companies in England to have a hydraulic sample extruder fitted with a UT100 thread and allowing me to use it.

Many individuals and organisations helped in providing permissions to access their land and field sites in north Buckinghamshire and I am very grateful for their support. They include members of the National Trust (Stowe), Buckinghamshire Geology Group, FCC Environment (April, Alison and Gillian), Anthony and Lois Houghton-Brown of Tingewick, Aylesbury Vale District Council and the many farmers who kindly allowed me access to their fields.

The laboratory and academic support staff in the Department of Geography and the Schofield Centre are thanked for the continual support, help and advice. In Geography, they include Steve Boreham, Chris Rolfe and Laura Healy. I thank Chris Jeans for taking the time to show me the ropes of his bespoke sample preparation methods for clay mineralogy.

I would like to acknowledge the individuals who were proper pioneers in working between the two disciplines of Quaternary geology and soil mechanics and achieved so much in doing so. I have been inspired and influenced by their work and endeavors throughout my research. They include Geoffrey Boulton, Mike Paul, John Hutchinson, Jackie Skipper, Fred Bell, Martin Culshaw, Peter Fookes and finally, Alec Skempton.

The project was funded as part of an EPSRC CASE studentship with Arup as the industrial partner. I would like to thank Tom Berry (formerly of Arup) for identifying the research opportunity, and Arup, including Matt Free, for supporting investment in it.

Thank you to all my friends and family for all their support, love and understanding. And thank you to my partner Kathryn for her love, support and patience and generally believing in me when I decided to take a career break to go back to university. She didn't really expect to be in a relationship with a student again.

Dedication

This thesis is dedicated to my uncle John who died in late 2017 after an on-going battle with cancer.

Abstract

Resilience is an important factor in the design and operation of new and existing linear infrastructure. Temporal and spatial variability in Quaternary, cold-climate processes, including deposition and weathering of glacigenic sediments and bedrock, subglacial drainage and permafrost development, has resulted in abrupt lateral and vertical anisotropy in the natural geotechnical state of the ground. The ability to anticipate vertical and lateral changes in the physical properties and structure of the shallow subsurface remains a major challenge for geotechnical design.

This research uses a combination of field and laboratory techniques to investigate the Middle Pleistocene history of part of north Buckinghamshire and its potential influence on geotechnical variability of till and Oxford Clay mudrocks. The project area was chosen because of its position relative to the proposed route of Great Britain's second highspeed railway (HS2) and its coincidence with a major Quaternary domain divide between lowland glaciated and non-glaciated, landscape assemblages.

A regional database of geotechnical properties and behaviour was constructed. The database was used to describe variability in geotechnical property and behaviour parameters, against which the results of the laboratory investigations were compared. Geotechnical laboratory analyses included single- and multi-stage triaxial tests to determine undrained shear strength parameters, stress paths and strength envelopes. Small-strain stiffness was analysed using Hall effect sensors in triaxial compression. Compressibility behaviour was examined using 1D consolidation tests. This was supplemented by index testing, clay mineralogy analysis, geological field logging and numerical dating of glacigenic sediments using optically stimulated luminescence (OSL) techniques. The results of the laboratory investigation, and database parameters, were interpreted against a national framework of spatial Quaternary Domains which relate similar geological and geomorphological landscape assemblages to their interpreted Quaternary history.

The research has demonstrated that there were at least two advances of glacier ice into the area, separated by the development of a large, proglacial ice-dammed lake. OSL dating has determined minimum ages of glacigenic sediment deposition between 145±10 ka and 205 ±13 ka. This implies that the glacial events are at least late Wolstonian in age but the OSL ages do not unequivocally discriminate between Middle Pleistocene glacial events. Direct field evidence for periglaciation occurs in the form of involutions in limestone bedrock and river

terrace gravels, sub-horizontal shears in till and Oxford Clay bedrock and frost-cracking within till-derived chalk clasts and micritic limestone bedrock.

There are no appreciable differences in the undrained behaviour of the Oxford Clay related to lithology or clay mineralogy. Geotechnical analyses suggest that the Oxford Clay is weaker and more compressible in areas that have not been previously glaciated, compared to those that have. Variability in undrained shear strength and secant shear modulus, G, is seen to be dependent on depth below ground level, regardless of Quaternary Domain. Variability in compressibility and secant effective strength parameters of the Oxford Clay are interpreted to be a function of proximity to a former Middle Pleistocene margin of the British Ice Sheet (BIS). Subglacial and periglacial shearing are interpreted to result in an increase in initial void ratio, increase in compressibility with a corresponding reduction in the secant angle of shearing resistance.

Chalk-rich tills are stiff, have low compressibility and have mobilised shear strengths up to 477 kPa. The strength and compressibility variability in the ground between Quaternary Domains and between Oxford Clay and till exposed at the ground surface, has important implications for the design of railway infrastructure which requires geological subgrade stiffness and strength for its long-term performance.

Notation

A	Activity
c	Cohesion
c′	Effective cohesion
C_c	Compression Index
C^*_c	Intrinsic Compression Index
C_{sec}	Coefficient of secondary ne dimensional (1D) consolidation
C_z	Coefficient of curvature
C_u	Coefficient of uniformity
c_u	Undrained shear strength
c_v	Coefficient of 1D consolidation
c_{vi}	Coefficient of isotropic (triaxial) consolidation
e	Void ratio
e_f	Final void ratio
e_i	Initial void ratio (also e_0)
e_L	Void ratio at a soil's Liquid limit
e^*_{100}	Void ratio at an effective vertical stress of 100 kPa
e^*_{1000}	Void ratio at an effective vertical stress of 1000 kPa
ε_a	Axial strain
η_{crit}	Critical effective stress ratio (pre-peak)
γ	Shear strain
$\varepsilon_{F=2}$	Shear strain mobilised at 0.5_{qmax}
g	Gravitational acceleration
G	Shear modulus
G_s	Specific gravity (particle density)
ICL	Intrinsic Compression Line
I_p	Plasticity Index
I_v	Void Index
k	Permeability
kPa	Kilopascal
kN	Kilonewton
km	Kilometres
LI	Liquidity Index
M	Critical effective stress ratio (post-peak)
m	Mass
m	Metres

mbgl	Metres below ground level
MC	Moisture content
MIS	Marine Isotope Stage
MN	Meganewton
MPa	Megapascal
m_v	Coefficient of volume compressibility
N	Newton
OCR	Overconsolidation ratio
OSL	Optically stimulated luminescence
p′	Mean effective stress invariant
′	Prime (‘dash’) denotes effective stress parameter or unit
Pa	Pascal
PSD	Particle-Size Distribution
ø′	Effective angle of friction
$ø'_{trans}$	Effective angle of friction at the stress ratio state corresponding to η_{trans}
$ø'_{0.4\%}$	Effective angle of friction at a mobilised strain of 0.4%
$ø_r$	Residual angle of friction
$ø'_p$	Effective peak angle of friction
q	Deviatoric stress
q_{max}	Maximum deviatoric stress
W_p	Plastic limit
ρ_B	Bulk density
ρ_D	Dry density
ρ_s	Particle density
ρ_w	Density of water
r_o	Initial compression ratio
r_p	Primary compression ratio
r_s	Secondary compression ratio
SCL	Sedimentation Compression Line
S_r	Degree of saturation
s	Seconds
σ	Total stress
σ′	Effective stress
σ_1	Principal stress axis (vertical)
σ'_1	Principal effective stress axis (vertical)
σ_3	Principal stress axis (horizontal)
σ'_3	Principal effective stress axis (horizontal)

σ_a	Total axial stress
σ_r	Total radial stress
σ'_p	Preconsolidation pressure (maximum vertical effective stress)
σ'_v	Vertical effective stress (also σ'_{vo})
τ	Shear stress
u	Pore(water) pressure
U	Degree of 1D consolidation
W_L	Liquid limit
YSR	Yield stress ratio

Contents

List of Figures

List of Tables

1 Introduction

The ability to anticipate vertical and lateral changes in the physical properties and structure of the shallow geological subsurface remains a major challenge for ground engineers. As well as variability between geological units, variability is known to exist within units of the same stratigraphical classification. Geological and geotechnical variability in natural engineering soils increases uncertainty in the design, construction and performance of infrastructure assets built on or in the ground.

The shallow subsurface in Great Britain (considered here to be ~ 60 m below ground level) comprises geological bedrock and natural and artificial Quaternary (superficial) deposits. The physical properties and behaviour of engineering soils have a major influence on the design and performance of structures built on, in or with them (Mitchell & Soga, 2005). Geotechnical ground investigation attempts to characterise the properties and behaviour of engineering soils to meet the design criteria of the intended use of the ground and avoid ground-based geohazards. This is often limited by the fact that data are obtained from a small sample dataset from which it is difficult to account for the full range of spatial variability in the ground even at site scale (Fookes, 1997; Culshaw, 2005). Geotechnical variability within and between sites is often responsible for 'unforeseen ground conditions'. It is a major cause of delays to ground investigation and negative impacts on longer-term infrastructure resilience and performance (Fookes, 1997; Culshaw, 2005; Griffiths & Stokes, 2008; de Freitas, 2009; Royse *et al.*, 2009).

Ground engineering in mid-latitude lowland landscapes affected by past cyclical glacial and periglacial processes intensifies the challenge of anticipating variability within engineering soils. Quaternary climate-driven events have the potential to change effective stresses and so change the original *in situ* state of pre-existing frost-susceptible bedrock and sediments. Quaternary sediments are characterised by engineering soils of mixed grain sizes ranging from clay to boulders and may also include slabs of bedrock. Periglacial weathering of geological bedrock induces post-depositional changes in effective stress through processes including growth and decay of segregated ice, solifluction and ice-wedging. The transition from one engineering soil type to another can change over short vertical and lateral distances (<10 m) making their properties difficult to generalise even at site-scale. Their physical properties and behaviour are influenced by a combination of cold-climate geological processes. They include glacial erosion, glacier-transport and deposition, loading by glacier-ice, ground-ice formation and periglacial weathering. Quaternary depositional and stress history therefore influences fundamental geotechnical behaviour which may change from

regional to site-scale, change within similar geological units and overprint the depositional and erosional histories of bedrock.

Quaternary geological history is not used consistently to interpret the geotechnical behaviour of Quaternary soils. Geotechnical measurements are rarely related to geological history or other measurements in similar materials beyond the site scale. Numerical values of geotechnical properties and behaviour are used at the site-scale to meet specific design criteria for which the ground investigation was undertaken. There is rarely an incentive or demand to relate these values to others in similar material beyond the site-scale or for an engineer to interpret them based on their mode of origin. Consequently, there is limited opportunity to investigate the regional variability of measured properties based on geological history. It is argued here that relating geotechnical measurements to geological processes of erosion, transport and deposition could improve ground design and avoid unexpected ground conditions on site.

The relationship between Quaternary history and geotechnical behaviour provides a means of anticipating geotechnical variability if spatial relationships between them can be established. Classifying engineering soils based on the geological principles of lithostratigraphy provides a tool to group similar engineering soils with shared geological history and properties. The research presented here aims to test the application of Quaternary geological history-stress history to engineering soils as a means of anticipating physical property variability by using geological principles of stratigraphy. This will be further developed to provide a predictive tool to enhance current and future infrastructure performance based on sediment deposition and modification during the Quaternary.

1.1 Project background

This research project was initiated by Tom Berry previously at Arup, in recognition of the geotechnical variability and hazards often associated with engineering soils and rocks that have been affected by the former cold-climate events of the Quaternary. Quaternary engineering soils, including weathered geological bedrock, are frequently encountered during ground investigations. Their geotechnical variability and potential geohazards pose significant uncertainty in the selection of geotechnical design parameters for new constructions and long-term performance of historical infrastructure, including railway earthworks. With the support of Professors Philip Gibbard and Malcolm Bolton at the University of Cambridge, along with partners including Network Rail, Tom secured funding for an EPSRC iCASE studentship.

During the research design phase, a major ground investigation in north Buckingham was identified. In 2014-2015, ground investigation for Phase 2 of Network Rail's East West Rail scheme was underway. The scheme aims to re-open the former Varsity Line between Cambridge and Oxford. The Phase 2 ground investigation between Bicester in the west and Milton Keynes in the east was contracted to Bam Ritchies with consultant supervision from WSP Parson Brinckerhoff. In consultation with Network Rail, permission was sought and given to access provisional data and to collect surplus, scheduled, but untested disturbed and undisturbed sediment samples.

During April and May 2017, I undertook a formally taught and examined 'permafrost and periglacial environments' course at the University Centre, Svalbard. My intention was to investigate present-day permafrost environments as an analogue for past periglacial conditions in southern Britain. I have used examples of data, information and photographs collected in Svalbard to supplement information in this thesis.

1.2 Thesis structure and terminology

The thesis comprises research drawn from the disciplines of Quaternary science and soil mechanics and aims to combine elements from both disciplines within the research theme of Quaternary engineering geology. This presents many challenges, including the description and classification of natural geological materials and research aims that satisfy the needs of both disciplines. It is difficult to write about geology and soil mechanics without using terms that are unfamiliar to readers from each discipline. Common terms and their meaning used in this thesis are highlighted in Table 1-1.

The terms engineering soil and geological bedrock are used throughout the thesis. This is based on the definition of soil as those geological materials that can be disaggregated by such gentle means as agitation in water (British Standards Institution, 1999). They are synonymous with geological sediment, superficial deposits and Quaternary deposits. Importantly, they include those elements of weathered bedrock that behave as soil. Engineering soils are distinct from pedogenic soils which are those soils in which plants grow and which possess distinct horizons reflecting biological activity, organic content and chemical leaching. Geological naming of different materials based on their lithology and relative geological age (lithostratigraphy) is maintained throughout. Where possible, geotechnical qualifiers are also used e.g. stiff, overconsolidated clay and silt of the Oxford Clay Formation.

Common terms used in this thesis and their meaning	
Bedrock	Taken to mean the geological parent material from which Quaternary

	sediments are derived. Despite the name, bedrock may include geological material that behaves as both engineering rock and soil.
Clast	A coarse-grained particle within a matrix of fine-grained particles, usually clay, silt and/or sand.
Deposit	Used in the same sense as soil and sediment.
Diamicton	A generic term to describe a soil whose components include variable mixtures of clay, silt, sand and gravel, commonly with cobbles and/or boulders. It is synonymous, but not exclusively associated with the glacial soil, till.
Matrix	An aggregation of fine-grained inorganic soil particles in which larger, coarse particles occur.
Soil	Used here in the engineering sense to mean those geological materials that can be disaggregated by such gentle means as agitation in water.
Sediment	Used in the same sense as soil.
Till	Geological sediment deposited by the direct action of glacier ice.

Table 1-1 Commonly used terms used in this thesis and their meaning.

All references to sizes of inorganic soil particles are in accordance with British Standards Code of Practice for Site Investigations terminology which is in turn consistent with BS EN 1997-2: 2007 Eurocode 7 (British Standards Institution, 1999, 2007; Norbury, 2012).

The thesis comprises five main parts:

1. Chapters 1,2,3 and 4 provide an analysis of the potential geotechnical consequences of former Quaternary glacial and periglacial processes in southern Britain and the geology and engineering geology of the Oxford Clay Formation and Quaternary deposits in north Buckinghamshire;
2. Chapter 5 describes the development of a conceptual geological ground model and Quaternary Domains which are used in Chapter 6 to provide a statistical analysis of selected geotechnical properties and behaviour;
3. Chapters 7 and 8 describe the field and laboratory methodologies used to investigate the nature and age of Middle Pleistocene deposits and the geotechnical properties and behaviour of till and Oxford Clay Formation along a northeast-southwest transect, perpendicular to the inferred Middle Pleistocene, glacial limit;
4. Chapter 9 synthesises and discusses evidence for the Middle Pleistocene history of north Buckinghamshire, its relationship to glaciated areas of the English Midlands and East Anglia, the spatial variability of geotechnical properties and behaviour and its relevance to Quaternary Domains as potential indicators of Quaternary geological history;
5. Chapters 10 and 11 provide conclusions and recommendations for future work.

All photographs, figures and materials are by the author except where stated otherwise or for clarification. All field and laboratory work was undertaken by the author with assistance or where stated.

1.3 Project area

The project area comprises parts of north Buckinghamshire including Milton Keynes and parts of Bedfordshire and north Oxfordshire (Figure 1-1) in south, central England approximately 80 km northwest of London. The project area was chosen for the following reasons:

- Its strategic location for future infrastructure development associated with Phase 2 of England's highspeed rail development programme, (HS2).
- Its location at the transition between glaciated and non-glaciated lowland British landsystems which provide a geographical domain boundary against which to investigate spatial variability in similar engineering soils.
- To investigate the glacial and periglacial history of a relatively little studied part of the British onshore Quaternary sequence and make comparisons with better-known sequences in the English south Midlands and East Anglia.

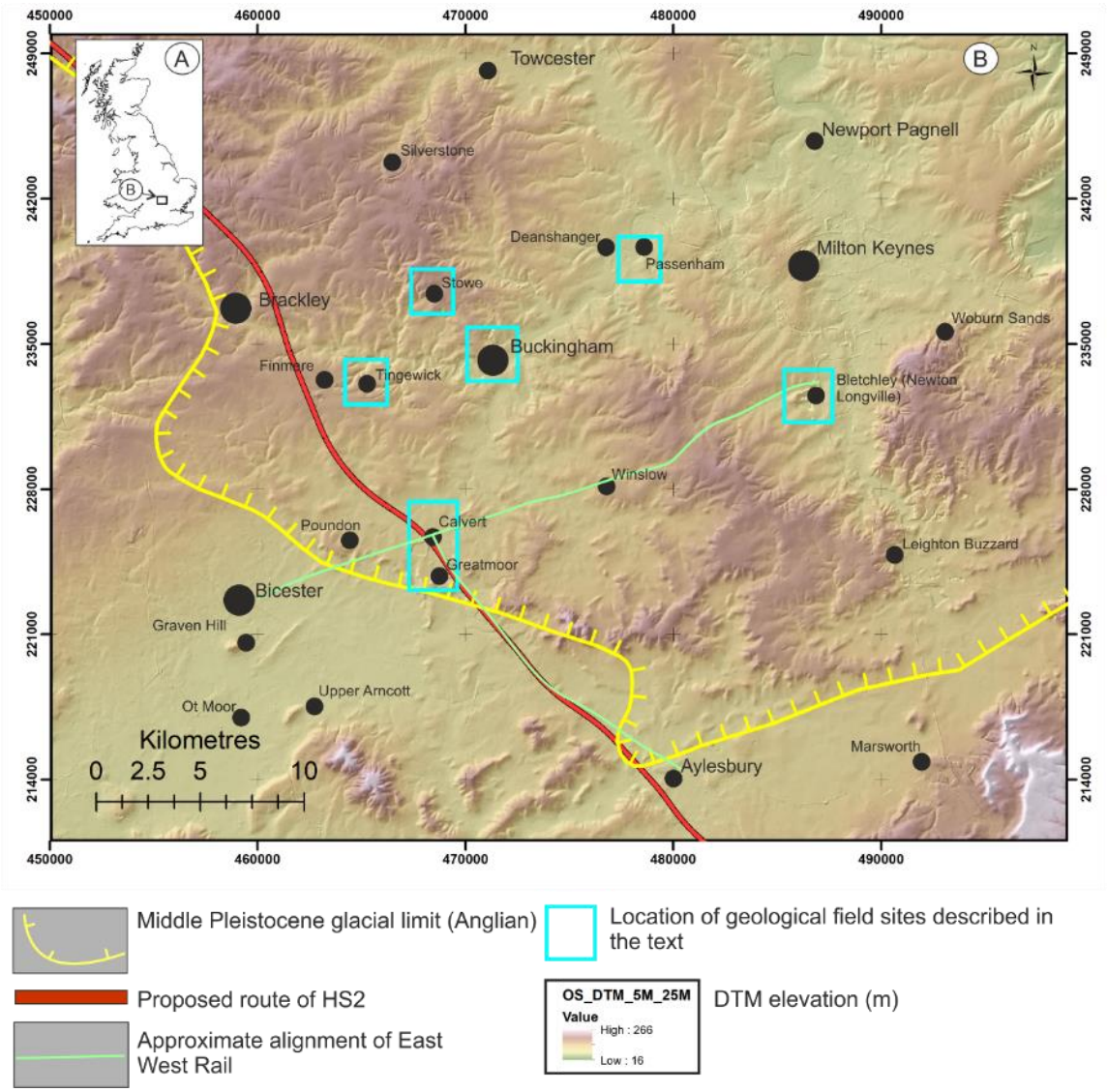

Figure 1-1 Project area, Anglian Stage glacial limit (described in Chapter 2, ticks on up-ice side) and proposed route of Highspeed 2 (HS2) rail route including key place names mentioned in the text. Geographical location with reference to Ordnance Survey Landform Profile 50 m resolution Digital Terrain Model (DTM) © Crown Copyright and Database Right [2018]. Ordnance Survey (Digimap Licence). Size of circles represent relative conurbation size.

The project area is underlain by bedrock comprising middle to late Jurassic mudrocks with sandstone and limestone. Areas underlain by Jurassic mudrocks are low-lying and form the broad northeast-southwest trending clay vale which in part includes the Vale of Aylesbury. Beds of gently-dipping limestone and/or sandstone crop out forming dipslopes orientated towards the southeast. Cretaceous limestone crops out to the south east of Aylesbury where it forms the northwest-facing escarpment of the Chiltern Hills. Quaternary deposits cap hills that form between the mainly northeast flowing river systems of the River Great Ouse and the southwest-flowing River Ray, the latter a tributary of the River Cherwell. A northwest-

southeast trending ridge within the Jurassic Oxford Clay Formation provides a drainage divide between the two catchments (Figure 1-2).

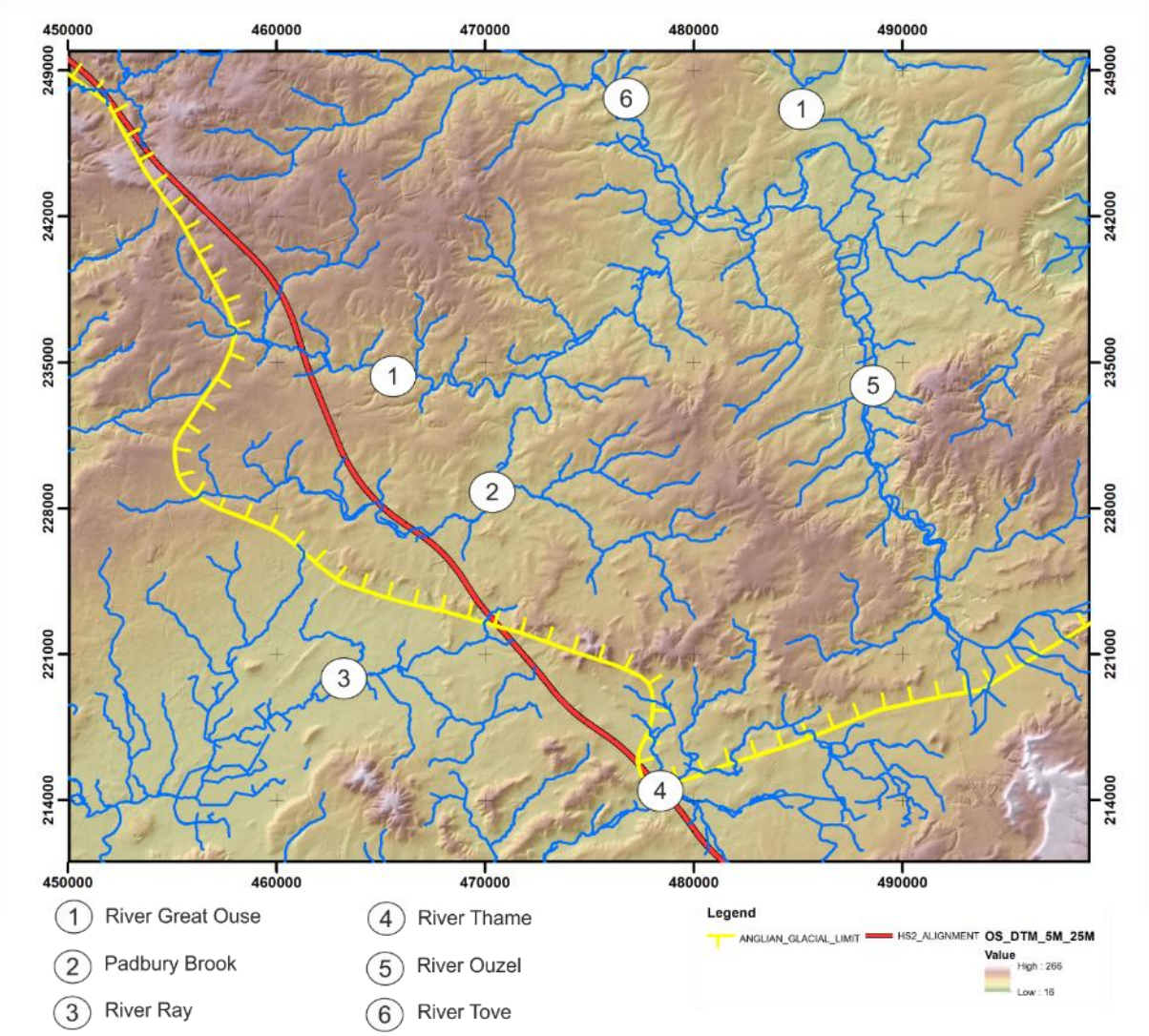

Figure 1-2 River drainage network within project area. Extent as Figure 1-1. Geographical location with reference to Ordnance Survey Landform Profile 50 m resolution Digital Terrain Model (DTM) © Crown Copyright and Database Right [2018]. Ordnance Survey (Digimap Licence).

1.4 Research hypothesis, aims and objectives

This research aims to test the hypothesis that the effects of former glacial and periglacial events in lowland Britain can be mapped and related to spatial variability in geotechnical properties and behaviour of till and frost-susceptible Oxford Clay Formation (hereafter referred to as Oxford Clay) bedrock. If the spatial patterns and types of glacial and periglacial activity can be mapped geographically, the degree of correlation with spatial variability in selected geotechnical parameters could then be compared. The hypothesis is based on the

theory that changes in effective stress in the ground are brought about by glacial and periglacial processes, including ground and glacier ice growth and decay.

The hypothesis also implies that the behaviour of frost-susceptible Oxford Clay is influenced by Pleistocene changes in effective stress when compared to its pre-Pleistocene geological sedimentation, burial and erosion, for two critical reasons. Firstly, its fine-grained lithology means that it is likely to be frost susceptible. During cyclic periods of Quaternary climatic cooling, it is probable that it was susceptible to the growth and decay of segregated ice lenses which is associated development of periglacial landforms and mechanical weathering. Secondly, it provided the glacier-bed interface during glaciation and is therefore likely to have been deformed through sub-glacial shearing.

In central southern England, the maximum extent of the British Ice Sheet (BIS) developed during Pleistocene glaciations and has traditionally been taken as the maximum extent of glacigenic deposits (Figure 1-1). The maximum extent of glaciation has generally been related to major low latitude glaciation in NW Europe during the Anglian Stage (Elsterian Stage of mainland Europe). Based on the presence of overlying temperate interglacial sediments, the Anglian Stage glaciation is correlated to Marine Isotope Stage (MIS) 12 (~480 ka). No numerical dating of these sediments exists in the north Buckinghamshire area.

1.4.1 Aims and objectives

The aim of this research is to apply an innovative approach, combining geological and geotechnical data and information, soil mechanics and Quaternary geological history to characterise geotechnical variability. The geological component was achieved by applying maps of Quaternary Domains to the description and stratigraphy of previously unrecorded field sections exposing Quaternary sediments, estimation of the timing of glaciation using Optically Stimulated Luminescence (OSL) and development of a conceptual ground model.

Geotechnical variability of till and Oxford Clay bedrock was quantified using newly acquired ground investigation data combined with existing ground investigation data within the British Geological Survey's (BGS) National Geotechnical Properties Database (NGPD). The assessment of geotechnical variability will be supplemented and compared to laboratory measurements of 1D compressibility, undrained shear strength, small-strain stiffness, bulk and particle density, plasticity and particle size. The influence of clay content on geotechnical behaviour will be investigated by measurement of clay mineral type using qualitative X-ray diffraction (XRD) in till and Oxford Clay.

The specific objectives of the research related to the thesis structure presented in Section 1.2, are:

1. **Geotechnical consequences of former glacial and periglacial processes**
    - Synthesise the potential geotechnical consequences of glacier and ground ice formation and degradation on Quaternary deposits and frost-susceptible Oxford Clay in part of the formerly glaciated and periglaciated landscape of lowland Britain;
2. **Geological ground model and geotechnical background**
    - Construct a conceptual geological ground model and Quaternary Domains using existing geological data and information, against which the results of field and laboratory investigations can be compared;
    - From existing geological and geotechnical data, construct a relational database and quantify the statistical range of geotechnical parameter values for till and Oxford Clay based on the spatial distribution of Quaternary Domains;
3. **Quaternary history and laboratory-based geotechnical behaviour**
    - Determine the timing and style of lowland Middle Pleistocene glaciation and periglaciation through field and laboratory investigation of sediments and landforms in north Buckinghamshire and, by stratigraphical comparison, determine its relationship to glacigenic sequences in the Central England and East Anglia;
    - Through laboratory experimentation, determine the 1D consolidation, undrained shear strength, effective stress secant angle of friction and stiffness of till and Oxford Clay and compare the results with regional statistical variability determined through construction of a database;
4. **Discussion and implications of Middle Pleistocene history for geotechnical variability**
    - Investigate the spatial variability in the results of laboratory and database derived geotechnical properties and behaviour by comparison with Quaternary Domains as a proxy for the likely glacial and periglacial influences on geotechnical variability.

2 Geotechnical consequences of Quaternary cold-climates in lowland Britain

2.1 The Quaternary Period

The Quaternary Period (2.6 Ma – present day) represents a geological interval of intensification in the frequency and magnitude of high to mid latitude glaciation. Cyclical variations in the amount and aspect of orbitally-controlled solar radiation reaching the Earth have been recognised from atmospheric proxy records preserved in marine sediments and ice-cores e.g. (Shackleton & Opdyke, 1973; Shackleton & Pisias, 1982; Lisiecki & Raymo, 2005). The relationship between isotope proxies and global changes in temperature and ice volume has enabled a chronostratigraphical hierarchy for the Quaternary Period to be established (Table 2-1). The Quaternary Period has been divided into Marine Isotope Stages (MIS) representing alternating cold (glacial) and temperate (interglacial) events. During cold stages in mid and high latitudes, ice sheets expanded along with corresponding fluctuations in the exposure of terrestrial environments to periglacial activity (Benn & Evans, 1998; Lowe & Walker, 2015).

<table>
<tr><th>Period</th><th>Epoch</th><th>MIS</th><th>Age (Ma)</th><th colspan="3">Northern Hemisphere Stages and substages</th></tr>
<tr><td rowspan="11">Quaternary</td><td rowspan="11">Middle Pleistocene</td><td rowspan="2"></td><td rowspan="2"></td><td colspan="2">NW Europe</td><td>British Isles</td></tr>
<tr><td>Holocene</td><td>1</td><td>0.017</td><td colspan="2">Holocene</td><td>Holocene</td></tr>
<tr><td></td><td>2</td><td>~0.02</td><td colspan="2">Late Weichselian</td><td>Late Devensian</td></tr>
<tr><td></td><td>3</td><td>~0.05</td><td colspan="2" rowspan="2">Middle Weichselian</td><td>Middle Devensian</td></tr>
<tr><td></td><td>4</td><td>~0.07</td><td rowspan="2">Early Devensian</td></tr>
<tr><td></td><td>5a
5b
5c
5d</td><td>~0.12</td><td colspan="2">Early Weichselian</td></tr>
<tr><td></td><td>5e</td><td>~0.13</td><td colspan="2">Eemian</td><td>Ipswichian</td></tr>
<tr><td></td><td>6</td><td rowspan="2">~0.39</td><td rowspan="2">Saalian</td><td>Warthe/Drenthe</td><td rowspan="2">Wolstonian</td></tr>
<tr><td></td><td>7</td><td>Schöningen, Reinsdorf
Fuhne</td></tr>
<tr><td></td><td>11</td><td>~0.40</td><td colspan="2">Holsteinian</td><td>Hoxnian</td></tr>
</table>

		12	~0.44	Elsterian		Anglian
		13-21		Cromerian Complex	Interglacial IV	
					Glacial C	
					Interglacial III	
					Glacial B	
					Interglacial II	
					Glacial A	Cromerian
			0.79		Interglacial I	Beestonian

Table 2-1 Quaternary chronostratigraphical framework for Britain and northwest Europe. Chronostratigraphical units below the Cromerian stage not shown. After Lowe & Walker (2015) and Cohen & Gibbard (2011).

During Quaternary glaciations in Great Britain, the British Ice Sheet (BIS) extended into southern Britain from ice accumulation centres in NW Scotland, the Lake District and North Wales (Ehlers *et al.*, 1991; Gibbard & Clark, 2011; Lowe & Walker, 2015). The influence of the Scandinavian Ice Sheet in Eastern England, sourced from the North Sea region has also been suggested (Ehlers & Gibbard, 1991; Lunkka, 1994; Clark, P L Gibbard, *et al.*, 2004; Ehlers *et al.*, 2011) but evidence for it has been questioned (Lee *et al.*, 2002; Davies *et al.*, 2011).

It is generally accepted that glaciation occurred on at least three occasions in Britain during the Devensian (Weichselian), Wolstonian (Saalian) and Anglian (Elsterian) Stages. The maximum terrestrial limits of glaciation during these stages is shown in Figure 2-1. Of these terrestrial glacial events, glaciation during the Anglian Stage was the most extensive, extending into southern England including present-day north London.

Evidence of glaciation in southern England beyond the southern extent of the inferred Anglian glacial limit is recognised by sediments and landforms of possible glacial origin in the Isles of Scilly (Hiemstra *et al.*, 2006). Beyond the Anglian Stage glacial limit, lowland Britain was exposed to multiple phases of non-glacial, cold-climate periglacial activity, including the development of permafrost, during cold stages from the beginning of the Quaternary Period (Ballantyne & Harris, 1994).

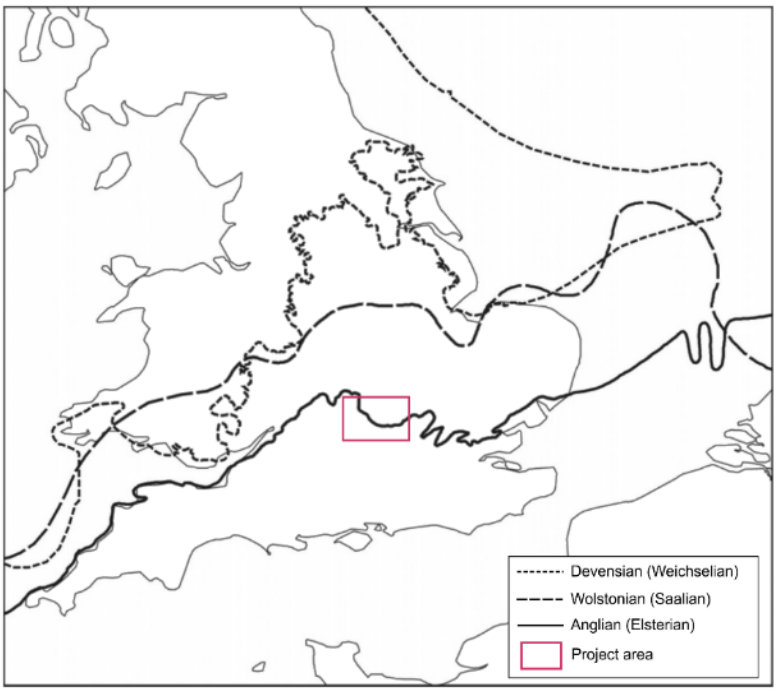

Figure 2-1 Interpreted glacial limits in southern Britain modified after Gibbard & Clark (2011).

Differential weathering under cold and temperate Quaternary climates has resulted in bedrock weakening and the production of deep zones of weathering in lowland southern Britain (Murton & Ballantyne, 2017). The extent of periglacial bedrock weathering generally decreases from south to north because of sub-glacial erosion during subsequent glaciations. Post-Anglian Pleistocene glacigenic sediments are similarly affected by periglacial weathering and modification during subsequent glaciation. Where ground temperatures remain at 0°C for two consecutive years or more, permafrost may form. The linkage between Mean Annual Air temperature (MAAT), Mean Surface Temperature (MST) and ground thermal diffusivity and conductivity provides a thermo-mechanical model on which to predict the potential formation of permafrost (French, 2007; Harris *et al.*, 2009; Murton & Ballantyne, 2017). The interpreted former extents of permafrost in southern Britain derived from abiotic and biotic temperature proxy evidence in the terrestrial periglacial record are shown in Figure 2-2.

Abiotic and biotic indicators provide evidence for the presence of past permafrost. Biotic evidence includes the beetle *Choleptera* and abiotic evidence includes thermal contraction cracks, involutions and pingos (Ballantyne & Harris, 1994). This evidence has been correlated to MAAT and used as a proxy in the reconstruction of palaeotemperatures.

During the period 74 – 59 ka in Great Britain, it is estimated that the mean temperature of the coldest month ranged between -32°C to -10°C (Huijzer & Vandenberghe, 1998). The

presence of structures characteristic of permafrost, including involutions and ice-wedge casts are associated with the regionally extensive 'Barham Arctic Soil' underlying Anglian-age glacigenic deposits in East Anglia (Rose & Allen, 1977; Kemp *et al.*, 1993). This also provides abiotic evidence for the presence of pre-Devensian permafrost. It is probable that this same climatic zone controlling permafrost aggradation, also developed during each of the previous glacial events in lowland Britain.

Terrestrial Quaternary sediments are widespread in Great Britain (Figure 2-3). Till alone covers over 30% of the British landmass (Entwisle & Wildman, 2010). The Quaternary sediments shown in Figure 5 are classified according to their lithology (sediment composition) and interpreted process of formation (genesis). Lithogenetic classification has been used to show the distribution of Quaternary sediments on geological maps at 1:50 000 scale in the UK (McMillan & Powell, 1999). McMillan *et al*. (2011) introduced a hierarchical classification and correlation of Quaternary and Neogene sediments in the UK on the basis of lithostratigraphy which developed the work of Mitchell *et al*. (1973) and Bowen (1999). This system is consistent with the lithostratigraphical classification of geological bedrock and allows correlation of similar layers of Quaternary sediments based on Group, Formation or Member.

This system is referred to throughout this thesis as a baseline stratigraphical reference. It is shown alongside other formal and informal stratigraphical terms where relevant. Importantly, lithostratigraphy is used increasingly to provides a fundamental basis on which to map, model and characterise Quaternary sediments including their geotechnical properties and behaviour (Northmore *et al.*, 2011; Culshaw *et al.*, 2017).

Figure 2-2 Extent of permafrost and seasonally frozen ground in Great Britain during the Devensian (Weichselian) Stage. Note north-south climate gradient. A to E after Huijzer & Vandenberghe (1998), F after Isarin (1997) and following the style of Murton & Ballantyne (2017). Modelled permafrost thicknesses for East Anglia and Dartmoor estimated from ground thermal properties (diffusivity and conductivity) and mean annual air and surface temperatures from Busby *et al*. (2016). E) shows discrepancy between numerical methods of Busby *et al*. (2016) which estimate thick permafrost and biotic and abiotic climate proxies used by Huijzer & Vandenberghe (1998) which shows discontinuous or sporadic permafrost in SW England.

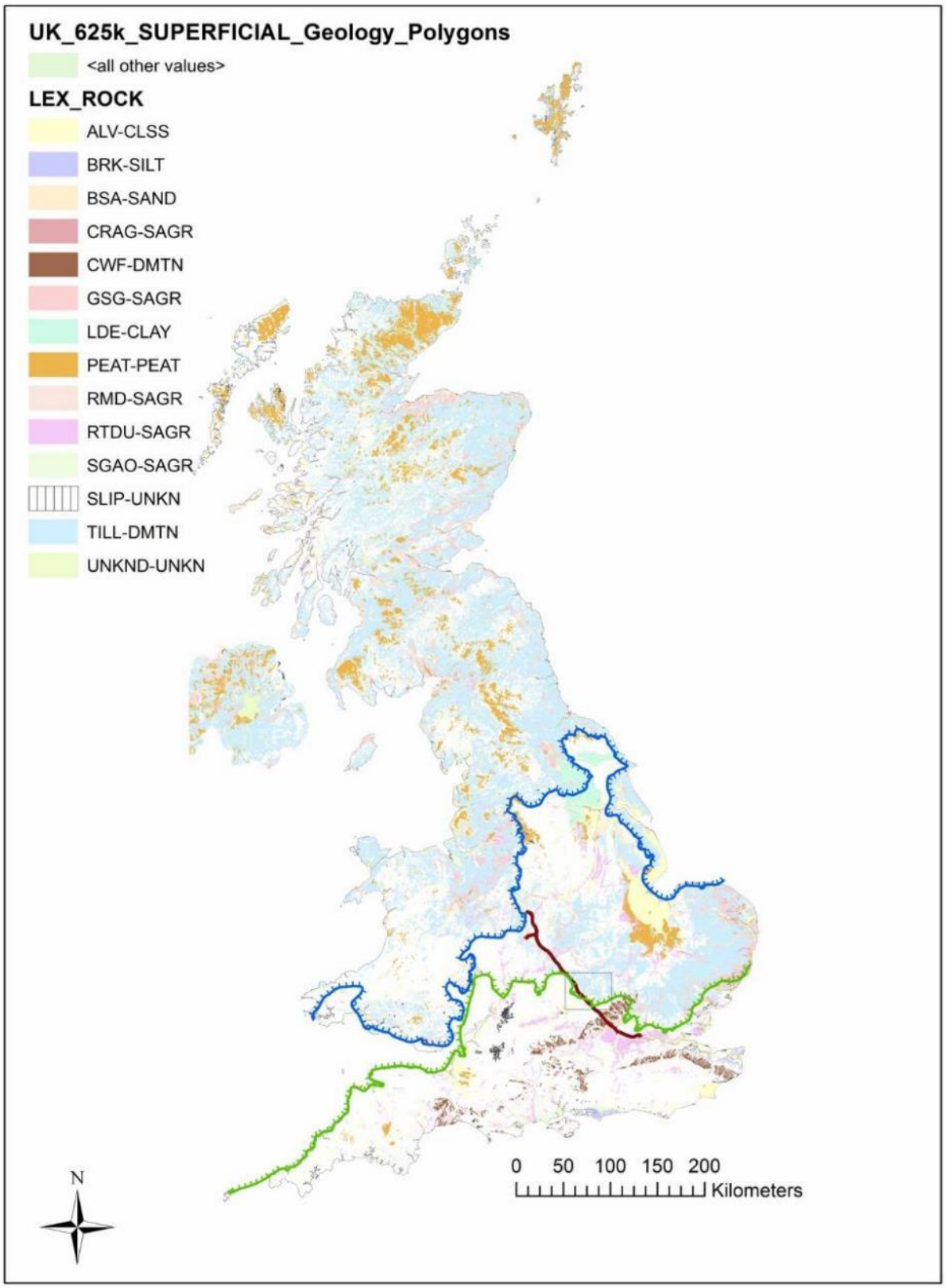

Figure 2-3 Distribution of Quaternary sediments and limits of glaciations in the United Kingdom. The Wolstonian Stage glacial limit not shown. 1:625 000 geological data used under licence from the BGS (licence number 2015/038). HS2 route alignment provided under Open Government Licence v1.0.

2.2 Geotechnical consequences

The processes of ground freezing, precipitation and subsequent decay of ground and glacier ice is known to change the geotechnical properties of engineering soils (Boulton & Paul, 1976; McGown & Derbyshire, 1977; Chamberlain & Gow, 1979; Boulton & Dobbie, 1993). The legacy of the geological events of the Quaternary have had a major effect on engineering geology in the shallow subsurface (Paul *et al.*, 1981). The events of the Quaternary are considered the most significant factors influencing the properties and behaviour of near-surface geological materials for civil engineering (Higginbottom & Fookes, 1970; Fookes, Gordon, *et al.*, 1975; Fookes, 1991, 1997; Hutchinson, 2001). As they are geologically young geological materials, the physical properties of primary glacigenic soils reflect the climatically-controlled geological processes of erosion, transport and deposition (Boulton & Paul, 1976; Culshaw *et al.*, 1991; Fookes, 1991). In contrast, freezing effects in glacial and non-glacial environments may modify the depositional state of primary glacigenic sediments and frost-susceptible soils.

Primary depositional geological processes influence soil properties including particle size, shape, mineralogy and fabric (Boulton & Paul, 1976; Paul *et al.*, 1981; Trenter, 1999). Post-depositional processes and changes in stress within the ground have the potential to alter the geotechnical behaviour of engineering soils and/or *in situ* geological bedrock. Changes in stress can be brought about by different processes including deposition, erosion, shear failure, groundwater level and flow, glacier-induced loading, freezing and thawing of ground-ice and mechanical weathering. Changes in total stress can be considered a result of geostatic loading either through sedimentation or loading by glacier ice. Changes in porewater pressure within the skeleton of a given volume of soil also take place in response to external stress change. When porewater pressure is considered, the net stress acting on the solid particles within a soil is termed effective stress and is given by:

$$\sigma' = \sigma - u$$

Equation 2-1

where σ′ is effective stress, σ is total stress and u is porewater pressure

This concept is fundamental in soil mechanics. It can also be usefully applied to interpret the likely stress changes experienced by a primary glacigenic deposit or geological bedrock in response to changes in groundwater conditions and glacier-ice growth and decay which result in volume change (Skempton & Weeks, 1976; Paul *et al.*, 1981; Hutchinson, 1991, 2001; Boulton & Dobbie, 1993; Boulton, 2010). Using total stress only had led to claims that the degree of overconsolidation in a till, for example, can be related to past preconsolidation

pressure as a function purely of ice thickness (Kazi & Knill, 1969). Boulton (1977), through a study of modern glaciers in Spitsbergen, Svalbard, demonstrated that sub-glacial drainage and post-depositional wetting and drying brought about changes in effective stress and consequently, degree of consolidation.

2.2.1 Ground freezing and glaciation

The mechanical behaviour of freezing, frozen and thawed soils is dependent on the proportion of, and interaction between, solid soil particles, frozen and unfrozen water and air within the skeleton of the soil. Volumetric expansion during the phase change of unfrozen water to ice by about 9% results in heave. In addition, the formation of ground ice results in the introduction of moisture which exceeds the moisture content in the unfrozen state. Excess ice contents in sandy, clayey silt between 11 and 90% were measured by the author in ice-rich permafrost in Adventdalen, Svalbard (Figure 2-4). Along with its subsequent degradation during thaw, ground heave and subsidence present one of the main geotechnical hazards in present-day permafrost environments (French, 2007).

The main types of ground ice of relevance for understanding former ground conditions in lowland Britain are pore, segregated, intrusive and wedge ice (Murton & Ballantyne, 2017). Pore ice is crystalline and generally forms in the pore space of granular materials whilst segregated ice forms in fine-grained sediments and rocks rich in silt and clay. Segregated ice lenses may be <10 mm to >10 m thick (Murton & Ballantyne, 2017). Intrusive ice forms as veins injected under pressure into frozen or partially frozen ground. Wedge ice forms by the aggradation of ice in pre-existing thermal contraction cracks. Ground ice growth is controlled by grain-size, mineralogy, hydraulic conductivity and porosity. A grain size of <0.075 (fine silt) is critical for the development of segregated ice. Fine-grained lithologies are said to be frost susceptible where segregated ice forms within their soil matrix.

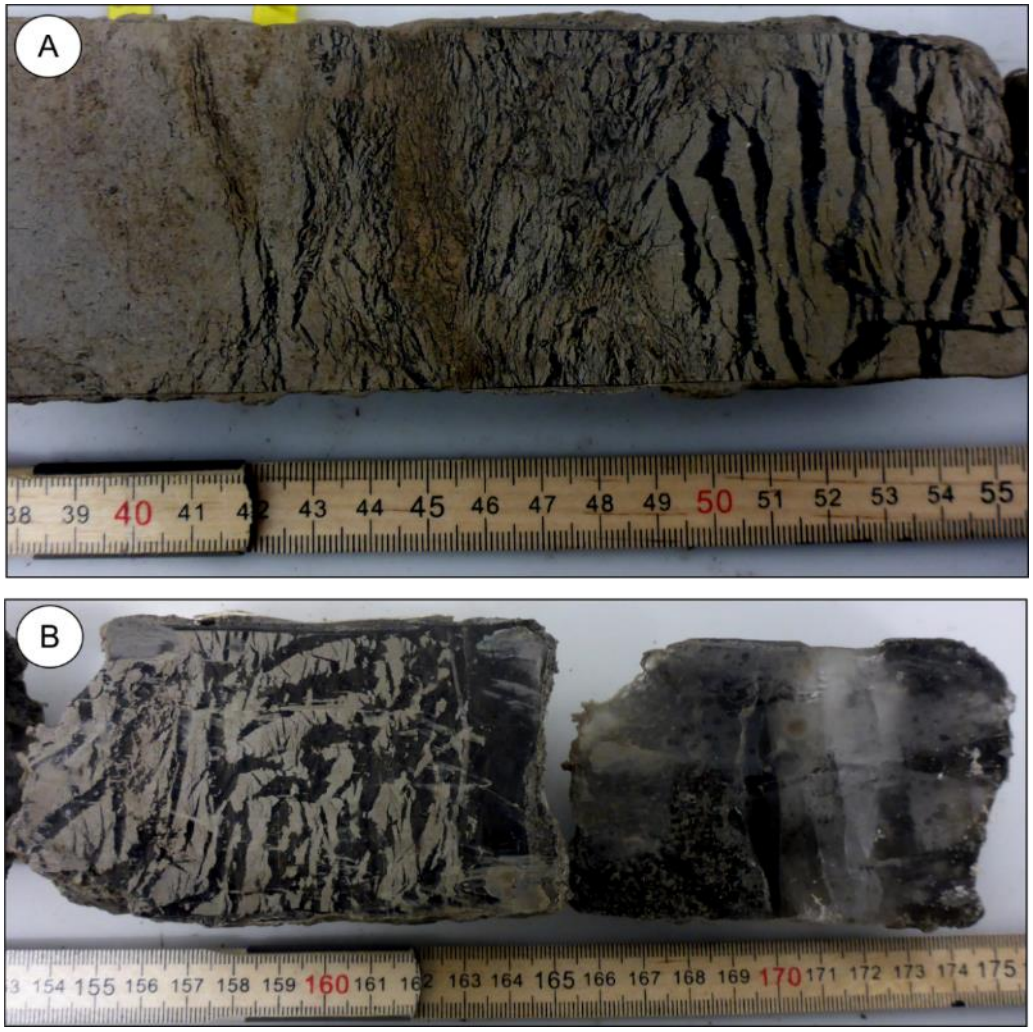

Figure 2-4 Segregated ice lenses grading downwards to massive-ice in icy sandy-silt, valley fill sediments, Adventdalen, Svalbard. A) Transition from thin ice laminations in the seasonally frozen active layer (<42 cm), thick laminations in the transition zone (40-49 cm) to thin beds of segregated ice in the permafrost zone, B). Massive-ice >165 cm. Photographs by Kasia Stachniak taken during group permafrost drilling and laboratory exercises in Svalbard. Depths are centimetres below ground level.

The thermo-mechanics of ground freezing are described by Williams & Smith (1989). The geotechnical effects of freezing and thawing on the consolidation characteristics of undisturbed and reconstituted fine-grained soils is described experimentally by Morgenstern & Nixon (1971), Nixon & Morgenstern (1973) and Konrad & Morgenstern (1981). In terms of the effects of freezing and thawing on geotechnical properties and behaviour, six processes are critical and are summarised below mainly from Williams & Smith (1989) and Konrad and Morgenstern (1981).

1. Differences in thermal conductivity and diffusivity result in differential cooling rates of the ground. During ground cooling, tensile horizontal stresses are established that result in the formation of vertical to sub-vertical thermal contraction cracks when the

tensile strength of the ground is exceeded. In plan view, thermal contraction cracks develop into a network of five or six-sided polygon nets. Thermal contraction cracks may become filled with sediment, snow and/or ice to form ice-wedges.

2. Groundwater acts as a weak solute and so its freezing point is depressed relative to pure water which freezes at 0°C. The implication is that unfrozen water can exist within the ground at temperatures below 0°C and that this is more common in soils with high porosity and low permeability (Figure 2-5). Soils with clay minerals will also retain unfrozen water adsorbed onto their crystal surfaces.
3. During ground freezing in soils of low permeability and high porosity, unfrozen water can migrate beyond the 0°C isotherm and freeze above it (in top-down freezing) in a zone referred to as the frozen fringe. Here, unfrozen water is drawn by capillary to the freezing front under temperature-induced potential energy gradients. At the freezing front, segregated ice forms as lenses parallel to the freezing accompanied by release of latent heat during the phase transition of liquid water to ice. Sub-horizontal discontinuities can form at the location of segregated ice-lens growth which have been experimentally shown to exist near the ground surface in top-down freezing and at the base of the active layer/top of permafrost in bi-directional freezing. In bi-directional freezing a desiccated zone forms where unfrozen water is drawn to surface-down and permafrost-up freezing fronts.
4. Thermally-induced potential energy gradients can induce suction pressures by capillary action and increase effective stress at the freezing front in frost susceptible fine-grained soils. Suction pressures upto 1MPa have been recorded in clayey and silty soils during cooling from 0°C to -0.75°C and up to 3.8 MPa when cooled to
   -1°C. Such suction pressures can therefore result in preconsolidation of soil by freezing (Chamberlain & Gow, 1979).
5. Permafrost forms where the ground remains at or below 0°C for at least two consecutive years. Permafrost is therefore defined based on temperature rather than ice-content of the ground. Consequently, permafrost can be ice-rich or ice-poor depending on grain size, availability of moisture and climate.
6. A seasonally freezing and thawing active layer, commonly between 1 and 3 m thick, is developed above permafrost where spring/summer temperatures exceed 0°C. The thickness of the active layer is dependent on factors including ground surface temperature during thawing, thermal conductivity of the soil, duration of the thawing season, dry density of the soil and the mass of frozen and unfrozen water (French,

2007). The rate and magnitude of thaw is controlled by the hydraulic conductivity of the host material and frozen or unfrozen material surrounding it.

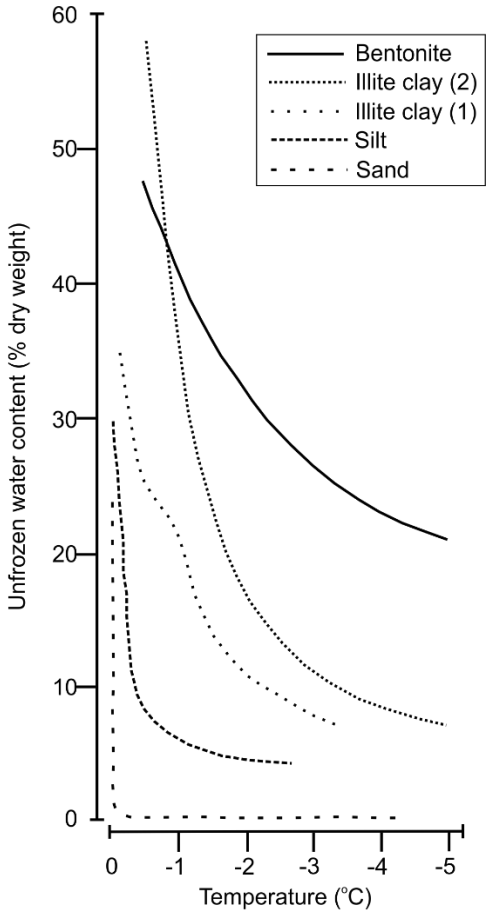

Figure 2-5 Influence of grain-size on the amount of unfrozen water remaining during freezing. Modified after Williams & Smith (1989). Below ~1.5°C water is adsorbed onto dominantly clay minerals.

Although complex and often superimposed through geological time, a summary of the probable geotechnical consequences of glacial and non-glacial freezing processes soils is given in the following sections and summarised in Figure 2-6. This summary is new and has been produced from consideration of geological and geotechnical literature. Geotechnical consequences are considered in the context of the type of geotechnical property or behaviour that could be affected. Glacial effects on the following properties and behaviour are considered with reference to till type. Freezing effects in glacial and non-glacial environments are considered with reference to fine-grained clay- and silt-rich sediments including till and fine-grained bedrock.

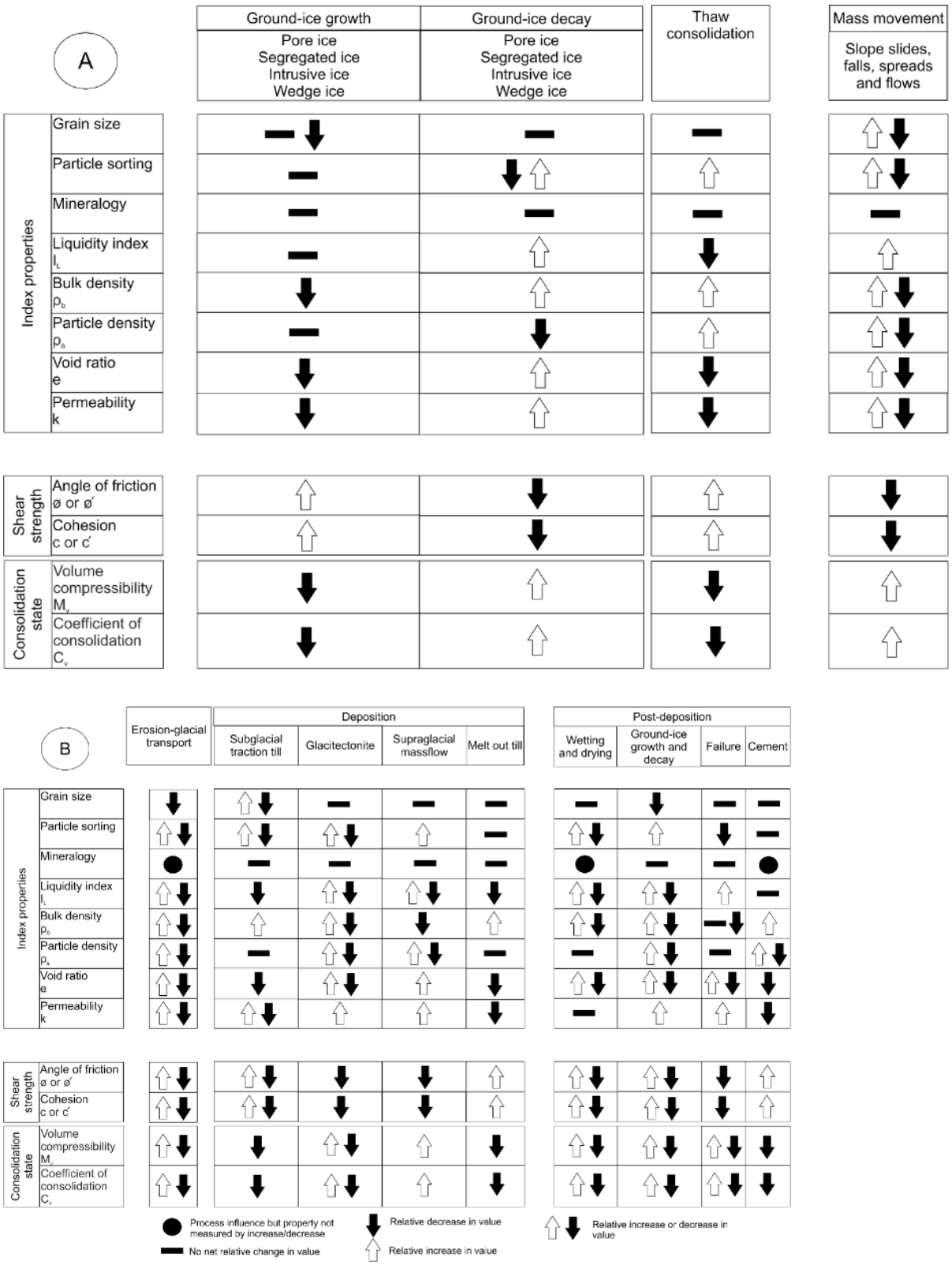

Figure 2-6 Examples of the effects of ground freezing (A) and till erosion, transport, depositional and post-depositional processes (B) on selected geotechnical properties and behaviour interpreted by the author. Summarised from sources including Morgenstern & Nixon (1971), Nixon & Morgenstern (1973), Boulton & Paul (1976), Paul *et al*. (1981), Konrad & Morgenstern (1981), Boulton & Hindmarsh (1987), and Williams & Smith (1989).

The revised and rationalised definitions of till types used here, are those from the outcomes of the Engineering Group of the Geological Society's Working Group on glacial and periglacial engineering geology (Culshaw *et al.*, 2017; Giles *et al.*, 2017). This classification rationalises previous classifications of till that have been used in Quaternary and engineering geology in the UK (e.g. McGown & Derbyshire, 1977; Trenter, 1999).

The four till types are referred to in Sections 2.2.2 to 2.2.7 where the process of deposition is significant in controlling geotechnical properties and behaviour. The four till types are briefly summarised from Giles *et al*. (2017) as:

- **Subglacial traction till**. Sediment deposited by a glacier sole either sliding over and/or deforming its bed, the sediment having been released directly from the ice by pressure melting and/or liberated from the substrate and then disaggregated and completely or largely homogenised by shearing;
- **Glacitectonite**. Rock or sediment that has been deformed by subglacial shearing but retains some of the structural characteristics of the parent material;
- **Supraglacial massflow**. Clast-supported, massive to crudely stratified or graded sediments of variable grain-sizes. Sedimentology of depocentres is complex due to multiple cycles of redeposition. Typical facies associations comprise interbedded sediments of mixed grain-sizes and discontinuous bodies of laminated lacustrine sediments and glaciofluvial sands and gravels. Internal disturbance is common and characterized by normal faulting, flow folding & soft sediment deformation.

2.2.2 Till particle-size and fabric

The particle-size distribution of Quaternary soils varies from well-graded silt and clay with cobbles and boulders, uniformly graded dense to loose sand and gravel, to laminated clay and silt and peat. The range of grain-sizes that are characteristic of Quaternary soils means that they do not conform to simplified models of soil behaviour based on clay and sand end-members (e.g. Barnes 2010; Shukla 2014). For simplicity, the significance of glacial and freezing effects on index properties is illustrated here with reference to till.

Debris that eventually becomes till is entrained within glacier ice from two main sources; subglacial erosion and supraglacial rockfall, debris-flow and avalanches. It is then transported on, within and below a glacier where it is then deposited in a range of sub-and supra-glacial environments. Debris-rich ice at the base of a glacier (Figure 2-7) is entrained at its sole as it overrides its basal bed which may be sediment or bedrock. Debris becomes entrained when

the frictional strength of the sediment or bedrock is exceeded by the shear stress at the base of the glacier (Benn & Evans, 1998).

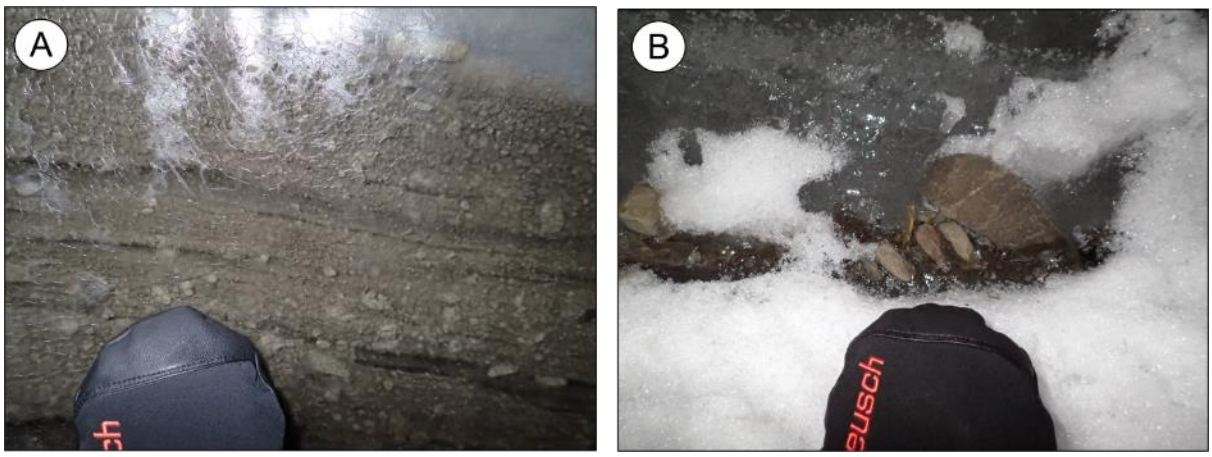

Figure 2-7 Debris-rich basal glacier ice in Svalbard observed by the author. A) Banded silt and fine to coarse sand debris in the Larsbreen Glacier. Banding is probably a result of basal shear, parallel to the glacier sole. B) Imbricated coarse gravel in the Longyearbreen Glacier. Glacier flow in B is from right to left. Mitt for scale.

In debris-rich zones at the glacier sole, particle-particle and particle-bed contacts are common. These particle contacts acting under basal shear stress induce mechanical grinding and erosion imparting a usually silt-grade 'rock flour' into the resulting till deposit (Boulton & Paul, 1976).

Sediment mineralogy is dependent on the nature of the source material and may only be modified by post-depositional weathering. Tills are often poorly-sorted (well-graded) sediments with multi-or bi-modal particle-size distributions (Sladen & Wrigley, 1983; Trenter, 1999). They are often referred to in the Quaternary geological literature using the non-genetic term diamicton although the term is not exclusive to till. Tills with 30-45% or more fine particles (fine sand or less) are matrix-supported with coarser particles acting as discrete particles (McGown & Derbyshire, 1977). Where the fines component is <15% the till is described as granular.

Particle-size, shape and degree of sorting is further modified by the environment of deposition. The particle-size distribution of subglacial traction tills is inherited from the source of the sediment and its degree of basal abrasion and particle-particle collisions. Melt-out is deposited by melting of ice in buried and detached masses of debris-rich ice typically near the margins of retreating glaciers (Giles *et al.*, 2017). Thinly-bedded and/or laminated sediment may be present if preserved during ice-melting. Supraglacial tills mass-flow and debris-flow tills are deposited by gravitational mass-movement. Their particle-size is

dependent on the source material and distance from the flow source. They are commonly clast-supported, poorly-sorted and crudely bedded (Giles *et al.*, 2017). Lenses of sand may be common. Glaciotectonites comprise subglacial traction till that has been deformed by subglacial shearing although retains some of the original character of the undeformed material (Giles *et al.*, 2017). Banding, representing discrete differences in grain size may be present in the parent material. Deformation may result in changes in particle-size as packages of sediment and/or bedrock are emplaced into the mass of the till.

The growth and decay of ground ice in Quaternary sediments is known to influence patterns of particle sorting. Involutions produced by thaw-induced, density-driven currents result in sediment mobilization and reworking (Murton & French, 1993; Murton *et al.*, 1995; French, 2007). Repeated freezing and thawing of moist, poorly-sorted soils has been shown to result in net downward migration of clay, silt and fine-sand and net upward migration of coarse particles within a soil column (Ballantyne & Harris, 1994). Mechanical sorting in the active layer induced by frost 'pull' or 'push' results in sorted or non-sorted forms of patterned ground including polygons, stripes, circles and earth hummocks. Post-depositional sorting produced by seasonal active-layer freezing and thawing may therefore modify the depositional fabric of a soil.

Physical weathering processes including frost wedging, frost splitting, frost scaling and granular disintegration can modify primary particle-size distributions in Quaternary soils and bedrock (Ballantyne, 2018). Field observation and laboratory experimentation have demonstrated the effectiveness of ice-segregation as a weathering mechanism in fine-grained rocks causing cracking and brecciation (Chandler, 1970; Skempton & Weeks, 1976; Murton *et al.*, 2006). Figure 2-8 illustrates examples of frost weathering in fine-grained rocks.

Salt effloresence occurs in salt-rich, high porosity sedimentary rocks with weak tensile strength in arid polar environments (Ballantyne, 2018). The precipitation and growth of salts including halite and gypsum has been shown to generate tensile stresses in the order of 15 MPa. Stresses of this magnitude can result in the formation and propagation of microcracks which enhance mechanical weathering.

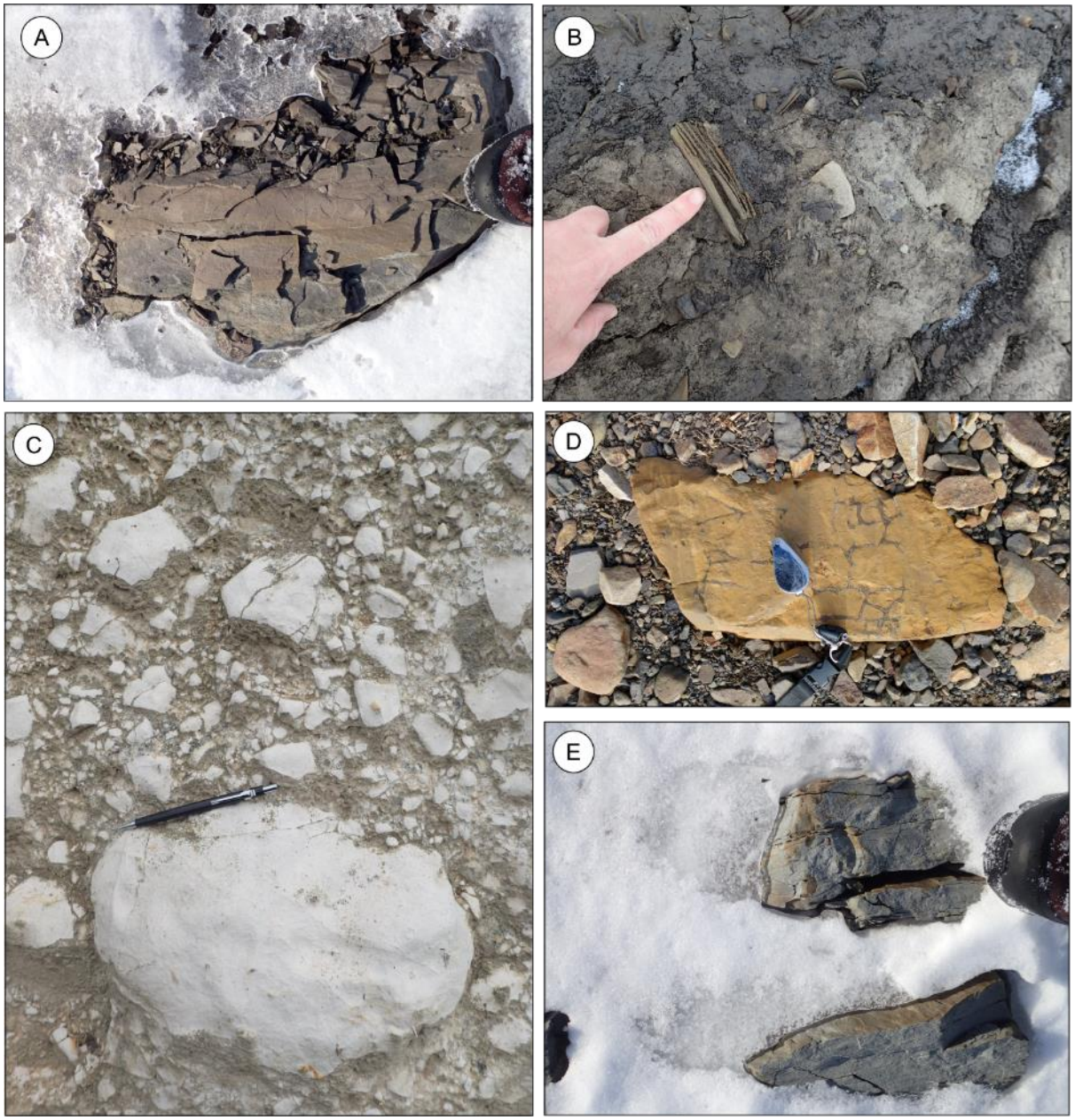

Figure 2-8 Examples of evidence of present day and relict frost weathering in fine-grained rocks. A) Frost wedging along vertical joints, and frost splitting parallel to bedding in sandy siltstone. B) Frost splitting parallel to bedding in sandstone clast within pingo-rampart debris. C) Type 2 brecciation of chalk (ice segregation). D) Polygonal ice-filled cracks. E) Frost splitting. A, B, D and E Adventdalen, Svalbard, C Pegwell Bay, Isle of Thanet, UK. Boot for scale in A and E. All photographs by the author.

2.2.3 Atterberg limits (plasticity)

The range of moisture contents at which a soil behaves as a liquid (liquid limit) and as semi-solid (plastic) are known as Atterberg limits and their difference describe a soil's plasticity index (PI). Specifications for reconstituting the <425μm fraction of soil, on which its plasticity determination is based, are given in e.g. Anonymous (1990) The threshold liquid (W_L) and plastic (W_p) limits are a function of the particle-size and mineralogy of the soil (e.g. Holtz *et al.*, 2011). Soils with clay minerals usually have higher liquid limit because of

adsorption of liquid water onto clay lattice layers. The ratio of the difference between the *in situ* moisture content (ω) of a soil and its plastic limit to its plasticity index defines its liquidity index (LI):

$$LI = \frac{\omega - W_p}{PI}$$

Equation 2-2

Soils whose LI values are close to or below 0 will behave in a brittle manner when unconfined, those with values between 0 and 1 will be plastic and those with LI >1 will be effectively liquid.

As a result, tills inherit their plasticity characteristics from the debris source, transport distance and post-depositional changes in grain-size.

2.2.4 Density

In considering changes in density, it is useful to view the skeleton of an unfrozen soil in terms of its component parts (Figure 2-9).

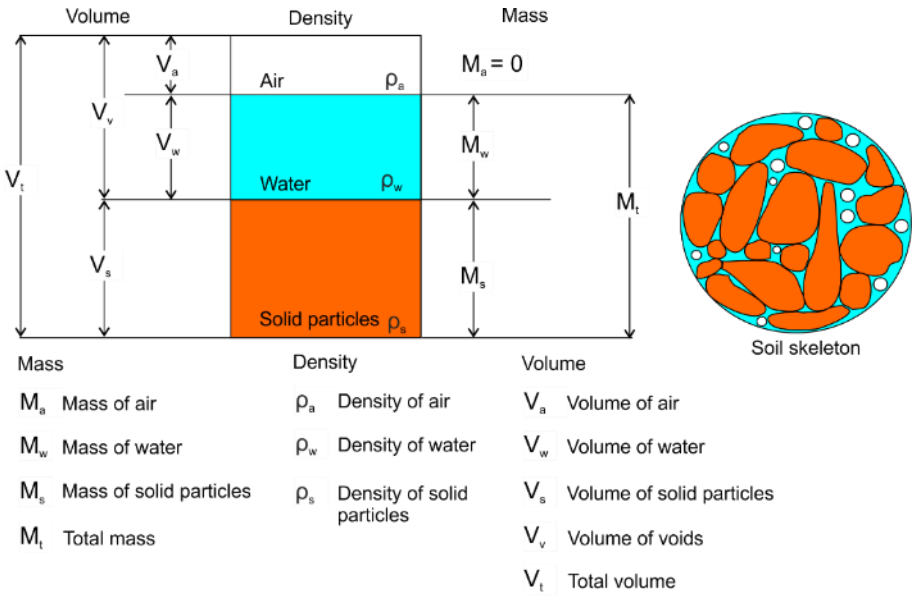

Figure 2-9 Conceptual unfrozen soil model and its components in terms of mass, volume and density produced by the author, based on Holtz *et al.* (2011). In a frozen soil, V_v will increase as volumetric expansion takes place during the phase transition from liquid water to ice.

The ratio between mass (M) and volume (V) is density (ρ):

$$\rho = \frac{M}{V}$$

The ratio of the volume of voids to the volume of solid particles is expressed as void ratio (e):

$$e = \frac{V_v}{V_s}$$

Void ratio is related to porosity (n) by:

$$e = \frac{n}{1 - n}$$

$$n = \frac{e}{1 + e}$$

Bulk (ρ_b), dry (ρ_D) and particle density (ρ_s) are properties that are susceptible to changes brought about by glacial and non-glacial cold-climate processes.

Particle density (specific gravity) refers to the ratio of the average density of solid particles to the average density of water. For tills, particle density is therefore a function of debris source area and distance of transport. It may be affected by post-depositional cementation where cement becomes a component part of the particles during particle density measurement.

Bulk density is the average mass of solid and liquid parts of a soil (assuming the mass of air ≈0) in a given volume. Assuming no particle disintegration, changes in bulk density are accompanied by expulsion (consolidation) or absorption (swelling) of water and therefore effective stress. In the former case, effective stress gradually increases and void ratio decreases as porewater pressures are dissipated. As effective stress decreases during swelling, void ratio increases. Void ratio also increases during the phase transition of liquid water to ice. Decreasing void ratio results in densification of the soil skeleton which may also correspond to increasing shear strength and a decrease in compressibility.

Dry density is a measure of the ratio of the mass of dry particles in a given soil mixture to its volume. Like particle density, changes in its value are dependent on debris source area and transport distance. Values of dry density may be increased if the soil skeleton is subjected to compaction-like effects including subglacial loading under high effective stresses.

The ratio between V_w and V_v is the degree of saturation (S_r):

$$S_r = \frac{V_w}{V_v}$$

Where $V_w = V_v$, $S_r = 1$. The depositional and post-depositional processes influencing S are complex. Primary deposition of till for example may decrease S_r in response to subglacial loading. Supraglacial mass-flow or remoulded subglacial till may result in increased values of S_r. The development of segregated ice draws porewater to a fine-grained soil's freezing front

so that on melting, the mass of water is increased relative to the unfrozen state of the soil and so S_r increases. Changes in groundwater levels contribute further to post-depositional changes in the value of S_r.

2.2.5 Permeability

Permeability is principally proportional to the square of the pore size available for fluid flow and therefore is also a function of porosity (or void ratio) and the nature and degree of connectivity between pores (void space) which may be wholly or partially filled with water. Consequently, any change in void ratio will be accompanied by a change in permeability. During freezing of a fine-grained soil, permeability decreases as liquid water is transformed to ice. On thawing, and presuming drainage is permitted, porewater is expelled, the void ratio decreases, porosity decreases and consolidation occurs. Connectivity between voids within the soil is also dependent on the size, shape (sphericity and angularity), degree of sorting and degree of packing of the solid particles.

Importantly, freezing and thawing within soils produces horizontal and subvertical cracks that can increase permeability (Chamberlain & Gow, 1979). Permeability is often anisotropic as the increase in vertical permeability is a greater magnitude than that in the horizontal plane.

In a subglacial depositional environment, changes in permeability are controlled by changes in effective stress. Changes in effective stress are dependent on the magnitude of applied stress, degree of saturation and the starting permeability of subglacial sediments or bedrock which governs rate and magnitude of drainage. Subglacial consolidation (Boulton & Paul, 1976; Boulton & Dobbie, 1993) and deformation (Boulton & Hindmarsh, 1987; Phillips & Lee, 2013; Lee *et al.*, 2017) may control changes in permeability. Assuming drainage is allowed, consolidation results in sediment densification as porewater is expelled and void ratio decreases. The initiation of brittle deformation structures introduces discontinuities. Discontinuities including geological faults may act as groundwater flow paths themselves and increase vertical and/or horizontal permeability. Displacement of geological layers of contrasting permeability may increase or decrease permeability of the deforming soil mass. Subglacial shearing has been shown to result in changes to the structures and density of sediment deposited beneath glacier ice. Subglacial shearing and its extent beneath the glacier sole, commonly results in the formation of two distinct layers, referred to as the A and B Horizons, where the A horizon (if present) overlies the B Horizon (e.g. Benn & Evans, 1998). The A Horizon is typically characterised by deformed sediment and is interpreted to form by shear-induced sediment dilation. This effect decreases with increasing depth beneath the

glacier sole. Subglacial shear deformation has been shown to decrease porosity and increase permeability in the upper A-Horizon of subglacial traction tills compared to the underlying B-Horizon (Boulton & Hindmarsh, 1987; Benn, 1995)

Within the supraglacial depositional environment, mass-flow processes may result in a less dense soil and more open fabric. Consequently, porosity and void ratio are likely to be higher.

2.2.6 Compressibility (consolidation state)

Suction pressures developed at the freezing front within fine-grained soils increase effective stress within the soil skeleton resulting in additional localised consolidation which could be considerable once the previous maximum preconsolidation has been exceeded (Chamberlain & Gow, 1979; Chamberlain, 1981; Williams & Smith, 1989). Plastic compression would continue until the soil reached its shrinkage limit. The expelled porewater thus also contributes to the formation of ice within the soil skeleton. The permeability of the soil will determine the rate of dissipation of excess porewater pressure and consequently the thaw consolidation ratio (Nixon & Morgenstern, 1973). If drainage is subsequently allowed or the vertical stress on the soil is increased by loading, re-loading and consolidation of the soil will occur.

The effective stress path that is taken by a fine-grained soil whereby cryostatic suction is developed and ice lenses form and degrade during one cycle of freezing and thawing is illustrated in Figure 2-10(1). In this hypothetical scenario, a normally consolidated soil lies on the virgin compression curve at an arbitrary point A where all excess porewater pressure has dissipated and so has an effective stress σ'_A and void ratio e_A. As freezing occurs, effective stress increases as large hydraulic potential gradients initiate suction and porewater is drawn to the freezing front. At point B the increase in freezing induced effective stress results in an effective stress of σ'_B and void ratio corresponding to e_B. This represents the maximum effective stress experienced by the soil. At the onset of temperature-induced thawing, the increase in porewater pressure reduces effective stress and induces swelling of the soil so that its void ratio increases to point C. Providing drainage is allowed, excess porewater pressure dissipates, effective stress increases and consolidation occurs to the final point D. The reduction in volume in the sample as a result of one cycle of freezing and thawing is therefore $e_A - e_D$. The sample is overconsolidated as its overconsolidation ratio (OCR) is >1:

$$OCR = \frac{\sigma'_{\mathrm{p}}}{\sigma'_{\mathrm{vo}}}$$

Equation 2-3

$$OCR = \frac{\sigma'_B}{\sigma'_D}$$

Equation 2-4

where σ'_p is preconsolidation pressure and σ'_{vo} is the *in situ* effective stress. Preconsolidation pressure represents the maximum previous effective stress experienced by the soil. At point C, the corresponding effective stress is termed residual stress and represents the remaining intergranular stress after completion of porewater pressure dissipation (Nixon & Morgenstern, 1973). It has been shown that the magnitude of difference between unfrozen and frozen-thawed degree of overconsolidation is greater in clay-rich soils than silt-rich soils (Figure 2-11 A and B).

Overconsolidation also results from multiple-freezing and thawing cycles (Figure 2-10(2)). The net amount of consolidation decreases with increasing effective (residual) stress (Nixon & Morgenstern, 1973). Importantly, overconsolidation during freezing is modified by subsequent drainage-dependent expulsion of porewater. Changes in the arrangement of soil particles accompany freezing and thawing so that clay and silt particles are aligned parallel to the plane of the freezing front and perpendicular to the direction of freezing (Chamberlain & Gow, 1979). In addition, horizontal and vertical discontinuities form because of the growth of segregated ice and suction tension within the soil skeleton (Chamberlain & Gow, 1979).

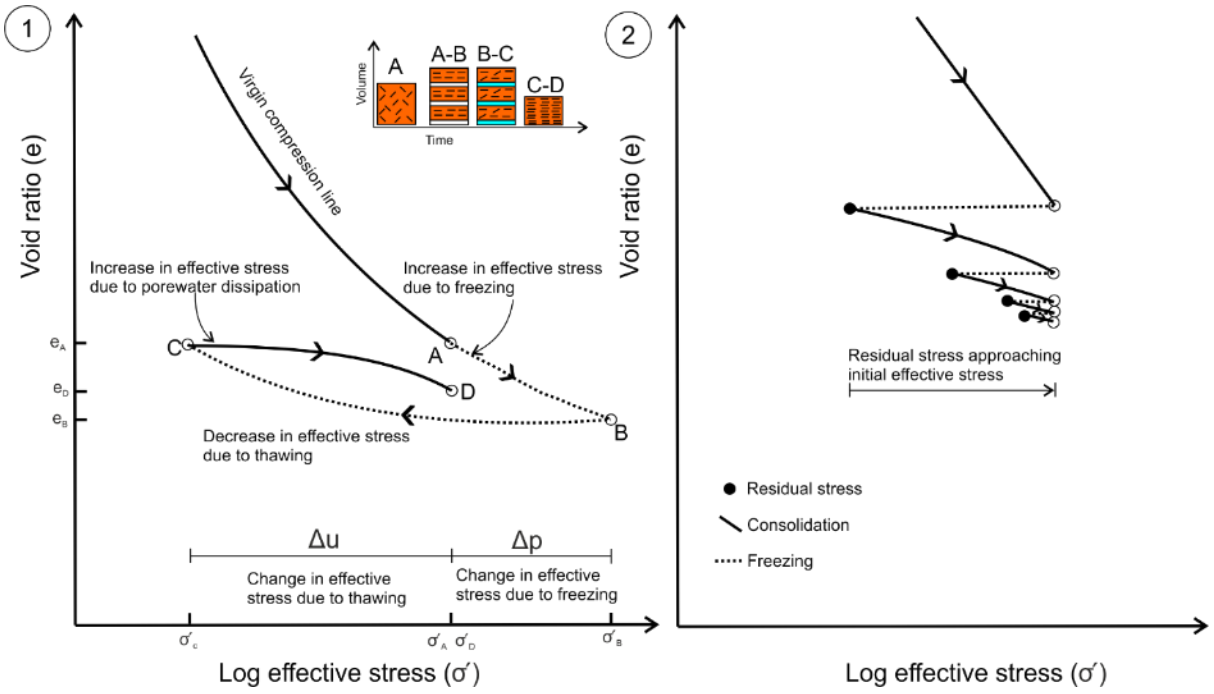

Figure 2-10 Consolidation effects of one cycle of freezing and thawing in a fine-grained soil (1). Consolidation effects of cyclic freezing and thawing under constant applied stress (2). By the author after Nixon &

Morgenstern (1973), Paul *et al.* (1981), and Chamberlain & Gow (1979). u is pore pressure, p is (suction) stress. Legend for soil model colours as for Figure 2-9 except in A-B where white represents ice.

The implication of effective (residual) stress during thaw-induced, one-dimensional, undrained thaw consolidation with higher the residual stress is that it will result in lowering the consolidation settlement, lowering the pore-pressure generated during thawing and increase the undrained shear-strength (Nixon & Morgenstern, 1973). The combined effect of these factors means that for a given value of effective stress, the coefficient of volume compressibility (m_v) is increased compared to a similar soil in its unfrozen and subsequently thawed state (Figure 2-11C).

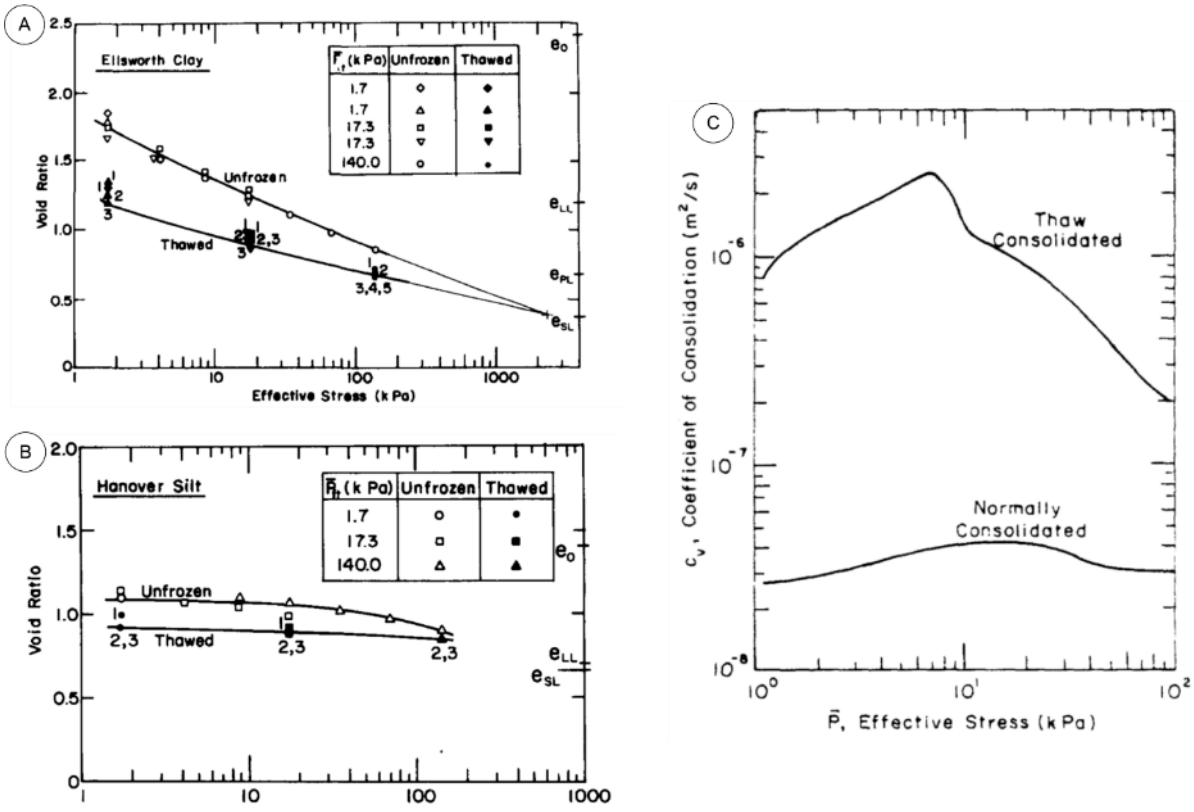

Figure 2-11 Consolidation effects of freezing and thawing for clay-rich (A) and silt-rich (B) soils after Chamberlain & Gow (1979). In each soil type, freezing and thawing moves the soil to a denser state and the magnitude of change decreases with increasing effective stress. C) Magnitude of effect on coefficient of consolidation (c_v) as a function of effective stress after Chamberlain (1981).

Subglacial changes in effective stress as a result of variations in groundwater discharge and flow, deformation and loading beneath glacier ice, have also been shown to account for differences in the consolidation state of glacigenic sediments (Boulton & Paul, 1976; Boulton & Dobbie, 1993). Sub-glacial loading by glacier ice causes an initial increase in porewater pressure. The resulting pressure gradient allows dissipation of excess porewater pressure by expulsion of porewater providing that drainage is allowed according to the theory of one-

dimensional consolidation. Porewater pressure is expected to be higher and consequently effective stress lower, in a subglacial environment compared to a non-glacial or periglacial setting (Boulton & Dobbie, 1993). This effect results from the supply of groundwater from melting ground ice or from flow derived from the sole of temperate glacier ice where the rate is governed by the permeability of the sediment. The flow is maintained by a water potential pressure gradient and so effective pressures are lowered. Only at lower permeabilities will effective stresses be increased. The lower the permeability, the greater the effective stress gradient needed to maintain a given groundwater discharge rate (Boulton & Dobbie, 1993). For sediments with permeabilities $<10^{-10}$ to 10^{-8}, the pressure gradient needed to maintain a given discharge rate increases above the pressure gradient that exists due to geostatic pressure. As a result, effective stresses are higher only in lower permeability subglacial sediments.

The grain-size of the subglacial substrate is a critical factor that controls basal glacier meltwater discharge and drainage. Subglacial sediments with high permeabilities permit drainage, flow and consolidation and result in higher effective stresses at the glacier sole than sediments of lower permeability. For sediments with lower permeability, drainage is impeded, effective stresses are increased and compressibility is reduced.

Changes in subglacial effective stress influence the magnitude of overconsolidation that would be expected if overconsolidation was due purely to gravitational loading by the combined weights of soil particles, unfrozen water and ice. If the subglacial substrate has a low permeability ($<10^{-10}$ to 10^{-8}) and promotes a high potential pressure gradient and low effective stress at the glacier sole, the increase in preconsolidation pressure with depth should be greater than gravitational (Boulton & Dobbie, 1993). In contrast, if the substrate has a high permeability ($>10^{-8}$) and promotes a low potential pressure gradient with a higher effective stress at the glacier sole, preconsolidation pressures should be approximately gravitational. This relationship was shown to be true for late Pleistocene, permeable tills on the east coast of Yorkshire and for Middle Pleistocene glaciolacustrine sediments in the Netherlands (Boulton & Dobbie, 1993).

2.2.7 Shear strength

The shear strength of a soil depends on a unique combination of normal effective stress, frictional resistance to shear and the tendency to dilate or expand in volume on being sheared. In terms of effective stress, shear strength is conventionally defined according to the Mohr-Coulomb failure criterion:

$$\tau = c' + \sigma'(tan\text{ø}')$$

Equation 2-5

where τ is shear resistance (shear strength) on a given plane, c′ is effective ('true') cohesion, σ′ is effective stress and tanø′ is the angle of shearing resistance related to friction (Figure 2-12A).

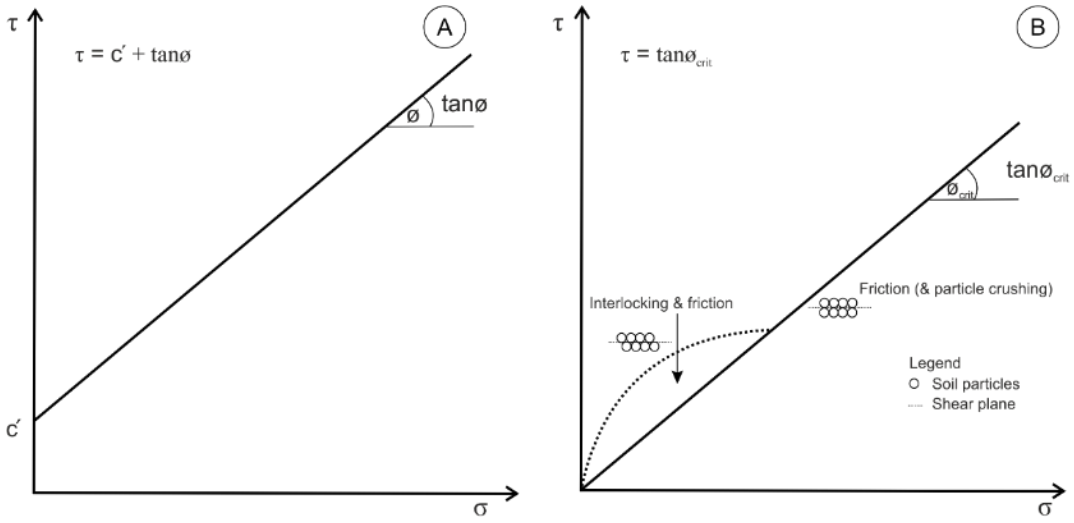

Figure 2-12 Mohr-Coulomb failure criterion A) and effect of dilatancy at low to intermediate effective stresses B). Modified after Knappett & Criag (2012).

While this model applies to loose soils, it does not represent the effect of dilatancy in dense, granular soils during shear at low to moderate effective stresses (Bolton, 1986). At low to moderate effective stresses, resistance to shearing is provided by friction and the interlocking of soils particles (Figure 2-12B). The magnitude of interlocking, and rate of dilatancy, depends on factors including mineralogy, particle roundness, grading and sphericity. In addition, if effective stress is equal to zero, shear stress must also be equal to zero for frictional resistance to shear. At low to moderate effective stresses, particle interlocking provides additional strength which must be overcome by volume increase and dilatancy as particles begin to move relative to each other and so the failure envelope is in fact curved. During this stage, tanø is not constant as suggested by the Mohr-Coulomb failure criteria. At a critical effective stress, dilatant behaviour ceases and frictional strength dominates so that tanø = ø$_{crit}$ at high effective stresses. This model predicts that regardless of initial state, all soils will reach a critical state where shear deformation occurs with no further change in effective stress.

Because of the curved failure envelope for dense granular soils and overconsolidated clays, envelope peak strengths are greater than their critical state values at low to moderate effective

stresses. Clays that possess zero or small interparticle bonding ($c' = 0$) must have failure envelopes that pass through the origin from the critical state as shown for dense sands in Figure 2-12b (Atkinson, 2007).

The temporary effects of ground freezing and thawing on undrained shear strength are complex. Physical effects are dependent on the magnitude and cause of changes in effective stress, ground ice type and its mechanical properties and the proportion of frozen and unfrozen water within the soil's skeleton. In general, freezing results in increased strength due to the increased cohesion between solid particles by cementation by ice, but this effect decreases at high confining stresses (Czurda & Hohmann, 1997). Frozen soil also displays time-dependent creep behaviour; exhibiting a similar behaviour to ice.

The effects of freezing and subsequent thawing on the shear strength of a soil can be summarised in four steps (Sage & D'Andrea, 1988). In its unfrozen state, a fine-grained soil is in its densest state with assumed tight packing of soil particles. On freezing and growth of ice lenses, solid particles become dispersed by ice and so the particle and bulk density decreases. On thawing, some degree of the freeze-induced dispersion particle packing is retained so that the soil is in its weakest, least dense state. Providing drainage is allowable during thawing, excess porewater will be expelled and consolidation will occur so that the density increases and shear strength increases towards its pre-frozen state.

For a frozen soil, short-term shear strength is a function of normal stress and temperature which influences cohesion. The temperature influence on the frictional component of strength is considered to be small (Czurda & Hohmann, 1997). Shear strength is time dependent; resistance to shearing decreasing with time, applied load and number of freeze-thaw cycles. Experimental investigation on the effects of unidirectional freezing in open and closed hydraulic systems, using clay and silt soils, was undertaken by Czurda & Hohmann (1997). The undrained shear strength of samples subjected to one cycle of open or closed-system freezing were measured using a shear-box device and compared to their unfrozen behaviour. All frozen samples, except for those with 86% kaolinite, exhibited an increase in shear strength parameters c and ø and that values for samples frozen in the open system most closely reflected those in their unfrozen state. The latter implies that the shear strength at the freezing front is similar to the unfrozen state. In the open system, differences in temperature between the upper and lower parts of the sample did not appear to influence ø. In the closed system, without such vertical temperature differences, c and ø were increased with values of c increased upto 10 times. Small differences in shear strength in the open system were

attributed to the original moisture content of the samples and differences in cation exchange capacity (cec) associated with clay minerals. Smectite-rich samples with high cec and high specific areas, influence the orientation of clay particles and their adsorbed water layers which in turn governs ice-lens formation and ice-bonding.

The relationship between shear strength and excess pore pressure developed in thawing soils has been established and used to explain failure of clay-rich solifluction material on slopes <3º (Hutchinson, 1974; Skempton & Weeks, 1976). Using the Mohr-Coulomb failure criterion, Skempton & Weeks showed that in undrained conditions, the ratio between pore pressure and geostatic pressure can be expressed as:

$$r_u = \frac{\gamma_w h}{\gamma z}$$

Equation 2-6

where γ_w is the unit weight of water, γ is unit weight of soil, h is piezometric height and z is depth. If γ is usually $2\gamma_w$, then r_u = ~0.5. Where r_u = 1, pore pressure is equal to geostatic pressure and therefore piezometric head would rise to a height equal to 2z. Skempton & Weeks (1976) calculated values of r_u between 0.83-0.93 assuming a depth of thaw of 2 m, thaw time of 3 months and c_v of 2.5m^2/year. Using these values of r_u and thaw depth, limiting slope angles between 1.3º-3.0º were calculated using effective strength parameters c′ = 1kN/m^2, ø′ = 14º and c′ = 0, ø′ = 18º respectively. The implications of these results are significant. They suggest that in fine-grained materials under previous thawing conditions where the rate of thawing exceeds the rate of consolidation, failure in the palaeo-active layer will occur along a plane on slopes whose angle is much less than in the temperate climate of present-day southern Britain (Hutchinson, 1974). Excess porewater is generated as a result of thawing and the corresponding increase in moisture content often exceeds the soil's liquid limit (Hutchinson, 1974).

Subglacial shear stresses are induced beneath glaciers and are a function of gravitational loading by ice and sediment and subglacial hydrogeology (Boulton & Dobbie, 1993). Strain is transmitted to the underlying sediment or geological bedrock and the substrate begins to yield initially elastically and then plastically as the substrate shear strength is mobilized. When the shear stresses beneath a glacier exceed the shear strength of the underlying substrate, the full shear strength is mobilized and the substrate fails. After reaching its peak strength, the substrate may continue to deform with increasing stress but with declining and ultimately zero shear strain. Average subglacial stresses are typically 60-120 kN/m^2 (Sladen & Wrigley,

1983; Boulton & Dobbie, 1993). If deformation representing failure is observed, the shear strength of the subglacial material must have therefore been below this value. Any measured value of shear strength above this reflects the effect of post-depositional processes including consolidation and cementation.

Thus, deformation of the subglacial substrate provides one mechanism of glacier motion in conjunction with sliding and deformation of the glacier ice itself (Benn & Evans, 1998). The consequence of this is that the substrate's shear strength has been partially or wholly mobilised and so its drained or undrained shear strength parameters are at a residual value.

The relationship between effective stress, subglacial groundwater flow and substrate permeability has been used to define critical conditions under which a glacier bed may or may not deform and under which drainage channels may or may not incise (Boulton & Paul, 1976; Boulton & Dobbie, 1993). These relationships determine the ultimate behaviour of a subglacially deformed substrate which is either a primary glacigenic deposit or bedrock. The critical effective stress conditions are summarised below from Boulton (1977), Boulton & Dobbie (1993) and Boulton & Hindmarsh (1987).

In conditions with no groundwater flow and with no applied stress, the vertical effective pressure gradient is equivalent to gravitational and is defined by:

$$\partial p'/\partial z = (1-n)(\rho_s - \rho_w)_g = (\partial p'/\partial z)_g$$

Equation 2-7

where p′ is effective pressure, z is depth, n is porosity, ρ_s is particle density, ρ_w is the density of water (1Mg/m^3), g is acceleration due to gravity (9.8m/s^2) and $\partial p'/\partial z$ is effective pressure gradient (partial differential).

When a load is applied a vertical stress is initiated which is initially taken up by an increase in water pressure. If drainage is permitted at the base and consolidation can take place, a potential vertical hydraulic gradient ($\partial\psi/\partial z$) is established. The complete effective pressure gradient is therefore:

$$\partial p'/\partial z = (\partial p'/\partial z)_g - (\partial\psi/\partial z)$$

Equation 2-8

As drainage progresses groundwater flow is initiated at a rate, v governed by Darcy's Law:

$$v = (-k/\rho_w g)\,(\partial\psi/\partial z)$$

Equation 2-9

where k is intrinsic permeability.

As groundwater is expelled, excess porewater pressure decreases until it reaches 0 where no more porewater is expelled. In this condition:

$$\partial p'/\partial z = (\partial p'/\partial z)_g$$

Equation 2-10

Beneath temperate glaciers in mid-latitudes, basal meltwater is supplied to the subglacial zone because of geothermal heating and movement-induced frictional heating. Consequently, groundwater is replenished into the consolidating subglacial sediment or geological bedrock. As a result, the condition of 0 porewater pressure is never reached and so effective stresses in subglacial zones with no or impeded drainage are less than those that would be expected in a non-glacial environment. This also accounts for reduced consolidation described in Section 2.2.6.

A subglacial hydraulic gradient must be maintained to allow drainage to continue for a given melt rate. The final basal effective pressure is therefore a combination of gravitational effective pressure and potential effective pressure needed to discharge meltwater for a given melt rate, m:

$$m = (-k/\rho_w g)\,(\partial\psi/\partial z)$$

Equation 2-11

And the final vertical effective pressure gradient will be:

$$\partial p'/\partial z = (\partial p'/\partial z)_g - (\partial\psi/\partial z) = (1-n)(\rho_s - \rho_w)_g - m\rho_{wg}/k$$

Equation 2-12

The relative magnitudes of the gravitational and hydraulic components will be determined by the permeability of the substrate. For a given melt rate, the vertical effective pressure gradient increases as the permeability decreases. For permeabilities $<10^{-8}$, effective pressures much greater than gravitational can occur. In addition, as permeability decreases with depth, the component of effective pressure due to hydraulic potential will increases in order to maintain a constant flow rate.

Where the subglacial substrate comprises weakly permeable basal till (aquitard) overlying permeable sediment (aquifer) and drainage is through groundwater flow (rather than film or erosive channel flow), meltwater is discharged vertically through till and into the aquifer. In the case where the permeability of the aquiclude is $<10^{-8}$, porewater potential pressure increases and a large potential pressure gradient is established across the aquiclude which exceeds the gravitational gradient. As a result, the effective stress at the glacier sole is reduced. In a second case, the permeability of the aquiclude is $>10^{-8}$. Drainage is permitted more easily than in the former case, porewater potential increases less and the effective pressure gradient across the aquiclude is reduced which is similar to the gravitational gradient.

Where the substrate comprises weakly permeable till (aquitard) overlying weakly permeable bedrock (aquiclude), meltwater flows from the glacier sole into and through the underlying till aquitard. Porewater pressure at the top of the aquitard increases and a large potential pressure gradient is established from the top to the base of the aquitard which is needed to drive groundwater flow towards the glacier margin. Assuming the permeability and flow rate remains constant, as the glacier margin is approached the height of the piezometric surface must increase to maintain the required flow rate. This occurs until the piezometric surface reaches the glacier surface at which point effective stress is 0 (total stress = porewater pressure) and the glacier becomes unstable.

The implications for the behaviour of the Middle Pleistocene BIS in lowland Britain are significant. Where the BIS was underlain by low permeability material over a permeable substrate (bedrock or sediment), high potential pressure gradients would be established which would be greater than the ice pressure minus the potential pressure at the top of the aquifer:

$$(m\rho_{wg}t/\mathrm{k}) > \rho_i - \psi_a$$

Equation 2-13

where ρ_i is ice pressure, ψ_a is hydraulic potential at the top of the aquifer and t is the thickness of the low permeability material overlying the aquifer. In this case, meltwater would accumulate on the surface of the low permeability layer and flow would then occur by channel or sheet flow.

In contrast, where the BIS was underlain by a permeable substrate which can transmit meltwater flow along a potential pressure gradient that keeps the potential pressure at the top of the aquifer low, the potential pressure at the top of the aquifer is less than the ice pressure.

In this case, water will not build up at the sole of the glacier and no further drainage route is needed.

The value of effective pressure at the glacier sole determines the shear strength of the substrate (either glacigenic sediment or bedrock) according to the Mohr-coulomb failure criterion. A critical effective pressure (p'_c) at which failure and deformation will occur is given by (modified from Boulton & Dobbie (1993)):

$$p'c = (\tau_b - c')/tan\emptyset'$$

Equation 2-14

where τ_b is basal shear stress.

The significance of subglacial effective pressures, hydraulic potential gradients and permeability under four different scenarios is illustrated in Figure 2-13.

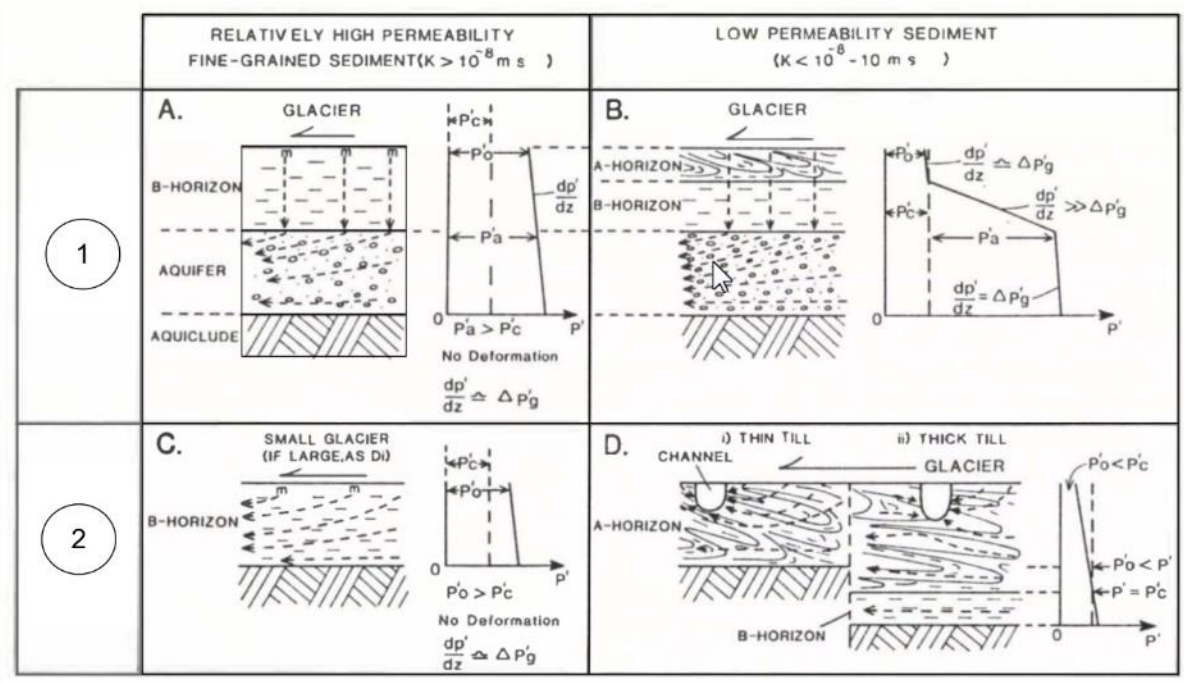

Figure 2-13 Five scenarios of effective stress gradient, permeability and till thickness that result in subglacial deformation and subglacial channelised drainage after Boulton & Dobbie (1993). Scenario 1, glacier ice underlain by permeable aquifer and aquiclude. Scenario 2, glacier ice underlain by aquitard. $\partial p'/\partial z$ is vertical effective pressure gradient, p'_a is pressure at the top of permeable substrate (aquifer), p'_c is critical effective pressure for deformation, p' is effective stress, $\Delta p'_g = (\partial p'/\partial z)_g$ = vertical effective pressure gradient due to gravity and p'_o is pressure at glacier sole. A-horizon includes subglacial deformation which is absent in the B-Horizon.

In Figure 2-13(A), subglacial vertical drainage through the till and into the permeable aquifer is good. Porewater pressures are dissipated and the p'_o is high. The vertical effective pressure

gradient is low and approximates the vertical effective pressure gradient due to gravity. $p'_o > p'_c$ and no deformation occurs.

In Figure 2-13(B), the permeability of the till is lower and drainage efficiency is lower compared to 14(A). Porewater pressure is increased at the top of the till so that $p'_o \leq p'_c$ and deformation occurs in the A-Horizon. A large effective pressure gradient is established beneath the A-Horizon where $\partial p'/\partial z > p'_c$ so that $\partial p'/\partial z > (\partial p'/\partial z)_g$ from the top of the B-Horizon to its base. Within the aquifer, $\partial p'/\partial z = (\partial p'/\partial z)_g$.

In Figures 2-13(C), 14(Di) and 14(Dii), there is no permeable aquifer in the subglacial zone. In Figure 2-12C, a relatively permeable till horizon overlies an aquiclude beneath a small glacier. Porewater pressures are dissipated and the corresponding value of p'_o is high. The permeability of the substrate is sufficient to facilitate groundwater flow. In terms of vertical effective pressure gradients, $\partial p'/\partial z = (\partial p'/\partial z)_g$. $p'_o > p'_c$ and no deformation occurs.

Figures 2-13(Di) and 14(Dii) illustrate the effect of till thickness variability. Low permeability till requires a large potential pressure gradient to transmit horizontal groundwater flow. At the glacier sole, porewater pressure is increased and so $p'_o < p'_c$. As p'_o tends to 0, deformation occurs and is accompanied by channelized drainage forming an A-Horizon. In terms of vertical effective pressure gradients, $\partial p'/\partial z = (\partial p'/\partial z)_g$. Where the till is thin, deformation occurs throughout and is represented entirely by an A-Horizon. Where till is thick, deformation ceases at the base of the B-Horizon where $p' > p'_c$.

The depth to which the deformed A-Horizon might extend (t_A) is dependent on the critical pressure required to cause deformation, the effective pressure at the glacier sole and the effective pressure gradient due to gravity:

$$t_A = \frac{p'_c - p'_o}{(\partial p'/\partial z)_g}$$

Equation 2-15

If p'_o is 0 (for example at the margin of the BIS underlain by low permeability bedrock) and assuming τb is 50-100kPa, c is 0-25 kPa ø is 12-30° and $(\partial p'/\partial z)_g$ is 10 kPa/m^{-1} then t_A ranges between 4 and 47 m. The implication is that most British lowland tills are therefore pervasively deformed throughout and that deformation also occurs within the B-Horizon. Differences in deformation style between the A and B-Horizons were observed by Boulton & Hindmarsh (1987) and Benn (1995) in exposed subglacial till in Iceland. The upper A-Horizon was dominated by ductile deformation structures while the underlying B-Horizon

showed evidence of brittle and ductile deformation including shear planes. This implies that because subglacial tills are re-moulded, their strength should decrease compared to their undeformed state. The ratio between the undeformed and remoulded strength is termed sensitivity (Skempton & Norhey, 1952). The sensitivity of Anglian-age tills in East Anglia have been measured and found to range between 1.08 – 1.67. Their undeformed and remoulded strengths are therefore similar and they can be classed as low sensitivity clays (Bell, 1991, 1992).

A further consequence of subglacial deformation on shear strength is that the A-Horizon exhibits a higher permeability, higher void ratio, lower density and lower strength compared to the underlying B-Horizon (Boulton & Paul, 1976; Boulton & Hindmarsh, 1987; Benn & Evans, 1998). Measurements at a retreating glacier margin in Iceland recorded a mean void ratio in the 0.4 m thick A-Horizon of 0.585 compared to 0.450 in the lower B-Horizon (Benn, 1995). In the same area, Boulton & Hindmarsh (1987) recorded a change in void ratio between 0.4 – 0.6 m falling from 0.55-0.6 above to 0.4-0.45 below. Benn (1995) also measured undrained shear strength using a field vane apparatus and recorded values in the B-Horizon about 1.5 to 2 times the values recorded in the A-Horizon. Dilatant behaviour in the B-Horizon during shear may account for the more open and weaker fabric observed in the A-Horizon as the till has been sheared to its critical state.

In contrast, variable shear strength and degree of consolidation depth profiles in glacigenic sediments have been observed in Denmark (Christoffersen & Tulaczyk, 2003) and offshore Norway (Sættem *et al.*, 1996). Using hand vane apparatus, Christoffersen & Tulaczyk (2003) measured changes in subglacial till shear strength. They observed a change at ~10 m where shear strength decreased downwards from ~160 kPa to <120 kPa. Alternating shear strength values from ~360 kPa to >800 kPa were observed in glacigenic sediments during offshore investigations in Norway (Sættem *et al.*, 1996).An alternating profile of shear strength and degree of consolidation does not conform to a conventional model of consolidation by sedimentation alone. Basal freeze-on was suggested by Sættem *et al*. (1996) as a potential mechancism to explain the alternating depth profile. Using a linked numerical thermal and mechanical model, Christoffersen & Tulaczyk (2003) also suggested basal freeze-on as a mechanism to explain the apparent variability. In this model, subglacial freezing occurs in response to climate-induced temperature gradients. Freezing in fine-grained sediments, as described in Section 2.2.1, generates high suction pressures and draws water to the freezing front. High suction pressure results in overconsolidation with respect to the sediments

unfrozen state and the upper part of the till layer is therefore denser and stronger than the lower part.

2.3 Summary

The processes described in Section 1.6 demonstrate that the influence of Pleistocene cold-climates is potentially significant for geotechnical property and behaviour characterization. Primary glacigenic sediments including till are influenced by variability in the patterns of erosion, transport and depositional style. Depositional and post-depositional changes in effective stress are critical factors in changing their consolidation state and shear strength.

Changes in effective stress brought about by the growth and decay of segregated ice in fine-grained sediments have the potential to change the consolidation and shear strength of primary glacigenic sediments as well as weathered Mesozoic mudrocks. The latter effect is important when interpreting the depth-dependent geotechnical behaviour of geological units including the Oxford Clay. If the magnitude of maximum effective stress brought about by ground freezing and thaw consolidation in the previous permafrost zone (~60 mbgl) exceeds that related purely to geological sedimentation and erosion, the previous overconsolidation signature will be wholly or partially removed. The same logic implies that the depositional history of till in areas beyond glaciation could be partially or wholly removed by subsequent changes in effective stress brought about by ground freezing.

Cyclic Quaternary climate changes further imply that post-depositional effective stress changes occurred on more than one occasion in lowland Britain; each event superimposed the last. It is assumed that subsequent changes in effective stress may only influence the final behaviour of a soil if its magnitude of maximum preconsolidation pressure exceeds that of previous events. Further, this effect may be laterally and vertically variable in any one soil profile because of variations in ground thermal regime, degree of saturation and erosion.

3 Geological background

A geological background for the Oxford Clay and Quaternary deposits is provided here that describes their sedimentology, geological history and processes of formation which may influence their geotechnical properties and behaviour. Reference to the geological background is then made when interpreting the results of field and laboratory analytical methods to determine the likely causes of variability.

The lack of exposures of Quaternary sediments and associated geomorphological features in north Buckinghamshire has meant that its glacial and periglacial history has received little scientific attention. In contrast, mudrocks of the Oxford Clay were previously exposed in former excavations for brickmaking. They provided sites for the investigation of their engineering geology and geotechnical behaviour.

Investigation of Quaternary sediments of relevance to Buckingham were undertaken in the Kettering and Northampton districts, north of the project area (Hollingworth & Taylor, 1946). This was further developed during drilling for potential sand and gravel resources in the northern part of the Buckingham area (Sumbler & Samuel, 1990). Geological surveys at the six-inch to one-mile scale were undertaken between 1895 and 1897 while surveys at the one inch to one-mile scale were undertaken in the 1860s. The latter geological maps were published as 'old series' one inch to one mile maps (1:63 360) as Sheets 45 and 46 (Green, 1864).

The geology of the regional area to the east was investigated in advance of the construction of the new town of Milton Keynes (Horton, 1970; Horton *et al.*, 1974). Recent geological investigation and survey at 1:10 000 and publication at 1:50 000 scale by the BGS was completed in 2000 for Buckingham (Sumbler, 2002) and Bedford (Barron *et al.*, 2010).

3.1 Geology of the Oxford Clay Formation

The Oxford Clay is a sedimentary rock and is part of the middle to late-Jurassic Ancholme Group. Its distribution in the project area is shown in Figure 3-1. It is interpreted as a marine, argillaceous clay, silty clay and clay-shale mudrock of Callovian to Oxfordian age (Cox *et al.*, 1992). In places, laterally persistent but thin (<0.3 m thick) limestone beds appear with impersistant beds of pyrite nodules and pyritic mudstone. Its upper part is weathered and occurs at outcrop and in boreholes as a greyish-brown clay with common gypsum crystals in the form of blades of selenite. The weathering characteristics of the Oxford Clay were

investigated by Russell & Parker (1979) following similar work on the characteristics of Lias Group mudrocks (Chandler, 1972) in the East Midlands (Table 4-3, Section 4.1.9).

Mudrocks of the Oxford Clay were deposited during a phase of marine transgression in southern Britain that followed a period of tectonic uplift, faulting and shallow marine sedimentation in the North Sea region (Hesselbo, 2012). In the project area, it was deposited within the palaeogeographic marine area of the East Midlands Shelf and with landmasses including the London Platform to the south. Environments of deposition in shallow marine and fully marine conditions in the East Midlands shelf are considered similar.

From oldest to youngest, it is divided into the Peterborough, Stewartby and Weymouth members (Table 3-1). Regionally, the Oxford Clay thins eastwards from 300 m in Wiltshire to ~ 76 m near Peterborough (Figure 3-2). This thinning is partly due to gradual onlap and thinning towards the structural block of the London Platform. It is also due to gradual erosion and overstep of the Weymouth Member. Its outcrop extends from southwest to northeast in the project area where it forms the centre of a shallow ‘clay vale’ bounded to the southeast by the Chiltern Hills and the northwest by the dipslopes of older Middle and Lower Jurassic rocks. Its regional dip is between 1º and 2º to the southeast. Its maximum thickness in north Buckinghamshire ranges from about 67 m in the west to about 62 m in the east (Sumbler, 2002).

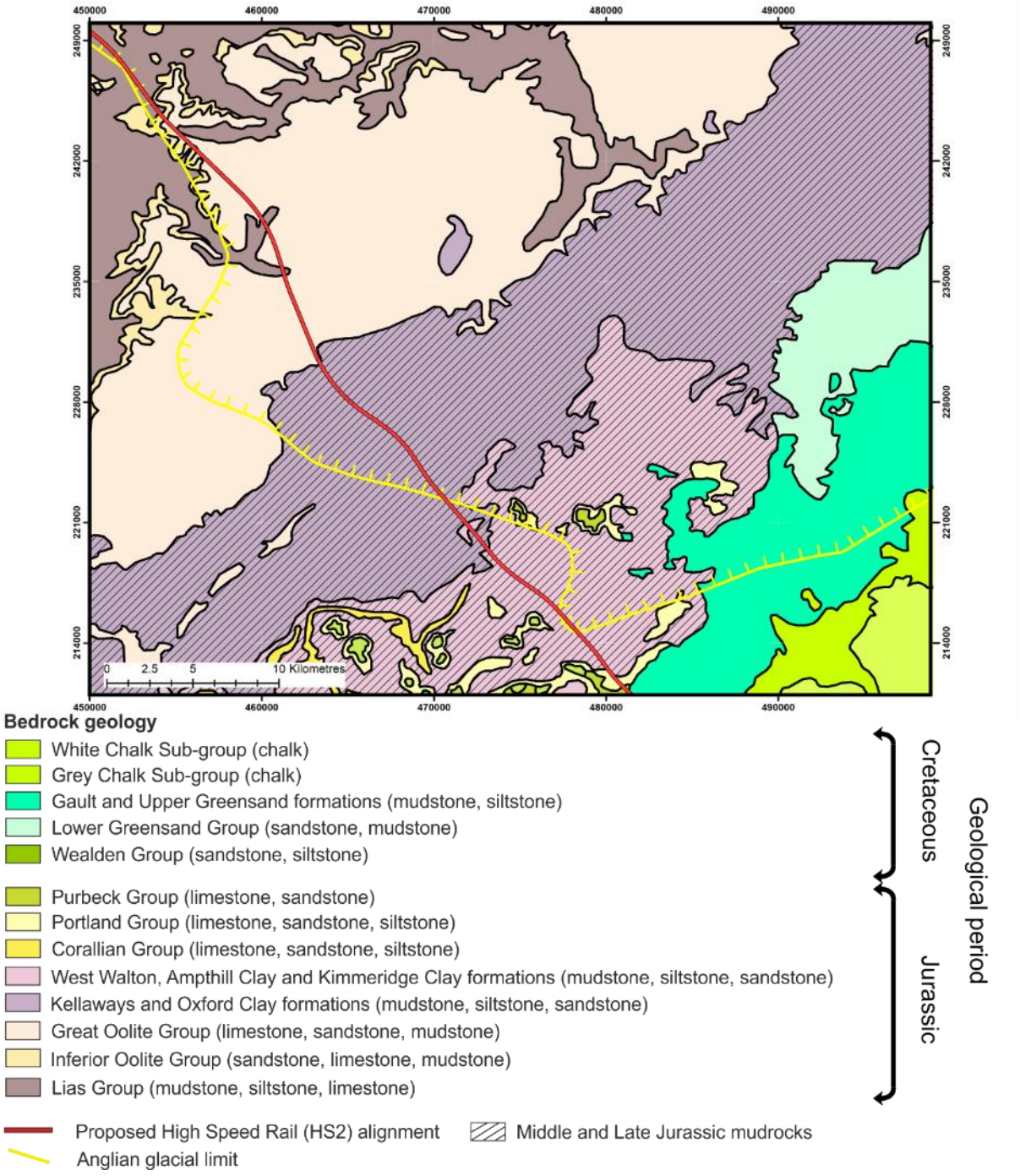

Figure 3-1 1:625 000 bedrock geology map of the project area highlighting the presence of Middle and Late Jurassic clays underlying the inferred Middle Pleistocene glacial limit. DigMapGB625 and glacial limit provided under licence from the BGS (licence number 2015/038). Glacial limit is interpreted as Anglian after Gibbard & Clark, 2011.

Stage	Zone	Sub-zone	Lithostra-	Description	Thickness

				tigraphy		(m)
Oxfordian	Lower	*Cardioceras cordatum*	*C. cordatum*	Weymouth Member	Light grey, silty mudstone with common bivalves	15 - 20
			C. costicardia			
			C.bukowskii			
		Quenstedtoceras mariae	*C. praecordatum*			
			C.scarburense			
Callovian	Upper	*Queenstedtoceras lamberti*		Stewartby Member	Light to medium-grey, slightly silty, calcareous blocky mudstone. Fossils are common and include bivalves and small, often pyritised ammonites. Beds of nodular cementstone, limestone (upto 0.3 m thick) and calcareous siltstone are common.	21 - 23
		Peltoceras athleta	*Upper Middle*			
			Lower	Peterborough Member	Interbedded greenish-grey, slightly blocky mudstone and brownish-grey, fissile, bituminous mudstone with abundant bivalves, belemnites and ammoniate fossils which are often pyritised. Septarian nodules are common and upto 1 m diameter within the *Acutistriatum* Band.	24 - 26
	Middle	*Erymnoceras coronatum*	*Kosmoceras grossouvrei*			
			Kosmoceras obductum			
		Kosmoceras jason	*Kosmoceras jason*			
			Kosmoceras medea			
		Lower Sigaloceras calloviense	*Sigaloceras enodatum*			

Table 3-1 Lithostratigraphy of the Oxford Clay Formation (modified after Sumbler, (2002) and Cox *et al*. (1992). Ammonite zones after Calloman (1969) reported in Jackson & Fookes, (1974).

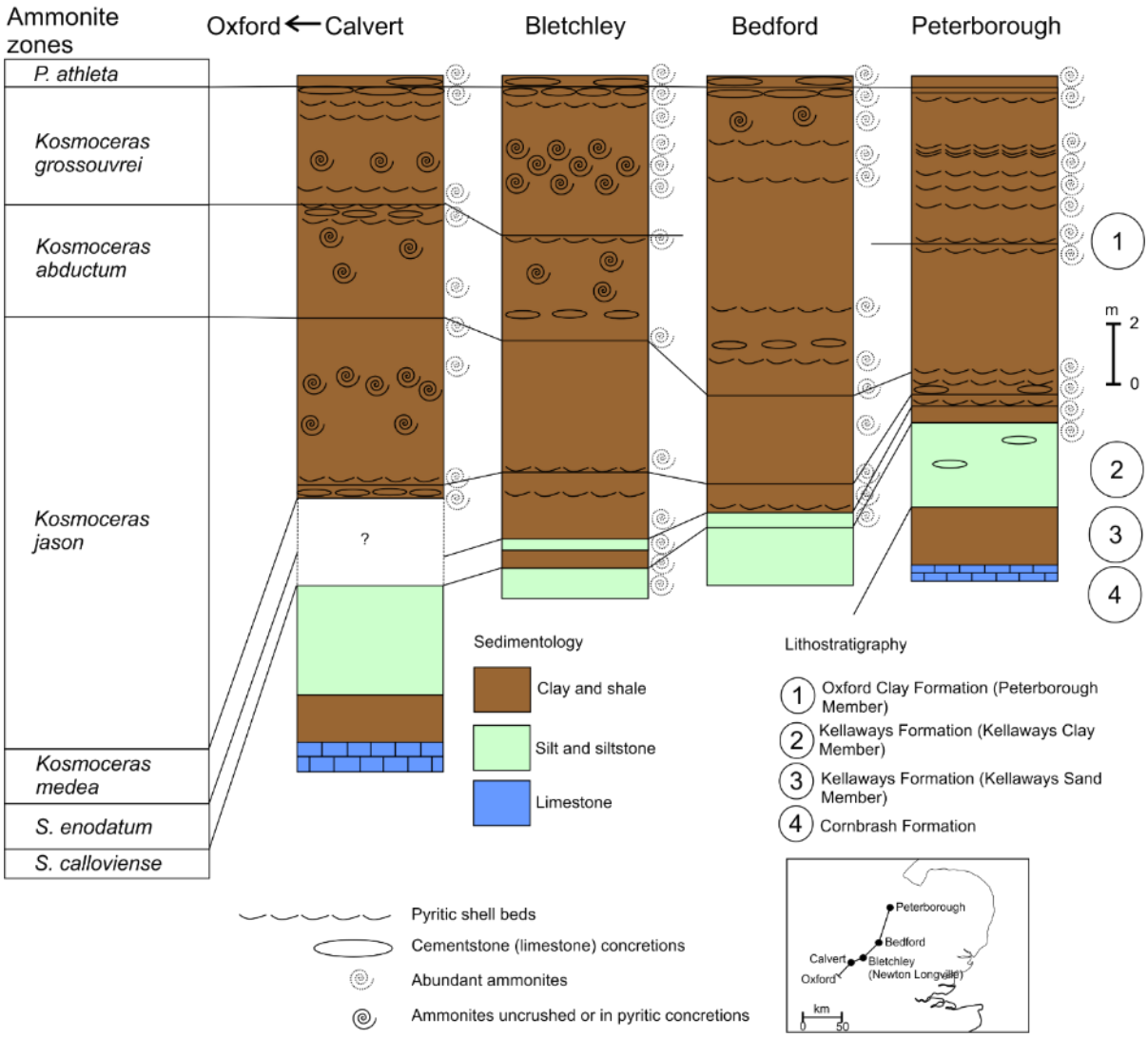

Figure 3-2 Lithostratigraphy and ammonite subzones of the Oxford Clay demonstrating thinning to the northeast after Callomon (1968).

3.2 Quaternary geology

The Quaternary geology of north Buckinghamshire has received relatively little scientific attention compared to other glaciated lowland regions including eastern England, East Anglia and parts of the Midlands. This is surprising considering its location at a critical glacial and periglacial Quaternary Domain boundary at the maximum limit of the British Ice Sheet (BIS).

To the north and northeast, the landscape has been glaciated and subsequently modified by multiple phases of periglaciation. To the south and southwest, periglacial conditions dominated during Pleistocene glacials in northern Britain. The Quaternary geology of the project area is shown in Figure 3-3.

There are three regions of lowland Britain that are potentially relevant to the glacial and periglacial history of north Buckinghamshire; the English Midlands (Leicestershire and

Gloucestershire), East Anglia and the Vale of St Albans. The Quaternary geology of these regions, their glacial and periglacial history and on-going debates concerning the timing and extent of Middle Pleistocene lowland glaciations is summarised below because the correlation of the Quaternary sequences of north Buckinghamshire with those in other areas of lowland Britain is not yet known.

3.2.1 Regional context: Middle Pleistocene fluvial systems

Prior to the onset of major terrestrial glaciation during the Middle Pleistocene, southern Britain was dominated by fluvial activity. Major river systems including the ancestral drainage system of the River Thames was superimposed on a landscape which had been tectonically uplifted to the west, under the influence of Paleogene and Neogene Alpine orogenic events (Gibbard & Allen, 1994; Gibbard & Lewin, 2003). Consequently, left-bank tributaries of the River Thames followed a drainage path parallel to the regional, southeast tectonic tilt of underlying Mesozoic bedrock before flowing east and northeast to drain into the North Sea Basin (Gibbard & Allen, 1994; Gibbard & Lewin, 2003; Belshaw *et al.*, 2014).

Fluvial sand and gravel of the Baginton-Lillington Member underlies glacigenic sediments of the Wolston Formation in central England (Shotton, 1953; Bridge *et al.*, 1998). Originally interpreted by Shotton (1953) as a northeast-southwest orientated, Wolstonian (Saalian) age 'proto-Soar' drainage system, they were re-interpreted as a component part of a pre-Anglian river system called the Bytham River by Rose (1987, 1989, 1994). This was based on re-interpretation of the age of the Wolston Formation as Anglian and therefore the underlying gravels as pre- or early-Anglian in age. On the basis of lithological and altitudinal correlation, authors including Lewis (1993), Lewis *et al*. (1999), Rose *et al*. (1999), (2009) and Lee *et al*. (2004)b correlated a sequence of 'Bunter'-rich sand and gravel underlying the Wolston Formation with sand and gravel of the Ingham Formation (Hey, 1976; Clarke & Auton, 1984) that underlies unequivocal Anglian-age glacigenic sediments in Norfolk. The orientation of this river system is perpendicular to southeastward-draining pre-glacial river systems recognised throughout southern Britain, however.

Work by Gibbard *et al*. (1992, 2009, 2012) on the eastern margin of the Fenland Basin, supported by Belshaw *et al*. (2014), suggested that the configuration of the Bytham River proposed by Rose (1987, 1989, 1994) could not have existed before the Anglian.

This was based partly on the orientation of the river system, the interpretation of fluvial gravels on the eastern margin of the Fenland as ice-marginal and demonstrating that the Fenland Basin did not exist in its present form before the Anglian Stage glaciation. Despite

this conclusion, disagreement persists and the presence, age and configuration of a pre-Anglian Bytham River or Wolstonian proto-Soar river is still debated (e.g. Lee *et al.*, 2017).

Northwest-southeast orientated spreads of sand and gravel in Bedfordshire and Hertfordshire have been termed the Milton and Letchworth formations (Belshaw *et al.*, 2014). They are interpreted as former left-bank streams of the ancestral River Thames, flowing southeastwards, parallel to geological bedrock dip, to join the main course of the ancestral Thames in Hertfordshire and Essex. Belshaw *et al*. (2014) also observe that gravels underlying glacigenic deposits including till, occupy low cols (either dry or with present-day water courses) in the Chiltern escarpment. These are interpreted as further evidence for the existence of northwest-southeast orientated, pre-Anglian, left bank drainage systems of the ancestral River Thames.

3.2.2 Regional context: Middle Pleistocene glacial geology of the English Midlands, East Anglia and Vale of St Albans

It is generally accepted that during the Middle Pleistocene, lowland Britain was glaciated on at least three separate occasions resulting in the deposition of a suite of Mesozoic-rich tills and associated glacigenic sediments across the Midlands and eastern England.

Evidence of Anglian Stage glaciation in lowland Britain is well-constrained in onshore and coastal localities in East Anglia. The dating of the Anglian Stage glaciation is generally constrained using U-Th, $\delta^{13}C$ and $\delta^{18}O$ isotopic compositions and biostratigraphical dating of organic-rich sediments which overlie till and are shown to correlate to MIS11 (Ehlers & Gibbard, 1991; Bowen, 1999; Rowe *et al.*, 1999; Candy, 2009; Preece *et al.*, 2009; Gibbard & Clark, 2011).

At least two post-Anglian glacial events are recorded in the sedimentary archives of eastern England. Evidence of glaciation during the Wolstonian (Saalian, MIS?11b-6) stage is preserved in fluvio-deltaic sediments on the eastern margin of the Fenland Basin (Gibbard *et al.*, 1992, 2009). Here, spreads of sand and gravel ('Skertchly Line') interpreted in part as fluvial and pre-Anglian in age (Rose *et al.*, 2001) were re-interpreted as glaciofluvial, delta fan deposits reportedly dated by Optically Stimulated Luminescence (OSL) dating to ~160 ka (Gibbard *et al.*, 2009, 2012).

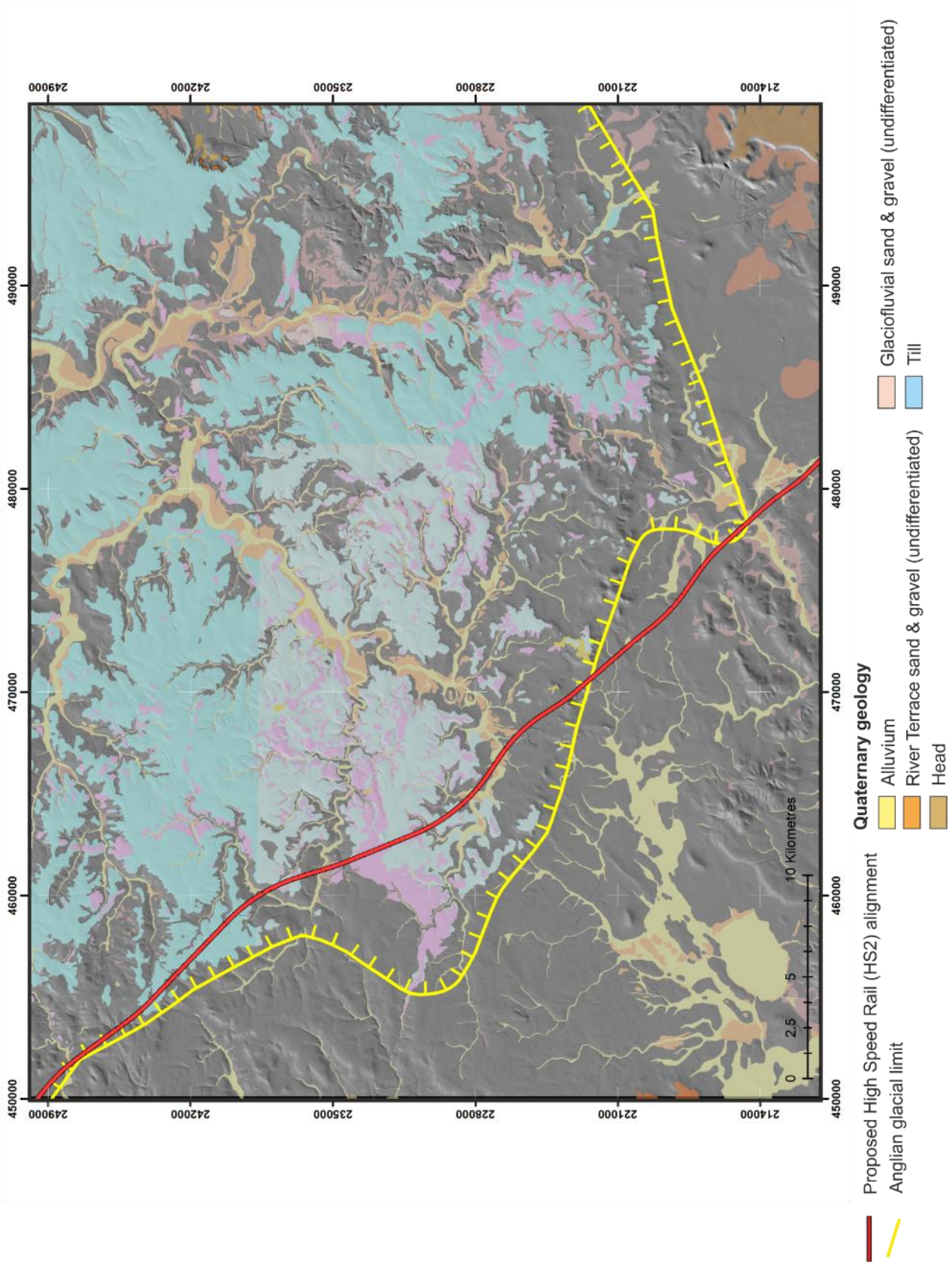

Figure 3-3 1:50 000 Quaternary geological map of north Buckinghamshire and surrounding area. DigMapGB50 and glacial limit provided under licence from the BGS (licence number 2015/038). Hillshade using Digital Terrain Model (DTM) © Crown Copyright and Database Right [2018]. Ordnance Survey (Digimap Licence). Glacial limit is interpreted as Anglian after Gibbard & Clark, 2011.

The youngest glacial event to have affected lowland southern Britain occurred during the late Pleistocene, Devensian (Weichselian, MIS4-2) Stage. Remnants of late Pleistocene glacigenic sediments, interpreted to have been deposited during the Devensian Stage glaciation are found in north Norfolk (Straw, 1960; Catt, 1991; Pawley *et al.*, 2006).

In contrast, the English Midlands are conspicuous by their absence of equivalent Middle Pleistocene organic deposits overlying till. Evidence of the timing of glaciation derived from absolute dating equivalent to East Anglia is absent. The timing of glaciation in the English Midlands is therefore inferred from stratigraphical correlation of lithologically similar glacigenic deposits and the correlation of river terraces. The latter correlation is usually based on altitude and lithology. As a result, the timing of glaciation has proved to be equivocal and glacigenic sediments in the English Midlands have been the subject of extensive study and debate concerning the timing of their deposition. They have been interpreted either as part of the Wolstonian Stage (Shotton, 1953, 1983; Rice & Douglas, 1991; Gibbard *et al.*, 2013) or the Anglian Stage (Sumbler, 1983, 2001; Rose, 1987; Bridge *et al.*, 1998).

Middle Pleistocene glacial deposits are found south of the Devensian (Weichselian) glacial limit across the English Midlands and East Anglia (Ehlers & Gibbard, 1991; Clark, Philip L Gibbard, *et al.*, 2004; Rose, 2009; Gibbard & Clark, 2011; Lee *et al.*, 2012).

The geographical location of the north Buckinghamshire area means that the Middle and Late Pleistocene geology of Eastern England, East Anglia as well as Central England are potentially relevant. A brief overview of the geology and stratigraphy in each of the regions is therefore given in the following sections.

3.2.2.1 English Midlands

Relatively little is known of the Quaternary geology in large areas of the English Midlands extending between the Vale of St Albans in the east (Gibbard, 1977) and the Cotswolds to the west (Shotton, 1953, 1976, 1983, Sumbler, 1983, 2001). It has been assumed that the area was glaciated only once and that it occurred during the Anglian Stage (e.g. Sumbler, 2002). The glacigenic deposits in the area have therefore been assumed to be of Anglian age. The Anglian Stage glacial limit in the English Midlands has been assumed to coincide with the maximum southerly extent of glacigenic deposits on published 1:50 000 geological maps (e.g. Clark *et al*., (2004), Ehlers *et al*., (2011) and Gibbard & Clark (2011).

The glacial and glaciofluvial sediments in the Rugby and Coventry areas were described by Shotton (1953, 1976, 1983), Bishop (1958), Rice (1981) Rice & Douglas (1991) and Bridge *et*

al., (1998) and interpreted as Wolstonian in age. They were correlated with glacigenic sediments in Leicestershire which were also believed to be Wolstonian in age (Rice, 1981; Rice & Douglas, 1991). The upper and lower clay-dominated sediments were interpreted as tills related to two different episodes of glacial advance, separated by thick laminated, pro-glacial glaciolacustrine deposits. The upper and lower tills were termed the Oadby and Thrussington Till members respectively. A summary of the lithostratigraphical schemes employed in the English Midlands is given in Table 3-2.

The Thrussington Till Member is matrix-supported and comprises two main facies (Rice, 1968, 1981). One 'Triassic' facies is 1 – 3 m thick, reddish-brown with green mottling and contains abundant Triassic-derived erratics including 'Bunter' quartz, fine-grained sandstone ('skerries') and quartzite. Other erratics are present including Lias Group limestones and Carboniferous coal. Southwest of Leicester, it passes laterally southeastwards into a second 'Chalky' facies with common Cretaceous chalk and flint erratics.

The Oadby Till in Leicestershire comprises matrix supported, sandy clay and silt rich in Cretaceous chalk, flint, middle Jurassic oolite clasts and a matrix derived from Lias Group clay. It is distinguished from the stratigraphically lower Thrussington Till by the increase in proportion of chalk and flint clasts and its dominant bluish-grey unweathered colour. Rice (1968) informally divided the Oadby Till into upper and lower tills where Lias Group and some Triassic erratics were dominant in the lower unit, while Cretaceous chalk and flint erratics were dominant in the upper unit. Southwest of Leicester, the Oadby Till is found interbedded with clay, silt and sand where they were interpreted as sub-aqueous flow tills (Rice, 1981).

Shotton (1953, 1976), Rice (1981)	**Horton *et al.* (1974) (Milton Keynes area)***	**Old *et al.* (1987) (Warwick District)**	**Bridge *et al.* (1998) (Coventry District)**	**Formation**	**Environment**
Dunsmore Gravel Member	Fluvioglacial deposits	Dunsmore Gravel Member	Anker Sand and Gravel; Dunsmore Gravel	Wolston	Meltwater
Oadby Till Member	Glacial lake deposits and Boulder clay with glacial sand and gravel	Oadby Till Member	Oadby Till Member		Glacial
Upper Wolston Clay Member		Upper Wolston Clay Member	Shawell Gravel Member		Meltwater
Wolston Sand and Gravel/Wigston Sand and Gravel members		Wolston Sand and Gravel Member	Wolston Sand and Gravel Member		Glaciolacustrine
Lower Wolston Clay Member		Lower Wolston Clay Member	Lower Wolston Clay Member		
Thrussington		Thrussington	Thrussington Till		Glacial

Till Member		Till Member	Member		
Baginton Sand and Baginton-Lillington Gravel Member	Sand and Gravel of unknown age	Baginton Sand and Gravel Member	Baginton Sand and Gravel Member	Baginton	Fluvial

Table 3-2 Glacial deposits of the English Midlands region modified after Gibbard *et al*. (2013). *Stratigraphical relationships in this area are poorly known and not stratigraphical names were applied by Horton *et al*. (1974) 'Chalky boulder clay' is interbedded with 'laminated lake clay' in Milton Keynes.

Reinterpretation and correlation of the glacial sequence with lithologically similar deposits, including chalk-rich till in East Anglia, led Perrin (1971), Sumbler (1983, 2001) and later Rose (1987, 1989, 2009) to interpret the sequence as Anglian in age. Sumbler (1983) further argued that the Oadby Till and Thrussington Till members did not represent different glaciations but were two lobes of the same ice-sheet. Gravels underlying the glacial sequence were interpreted as fluvial in origin. The underlying Baginton Sand and Gravel Member were considered by authors including Shotton (1953) to be part of northeasterly flowing, Wolstonian proto-Soar river system. In contrast, following reinterpretation of the glacial sequence as Anglian in age, Rose (1989, 1994, 2009), Rose *et al*. (2001) and Lee *et al*. (2012) considered them part of an extensive pre-Anglian 'Bytham' river system that extended from the Midlands area, across the Wash and into the North Sea via East Anglia. Growing evidence for post-Anglian, pre-Devensian glaciation along the margin of the Fenland in Norfolk and reconsideration of the stratigraphical evidence in the west Midlands has demonstrated that the deposits of the Birmingham area might be Wolstonian in age but this is yet to be established (Gibbard *et al.*, 1992, 2012).

The relationship of the glacigenic sequences in north Buckinghamshire and those of Moreton-in-Marsh, Gloucestershire has not been established. The glacigenic sequence of Moreton-in-Marsh crops-out as a conspicuous outlier surrounded by Jurassic mudstone and separated from the main spread of Midlands glacigenic deposits to the north and east. The glacigenic sequence here was described by Shotton (1953) and Bishop (1958). Both correlated the sequence of sand and gravel, laminated clay and tills with stratigraphically similar sequences in the Midlands and therefore interpreted them as belonging to a Wolstonian age glaciation which included the development of a large proglacial lake called Lake Harrison by Shotton (1953). Following the re-interpretation of the age of the Wolston glacigenic deposits in the Midlands as Anglian, Sumbler (1983) argued that the sequence in Moreton-in-Marsh should therefore also be considered Anglian and in terms of MIS chronology placed them within MIS 12 to 10. Sumbler (1995, 2001) also correlated the Moreton-in-Marsh glacigenic sequence with river terraces of the Evenlode Valley in the upper Thames and the River Thame. He

correlated the flint-rich gravels of the Wolvercote Terrace of the upper Thames with glacigenic deposits in Moreton-in-Marsh. Sumbler (1995) further related the chalk-rich glacigenic deposits near Aylesbury with the Blackditch Terrace of Thame and by topographical correlation related the Blackditch and Wolvercote terraces. Sumbler (Sumbler, 1995, 2001) therefore argued that the glacigenic deposits in Moreton-in-Marsh were equivalent to those in the Thame Valley near Aylesbury and that they were Anglian in age although he related them to MIS 12 to 9 (i.e. incorporating post-Anglian stages).

3.2.2.2 East Anglia

East Anglia, in eastern England, includes the counties of Norfolk, Suffolk and parts of Cambridgeshire. East Anglia contains one of the best terrestrial archives of Middle Pleistocene glaciation in northern Europe. Consequently, it has received much scientific attention and has played a key role in the development of ideas concerning lowland glaciation in Great Britain and its correlation with mainland Europe for over 100 years. Despite, or perhaps because of this, the timing, extent, number and correlation of glaciations represented by the widespread glacigenic deposits remains the subject of debate and on-going modification.

Different stratigraphical approaches have been used to attempt to unravel the often complex glacigenic sequences exposed in East Anglia and especially the coastal sequences of north Norfolk. They include, lithostratigraphy (Reid, 1882; Baden-Powell, 1948; West & Banham, 1968; Hart & Boulton, 1991; Lunkka, 1994; Lee *et al.*, 2002; Lee *et al.*, 2004a), chemostratigraphy (Perrin *et al.*, 1979; Scheib *et al.*, 2011) and most recently tectonostratigraphy and glacidynamic parasequences (Lee & Phillips, 2013; Lee *et al.*, 2013, 2017). A summary of the lithostratigraphical schemes for the glacial deposits of north Norfolk is given in Table 3-3 and the revised lithostratigraphical scheme proposed by Hamblin *et al*. (2005) and Lee *et al*. (2004a) in Table 3-4. The revised chronology has been challenged (Banham *et al.*, 2001; Preece *et al.*, 2009; Gibbard & Clark, 2011) with some researchers preferring the application of the scheme suggested by Lunkka (1994), for example. The scheme proposed by Lee *et al*. (2004) and Hamblin *et al*. (2005) has been criticised because of their rejection of biostratigraphical evidence and the weakness of assigning MIS sequences by counting forward or backwards and assigning each till unit to a separate MIS Stage (Preece *et al.*, 2009; Gibbard & Clark, 2011).

Despite the on-going stratigraphical and chronological debate, it is generally accepted that two phases of Middle Pleistocene glaciation are represented by the glacigenic sediments in

East Anglia. The oldest Middle Pleistocene glacigenic deposits of East Anglia have traditionally been associated with the Anglian Stage. The proposal by Lee *et al*. (2004) and Hamblin *et al*. (2005) that there is lithostratigraphical evidence for pre-Anglian glaciation (?MIS16) in East Anglia is equivocal and was challenged by Preece *et al*. (2009). Interpretation of the 'Tottenhill' glacial sequence on the eastern margin of the Fenland Basin (Gibbard *et al.*, 1992, 2009) has established evidence for post-Anglian, pre-Devensian, Wolstonian Stage glaciation in the region.

Banham (1968)		**Hart & Boulton (1991)**	**Lunkka (1994)**	**Bowen *et al*. (1999)**
Contorted Drift and associated deposits	Brick Kiln Dale Gravels Gimingham Sands		Lowestoft Till Formation, Marly Drift Member	Lowestoft Formation
	Third (3rd) till Mundseley Sands	Walcott Diamicton Member	Cromer Diamicton Member Mundesley Diamicton Member	North Sea Drift Formation
Cromer till	Second (2nd) till Intermediate Beds First (1st) till	Eccles Diamicton Member	Walcott Diamicton Member	
		Happisburgh Diamicton Member	Happisburgh Diamicton Member	

Table 3-3 Glacial stratigraphy in Norfolk prior to revision by Hamblin *et al*. (2005) and Lee *et al*. (2004).

Formation	**Members**	**Proposed MIS stage**	**Provenance**
Briton's Lane	Briton's Lane Sand and Gravel	6	North Sea, Scandinavia, Northern Britain
Sherringham Cliffs	Weybourne Town Till	10	North Sea
	Runton Till		North Sea, Northern Britain
	Bacton Green Till (3rd Cromer till)		
Lowestoft	Walcott Till (2nd Cromer till)	12	North east and eastern Britain
	Lowestoft Till		
Happisburgh	Corton Till	16	North Sea, north Britain
	Happisburgh Till (1st Cromer till)		

Table 3-4 Revised Lithostratigraphical scheme for north Norfolk (J R Lee *et al.*, 2004; Hamblin *et al.*, 2005). Note correlation of the Walcott till (2nd Cromer till) with the Lowestoft Formation in this revised scheme.

The Anglian Stage glaciation in East Anglia was associated with a lobe of the BIS that extended into southern Britain north of the present-day River Thames. Here, it deposited matrix-supported diamictons with abundant chalk clasts and Jurassic clays within the matrix, belonging to the Lowestoft Till Member of the Lowestoft Formation (Perrin *et al.*, 1979).

The chalk-rich tills of the Lowestoft Formation were believed to have been deposited contemporaneously with the 'North Sea Drift' Formation by an oscillating lobe of the Scandinavian Ice Sheet (SIS) and its interaction with the BIS (Baden-Powell, 1948; Lunkka, 1994). This resulted in deposition of a glacigenic sequence of sandy tills, including the

informally named ‘Three Cromer Tills’ of the North Sea Drift Formation, separated by either outwash or glaciolacustrine sediments (Reid, 1882). However, the presence of Scandinavian ice in the region was questioned by authors including Lee *et al*. (2002) who suggested that rare Scandinavian erratics, including Oslofjord rhomb porphyry, were reworked from the floor of the North Sea and that glacigenic deposits are of entirely British origin based on the overwhelming dominance of British materials. The Lowestoft Formation, including the informal ‘Marly Drift’ facies, was believed to have been deposited by eastward-directed advance of part of the BIS from the north or northwest during a temporary retreat of the SIS (Lunkka, 1994). Each of the tills were thought by Lunkka (1994) to represent four, separate glacial advances into the East Anglia area. Each intervening unit represented glacial retreat and deposition of outwash sands or glaciolacustrine sediments into an ice-dammed pro-glacial lake in the present-day North Sea region. Although deposition of the tills was believed to be dominantly terrestrial, Eyles *et al*. (1989) and Zalasiewicz & Gibbard (1988) suggested that tills of the North Sea Drift Formation were at least in part waterlain, possibly into an intermittent pro-glacial lake in the present-day North Sea region (e.g. the Mundsley Diamicton of Lunkka (1994) and equivalent deformed Bacton Green Till Member of Lee & Phillips (2008)).

Despite the debate and differences of opinion on the timing, extent and stratigraphical correlation of the glacial sequence in north Norfolk, three broad assemblages of sediments can be summarised, based on their lithostratigraphical relationships. The lower sequence comprises the sandy tills of the ‘North Sea Drift’ Formation deposited by an oscillating lobe of North Sea ice. The middle sequence comprises an assemblage of matrix dominated tills with abundant chalk erratics and Jurassic-rich derived silt and clay. This assemblage includes the ‘Marly Drift’ and the Lowestoft Till Member of the Lowestoft Formation of north Norfolk and southern Britain. It is believed to have been deposited by part of the BIS entering the East Anglia region form the north or northwest. The final assemblage in north Norfolk comprises a deformed sequence of glacigenic sediments referred to as the ‘Contorted Drift’.

The glacigenic sequence exposed in north Norfolk is complicated by evidence of pervasive brittle and ductile deformation, increasing in intensity towards the northwest (Hart, 1990; Hart *et al.*, 1990; Hart & Boulton, 1991). Previously generalised and described informally as ‘Contorted Drift’ (Reid, 1882), structures including low-angle thrusts, back thrusts, overturned folds and basal decollement surfaces have been interpreted at the outcrop and microscale by Phillips *et al*. (2002), Burke *et al*. (2009), Lee *et al*. (2013), Vaughan-Hirsch *et*

al. (2013) and Lee et al. (2017). Most recently, Lee *et al*. (2017) have applied a tectonostratigraphic approach to the glacigenic sequences in north Norfolk.

By identifying structural and stratigraphical boundaries to map regionally significant, tectonostratigraphic- parasequence units, they have been able to infer the sequence of glacial events using tectonostratigraphy. This relies on the interpretation of compressional brittle and ductile deformation structures as originating in either a pro-glacial or ice-marginal setting. Packages of glacigenic sediments and associated upper and lower sedimentary or glacitectonic detachment surfaces have been identified and mapped. On the assumption that each detachment surface represents an oscillation of the BIS, Lee *et al*. (2017) identified six individual advances into north Norfolk. The tectonostratigraphical scheme is summarised in Figure 3-4.

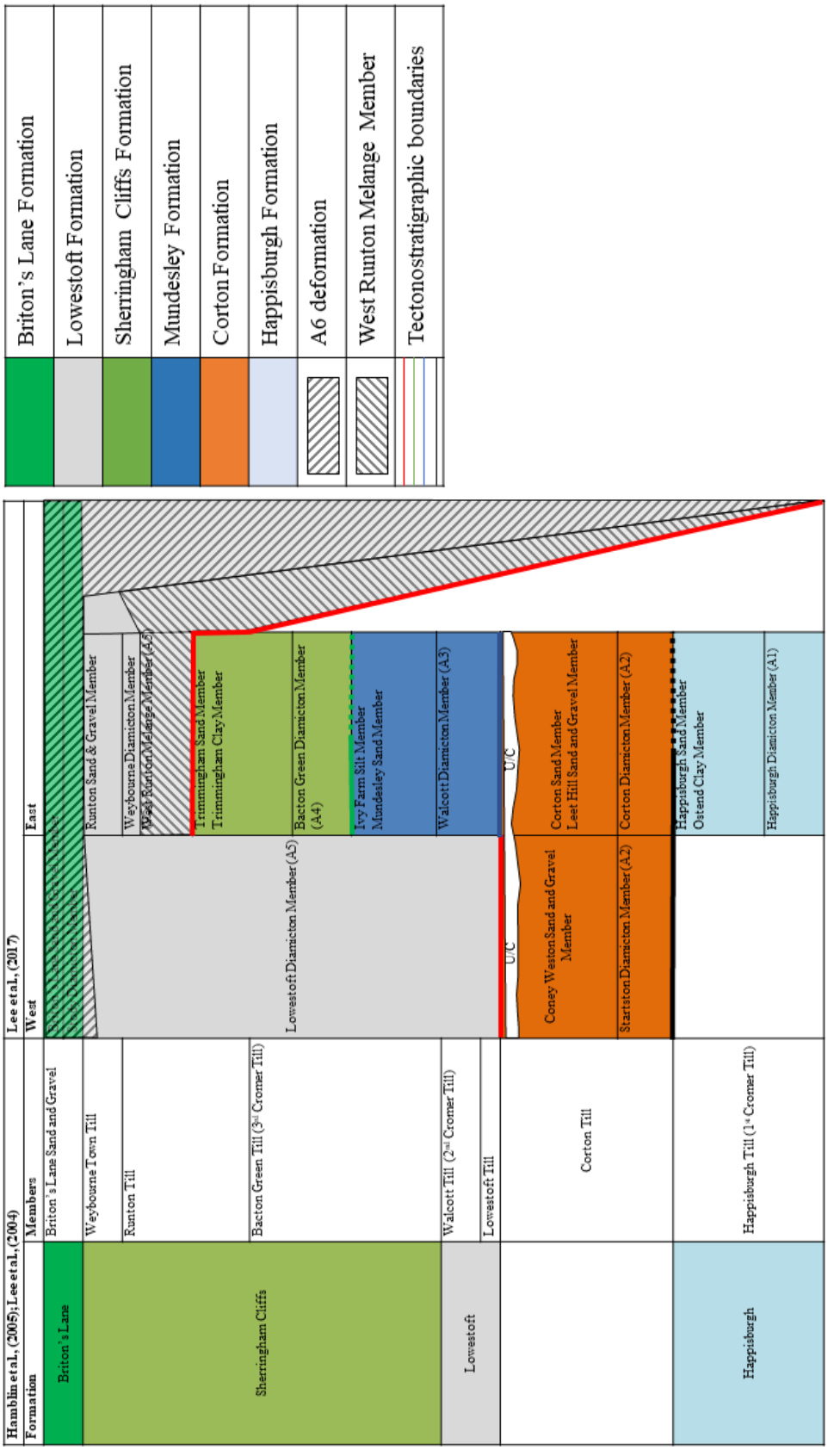

Figure 3-4 Tectonostratigraphic scheme for the glacial deposits of north Norfolk after Lee *et al*. 2017. Lithostratigraphic nomenclature from Hamblin *et al*. (2005) and Lee *et al*. (2004). A6 deformation is equated with the 'Contorted Drift' glacitectonite.

3.2.2.3 Vale of St Albans

The Vale of St Albans area is located at the margin of the maximum extent of the BIS during Anglian glaciation. This critical area provided evidence for the interaction of the BIS and the pre-Anglian drainage of the River Thames and its subsequent diversion. It is considered here as a proxy for Anglian ice-marginal dynamics and sedimentation in lowland Britain. It is located on the eastern dipslopes of the Chiltern Hills and glaciation here is believed to have been contemporaneous with that in north Buckighamshire although no unequivocal evidence is available to support it.

The Quaternary geology of the Vale of St Albans was studied in detail by Gibbard (1977). Numerous pits, quarries and boreholes provided evidence to establish the detailed sedimentology and stratigraphical relationships between glacigenic, fluvial and organic deposits. Thirteen lithostratigraphical units were identified. Most were assigned to the Anglian glaciation comprising at least two major advances marked by chalk-rich tills and glaciolacustrine sediments deposited following blocking of eastward directed fluvial drainage of the proto-Thames. The stratigraphical sequence for the pre-Anglian and Anglian deposits in the Vale of St Albans is shown in Table 3-5.

Gibbard (1977) showed the glacigenic sequence in the Vale of St Albans could be correlated with the glacigenic assemblages in Hitchin. The deposits here occupy a broad 'drift-filled' channel that extends across the Chiltern Hills and is drained by the valleys of the Rivers Hiz near Hitchin and Beane near Stevenage. All of the deposits occur within the valley with the exception of the Lower Westmill Gravel which is not seen northwest of Stevenage.

To the east of the Vale, glacigenic deposits infilling a depression in the Chalk Group bedrock surface near Bishop's Stortford were correlated with the Vale of St Albans. Here only one 'chalky' till is represented and interpreted to correlate with the Eastend Green Till.

Vale of St Albans		**Sedimentology**	**Palaeoenvironmental interpretation**	**Age**
West	East			
Smug Oak Gravel		Cross-bedded gravel with sand lenses (81-84% flint), (11-17% vein quartz and quartzite). Small-scale faults and ice-wedge casts	Westward flowing glaciofluvial river system sourced from northeastward retreating glacier ice. Periglacial	
Eastend Green Till	Eastend Green Till	Light-grey to blue-grey till with abundant chalk erratics. Clast orientation change from ESE-WNW at base to ENE-WSW above	Two-stage glacial advance from the northeast. Southwest fluvioglacial flow and northeast directed fluvial flow. Second-stage glacial advance diverts ancestral Thames into its present-day course. *In situ* glacier ice stagnation and	'Anglian II'

			formation of kettle holes.	
Moor Mill Laminated Clays		Silty clays, laminated in part	Glaciolacustrine. Ice-dammed, pro-glacial lake.	
Westmill Gravel	Westmill Upper Gravel	Gravel lenses with cross-bedded sand beds (2-25% chalk)	Fluvial. Braided river northeast and southwest flow confluence. *In situ* glacier stagnation. Permafrost. Re-advance of Ware till glacier	'Anglian I'
	Ware Till	Light to dark grey, weathered brown, matrix-supported with common chalk erratics	Valley glaciation. Advance of glacier ice from northeast. Waterlain in part. Solifluction.	
	Watton Road Laminated Silts	Brown, laminated, clayey silt with concave shear planes	Glaciolacustrine. Pro-glacial ice-dammed lake during advance of Ware till ice.	
	Westmill Lower Gravel	Gravel and cross-bedded sand. Gravel is flint rich (75-91%) with quartz and vein quartz (9-17%). Ice-wedges	Fluvial. Braided river. Ancestral Thames. Permafrost.	
Leavesden Green Gravel		Horizontally-bedded, flint-rich gravel with quartz and vein quartz	Eastward flowing braided river. Ancestral Thames	Pre-Anglian

Table 3-5 Sedimentology and palaeoenvironmental interpretation of the glacigenic and fluvial deposits of the Vale of St Albans after Gibbard (1977). Anglian I and II are informal events recognised in the Vale.

3.2.2.4 Regional stratigraphical correlation between the English Midlands and East Anglia

Stratigraphical correlation between the Midlands and East Anglia has been attempted on the basis of lithostratigraphy and till fabric analysis (Baden-Powell, 1948; West & Donner, 1956; Ehlers & Gibbard, 1991; Fish & Whiteman, 2001; Hamblin *et al.*, 2005; Rose, 2009; Lee *et al.*, 2011) and chemostratigraphy (Perrin *et al.*, 1979; Scheib *et al.*, 2011). A correlation between glacigenic deposits in north Buckinghamshire and those of East Anglia and the English Midlands has yet to be established. Regional stratigraphical correlation is summarised here to provide a stratigraphical framework against which the results of field and laboratory investigations will be compared in Sections 8 and 9.

The calcium-carbonate and chalk-rich diamictons of the Lowestoft Till Member (Lowestoft Formation) and 'Marly Drift' of the 'North Sea Drift Formation' of East Anglia have proved critical in attempts to correlate glacial sequences in the English Midlands and East Anglia (Wood, 1880; Baden-Powell, 1948; West & Donner, 1956; Perrin *et al.*, 1979; Allen *et al.*, 1991; Fish & Whiteman, 2001).

The 'Chalky Boulder Clays' of Norfolk and Suffolk were previously divided into an upper and lower division, referred to as the Gipping and Lowestoft Boulder Clays respectively (Baden-Powell, 1948). The 'Lowestoft Boulder Clay' comprises matrix-dominated tills with abundant chalk erratics and Jurassic clay and silt within the matrix. The 'Gipping Boulder

Clay' was originally interpreted as a pale brown and younger till, separated from the 'Lowestoft Boulder Clay' by interglacial deposits (West & Donner, 1956). It is now generally considered that the 'Gipping Boulder Clay' is in fact a weathered product of the 'Lowestoft Boulder Clay' (e.g. Perrin *et al.*, 1979; Lewis, 1999). In contrast, recent statistical analysis of the geochemistry of chalk-rich tills in the region raises the possibility that two 'chalk-rich' till facies exist that are associated with two separate glacial events (Scheib *et al.*, 2011). The 'Chalky Boulder Clay/Lowestoft Boulder Clay' of East Anglia was correlated by with tills of Pennine derived-ice in the Midlands and the English Midlands by West & Donner (1956) using clast fabric analysis. They identified three glacial events in East Anglia and the Midlands and included the 'Gipping' event as a separate glaciation. Their 'Lowestoft Advance' was correlated with Pennine derived ice that deposited Midlands tills and their chalk-rich, 'Lowestoft Boulder Clay', correlatives in East Anglia. The sequence was regarded as being deposited during the Anglian Stage.

Investigation of carbonate content, particle-size and erratic type, led Perrin *et al*. (1979) to correlate the Lowestoft Till of East Anglia with lithologically similar tills forming extensive till sheets in southern Britain. Perrin *et al*. (1979) termed this group of tills the 'Lowestoft Type' and distinguished them from the North Sea Drift Formation, including its 'Marly Drift'. As a result, Perrin (1979) correlated all matrix-supported and chalk-rich tills of southern Britain ('Lowestoft Type') with the Lowestoft Till member of East Anglia and by implication, regarded them as Anglian in age. Perrin's correlation however, does not take account of the fact that the Lowestoft Till Member in East Anglia was associated with advance of the BIS from the north or northwest (Pennine derived).

Following lithostratigraphical revision of the glacigenic assemblages in East Anglia, the sequence was related to separate glacial events ranging in age from MIS16 to MIS6 (Lee *et al.*, 2004 b; Hamblin *et al.*, 2005). This was in contrast to authors, including Lunkka (1994), who considered the glacigenic sequence to be entirely of Anglian age. Hamblin *et al*. (2005) and Lee *et al*. (2012) correlated the Thrussington Till Member of the English Midlands with the Lowestoft Till Member (Lowestoft Formation) of East Anglia and related them both to glaciation during the Anglian Stage. Lee *et al*. (2012) tentatively correlated the overlying sediments of the Sherringham Cliffs Formation including the Bacton Green Till Member (3rd Cromer till) and Weybourne Till Member, with the Oadby Till Member. They interpreted deposition of these sediments during glaciation in the Wolstonian (?MIS10) Stage. Using tectonostratigraphy, Lee *et al.* (2017) tentatively correlated tectonostratigraphical unit A6 with a younger glacial event associate with ice advancing westwards through the Fen Basin.

This was also consistent with geochemical evidence from chalk-rich tills of the Midlands and East Anglia (Scheib *et al.*, 2011).

The age and stratigraphy of glacial deposits in the English Midlands, south of the Devensian Stage glacial limit, has been the subject of much debate and research over the past 50 years. The correlation of the Anglian age Lowestoft Formation in East Anglia with other chalk-rich tills in the English Midlands is problematic. Firstly, the Lowestoft Till Member of East Anglia is interpreted to have been deposited by a Pennine-sourced portion of the BIS that advanced into East Anglia form the north or northwest (Rose, 1992; Clark, P L Gibbard, *et al.*, 2004; Lee *et al.*, 2017). If the chalk-rich tills in the Midlands were deposited as part of this same advance, chalk-rich lithologies could not have been included at this time as the bedrock sources of Chalk existed to the east and so must have been incorporated subsequently.

Lee *et al*. (2012) explain this by interpreting deposition of potentially equivalent diamictons of the Sherringham Cliffs Formation to have occurred during a younger ?MIS 10 event. Secondly, the Wolston Formation glacigenic sequence of the Midlands was considered to have been deposited during the Wolstonian Stage and therefore younger than the sequence in East Anglia. Acceptance of the age of the Midlands' chalk-rich tills as Anglian, led to the re-interpretation of the Midlands Wolston Formation as itself Anglian in age (Rose, 1987, 2009; Lee *et al.*, 2012). Supporting this interpretation on the basis of correlation with terraces of the Upper River Thames, Sumbler (2001) advocated an Anglian age for the glacigenic deposits in Moreton-in-Marsh, Gloucestershire, themselves originally interpreted as Wolstonian by Shotton (Shotton, 1953, 1983). This re-interpretation has held for many years but has since been challenged by Gibbard *et al*. (2013) who argued that the original interpretation of Wolstonian be reinstated for the Midlands' Wolston Formation.

The relative stratigraphical relationships of the Wolston Formation in the Midlands is not in doubt. The stratigraphical relationships in East Anglia remain the subject of on-going research with tectonostratigraphy providing the most recent understanding of the timing and number of glacial events in the region. Despite this evolving stratigraphical relationships, three hypotheses of relevance to north Buckinghamshire, revealed by a review of the literature, remain with consensus yet to be reached. They are:

1. The glacigenic sequences in the English Midlands and East Anglia were all deposited by oscillations of North Sea and 'Pennine' ice lobes of the BIS during the Anglian Stage.

2. The glacigenic sequences in East Anglia were deposited during oscillations of North Sea and 'Pennine' ice lobes of the BIS during the Anglian Stage and the glacigenic sequences in the Midlands were deposited by a subsequent glaciation during the Wolstonian Stage.
3. A hybrid of 1 and 2 where the Thrussington Till member of the Wolston Formation and the Lowestoft Till Member of East Anglia was deposited by a 'Pennine' lobe of the BIS during the Anglian Stage and the Oadby Till Member by a North Sea lobe of the BIS during the Wolstonian Stage (?MIS 10 or 6).

The implication of 1 is that the re-interpretation of the Midlands' glacigenic sequences as Anglian in age remains and that the arguments against it made by Gibbard *et al*. (2013) are rejected. Given the counter arguments stated above, this rejection is not supported here. If hypothesis 2 is accepted, the implication is that there is a geographical boundary between the late Wolstonian Stage glacigenic sequence in the Midlands and the Anglian Stage glacigenic sequence of East Anglia as mapped by Gibbard & Clark (2011). Hypothesis 3 relies on the acceptance of Anglian Stage glaciation in the Midlands to deposit the basal Thrussington Till Member with sediments of the Oadby Till Member and intervening glaciolacustrine sediments deposited over it during ?MIS 10 or 6. If hypothesis 2 is accepted, hypothesis 3 must be rejected.

3.2.3 Regional context: periglacial geology

Frost-susceptible clay and silt-rich bedrock and Quaternary sediments in southern Britain are likely to have been subject to ground ice growth and degradation during multiple episodes of cold-climate development in the Quaternary. In lowland Britain, sediments, landforms and structures associated with periglacial activity and permafrost are common (Ballantyne & Harris, 1994; French, 2007). They include solifluction (Skempton & Weeks, 1976; Hutchinson, 1991), involutions and ice-wedge psuedomorphs (Rose & Allen, 1977; Murton *et al.*, 2015), loess (e.g. Antoine *et al.*, 2003), thermokarst depressions (West, 1991; Boreham, 1996) and bedrock brecciation (Chandler, 1972; Murton, 1996). Anomolous depressions in geological rockhead in London have also been suggested as the former sites of pingos (Berry, 1979; Hutchinson, 1980; Banks *et al.*, 2015).

On geological maps, 'head' is a genetic term and is often synonymous with periglacial solifluction deposits but can also include recent slope and hillwash deposits. Head is recognised where it infills valleys or forms fans at the mouths of dry-valleys and is recognised throughout southern Britain (Ballantyne & Harris, 1994; Murton & Ballantyne, 2017). For

example, at least three generations of incised sheets of 'head' are recognised in Bedford (Barron *et al.*, 2010). The sediments are lithologically similar to their parent materials and comprise, angular gravel or cobbles in a generally silty or clayey matrix.

Regions in southern Britain underlain by clay and silt-rich bedrock have been shown to be susceptible to the formation and degradation of ground ice, typically in the form of segregated-ice lenses, periglacial erosion and the formation of thermokarst (Ballantyne & Harris, 1994; Murton & Ballantyne, 2017). Circular depressions in the landscape of the Fenlands have been attributed to thermokarst lake formation (West, 1991). Here, groundwater-fed springs and surface meltwater result in the formation of lakes above permafrost beyond the maximum extent of glaciation. Thermally driven erosion during thaw (backwearing) results in the erosion of the lake margins and associated deposition of locally-derived solifluction sediments (Murton, 2001). The latter process has been invoked by West (1991) to explain the formation of the Fenland 'Crowland Bed'. Circular or near-circular depressions are shown on geological maps in north Buckinghamshire. Thermokarst has not been directly invoked as a factor in their formation but features developed over frost-susceptible bedrock, including that of Ot Moor (Ambrose & Horton, 1991) may be related to thermokarst degradation.

3.2.4 Quaternary geology of north Buckinghamshire, including Milton Keynes

The descriptions of the Quaternary geology in the following section focuses on the geographic region of north Buckinghamshire. Given the proximity and potential relevance of sequences in Milton Keynes, Bedfordshire and part of north Oxfordshire, reference is also made to these regions.

Investigation of Quaternary sediments of relevance to north Buckinghamshire were undertaken in the Kettering and Northampton area (Hollingworth & Taylor, 1946) to the north of the project area. This was further developed during borehole drilling for potential sand and gravel resources in the northern part of the Buckingham area (Sumbler & Samuel, 1990). Geological surveys at the six-inches to one mile were undertaken between 1895 and 1897

while surveys at the one inch to one-mile scale were undertaken in the 1860s. The latter geological maps were published as 'old series' one inch to one mile maps (1:63 360) as Sheets 45 and 46 (Green, 1864).

The geology of the regional area to the east was investigated in advance of the construction of the new town of Milton Keynes (Horton, 1970; Horton *et al.*, 1974). Recent geological investigation and survey at 1:10 000 and publication at 1:50 000 scale by the BGS was completed in 2000 for Buckingham (Sumbler, 2002) and Bedford (Barron *et al.*, 2010) and reference is made to these results in the following sections.

3.2.4.1 Pre-Anglian sediments and geological rockhead topography

The elevation of geological rockhead in parts of East Anglia and Cambridgeshire is known to be variable and in places incised into sediment-filled depressions interpreted as tunnel valleys (Woodland, 1970; Bricker *et al.*, 2012; van der Vegt *et al.*, 2012). Tunnel valleys are believed to form sub-glacially through meltwater erosion and subsequent infill beneath continental ice-sheets (van der Vegt *et al.*, 2012). Sediment-filled depressions in the geological rockhead surface in parts of north Buckinghamshire, Bedfordshire and Northamptonshire have also been identified (Thompson, 1896).

Sumbler (2002) identified a broad, northeast-southwest trending valley cut into geological rockhead extending from south of Buckingham and decreasing in elevation towards Maids Moreton [SP 704 356], also filled with glacigenic sediments, including glaciolacustrine sediments. The buried valleys occur beneath the present-day valleys of the rivers Nene and Great Ouse and their tributaries where they trend either northeast-southwest or north-south. Their distribution in relation to other buried valleys of southeastern England is shown in Figure 3-5.

The origin of sediment-filled valleys in north Buckinghamshire, Bedfordshire and Northamptonshire remains unresolved. Tunnel valleys are typically filled with coarse-grained sediment at their base reflecting high-energy, sub-glacial fluvial deposition. Silty sand, sand, laminated clay and silt with interbedded till are characteristic of the buried valleys in the north Buckinghamshire region; coarse-gained sand and gravel appears to be absent. Horton (1970) considered their most likely origin to be related to fluvial and/or glaciofluvial erosion prior to the onset of glaciation. A model for the subglacial, effective stress conditions that could result in the formation of buried channels is described in Section 1.6.4.

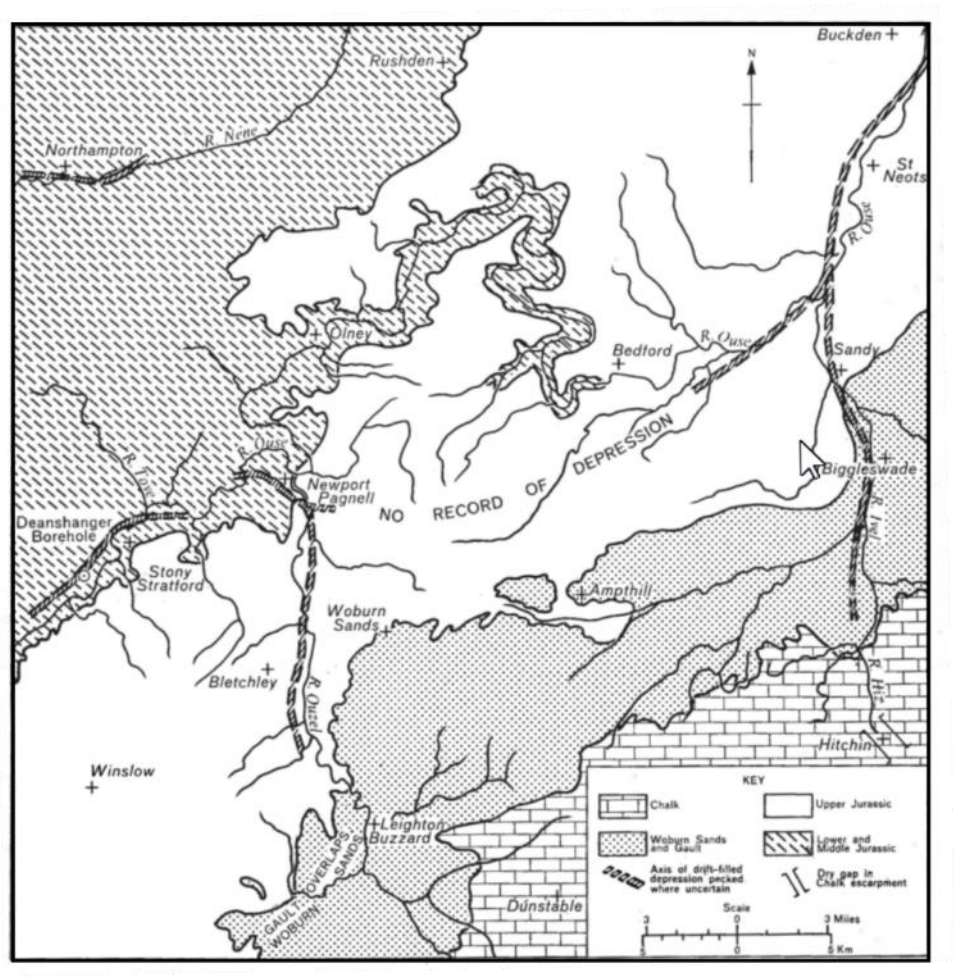

Figure 3-5 Distribution of depressions in geological rockhead in parts of Bedfordshire, Hertfordshire and Cambridgeshire interpreted as buried valleys after Horton *et al.* (1974).

Undifferentiated sand and gravel deposits were interpreted to underlie glacigenic deposits in the Buckingham area (Sumbler, 2002). He described scattered patches of quartz and quartzite-rich gravels and tentatively correlated them with the fluvial terrace deposits of the Hanborough Member of the Upper Thames region (Sumbler, 1995). Alternatively, these deposits may represent glaciofluvial outwash sediments associated with the early onset of glaciation and the advance of an ice-sheet into the area from the north or northeast. Limestone-rich gravel occurring at the base of the glacigenic sequence in the Buckingham area may also provide further evidence of pre-glacial fluvial or glaciofluvial sedimentation. Outcrops of this gravel occur in a disused railway cutting near Finmere [SP 642 343] and Maids Moreton [SP 715 350].

Sand and gravel terraces within the valley of the River Great Ouse at Haversham [SP 830 431], north of Milton Keynes comprise rounded to sub-rounded gravel of local Jurassic limestone with minor proportions of ‘Bunter’ and ironstone clasts (Horton *et al.*, 1974). They are seen to directly overlie Jurassic bedrock and appear to be overlain by till. Horton *et al.*

(1974) noted that the clast content differed from the Chalky Boulder Clay (*sic*) but compared to an unspecified adjacent till in the valley. He tentatively associated these gravels with limestone-rich gravels in Northampstonshire where they were seen to underlie 'Chalky Boulder Clay' (sic) and overlie a 'Lower Boulder Clay' (Hollingworth & Taylor, 1946). The gravels are interpreted as either pre-glacial fluvial or glaciofluvial deposits (Horton *et al.*, 1974). If they are glaciofluvial, they are inferred to have been sourced from a lobe of BIS whose provenance is interpreted to be from the north or northeast.

In the Bedford, Wellingborough, Northampton and Towcester area, sand and gravel deposits interpreted as fluvial in origin have been assigned to the Milton Formation (Barron *et al.*, 2006, 2010). Milton Formation sediments comprise locally-derived clasts mixed with sand sourced from Triassic sandstones of the West Midlands (Barron *et al.*, 2010). They are interpreted to have been deposited in braided streams, partially cut into underlying geological bedrock.

In the Buckingham area pre-glacial sand and gravel deposits may also correlate with the Milton Formation of Belshaw *et al*. (2014) and form part of left-bank tributary of the ancestral Thames river system.

3.2.4.2 Glacigenic sediments

In the north Buckinghamshire area, glacigenic deposits are commonly >10 m thick. In the BGS Deanshanger borehole [SP 7652 3880], over 60 m of interbedded matrix-supported clayand stilt with chalk casts and laminated clay, silt and sand were proved and interpreted to infill a buried valley adjacent to the River Great Ouse. Green (1864) identified a three-fold division what he interpreted as glacigenic deposits in the Buckingham, Bicester and Brackley area (Table 3-6). He noted that the glacigenic deposits are found on interfluves and concluded that they once formed an extensive spread which has subsequently been dissected by periglacial weathering and post-glacial fluvial incision.

Stratigraphy	**Sub-division**	**Palaeoenvironment**
Low Level or Valley Gravels	-	Fluvial
Clays and gravels of the Boulder or Glacial Period	- Clean gravels without clay - Stiff blue clay with occasional pebbles and large, angular ice-scratched boulders -Clayey and dirty gravels	Glacial, glaciofluvial

Table 3-6 Glacigenic geology of the Buckingham district identified by Green (1864). Relative stratigraphical order uncertain.

Green (1864) described ‘clean gravels’ comprise generally well-rounded gravel of Jurassic oolites, flint, quartz pebbles, blocks of ‘slate’ and occasional gneiss, granite and other igneous rocks of unknown provenance. They display irregular bedding, varying grain-size, apparent cross-bedding and are well to poorly-sorted.

The ‘stiff blue clay’ was previously exposed in small pits and railway cuttings in the Buckingham area. Green (1864) observed stiff blue clay with occasional ‘pebbles’ and boulders. The boulders comprised Jurassic limestone, ‘quartz blocks’, vein quartz and probable Carboniferous sandstone and limestone. ‘Ice scratches’ were observed on the boulders of probable Carboniferous sandstone and limestone but not on the clasts of Jurassic rocks. Locally, in Buckingham, chalk, ‘chalk rock’ and flints were observed. In places the gravel is observed to be cemented by iron oxide, interpreted by Green as post-depositional weathering.

The third division recognised by Green was that of clayey, ‘dirty’ gravels which were commonly associated with ground underlain by Jurassic Oxford Clay and Kimmeridge Clay formations. The term ‘dirty’ is interpreted to indicate the presence of abundant silt or clay. The gravels comprise abundant flint and quartz with minor amounts of locally-derived clasts.

The stratigraphical relationships within Green’s ‘Boulder or Glacial Period’ are not known but a former exposure to the west of Buckingham was described by Green and is shown in Figure 3-6.

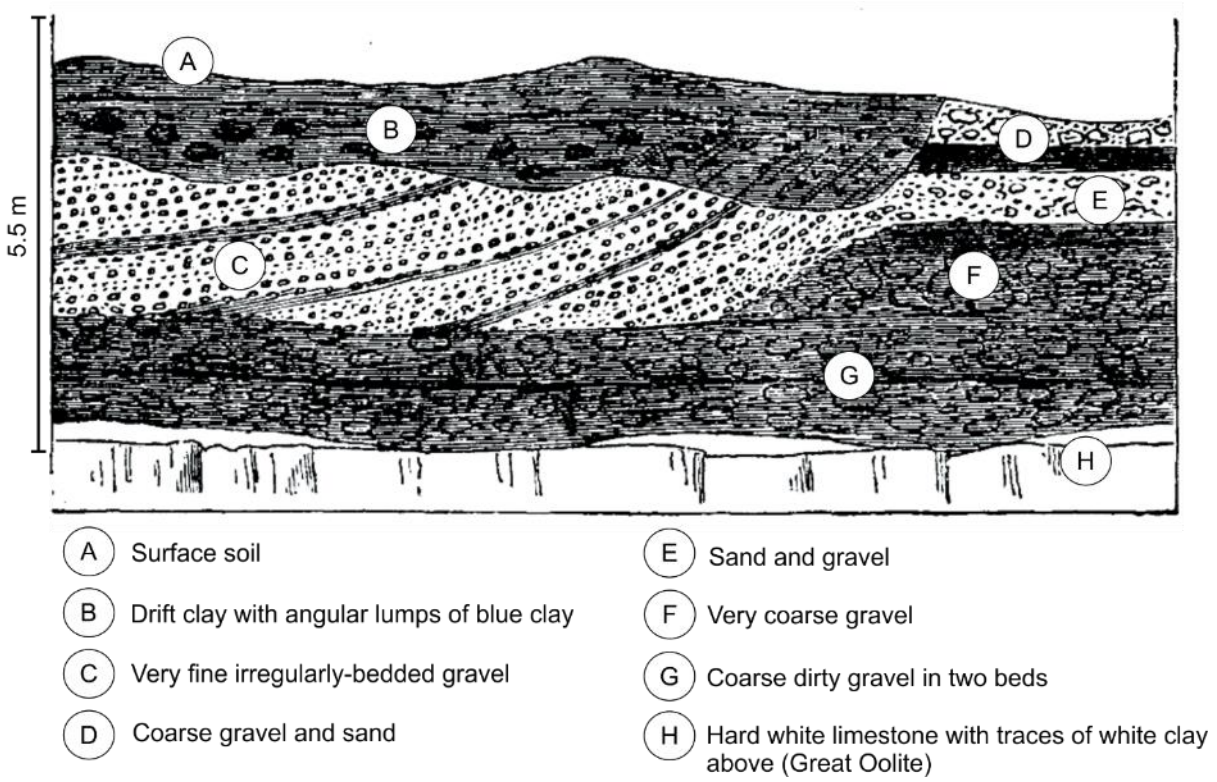

Figure 3-6 Section in a former pit 'two miles to the west of Buckingham on the Bicester Road' modified after Green (1864). The exact location is unknown but is interpreted to be near Tingewick [SP 6580 329].

'Stiff blue clay' was observed to underlie and interdigitate with clean gravels and in conjunction with the presence of far travelled erratics. Green tentatively interpreted the clay deposits as the oldest in the sequence. The presence of deformed and contorted sediments (see Section 3.3.4.6), may indicate sub-glacial or ice-marginal deformation, but Green suggested that the gravels were deposited in a marine setting. The inferred age for the glacigenic deposits was given as post-Pliocene (Green, 1864).

Sumbler (2002) also identified matrix-supported tills in the Buckingham area which he interpreted as till. till comprises grey 'gritty' clay matrix with abundant erratics of chalk, flint, quartz, quartzite, Jurassic limestone, Carboniferous sandstone and limestone, and various unspecified igneous rocks (Sumbler, 2002). Erratics range in grain-size from silt to rare boulders. This till was termed the Oadby Till Member by Sumbler (2002) correlating it on the basis of lithology, with the assumed Anglian-age 'Chalky Boulder Clay' of the English Midlands and East Anglia following Perrin *et al*. (1979). Olive-grey to dark grey, matrix-supported clay and silt with clasts, weathering to yellowish brown in Bedford is interpreted as till. It comprises silty, variably sands clay with abundant clasts of chalk, flint, Jurassic limestone, sandstone and ironstone, quartzite, quartz and Carboniferous limestone and

sandstone as cobbles and boulders with rare igneous lithologies (Barron *et al.*, 2010). The till is 0 to 25 m thick and its base generally occurs above 80 to 85 m OD.

Only one unit of till was interpreted in the Buckingham area. Sumbler (2002) noted that the lower 'few metres' of his Oadby Till Member differed from overlying till. He described dark grey and sandy till with relatively few pebbles. Geological surveys at the 1:10 000 scale in the nearby Bedford, Towcester and Wellingborough areas identified at least one other till unit that was interpreted to occur stratigraphically below the dominant chalk-rich till of the region (Barron *et al.*, 2006, 2010). The older till is characterised by a lack of chalk and flint erratic clasts and a greater proportion of Triassic-derived 'Bunter' quartz, quartzite and locally derived clasts. In Bedford it comprises dark bluish-grey matix-supported till with mainly Jurassic limestone and ironstone, some quartz and quartzite, Jurassic fossils, rare flint and very rare chalk. In the valley of the River Ouzel it is interpreted to underlie the main 'Chalky Boulder Clay' and comprises grey, 'gritty' textured clay with 'Bunter' pebbles (*sic*), local limestone and fossils including ossicles of *Pentacrinus* and *Gryphaea*, minor weathered flints and calcareous concretions (Hollingworth & Taylor, 1946). Rafts of Jurassic bedrock are also present (Horton, 1970). It is up to 24 m thick and rests directly on bedrock or on laminated clay and silt in the Northamptonshire area (Hollingworth & Taylor, 1946; Barron *et al.*, 2010).

The stratigraphically lower till was referred to as the Bozeat Till by Barron *et al*. (2010) and the Lower Boulder Clay by Hollingworth & Taylor (1946). The Bozeat Till has been correlated with the Thrussington Till of the English Midlands and the Lowestoft Formation of East Anglian by Lee *et al*. (2012).

Chalk-rich diamicton interpreted as till crops out in Milton Keynes, Bedfordshire and Northamptonshire. It forms an extensive deposit preserved on interfluves between the tributaries of the River Great Ouse and Nene or in buried valleys. The till comprises grey, silty clay with abundant fine gravel erratics of chalk with some larger, ice-striated clasts (Horton *et al.*, 1974). Other erratics include angular flint, 'Bunter'-derived quartz and quartzite, Jurassic limestone, mudstone and fossils. Large erratics of Mesozoic bedrock clay have also been recorded at the base and interpreted as rafts incorporated within the till (Horton, 1970; Horton *et al.*, 1974). The chalk-rich till in the Milton Keynes and Bedfordshire area has been correlated with the 'Chalky Boulder Clay' (Lowestoft Formation) of Perrin (1979).

If two tills with different clast assemblages are present it may suggest that each is a product of two separate glaciations. This may reflect an earlier Anglian and later Wolstonian glaciation. Alternatively, the two tills may be the product of one glaciation and their contrasting composition may reflect local variation in sediment source. Sumbler (2002) considered the Buckingham Oadby Till Member and its two facies to be the product of oscillations of different lobes of the same Anglian-age advance of the BIS.

A borehole, SP 73NE2, drilled in 1964 by the then Institute of Geological Sciences (IGS) near Deanshanger [476520 238800] proved 61.7 m of glaciolacustrine and fluvio-lacustrine sediments, interbedded and overlain in their upper part with chalk-rich till. A summary of the sequence proved in borehole SP 73NE2 is shown in Figure 3-7. Photographs taken of the remaining bulk samples archived in the National Geological Repository at the British Geological Survey are shown in Figure 3-8. Glaciolacustrine deposits also occur on the western margin of the River Ouzel [SP 487 324].

The glaciolacustrine sediments are dominated by a fining-upwards sequence of bedded and channelised sand and laminated to poorly-bedded silt, clay and sand with common lenses or beds of till. A lower unit of silty sand is separated from an overlying unit of laminated clay, silt and sand by till with a chalk-rich erratic assemblage. Till occurs throughout as beds or lenses with gradational contacts with laminated silt and clay. Chalk erratics are seen to depress laminations below with draped laminations over them. Ductile and brittle deformation is common within the laminated sequence where it is overlain and interbedded with till. High and low-angle normal and reverse faults and overturned folds are present. Folds limbs are faulted (e.g. Figure 3-8G). The bases of sand beds are often sharp and erosional. Chalk is present throughout as fine to medium-grained sand or fine gravel clasts. Channelised sand beds with scattered ‘Bunter’ quartzite, carbonaceous fragments, chalk and quartz clasts are common at the base of the sequence.

The sequence is interpreted as fluvio-lacustrine where subaqueous delta sands were deposited at the base, fining upwards into laminated glaciolacustrine sediments (Horton, 1970; Horton *et al.*, 1974). Lenses and beds of chalk-rich till were interpreted as debris released either from floating icebergs or subaqueously as flow tills from a proximal ice-margin. Proglacial lakes were interpreted to be dammed by glacier ice to the north and/or northeast and constrained by bedrock to the west.

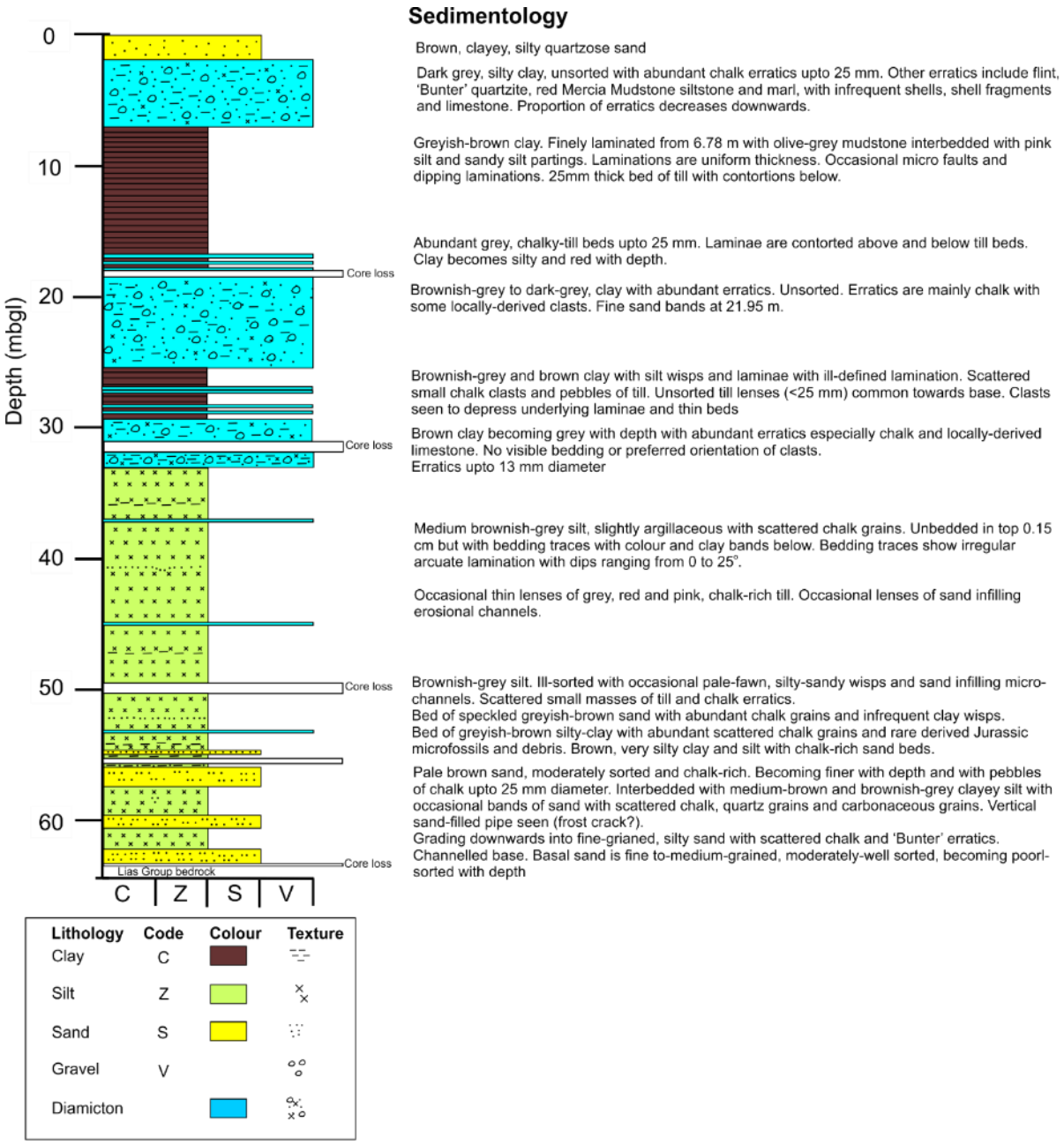

Figure 3-7 Summary of borehole log SP 73NE2 (Deanshanger/Manor Farm Towcester 10) produced by the author from interval 0 – 63.4 mbgl.

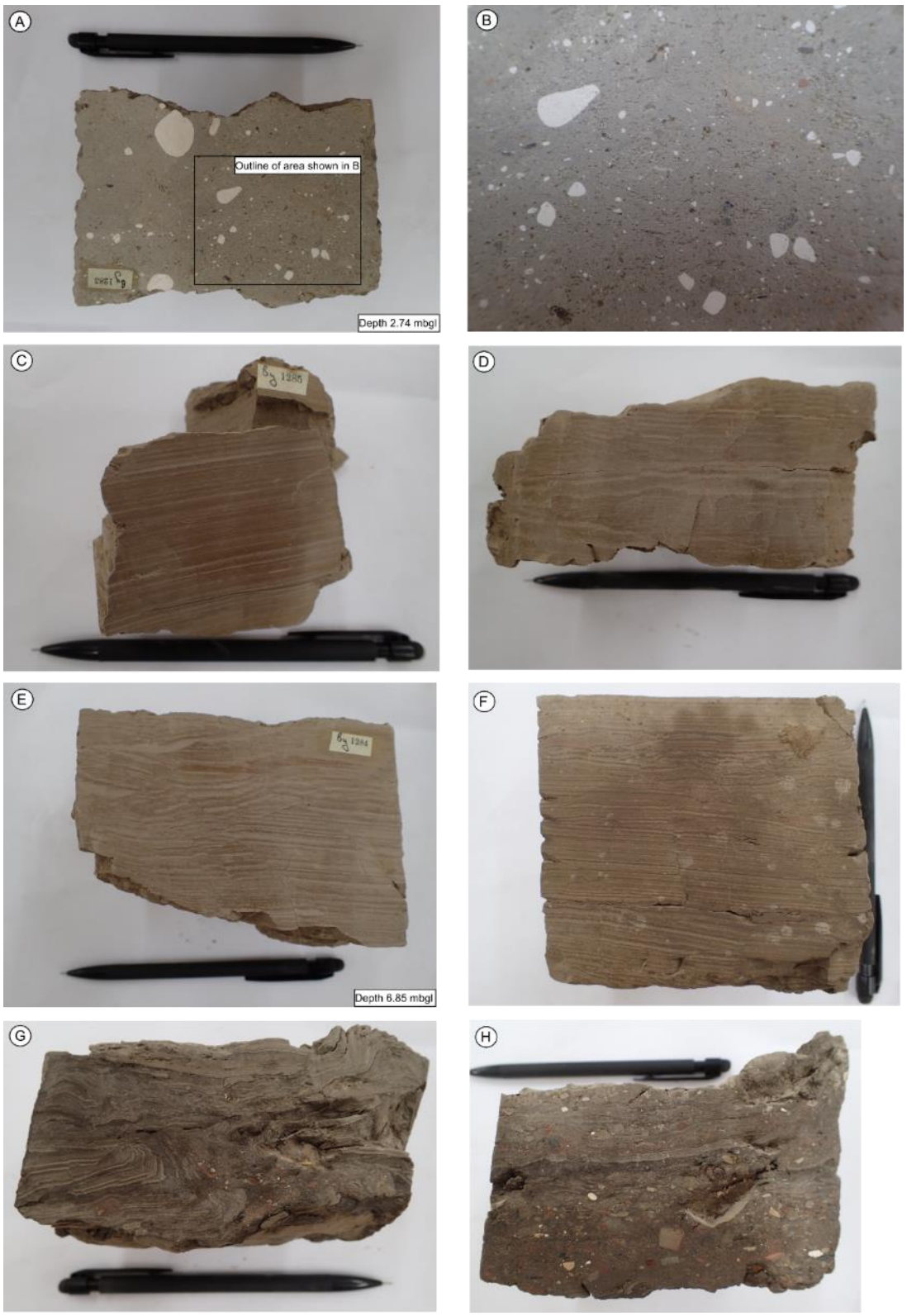

Figure 3-8 Bulk samples from BGS borehole SP 73NE2 (Deanshanger/Manor Farm Towcester 10) from interval 1.7 – 63.4 mbgl. Individual depths and way-up unknown except where indicated. A) Matrix-supported, poorly-sorted, till with well-rounded fine gravel of chalk. B) Close-up of A. C) Parallel-laminated clay (dark) and silt (light). D) As C with common high-angle normal micro faults. E) As D with low-angle normal and reverse microfaults. F) As E with low angle slump structures. G) Folded and faulted laminated silt and clay with chalk-

rich till. H) Interlaminated diamicton, clay and silt with possible dropstones of erratics and till clasts. Pencil is 140 mm long. All photographs by the author. For further description see Horton (1970).

Glaciolacustrine deposits are present in the Buckingham area. They are not well exposed, although Sumbler (2002) interpreted 'undifferentiated glacial deposits' as glaciolacustrine in origin. In addition to a probable east-west trending buried valley in the Stony Stratford area [SP 790 400], this raises the possibility that buried valleys may extend into the Buckingham area as suggested by Sumbler (2002).

In Buckingham, glaciofluvial sediments comprise poorly-sorted flint-rich gravels and sand that occur below, within and above till. They are probably the same sediments described as the 'clean gravels' described by Green (1864). The thickness of the unit is variable. In Stowe Park [SP 672 376], 18 m of poorly-sorted gravel with cobbles and boulders are exposed and interpreted as englacial, glaciofluvial sediments. Sheet-like sediment-landforms were interpreted by Sumbler (2002) as outwash sandur deposited in front of a retreating ice-margin.

Sand and gravel overlain by chalk-rich till is exposed in the valley of the River Ouzel in the Milton Keynes area where they overlie the Oxford Clay (Horton *et al.*, 1974). The sand and gravel comprise poorly-sorted to well-graded gravel with chalk, flint, limestone and 'Bunter' pebbles and seams of fine gravel. Sands are dominated by quartz and chalk, and moderately-sorted. Along with beds of silt and silty clay, they are cross-bedded. Sand and gravel interbedded with till is recorded in Northamptonshire and may also occur in areas including Newton Longville [SP 854 308]. Sand and gravel overlying till occurs to the southwest of Milton Keynes where between 0.91 and 6.4 m of variably clayey, sand and gravel and sandy flint-rich gravel are exposed or proved in boreholes. It forms a weak terrace feature and its base occurs above 67 m OD. Sand and gravel deposits associated with till are interpreted as glaciofluvial in origin.

3.2.4.3 River Terrace sediments

The 'low-level gravels' of Green (1864) are associated with terraces of local significance along the course of the River Great Ouse and its tributaries. Sumbler (2002) identified at least two River Terrace aggradations comprising quartz and quartzite-rich gravel, probably reworked from glacigenic sediments along the course of the River Great Ouse. Second Terrace sediments form a bench in the landscape, ~5 m above the floodplain. First Terrace sediments form a bench ~2 m above the floodplain with gravel passing beneath alluvium. Terrace sediments associated with the tributaries of the River Great Ouse contain a higher proportion of silt than those of the main river valley.

The river terraces of the River Great Ouse and their Pleistocene history has been described by Boreham *et al*. (2010). Four terraces of the upper River Great Ouse have been identified and correlated with equivalents in the Wash Basin. They range in age from Wolstonian (~MIS 10) to late Devensian (MIS 2).

Investigation of the lithological and altitudinal correlation of the river terraces of the upper Thames and their relation to river valleys including the Cherwell and Evenlode was undertaken by Sandford (1924), Bishop (1958) and Briggs & Gilbertson (1980). A summary of the terrace sequence in the upper Thames is given in Table 3-7 together with their correlation to the River Thame (Sumbler, 1995) and the River Ray, a tributary of the River Cherwell (Ambrose & Horton, 1991).

<table>
<tr><th>MIS stage</th><th>Upper Thames (Briggs & Gilbertson, 1980)</th><th>Thame (Sumbler, 1995)</th><th>River Ray (Ambrose & Horton, 1991)</th></tr>
<tr><td>1</td><td>Alluvium</td><td>Alluvium</td><td>Alluvium</td></tr>
<tr><td rowspan="2">2-4</td><td>Later Floodplain terrace</td><td>Quarrendon terrace</td><td rowspan="2">First terrace

Second terrace</td></tr>
<tr><td>Earlier Floodplain terrace</td><td>Ickford terrace</td></tr>
<tr><td rowspan="2">5</td><td>Wolvercote Channel</td><td>-</td><td rowspan="3">Third terrace</td></tr>
<tr><td>Upper Summertwon-Radley terrace</td><td rowspan="2">Shabbington</td></tr>
<tr><td>6-?10</td><td>Lower Summertwon-Radley terrace</td></tr>
<tr><td rowspan="2"></td><td>Wolvercote terrace</td><td>Blackditch terrace</td></tr>
<tr><td rowspan="2">Hanborough terrace</td><td rowspan="2">Chilworth terrace</td><td rowspan="3">-</td></tr>
<tr><td>11</td></tr>
<tr><td>12</td><td>Plateau Drift</td><td>Three Pigeons/Tiddington terraces?</td></tr>
</table>

Table 3-7 Tentative correlation of terraces in the upper Thames, Thame and River Rey (River Cherwell tributary) relevant to the north Buckinghamshire area.

The correlation of the river terraces of the River Great Ouse to those of the upper Thames river system is uncertain. Sumbler (2002) correlated Second terrace sediments with the composite Summertown-Radley Member and the First terrace with the Northmoor Member of the upper Thames succession. The lower part of the Summertown-Radley Member is assigned to ?MIS6 and its upper part to MIS 5 while the Northmoor Member is assigned to MIS 4-2 (Gibbard, 1999). Altitudinal correlation of the terraces of the River Ray with the upper Thames suggest that it developed in the late Wolstonian Stage with deposition during the Devensian (Ambrose & Horton, 1991). The Blackditch/Wolvercote Terraces are altitudinally-

correlated with glacigenic deposits in the Thame catchment in the area of Stewkley [SP 850 263] (Sumbler, 1995).

3.2.4.4 Alluvium

Alluvial sediments are associated with the River Great Ouse and its tributaries and are confined to their floodplains. Alluvial sediments are upto 2.5 m thick and comprise clay, sandy clay and silt with some peat lenses (Sumbler, 2002). A gravel 'lag' is commonly present at the base and may also occur as lenses.

3.2.4.5 Tufa and Peat

Small areas of peat and tufa are noted in the Buckingham area but their distribution and thickness are not known (Sumbler, 2002).

3.2.4.6 Periglacial geology and structures of glacial or periglacial origin

Evidence for the presence of past permafrost in Buckinghamshire has been shown at Marsworth [SP 933 141], near Aylesbury (Murton *et al.*, 2001, 2015). Here, clayey, silty and gravelly sediments preserve evidence of thermal contraction cracks, chalk bedrock fracture, fluvial activity, involutions, mass-movement and deposition of loess and coversand. The authors attribute the main phase of periglacial activity to MIS 6 (Wolstonian).

'Head' is recognised in valleys in Buckingham and Bedford (Sumbler, 2002; Barron *et al.*, 2010). It is also possible that 'head' exists over a much wider area than shown on 1:50 000 scale geological maps, especially in areas underlain by fine-grained bedrock lithologies.

Brittle or ductile deformation structures may be present in Quaternary sediments or geological bedrock where they have been subject to glacial and/or periglacial induced changes in effective stress. Large-scale, sub- to pro-glacial deformation associated with the Middle Pleistocene BIS have been recognised in lowland Britain (Rice, 1981; Hopson, 1995; Lee *et al.*, 2013; Phillips & Lee, 2013). Similar glacitectonic structures have not been unequivocally identified in the Buckingham area but their presence in a former ice-marginal setting cannot be discounted. Sumbler (2002) and Horton (Horton, 1970) refer to 'rafts' of Jurassic bedrock within till proved in boreholes to the northeast of Buckingham. It is not known if these features represent true glacitectonically-emplaced rafts or boulders of bedrock incorporated into till.

Green (1864) demonstrated that glacigenic sand and gravel in Buckingham showed evidence of brittle and ductile glacigenic deformation (Figure 3-9). At Tingewick [SP 650 320], the gravels are displaced by a steeply dipping fault. Folded sand and gravel-dominated beds with

subvertical dips were seen in former sand and gravel pits in Foscott, Maids Moreton [SP 700 350] and overlain by deformed clay beds at Tile House Farm [SP 694 396].

Structures interpreted to be the result of cambering and valley-bulging are present in the area to the north of Buckingham (Horton *et al.*, 1974). Valley bulging results in the ductile deformation of sediment or rock in valleys where lateral stress is released through erosion. Folds associated with valley bulging are often associated with cambering in an up-slope direction. Cambering and valley-bulging are common where permeable and generally strong rock overlies weaker and less permeable rock (Parks, 1991) and have been recognised in areas of Jurassic outcrops where permeable limestone and sandstone caps hills overlying mudrocks (Chandler, 1970; Hutchinson, 1991).

Structures interpreted to be the result of valley-bulging were also observed in the former brickworks site at Bletchley [SP 320 860] according to Horton *et al*. (1974). At the Bletchley site, mudstone of the Oxford Clay has been folded into open and inclined folds (Figure 3-10E). Folded rocks of the Oxford Clay are overlain by terrace gravel with involution structures providing evidence of degradation of ice-rich permafrost.

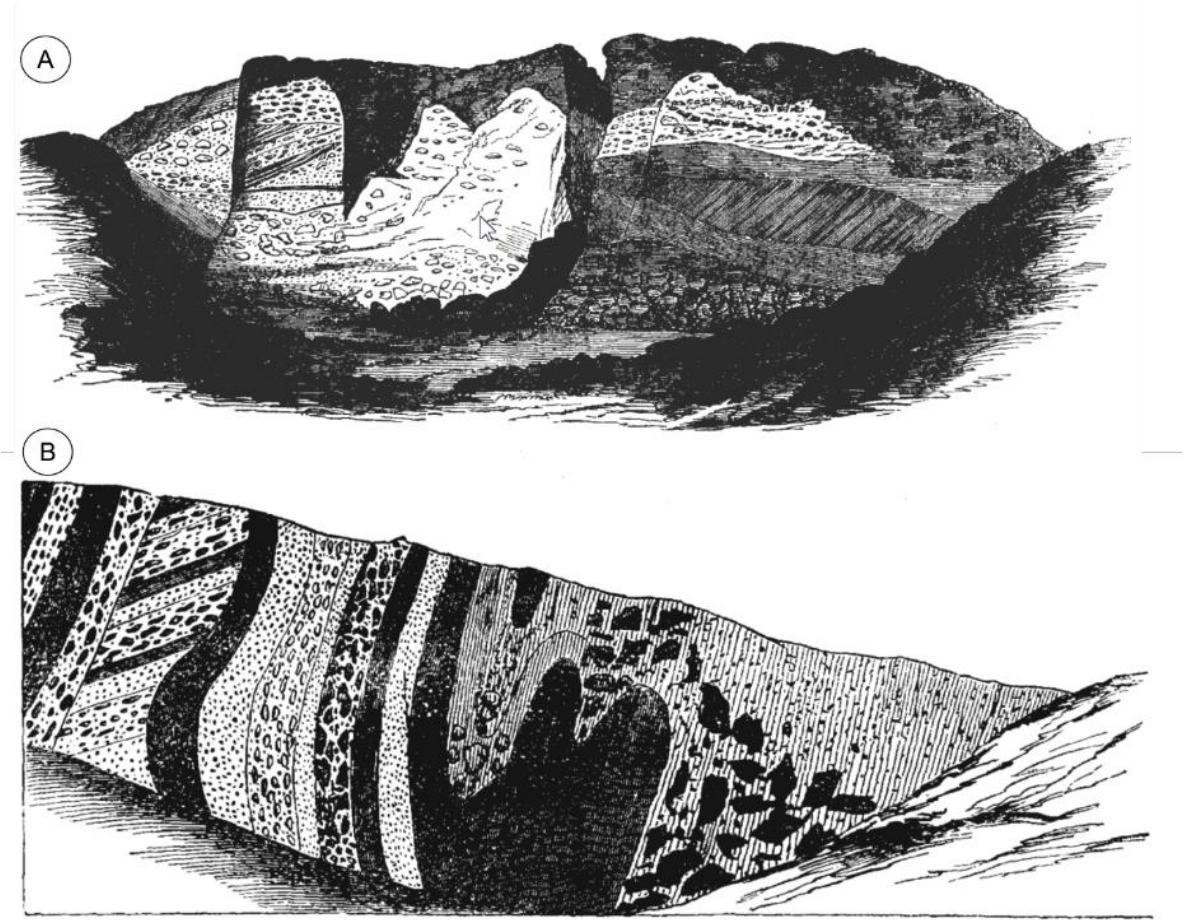

Figure 3-9 Brittle and ductile deformation structures within glacigenic sediments in north Buckinghamshire after Green (1864). A) Former pit in Tingewick [SP 6530329], cross-bedded gravels and sand displaced by a normal fault. B) Vertical and sub-vertical beds of gravel and sand associated with apparently tight, upright folds, near Foscott [location interpreted to be near SP 710 357].

Landslides are shown on the geological map of Buckingham. They are associated with the failure of mudstones and clay of the Kimmeridge Clay Formation where it is overlain by the Portland, Purbeck and Whitchurch Sand Formations.

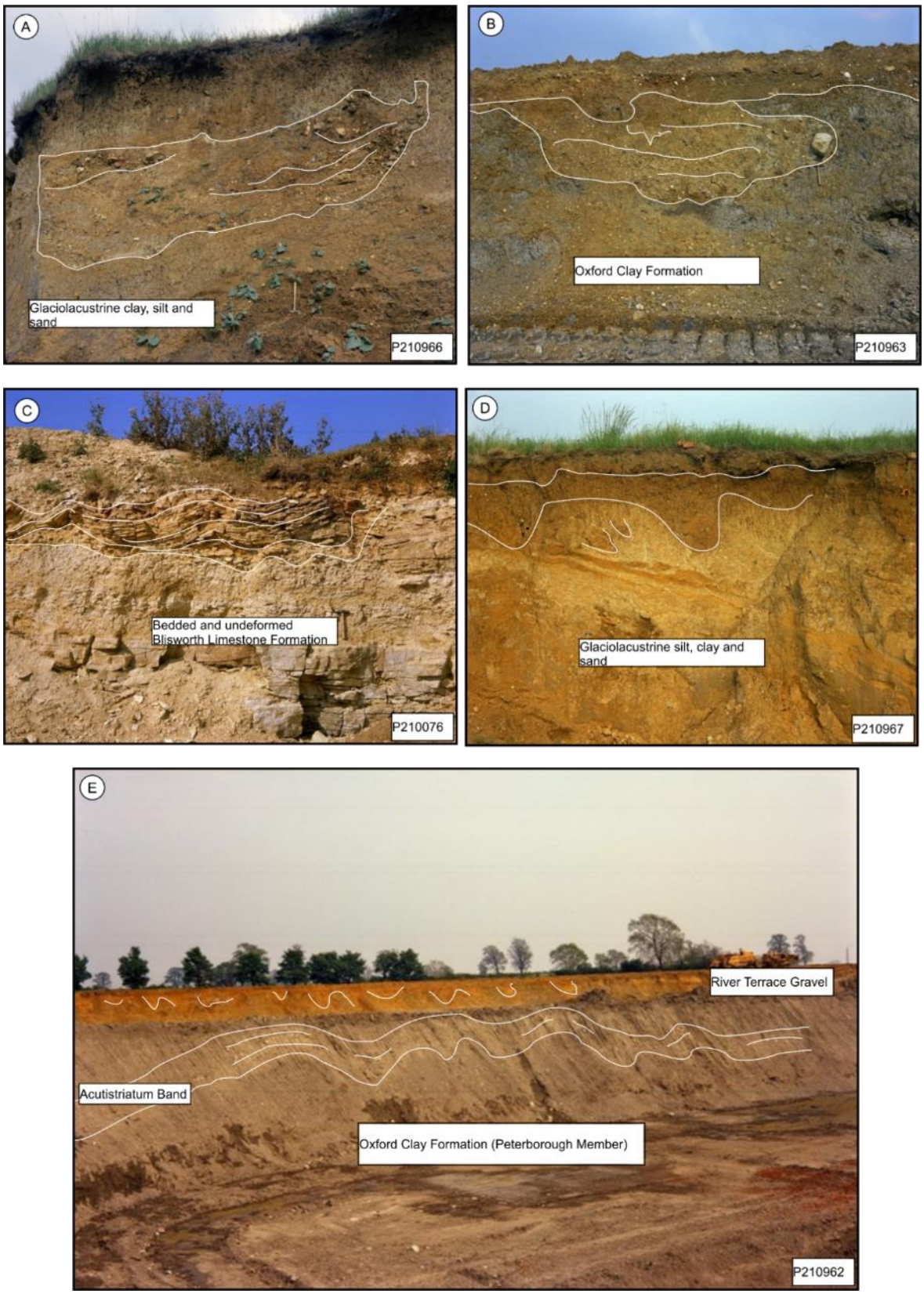

Figure 3-10 Examples of probable periglacial features in north Buckinghamshire. P numbers refer to BGS Geoscenic codes (geoscenic.bgs.ac.uk). A) Involution, Fletton Quarry, Bletchley, Milton Keynes [4855 2325]. B) Involution, Newton Longville (Bletchley), Milton Keynes [4855 2325], hammer for scale. C) Involutions as folds in thinly-bedded limestone, Deanshanger [4755 2395], hammer for scale. E) Involutions in River Terrace

Gravel overlying ductile deformation (valley bulging?) in Peterborough Member, Newton Longville (Bletchley), [4855 2325].

3.2.4.7 Biostratigraphy and till provenance

Investigation of the palynology of tills from north Buckinghamshire and Bedfordshire was carried out by the British Geological Survey as part of an assessment of sand and gravel resources (Boon, 2007; Riding, 2008). Palynomorphs are dominated by middle and late Jurassic miospores with some from Carboniferous, late Triassic, early Jurassic and Cretaceous assemblages. This led Riding (2008) to conclude that the till sheet from which the samples were taken was relatively homogenous and that the provenance of the till was derived from the northeast. This general direction agreed with that using chalk micropalaeontology, proposed by Fish & Whiteman (2001).

3.2.5 Synthesis of the glacial evolution of southern Britain

Summarising sections 2.42 to 2.4.5.1, the various models of the glacial evolution of the south Midlands and East Anglia are shown in Figures 3-11 and 3-12.

Before 2017, the conceptual models of the glaciation evolution of southern Britain illustrated at least advances of glacier ice during the Middle Pleistocene. Based on clast lithology and orientation, West & Donner (1956) interpreted two events, an early event sourced from the north and northwest, and a younger event from the Fenland region to the east (Figure 3-11, 1B). This two-phase model was re-defined as a single-phase by Perrin *et al*. (1979) based on clast lithology and geochemistry and the re-interpretation of West & Donner's younger advance as a weathering horizon in older till (Figure 3-11, 1C). The two-phase model was re-introduced by Rose (1992). He recognised an older, Triassic-rich till (Thrussington/Bozeat) in the English Midlands and associated it with the early advance of a Pennine-derived ice lobe of the BIS, (Figure 3-11, 1D). A later advance from the east, of a North Sea ice lobe of the BIS was associated with deposition of chalk-rich tills of the Oadby Member. Fish & Whiteman (2001) interpreted a two-phase model but with ice-advance into southern Britain from the north and northeast before fanning eastwards into East Anglia. An eastward shift in the direction of ice advance was interpreted as a result of partial retreat of lobe of the Scandinavian Ice Sheet which was located in the North Sea region at that time. A two-phase glacier advance involving an older advance of a Pennine ice lobe of the BIS advancing from the northwest and a later eastward advance from the Fenland region was advocated by authors including Hamblin *et al*. (2005) and Rose (2009).

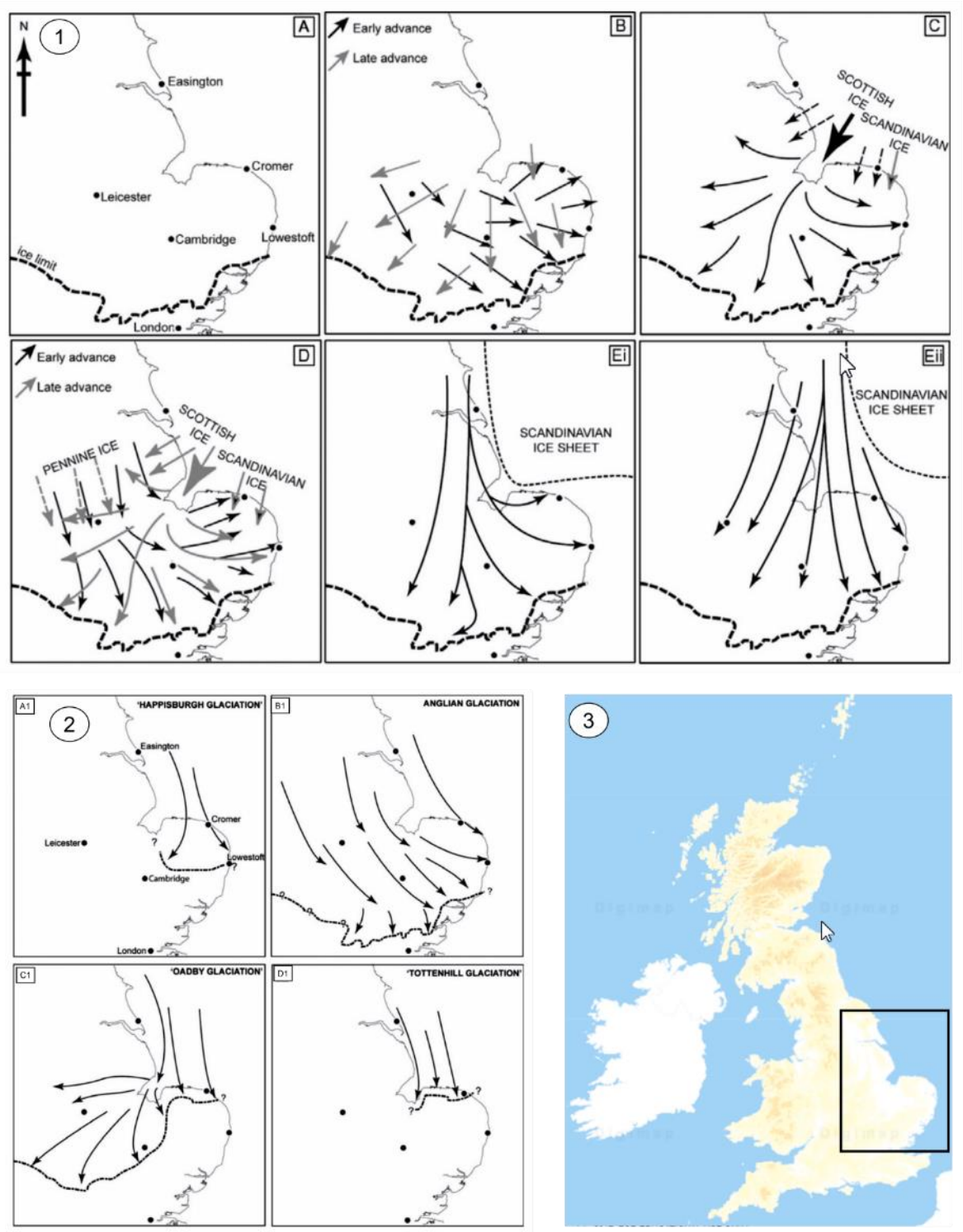

Figure 3-11 Middle Pleistocene glacial evolution of southern Britain modified after Lee *et al*. (2011) from literature prior to 2017. 1 A) location map of region highlighted in 3. B) Ice flow paths of West & Donner (1956); early Anglian advance and later 'Gipping'/Wolstonian advance. C) Single Anglian stage advance of Perrin *et al*. (1979) including Jurassic and chalk-rich facies of the Lowestoft Formation, North Sea Drift, Calcethorpe, Wragby and 'Marly Drift'. D) Two phase model of Rose (1992); early 'Pennine' advance including Triassic-rich Thrussington Till and Jurassic-rich Lowestoft Till Member followed by North Sea advance and deposition of chalk-rich Oadby Till Member. Ei) and Eii) Two phase model of Fish & Whiteman (2001), the later source area shifted to the east by retreat of Scandinavian Lobe of North Sea ice? 2) A1-D1 4 event glacial

evolution model after Hamblin *et al*. (2005), Rose (2009) and Clark *et al*. (2004). A1) 'Happisburgh Glaciaion (?MIS16), B1) Anglian Glaciation (MIS12), C1) 'Oadby Glaciation' (?MIS10) and D1) Tottenhill Glaciation (Gibbard *et al.*, 1992). 3 Location map.

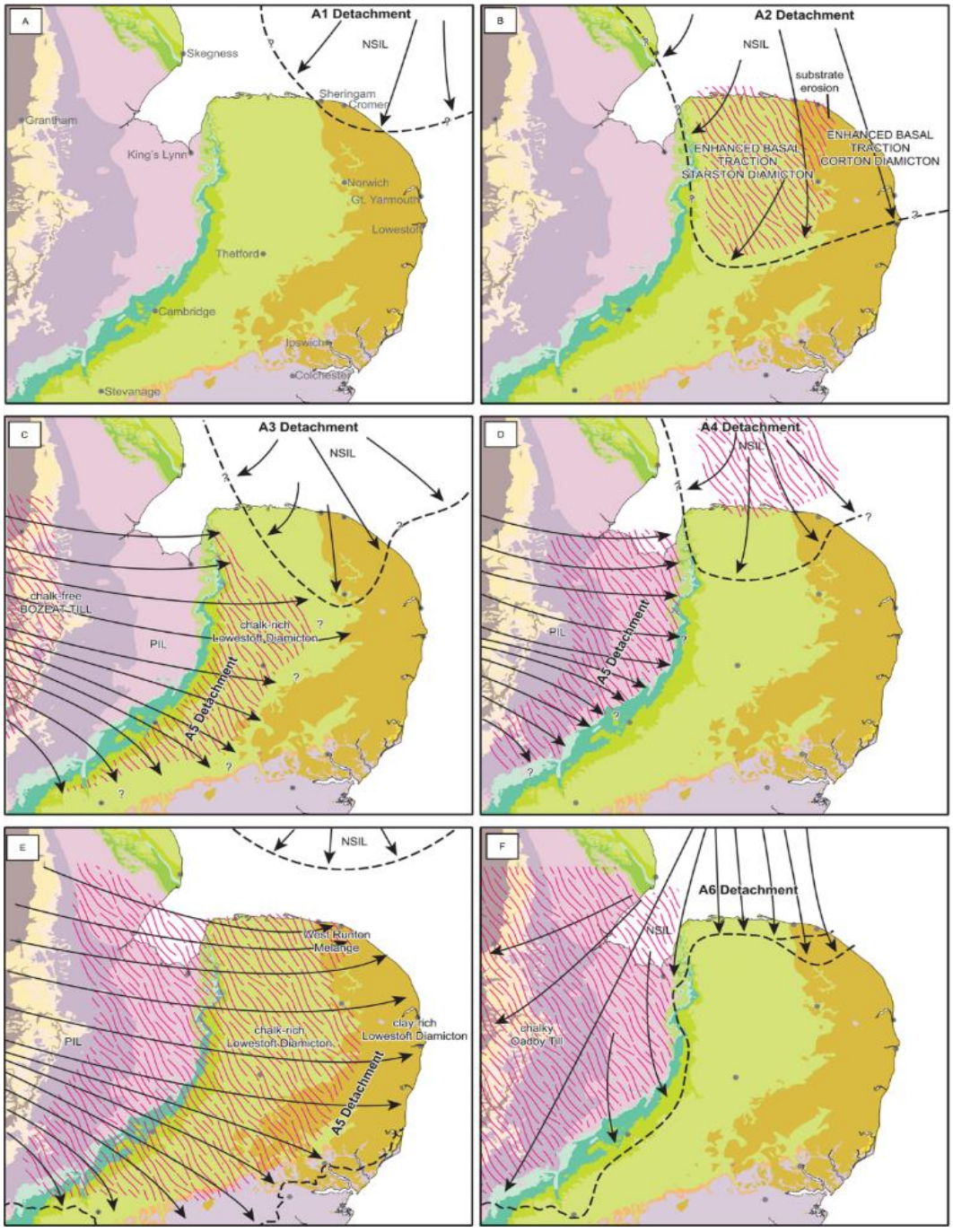

Figure 3-12 Middle Pleistocene glacial events of the Midlands and Eastern England using tectonostratigraphy in north Norfolk after Lee *et al*. (2017). Refer to Figure 3-4 for description of tectonostratigraphic parasequences. A) NSIL advance and deposition of Habbisburgh Diamicton Member. B) NSIL advance and deposition/accretion of Startston and Corton Diamicton members. C) A3 and A5 detachments. Accretion of Walcott Diamicton Member in NE Norfolk and Lowestoft Diamicton Member in the west. Thrussington/Bozeat till Member in the Midlands (also Phase C of Lunkka 1994). D) A4 and A5 detachments. Accretion of Bacton Green Diamicton Member, erosion of Jurassic mudrocks in the Fen Basin and accretion of the Lowestoft Diamicton Member (part of Phase D of Lunkka 1994). E) Main A5 detachment. Erosion of Jurassic mudrocks in the Fen Basin, erosion of

Chalk bedrock, local accretion of Lowestoft Diamicton Member in the west, Weyboune Diamicton Member in the north, Jurassic-rich Lowestoft Diamicton Member in the east (extensive till sheet), widespread glacitectonic deformation in NE Norfolk and creation of the West Runton Melange Member, F) Glacitectonism and oscillating ice-margin in NE Norfolk (part of Phase F of Lunkka 1994), breaching of the Wash basin, erosion and deposition of the Oadby till Member. PIL – Pennine Ice Lobe, NSIL – North Sea Ice Lobe. Geological legend as Figure 3-1.

The revision of the stratigraphical relationships in East Anglia using tectonostratigraphy, enabled Lee *et al*. (2017) to interpret the glacial of southeast England as a dynamic interplay between ice lobes of the BIS soured either from the Pennine or North Sea regions (Figure 3-12). This re-interpretation enabled multiple phases of glacier advance to be identified locally. Regionally significant events are associated with older, southwest directed Pennine ice lobe advances and a younger event (detachment event A6, Figure 3-12, 3F) from an eastward directed advance of a North Sea ice lobe. The latter model associated older glacial events with those during the Anglian stage and the younger event, post-Anglian Stage and tentatively associated with glaciation in MIS10.

4 Engineering geological background

4.1 Engineering geology of the Oxford Clay Formation

To establish the regional geotechnical behaviour of the Oxford Clay and till, against which laboratory results will be compared, a literature review is provided here.

The Oxford Clay is classified as an overconsolidated, very stiff fine soil/weak mudstone (Cripps & Taylor, 1987; Dobbs *et al.*, 2012). Regionally, it comprises very stiff clay to very weak mudstone weathering to fissured soft to stiff clay. It is generally very low to low permeability with groundwater flow dominantly through discontinuities, especially in its fissured top few metres. It also includes fissured, very weak siltstone and is calcareous in part. Laminations and thin horizontal to sub-horizontal bedding is common.

The engineering geology of the Oxford Clay in north Buckinghamshire was investigated by the then Institute of Geological Sciences (now the British Geological Survey) prior to the development of the new town of Milton Keynes in the 1960s (Cratchley *et al.*, 1969). The results of the Milton Keynes investigation were summarised in a large-format and unpublished data table which provided the basis for engineering geological classification 1:50 000 geological maps in use today. Cratchley *et al*. (1969) considered the Oxford Clay a uniform material on the basis of its Jurassic, marine palaeoenvironment of deposition. The qualitative and quantitative parameters for the Oxford Clay are shown in Table 4-1. Their interim report is incomplete although the authors attempted to map the spatial variability in index properties using contours of values. For example, Liquid Limit was mapped and showed a gradual and small amplitude trend from northwest to southeast. Values varied only within 8%. Local differences from the regional trend were mapped and interpreted to be a result of differences in primary Jurassic palaeoenvironments of deposition. They concluded that the Oxford Clay was relatively uniform, stiff, fissured, silty clay.

The geotechnical properties and behaviour of Mesozoic mudrocks including the Oxford Clay were summarised by Cripps and Taylor (1987) and Bell (1992). Their results are summarised in Table 4-2. The results were based on site-specific investigations in north Buckinghamshire and Bedfordshire by authors including Jackson and Fookes (1974), Parry (1972) and Burland (1977). The effects of weathering were investigated by Jackson (1973) in Cambridgeshire, Russell and Parker (1979) and Russell *et al*. (1978). More recently, an advanced geotechnical experimental programme on Mesozoic mudrocks including the Oxford Clay, was undertaken by Hosseini Kamal (2012).

Engineering Geological Unit	**Lithology**	**Cementation**	**Hardness (consistency)**	**Compactness**

Uniform silty clay	Pyritised, calcareous silty clay. Occasionally bituminous	None	Stiff	Compact
Fissility	**Fissuring intensity**	**Bedding**	**Colour (unweathered/weathered)**	**Mineralogy**
None	Low/Moderate	Laterally persistent, even	Blue grey and olive grey/Dark brown	Carbonate, illite, trace kaolinite, mica and quartz
Inclusions	**Variability**	**Liquid limit (W_L) range**	**Plastic limit (W_p) range**	**Plasticity Index (I_p)**
Shells, lignite	Low	50-75	20-30	30-45
Liquidity Index (LI) range	**Particle Density (Mg/m^3)**	**Bulk Density (ρ_b) range (Mg/m^3)**	**Intact undrained strength S_u (kN/m^2)**	**Sulphate (% dry weight)**
(-0.3) – (-0.1)	2.6	1.9-2.1	100-250	0-15
Swelling pressure	**Strength variation**	**Compressibilty variation**	**Slope stability (pre-existence of slips)**	**Slope stability (pre-existence of slips)**
Fairly low, occasionally moderate	Low	Low	None	Minor solifluction
Slope stability (maximum slope anlge)				
Average 15°				

Weathering where buried by Quaternary deposits		
Zones:	Major	Minor
Thickness(m):	0-0.5	0-1.0
Dessication jointing intensity:	High	Moderate
Colour:	Mid-brown	Brown-grey

Weathering where not buried by Quaternary deposits			
Zones:	Soil	Major	Minor
Thickness(m):	0-0.5	0.5-2.0	1.0-3.0
Dessication jointing intensity:	-	High	Moderate
Colour:	Dark brown	Mid-brown	Brown-grey

Table 4-1 Selected engineering geological parameters for Oxford Clay in the Milton Keynes area after Cratchley *et al*. (1969).

Property	**Stewartby Member**	**Peterborough Member**	
	Unweathered	**Weathered**	**Unweathered**
Liquid limit, W_L	(58) 53-63[a]		(60) 45-75
Plastic limit, W_p	21-23[a]		(33)

			18-47
Plasticity Index, I_p	31-39		12-50
Clay fraction % (< 2μm)	(64) 60-68		(52) 30-70
Void ratio, e		0.41-0.18[b]	0.42-0.96[b]
Natural moisture content, ω (wt %)	(25) 22-28[a]	(29) 17-36[c]	(21) 15-32[c]
Particle density, ρ_s (Mg/m^3)			2.53-2.73
Bulk density, ρ_b (Mg/m^3)	(2.03)	1.71-2.1	(2.03) 1.84-2.05
Undrained shear strength, S_u (kN/m^2)	(110-360) 45-510[a]	52-93	(360-1100) 96-1300
Effective cohesion, c´ (kN/m^2)	10	0-20	10-216
Effective angle of friction, ø´ (°)	31	21.5-28	23-40
Residual angle of friction, $ø_r$ (°)	15		(18) 12.5-18.5
Coefficient of volume compressibility, mv (m^2/MN)	(0.077) 0.046-0.12[a]		0.003-0.12[a]
Coefficient of consolidation, c_v (m^2/yr)	(0.16) 0.40-1.27[a]		(0.93) 0.49->40
Modulus of elasticity, E (MN/m^2)	(40) 10-70[a]		(50-135) 45-230
Permeability, k (m/s)			$5*10^{-10}$

Table 4-2 Summary property ranges for Oxford Clay after Cripps & Taylor (1987). Assumes 'middle Oxford Clay' and 'lower Oxford clay' are equivalent to Stewartby and Peterborough formations respectively. Values in parentheses show the mean or typical value. [a]may include some weathered material. [b] from particle density, bulk density and moisture content. [c] stratigraphical division not specified.

4.1.1 Particle fabric

Few macro- and micro-fabric studies of the Oxford Clay are available in the literature. Fabric is taken here to describe the arrangement of solid particles, their shape, sorting and inclusion of features including discontinuities.

In Stewartby, Parry (1972) investigated the micro- and macro-fabric of the Oxford Clay. At the outcrop scale, Parry observed laminated and thinly-bedded clay-shale with closely to very closely spaced discontinuities. An interpretation of Parry's observations, not described in the corresponding paper, is presented in Figure 4-1. The presence of lithorelicts has been interpreted following the investigations of Lias Group mudrocks by Chandler (1972). This author interpreted gravel-sized fragments of mudstone and clay as remnants of *in situ* material that had been periglacially weathered and breacciated by the *in situ* growth of segregated ice during the Pleistocene. In Chickerell (Dorset) and Yaxley (Cambridgeshire), Jackson (1973) observed alternations of 'hard' and 'soft' beds at outcrops exposed for seven or more years, in

the Peterborough Member (*K.Grossoveiri* and *Lower Peltaceras Athleta* sub-zones) and is shown in Figure 4-2.

Using scanning electron microscopy (SEM), Jackson (1973) concluded that the hard bands resulted from a higher degree of preferential alignment of clay particles compared to the 'soft' bands. The higher degree of clay particle alignment was interpreted to be a result of differences in sedimentation rate during primary deposition whereby higher rates of deposition results in higher degree of particle alignment.

The degree of preferred alignment of clay particles at the microscopic scale was further investigated by and Parry (1972) in Stewartby. Using an SEM with variable magnification, Parry observed strong orientation of platy clay minerals. Two examples are given Figure 4-3.

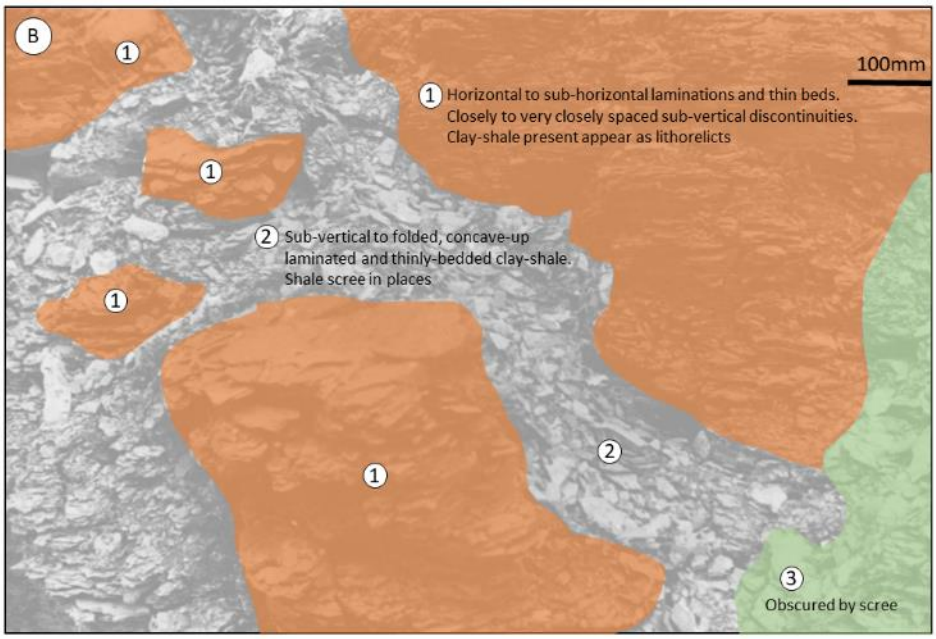

Figure 4-1 A) Unweathered Oxford Clay after Parry (1972), B) Interpretation by the author.

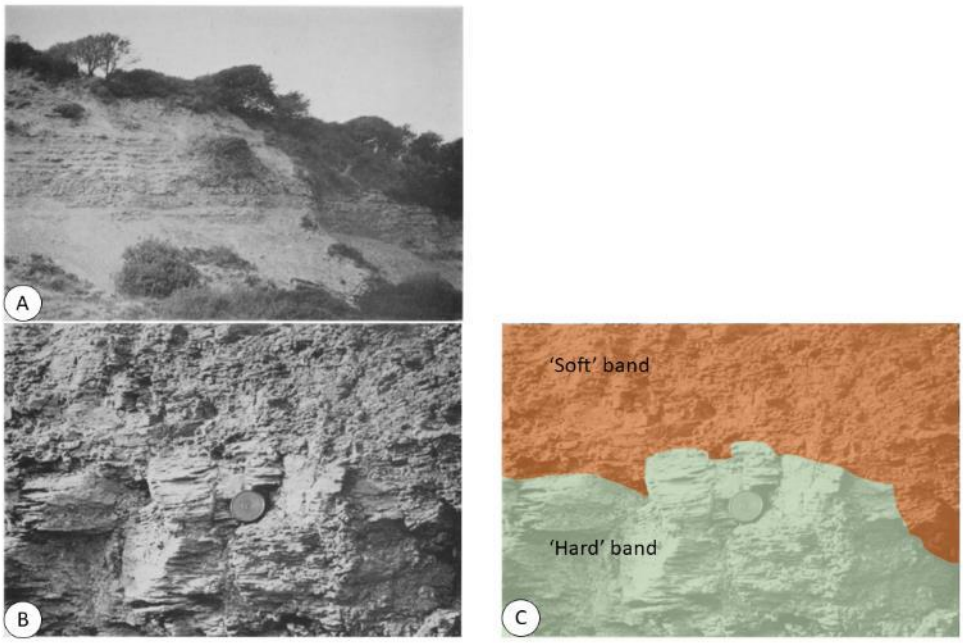

Figure 4-2 Peterborough Member outcrop fabric observed by Jackson (1973) at Chickerill, Dorset also seen at Yaxley, Cambridgeshire. A) Outcrop overview of alternating beds of 'hard' and 'soft' clay and clay-shale. 'Hard' bands are relatively more resistant to weathering and stand proud of 'soft' bands B) Close-up view of part of outcrop face in A), C) Interpretation by the author.

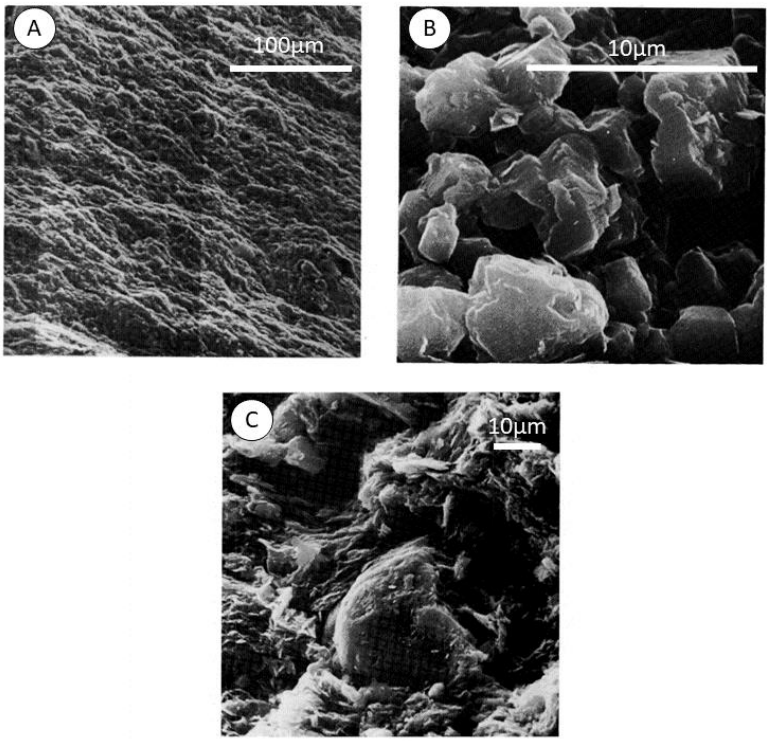

Figure 4-3 Oxford Clay Scanning Electron Microscope (SEM) images from Parry (1972). A) orientated clay particles resulting in cleavage, B) orientated kaolin particles, C) orientated clay particles surrounding a silt grain.

The preferential orientation of clay particles has been shown to influence patterns of weathering (Jackson, 1973), drained and undrained shear strength (Jackson & Fookes, 1974; Parry *et al.*, 2014) and compressibility (Jackson & Fookes, 1974). Preferential orientation results in the increased proportion of clay particles with face-to-face or edge-to-edge contacts, increasing effective contact area, increased cohesion and thus increasing interparticle bonding. Russell and Parker (1979) state that clay particles are bonded as a result of authigenic cementing or ionic bonding via adsorbed cations onto the negatively charged clay crystal lattice. They also state that ionic activity and authigenic crystal growth will be more active at crystal edges rather than faces and so bonds will develop there more easily.

4.1.2 Atterberg limits (plasticity)

Typical values for liquid limit (W_L), plastic limit (W_p), plasticity Index (I_p), natural moisture content (ω), bulk density (ρ_b) and particle density (ρ_s) are shown in Tables 4-1 and 4-2 and Figures 4-4 and 4-5. From these plots, the Oxford Clay is classified as a high to very high plasticity clay or silt. As part of their investigation on the depth of burial of the Oxford Clay, Jackson & Fookes (1974) showed that there was little variability with depth in liquid and plastic limits above the *K.jason* zone in the Peterborough Member at Bletchley and Calvert (Figure 4-4). Above these zones, values of liquid and plastic limits are typically 70% and 30% respectively. This in agreement with the investigation carried out in the Peterborough member

of Bedfordshire by Parry (1972) where the mean values for W_L and W_p were 70% and 25% respectively. The Peterborough Member at Whittlesey neat Peterborough shows W_p values between ~ 15% and 23% and W_L values between 65% and 73% (Burland *et al.*, 1977).

Variability below the *K.jason* zone at Bletchley reflects changes in clay content whereby higher clay content results in higher liquid limit values and lower activity values. Activity is defined as:

$$Activity = \frac{I_p}{C}$$

Equation 4-1

where I_p = Plasticity index (%)

C = Clay (<0.002 mm) content (%)

Aggregation ratio (Davis, 1967) has been used to measure the resistance of a sediment to full dispersion where aggregated particles may be present. It is defined as:

$$\textbf{\textit{A}ggregation ratio (Ar)} = \ (\%\ \textbf{clay mineral})/(\%\ \textbf{clay size})$$

Equation 4-2

where, % clay mineral = percentage of clay measured by X-Ray Diffraction (XRD)

% clay size = percentage clay size measure during particle-size analysis (PSA)

Values greater than one indicate the potential for poor dispersal of aggregated particles during PSA. The values in Figure 4-4, demonstrate the percentage of clay obtained from mineralogical analyses is consistently higher than the values obtained from PSA and highlight the potential for particle aggregation within the Oxford Clay. The presence of carbonate as a cementing agent has been reported as a possible reason for this (Jackson & Fookes, 1974).

Moisture content values were observed by Jackson and Fookes (1974), Parry (1972) and Burland *et al*. (1977) to decrease with depth. For example, at Stewartby [TL 024 022], Parry measured moisture content values of 32% at 3 m below ground level (mbgl) and 26% at 14 m (bgl). Burland *et al*. (1977) measured moisture contents varying from ~ 21% at 4 mbgl to ~ 15% at 14 mbgl. Moisture contents exceeded ~ 27% in the weathered zone described as 'callow' by Burland *et al*. (1977).

Moisture content values are generally close to or at the W_p giving liquidity index (I_L) values close to or below zero indicating their potential to behave as a solid. For example, Jackson

and Fookes (1974) measured liquidity index values between -0.44 and -0.03 for sites in Buckinghamshire, Bedfordshire and Cambridgeshire.

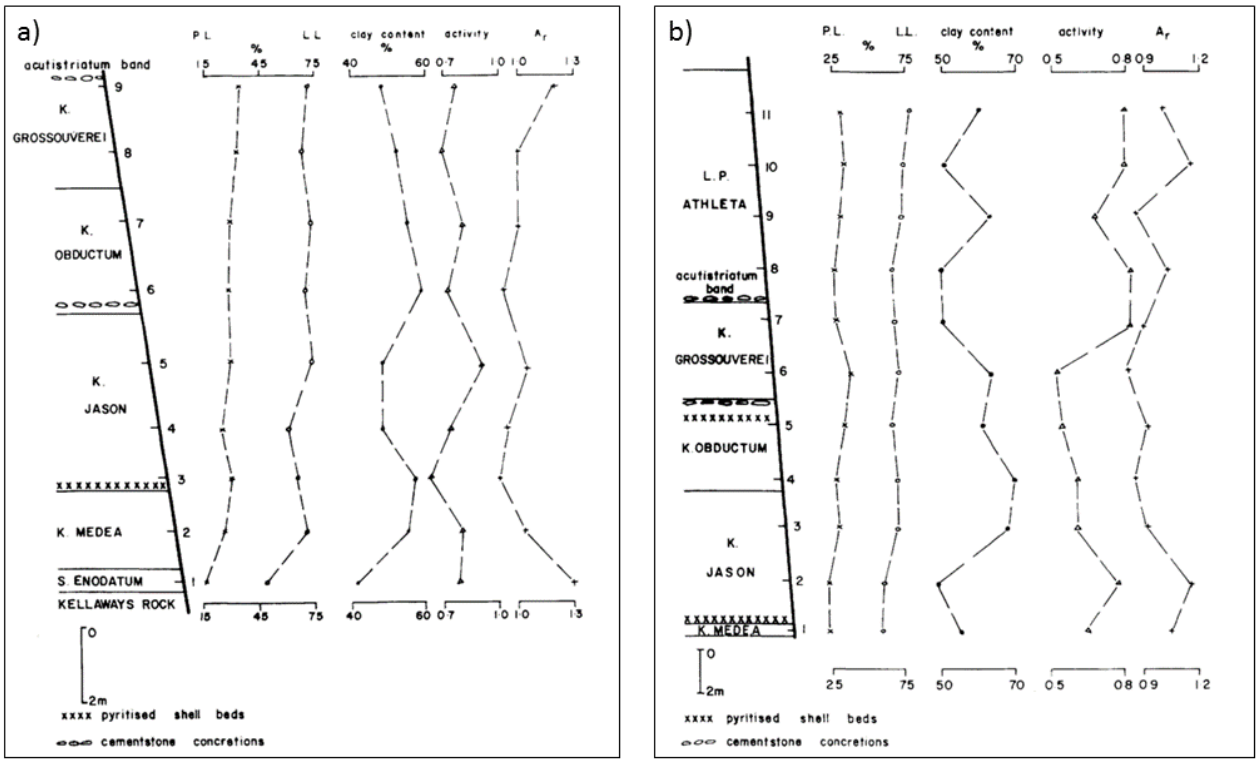

Figure 4-4 Depth variability in index properties correlated to stratigraphical zones and sub-zones at Bletchley (a) and Calvert (b), after Jackson & Fookes (1974).

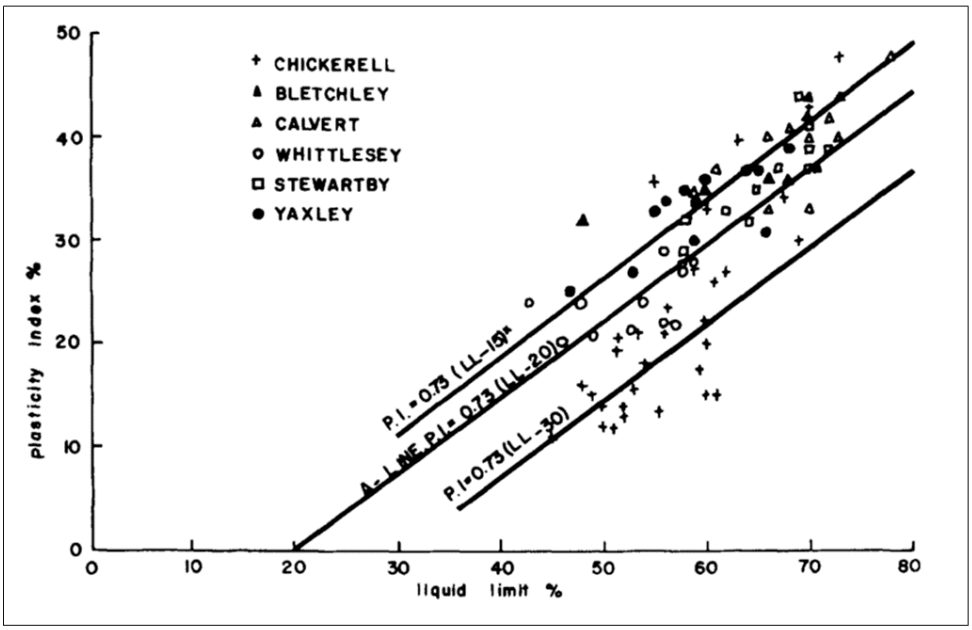

Figure 4-5 Oxford Clay plasticity, after Jackson & Fookes (1974).

Burland *et al*. (1977) showed that the unit weight of the Oxford Clay is fairly uniform with depth at 19.9 kNm^2.

4.1.3 Permeability

Calculated values of permeability (k) taken from *in situ* groundwater rebound measurements for the Peterborough Member were 3.5 x 10^{-9} m/s and 5 x 10^{-11} m/s in the horizontal and vertical directions with respect to bedding respectively (Parry, 1972).

Using measured values of c_v and m_v derived from 1D consolidation tests for different stress increments, (Jackson & Fookes, 1974), k can be estimated from (Head & Epps, 2011):

$$k = m_v c_v \rho_w g$$

Equation 4-3

where units are c_v (m^2/s), m_v (m^2/N), ρ_w (kg/m^3) and g (m/s^2).

Using equation 4-3, permeability values for the Peterborough Member parallel to bedding ranged from 6.11 x 10^{-11} m/s to 9.05 x 10^{-11}. Values perpendicular to bedding ranged between 1.66 x 10^{-12} to 3.48 x 10^{-12} m/s.

4.1.4 Compressibility

The compressibility of a material describes its densification because of the expulsion of porewater due to the application of static or dynamic stress. For most purposes the application of stress is unidirectional and vertical. Expulsion of porewater is dependent on the length of the drainage path and permeability. The rate of consolidation is described by the coefficient of consolidation (c_v) and the amount by the coefficient of volume compressibility (m_v). The compressibility of the Oxford Clay has been investigated by Jackson and Fookes (1974) as part of their investigations of the effects of deep burial. Using specimens trimmed from undisturbed block samples, parallel and perpendicular to bedding, Fookes and Jackson used a special oedometer with combined temperature and loading measurement to consolidate to a maximum pressure of 1.72 MPa.

They found that values for c_v and m_v varied depending on the stress applied and the orientation of bedding in the sample to the direction of applied stress. Values of c_v exceeded 40 m^2/yr for samples cut perpendicular to bedding and varied between 0.27 and 0.61 m^2/yr for specimens cut parallel to bedding. Highest values were obtained from specimens at Calvert. Values for m_v ranged between 0.0117 m^2/MN and 0.0234 m^2/MN for specimens cut

perpendicular to bedding and between 0.0223 m^2/MN and 0.112 m^2/MN for specimens cut parallel to bedding.

The maximum depth of burial of the Oxford Clay was estimated by Fookes and Jackson (1974) to be between 472 m and 811 m in Buckinghamshire and between 460 m and 661 m in Bedfordshire. Using the graphical Casagrande method (Holtz *et al.*, 2011) to estimate former preconsolidation pressures from the yield point on a void ratio-log pressure plot, they estimated an effective preconsolidation pressure equivalent to an overburden of ~ 91 m. To explain the lower degree of overconsolidation than would be expected, they inferred factors including glaciation and solifluction as possible mechanisms that would reduce inter-particle bonds and weaken the material.

4.1.5 Shear strength

Undrained shear strength was measured by Parry (1972) using 100 mm x 200 mm cylindrical specimens trimmed from U100 samples taken using shell and auger drilling methods at Stewartby [TL 024 422]. Parry showed that undrained shear strength in the Peterborough Member increased with increasing depth below ground level and with decreasing moisture content. Undrained shear strength values of 95kN/m^2 and 165kN/m^2 were reported at depths of 2.5 and 13.7 mbgl respectively. Burland *et al*. (1977) reported undrained shear strength increasing with depth from 50 kN/m^2 to 1200 kN/m^2 with average values of c´ and ø´ of 80 kN/m^2 and 28º. The rate of increase in undrained strength was seen to be greater in the Peterborough Member compared to the Stewartby Member. Experiments on specimens orientated parallel to bedding gave undrained shear strength values upto 1.7 greater than vertically-orientated specimens.

Drained triaxial experiments conducted at effective normal stresses (σ_3´) of 70, 140 and 210kPa and a strain rate of 0.0012mm/min to 20% strain are illustrated in Figure 4-6 and the results summarised in Table 4-3.

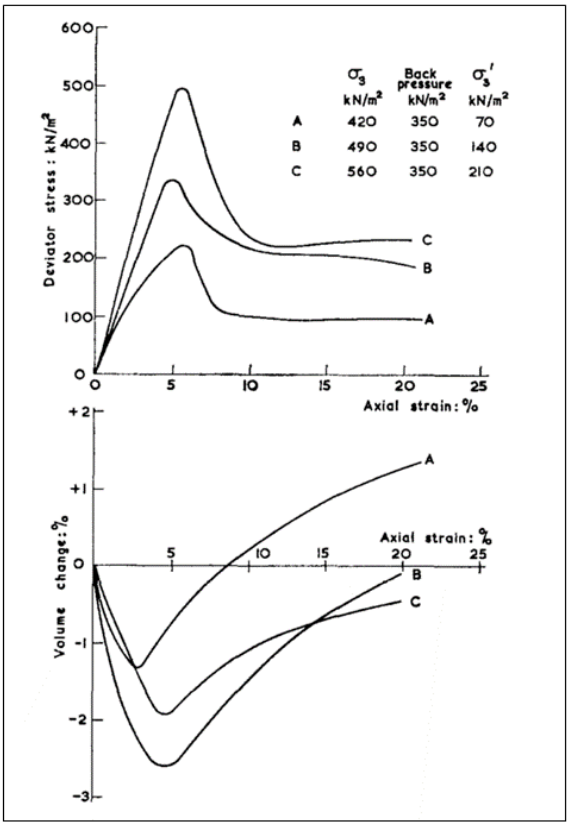

Figure 4-6 Drained peak and 20% stress-strain curves for the Peterborough Member, Stewartby (after Parry 1972).

Depth	**Peak strength parameter**		**20% axial strain strength parameters**	
m	c´	ø´	c´	ø´
5	0	28.0 º	0 º	20.0 º
8	25	29.5 º	15.0 º	18.0 º

Table 4-3 Drained peak and 20% strain effective stress strength parameters for the Peterborough Member, Stewartby (after Parry 1972).

In triaxial compression each test specimen showed initial volumetric decrease with increasing stress towards peak deviator stress. Just before reaching peak deviator stress, volumetric increase occurs and continues upto and beyond peak stress. Beyond peak stress, volumetric expansion is accompanied by increasing strain with constant deviator stress.

Using drained shear box experiments, Parry (1972) investigated the influence of lamination on shear strength by preparing 38x78 mm cylindrical specimens, parallel, perpendicular and 30º relative to the laminated fabric of the samples. The results are shown in Table 4-5.

Direction of specimen relative to	**Peak**		**Residual**	
	c'_p	**$ø'_p$**	**c'_r**	**$ø'_r$**

lamination				
Horizontal	10	21.5º	0	13º
Vertical	20	32.5º	0	13º
30º to horizontal	20	21.5º	0	13º

Table 4-4 Peak and residual shear strength values for the Peterborough Member, Stewartby (after Parry, 1972).

For each orientated specimen, strength increased with increasing normal stress. The orientation of the samples had the greatest effect on the displacement at peak strength and rate of strength degradation from peak to residual. This behaviour was also observed by Burland *et al*. (1977) in drained shear box experiments. Displacement values at peak were between 4 – 6 mm for vertically-orientated specimens and 2.7 – 4 mm for horizontal and 30º to horizontal specimens. This is consistent with the results obtained from orientation-specific shear box experiments carried out by Jackson & Fookes (1974) at a rate of strain of 0.000192 mm/min and those of Burland *et al*. (1977). The rate of reduction in shear strength following peak was more rapid in the horizontal compared to 30º to horizontal and vertically-orientated specimens. Jackson & Fookes (1974) found that values of ø′ and $ø'_r$ were about 10º and 2º higher respectively in vertically orientated, compared to horizontally-orientated specimens. For horizontally-orientated specimens, Burland *et al*. (1977) found peak strength values of $ø'_p$ = 27.5º, c'_p = 80 kN/m2 and residual strength values $ø'_r$ = 13º and c'_p = 3.5 kN/m^2. For samples on which shear was observed to have occurred parallel to bedding, shear strength values were close to residual. The implication for design, stated by Parry (1972), is that shear strength may be at residual towards the toe of a slope and at or just below peak towards its top.

Shear strength anisotropy, defined by the ratio of horizontal to vertical shear strength, was investigated using a modified shear vane by Russell *et al*. (1978). They showed for five depth profiles that shear strength anisotropy was relatively constant at 0.7 below about 6.5 mbgl, increasing to 2 at depths < ~6.5 m before decreasing to 1 at depths < 1 m. Russell *et al*. (1978) related this pattern to weathering where in addition to a downwards decrease in moisture content, the observed increase in anisotropy correlated with an upward increase in the proportion of gypsum and decrease in the proportion of pyrite and calcite.

Russell & Parker (1979) showed that both drained and undrained shear strength decrease with increasing weathering and that the greatest difference occurred between weathering grades I and II i.e. at the base of the weathering zone. They also found negative correlations between undrained shear strength and moisture content and that the degradation of illite was correlated with increasing degree of weathering and decreasing shear strength.

The drained and undrained shear strength of the Oxford Clay is therefore anisotropic. Anisotropic strength behaviour is a result of mechanical and chemical weathering and preferential orientation of clay particles parallel to bedding in unweathered samples. The degradation of interparticle bonds and dissolution of calcite cement is thought by Russell and Parker (1979) to account for reduction in shear strength. They observe however that calcite can be introduced into shallow parts of the Oxford Clay from weathering of overlying calcite-rich Quaternary sediments.

4.1.6 Clay mineralogy

Deposition of the Oxford Clay in a Callovian-Oxfordian marine basin in southern Britain resulted in a relatively uniform clay mineralogy. Detrital clay minerals, derived from weathering of Palaeozoic and Mesozoic rock sources are characterised by mica, kaolin and poorly-defined assemblages of mixed layer smectite-mica-vermiculite (Jeans, 2006). During the Oxfordian, the detrital component was completely or partially replaced by authigenic clay minerals comprising glauconite or smectite in marine sediments. The change from detrital to authigenic clay minerals is associated with a change in sedimentology and related to tectonic uplift and volcanicity in the North Sea region (Jeans, 2006).

Using X-ray diffraction analysis (XRD) of the <2µm component, Perrin (1971) examined three samples belonging to the Peterborough Member of the Oxford Clay in Buckinghamshire and Bedfordshire. The samples contained 65 – 80% mica and 20 – 35% kaolinite with trace amounts of vermiculite and smectite and non-clay mineral quartz. Regionally, Jeans (2006) reported on an additional 22 samples dominated by mica, poorly defined, mineralogically-collapsible minerals and kaolin with chlorite present in trace amounts. One sample from the Weymouth Member identified 80% mica and 20% kaolin with trace amounts of chlorite and vermiculite.

Using quantitative XRD on the orientated, clay-sized fraction derived from sedimentation analysis, Jackson & Fookes (1974) identified kaolin, mica (Illite), chlorite and illite/montmorillinite mixed-layer components as the dominant clay minerals in the <2 µm size fraction (Figure 4-7). Non-clay minerals included trace and <4% non-clay quartz and feldspar.

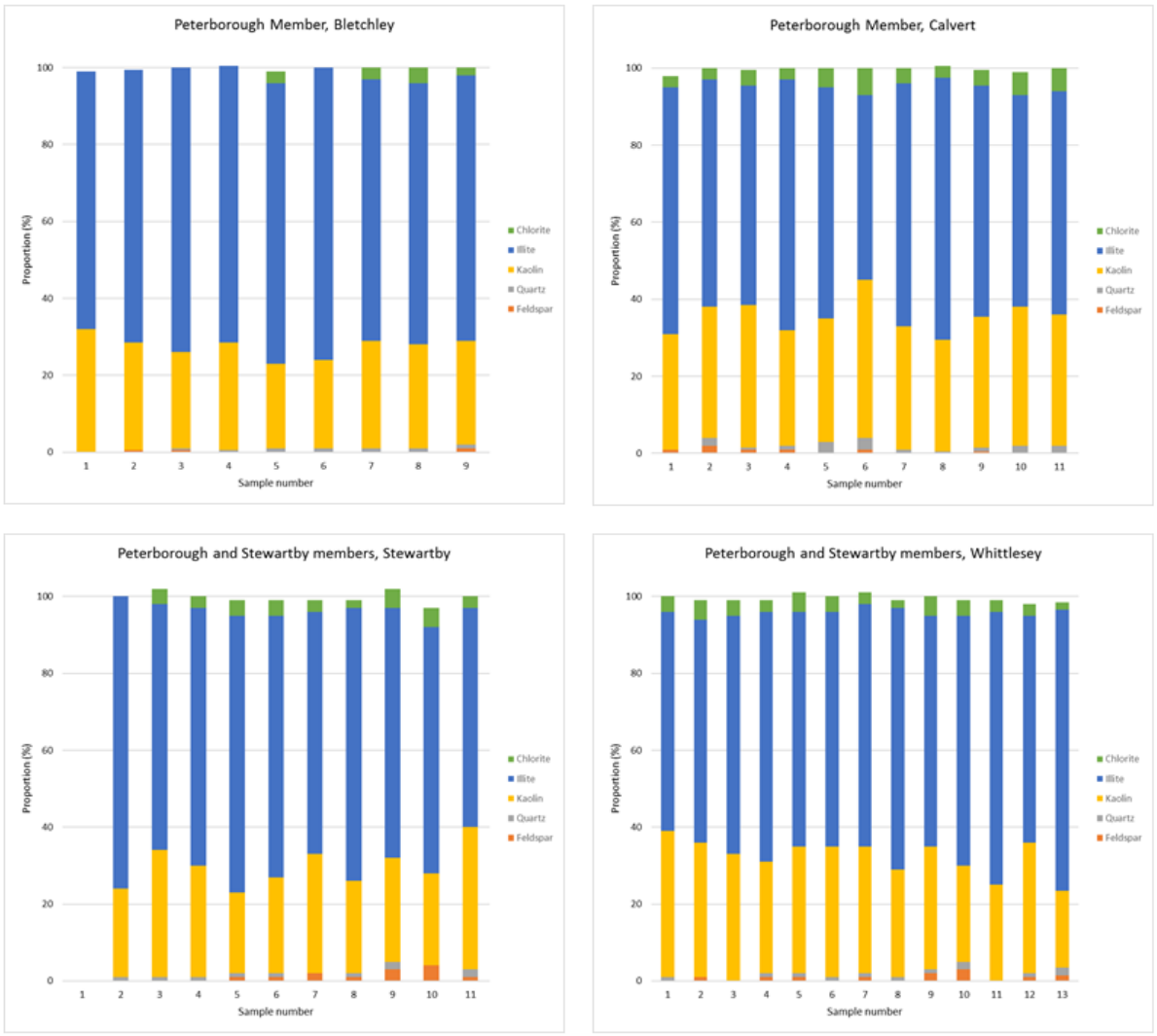

Figure 4-7 Clay mineralogy as determined by XRD on the <2µm size fraction for using data from selected sites from Jackson and Fookes (1974). Some samples exceed 100% by proportion using reported data. Trace minerals excluded from calculation. No data for Sample 1, Stewartby.

4.1.7 Weathering

The geotechnical effects of chemical and physical weathering and its classification (Table 4-3) has been investigated in by Russell and Parker (1979), Russell *et al*. (1978) and Jackson (1973) following the work on Lias Group clays by Chandler (1972). Based on chemical and mineralogical analysis of weathering profiles of five sites across the outcrop of the Oxford Clay, Russell and Parker (1979) demonstrated that weathering effects extend to a maximum depth of 10 m but generally < 6 m to the top of weathering grade (WG) 1. At Stewartby in Bedfordshire [TL 024 422], Parry (1972) showed that the depth of weathering based on colour change extend to depths between 3 and 7.5 m. Russell and Parker noted that the correlation between indicators of weathering and depth is not straightforward but that consistent trends are observed. Moisture content decreases with depth except for a shallow (< ~1 m) zone of

desiccation in near surface WG 4. The oxidation of sulphides including pyrite (FeS_2) to produce sulphuric acid (H_2SO_4) and ferric oxides (Fe_2O_3) and its combination with calcium carbonate to precipitate gypsum ($CaSO_4.2H_2O$) is common in Mesozoic mudrocks in Great Britain. Gypsum and Jarosite as indicators of weathering were found at depths generally of < 6 m. Gypsum was also found in higher concentrations at the base of fissures that extended through the weathering profile to the top of WG 1 sediments.

The informal term ‘callow’ has been applied to the Oxford Clay that encompasses unspecified grades of weathering (Parry, 1972; Burland *et al.*, 1977). The terms is often applied to describe a zone extending from ground level to ~ 2 m that includes gravel and lenses of sand in a matrix of clay and silt. It has been suggested by Parry (1972) that the origin of this material is either glacial outwash or periglacial solifluction.

Water content **A) Range** **B) B)Liquidity index**	A) 32-36% B) 0->0.12	-	A) 27-32% B) -0.03-0.08	A) 23-27% B) -0.15-(-0.05)	A) 19-25% B) -0.34-(0.14)	A) 14-19% B) -0.57-(-0.38)

Zone	Visual description	Fabric (based on thin sections)	Discontinuities A) Fissure spacing B) Shears	Chemistry A) $CaCO_3$ B) $H_20.CaSO_4$ (form)
Solifluction/ landslide	Mottled light grey/brown, clay becoming grey with depth; considerable oxidation near surface (with frequent small haematite pellets); minimal oxidation at depth (i.e. >3 m); extensive gleying at shallow depths	0-2 m Heterogeneous with small (<1 mm) rotated lithorelics; >2 m rotated lithorelics (upto 30mm) otherwise Zone III	A) apparently intact (except for dessication cracks) at shallow depths; as Zone III at greater depths B) as Zone II	A) 0-4% B) none observed
IV	Superficial material of various origins including head. Often with flint and chalk fragments; dessicated compared to underlying clay	-	-	-
III	Fissured clay with light grey (gleyed) fissure surfaces; centres of lithorelicts seen to be pale brown (oxidised)	Lithorelicts (upto 30 mm) have horizontal bedding; matrix occupies <50% of section, is often gleyed and where limited in extent is usually sheared,; larger areas of matrix show orientated bands	A) 10-30 mm B) Minor shearing in gleyed fissures is common	A) 5-6% B) common; often sugary gypsum crystals
IIb	Grey/blue-grey clay with brown (oxidised) areas typically along and beyond fissures making up 30-60% of the clay	As Zone I but with brown staining usually in areas parallel to fissures	A) 20-100 mm B) minor shears, 1-2 mm displacement, sometimes associated with oxidation	A) 0-5% B) large gypsum crystals
IIa	Blue-grey clay/soft mudstone; oxidation on surfaces of fissures only	As Zone 1 but with brown staining only along fissures. Laminar fabric visible, stony	A) 20-100 mm B) no shears	A)1-6% B) some
I	Dark, blue-grey, silty, firm clay; no oxidation	Horizontal laminar fabric	A) >100 mm B) no shears	A) 1-7% 2) none observed

Table 4-5 Weathering grade classification for the Oxford Clay (after Chandler (1972) for Lias Group mudrocks, excluding F_2O_3/FeO ratios and Russell and Parker (1979).

4.1.8 Tectonic structures

Structures reflecting both brittle and ductile deformation have been observed at outcrop scale in clays and mudrocks of the Oxford Clay. Those structures interpreted to be related to the effects of Quaternary glaciation and periglaciation are described in Section 2.4.6.7.

1:50 000 scale geological maps show few geological faults affecting the Oxford Clay in north Buckinghamshire. Northeast-southwest trending faults are shown at geological rockhead in

the area around Islip [SP 526 141] and Ambrosden [SP 606 197]. They are displaced by geologically-younger northwest-southeast trending faults. Parry (1972) observed a series of northwest-southeast and west-northwest-east-southeast trending normal faults at outcrop in Stewartby with throws to the south of between 3 and 12 m.

Joints and fissures, increasing in frequency with decreasing depth below ground level, were observed in the Stewartby Member by Burland *et al*. (1977) at Whittlesey. Equal area stereogram plots of fissure orientation and inclination are shown in Figure 4-8.

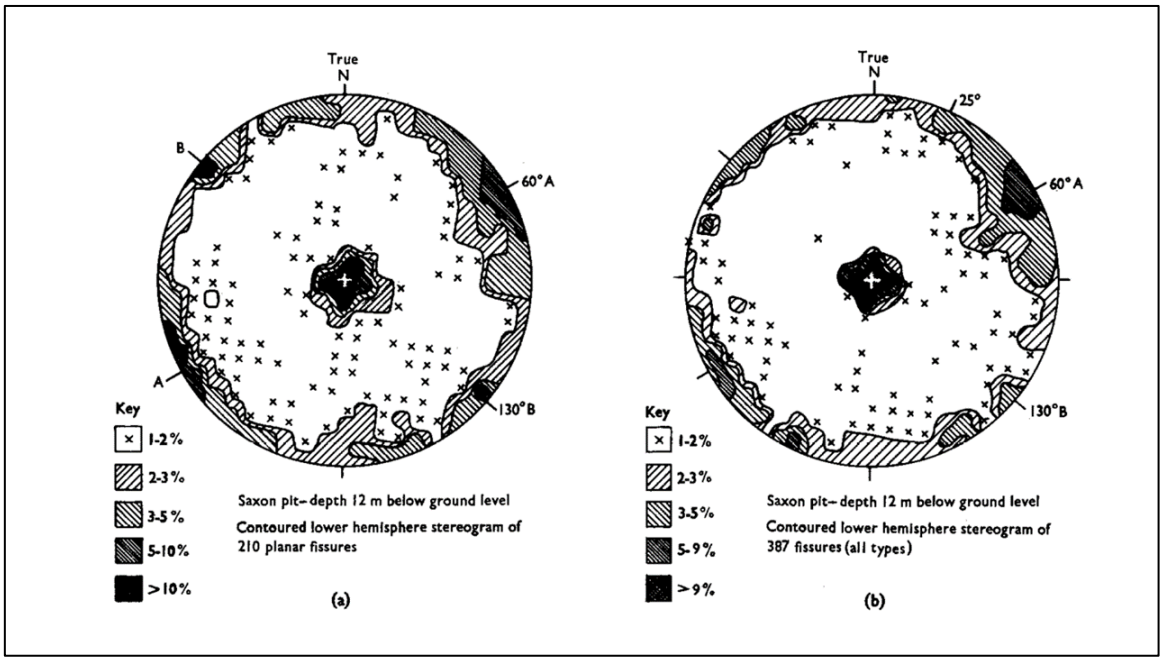

Figure 4-8 Fissure orientation and inclination in the Stewartby member, Whittlesey after Burland *et al.* (1977) plotted on Lambert equal-area stereonet. A) planar, b) non-planar.

Fissures were defined by Burland *et al*. (1977) as those discontinuities of limited extent (<1 m) typically 10 – 150 mm and which do not cut bedding planes. Figure 4-8 shows two dominant inclination orientations (A and B); 60º (strike 150º) and 130º (strike 210º). Two dominant dip amounts are evident; near vertical, plotting near the centre of the stereogram and near horizontal plotting near the great circle. Burland *et al*. (1977) interpreted that these structures were formed by removal of vertical stress during erosion of overburden. Weathering and tectonic origins were also proposed as contributory mechanisms.

Ductile deformation affecting the older rocks beneath the Oxford Clay is evident by folding in the northeast-southwest trending Charlton anticline (Sumbler, 2002). Middle Jurassic rocks are folded into an asymmetrical anticline where dips are steepest (up to 6º) on its northwestern side. The anticline overlies the deep-seated Charlton Axis and so may be associated with

reactivation of faults associated with the basement structure. The Charlton anticline is faulted on along its northwestern limb.

4.1.9 Summary

Palaeoenvironmental conditions during deposition of the Oxford Clay are considered to have been relatively uniform. Subsequent depth of burial and removal of geological overburden are considered insufficient to explain differences in geotechnical properties and behaviour. Differential preferential alignment of clay particles has been shown to influence differences in compressibility and both drained and undrained shear strength behaviour. Mechanical and chemical weathering are further post-depositional processes which influence patterns of behaviour as a result of degradation of interparticle ionic bonds and cement and the introduction of discontinuities. Slope failures are common in the weathered zones of overconsolidated mudrocks.

Spatial patterns of geotechnical variability and their causes are little known. The effects of glacial and periglacial processes were referred to by Parry (1972) and Jackson & Fookes (1974) but their effects were not quantified. The effects of glaciation (overburden, sub- and pro-glacial drainage) and growth of segregated in frost susceptible Mesozoic mudrocks in lowland periglaciated areas remains under represented in the literature.

4.2 Quaternary Engineering Geology

The engineering geology of north Buckinghamshire has received relatively little scientific attention. National schemes related to Quaternary geohazards and attempts to rationalize geotechnical variability based on landsystems and domains are briefly reviewed. A review of literature related specifically to the geotechnical characterization of tills in north Buckinghamshire and adjacent areas is then given.

4.2.1 Geotechnical characterisation of Quaternary engineering soils

Bell (1992) associated engineering soils of Quaternary age with geotechnical variability including low density, low strength, high compressibility, high permeability, collapsibility, high shrink-swell potential and shallow groundwater. Bell (1992) argued that if problematic Quaternary soils cannot be removed, most site-based remedial work is concerned with the management of groundwater and improving soil strength to reduce settlement and prevent soil failure.

Following the development of soil mechanics as a discrete discipline within civil engineering, a large body of evidence on the geotechnical characterisation of Quaternary soils began to develop from the 1960s. Research focused initially on sediments including loess (Fookes & Best, 1969; Northmore *et al.*, 1996), landforms and processes associated with mass movement (Chandler, 1970; Higginbottom & Fookes, 1970; Hutchinson, 1974, 1992; Skempton & Weeks, 1976) and those with specific ground engineering problems including rockhead anomalies (‘pingos’ or ‘scour hollows’) in central London (Berry, 1979; Hutchinson, 1980).

In recognition of the wide spatial extent of primary glacigenic deposits and their frequency of investigation in construction, research began to focus on the geotechnical properties and behaviour of tills (Kazi & Knill, 1969; McGown, 1971).

This applied research led to a major conference that synthesised current knowledge of till properties, behaviour and its implications for ground investigation and geotechnical design (Cocksedge & Hight, 1975; Fookes, Gordon, *et al.*, 1975; Fookes, Hinch, *et al.*, 1975; Marsland, 1975; McGown *et al.*, 1975).

Although there was much applied research being carried out, these studies lacked rigorous scientific information on the processes of formation and depositional environments of tills and their potential influence on geotechnical properties and behaviour. This was addressed by using temperate glaciers in Iceland and polar glaciers in Spitsbergen, Svalbard as modern analogues for Pleistocene ice-sheets in Great Britain (Boulton, 1968a, 1968b, 1970, 1975,

1977). This work led to the first attempts to relate former processes of glacier debris transport and deposition to geotechnical properties including particle grading, plasticity, bulk density and consolidation state (Boulton, 1975, 1977; Boulton & Paul, 1976; McGown & Derbyshire, 1977). Paul *et al*. (1981) integrated knowledge of effective stress, critical state soil mechanics and glaciology to provide a geotechnical basis with which to understand and interpret processes of Pleistocene till deposition in Great Britain.

Before the initiation of the Engineering Group of the Geological Society's Working Group on glacial and periglacial geology and geomorphology, the last major Quaternary geology initiative took place in the late 1980s. This research effort culminated in the publication of 61 papers explicitly related to Quaternary engineering geology (Forster *et al.*, 1991).

4.2.2 Quaternary engineering geology of north Buckinghamshire

With exception of geotechnical investigations in advance of the development of the new town of Milton Keynes (Cratchley *et al.*, 1969), there is no known published information on the engineering geology of north Buckinghamshire. This section therefore refers to the engineering geology of glacigenic deposits, interpreted to be equivalent in age and provenance, in parts of Hertfordshire and East Anglia. The review describes geotechnical properties and behaviour of tills only.

Deposits of till derived based on 1:625 000 scale geological maps are classified as fine-layered till comprising firm to very stiff or hard, slightly gravelly, sandy clay with interbeds of laminated clay/silt and beds and lenses of sand. It is described as fissured, especially in the upper few metres where permeability is often increased through discontinuities (Dobbs *et al.*, 2012).

The geotechnical properties of the two tills described in Section 3.3.4.2 were investigated in the Milton Keynes area (Cratchley *et al.*, 1969). Their stratigraphical relationships are unknown but are considered here to be two facies within the Oadby Till Member ('chalky boulder clay'). The 'lower' clay-rich till is up to 30 m thick and comprises firm, blue-grey to mid-brown when weathered, unsorted, pebbly (*sic*) clay with low to moderate fissure intensity. Lenses of sand and silt are common as are cobble clasts of flint and chalk. The 'upper' till is upto 5 thick and comprises light-brown to reddish-brown when weathered, stiff to hard, unsorted, sandy silt with some clay and pebbles (*sic*). Cobbles including flint and chalk are present as are lenses of clay.

4.2.2.1 Particle-size and fabric

The particle-size distribution of tills is commonly well-graded (poorly sorted), bi- or multi-modal and is often gap-graded in the coarse silt/fine sand fraction (McGown, 1971; Trenter, 1999). Particle-size analyses of Anglian tills in the Vale of St Albans and Norfolk are shown in Figure 4-9. Each of these tills were previously interpreted as 'Lodgement Tills' but are here interpreted as subglacial traction tills using the classification of (Giles *et al.*, 2017). The particle-size distributions show that the tills are well-graded and dominantly matrix supported (40-80% finer than silt grade) with the tills of the Lowestoft Formation and the Vale of St Albans with the highest proportion of silt and clay. The latter observation for the tills of the Vale of St Albans may reflect the dominant proportion of matrix material derived from underlying Jurassic mudrocks deposited at the margin of the Anglian margin of the BIS.

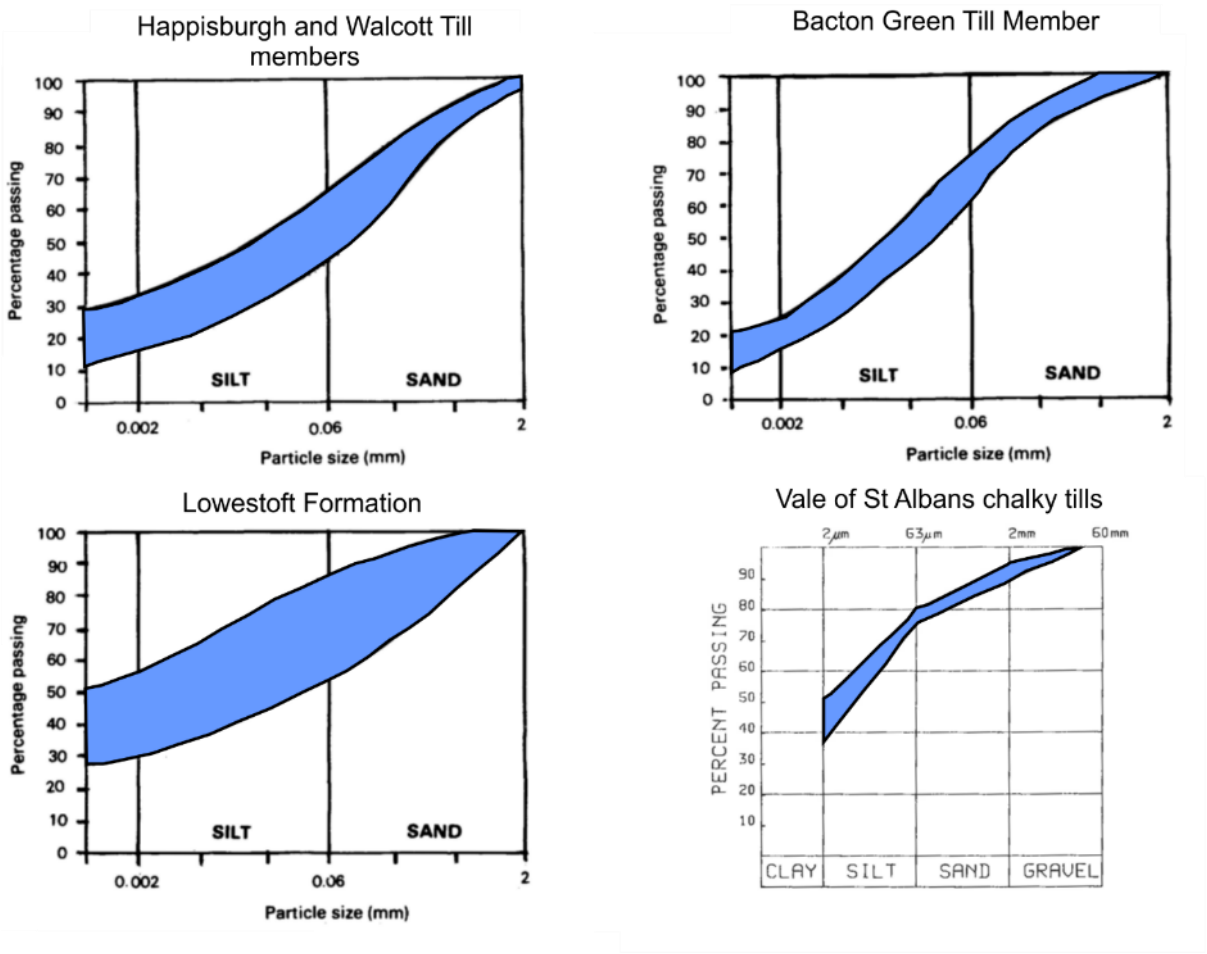

Figure 4-9 Particle-size grading envelopes for samples of Anglian till in Norfolk (Lowestoft Formation, Happisburgh, Walcott and Bacton Green members) and the Vale of St Albans modified after Bell (1991) and Paul & Little (1991).

4.2.2.2 Atterberg limits (plasticity)

The particle (grain) size and mineralogy of till is a function of its debris source, mechanism of transport and style of deposition. The relationship between liquid limit and plasticity index for undisturbed tills in Svalbard, Iceland and the Alps shows a linear relationship above liquid limit values of ~22-24, called the T-line (Boulton & Paul, 1976). The T-line is parallel but above the A-line of Casagrande which is routinely used on plots of plasticity index and liquid limit (Casagrande, 1932). The position of any point on or near the T-line is dependent on the proportion of clay minerals and particle-size; the greater the proportion of particles larger than clay, the lower the liquid limit. Investigation of Anglian tills in the Vale of St Albans illustrates this (Little & Atkinson, 1988). The plasticity index and liquid limit for samples of the Eastend Green Till (Holwell Hyde and Westmill), Ware Till (Holwell Hyde and Foxholes) and the Westmill Middle Till (Westmill) are shown in Figure 4-10 using the stratigraphical terminology of Gibbard (1977). These results show that the tills are intermediate to high plasticity. Their activity ranges between 0.57 - 0.73.

The liquidity index values vary between -0.07 - 0 indicating that the *in situ* moisture content is less than the plastic limit. Anglian tills at the former Building Research Establishment test site north of Watford, Hertfordshire show similar values (Marsland & Powell, 1991). Here, *in situ* moisture contents vary between ~15 to 22% above 6.8 mbgl increasing to ~25% below. *In situ* moisture content values are close to or at their plastic limit and so values for liquidity index are <0. Activity ranges between 0.58 – 0.72 and bulk density ranges between 2.0 – 2.2 Mg/m^3.

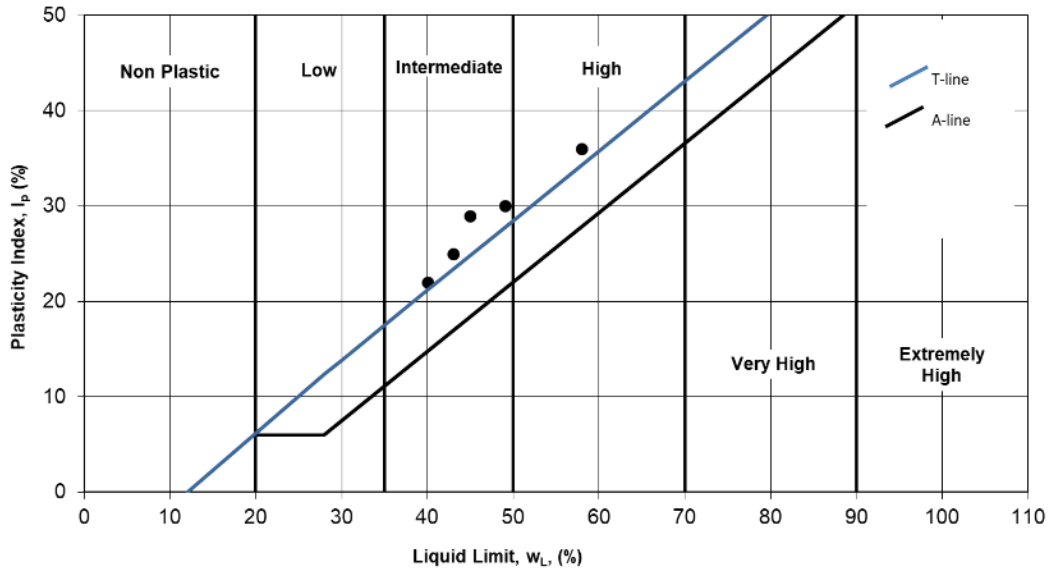

Figure 4-10 Plasticity plot by the author of tills in the Vale of St Albans using data from Little & Atkinson (1988).

Cratchley *et al*. (1969) investigated the geotechnical properties of presumed Anglian 'chalky-boulder-clay' in Milton Keynes. The Atterberg limits, liquidity index, particle and bulk densities for tills in Milton Keynes are summarised in Table 4-7.

	W_L	W_P	I_p	LI	ρ_s	ρ_b (Mg/m^3)
'Lower' Clay-rich till (Oadby Till Member)	40-60	20-30	20-30	(-0.1)-0.2	2.45-2.6	1.8-2.0
'Upper' Sandy Till (Oadby Till Member)	30-50	15-25	15-25	(-0.1)-0.1	2.6-2.75	2.0-2.3

Table 4-6 Summary index properties of two till types identified by Cratchley *et al*. (1969).

The variability of Atterberg limits, liquidity index, particle density and bulk density in the tills of Milton Keynes were investigated at 1 m and 0.2 m regular grid intervals from a temporary trench exposure (Denness, 1974). The results of the spatial variability are shown in Figure 4-11. They show that the magnitude of variability in each of the properties is similar between samples taken at 1 and 0.2 m. The apparent trend of lower values of liquid limit, plastic limit and liquidity index within the central part of the trench may reflect primary differences in lithology and mineralogy (Denness, 1974). It is also possible that liquidity index and bulk density changes reflect changes in moisture content with depth where samples taken closer to the ground surface may be desiccated, consequently increasing liquidity index and decreasing bulk density.

In East Anglia, the geotechnical properties of tills of Anglian age were investigated by Bell (1991) and summarised together with a comparison to tills of Devensian-age (Bell, 1992). A summary of the maximum, minimum and mean values for moisture content, liquid limit, plastic limit, plasticity index and activity is given in Table 4-8. The plasticity of the Anglian-age tills described by Bell (1991) is shown in Figure 4-12 in comparison to Devensian-age till exposed at Hunstanton, Norfolk.

The results from Bell (1991) indicate that Anglian-age tills are low to intermediate plasticity and generally inactive. The higher plasticity of the Lowestoft Formation till probably reflects its greater clay content than other tills shown. The *in situ* moisture content of the Lowestoft Formation, 'North Sea drift Formation' (Happisburgh Till Member and Walcott Till Member) are slightly below their plastic limits giving liquidity indices <0. The *in situ* moisture contents

of the Bacton Green Till in contrast are higher than their plastic limits giving liquidity indices >0. The tills of the Lowestoft Formation, Happisburgh Till Member and Walcott Till Member are therefore stiffer than those of the Bacton Green Till Member (Cromer Diamicton of the Contorted Drift/ 'North Sea Drift' Formation).

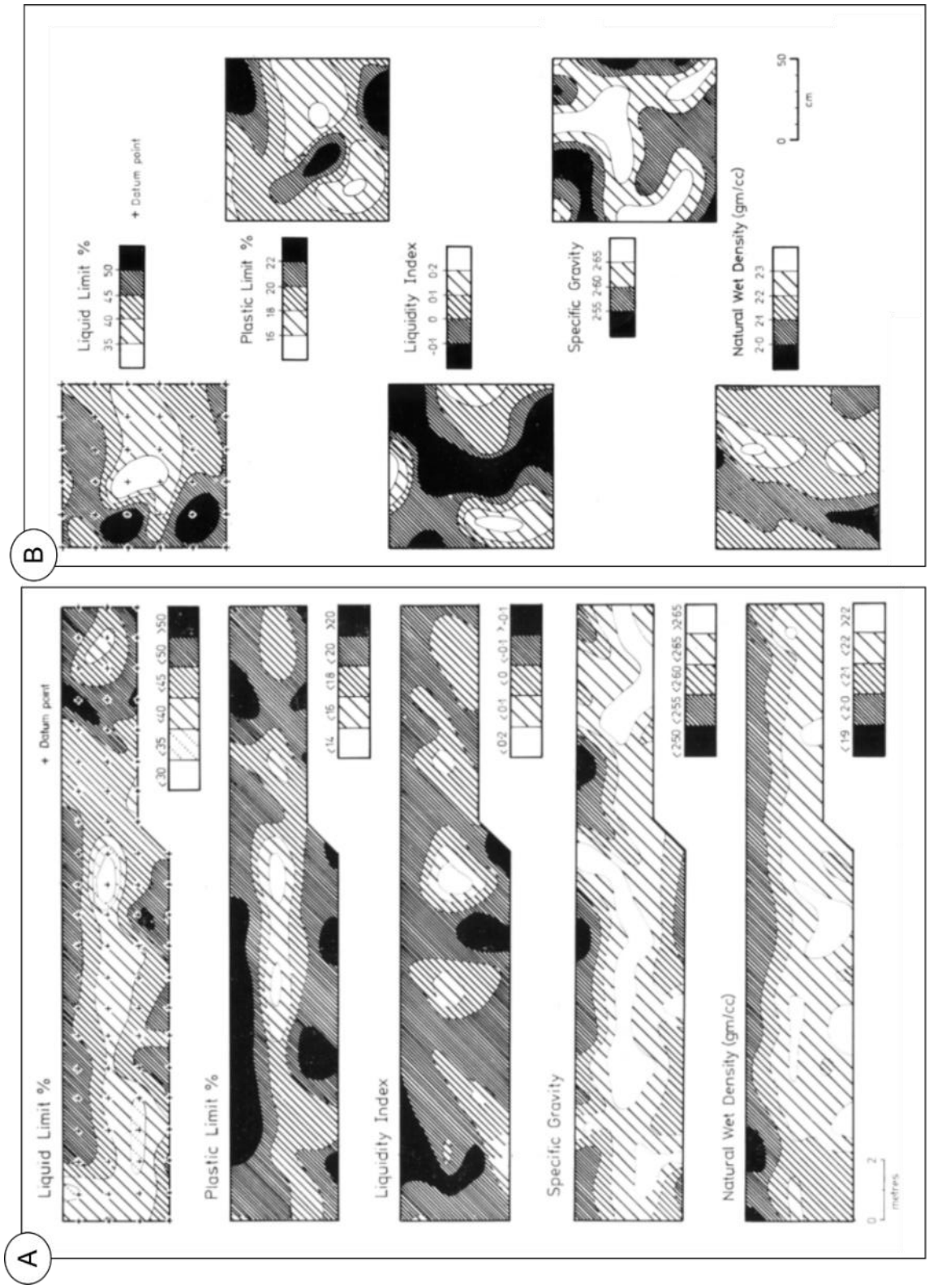

Figure 4-11 Geotechnical variability in liquid limit, plastic limit, liquidity index, particle density (specific gravity) and bulk density (wet density) after Denness (1974). A) Variability at 1 m sampling interval. B) variability at 0.2 m sampling interval within a randomly selected 1 m^2.

	ω	W_L	W_p	I_P	LI	Activity
Lowestoft Formation ('Marly Drift' facies)						
Max	25.2	45(IP)	23	23	0.07	1.00
Min	22.4	32(L)	15	15	-0.19	0.75
Mean	23.6	37(IP)	18	20	-0.02	0.85
Bacton Green Till Member ('Contorted Drift/North Sea Drift Formation')						
Max	18.9	29(L)	18	13	0.33	0.80
Min	13.2	19(L)	9	8	0.07	0.65
Mean	15.6	25(L)	14	11	0.16	0.75
Happisburgh and Walcott Till members ('First and Second Cromer Tills of the North Sea Drift Formation')						
Max	15.8	40(IP)	20	24	-0.16	0.95
Min	11.9	27(L)	14	13	-0.18	0.65
Mean	13.2	35(IP)	17	19	-0.17	0.80

Table 4-7 Maximum, minimum and mean values for moisture content (ω), liquid limit (W_L), plastic limit (W_p), plasticity index (I_p), liquidity index (LI) and activity for Anglian tills in East Anglia after Bell (1991). Stratigraphical terminology is after Hamblin *et al*. (2005) with reference to alternative terminology as used by Bell (1991). Intermediate plasticity (IP), low plasticity (LP).

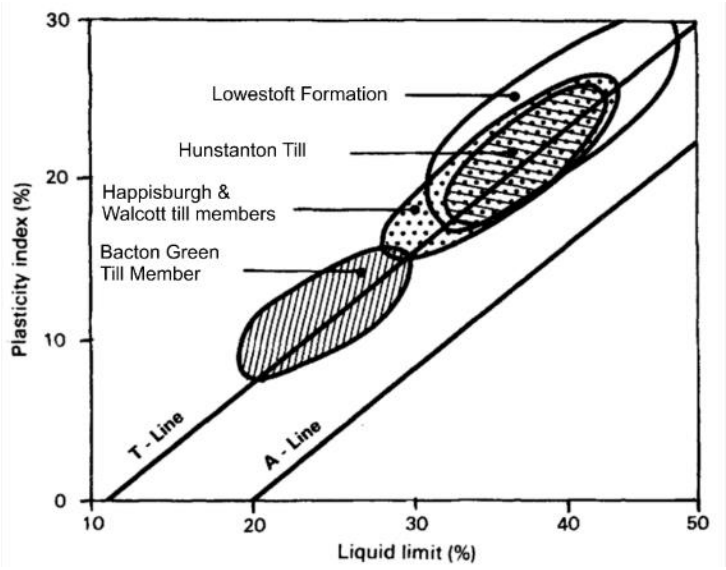

Figure 4-12 Plasticity of Anglian-age and Devensian-age (Hunstanton Till) tills in Norfolk from Bell (1991).

4.2.2.3 Permeability

The permeability (k) of the tills in the Vale of St Albans was investigated using values of c_v and m_v derived from 1D consolidation tests on undisturbed and reconstituted samples and equation 4-3 (Little, 1988). Reconstituted samples are those that have been thoroughly destructured and mixed at a water content usually 1.5 to 2 times the sample's liquid limit.

Values of k for reconstituted tills ranged between $1.29x10^{-11}$ to $7.29x10^{-13}$ whilst values vertical permeability for undisturbed till ranged between $9.46x10^{-13}$ to $1.12x10^{-10}$. Values in the horizontal direction range between $1.06x10^{-9}$ to $2.72x10^{-13}$. Little (1988) observed that there is little significant variation in permeability between the horizontal and vertical drainage directions because of the matrix-supported nature of the tills. In this case, matrix permeability is dominant rather than permeability of the coarser clasts within the matrix.

4.2.2.4 Compressibility

1D compression tests were carried out by Paul & Little (1991) on undisturbed and reconstituted (at 20% moisture content) chalk-rich tills in the Vale of St Albans corresponding to the Eastend Green Till (Holwell Hyde and Westmaill), Ware Till (Holwell Hyde and Foxholes) and the Westmill Middle Till (Westmill). All of the tills are matrix-supported and stiff to hard. They comprise 10-15% sand, 40% silt and 40-50% clay (Paul & Little, 1991) Undisturbed samples were taken by inserting 75 mm oedometer sample rings directly into till. Samples were taken parallel and perpendicular to the ground surface to permit estimation of compressibility in both directions. The results of the 1D oedometer experiments are shown in Figure 4-13 for reconstituted and undisturbed samples taken parallel to the ground surface.

The 1D oedometer results demonstrate the effects of samples reconstitution. The effects of previous consolidation and particle bonding are removed so that reconstituted samples are less dense and more compressible compared to undisturbed samples.

The oedometer-derived coefficient of consolidation (c_v) ranges between 0.25 m^2/yr – 11.76 m^2/yr for undisturbed samples and 0.13 m^2/yr – 5.94 m^2/yr for reconstituted samples (Little, 1988). Similar values were obtained using 1D consolidation experiments for Anglian tills in north Norfolk where values for c_v ranged between 0.84 m^2/yr – 3.81 m^2/yr and values for m_v ranged between 0.094 m^2/MN – 0.241 m^2/MN (Bell, 1991) The magnitude of overconsolidation is inversely proportional to c_v for undisturbed samples and magnitude of effective stress for undisturbed and reconstituted samples (Little, 1988; Bell, 1991).

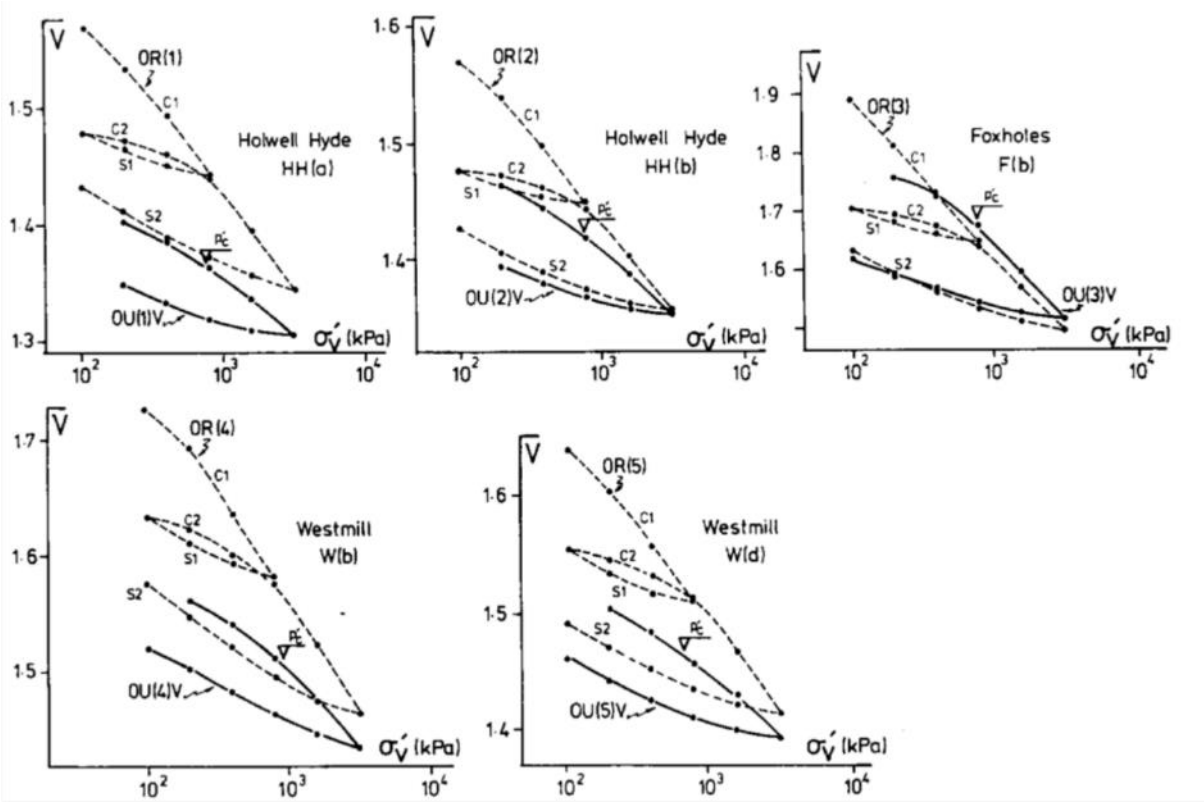

Figure 4-13 Results of 1D oedometer experiments on Anglian tills in the Vale of St Albans after Little (1988). Localities Holwell Hyde (HH), Foxholes (F) and Westmill (W). V=1+e, σ'_v = vertical effective stress and p'_c = estimated preconsolidation pressure using Casagrande graphical method. C1, C2 = compression stages, S = swelling stage.

In addition, for a given value of overconsolidation, values of c_v for undisturbed samples were greater than those for reconstituted samples. This suggests that the effects of deposition and burial that could promote drainage (e.g. bedding/lamination, sand lenses) are destroyed in the reconstituted samples (Little, 1988).

Preconsolidation pressures estimated using the Casagrnade graphical method ranged between 690 kPa – 930 kPa for those samples taken parallel to the ground surface in the Vale of St Albans (Little, 1988). Using the Eastend Green Till as an example and accounting for erosion, Little estimated that the original preconsolidation pressure at the Holwell Hill site was 2000 kPa, corresponding to an ice-sheet thickness of 200 m. The apparently lower value of estimated preconsolidation was accounted for by post-depositional weathering and periglacial activity. A preconsolidation pressure of 2000 kPa was also estimated for the same tills but using critical state theory from isotropically consolidated-undrained till samples (Atkinson & Little, 1988).

4.2.2.5 Shear Strength

Tills in north Buckinghamshire, Hertfordshire and Norfolk were previously classified as lodgement tills for engineering purposes (Eyles, Dearman, *et al.*, 1983; Trenter, 1999). The drained and undrained shear strength of lodgement tills was considered to be a function of their overconsolidated and dense state, and presence of depositional and post-depositional discontinuities including shear planes and freeze-thaw tension cracks (Sladen & Wrigley, 1983; Trenter, 1999).

Unconfined, shear-box and triaxial experiments were carried out on firm and stiff Anglian tills in Norfolk to determine their peak and residual shear strengths and stress-strain behaviour (Bell, 1991). The results are summarised in Table 4-9.

	Shear strength (UCS) kN/m^2		**Cohesion, c kNm^2**			**Angle of shearing resistance, ø**		
	Intact	**Remoulded**	**c_u**	**c´**	**Residual c_r**	**$ø_u$**	**ø´**	**Residual $ø_r$**
Lowestoft Formation ('Marly Drift' facies)								
Max	60	47	49	16	0	3	28	25
Min	52	35	16	7	0	0	21	16
Mean	55	41	27	11	0	1	24	21
Bacton Green Till Member ('Contorted Drift/North Sea Drift Fm')								
Max	90	84	46	20	3	10	33	25
Min	62	38	20	6	0	3	27	20
Mean	80	68	26	11	1	6	30	22
Happisburgh and Walcott Till members ('First and Second Cromer Tills of the North Sea Drift Fm')								
Max	112	94	48	19	5	6	32	29
Min	77	70	26	12	0	2	26	18
Mean	88	78	35	14	3	4	29	23

Table 4-8 Summary of drained and undrained shear strength parameters for Anglian till in Norfolk after Bell (1991). UCS = unconfined compressive strength, c_u and $ø_u$ from quick undrained triaxial experiment, c´ and ø´ from consolidated undrained triaxial experiments and c_r and $ø_r$ from shear-box experiments. Undrained strength = 0.5 shear strength at failure in UCS.

Values for the ratio of the undisturbed to remoulded strength of the tills describing its sensitivity were <2 and so are low sensitivity. In contrast, undrained shear strength measured using hand and motorised shear vane apparatus, showed sensitivity values between 3.72 – 5.78 when measuring undisturbed and reconstituted shear strengths in Anglian tills in the Vale of St Albans (Paul & Little, 1991). Maximum undrained shear strength values for undisturbed values ranged between 400kPa – 500 kPa with remoulded and reconstituted samples values between 65 kPa – 100 kPa. The increase in sensitivity values and reduction in undrained shear strength in reconstituted and remoulded samples, were interpreted to be because of the presence of calcite cement in the chalk-rich till whose bonds were destructured during reconstitution of the samples.

Critical state soil mechanics theory (Schofield & Wroth, 1968) was applied to the investigation of undrained shear strength of intact and reconstituted till in the Vale of St Albans by Atkinson & Little (Atkinson & Little, 1988). 38 mm diameter, cylindrical samples were obtained from Holwell Hyde and tested under isotropically consolidated-undrained triaxial conditions with external measurement of strain. Stresses between 50 and 1600 kPa were applied corresponding to overconsolidation rations between 1 – 32.

Figures 4-14A and 4-14BB shows effective stress paths for intact samples in consolidated-undrained conditions in triaxial shear where:

$$p' = \frac{1}{3}(\sigma'_a + 2\sigma'_r)$$

Equation 4-4

$$q = \sigma'_a - \sigma'_r$$

Equation 4-5

where p′ is mean effective stress, q is differential or deviatoric stress, σ'_a is axial (vertical) stress and σ'_r is radial stress in the σ_2 and σ_3 directions.

The stress paths in Figures 4-14A and B for undisturbed samples are typical for overconsolidated soils. At high effective stresses their stress paths approach the failure surface by deviating to the left as mean stress decreases, before deviating right along the failure plane in p′-q′ space. When plotted as stress ratio (q′/p′) the normally consolidated, reconstituted samples in Figure 4-14C approach a unique stress ratio-strain line for strains ~6%. For overconsolidated, reconstituted samples in Figure 4-14D, a peak stress ratio is reached before approaching a critical state line with increasing strain. Undisturbed samples in Figure 4-14E and F show a similar stress ratio-strain behaviour to overconsolidated, reconstituted samples. Critical states with increasing strain were only reached by light and normally consolidated samples. Heavily overconsolidated samples did not reach a critical state with large strains but did show a prominent peak stress ratio.

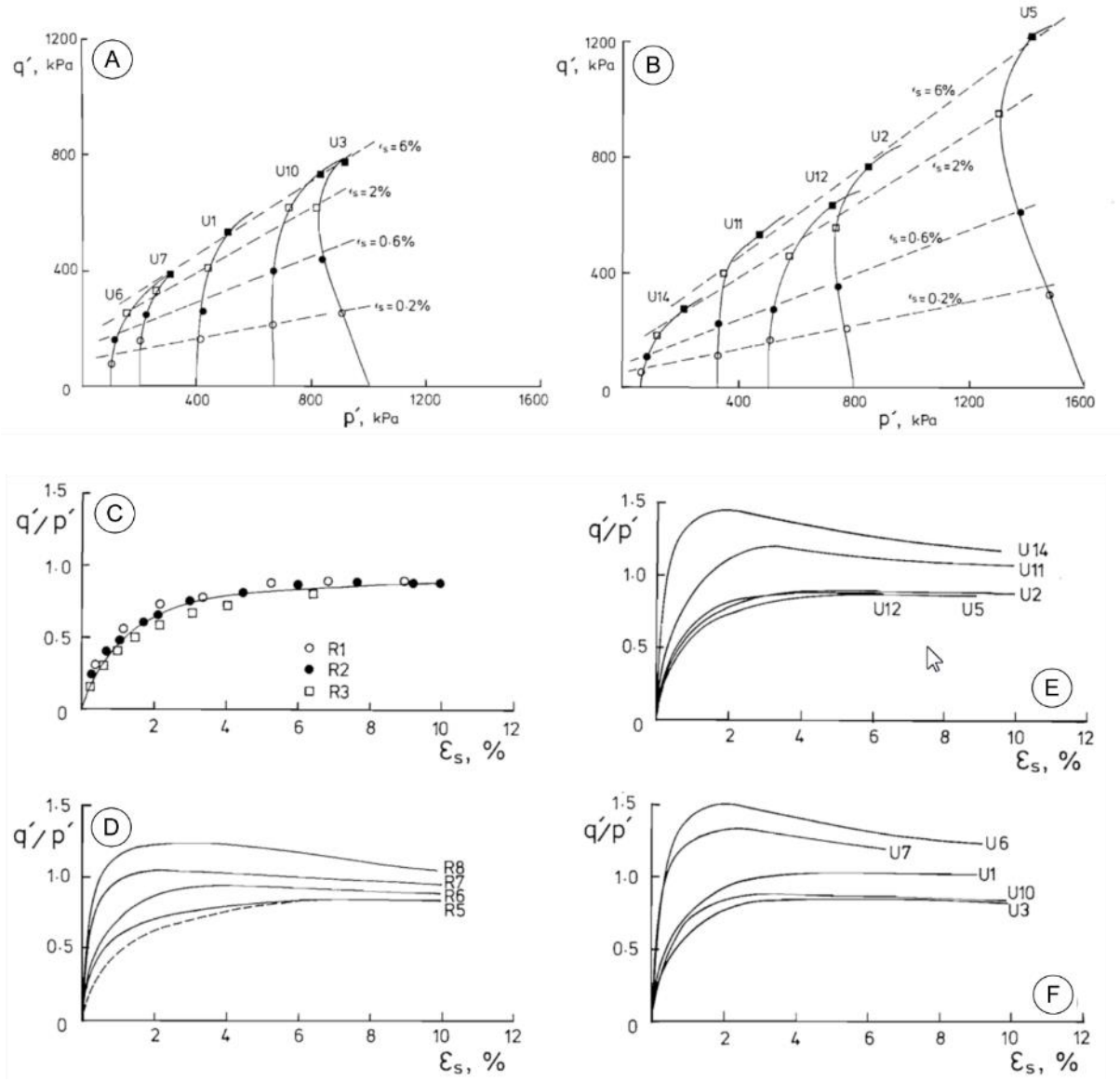

Figure 4-14 Stress path plots for intact and reconstituted tills form the Vale of St Albans in undrained Triaxial conditions after Atkinson & Little (1988). A) and B) Effective stress paths for intact samples. C) and D) Effective stress ratio-shear strain plots for normally consolidated (C) and overconolsolidated (D) reconstituted (R) samples. E) and F) Effective stress ratio-shear strain plots for undisturbed (U) samples. ε_s is deviatoric strain.

4.2.2.6 Stiffness

The stiffness of a soil describes the amount and rate of strain in response to the application of stress. Undrained shear stiffness (G_u) is described by:

$$G_u = \frac{\partial q}{\partial \gamma}$$

Equation 4-6

where q is deviator stress and γ is shear stregth (modified after Atkinson & Little, 1988). Undrained shear stiffness can be related to other deformation moduli by:

$$G_{\mathrm{u}} = \frac{1}{3} E'_{\mathrm{u}} = G' = \frac{E'}{2(1+\nu')}$$

Equation 4-7

Where, in terms of effective stress, G′ is shear modulus, E′u is undrained Young's modulus and ν′ is Poisson's ratio. As soils exhibit non-linear stress-strain behaviour, two types of shear moduli describe their behaviour; secant and tangent where secant stiffness describes the ratio of deviator stress to shear strain for any increment of change in the elastic and plastic ranges of soil deformation. Tangent modulus describes the partial differential of change. An example of laboratory-derived stress-strain behaviour exhibited by undisturbed Anglian till from Holwell Hyde in the Vale of St Albans is shown in Figure 4-15.

These results demonstrate the decrease in tangent stiffness with increasing strain. When normalised by initial effective pressure and plotted against overconsolidation ratio, tangent stiffness increases with increasing overconsolidation ratio for undisturbed and reconstituted samples. Values are similar between undisturbed and reconstituted samples at small values of overconsolidation ratio. At large values, undisturbed samples are stiffer by approximately 20%. This contrasts with the results of triaxial experiments relating OCR with the ratio between mobilised shear strength, τ_{mob} (expressed as τ_{mob}/c_u) and mobilisation strain using reconstituted kaolin clay (Vardanega *et al.*, 2012). The authors found that for moderate stresses ($0.2<\tau_{mob}/c_u<0.8$), the amount of strain mobilisation increased with increasing OCR.

Geologically-derived estimates of ground stiffness beneath rail track ballast have been calculated by Gunn *et al*. (2003). Gunn *et al*. (2003) showed that relationships between soil density, effective stress and shear wave velocity could be used to estimate soil stiffness. Further, they showed that lithostratigraphically grouped engineering soils with similar effective stress-controlled lithological, density and shear wave velocity properties could be used to derive small-strain shear modulus (G) using geological maps.

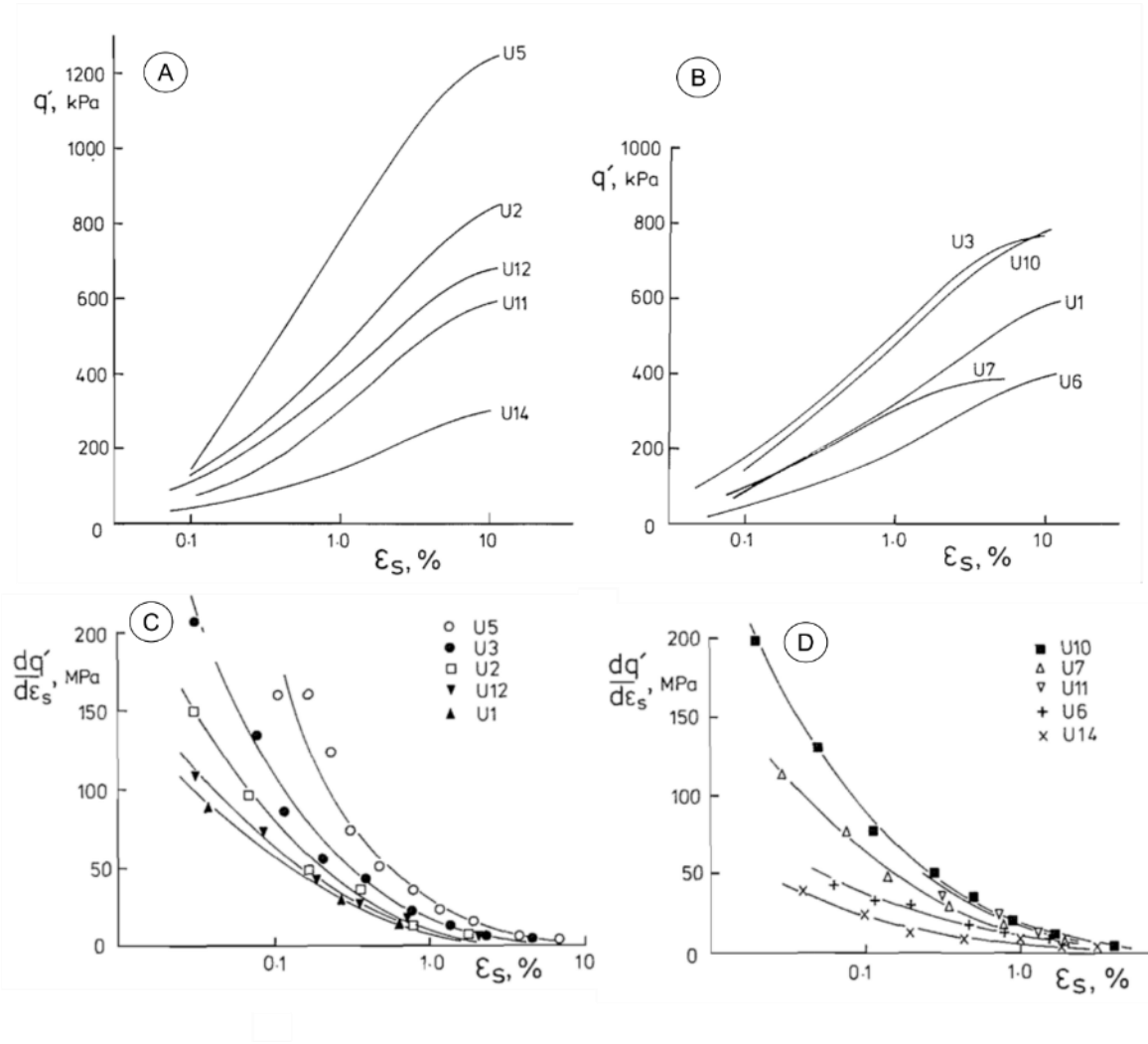

Figure 4-15 Stress strain behaviour of undisturbed Anglian tills from the Vale of St Albans after Atkinson & Little (1988). A) and B) Stress-shear strain. C) and D) Tangent stiffness parameters which are also equal to Young's undrained modulus.

5 Ground model

A geological ground model was established against which the results of laboratory experiments and inferences relating to the glacial and periglacial history of the project area could be made. The development of the ground model followed three phases; conceptual ground model from the literature review, creation of 2D geological profiles in selected geographic areas and thirdly, field-site selection and sedimentary logging. The aim was to progressively build and develop a ground model to establish the relative order of superposition of glacigenic sediments which could then be used to infer the glacial and periglacial event history of the area, the structure and degree of weathering affecting the Oxford Clay and their similarity or difference relative to the inferred limit of the BIS. Quaternary Domains (Booth *et al.*, 2015) were selected as an appropriate means of comparing spatial variability in sediments and their properties and form a part of the conceptual glacial and periglacial framework of the project area.

5.1 Conceptual ground model from literature review

Considering the Quaternary literature review, a conceptual ground model was established and is shown in Figure 5-1. The development of this style of conceptual model follows the style and recommendations established by authors including Fookes (1997) and Culshaw (2005).

The conceptual ground model highlights the potential for:

- Variable depth of weathering, including the effects of periglaciation, in dominantly clay-rich bedrock;
- Variability in the elevation of geological rockhead, including the potential presence of buried valleys infilled with glacigenic sediment comprising laminated clay and silt, lenses of sand and/or gravel and till;
- Glacitectonic disturbance of bedrock.

The next phase of development of the ground model was to map Quaternary Domains and to assess the probable geological ground conditions associated with each.

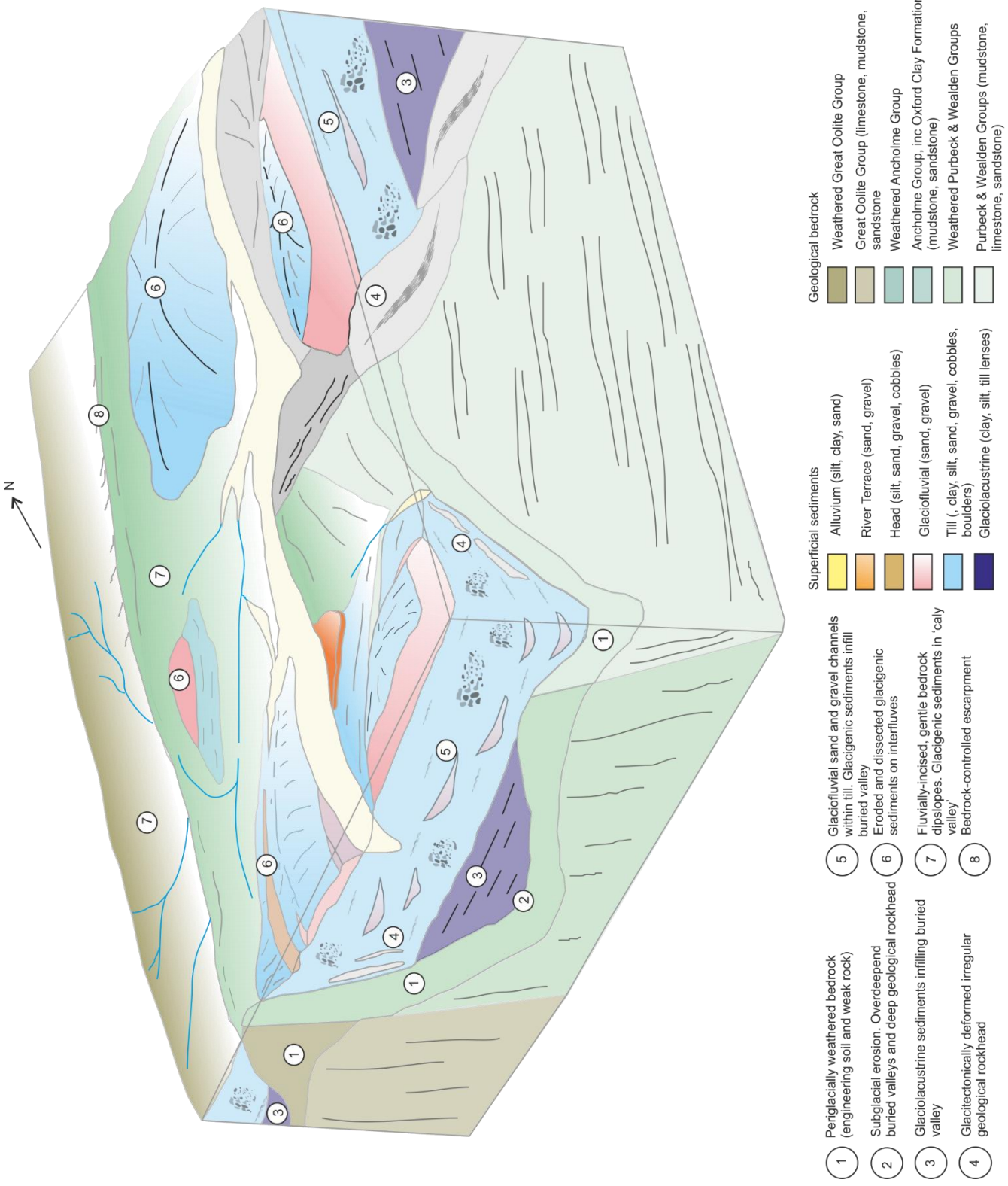

Figure 5-1 3D conceptual ground model for the project area. Not to scale.

5.2 Quaternary Landsystems and Domains

The geological complexity associated with glacial and periglacial sediments and landforms requires an approach that relates the complex assemblage of sediments and landforms, to their mechanism of transport and deposition. Landsystems represent landscape facets and sediment-landform assemblages that share similar characteristics and geological history. The advantage of the landsystem approach is that it provides a methodology to group together related processes, landforms and sediments into genetically related assemblages. For engineering geology and geotechnical engineering, it provides a tool to group together similar sediments and to compare their physical properties and behaviour based on their inferred process of deposition and post-depositional changes.

A threefold glacial landsystem approach comprising 'Lodgement Till Plain', 'Glaciated Valley' and 'Fluvioglacial-Ice-Contact' was proposed for formerly glaciated areas of Great Britain (Fookes, Gordon, *et al.*, 1975). This system was later modified in terminology to subglacial, supraglacial and glaciated valley landsystems for North America (Eyles, 1983). In Great Britain, the same conceptual glacial landsystems classification was further modified with the addition of one periglacial landsystem (Eyles & Dearman, 1981; Eyles, Dearman, *et al.*, 1983). The lowland area of southern Britain lying between the Devensian and Anglian glacial limits was classified within the subglacial landsystem and generalised as a lodegment till terrain. Tills in the 'Lodgement Till' terrain were characterised as well-graded (poorly-sorted), clast-supported or matrix-supported. Matrix-supported tills comprise those whose matrix is often >50% clay and silt so that larger particles including gravel act as discrete particles within the matrix. Areas beyond the Anglian limit were classified as part of the periglacial landsystem.

The conceptual landsystem approach as a means of attempting to characterise similar glacial and periglacial materials was advocated as a suitable way to develop geological ground models for civil engineering (Fookes, 1997; Hutchinson, 2001). The differentiation of glacial landsystems on the basis of subglacial, subaerial and subaqueous deposition for civil engineering purposes has recently been emphasized by Evans (Evans, 2017). Within a four-fold classification, the glaciated areas of lowland Britain are classified as 'Ice-sheet-related landsystems'. They are subdivided into 'hard' and 'soft' bedded areas based on subglacial bed type. In common with parts of lowland Britain, north Buckinghamshire is largely underlain by 'soft' bedrock comprising Mesozoic mudrocks.

The development of conceptual ground models has been widely advocated in Great Britain to maximise the use of data, information and scientific knowledge about landscape-forming processes and their influence on geotechnical design (Fookes, 1991, 1997; Culshaw, 2005). This led to the generation of deterministic and stochastic three-dimensional (3D) computer models of the ground to support civil engineering and environmental protection activities (Royse *et al.*, 2009; Price *et al.*, 2010; de Beer *et al.*, 2012; Van Der Meulen *et al.*, 2013; Kearsey *et al.*, 2015).

Most recently, the concept of two-dimensional (2D) landsystems and conceptual 3D ground models have been combined to map glaciated and non-glaciated Quaternary Provinces and Domains in Great Britain (Booth *et al.*, 2015), including their direct application to groundwater recharge assessments (e.g. McMillan *et al.*, 2000). Within the Province-Domain hierarchy, Domains are the lower hierarchical level and defined on the extent of glaciation, periglacial activity and the anticipated geometrical relationship between Quaternary sediments and underlying bedrock. Within the scheme of Booth *et al*. (2015), north Buckinghamshire is spatially correlated with the 'Dissected Superficial Deposits Domain' (Figure 5-2). Within this Domain, it is expected that thick glacigenic sediments overlying bedrock are present on the interfluves of present-day river systems. Underlying the present-day river systems within the Domain are deep, buried valleys filled with glacigenic sediments. Mass-movement deposits including solifluction and landslides are common.

The domains approach provides a qualitative, conceptual framework with which to anticipate variability within Quaternary sediments and bedrock affected by glacial action and ground ice growth and degradation. Despite the authors claims that it provides a quantitative spatial characterisation, it merely sums and expresses as percentages, the amounts of different Lithogenetic classes presented on geological maps within each Domain. It does not provide any information on geotechnical properties or its variability. Northmore *et al*. (2011) described the application of lithostratigraphy to geotechnical characterisation on the assumption that similar geological units should possess the same properties and behaviour.

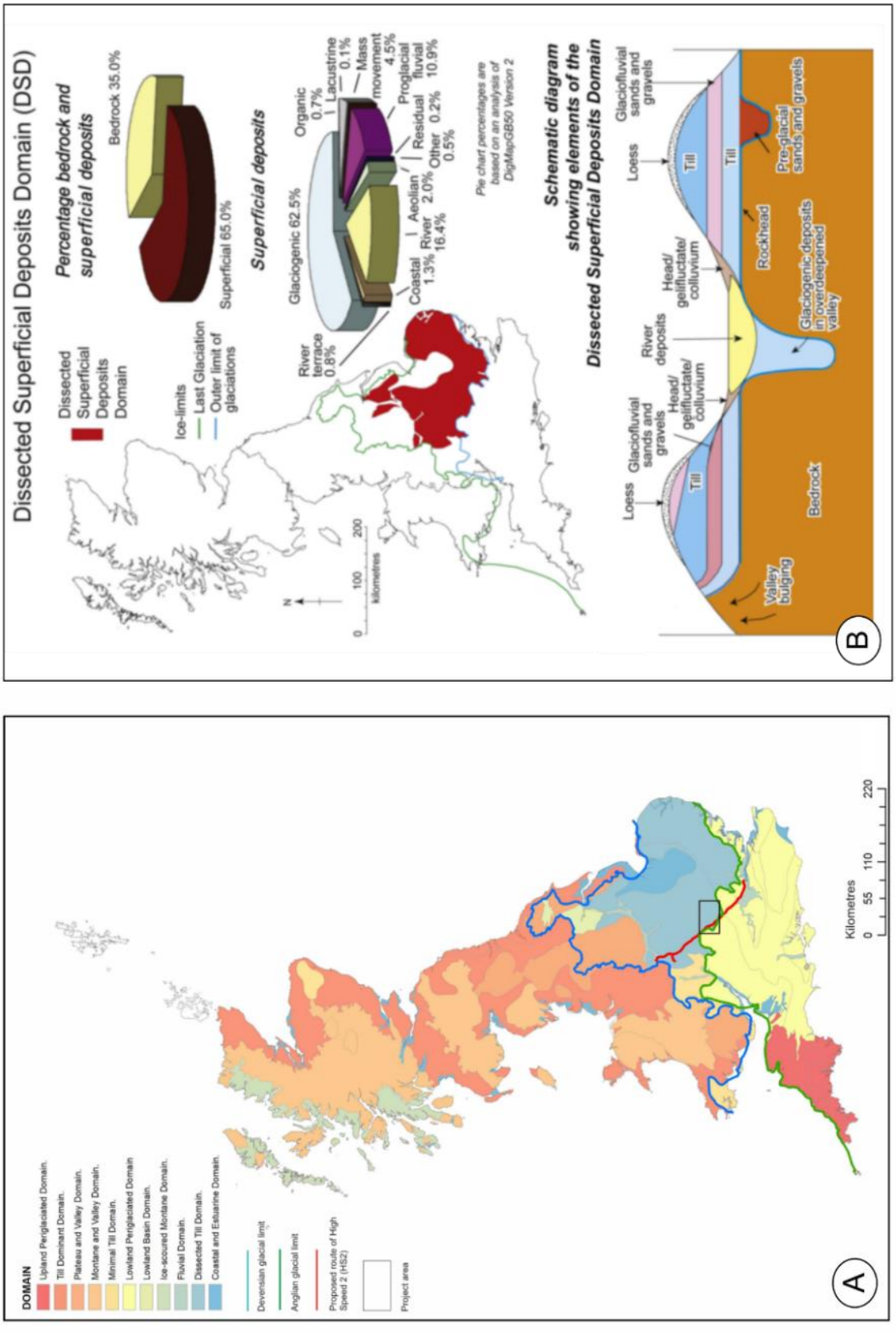

Figure 5-2 Quaternary Provinces and Domains in Great Britain. A) National distribution. B) Dissected Superficial Deposits Domain including summary percentages for bedrock and Quaternary spatial distribution and schematic cartoon of their geometrical relationships from Booth *et al*. (2015). Geological data used under licence from the BGS (licence number 2015/038). HS2 route alignment provided under Open Government Licence v1.0.

5.2.1 Quaternary Domains in north Buckinghamshire

To test the degree of similarity or difference in geotechnical properties of till and Oxford Clay in different locations, Quaternary Domains (QD) were spatially defined by subdividing the 'Dissected Superficial Deposits Domain' and the 'Lowland Periglaciated Domain' of Booth *et al*. (2015). Bedrock geology, the present-day presence or absence of Quaternary sediments and areas within or beyond the inferred limit of Middle Pleistocene glaciation, were used to define the Domains which are shown schematically in Figure 5-3 for the Oxford Clay and Late Jurassic mudrock formations.

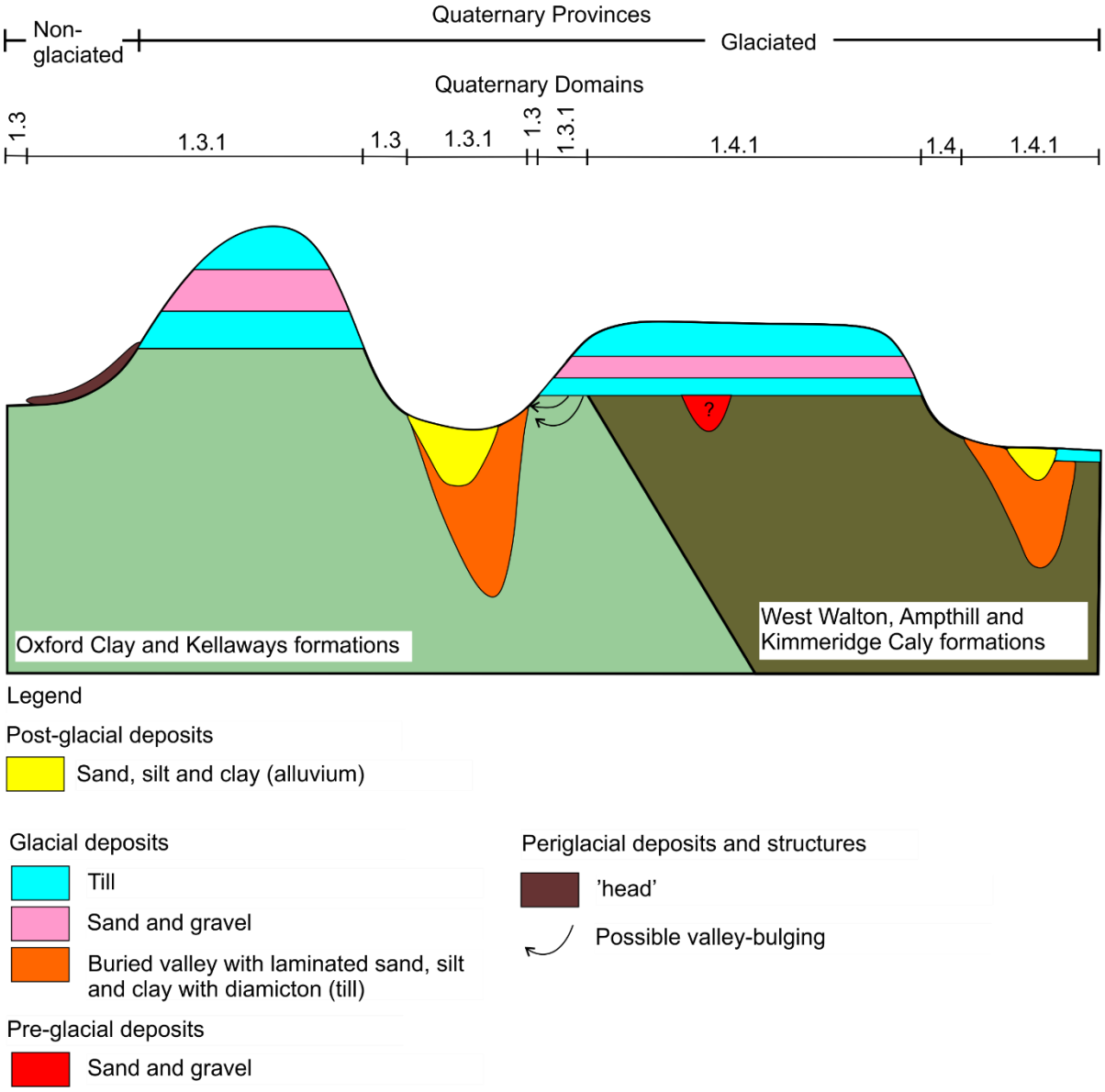

Figure 5-3 Schematic cartoon of Quaternary Domains underlain by the Oxford Clay and the West Walton, Ampthill and Kimmeridge Clay formations. Not to scale.

The use of underlying bedrock type as a criterion was chosen as it was interpreted that sediments making-up the matrix of the tills would be determined by the type of bedrock that

had previously formed the subglacial substrate, over which any glacier ice would have travelled. The Oxford Clay spans both the glaciated 'Dissected Superficial Deposits Domain' and non-glaciated 'Lowland Periglaciated Domain'. The Oxford Clay therefore provides an opportunity to compare its properties and behaviour between areas that were glaciated and subsequently periglaciated, and those where only periglacial processes, including the growth and degradation of segregated ice, operated.

Digital 1:625 000 bedrock geological maps were combined with 1:50 000 Quaternary geology maps using a series of spatial queries in ArcMap 10. The spatial definition of the Domains therefore assumes that the mapped geological boundaries are accurate, within the uncertainty associated with geological maps. Importantly, unmapped Quaternary sediments in bedrock-only Domains may in fact be present. The output of this exercise is shown in Figure 5-4.

QD prefixed with 1 or 2 refer to glaciated and non-glaciated provinces as defined by Booth *et al*. (2015). Province 1 corresponds to a geographic area in which it is interpreted that it was previously glaciated and periglaciated. In contrast, parent Domain 2 is interpreted to be non-glaciated and influenced by non-glacial, periglacial processes only. The Quaternary Domains, and their subdivisions, are summarised in Table 5-1.

The codes applied to the Domains are based on the progressive decrease in geological age of bedrock in each province numbered in increasing age from 1 to 4. Suffix 1 in any Domain indicates that the Domain is overlain by Quaternary sediment. Those Domains without suffix 1 indicate that no Quaternary sediment is present today but may have either not been deposited or subsequently removed by erosion since deposition.

The Domain framework was established to test its validity as a spatial proxy for geotechnical variability on the assumption that each Domain had a similar geological history. The first step to test the validity of the Domain approach, and the conceptual ground model in Figure 5-1, was to construct 2D geological profiles using ground investigation data proved in shallow boreholes.

Domain	**Domain Code**

description	Bedrock[1] Glaciated - Periglaciated	Bedrock_Quaternary[2] Glaciated-Periglaciated	Bedrock[1] Periglaciated	Bedrock_Quaternary[2] Periglaciated
Late Jurassic mudrocks (West Walton, Ampthill and Kimmeridge Clay Formations)	1.4	**1.4.1**	2.4	2.4.1
Late Jurassic mudrocks, sandstones (Kellaways and Oxford Clay formations)	**1.3**	**1.3.1**	**2.3**	2.3.1
Middle to Late Jurassic limestones, sandstones and mudrocks (Inferior and Great Oolite Groups)	1.2	**1.2.1**	2.2	2.2.1
Early to Middle Jurassic mudrocks (Lias Group)	1.1	**1.1.1**	2.1	2.1.1

Table 5-1 Quaternary Domains in north Buckinghamshire defined in this study. Highlighted Domain codes indicate those for which geotechnical samples were obtained either for till and/or Oxford Clay. **[1]** no Quaternary sediments overlying bedrock but may include unmapped 'head'. **[2]** no Quaternary sediments overlying bedrock but may include unmapped 'head', sediments may have previously been deposited but subsequently removed by erosion. **[3]** Quaternary sediments present overlying bedrock.

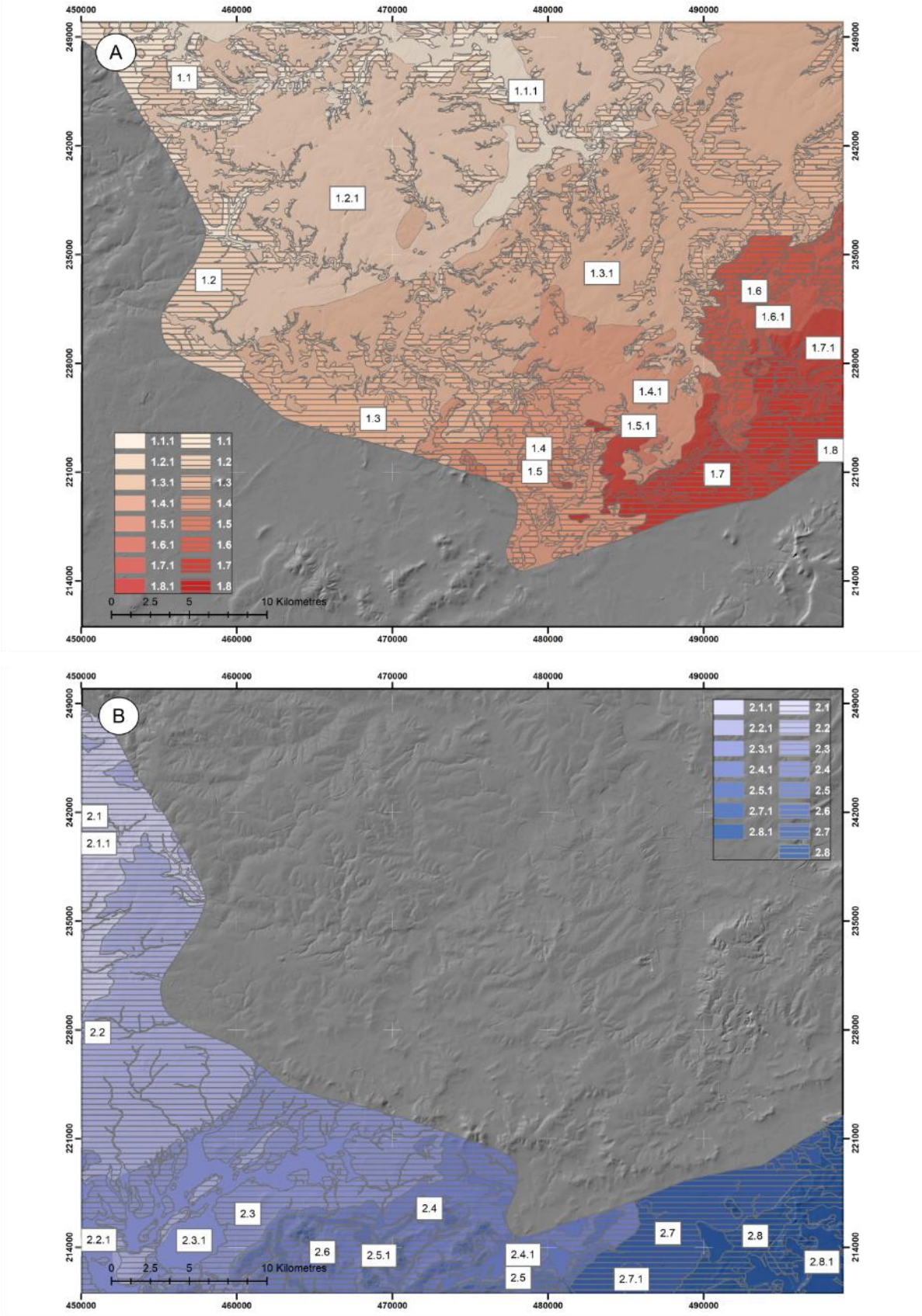

Figure 5-4 Quaternary Domains in north Buckinghamshire. A) Glaciated and periglaciated. B) periglacial, non-glaciated. Ordnance Survey Landform Profile 50 m resolution hillshade DTM © Crown Copyright and Database Right [2018].

5.2.2 2D geological profiles

SubsurfaceViewer®MX software was used to construct nine representative geological cross-sections in Buckingham. 5939 digital geological records from existing boreholes were available in the project area. Digital borehole data came from three main sources listed below:

1. The BGS's Single Onshore Borehole Index (SOBI) and Borehole Geology (BOGE) databases;
2. Manual borehole coding for this research;
3. Preliminary geological data from Network Rail's, East West Rail ground investigation project.

The location of these boreholes and their maximum depth of drilling is shown in Figure 5-5. Borehole records within the BGS's databases are compiled from a range of ground investigations, undertaken for different purposes and at different times. Because of this, the geological descriptions in the boreholes are of variable quality. In addition, the purpose of digital coding of borehole records undertaken by BGS, influenced the detail to which geological data was coded. For example, 50% of the available borehole data only codes the thickness of Quaternary sediments and depth to geological rockhead and contains no description or subdivision of Quaternary or bedrock layers.

Consequently, only boreholes data that were processed and coded by BGS for projects requiring geological subdivision and detailed coding were chosen for the construction of 2D geological profiles. Records derived from the BGS's National Geotechnical Properties Database (NGPD) and those records interpreted for recent BGS 3D geological modelling projects were prioritised for selection in Buckingham.

The uneven, spatial distribution of borehole records reflects the purpose for which they were drilled. Linear route ground investigation is reflected in schemes including East West Rail, upgrade of roads including the M40 and A43, and the construction of the new town of Milton Keynes in the 1960s. The borehole data is further limited by depth of drilling. 75% of the boreholes are <10 m in drilled length and 10% >20 m. To attempt to improve the distribution of records whose depth of drilling was >15 m, manual borehole data coding was undertaken for this research. 179 borehole records were coded. Digital coding of lithology was undertaken according to the primary, secondary and remaining components of each geological layer according to the scheme proposed by Cooper *et al*. (2006). The scheme is consistent with the recommendations of BS5930:1999+A2:2010 and based on codes representing the primary grain sizes of clay (C), silt (Z), sand (S), gravel (V), cobbles (L) and boulders (B).

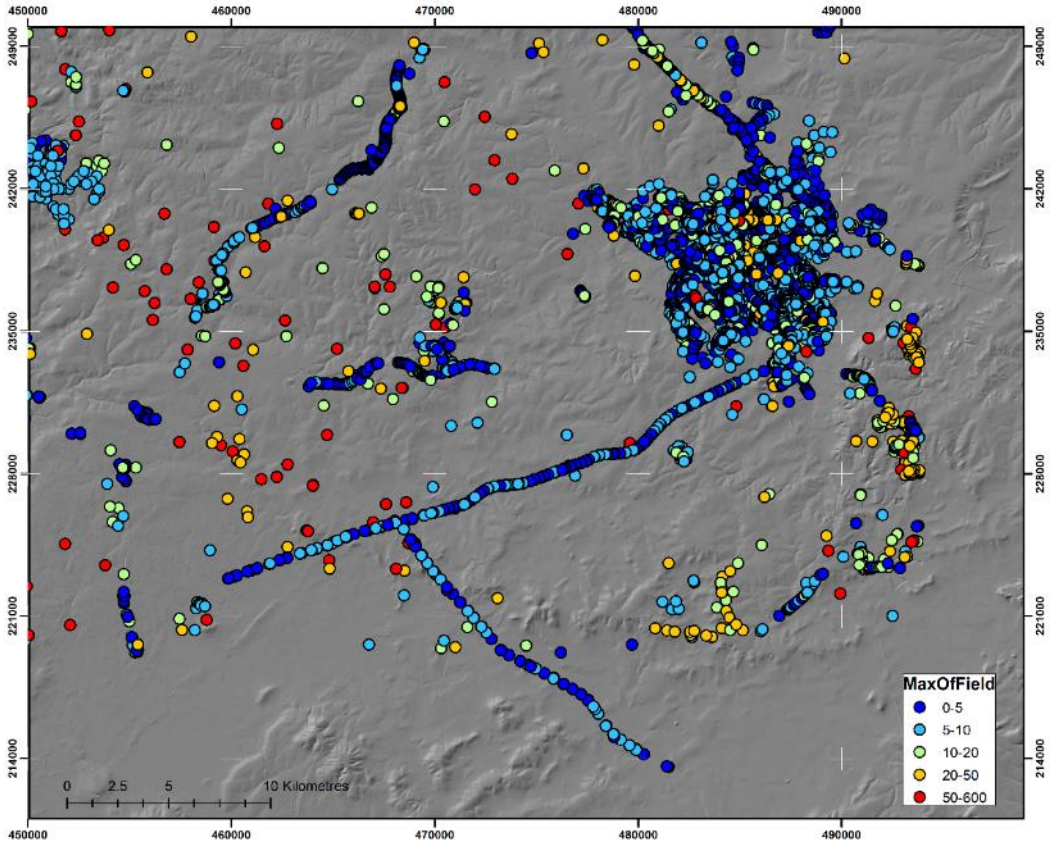

Figure 5-5 Location of borehole records with digital geological data classified according to their maximum depth of drilling (m). Ordnance Survey Landform Profile 50 m resolution hillshade DTM © Crown Copyright and Database Right [2018].

To create 2D geological profiles, SubsurfaceViewer®MX, requires project files that define the relative stratigraphical order of each geological layer, borehole location, downhole geological data and digital terrain model (DTM). A list of the files and their metadata is given in Table 5-2.

To develop the ground model, geological layers were correlated between boreholes based on their composition (lithology) and their interpreted lithogenetic classification. The legend for the correlated lithogenetic layers and the lithological data recorded in each borehole log is given in Figure 5-6 and used for each of the cross-section profiles shown in Figures 5-7 to 5-15.

File	Comment
DTM	Derived from Ordnance Survey 50 m resolution Landform Profile dataset. Accessed under licence from the EDINA Digimap service April 2015. ASCII format converted to TIN.

File	Comment
General Vertical Section (.gvs)	Created for Buckingham modified using the stratigraphy of Sumbler (2002), Barron et al., (2010) and Green, (1864).
Legend (.gleg)	Created for Buckingham using colours consistent with those on 1:50 000 scale geological maps (DigMapGB50).
DigMapGB50	ESRI shapefile of 1:50 000 bedrock, superficial, artificial and mass movement data.
Raster maps	Georegistered raster maps of 1:250 000 scale topography.

Table 5-2 SubsurfaceViewer®MX model files for north Buckinghamshire.

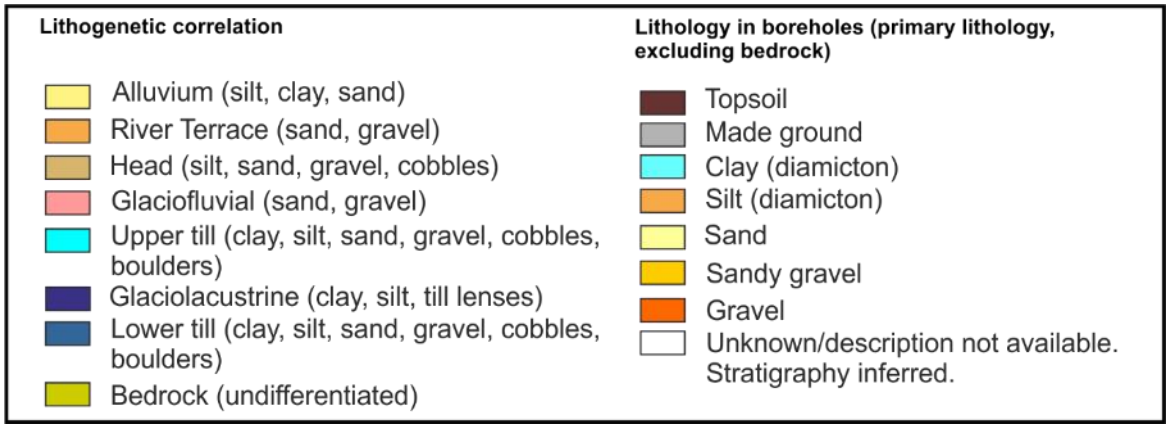

Figure 5-6 Legend for geological cross-section profiles.

5.2.2.1 Geological profile 1 (Quaternary Domains, QD 1.2 and 1.2.1)

Geological profile 1 is shown in Figure 5-7.

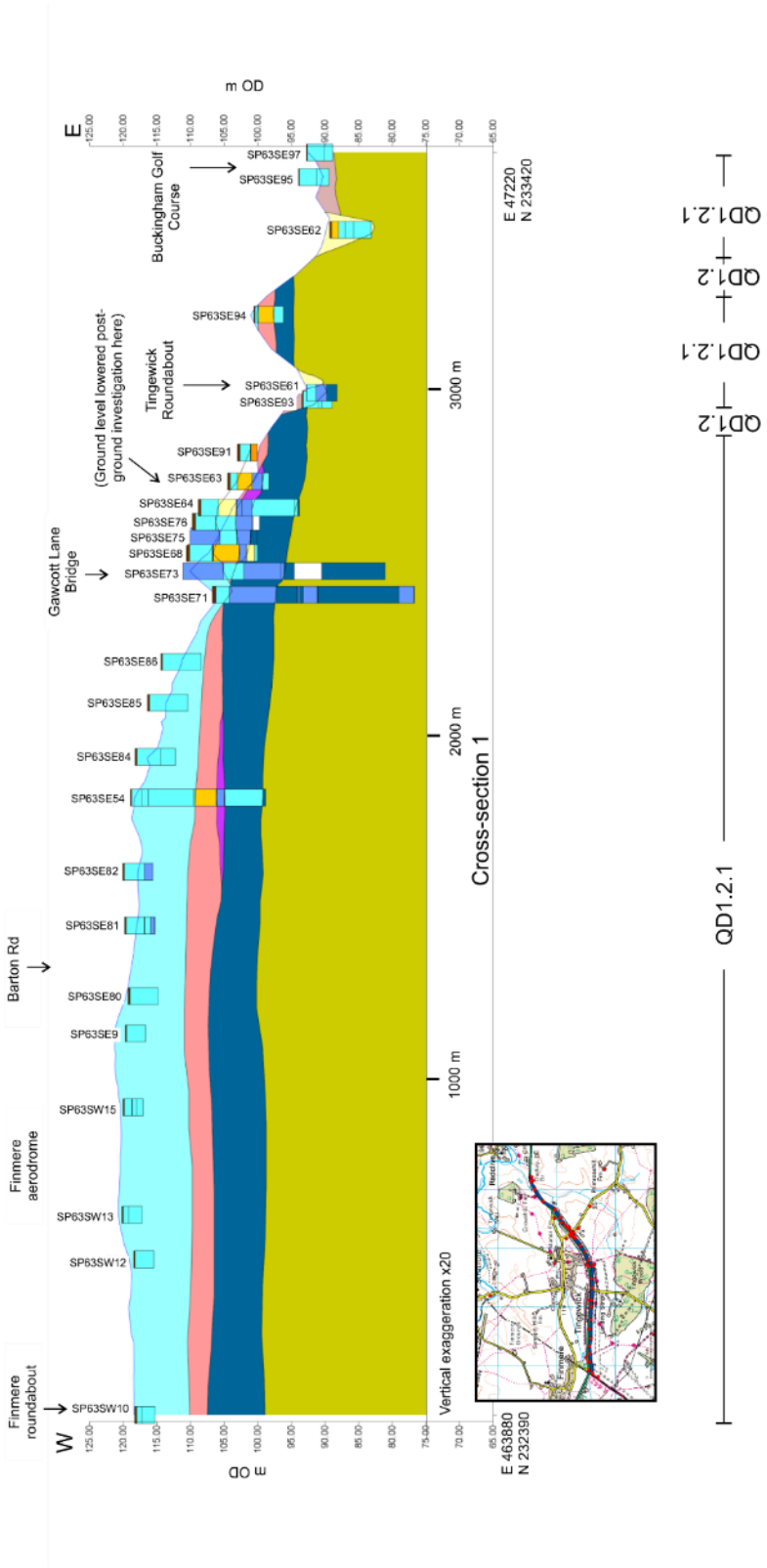

Figure 5-7 Geological profile 1, Tingewick. Legend shown in Figure 5-6. Ordnance Survey data © Crown Copyright and Database Right [2018]. Ordnance Survey (Digimap Licence).

Lithogenetic correlation and interpretation shows that the western part of Profile 1 is characterised by up to 20 m of glacigenic sediments preserved on the interfluves between the

present-day drainage system of the River Great Ouse. The contact between glacigenic sediments and underlying bedrock is interpreted to be uniform.

Glacigenic sediments comprises two distinct layers of till, separated by variably laminated and bedded sand and/or gravel. The upper till comprises fine to coarse gravel and cobbles of chalk, flint and limestone and its base elevation decreases towards the east. The lower till contains gravel of ‘Bunter’ quartzite, limestone and some chalk. The glacigenic sequence is incised to the east by tributaries of the River Great Ouse. It has also been partially removed during excavation for the new cutting in the A421, Tingewick By-pass.

5.2.2.2 Geological profile 2 (Quaternary Domains, QD 1.2, 1.3, 1.2.1 and 1.3.1)

Geological profile 2 is shown in Figure 5-8.

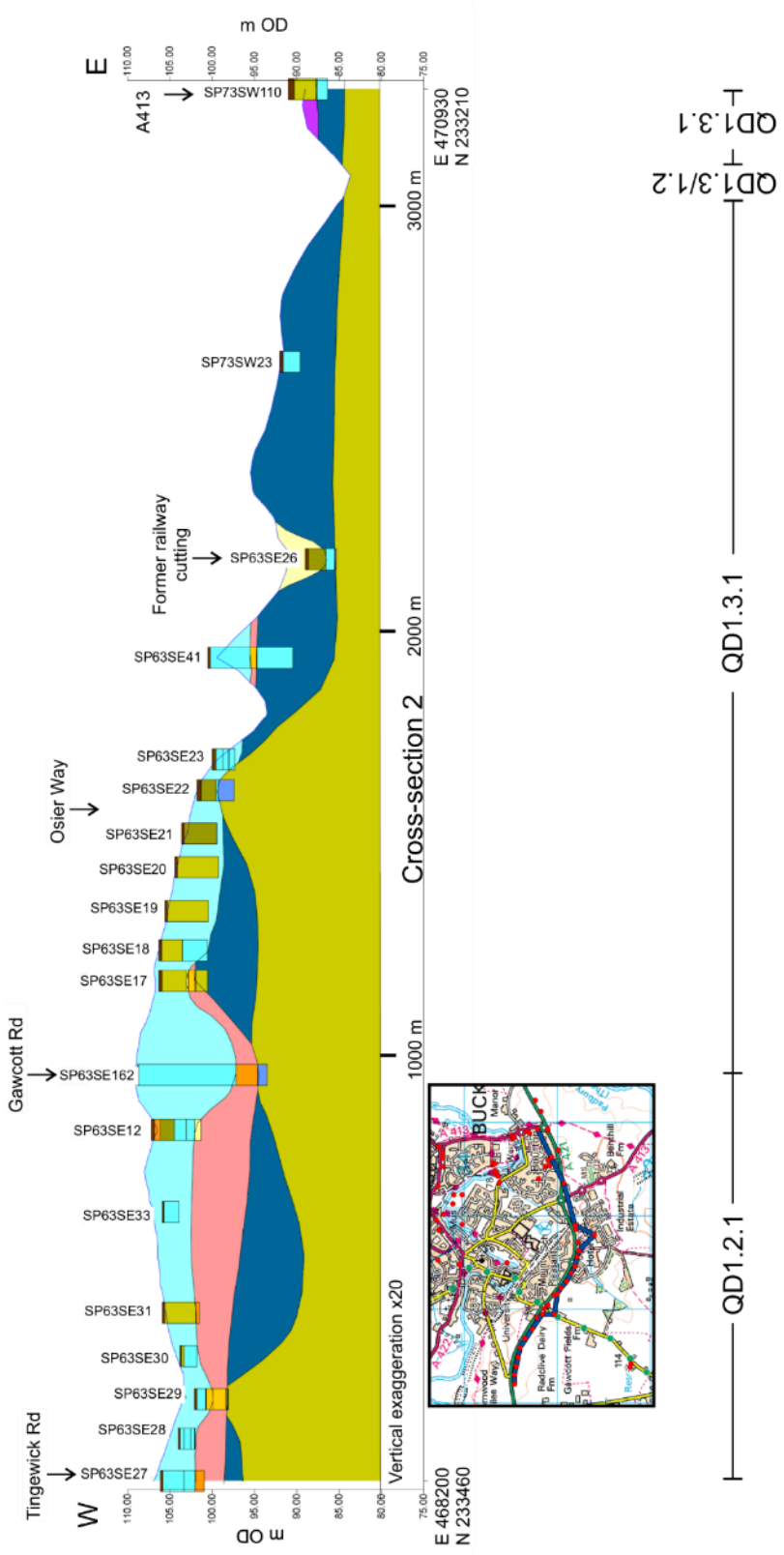

Figure 5-8 Geological profile 2, Buckingham By-pass. Legend shown in Figure 5-6. Ordnance Survey data © Crown Copyright and Database Right [2018]. Ordnance Survey (Digimap Licence).

Geological profile 2 is characterised in the west by glacigenic sediments overlying bedrock and which become incised by tributaries of the River Great Ouse to the east. The geometry of the contact between bedrock and overlying glacigenic sediment is unknown but interpreted to be undulating, and possibly channelized, based on the elevation of geological rockhead proved in boreholes.

The glacigenic sequence is interpreted to be characterised by two units of till separated by sand and/or gravel. The upper till comprises firm to stiff, matrix-supported silt and clay with fine to coarse gravel and cobbles of chalk, flint, limestone and sandstone. It is not present to the east where it was either not deposited or subsequently removed by erosion. Till exposed at the ground surface, to the east, is interpreted to be the lowermost till proved to the west.

5.2.2.3 Geological profile 3 (Quaternary Domains, QD 1.2.1 and 1.3.1)

Geological profile 3 is shown in Figure 5-9.

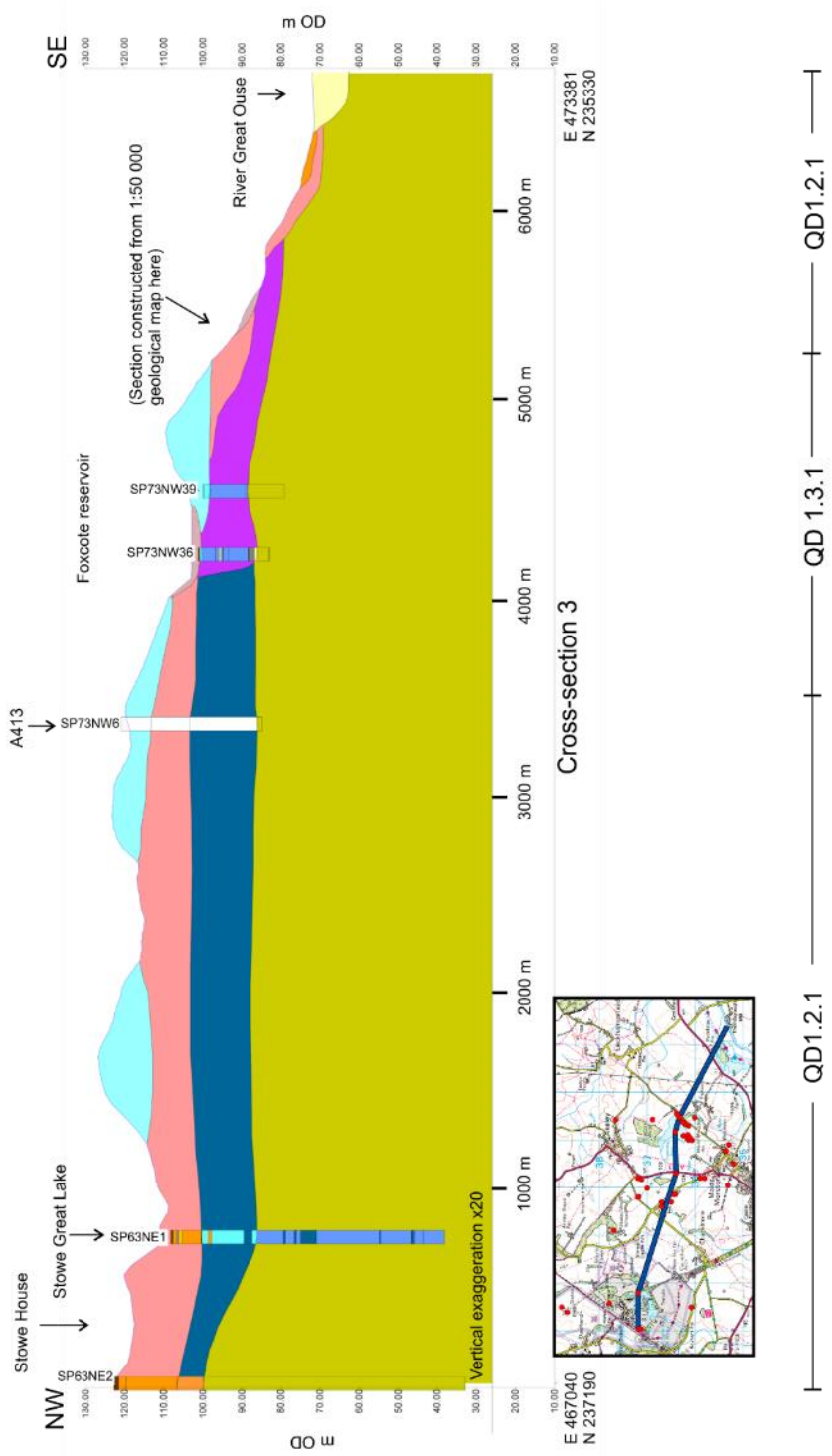

Figure 5-9 Geological profile 3, Stowe to Maids Moreton. Legend shown in Figure 5-6. Ordnance Survey data © Crown Copyright and Database Right [2018]. Ordnance Survey (Digimap Licence).

Probably interbedded sand and gravel, upto 15 m thick is proved to the west, making up much of the ground around Stowe House and school [SP 674 374]. Here, sand and gravel overlies till, which when traced southeastwards, is shown to correlate with the lower till identified in

geological profiles 1 and 2. In the area of Foxcote reservoir [SP 712 364], laminated clay, silt and sand is proved and is interpreted as glaciolacustrine. The nature of the contact between the glaciolacustrine sediments and lower till is uncertain but is interpreted to be erosional. Glaciolacustrine sediments therefore overlie and incised surface which may be the northwestern edge of the buried valley beneath the course of the River Great Ouse, proved in the BGS Deanshanger borehole (see Section 3.3.4.2).

5.2.2.4 Geological profile 4 (Quaternary Domains, QD 1.2.1 and 1.3.1)

Geological profile 4 is shown in Figure 5-10.

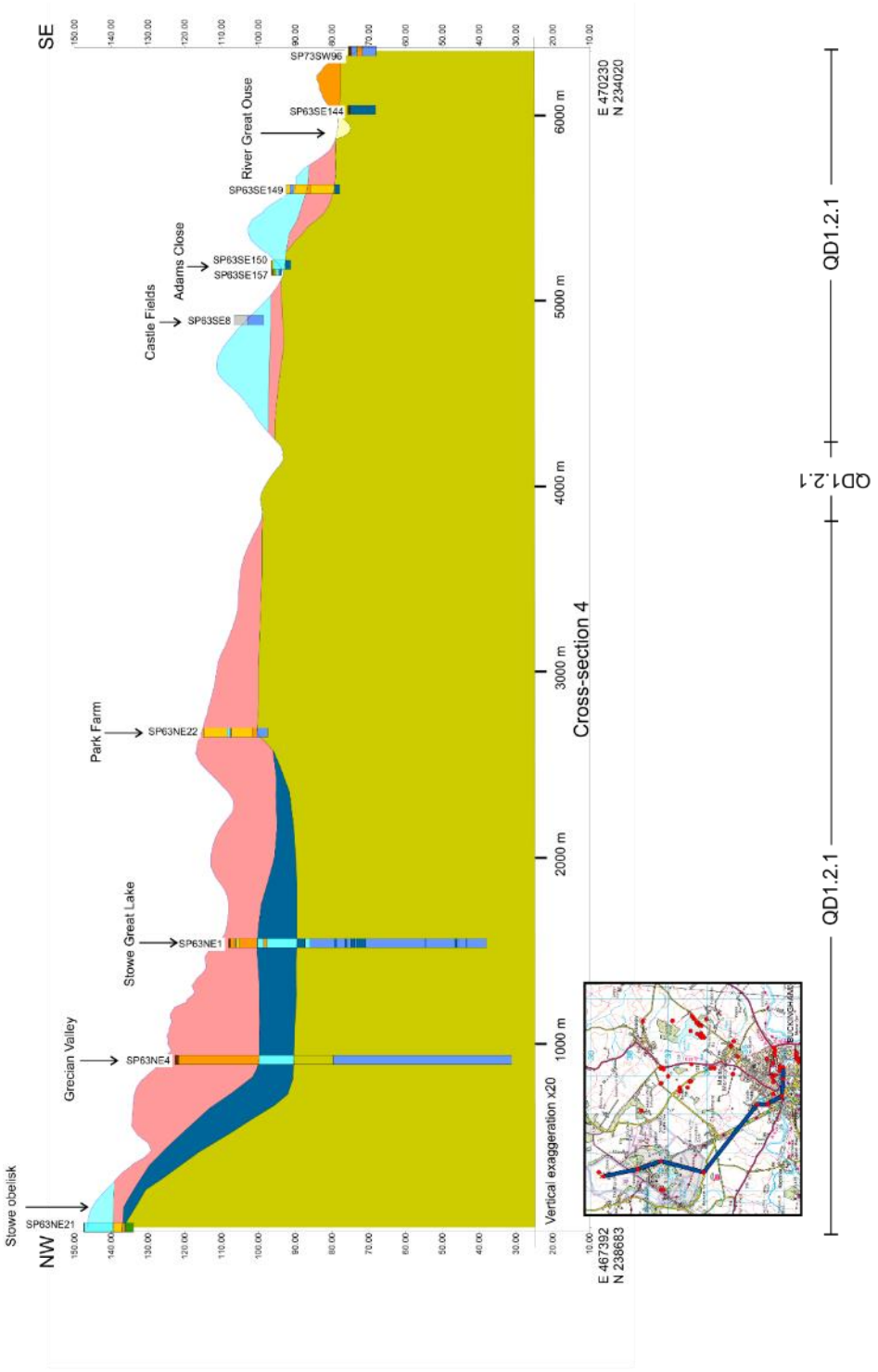

Figure 5-10 Geological profile 4, Stowe to Buckingham. Legend shown in Figure 5-6. Ordnance Survey data © Crown Copyright and Database Right [2018]. Ordnance Survey (Digimap Licence).

Glacigenic sediments comprising variably sandy and gravelly, matrix-supported clay and silt interpreted as till, overlain by sand and gravel, is proved around Stowe House to the northwest of the profile. The sediments here are interpreted to occupy a broad valley within

underlying bedrock, as proved by the elevation of bedrock recorded in boreholes SP 63NE21 and SP 63NE22.

Similar deposits of sand and gravel are proved in Buckingham [SP 696 340] where they are overlain by sediments interpreted as till. The till here comprises stiff, bluish-grey, matrix-supported gravel of chalk and flint. Gravels, probably associated with river terraces of the River Great Ouse, occur to the southeast of the section.

5.2.2.5 Geological profile 5 (Quaternary Domains, QD 1.2.1 and 1.3.1)

Geological profile 5 is shown in Figure 5-11.

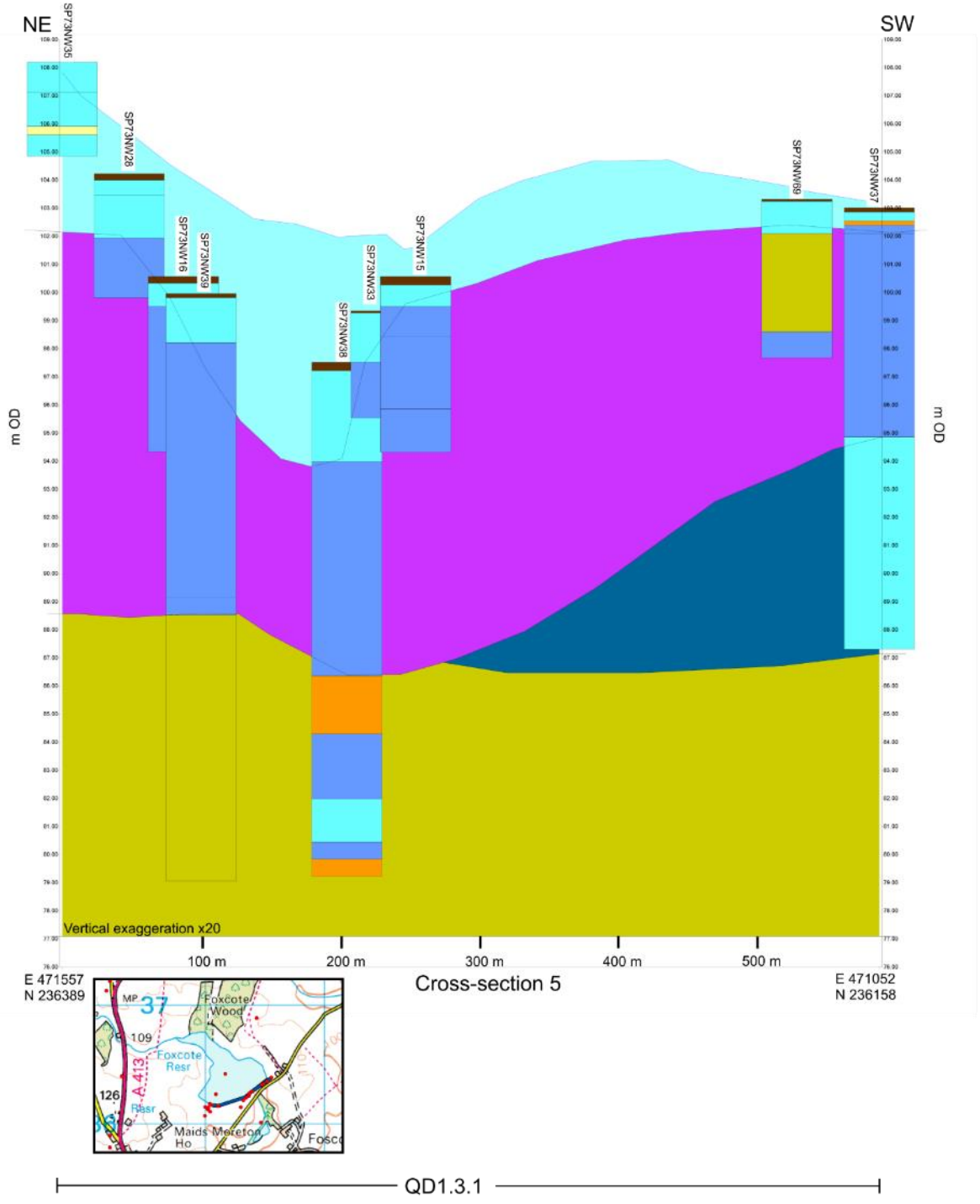

Figure 5-11 Geological profile 5, Foxcote Reservoir. Legend shown in Figure 5-6. Ordnance Survey data © Crown Copyright and Database Right [2018]. Ordnance Survey (Digimap Licence).

The geological profile at Foxcote reservoir proves upto 13 m of laminated silt and clay with some sand beds, interpreted as glaciolacustrine sediments. They are overlain by chalk-rich, matrix supported, variably sandy and gravelly silt and clay, interpreted as till. The decreasing

elevation of the base of the till between boreholes SP 73NW16 and SP73NW 15, suggests that the glaciolacustrine sediments may be incised.

Borehole SP 73NW37 demonstrates that glaciolacustrine sediments overlie a lower till. This till appears to occupy a low in underlying bedrock as it does not pass to the northeast.

5.2.2.6 Geological profile 6 (Quaternary Domains, QD 1.3, 1.3.1, 2.3 and 2.3.1)

Geological profile 6 is shown in Figure 5-12.

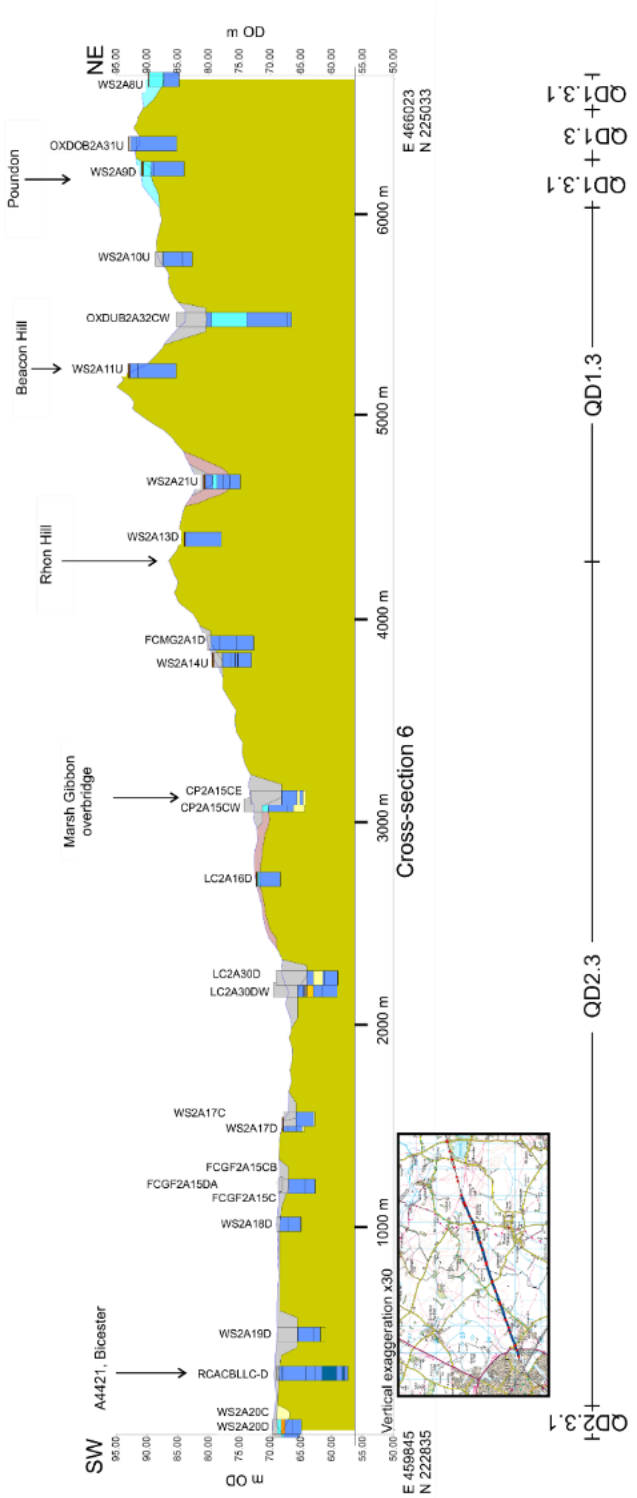

Figure 5-12 Geological profile 6, Bicester to Calvert. Legend shown in Figure 5-6. Ordnance Survey data © Crown Copyright and Database Right [2018]. Ordnance Survey (Digimap Licence).

The ridge around Poundon and Beacon Hill [SP 647 247] has been conventionally taken as the maximum extent of glacier ice in the region. Boreholes to the northeast prove thin (<5 m) chalk-rich till directly overlying bedrock. Glacigenic sediments appear to be absent southwest

of Beacon Hill. Small patches of sandy and gravelly silt and clay, interpreted as ‘head’, infill valleys and flank the tributaries of the River Ray, which flows southwest to drain into the River Cherwell around Islip [SP 523 137].

5.2.2.7 Geological profile 7 (Quaternary Domains, QD 1.3.1, 1.4.1 and 1.3)

Geological profile 7 is shown in Figure 5-13.

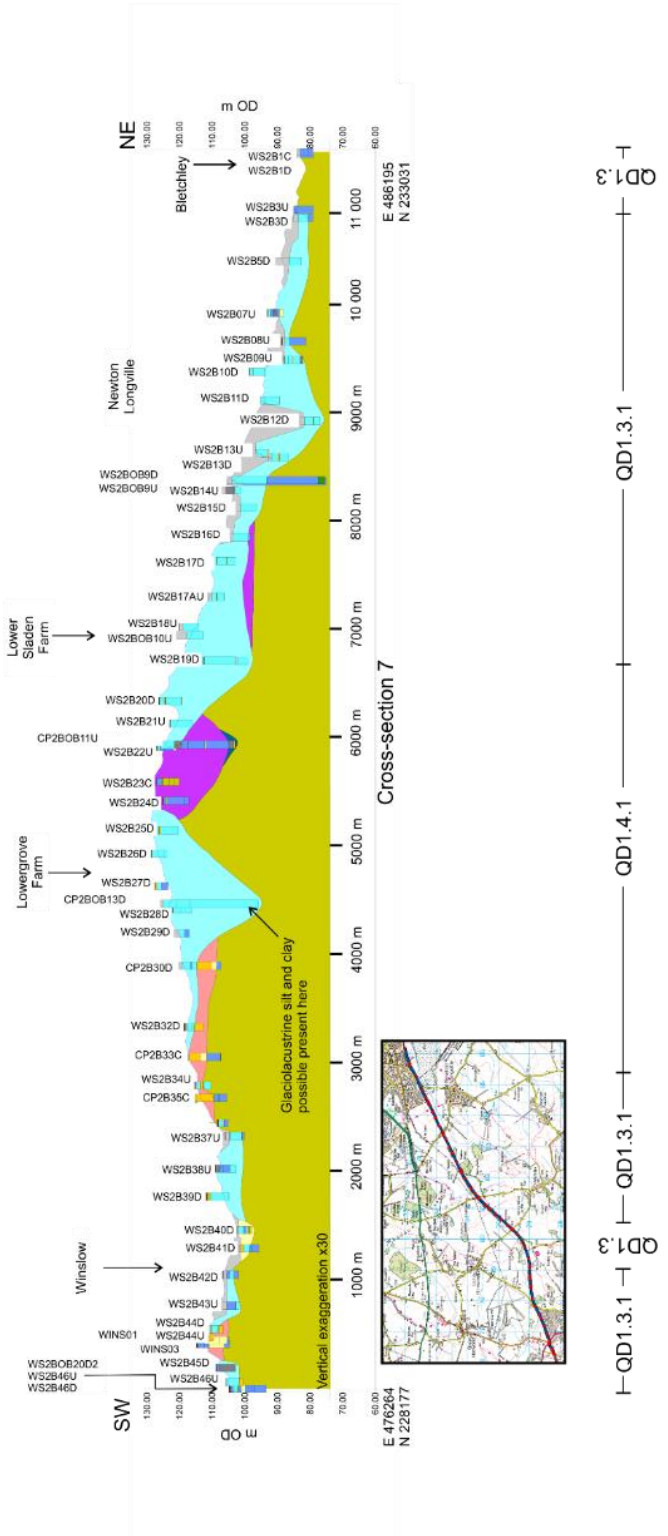

Figure 5-13 Geological profile 7, Winslow to Bletchley. Legend shown in Figure 5-6. Ordnance Survey data © Crown Copyright and Database Right [2018]. Ordnance Survey (Digimap Licence).

Thick (upto 40 m) glacigenic sediments overlie bedrock whose elevation varies between ~80 and 130 m aOD. The thickest glacigenic sediments occupy apparent valleys in the bedrock surface.

To the southwest, chalk-rich till variably overlies low-lying bedrock and sand and gravel. To the northeast, chalk-rich till either infills apparent valleys or caps glaciolacustrine sediments which in borehole CP2OB11U are ~15 m thick. Here till and glaciolacustrine sediments overlie a second till, which may either be equivalent to the lower till proved in profiles 1 and 2 or a second layer of chalk-rich till, interbedded with glaciolacustrine silt, clay and sand.

The base elevation of the chalk-rich till falls northeastwards from ~120 to 76 m aOD where it occupies a further valley feature in the bedrock surface.

5.2.2.8 Geological profile 8 (Quaternary Domains, QD 1.3 and 1.3.1)

Geological profile 8 is shown in Figure 5-14.

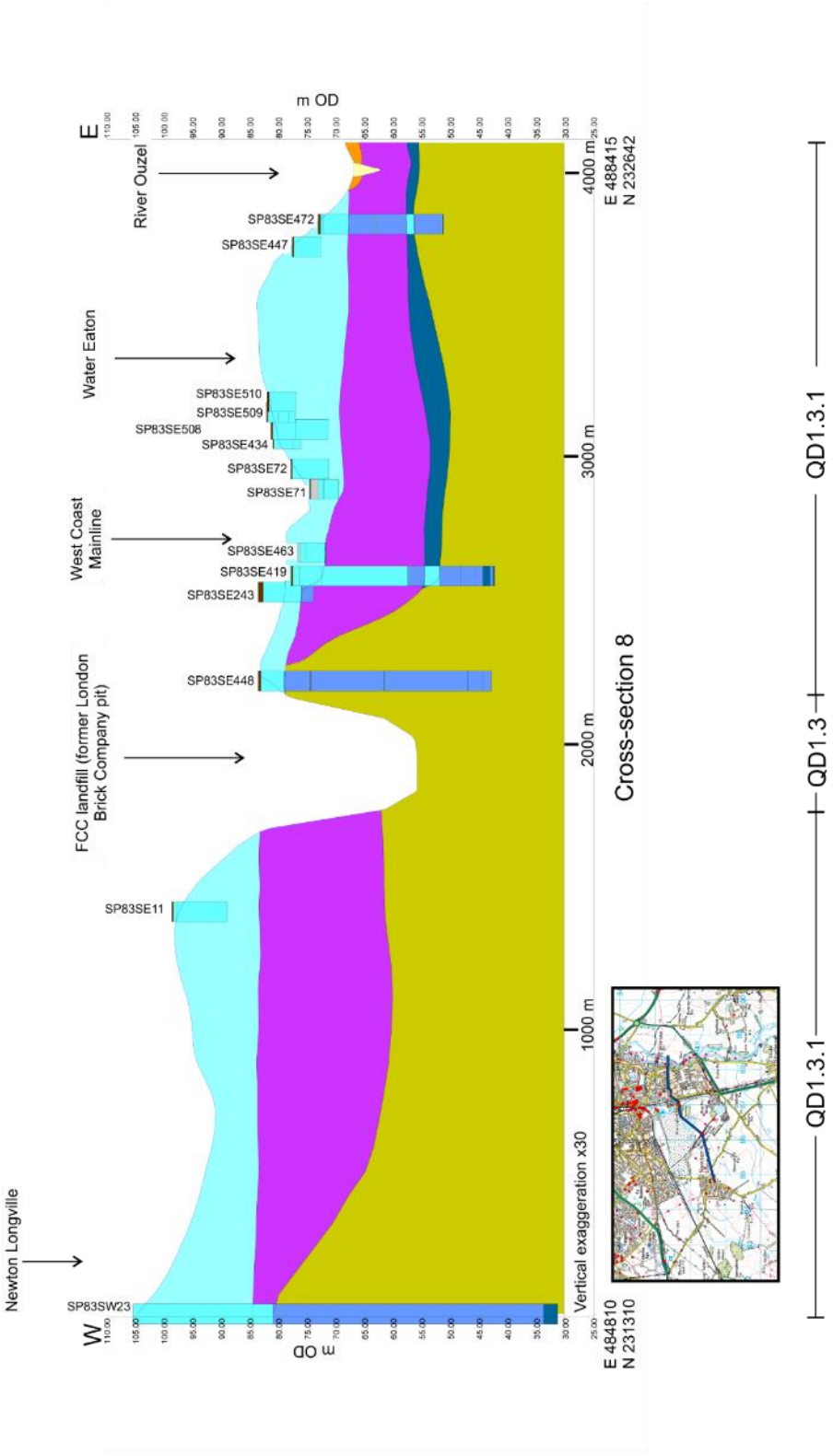

Figure 5-14 Geological profile 8, Bletchley and the River Ouzel. Legend shown in Figure 5-6. Ordnance Survey data © Crown Copyright and Database Right [2018]. Ordnance Survey (Digimap Licence).

Geological profile 8 partially crosses the former brick pit at Bletchley [SP 868 326] which is now a recycling and landfill site. The profile shows that thick (~12 m) glaciolacustrine sediments comprising laminated silt, clay and sand are present to the west and pass eastwards

beneath the current course of the River Ouzel. Here, they are overlain by chalk-rich, matrix-supported till. The glaciolacustrine sediments appear to infill a buried valley.

5.2.2.9 Geological profile 9 (Quaternary Domains, QD 1.3 and 1.3.1)

Geological profile 9 is shown in Figure 5-14.

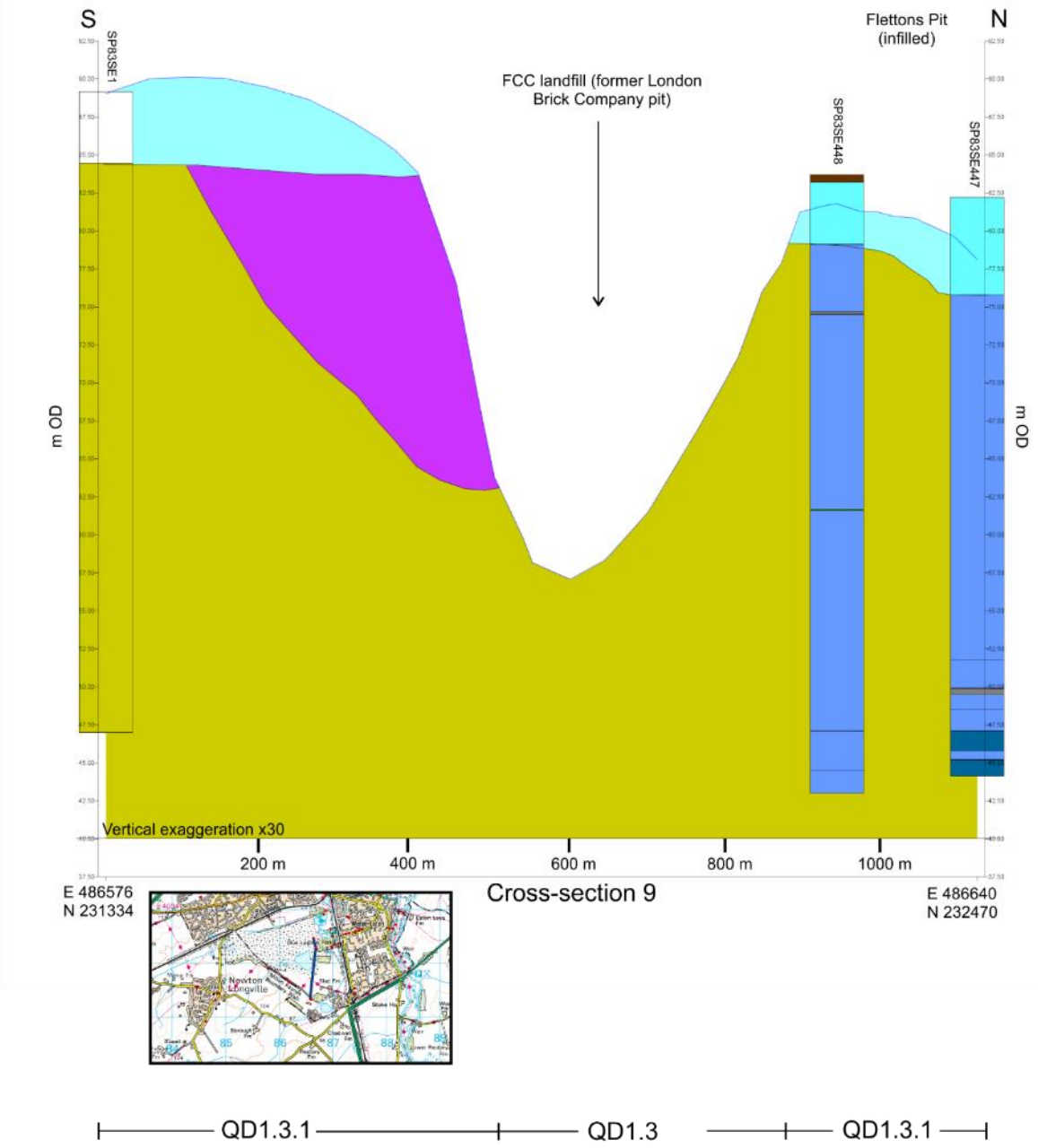

Figure 5-15 Geological profile 9, Bletchley. Legend shown in Figure 5-6. Ordnance Survey data © Crown Copyright and Database Right [2018]. Ordnance Survey (Digimap Licence).

Geological profile 9 sows that chalk-rich till overlies bedrock in the FCC landfill site. The presence of glaciolacustrine sediments is inferred from the 1:50 000 scale geological map.

6 Statistical analysis of regional geotechnical properties

To further investigate the validity of the Quaternary Domain approach, representative geotechnical parameters were investigated by comparing their values between each Domain. A geographical framework describing the variability in geotechnical properties and behaviour of till and Oxford Clay was established by designing and populating a relational database in Microsoft Access ™. The aim was to establish a statistical description and visualization of the variability in geotechnical parameters described by the spread of their values as quartile ranges about a median. The application of different statistical techniques to geotechnical data is discussed by Hallam (1990). In summarising an extensive literature review, Hallam concluded that non-parametric (rank) statistical analyses are appropriate for geotechnical data. This is based on the observation that geotechnical parameter values do not generally fit a 'normal' Gaussian distribution as the mean values within a population can be skewed by high values within the tails of their distribution. Therefore, parametric methods for statistical data exploration that assume a Gaussian distribution and can be defined by their mean and standard deviation, are not suitable for non-Gaussian geotechnical parameter analysis.

Non-parametric methods for data analysis do not assume any underlying distribution of data population. Hallam (1990), concluded that methods which rank data in numerical order and are then defined based on the proportion of data about a median value. This is defined based on the interquartile range (IQR) which represents the proportion of data between 25% and 75% of a population. A suitable of visualizing interquartile ranges is using Box and Whisker plots where the height of the boxes represents the IQR and the 'whiskers' represent the upper and lower quartiles (Figure 6-1). Data outliers are calculated from 1.5IQR. This approach, following that proposed by Hallam (1990) has been used extensively by the British Geological Survey to present geotechnical data variability for individual geological formations including the Mercia Mudstone Group, Lias Group and Lambeth Group (Hobbs *et al.*, 2012; Entwisle *et al.*, 2013).

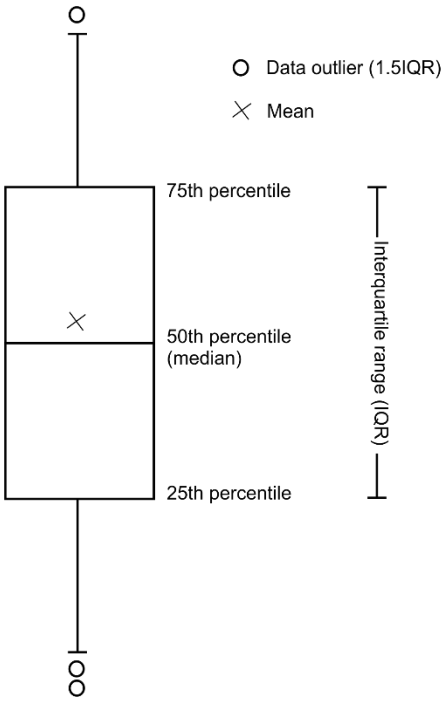

Figure 6-1 Definition of a Box and Whisker plot.

A similar approach is adopted here to describe the geographic spread of selected parameter values for till and Oxford Clay samples within the project area and to determine representative upper- and lower-bound values within each of the Quaternary Domains defined in Section 5. The IQR is shown in all Box and Whisker plots where the minimum number of data is >5. An extend box plot can be used where additional percentiles corresponding to 0.5%, 2.5%, 5%, and 10% are plotted (Hallam, 1990). These values are not plotted here but are summarised in associated tables for each parameter. The number of percentile divisions is given based on the number of data available. Where n >500, all are plotted, where n >100<499, the 0.5 percentile is omitted and where n >25<99, the 05 and 2.5 percentiles are omitted.

Two limitations of Box and Whisker plots identified by Hallam (1990) are:

1. Calculation of outlier values using 1.5IQR. Data points lying within the tails of a population of a geotechnical parameter may be valid and significant and should not treated as outliers. Therefore, the method of outlier calculation may be too simplistic. In this research, all outlier values are presented.
2. The conventional Box and Whiskers plot gives no information in the tail areas. The software used for this research did not allow further percentiles to be included, but they are presented as tabulated data instead.

6.1 Geotechnical database

It is assumed that any geotechnical parameter value is a true reflection of the natural state and/or behaviour of the soil being sampled. It is hoped that any variation within and between parameters represents their natural variability. However, it is likely that all soil samples are, to some extent, affected by processes which may change their natural state. It is important to note the limitations and potential influences on individual parameter values derived from existing laboratory tests and which are used in the project database. The following is based in part on that discussed by Hallam (1990).

- Data are derived from laboratory results associated with ground investigations of different ages, undertaken by different consultants and contractors and for different purposes. Variability in consistency of testing methods, standards and quality is likely to be reflected in the dataset. This applies even to index level tests as reported recently in a survey which compared the results of determinations for liquid limit, plastic limit and particle size (Anonymous, 2018). In this survey, reported values for liquid limit for example, taken from the same soil, varied between 48% and 57%.
- Natural variability. Variability results from the geological history of the soil and natural geological and hydrogeological changes, including effective stress and groundwater. It is this that it is hoped can be distinguished and accounted for.
- Sampling and handling. Extracting a soil sample from the ground and then packing, transporting and preparing it for analysis, all have the potential to change the natural, *in situ* state of the sample.
- Testing. Undertaking the test itself, carrying specimens between a preparation bench and the apparatus, leaving specimens uncovered, loading specimens, may introduce random and systematic errors into the results of the test.
- Data transfer. Despite the introduction of standards for the digital collection and transfer of geotechnical data, errors of data entry may persist.
- Geological interpretation. Grouping specimen data for analysis relies on their geological interpretation so that similar engineering geological units can be compared. This is often subjective and so mistakes and bias may influence the geological interpretation of any one specimen.

As a result, the data presented here are used to provide a regional synthesis of geotechnical property and behaviour variability, against which the results of laboratory experiments can be compared. The intention is to provide summary statistics and it is not intended that they are used design-specific values.

6.1.1 Sources of geotechnical data

Geotechnical data is sourced from ground investigations related principally to linear route infrastructure, earthworks and works for housing, including the development of the new town of Milton Keynes. The data is therefore either spatially clustered or spread along narrow, linear routes. As a result, no attempt has been made to apply geostatistical methods of analysis.

Data within the BGS's National Geotechnical Database (NGPD) was provided for the project for the geographic extent shown in Figure 1-1. Data within the NGPD is collected and processed by BGS to be compatible with the Association of Geotechnical and Geoenvironmental Specialist's (AGS) electronic data transfer format for digital geotechnical and environmental data (Associaiton of Geotechncial and Geoenvironmental Specilaists, 2004). Data is either processed and imported directly from AGS format files, or manually interpreted from reports describing the results of laboratory analyses (Self *et al.*, 2012).

The structure of the NGPD was modified to build a project-specific relational database whose structure is shown in Figure 6-2. Only those geotechnical parameters shown in Figure 6-1 were chosen for analysis. A unique identifier is used for each borehole and sample and used as a primary key to link all tables. Additional data was acquired and used to supplement the NGPD. Geotechnical data derived from Network Rail's East West Rail ground investigation and FCC Environment's Energy From Waste (EFW) scheme was identified and processed. Provisional EWR ground investigation data was received in AGS Version 3.1 and Energy From Waste data was received as hard copy reports from which digital data was manually input into the database. In total, an additional 5150 samples were added from these two ground investigations.

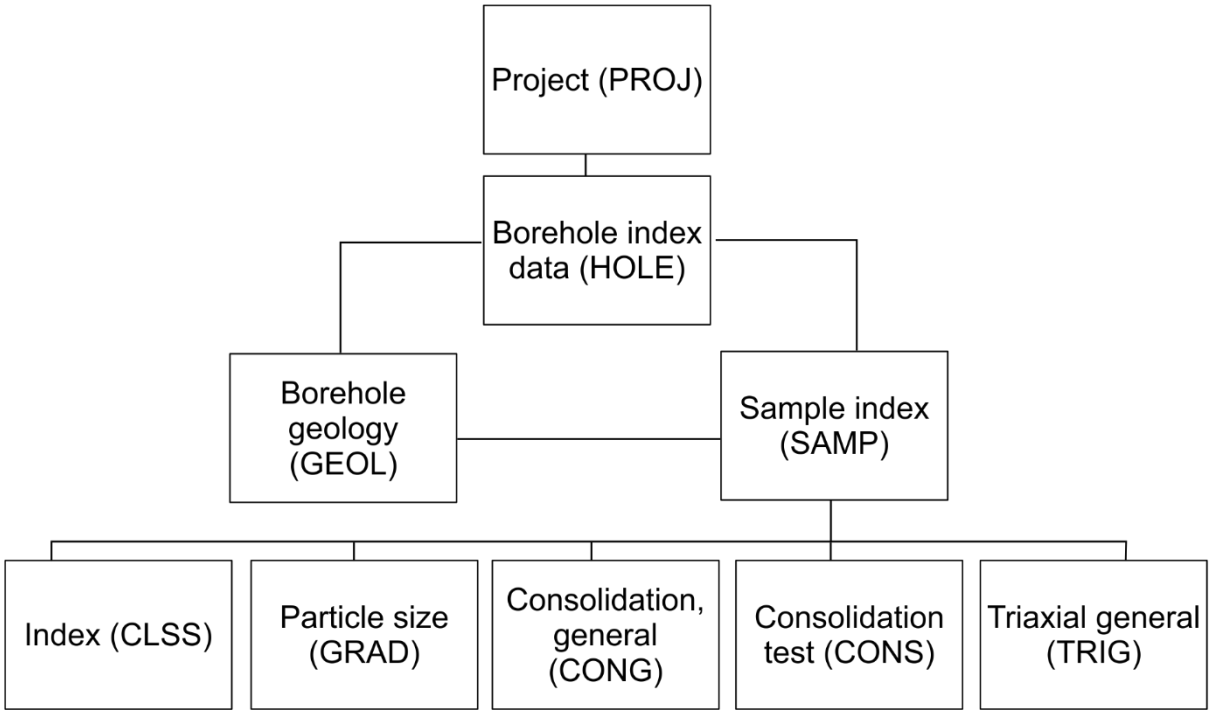

Figure 6-2 Structure of the north Buckinghamshire geotechnical database. Abbreviations in parantheses corresponds to AGS group names.

6.2 Data analysis

Geotechnical data are subdivided based on the Quaternary Domains defined in Section 5 and according to geological unit. The Oxford Clay is analysed at formation level and has not been subdivided according to Member status. Not all Quaternary Domains are represented in each class of geotechnical data if the number of data was <5. The geographic location of geotechnical samples within the project database is shown in Figure 6-3.

There are 8554 records that contain at least one value for values of liquid limit (W_L), plastic limit (W_P) or moisture content (ω) for all geological units in the database. Records without values for either liquid limit or plastic limit and non-plastic samples were excluded from the analysis of those parameters. Values for plasticity index (I_p) and liquidity index (LI) were calculated according to the equations described in Section 2.2.3. Records without measured moisture content values were excluded from the calculation of liquidity index.

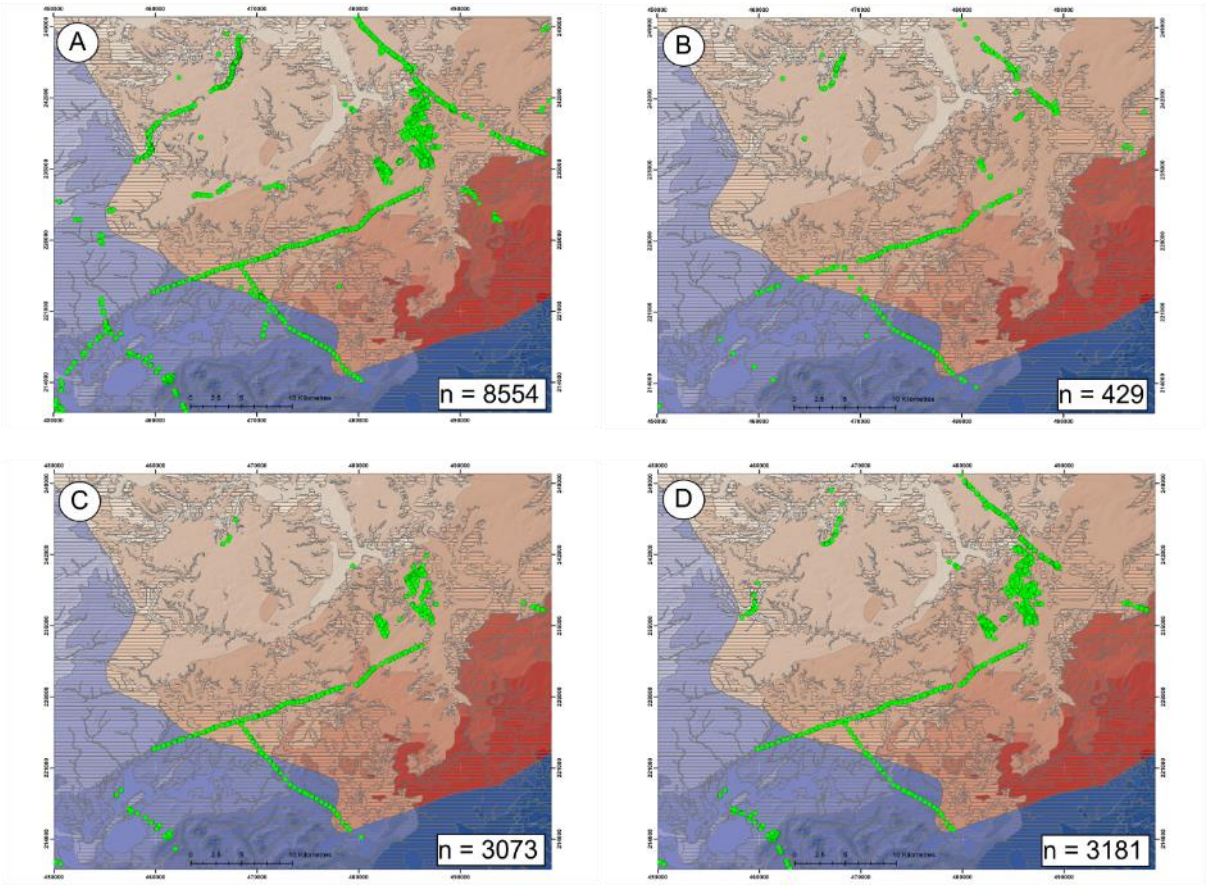

Figure 6-3 Location of geotechnical sample records with at least one record for each class of data prior to analysis by domains classification. A) CLSS (plasticity, moisture content). B) GRAD (particle size grading). C) CONS (consolidation test). CONG (consolidation general not plotted as it duplicates CONS locations). D) TRIG (undrained shear strength parameters from triaxial tests). Legend for Quaternary Domains as in Figure 5-3.

6.2.1 Atterberg limits and moisture content (till)

The analyses of plasticity for all data are shown on Casagrande plots as W_L *versus* I_P in Figure 6-4 and subdivided for each Quaternary Domain in Figures 6-5 and 6-6.

The analysis shows that tills are generally low to intermediate, and exceptionally high to very high plasticity. The possible effects of bedrock type are illustrated when the data are plotted according to Domain type. Tills in Domain 1.2.1 plot above the T-line of Boulton & Paul (1976) and with one exception, plot above the A-line. Tills in Domain 1.3.1 are spread above and below the T-line and generally above the A-line. In contrast, tills in Domain 1.4.1 generally plot below the T-line.

Non-parametric analysis of the data using Box and Whisker plots are shown in Figures 6-7 to 6-11 and Tables 6-1 to 6-5.

Median values for liquid limit are between 40% and 50% but greater variation is seen in values for plastic limit whose median values range between 16 and 20. The variability in

plastic limit accounts for the corresponding variation in plasticity index whose median values are between 19% and 20% in Domains 1.4.1 and 1.3.1 compared to 16% and 18% in 1.2.1 and 1.6.1. This variability is interpreted to be a result of the presence of a greater proportion of granular material derived from underlying bedrock in Domains 1.2.1 and 1.6.1, lowering the plastic limit. In contrast, Domains 1.3.1 and 1.4.1 are underlain by clay- and silt-rich mudrocks and so their plastic limit is higher.

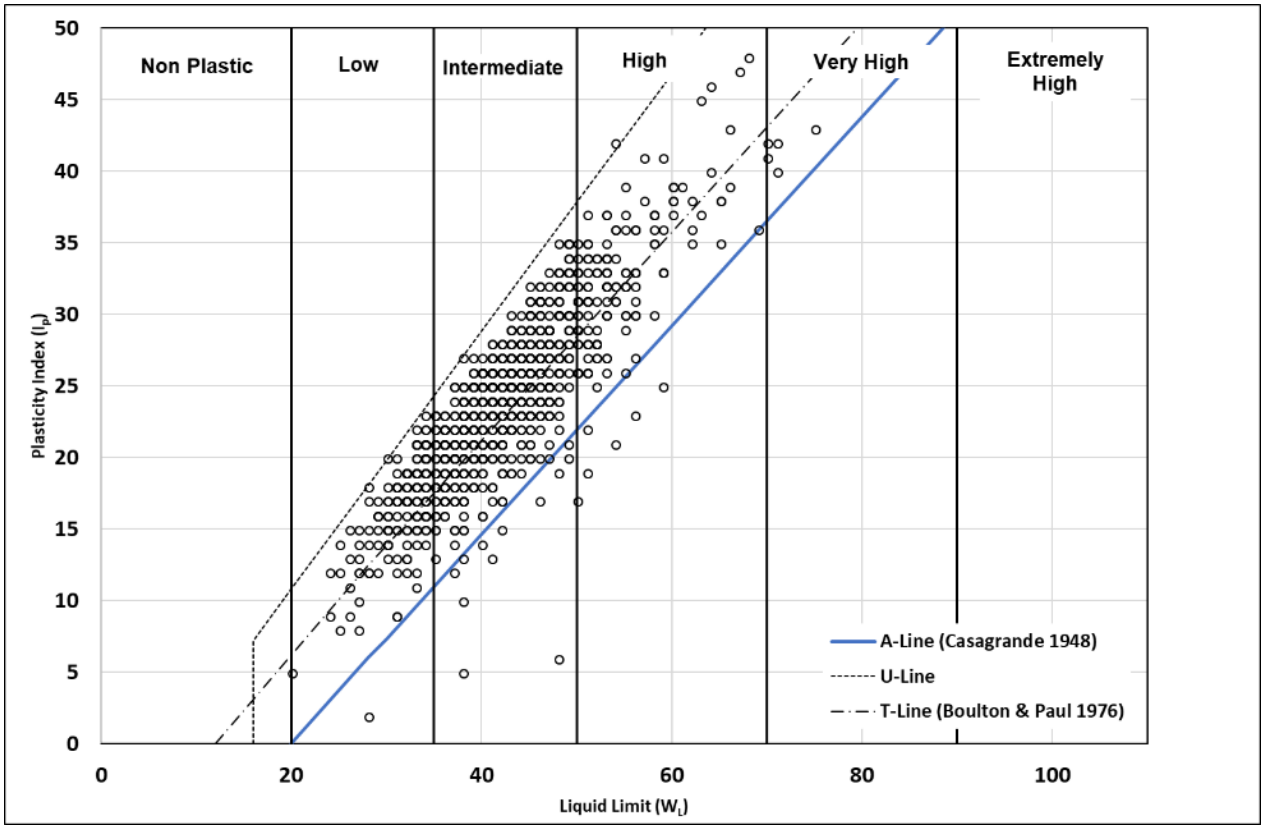

Figure 6-4 Plasticity plot for till, all Domains.

Median values for moisture content are 17% or 18% so that moisture content values plot close to the plastic limit values across all Domains. This is reflected in the ranges of values for liquidity index, where values lie close to 0 suggesting that the state of most of the till samples are close to their plastic limits.

To investigate the effects of depth on moisture content and plasticity values, depth plots are shown in Figure 6-12. Although there is scatter in the data, changes with depth are noticeable. Values for plastic and liquid limit decrease to ~2 mbgl, before reaching lower bound values with less scatter below ~5 mbgl. This may reflect the depth of weathering within the till but it is unlikely that depth of weathering in a glacial soil subjected to subsequent periglacial weathering shows a simple increasing depth-decreasing weathering profile.

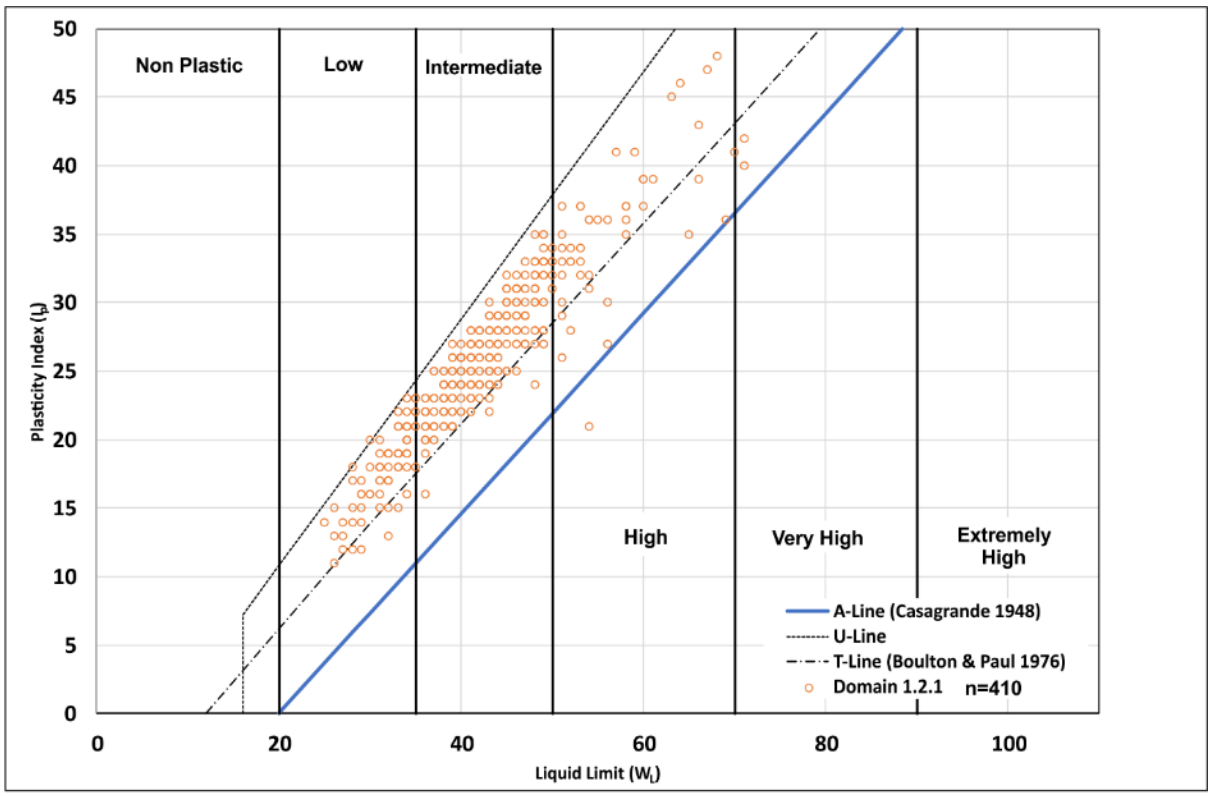

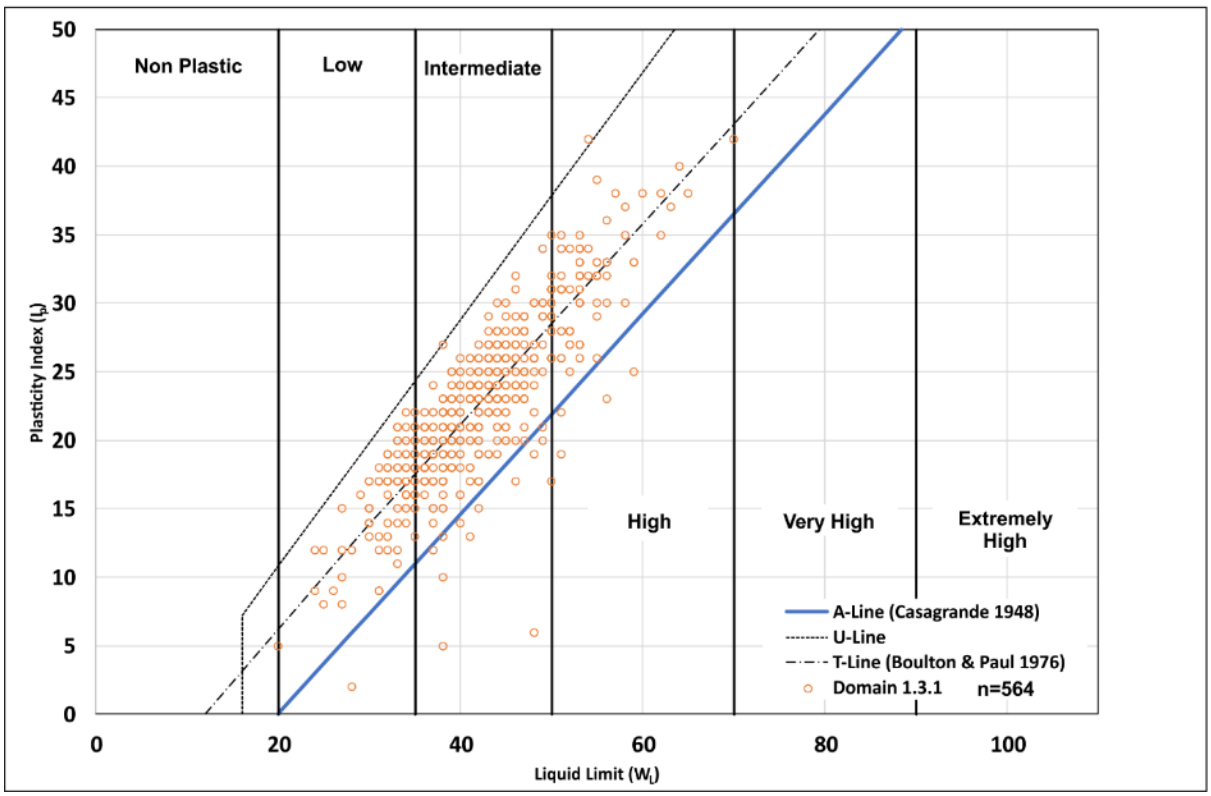

Figure 6-5 Plasticity plot, Domains 1.2.1 and 1.3.1, till.

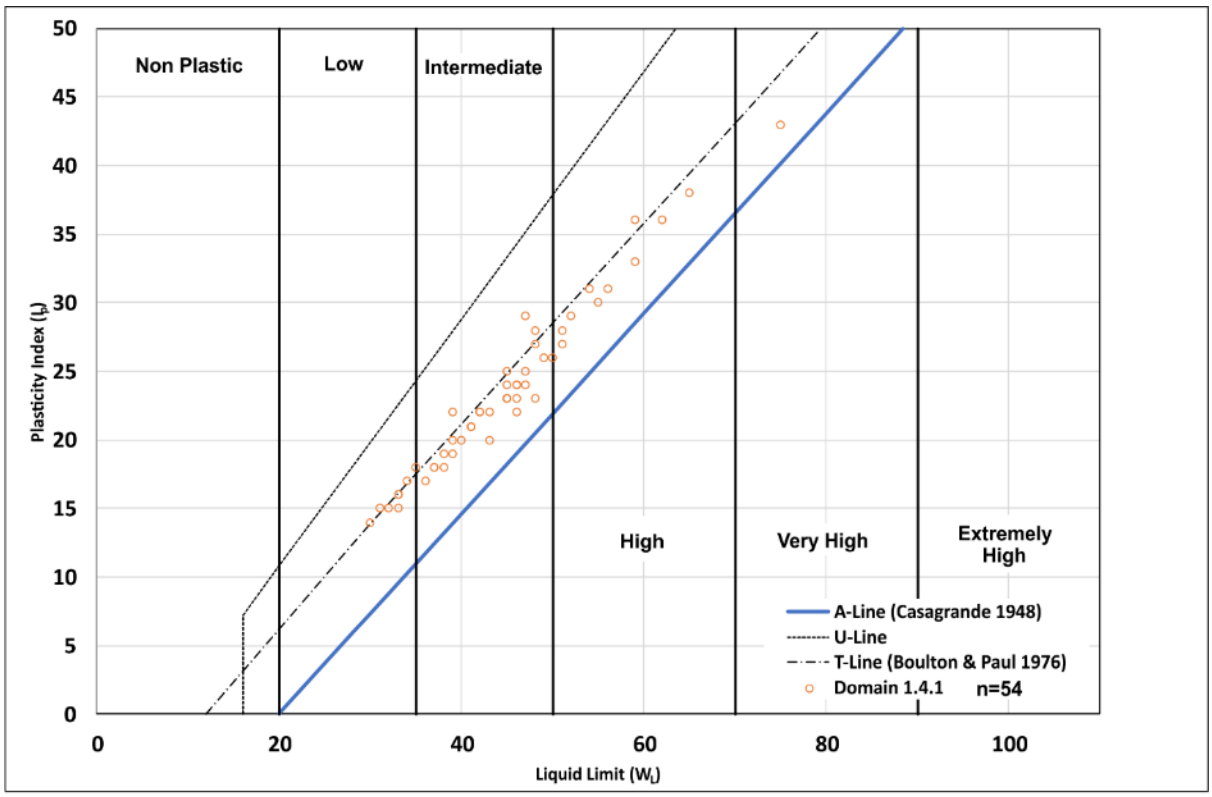

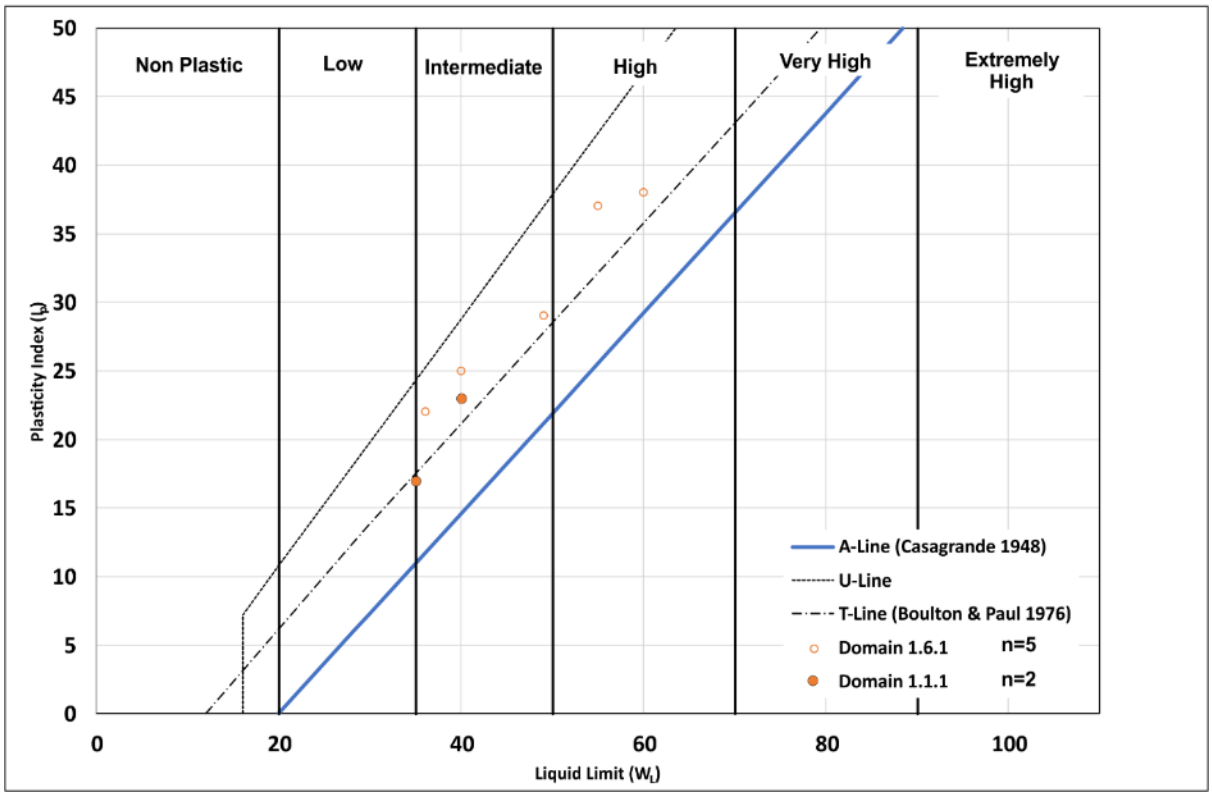

Figure 6-6 Plasticity plot, Domains 1.1.1, 1.4.1 and 1.6.1, till.

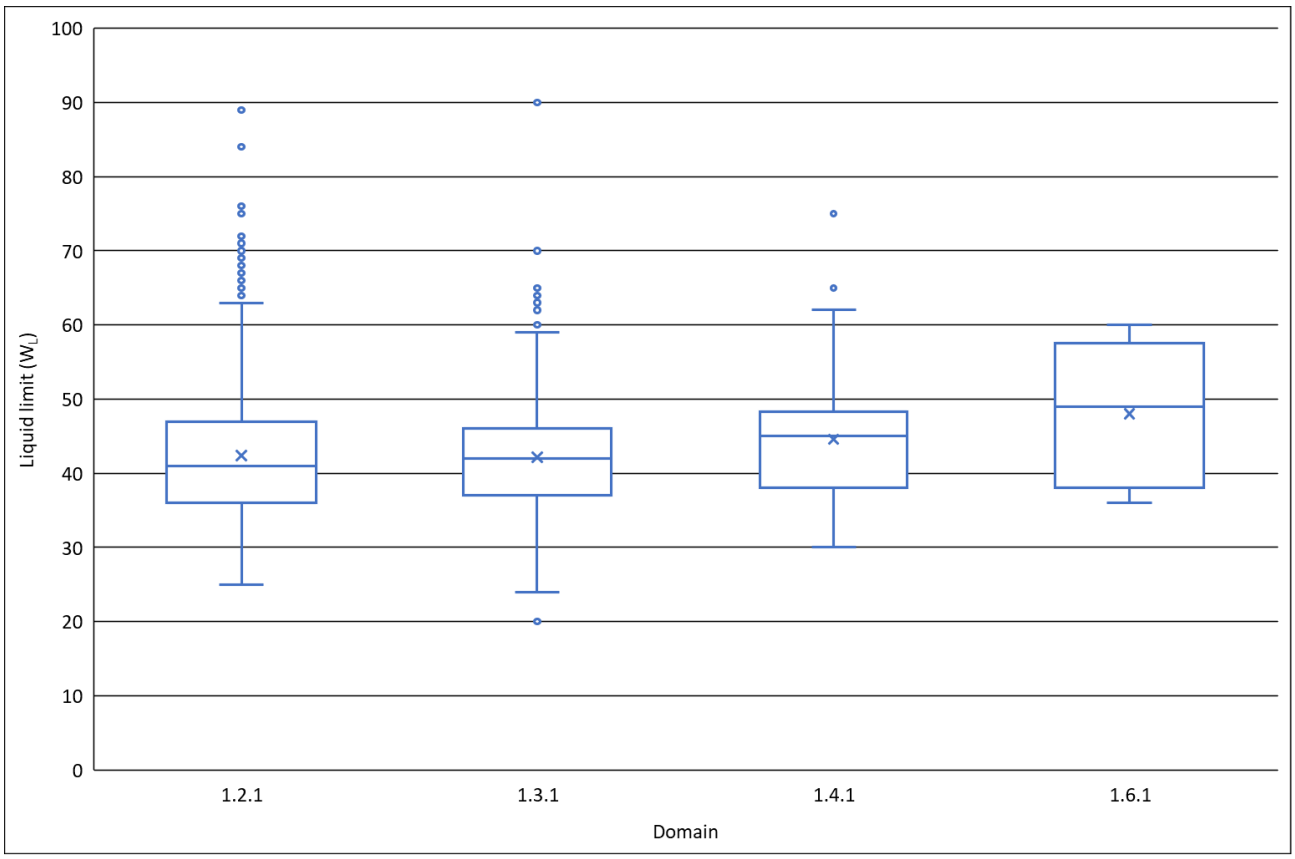

Figure 6-7 Box and Whisker plot for values of liquid limit, till.

Liquid Limit (W_L)					
	Domain 1.1.1	**Domain 1.2.1**	**Domain 1.3.1**	**Domain 1.4.1**	**Domain 1.6.1**
Maximum	NA	89	90	75	60
99.5	NA	NA	64	NA	NA
97.5	NA	67	57	NA	NA
90	NA	52	52	56	NA
75	NA	47	46	48	NA
50	NA	41	42	45	29
25	NA	36	37	38	NA
10	NA	32	33	33	NA
2.5	NA	28	30	NA	NA
0.5	NA	NA	25	NA	NA
Minimum	NA	25	20	30	36
n	2	411	564	54	5

Table 6-1 Percentile ranges for liquid limit, till. NA = range not calculated based on number of data.

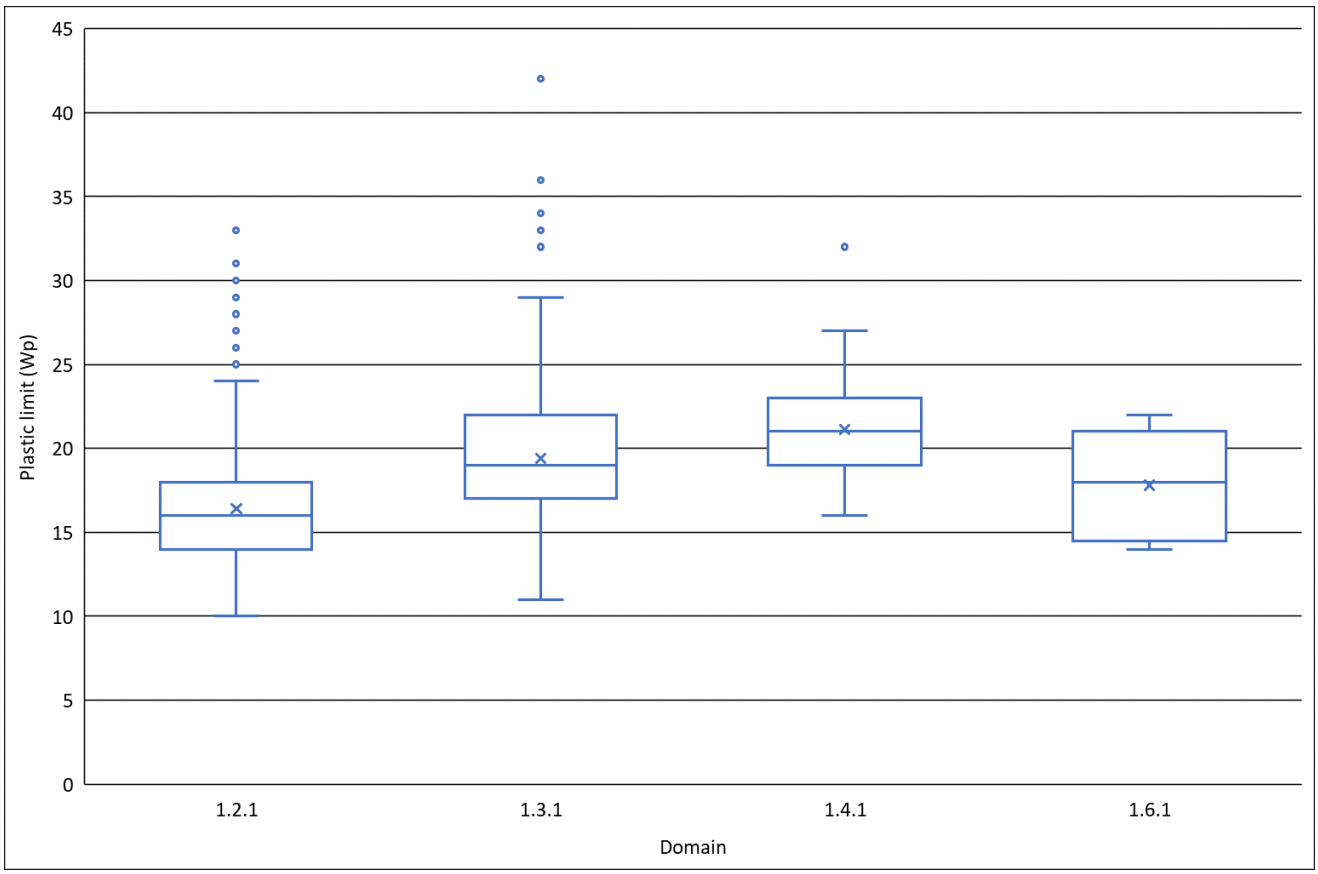

Figure 6-8 Box and Whisker plot for values of plastic limit, till.

Plastic Limit (W_P)					
	Domain 1.1.1	**Domain 1.2.1**	**Domain 1.3.1**	**Domain 1.4.1**	**Domain 1.6.1**
Maximum	NA	33	42	32	22
99.5	NA	NA	33	NA	NA
97.5	NA	26	28	NA	NA
90	NA	20	24	25	NA
75	NA	18	22	23	NA
50	NA	16	19	21	18
25	NA	14	17	19	NA
10	NA	10	15	17	NA
2.5	NA	12	13	NA	NA
0.5	NA	NA	12	NA	NA
Minimum	NA	10	11	32	14
n	2	410	564	54	5

Table 6-2 Percentile ranges for plastic limit, till. NA = range not calculated based on number of data.

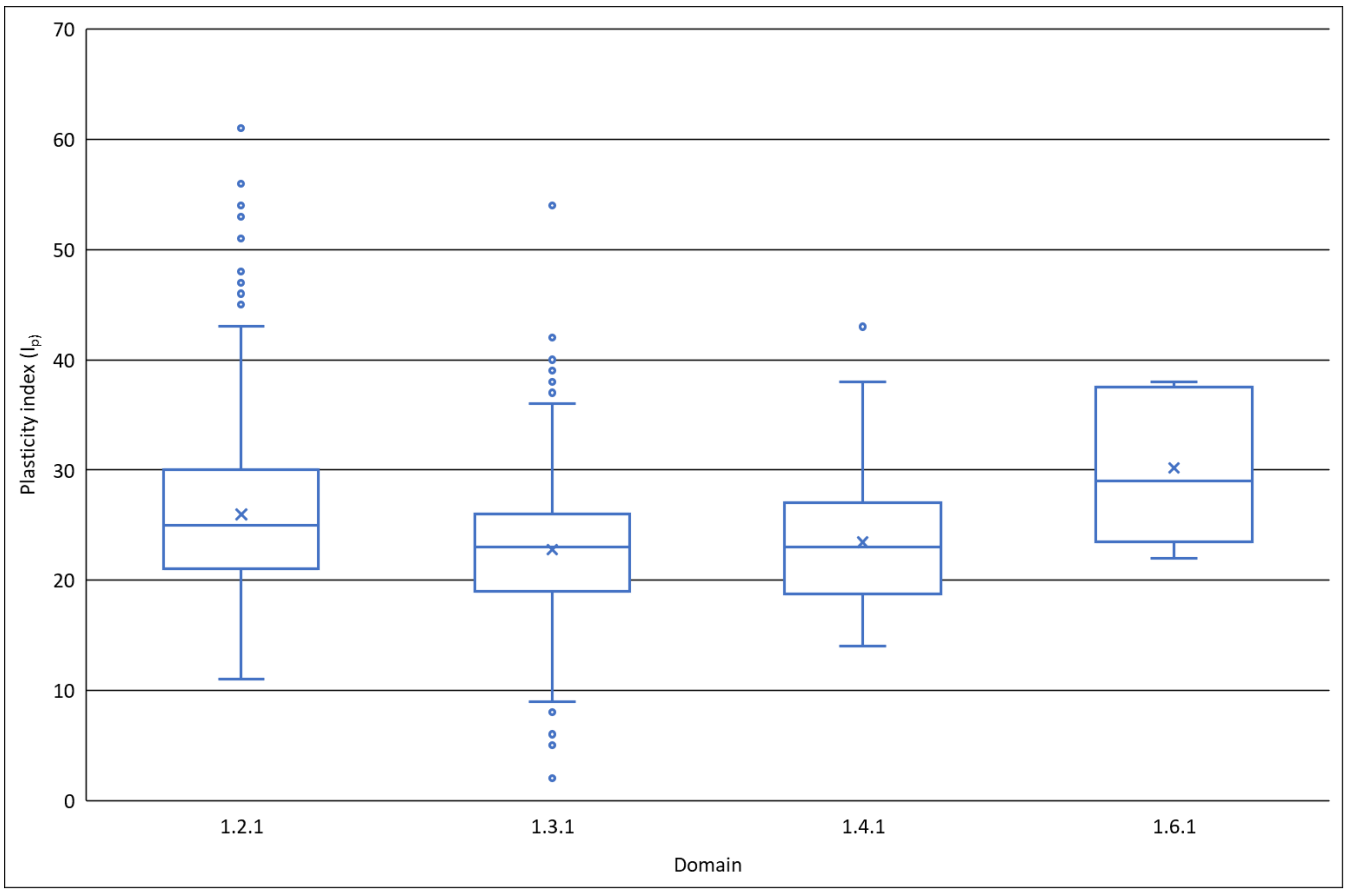

Figure 6-9 Box and Whisker plot for values of plasticity index, till.

Plasticity Index (I_P)					
	Domain 1.1.1	**Domain 1.2.1**	**Domain 1.3.1**	**Domain 1.4.1**	**Domain 1.6.1**
Maximum	NA	61	54	43	38
99.5	NA	NA	40	NA	NA
97.5	NA	42	35	NA	NA
90	NA	34	30	31	NA
75	NA	30	26	27	NA
50	NA	25	23	23	29
25	NA	21	19	19	NA
10	NA	18	16	16	NA
2.5	NA	21	12	NA	NA
0.5	NA	NA	6	NA	NA
Minimum	NA	11	2	14	22
n	2	410	564	54	5

Table 6-3 Percentile ranges for plasticity index, till. NA = range not calculated based on number of data.

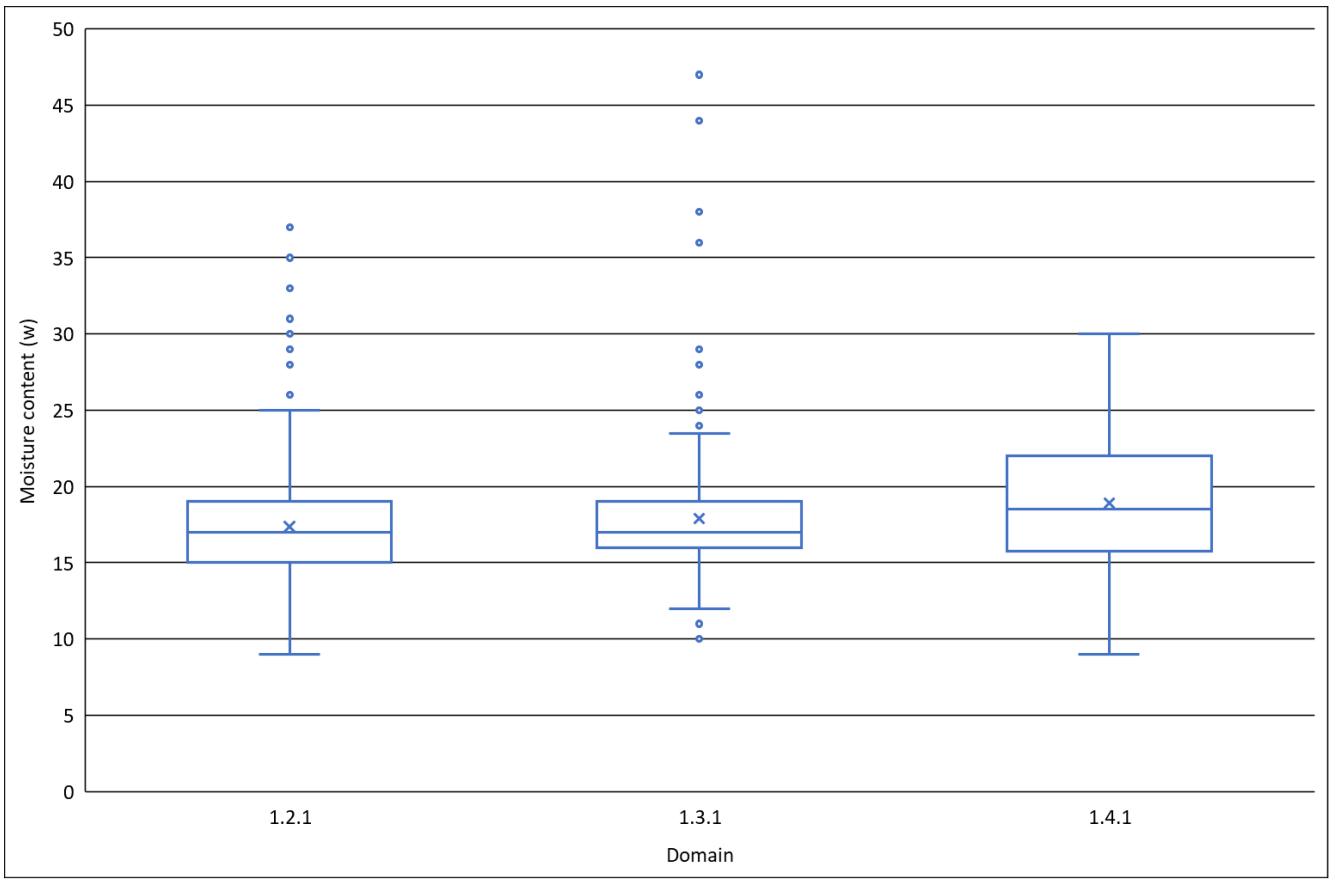

Figure 6-10 Box and Whisker plot for values of moisture content, till.

Moisture content					
	Domain 1.1.1	**Domain 1.2.1**	**Domain 1.3.1**	**Domain 1.4.1**	**Domain 1.6.1**
Maximum	NA	37	47	30	NA
99.5	NA	NA	38	NA	NA
97.5	NA	26	25	NA	NA
90	NA	22	22	23	NA
75	NA	19	19	22	NA
50	NA	17	17	19	NA
25	NA	15	16	17	NA
10	NA	13	14	15	NA
2.5	NA	11	13	NA	NA
0.5	NA	NA	11	NA	NA
Minimum	NA	9	10	9	NA
n	5	343	546	54	0

Table 6-4 Percentile ranges for moisture content, till. NA = range not calculated based on number of data.

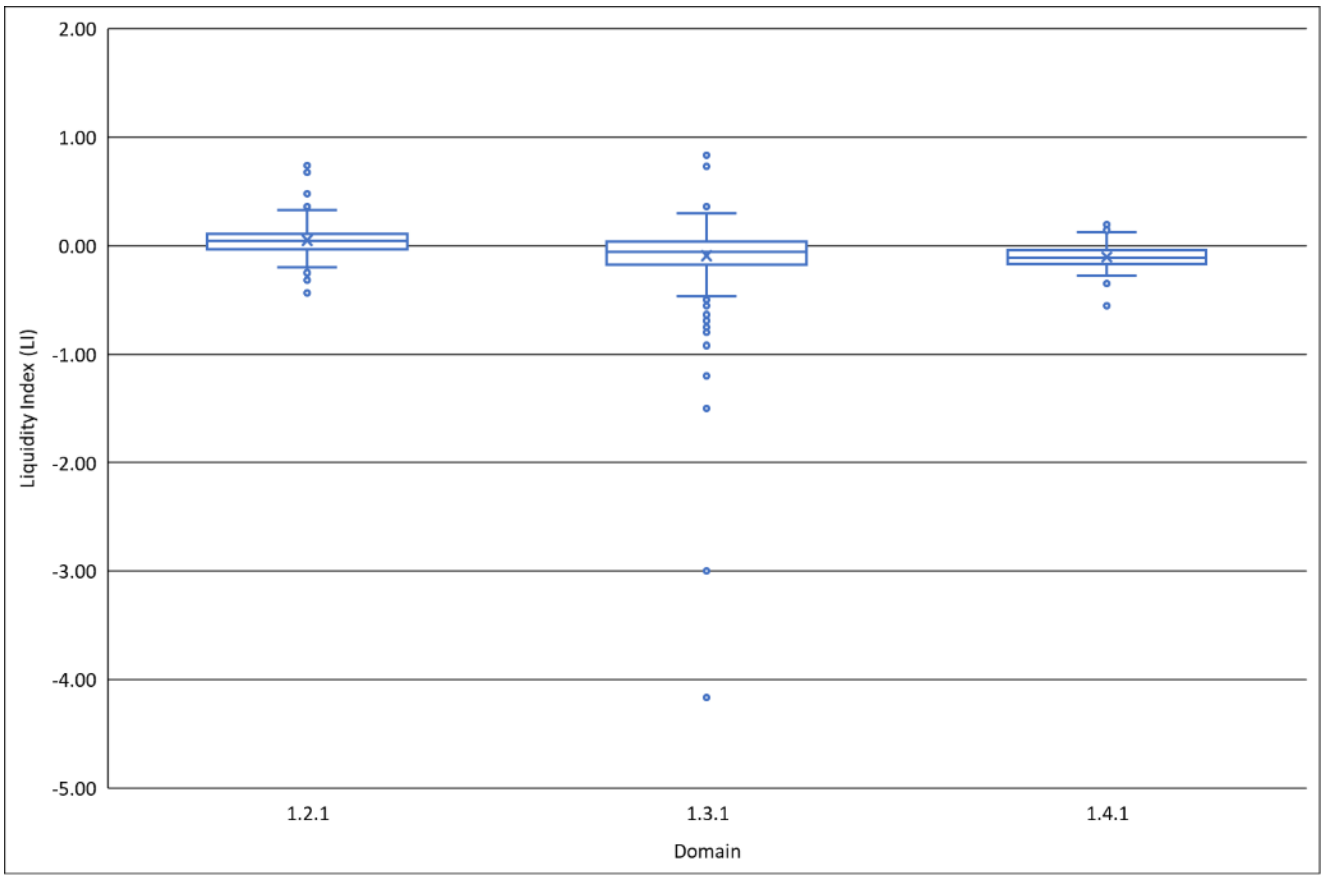

Figure 6-11 Box and Whisker plot for values of liquidity index, till.

Liquidity Index (I_L)					
	Domain 1.1.1	**Domain 1.2.1**	**Domain 1.3.1**	**Domain 1.4.1**	**Domain 1.6.1**
Maximum	NA	0.74	0.83	0.19	NA
99.5	NA	NA	0.38	NA	NA
97.5	NA	0.32	0.23	NA	NA
90	NA	0.19	0.11	0.05	NA
75	NA	0.11	0.04	-0.04	NA
50	NA	0.05	-0.06	-0.12	NA
25	NA	-0.03	-0.17	-0.16	NA
10	NA	-0.09	-0.29	-0.22	NA
2.5	NA	-0.18	-0.52	NA	NA
0.5	NA	NA	-1.28	NA	NA
Minimum	NA	-0.44	-4.17	-0.56	NA
n	2	343	546	54	0

Table 6-5 Percentile ranges for liquidity index, till. NA = range not calculated based on number of data.

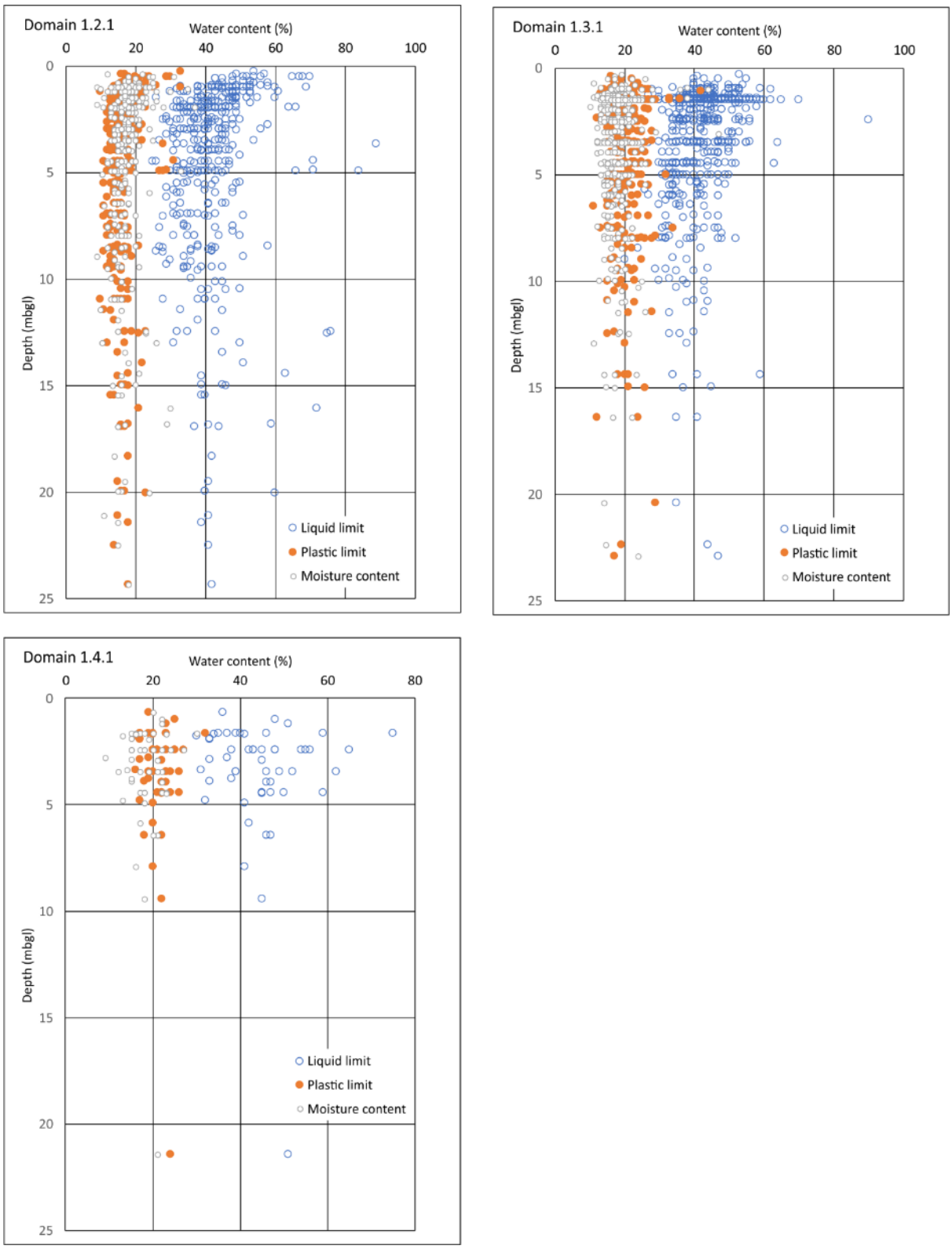

Figure 6-12 Depth *versus* plastic limit, liquid limit and moisture content, till.

6.2.2 Atterberg limits and moisture content (Oxford Clay)

The analyses of plasticity for all data are shown on Casagrande plots as W_L *versus* I_P in Figure 6-13 and subdivided for each Quaternary Domain in Figures 6-14 and 6-15.

The Oxford Clay is generally intermediate to high, and occasionally high to very high plasticity with some values in Domains 1.3 and 1.3.1, extremely high. There appears to be little variation in plasticity between Domains.

Non-parametric analysis of the data using Box and Whisker plots are shown in Figures 6-16 to 6-20 and described in Tables 6-6 to 6-10.

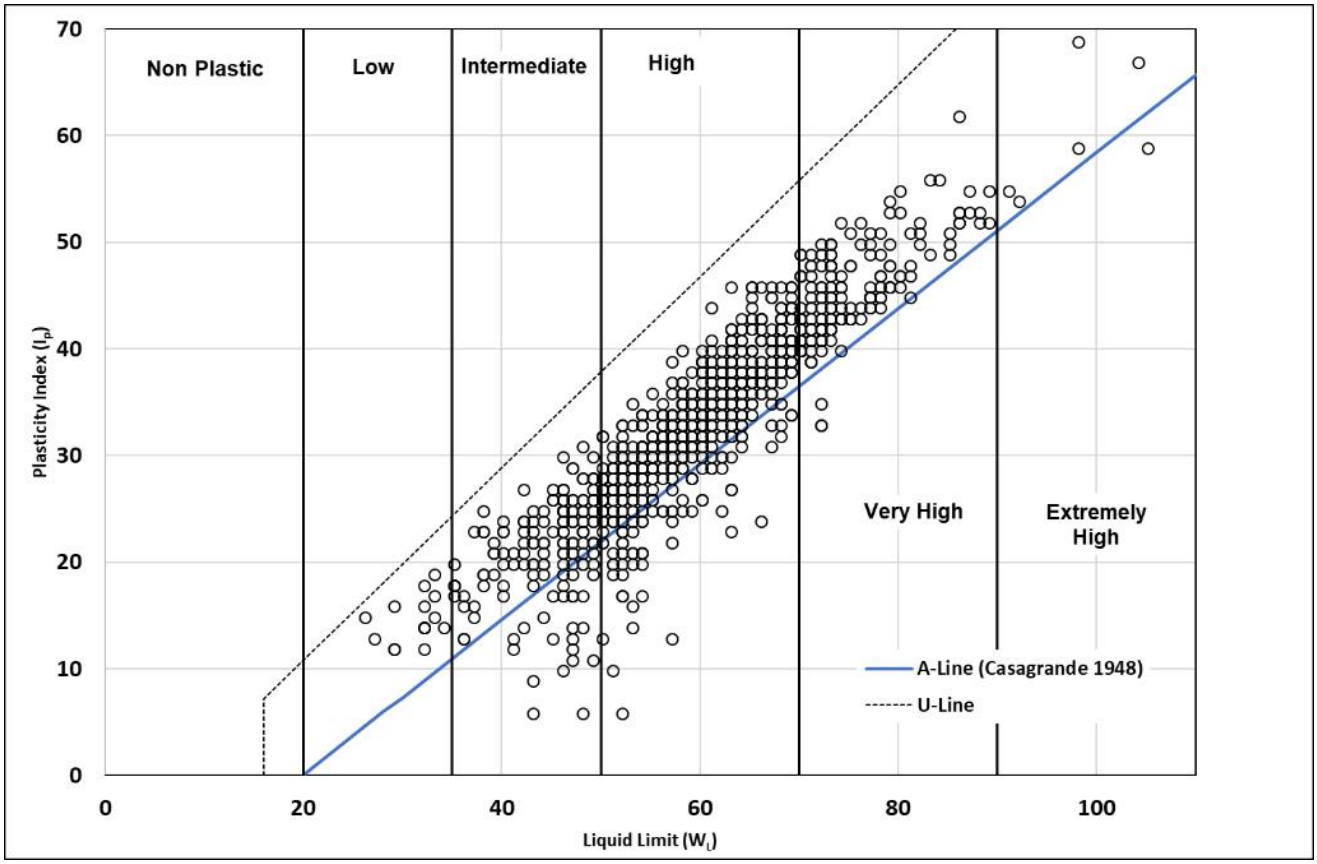

Figure 6-13 Plasticity plot for the Oxford Clay, all Domains.

There is a noticeable difference in values of liquid limit between samples from parent Domains 1 and 2. Those from Domains 1.3 and 1.3.1 have median values of 62% whilst those from Domain 2.3 and 2.3.1 have median values between 51% and 55%. As values for plastic limit are similar between all Domains, the difference in liquid limit accounts for the variation seen in plasticity index where values in Domains 1.3 and 1.3.1 are higher than those in Domains 2.3 and 2.3.1 (Figure 6-19). The reason for the difference in liquid limit is unknown. Differences in clay mineralogy are slight (See section 8) and so differences in grain sizes are likely to influence difference in liquid limit. Primary lithological differences in sedimentology

between members within the Oxford Clay could be an explanation. A second alternative is that there is a greater proportion of granular material in parent Domain 2 because of the greater length of time that this Domain was exposed to purely periglacial activity, compared to the Oxford Clay in parent Domain 1.

When plotted against depth below ground level there is a large spread of values (Figure 6-21). There is large variation in values of plastic and liquid limit below 8 – 10 mbgl in Domains 1.3 and 1.3.1 and 5 – 8 mbgl in Domains 2.3 and 2.3.1. The variation to a depth upto 10 mbgl probably reflects variation in the depth and style of weathering which influences particle-size and clay mineralogy.

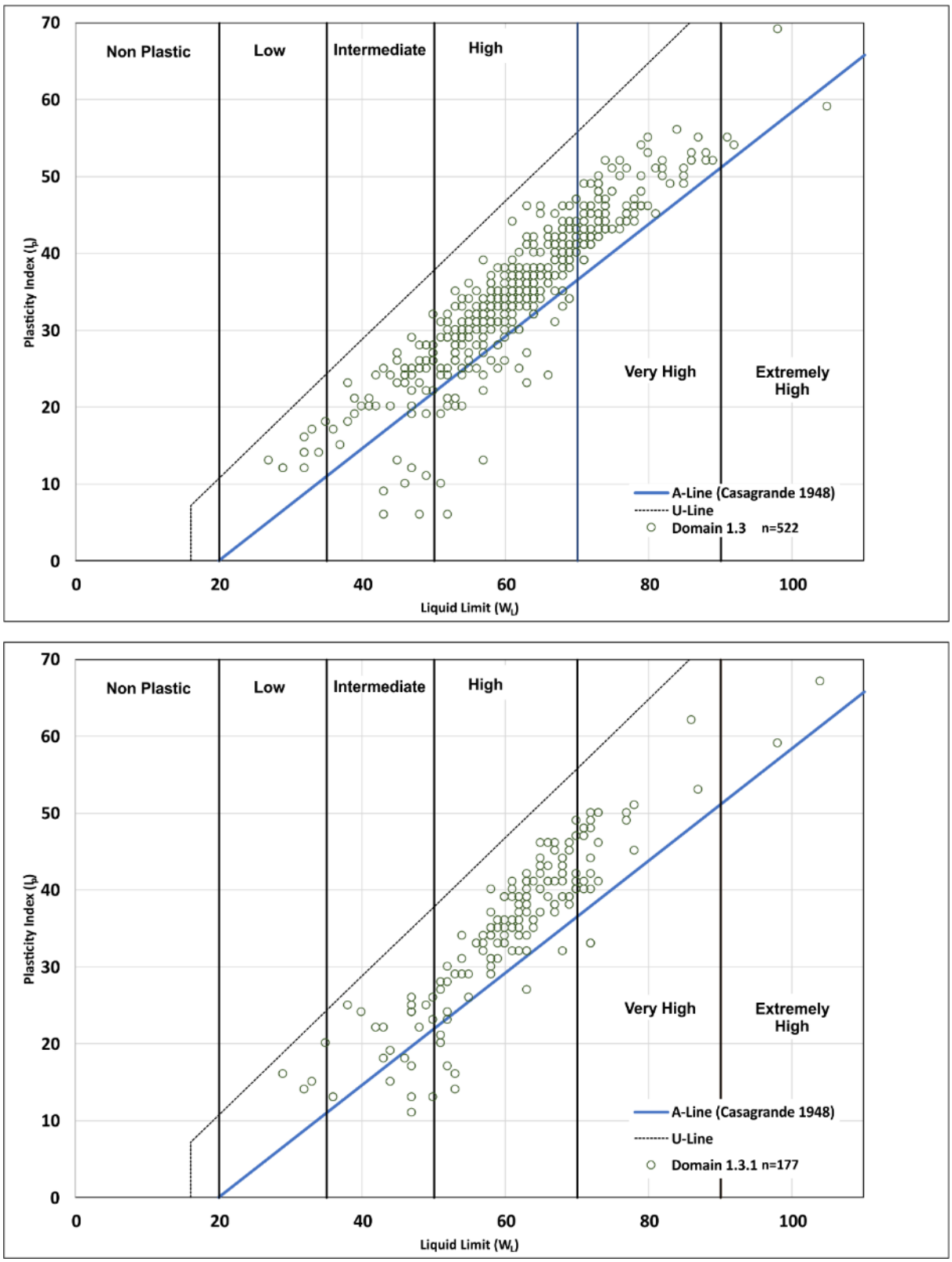

Figure 6-14 Plasticity plot, Domains 1.3 and 1.3.1, Oxford Clay.

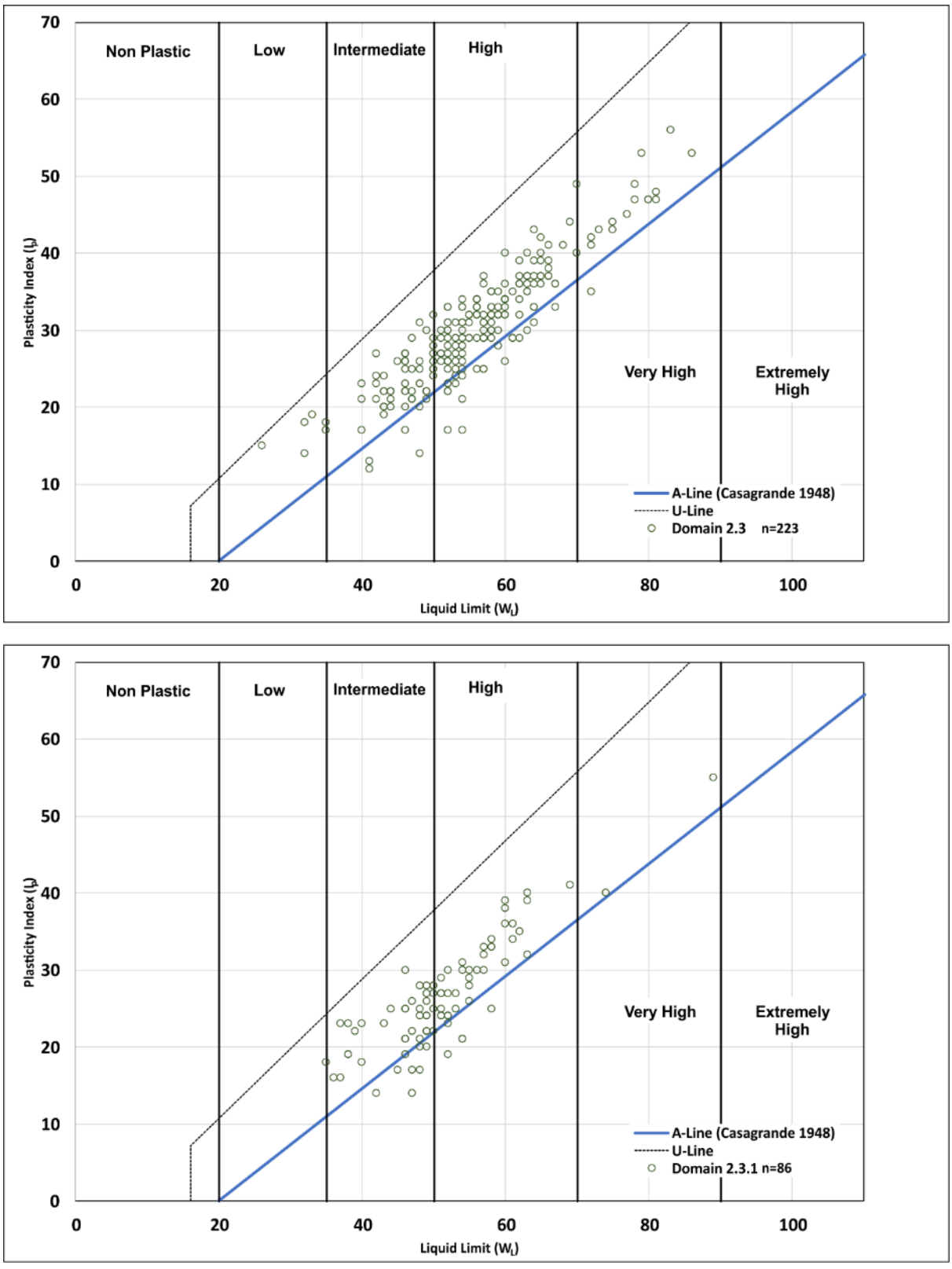

Figure 6-15 Plasticity plot, Domains 2.3 and 2.3.1, Oxford Clay.

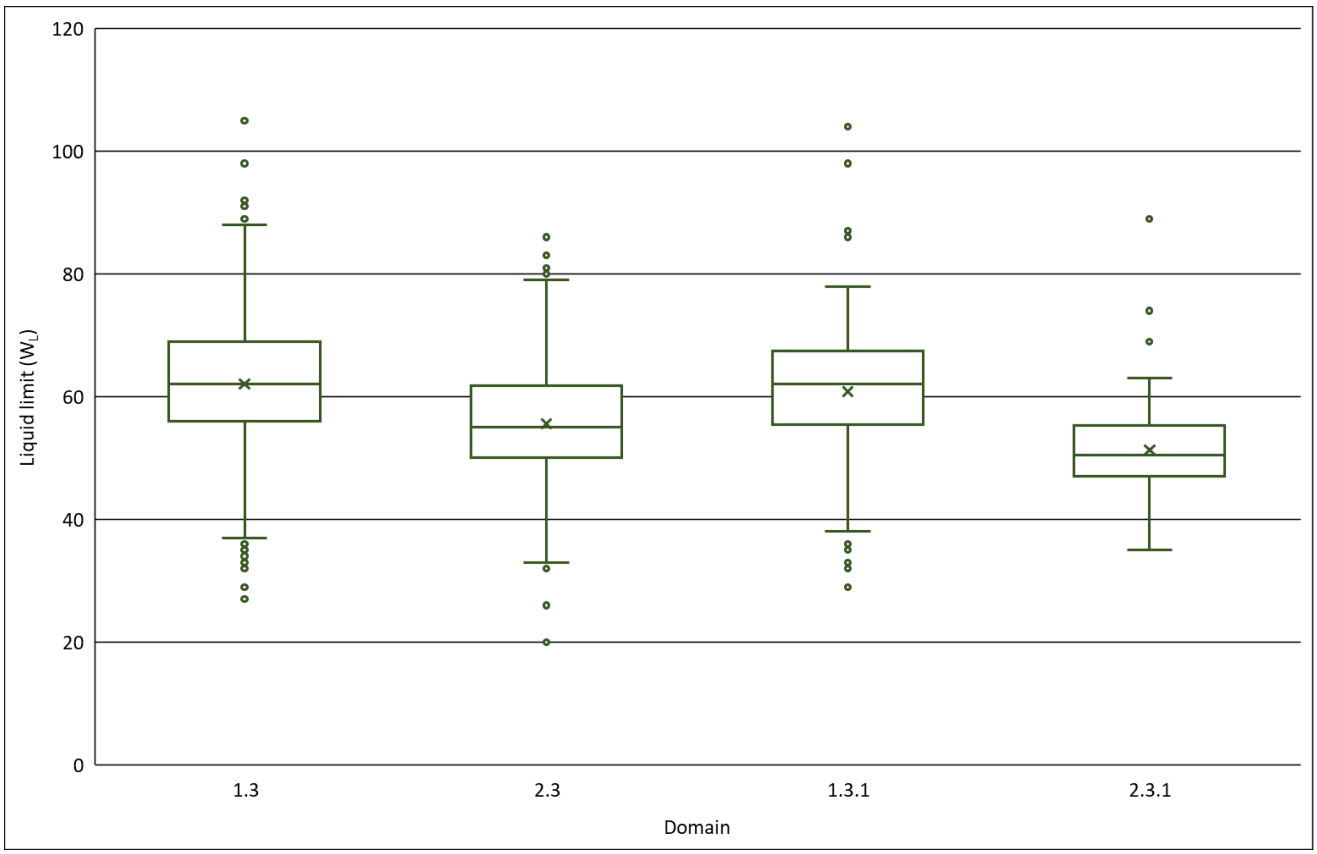

Figure 6-16 Box and Whisker plot for values of liquid limit, Oxford Clay.

Liquid Limit (W_L)				
	Domain 1.3	**Domain 1.3.1**	**Domain 2.3**	**Domain 2.3.1**
Maximum	105	104	86	89
99.5	91	NA	NA	NA
97.5	85	78	79	NA
90	74	72	67	61
75	69	67	61	55
50	62	62	55	51
25	56	56	50	47
10	49	47	44	40
2.5	38	36	35	NA
0.5	31	NA	NA	NA
Minimum	27	29	20	35
n	522	177	224	86

Table 6-6 Percentile ranges for liquidity limit, Oxford Clay. NA = range not calculated based on number of data.

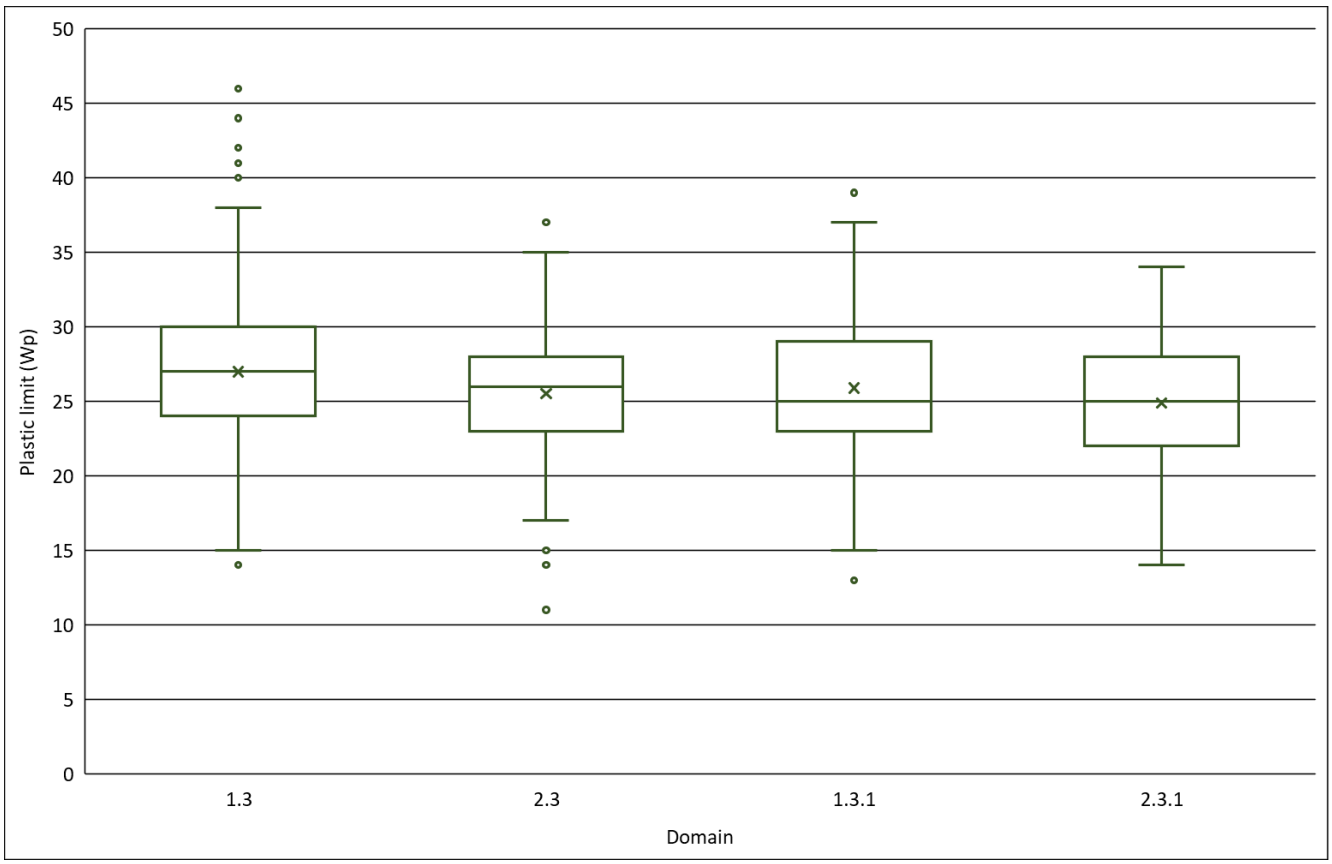

Figure 6-17 Box and Whisker plot for values of plastic limit, Oxford Clay.

Plastic Limit (W_P)				
	Domain 1.3	**Domain 1.3.1**	**Domain 2.3**	**Domain 2.3.1**
Maximum	46	39	37	34
99.5	43	NA	NA	NA
97.5	36	37	34	NA
90	32	31	31	31
75	30	29	28	28
50	27	25	26	25
25	24	23	23	22
10	22	21	20	20
2.5	18	18	17	NA
0.5	16	NA	NA	NA
Minimum	14	13	11	14
n	522	177	223	86

Table 6-7 Percentile ranges for liquidity limit, Oxford Clay. NA = range not calculated based on number of data.

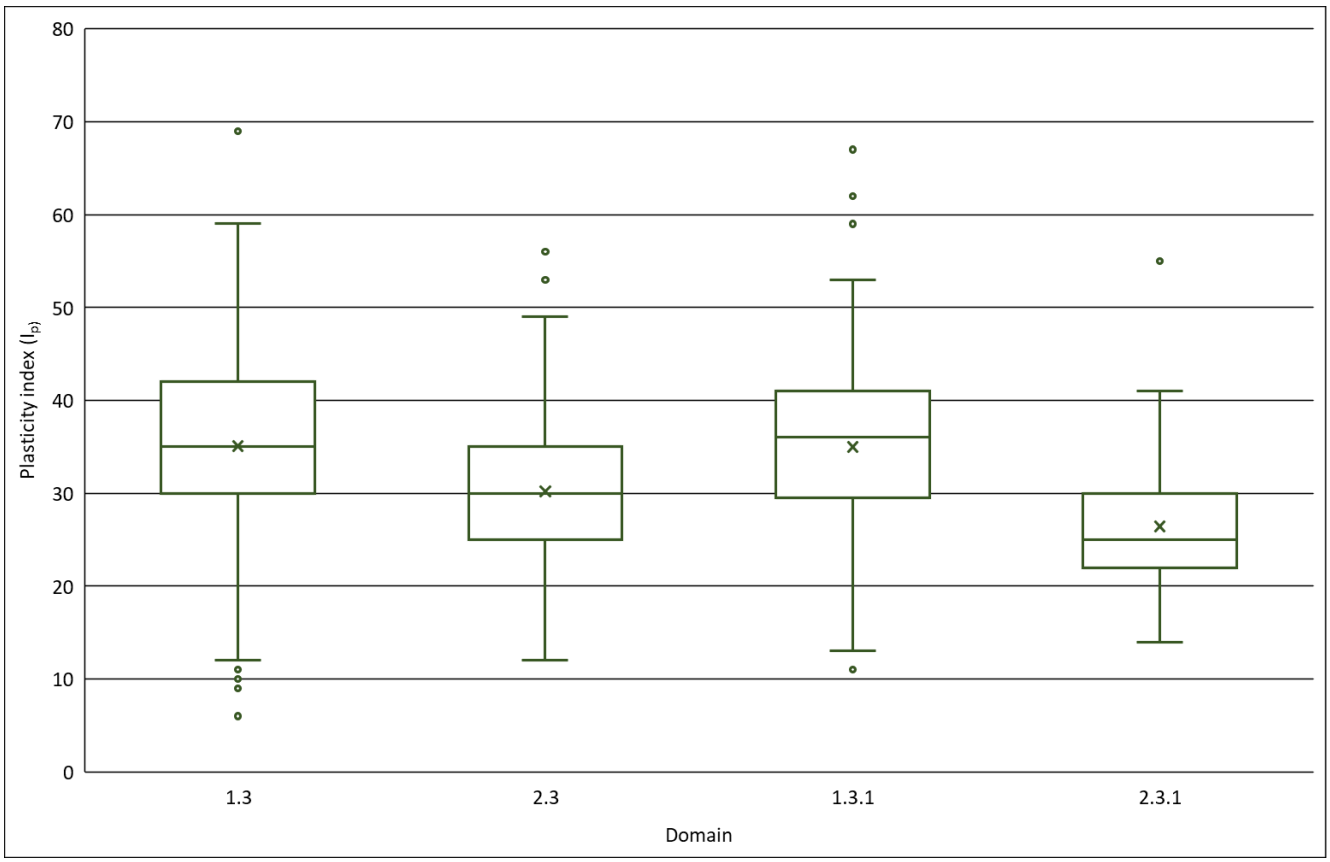

Figure 6-18 Box and Whisker plot for values of plasticity index, Oxford Clay.

Plasticity Index (I_p)				
	Domain 1.3	**Domain 1.3.1**	**Domain 2.3**	**Domain 2.3.1**
Maximum	69	67	56	55
99.5	55	NA	NA	NA
97.5	52	51	47	NA
90	46	46	40	36
75	42	41	35	30
50	35	36	30	25
25	30	30	25	22
10	24	20	21	19
2.5	13	13	17	NA
0.5	8	NA	NA	NA
Minimum	6	11	12	14
n	522	177	222	86

Table 6-8 Percentile ranges for plasticity index, Oxford Clay. NA = range not calculated based on number of data.

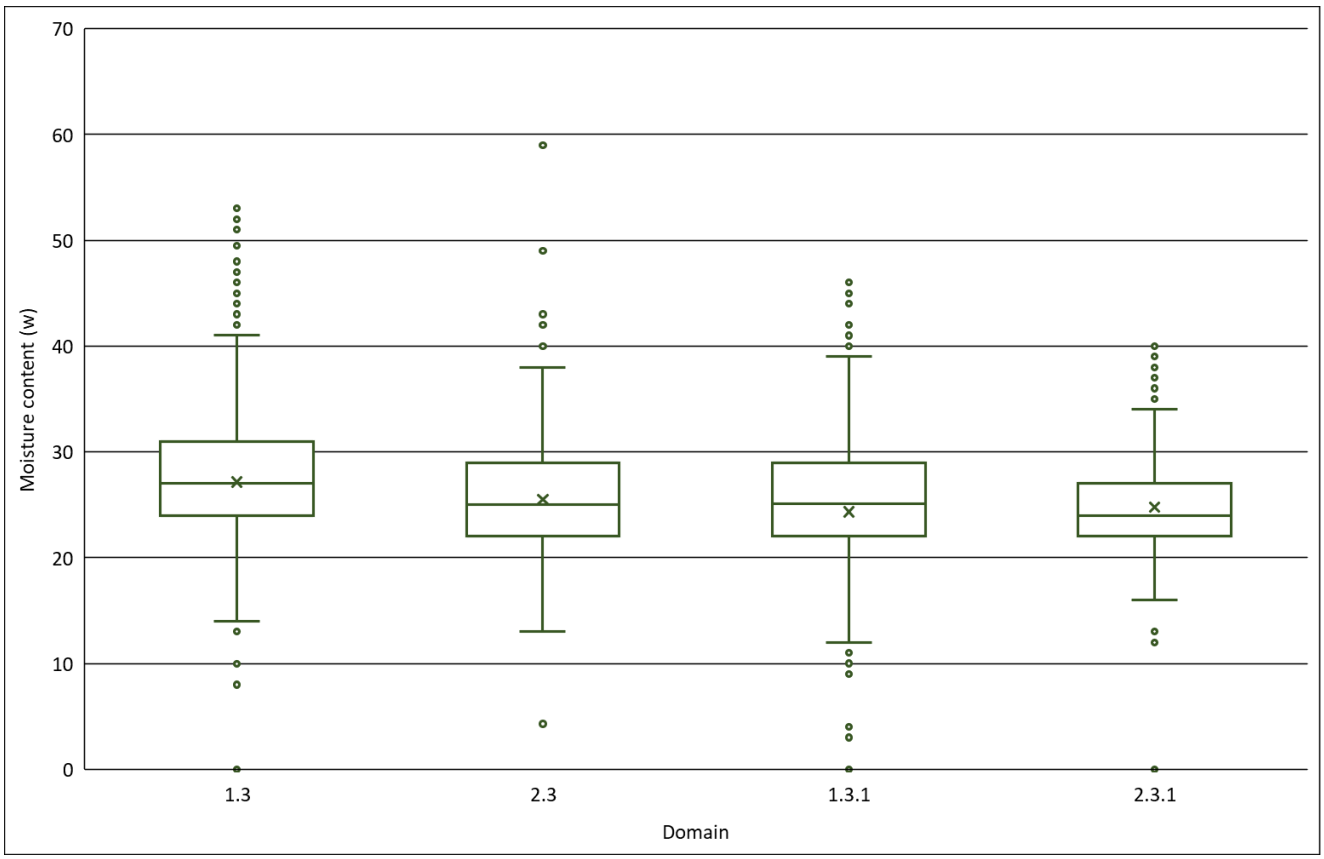

Figure 6-19 Box and Whisker plot for values of moisture content, Oxford Clay.

Moisture content				
	Domain 1.3	**Domain 1.3.1**	**Domain 2.3**	**Domain 2.3.1**
Maximum	53	46	59	40
99.5	49	43	NA	NA
97.5	40	39	37	38
90	35	33	33	32
75	31	29	29	27
50	27	26	25	25
25	24	23	22	22
10	21	19	20	19
2.5	18	14	15	17
0.5	14	9	NA	NA
Minimum	8	3	4	12
n	918	523	358	121

Table 6-9 Percentile ranges for moisture content, Oxford Clay. NA = range not calculated based on number of data.

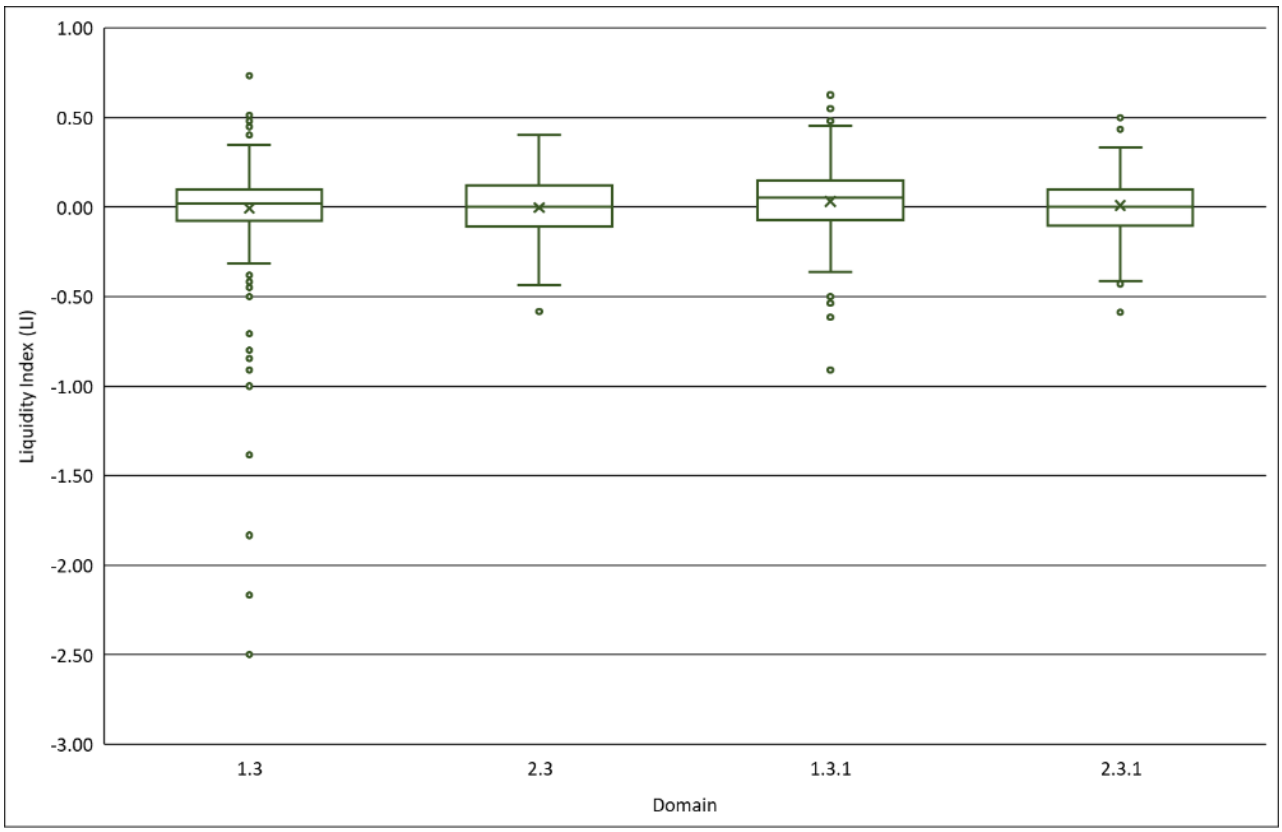

Figure 6-20 Box and Whisker plot for values of liquidity index, Oxford Clay.

Liquidity Index (I_L)				
	Domain 1.3	**Domain 1.3.1**	**Domain 2.3**	**Domain 2.3.1**
Maximum	0.73	0.63	0.40	0.50
99.5	NA	NA	NA	NA
97.5	0.32	0.40	0.30	NA
90	0.19	0.26	0.19	0.27
75	0.10	0.15	0.12	0.09
50	0.02	0.05	0.00	0.00
25	-0.08	-0.07	-0.11	-0.10
10	-0.17	-0.22	-0.23	-0.23
2.5	-0.46	-0.42	-0.34	NA
0.5	NA	NA	NA	NA
Minimum	-2.50	-0.91	-0.58	-0.59
n	499	143	223	85

Table 6-10 Percentile ranges for liquidity index, Oxford Clay. NA = range not calculated based on number of data.

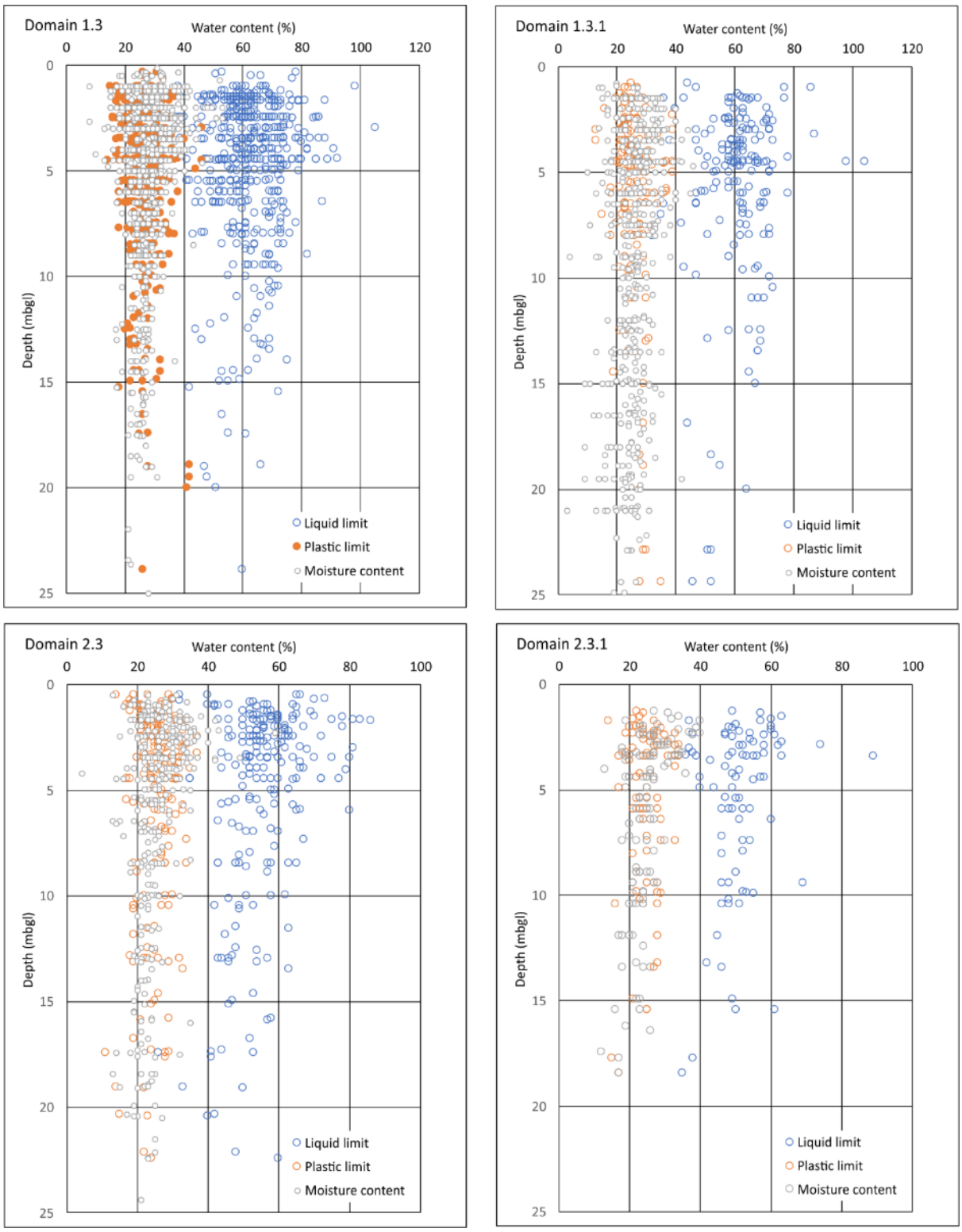

Figure 6-21 Plasticity-depth plots for the Oxford Clay classified according to Domain.

6.2.3 Particle-size (till)

There are 70 unique records in the project database for samples interpreted as till within parent Domain 1. Samples interpreted as ‘cohesive glacial deposits’ derived from the East West Rail project were also included in this analysis. Samples interpreted as till but included in Domains other than parent Domain 1, were excluded.

The results for all 70 samples, undivided by Domain are shown in Figure 6-22 where they are presented as percentiles. Referring to the median particle-size trend, sediments interpreted as till are slightly, gravelly, slightly sandy, silty to slightly silty, clay. The depression in the 25 to 2.5 percentile in the medium-sand to coarse-silt range and gravel range is a result of the presence of granular lenses of sand and gravel within the till. This is confirmed when the results are subdivided based on their Domain classification (Figures 6-23 and 6-24).

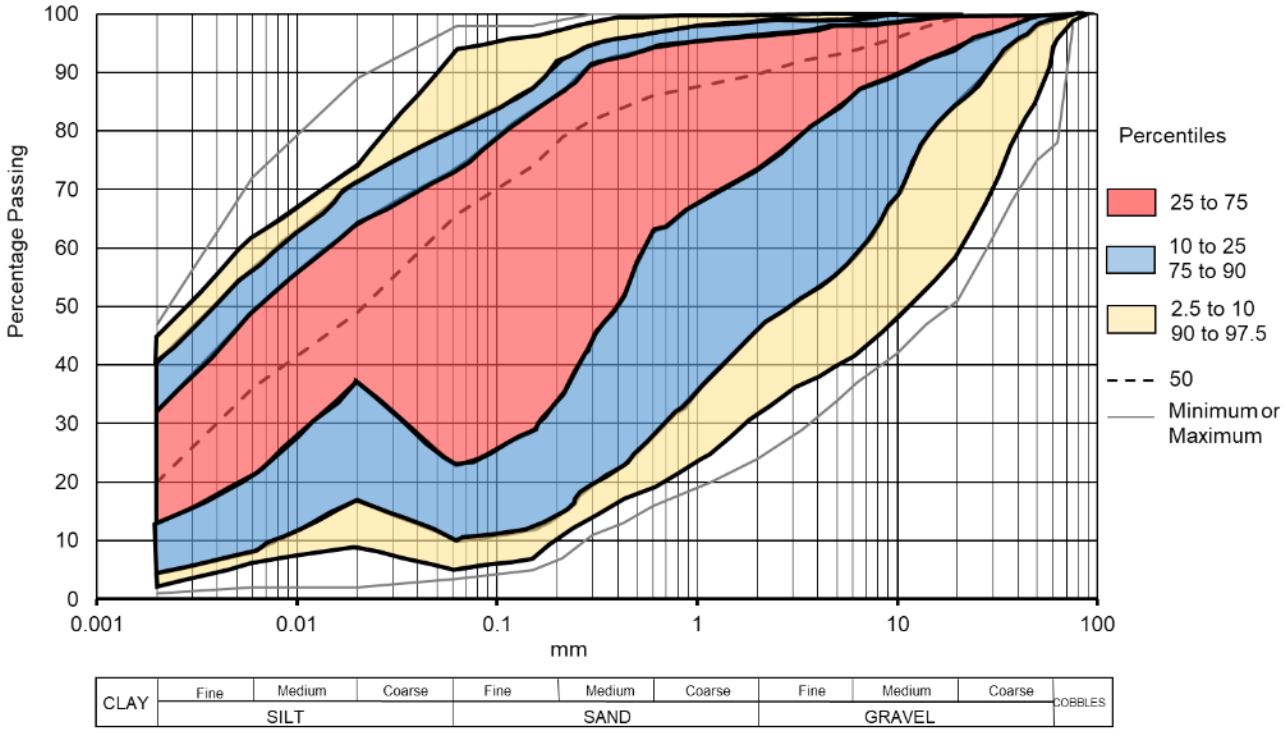

Figure 6-22 Particle-size grading curves summarised as percentiles for till, all Domains.

Tills in Domain 1.3.1 for example, are evenly divided into granular sand and gravel facies and silt- and clay-dominated facies representing matrix-supported, sandy and gravelly clay and silt.

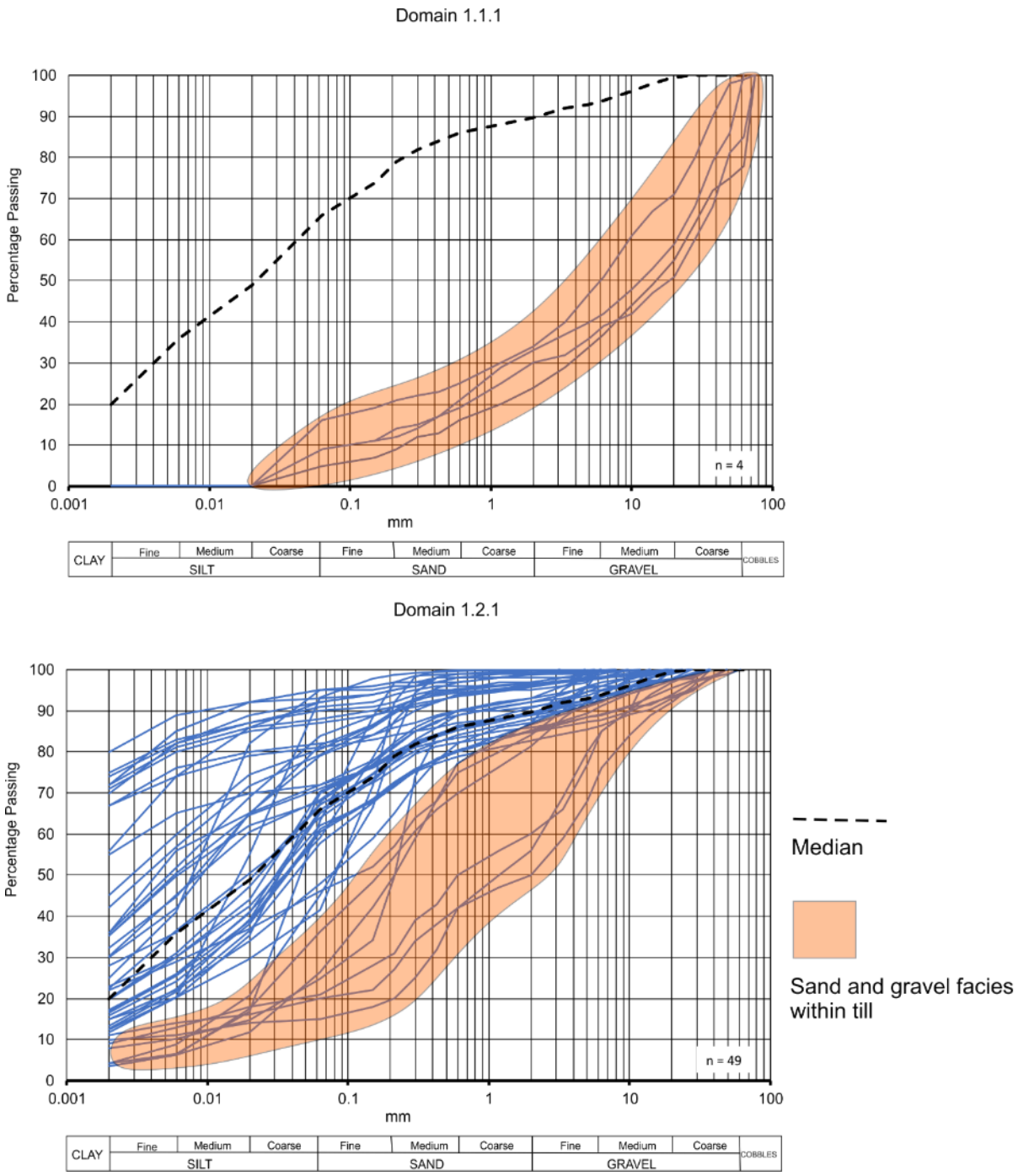

Figure 6-23 Particle-size grading curves for till within Domains 1.1.1 and 1.2.1. Median particle-size curve for all till samples shown.

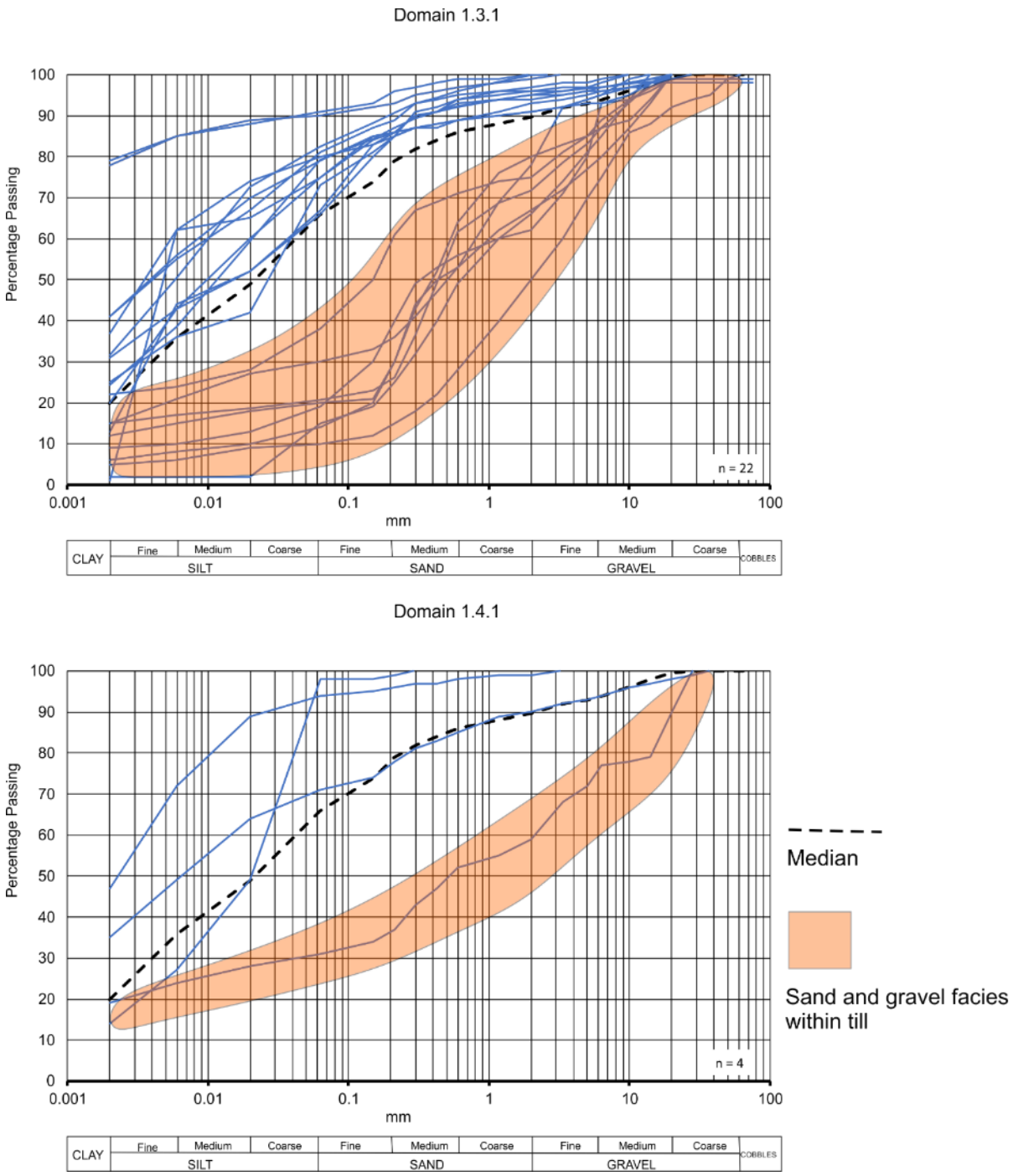

Figure 6-24 Particle-size grading curves for till within Domains 1.3.1 and 1.4.1. Median particle-size curve for all till samples shown.

6.2.4 Particle-size (Oxford Clay)

The analysis of the particle-size grading curves for all samples taken from the Oxford Clay, shows that it is a slightly sandy, silty clay (Figure 6-25). There is little variation across grain size for value in the upper 50th percentile. In contrast, the lower 50th percentile shows a large range of values.

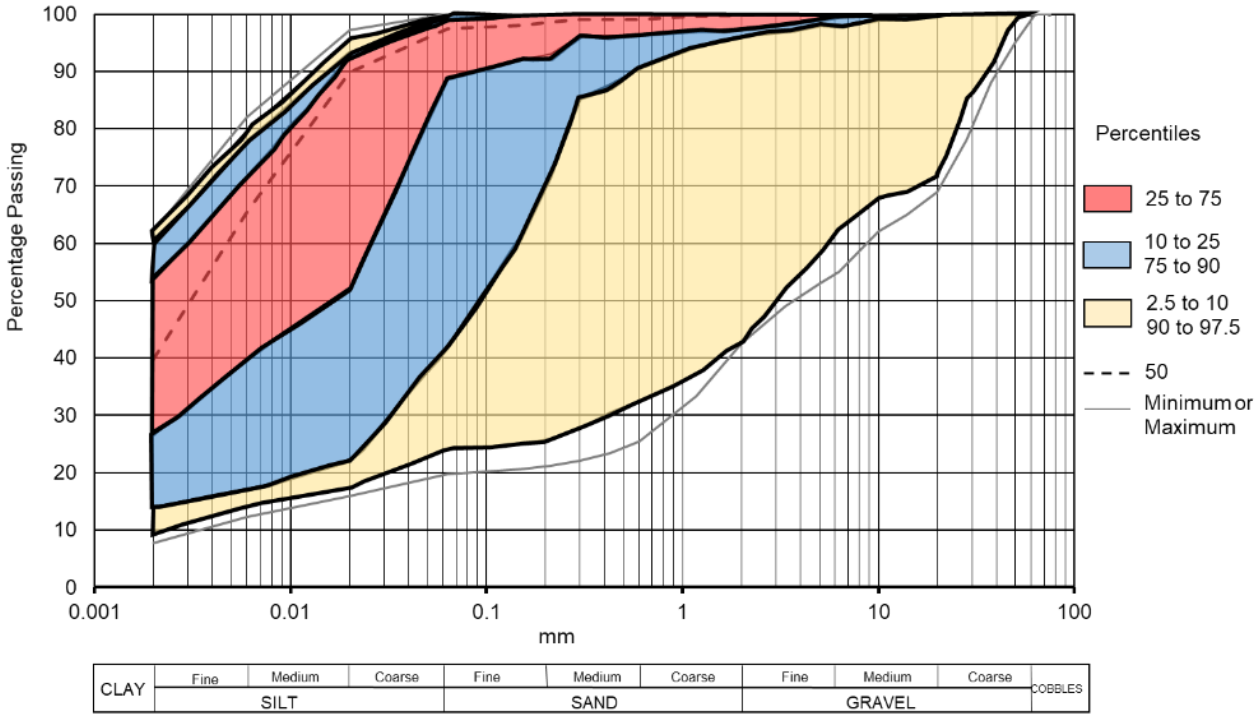

Figure 6-25 Particle-size grading curves summarised as percentiles for the Oxford Clay, all Domains.

The reasons for the large range of values in the lower 50th percentile are evident when individual grading curves are plotted by Domain subdivision (Figures 6-26 and 6-27). These values are associated with samples from two different populations. The first are samples taken from <5 mbgl and include granular material including sand and quartzite gravel. It is possible that this material in fact represents solifluction 'head'. The second population are those samples >5 mbgl where sand or gravel sized fragments of either fossils or crystals of gypsum are present. It was not possible to validate the individual sample preparation methods and so it is also possible that the granular components of particle-size grading for the Oxford Clay are aggregates of clay and silt not broken down during sample preparation.

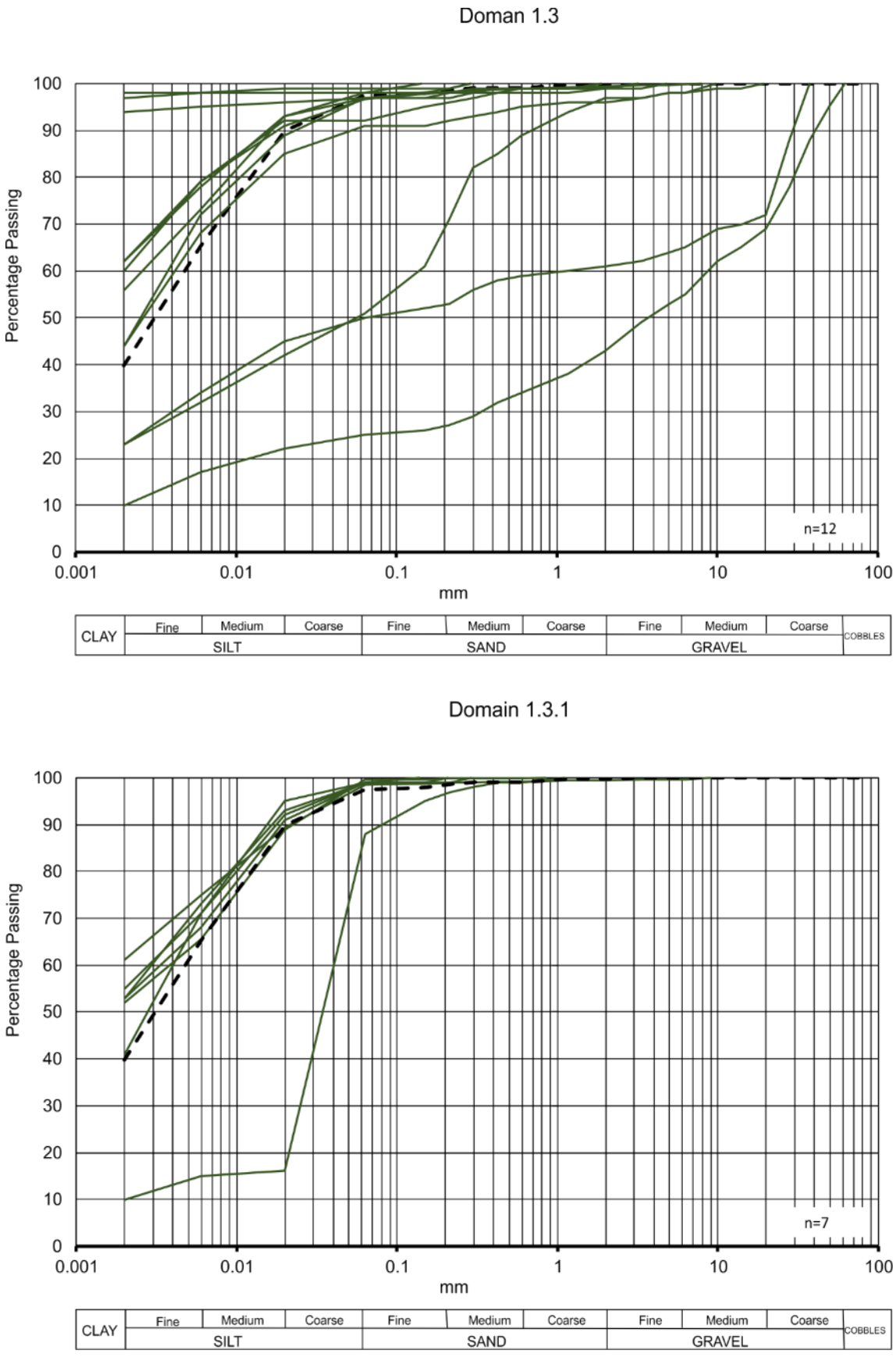

Figure 6-26 Particle-size grading curves for Oxford Clay, Domains 1.3 and 1.3.1. Median grading curve for all samples shown.

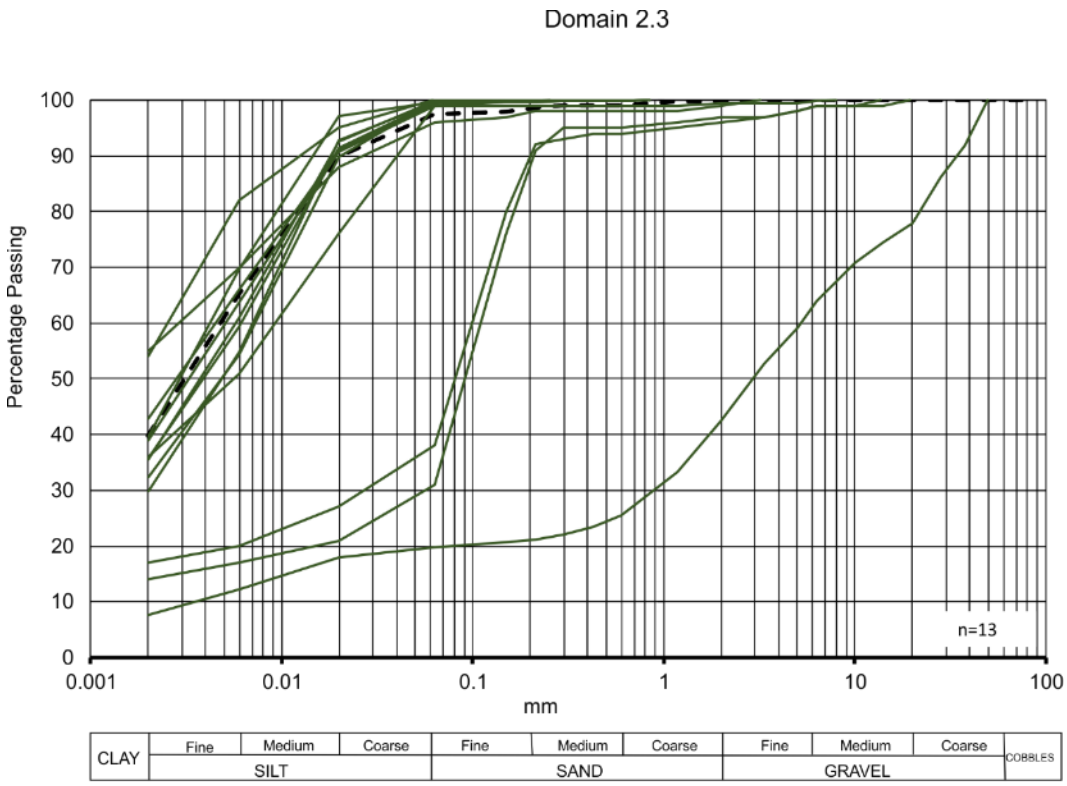

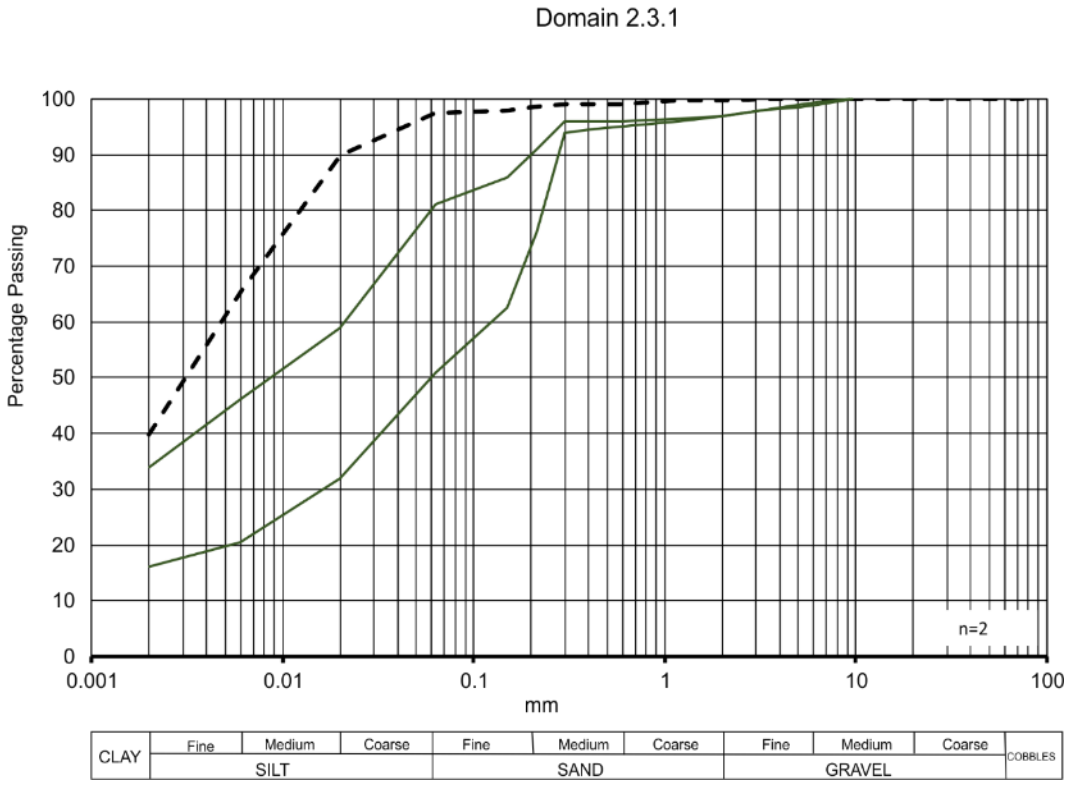

Figure 6-27 Particle-size grading curves for Oxford Clay, Domains 2.3 and 2.3.1. Median grading curve for all samples shown.

6.2.5 Consolidation (till)

There are 3073 records of consolidation test data within the project database, of which, 164 are interpreted as till samples including those classified as 'cohesive glacial deposits'. All

loading records are derived from laboratory, 1D oedometer experiments where the stress interval between each increment was doubled. To compare the results of consolidation test data, values for the coefficient of volume compressibility (m_v) and those for the coefficient of consolidation (c_v) were chosen for stress increments of 200 and 400 kPa.

For till, only Domain 1.3 contains data with >5 records and so inter-Domain comparison was not possible. The percentile range for each stress increment for values of m_v and c_v is shown in Figures 6-28 and 6-29 and the corresponding data are summarised in Tables 6-11 and 6-12. Values for m_v decrease with increasing stress. Median m_v values of 0.09 and 0.1 m^2/MN indicate that the till has low compressibility according to the compressibility classification given in Head & Epps (2011).

Values of c_v also decrease with increasing stress. Median values vary between 2.6 and 6.08 m^2/yr. Over both stress ranges there is a greater range of values in the upper 50th percentile compared to those in the lower. Values of c_v over both stresses show a large range of data that are classified as outliers.

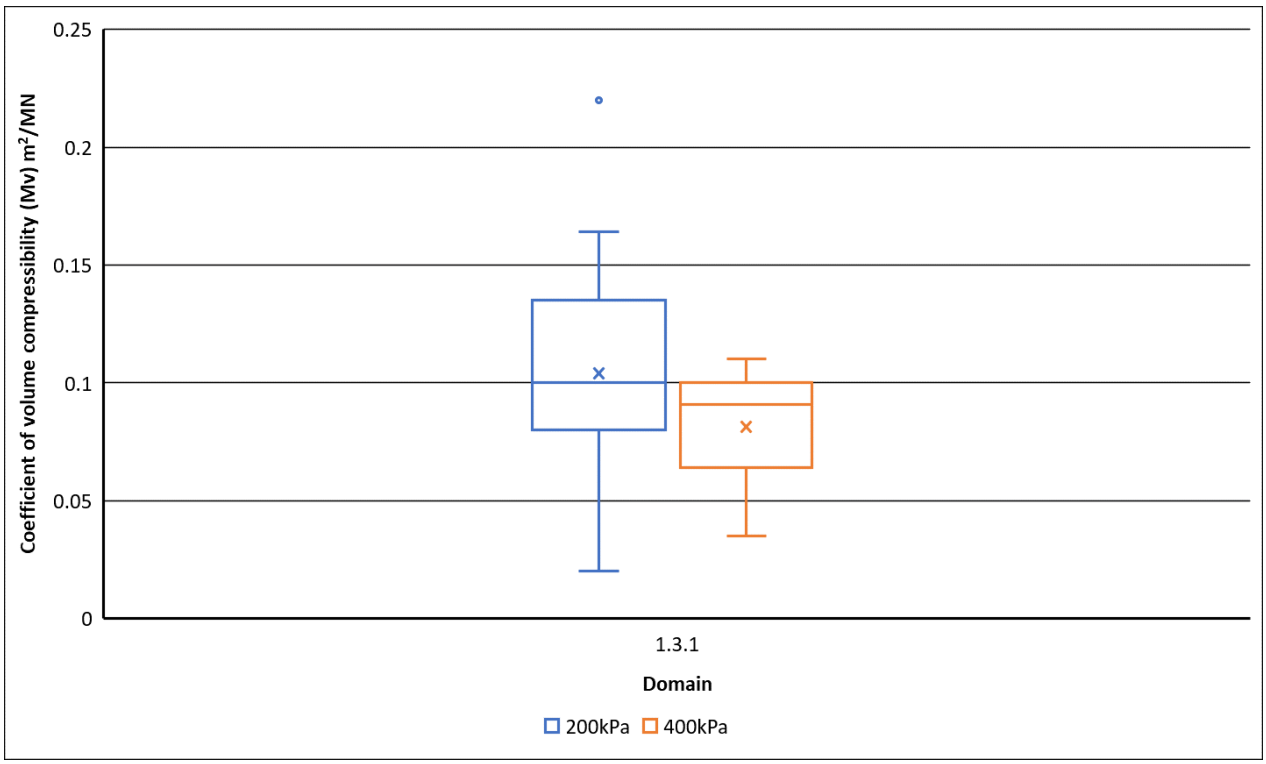

Figure 6-28 Comparison of values for m_v for stresses 200 and 400kPa, till Domain 1.3.1.

Coeffecient of volume compressibility (Mv), m^2/MN		
	Domain 1.3	
	200kPa	400kPa
Maximum	0.22	0.11
99.5	NA	NA
97.5	NA	NA
90	0.16	NA
75	0.13	0.10
50	0.10	0.09
25	0.08	0.06
10	0.04	NA
2.5	NA	NA
0.5	NA	NA
Minimum	0.02	0.04
n	19	12

Table 6-11 Percentile ranges of m_v for stresses of 200 and 400 kPa for till in Domain 1.3.1. NA = range not calculated based on number of data.

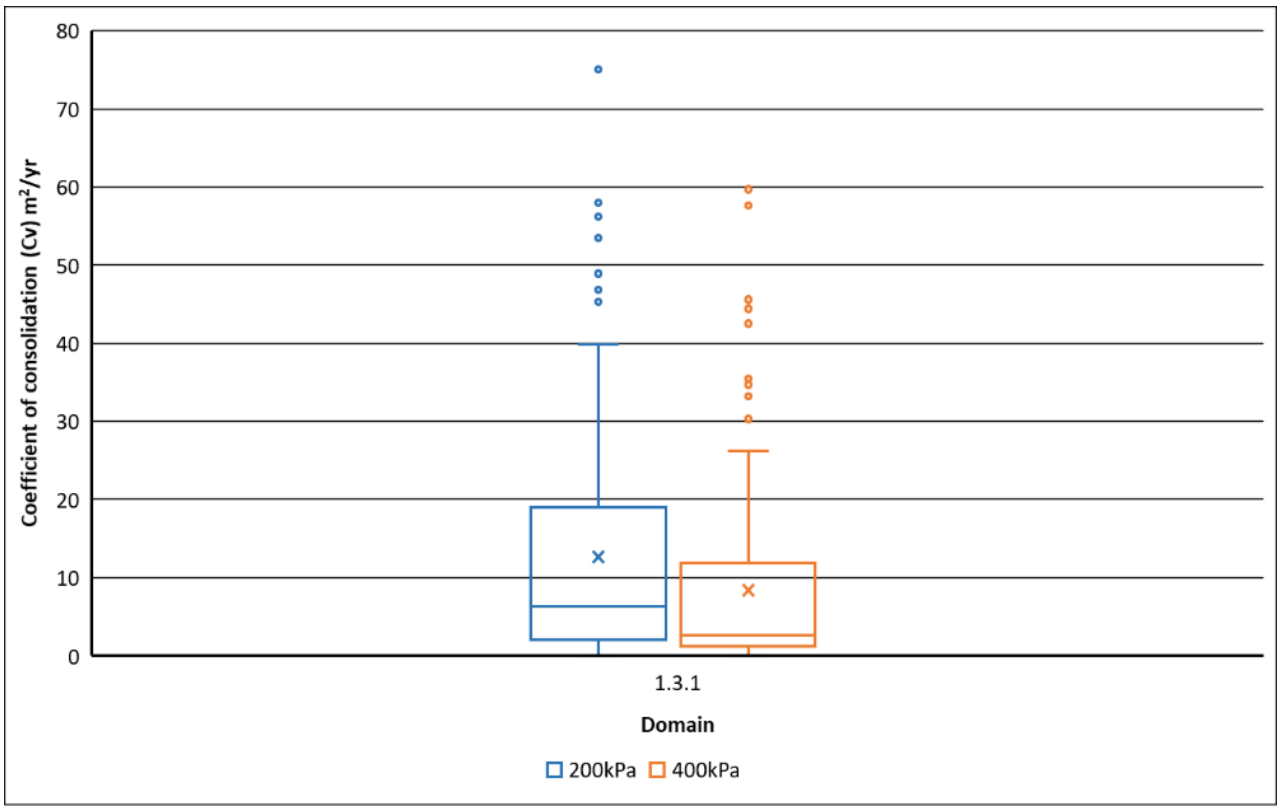

Figure 6-29 Comparison of values of c_v for stresses 200 and 400 kPa in Domain 1.3.1 for till.

Coeffecient of compressibility (Cv), m^2/yr		
	Domain 1.3	
	200kPa	400kPa
Maximum	75	60
99.5	NA	NA
97.5	50.97	44.72
90	37.46	25.60
75	18.15	11.05
50	6.08	2.60
25	1.95	1.20
10	1.00	0.51
2.5	0.46	0.32
0.5	NA	NA
Minimum	0.09	0.08
n	143	135

Table 6-12 Percentile ranges of c_v for stresses of 200 and 400 kPa for till in Domain 1.3.1. NA = range not calculated based on number of data.

6.2.6 Consolidation (Oxford Clay)

There are 125 records for values of m_v and c_v in the project database for samples interpreted as Oxford Clay. Parameter values for stress increments 200 and 400 kPa are ranked and

summarised as Box and Whisker plots in Figures 6-30 and 6-31 and described in Tables 6-13 and 6-14.

Values for m_v decrease with increasing stress increment across all Domains for which there is data. The number of data within the 200 kPa stress range is low making inter-Domain comparison difficult. Comparison of values within the 400 kPa stress range show a decrease in median values within the non-glaciated, parent Domain 2 compared to the glaciated parent Domain 1. The is an increase in median values from non-glaciated Domains 2.3 to 2.3.1.

Comparing values for c_v, there is a decrease in values with increasing stress, except in Domain 2.3, where the median and IQR increase. Median values of c_v are generally higher in glaciated Domains 1.3 and 1.3.1 compared to non-glaciated Domains 2.3 and 2.3.1. The IQR is less in the Oxford Clay in Domains currently overlain by Quaternary sediments compared to those that are not. Domains 1.3 and 2.3 are characterised by a wide IQR and high-value outliers that extend above the 75th quartile which also causes an increase in the mean, beyond the IQR.

Referring to the median values for m_v, the Oxford Clay can be classified as a medium compressibility using the classification of Head & Epps (2011). Median values are comparable to values for weathered 'brown London Clay' (Head & Epps, 2011).

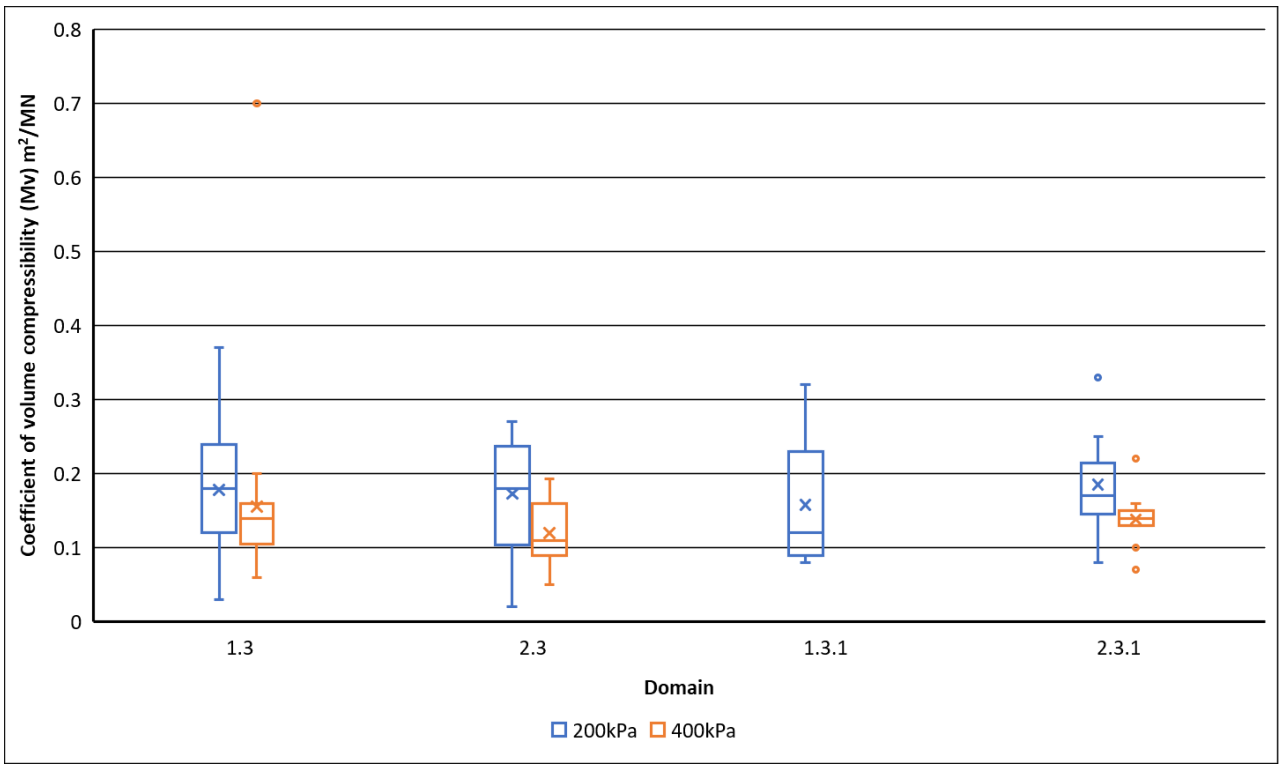

Figure 6-30 Box and Whisker plot for m_v, Oxford Clay.

Coeffecient of volume compressibility (Mv), m^2/MN								
	Domain 1.3		Domain 1.3.1		Domain 2.3		Domain 2.3.1	
	200kPa	400kPa	200kPa	400kPa	200kPa	400kPa	200kPa	400kPa
Maximum	0.37	0.70	0.32	NA	0.27	0.193	0.33	0.22
99.5	NA	NA	NA	NA	NA	NA	NA	NA
97.5	NA	NA	NA	NA	NA	NA	NA	NA
90	0.27	NA	NA	NA	0.27	0.17	NA	NA
75	0.24	0.16	NA	NA	0.23	0.15	0.21	0.15
50	0.18	0.14	0.12	NA	0.18	0.11	0.17	0.14
25	0.13	0.12	NA	NA	0.11	0.09	0.15	0.13
10	0.06	NA	NA	NA	0.07	0.07	NA	NA
2.5	NA	NA	NA	NA	NA	NA	NA	NA
0.5	NA	NA	NA	NA	NA	NA	NA	NA
Minimum	0.03	0.06	0.08	NA	0.02	0.05	0.08	0.07
n	59	24	9	4	36	27	13	11

Table 6-13 Percentile ranges of m_v for stresses 200 and 400 kPa for the Oxford Clay. NA = range not calculated based on number of data.

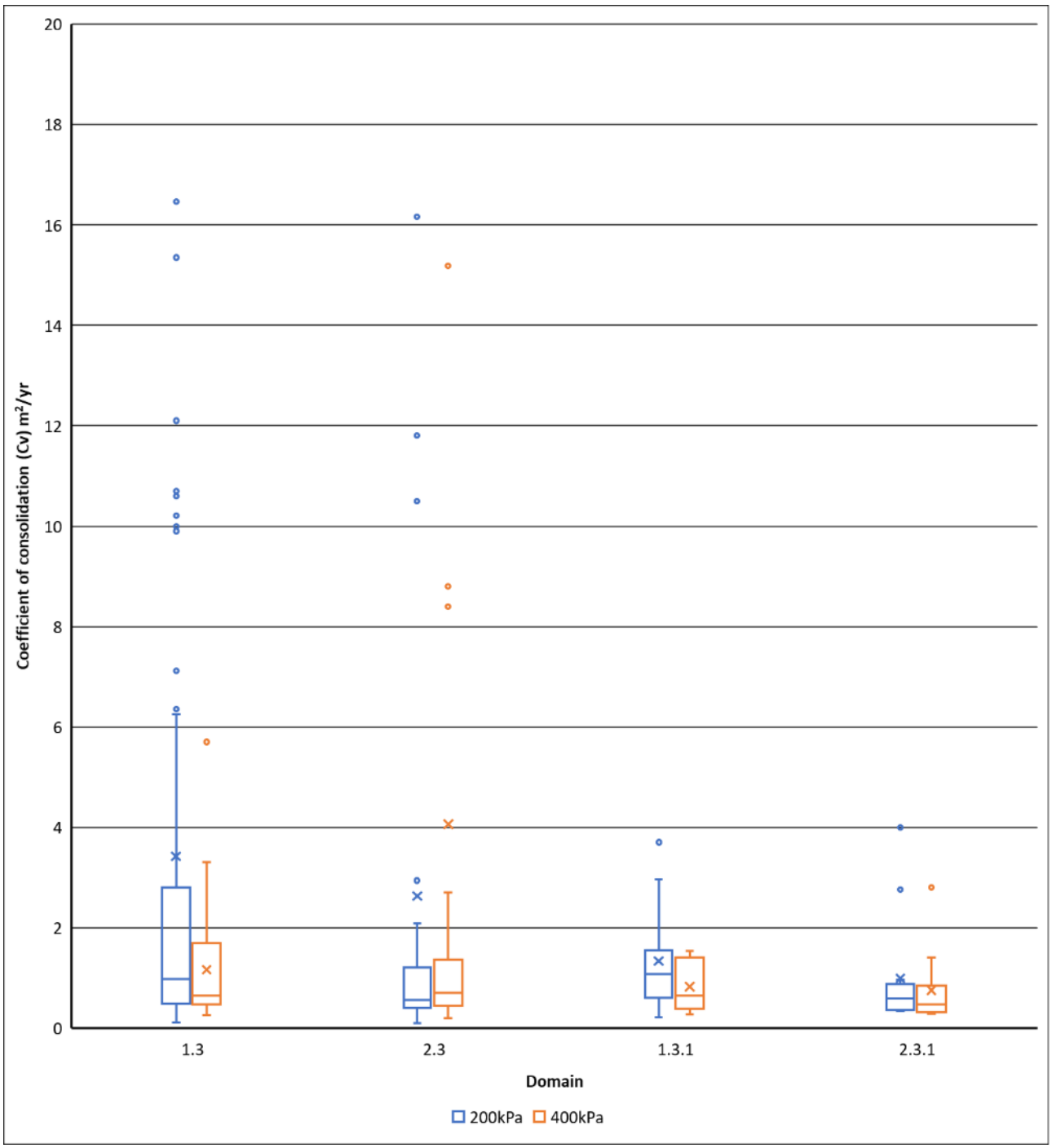

Figure 6-31 Box and Whisker plot for c_v, Oxford Clay. Three outlier values >20 m^2/yr omitted for clarity.

Coeffecient of compressibility (Cv), m^2/yr								
	Domain 1.3		Domain 1.3.1		Domain 2.3		Domain 2.3.1	
	200kPa	400kPa	200kPa	400kPa	200kPa	400kPa	200kPa	400kPa
Maximum	39.4	6	3.7	1.54	30.8	60.4	6.53	2.8
99.5	NA	NA	NA	NA	NA	NA	NA	NA
97.5	NA	NA	NA	NA	NA	NA	NA	NA
90	10.15	2.46	NA	NA	7.48	8.56	NA	NA
75	2.70	1.61	1.55	1.32	1.17	1.18	1.49	0.7
50	0.98	0.65	1.07	0.65	0.56	0.70	0.66	0.48
25	0.49	0.48	0.63	0.43	0.40	0.47	0.49	0.35
10	0.28	0.30	NA	NA	0.28	0.33	NA	NA
2.5	NA	NA	NA	NA	NA	NA	NA	NA
0.5	NA	NA	NA	NA	NA	NA	NA	NA
Minimum	0.12	0.26	0.22	0.27	0.1	0.2	0.35	0.29
n	74	39	15	10	35	27	11	11

Table 6-14 Percentile ranges of c_v for stresses 200 and 400 kPa for the Oxford Clay. NA = range not calculated based on number of data.

6.2.7 Undrained shear strength (till)

There are 1374 records for samples classified as till, within the project database. All records are derived from laboratory triaxial tests on samples whose diameter ranges between 38 and 107 mm. Unconsolidated undrained (UU) single stage (n=663) and multi-stage (n=663) triaxial tests, without measurement of pore pressure, are the most common. Other test types are single and multi-stage consolidated undrained (CU) with measurement of pore pressure (n=44) and consolidated drained (CU), (n=4). The latter four records were excluded from the following analysis.

Values of undrained shear strength are recorded in the database as undrained cohesion, C_u for UU tests. Strength parameters for CU tests are reported as undrained cohesion (c′) and undrained angle of shearing resistance (ø′). Because of the low numbers of samples with effective strength parameters, only values of C_u are analysed here. As values of undrained shear strength are not a material property but dependent on, for example, magnitude of stress, the results shown here are used to determine probable upper and lower bound limits only.

Box and Whisker plots for C_u are shown in Figure 6-32 and the data summarised in Table 6-15. Based on the median values, the samples can be described as very stiff. The IQR and median values decrease from Domain 1.2.1 to Domain 1.4.1. Median values for C_u decrease from 270 to 179 kN/m^2. This trend is also a geographic and geological one with values decreasing from northwest to southeast. The northwest-southeast geological trend is reflected

in the nature of the underlying bedrock. Domain 1.2.1 is underlain Middle Jurassic limestone, sandstone and mudrocks whilst Domains 1.3.1 and 1.4.1 are underlain by Middle and Late Jurassic mudrocks, whose age increases to the southeast. It appears therefore that the underlying bedrock type may influence the undrained shear strength of till; higher median values associated with granular bedrock and lower values associated with fine-grained bedrock.

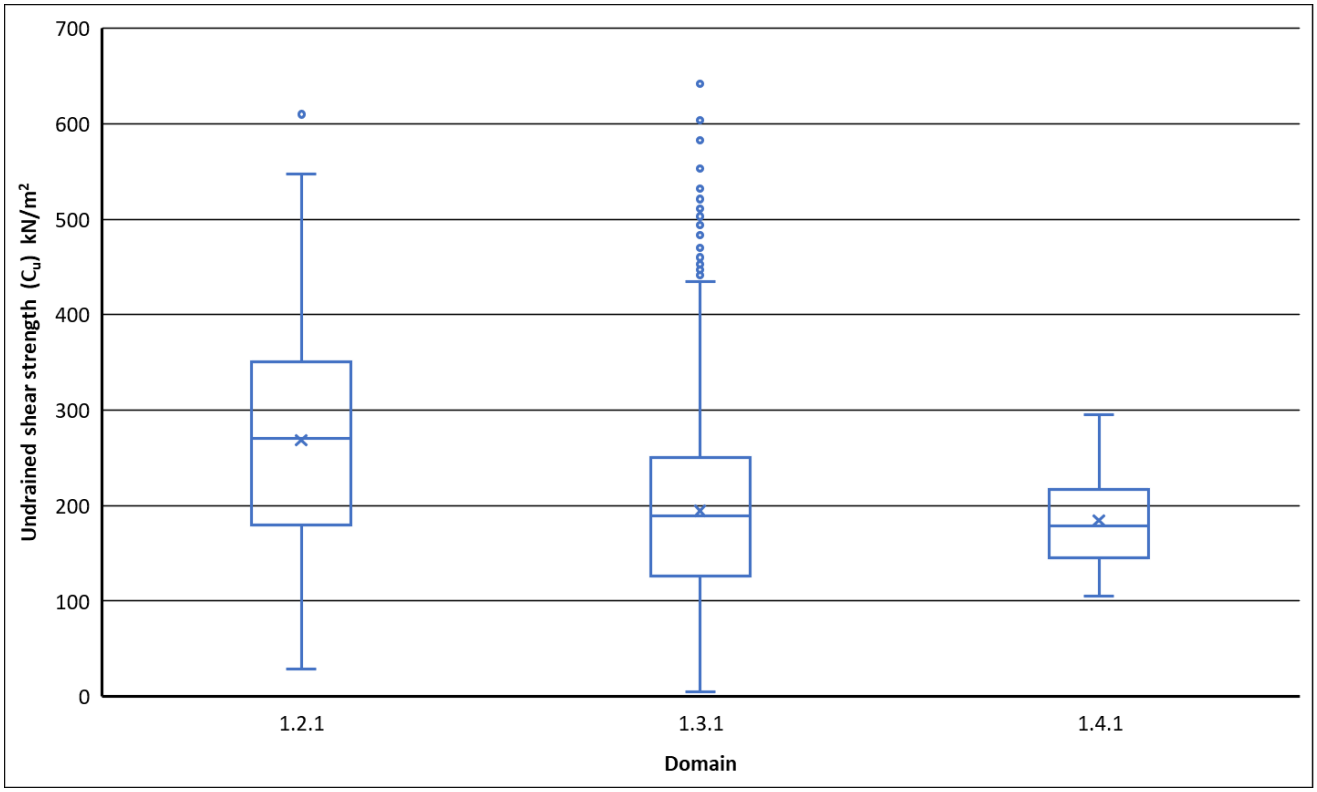

Figure 6-32 Box and Whisker plots of undrained shear strength for Till.

	Domain 1.2.1	Domain 1.3.1	Domain 1.4.1
Maximum	610	642	295
99.5	NA	518.21	NA
97.5	505	429.025	NA
90	437	315.4	NA
75	350	250	206
50	270	189	179
25	181	126	147
10	106	80	NA
2.5	45	40	NA
0.5	NA	20	NA
Minimum	29	5	105
n	220	1094	16

Table 6-15 Summary rank statistics for undrained shear strength, till. NA = range not calculated based on number of data.

The relationship between liquidity index and undrained shear strength has been established for fine-grained soils (Wroth & Wood, 1978; Vardanega & Haigh, 2014). Vardanega & Haigh (2014), based on data from fall cone tests, established that the transition in undrained strength between a soil's liquid and plastic limit increases a factor of ~35. To test this relationship using data within the project database, liquidity index-undrained shear strength were plotted and are shown in Figure 6-33.

The liquidity index-undrained shear strength plot in Figure 6-33 shows differences between Domains. Those data in Domains underlain by mudrocks (1.3.1 and 1.4.1) generally plot below or close to the curve defined by Wroth & Wood (1978) while those data in Domains underlain by granular bedrock (1.2.1) plot above it. This suggests that for any given value of undrained shear strength, those in Domains 1.2.1 are closer to their liquid limits than those in Domains 1.3.1 and 1.4.1 which must be closer to their plastic limits to mobilise the same strength.

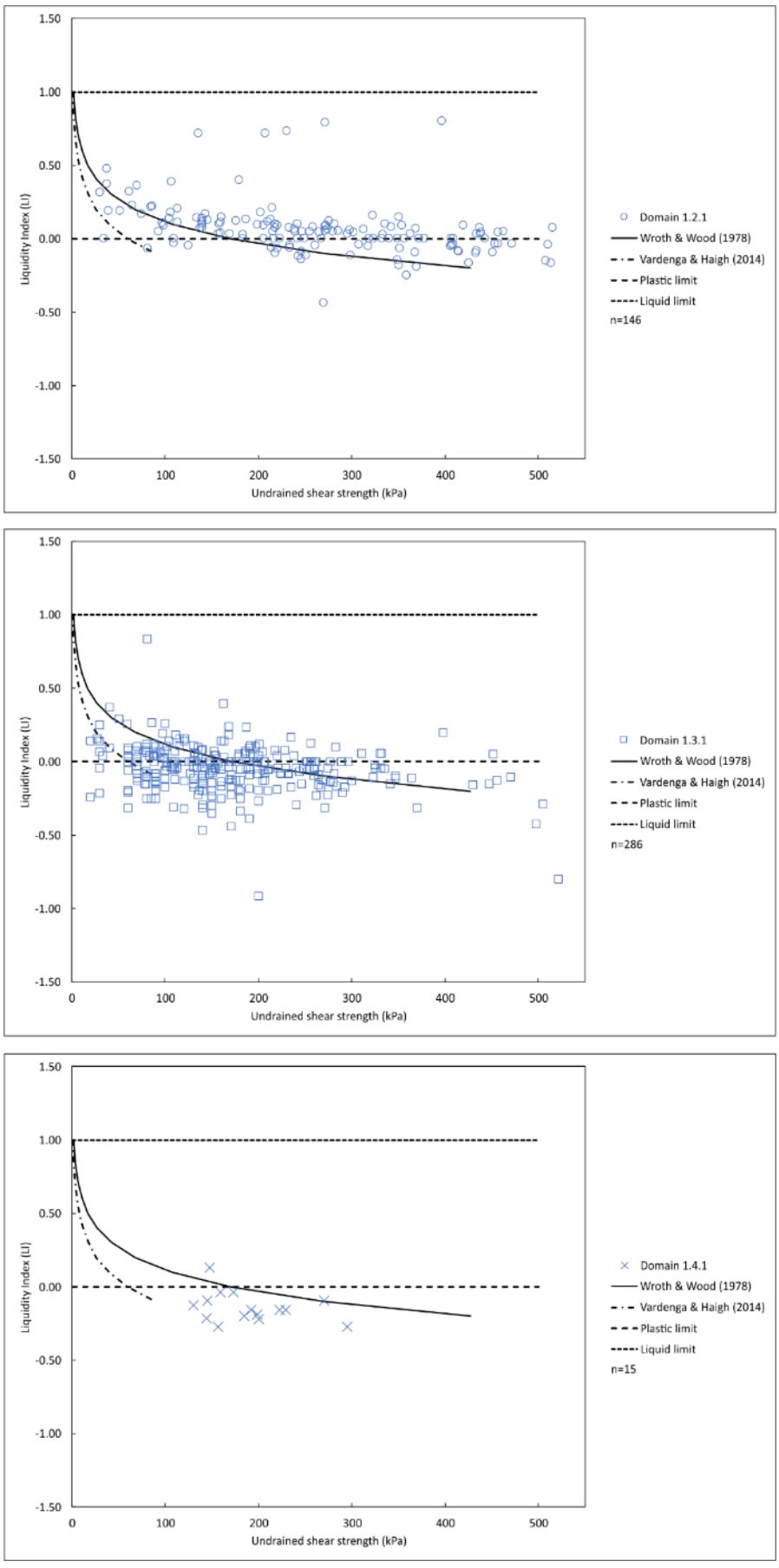

Figure 6-33 Liquidity index-undrained shear strength relationship for till.

6.2.8 Undrained shear strength (Oxford Clay)

There are 712 values of undrained shear strength for samples classified as Oxford Clay within the project database. Data are all derived from undrained triaxial tests on samples between 38 and 106 mm diameter. Triaxial tests are either UU or CU, single- or multi-stage experiments.

Percentile values are presented as Box and Whisker plots in Figure 6-34 and described in Table 6-16.

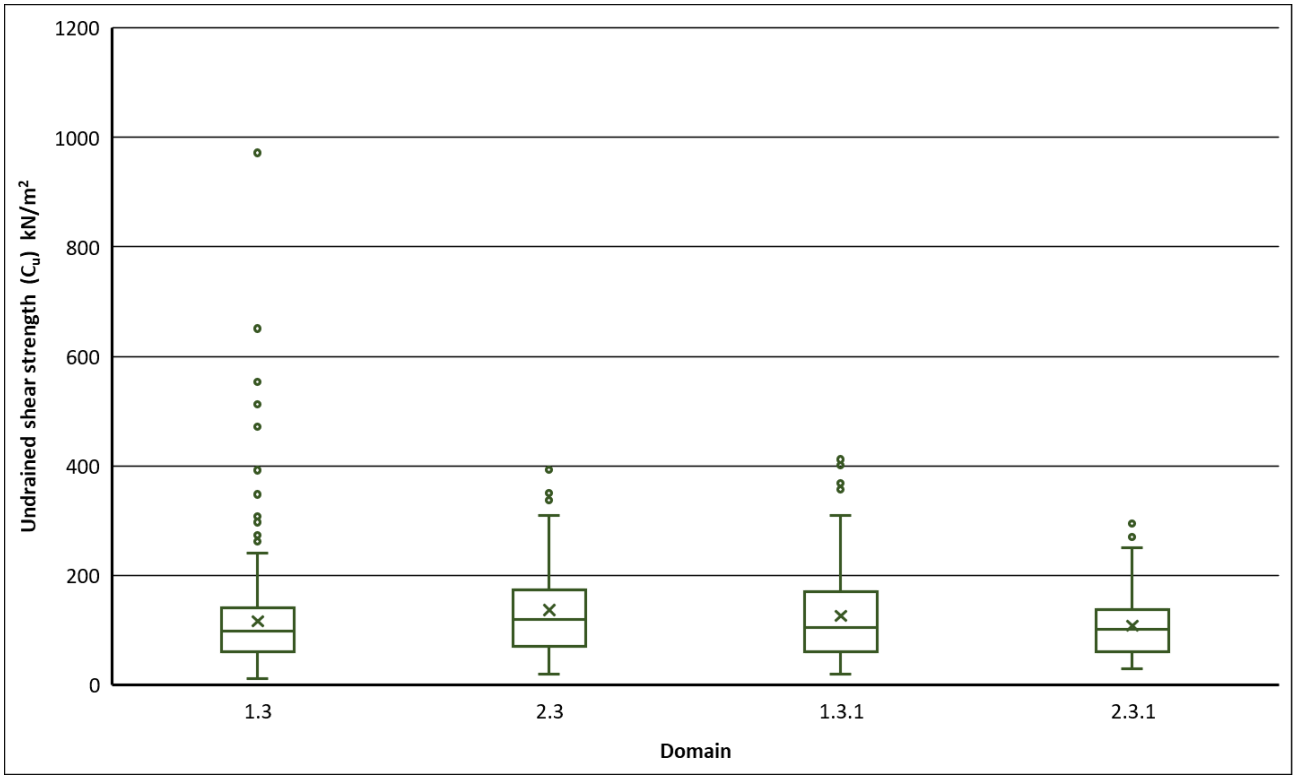

Figure 6-34 Box and Whisker plots of undrained shear strength for Oxford Clay.

Based on the median values for undrained shear strength, Oxford Clay samples can be classified as stiff. There is no noticeable difference in median values between Domains. Median values are slightly higher in Domains in 2.3 and 1.3.1, as are their IQR values.

To investigate the overall relationship between undrained shear strength and depth, values of Cu were plotted against depth below ground level (Figures 6-35 and 6-36). There is no distinct linear relationship between C_u and depth below ground level within each Domain. Between 0 and 10 mbgl, values are scattered. High values exceeding 200 kN/m^2 are seen and maybe associated with desiccation at shallow depths.

Undrained shear strength (C_u)				
	Domain 1.3	**Domain 1.3.1**	**Domain 2.3**	**Domain 2.3.1**
Maximum	972	412	393	295
99.5	NA	NA	NA	NA
97.5	302	310	NA	NA
90	198	221	251	181
75	140	170	172	133
50	99	105	119	102
25	60	60	75	60
10	40	49	51	40
2.5	30	30	NA	NA
0.5	NA	NA	NA	NA
Minimum	12	20	19	30
n	349	219	75	44

Table 6-16 Summary rank statistics for undrained shear strength, Oxford Clay. NA = range not calculated based on number of data.

Domain 1.3.1 is characterised by a uniform spread of values between 200 and 300 kN/m^2. In contrast, values in Domains 1.3 and 2.3 are characterised by a reduction in undrained shear strength between ~7-12 mbgl in Domain 1.3 and 6-8 and then 9-17 mbgl in Domain 2.3. This may be related to the zonation in plasticity values discussed in Section 6.2.2 but it is not possible to relate them directly.

Instead, the relationship between undrained shear strength and plasticity was investigated using liquidity index. The results are shown in Figures 6-37 and 6-38. The relationships generally follow that of Wroth & Wood (1978) but plot slightly below their best-fit line. There is little variation in liquidity index between Domains. Moisture content values plot close to values for plastic limit meaning that the liquidity index is generally close to, or slightly above, 0.

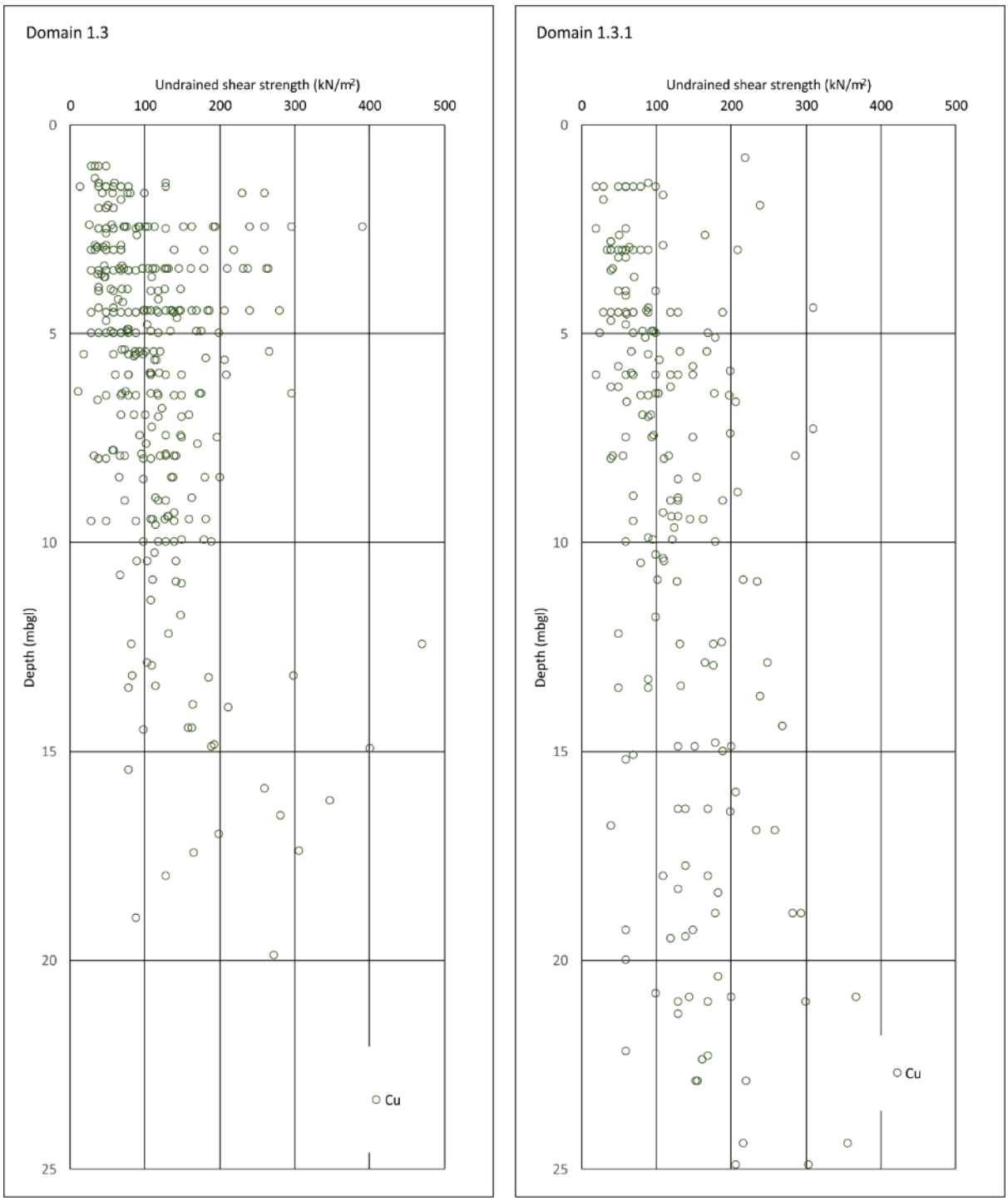

Figure 6-35 c_u *versus* depth for the Oxford Clay, Domains 1.3 and 1.3.1.

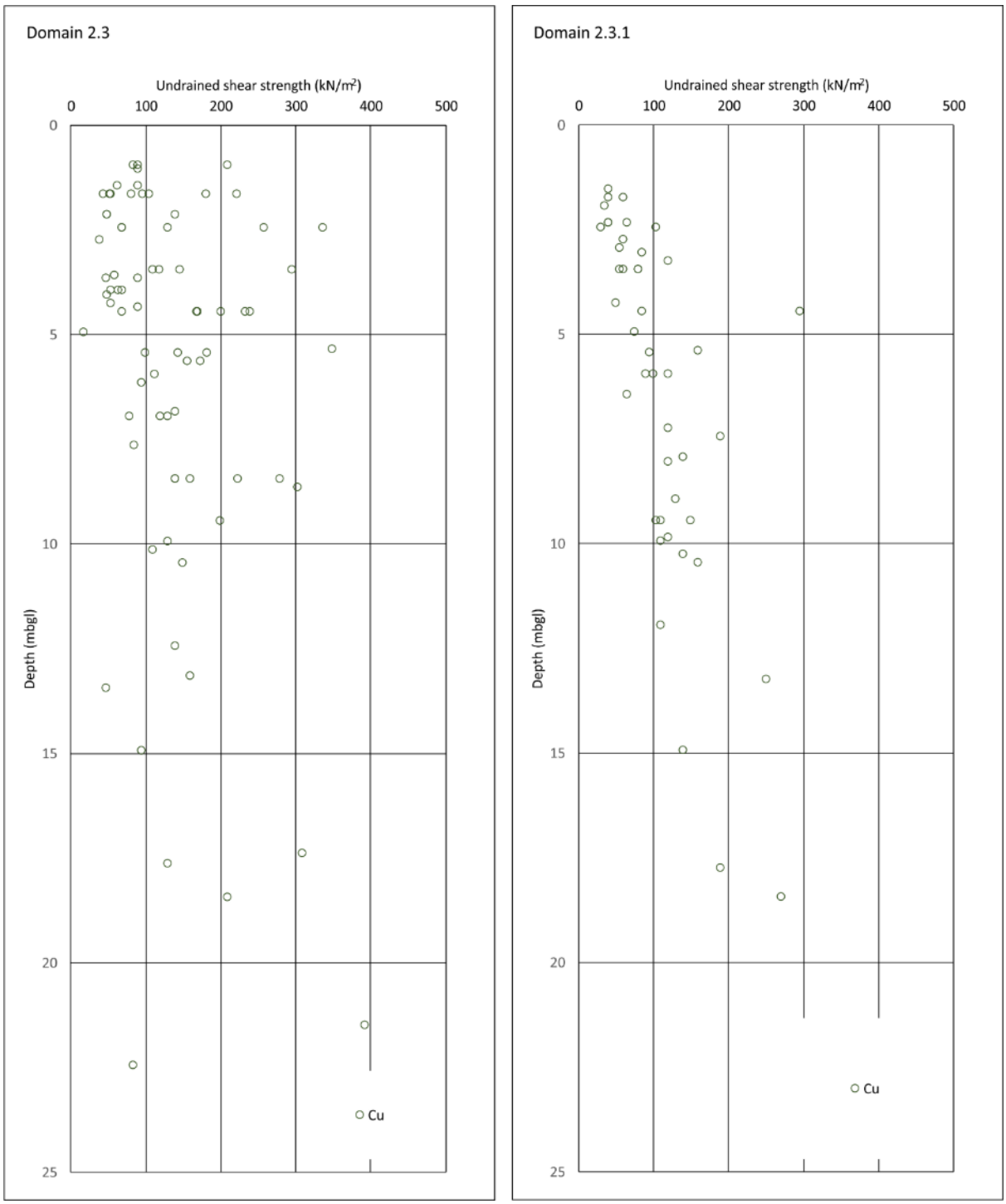

Figure 6-36 c_u *versus* depth for the Oxford Clay, Domains 2.3 and 2.3.1.

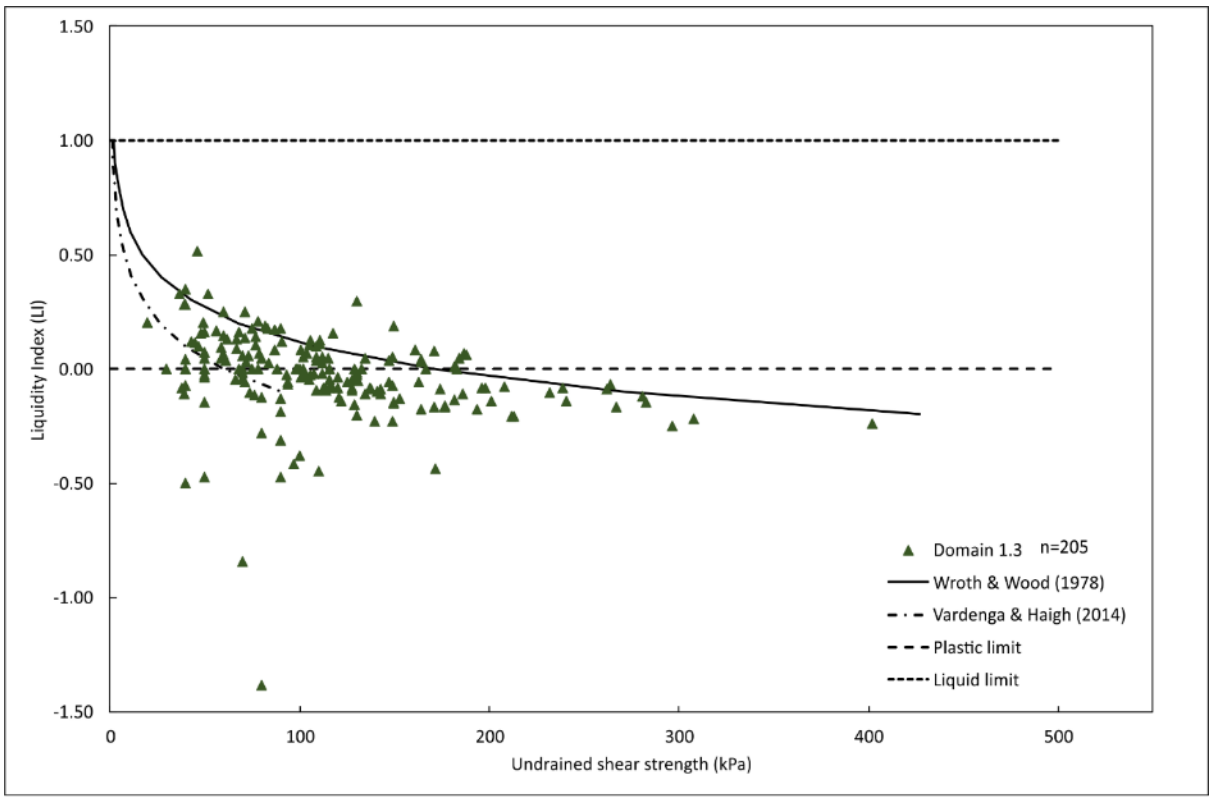

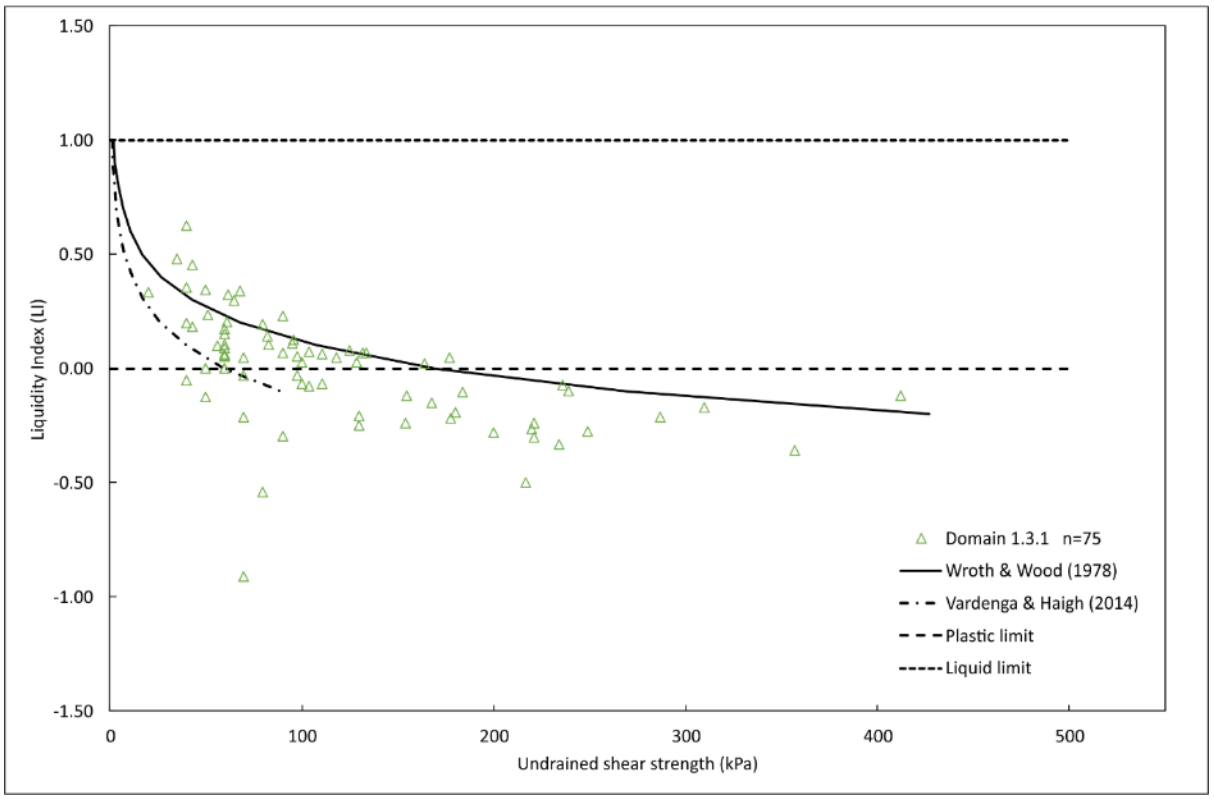

Figure 6-37 Liquidity index-undrained shear strength relationships for the Oxford Clay, Domains 1.3 and 1.3.1.

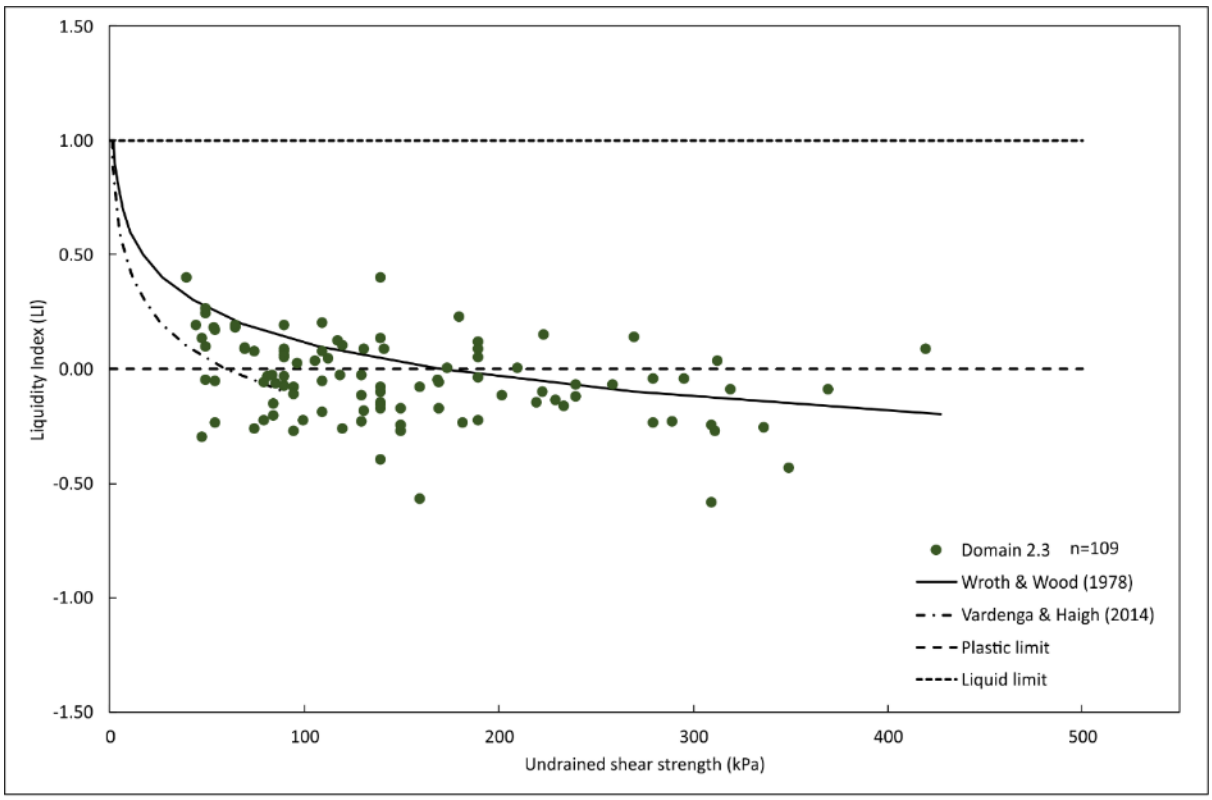

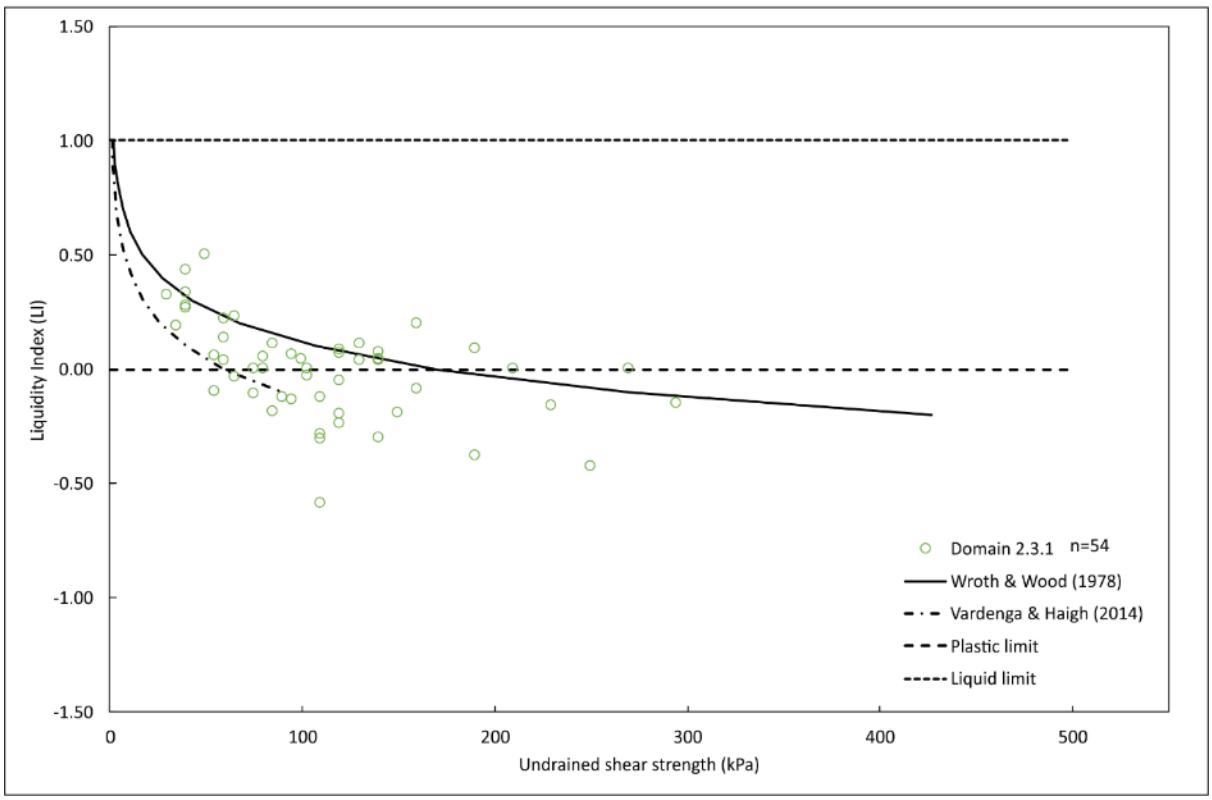

Figure 6-38 Liquidity index-undrained shear strength relationships for the Oxford Clay, Domains 2.3 and 2.3.1.

7 Field and laboratory methods

A geological field investigation and programme of geotechnical laboratory testing and experimentation was undertaken. This section describes the geological field, and geological and geotechnical laboratory methodologies used. The results and analyses are described in Section 8. This section is divided into geological field and laboratory methods (Sections 7.3 and 7.4) and then geotechnical laboratory methods (Section 7.5).

The objectives of the geological field investigations were to establish the composition, fabric and relative stratigraphical relationships within and between glacigenic sediments and underlying bedrock and to test evidence for their potential stratigraphical relationship with the English Midlands, Vale of St Albans and East Anglia. This was accomplished through examination of previously undescribed sedimentary exposures in former or active pits and quarries and their correlation with geological records from existing boreholes surrounding them (Section 5.2.2).

The objectives of the geotechnical investigation were to characterise fundamental index properties of till and Oxford Clay and their empirical relationship to geotechnical behaviour expressed as undrained shear strength, stiffness and compressibility. The variability in their parameter values could then be interpreted relative to their depth below ground level, spatial proximity to the Middle Pleistocene glacial limit of the BIS and their Quaternary Domain classification. The laboratory investigation therefore aimed to supplement the statistical analysis in Section 6 and to allow spatial comparison between specimens of the same geology within different Domains. Any differences or similarities identified, could then be related to their Quaternary geological history which differs between Provinces and Domains (Section 5.2.1).

The Oxford Clay provides an important geological reference to investigate the potential effects of glacial and/or periglacial processes. It crops out within different glacial and periglacial Quaternary Domains. Assuming its pre-Quaternary geological history was similar, as suggested by Jackson & Fookes (1974), it is assumed that differences in its properties and behaviour reflect its Quaternary history. These differences could then be mapped and compared to Quaternary Domains and field observations, to intepret the likely glacial and/or periglacial process that may have acted to influence changes in their properties and behaviour. The magnitude of variability at local to regional scale was then assessed by comparing the results of index, compressibility, undrained shear strength and stiffness derived from

laboratory investigation to the regional and ground investigation-specific variability determined from the analysis in Section 6, for each geological unit.

The index properties, selected based on their importance for geotechnical design and described in this section, were particle-(grain-) size, moisture content, Atterberg limits (plasticity), bulk density and particle density. Geotechnical behaviour was characterised in terms of compressibility, undrained shear strength and small-strain stiffness. Compressibility was measured in one-dimension (1D) using a 1D oedometer; undrained shear strength and small-strain stiffness were measured using triaxial apparatus in isotropically consolidated, undrained (CIU) conditions. Qualitative clay mineralogical analyses using X-ray diffraction (XRD) was also undertaken to investigate the potential relationship between the type of clay minerals present and plasticity, compressibility and undrained shear strength. The extent to which the clay mineralogy of matrix-dominated tills resembled that of the underlying Oxford Clay was also investigated.

7.1 Rationale for geological field-site selection

Selection of the field sites was based on their accessibility and spatial relationship to the inferred Anglian glacial limit of the BIS. The aim was to provide a southwest-northeast orientated transect through the Quaternary sequence in a direction interpreted to be parallel to former direction of advance and retreat of the BIS (see Figures 1-1 and 3-11). Site locations were chosen were chosen to provide potential exposures of geological layers proved by borehole drilling as part of Network Rail's, East West Rail (EWR) ground investigation.

Sites were also selected where they had been referred to in the literature but where description of the sediments or bedrock was missing on not provided. Five sites were selected, listed from southwest to northeast:

1. Home Farm, Stowe Park [SP 671 376];
2. Buckingham Sand Pit [SP 700 344];
3. Calvert [SP 698 227];
4. Newton Longville (Bletchley) [SP 869 322];
5. Passenham [SP 775 394].

A sixth site at Finmere [SP 625 326], adjacent to the proposed route of HS2, was selected and access agreed but was placed into administration before detailed geological investigation could begin. The locations of the field sites are shown in and their regional setting is shown in Figure 1-1. Field sites without good exposure but where useful examination of small cuttings,

overgrown pits and field brash could be made were also visited. These sites included Tingewick [SP 6530329], Poundon [SP 635 253] and Finmere Airfield [SP 641 323].

Sediment samples for numerical dating using Optically Stimulated Luminescence (OSL) were collected from Newton Longville, Buckingham Sand Pit and Home Farm, Stowe. Samples for determination of the clay mineralogy of till and Oxford Clay were selected from Buckingham Sand Pit, Calvert, Newton Longville, Passenham and Tingewick.

7.2 Sample selection, transport and handling

Undisturbed and disturbed sediment samples were derived from two main sources; disturbed bulk samples collected from field sites and undisturbed, ultra-thin walled (UT)100 cylindrical samples derived from the EWR ground investigation. The availability of disturbed, bulk and undisturbed, cylindrical UT100 samples from the EWR ground investigation was assessed at PSL Laboratories in Doncaster. Sediment samples scheduled but untested as part of the EWR project were collected in-person from the warehouses of PSL. Bulk and UT100 samples were stored in PSL's warehouse on shelved and open pallets. Most UT100 samples were stored horizontally but some were stored vertically.

Field and EWR-derived samples were chosen to compliment the results of existing geotechnical laboratory analysis results undertaken for ground investigation projects and which formed the basis of the statistical analysis in Section 6. The selection criteria were subjective; prioritising samples that enhanced spatial coverage and depth relative to the Middle Pleistocene limit of the BIS and Quaternary Domains. Samples > 10 mbgl were chosen to complement the EWR ground investigation whose focus, except for bridge crossings, was on ground characterisation <10 mbgl. Results of particle density, bulk density, particle-size analyses, Atterberg limits and single-stage triaxial compression analyses were used to directly supplement existing ground investigation data. The 1D consolidation and multi-stage triaxial compression analyses were designed to complement existing ground investigation data in two ways. Firstly, unless the swelling pressure exceeded the first stress increment, nine load-unload stages were used in the 1D consolidation analysis, compared to between four and six used for commercial analysis. Secondly, for selected samples, multi-stage triaxial analyses with measurement of small-strain stiffness were performed. For existing ground investigation data, most commercial laboratory triaxial tests comprised single-stage, 'quick' unconsolidated-undrained analyses. The objective of the analyses presented here was to provide estimates of small strain stiffness (~0.1%) and by using multi-

stage analyses, to increase the confidence in the measurement of undrained shear strength parameters, not routinely carried out in commercial laboratories.

Ideally the samples collected would be evenly distributed within and between Domains to provide representative laboratory results. However, the availability of samples from the EWR ground investigation, and the location of the field sites limited this. 1D consolidation and multi-stage triaxial experiments were undertaken on specimens prepared from UT100 samples, from the Oxford Clay in Domains 1.3, 1.3.1 (glaciated Province) and 2.3 (non-glaciated Province) and in Domain 1.4.1 (glaciated Province) for till. Bulk samples from the Oxford Clay were analysed in Domains 1.3, 1.3.1 and 2.3 and for till from Domains 1.1.1, 1.2.1, 1.3.1 and 1.4.1. Bulk samples for sediments interpreted to be from alluvium and river terrace deposits were analysed from Domains 1.1.1 and for glaciolacustrine sediments, from Domain 1.3.1.

After visual inspection, samples were lifted, carried and placed horizontally onto a pallet, then transferred to a van and driven to the Lord's Bridge storage area near Barton, Cambridge. Here, the external condition of each sampling tube was checked to ensure that end caps were in place and that the soft wax seal between the end cap and sample was still intact. Samples without end caps or where after visual observation, the wax seal was seen to be broken, were not used for strength, stiffness or compressibility experiments. Samples were stored horizontally onto shelves ready for collection, extrusion and testing (Figure 7-1A).

EWR samples were taken using either dynamic windowless samples or percussive shell and auger methods using thick-walled U100 or thin-walled UT100 samples. Samples taken after standard penetration testing (SPT) were treated as disturbed, bulk samples. Disturbed, and a small number of bulk samples, were also collected.

Open-tube, thick-walled U100 samples are considered Type 1 or 2 samples when they are obtained dynamically from normally or overconsolidated fine-grained sediments (Association of Geotechnical and Geoenvironmental Specialists, 1998; Gosling & Baldwin, 2010). Type 1 samples are suitable for all geotechnical laboratory experiments including strength and compressibility. Type 2 samples should be restricted to classification tests including particle-size determination, moisture content, plasticity, density and some experiments to determine remoulded strength. Open-tube, thin-walled, UT100 samples offer advantages over U100 samples taken with a plastic liner. UT100 samplers reduce the edge taper angle to 5º, area ratio (Ca) to <15% and inside clearance ratio (Ri) to <0.5% (Gosling & Baldwin, 2010). These improvements mean that UT100 samples can be classified as Type 1 according to

Gosling & Baldwin (2010). Only UT100 samples were used for strength, small-strain stiffness and compressibility experiments.

There were no UT100 sample extrusion facilities within the University or BGS. The samples were therefore extruded using the facilities at Oakley Soils in Bury St-Edmunds. Samples were collected when needed from Lord's Bridge and transported by car in hard, plastic containers to prevent rolling. The end caps of the samples were removed and the condition of the wax seal checked again. All samples had been filled with soft wax to the internal wall of the sample tube. Any samples where the wax seal had peeled away from the wall of the sampler were extruded but not used for strength, small-strain stiffness or compressibility experiments. Samples were extruded vertically using a hydraulic extruder fitted with a UT100 thread (Figure 7-1B). Each sample was carefully removed from the extruder, wrapped in multiple layers of cling-film and finally wrapped in bubble-wrap before being placed into 110 mm cut plastic pipe and wrapped again in clingfilm. The samples were placed horizontally into hard plastic boxes lined with bubble wrap and soft polystyrene packaging to minimize disturbance during transportation (Figure 7-1C). The samples were then driven by car to the geotechnical laboratories at the BGS where they were stored horizontally in a temperature-controlled cool room ready for testing. This procedure was followed for each batch of samples as and when they were needed.

A summary of the sediment samples used for geological and geotechnical characterisation is given in Table 7-1 and their location shown in Figure 7-2.

Figure 7-1 Undisturbed (intact) sediment sample storage, handling and transportation. A) Horizontal UT100 sample storage at Lord's bridge, Barton, Cambridge. B) Vertical extrusion of UT100 sample at Oakley Soils, Bury St-Edmunds. Soft wax is visible at the top of the partially extruded sample. C) Extruded UT100 samples, wrapped in cling film, bubble wrap and inserted into 110 mm plastic pipe before placing into plastic boxes filled with polystyrene foam and bubble wrap for transport to BGS laboratories.

Sample details								Laboratory analyses								
Sample name	Geology (Weathering grade, WG)[1]	Quaternary Domain	Depth to top of sample (mbgl)	Depth to base of sample (mbgl)	Sample type[2]	Date sample taken (ddmmyyyy)[3]	Date sample tested[4]	Particle Size Analysis (PSA)	Particle Density, ρ_s (Specific Gravity)	Bulk Density, ρ_B	Loss on Ignition (LOI)	[redacted] [3]	Atterberg (plasticity)	1D consolidation	Triaxial (multi stage) with Hall effect sensors	Clay X-Ray Diffraction (XRD)	Optically Stimulated Luminescence (OSL)[5]
CR022794	OXC_STW(IIb)	1.3	1.5	1.95	UT100	17/06/2015	16/02/2017	.	●	●	●	●	●	●		●	
CR023761	OXC_PET(IIa)	1.3	11.5	11.95	UT100	17/06/2015	28/02/2017	●	●	●	●	●	●	●	●	●	
CR023766	OXC_PET(IIa)	1.3	14.0	14.45	UT100	17/06/2015		●			●					●	
CR023247	OXC_PET(III)	2.3	2.0	2.45	UT100	26/05/2015	17/03/2017	●	●	●	●	●	●	●	●	●	
CR020746	OXC_PET(III)	2.3	1.2	1.65	UT100	27/05/2015	06/04/2016	●			●	●	●			●	
CR011958	TILL	1.4.1	13.5	13.95	UT100	18/06/2015	09/03/2017	●	●	●	●	●	●	●	●	●	
CR011968	TILL	1.4.1	19.5	19.95	UT100	18/06/2015		●			●					●	
CR011963	TILL	1.4.1	16.5	16.95	UT100	18/06/2015	17/03/2016	●	●		●	●	●			●	
CR011961	TILL	1.4.1	15.0	15.95	D	18/06/2015		●			●	●	●			●	
CR011953	TILL	1.4.1	10.5	10.95	UT100	18/06/2015	11/03/2016	●	●		●	●	●			●	
CR011981	TILL	1.4.1	27.0	27.45	D	18/06/2015		●			●	●	●			●	
CR011973	TILL	1.4.1	22.5	22.95	UT100	18/06/2015	14/03/2016	●	●		●	●	●			●	
CR011971	TILL	1.4.1	21.0	21.45	D	18/06/2015		●	●		●	●	●			●	
CR011966	TILL	1.4.1	18.0	18.45	D	18/06/2015		●			●	●	●			●	
CR011976	TILL	1.4.1	24.0	24.45	D	18/06/2015		●			●	●	●			●	
CR005904	OXC_STW(III)	1.3	1.5	1.95	UT100	16/01/2015	24/11/2016	●	●	●	●	●	●	●	●	●	
CR005942	OXC_PET(IIa)	1.3	24.0	24.45	UT100	16/01/2015	17/12/2016	●	●	●	●	●	●	●		●	
CR005869	OXC_PET(IIb)	1.3	12.0	12.45	UT100	13/01/2015		●			●	●				●	
CR005864	OXC_PET(IIb)	1.3	9.0	9.45	UT100	13/01/2015	07/12/2016	●	●	●	●	●	●	●	●	●	
CR005859	OXC_PET(IIb)	1.3	6.0	6.45	UT100	13/01/2015		●			●					●	
CR005853	OXC_STW(III)	1.3	3.5	3.95	UT100	13/01/2015		●			●	●	●			●	
CR021545	OXC_WEY(I)	1.3.1	8.8	9.25	UT100	22/04/2015	04/4/2017	●	●	●	●	●	●	●		●	
SP211016_1	TILL	1.2.1	UNK	UNK	B	21/10/2016		●			●	●	●			●	
SP211016_8	TILL	1.2.1	UNK	UNK	B	21/10/2016		●			●	●	●			●	

Table 7-1 Geological and geotechnical sample inventory. [1]Oxford Clay (OXC), Peterborough Member (OXC_PET), Stewartby Member (OXC_STW) and Weymouth Member (OXC_WEY), glaciolacustrine deposits (GLLD), alluvium (ALV), river terrace deposits (RTD) and glacigenic deposits undifferentiated (GLAC_UNDIFF). [2]Thin-walled (UT100), bulk (B) and disturbed (D). [3]Removed from the ground during ground investigation for East West Rail or hand-dug from field sites. [4]Date sample first tested for 1D consolidation to triaxial. [5]Moisture content and PSA undertaken on equivalent duplicate samples from the same location as those for OSL.

Sample details								Laboratory analyses								
Sample name	Geology (Weathering grade, WG)[1]	Quaternary Domain	Depth to top of sample (mbgl)	Depth to base of sample (mbgl)	Sample type[2]	Date sample taken (ddmmyyyy)[3]	Date sample tested[4]	Particle Size Analysis (PSA)	Particle Density, ρ_s (Specific Gravity)	Bulk Density, ρ_B	Loss on Ignition (LOI)	Moisture content, ω	Atterberg (plasticity)	1D consolidation	Triaxial (multi stage) with Hall Effect	Clay X-Ray Diffraction (XRD)	Optically Stimulated Luminescence (OSL)[5]
SP191016_7	TILL_SAND	1.3.1	3.0	3.0	B	19/10/2016		●			●	●					
SP191016_8	TILL_SAND	1.3.1	2.5	2.5	B	19/10/2016		●			●	●					
SP250916_2	GLLD	1.2.1	1.0	1.0	B	25/09/2016		●			●	●					
SP250916_3	TILL	1.2.1	1.0	1.0	B	25/09/2016		●			●	●	●			●	
SP11102016_1	TILL	1.2.1	4.0	4.0	B	11/10/2016		●			●	●	●			●	
SP191016_2	TILL	1.3.1	4.4	4.4	B	19/10/2016		●			●	●	●			●	
180815_SPRICE_2	OXC_PET	1.3.1	~20.0	~20.0	B	18/08/2015		●			●	●	●			●	
SP261016_5	TILL	1.1.1	2.0	2.0	B	26/10/2016		●			●	●	●			●	
SP191016_9	'HEAD'	1.2.1	0.5	0.5	B	19/10/2016		●			●	●					
SP11102016_3	SAND_GRAVEL	1.2.1	2.0	2.0	B	11/10/2016											
SP261016_2	ALV	1.1.1	1.0	1.0	B	26/10/2016		●			●	●	●				
SP261016_3	RTD	1.1.1	1.5	1.5	B	26/10/2016		●									
SP120617_1	GLLD	1.3.1	6.7	6.7	B	12/06/2017		●			●	●	●				
SP120617_2	GLLD	1.3.1	7.0	7.0	B	12/06/2017		●			●	●	●				
SP080417_8	GLAC_UNDIFF	1.2.1	5.46	5.46	B	08/04/2017		●			●	●					
SP070417_3	GLLD	1.3.1	5.96	5.96	B	07/04/2017		●			●	●					
SP070417_6	GLLD	1.2.1	13.0	13.0	B	07/04/2017		●			●	●					
SP080417_4	GLAC_UNDIFF	1.2.1	9.86	9.86	B	08/04/2017		●			●	●					
SP070417_1	GLLD	1.3.1	5.34	5.34	B	07/04/2017											●
SP070417_5	GLLD	1.2.1	13.0	13.0	B	07/04/2017											●
SP080417_1	GLAC_UNDIFF	1.2.1	9.86	9.86	B	08/04/2017											●
SP080417_5	GLAC_UNDIFF	1.2.1	5.46	5.46	B	08/04/2017											●

Table 7-1 continued.

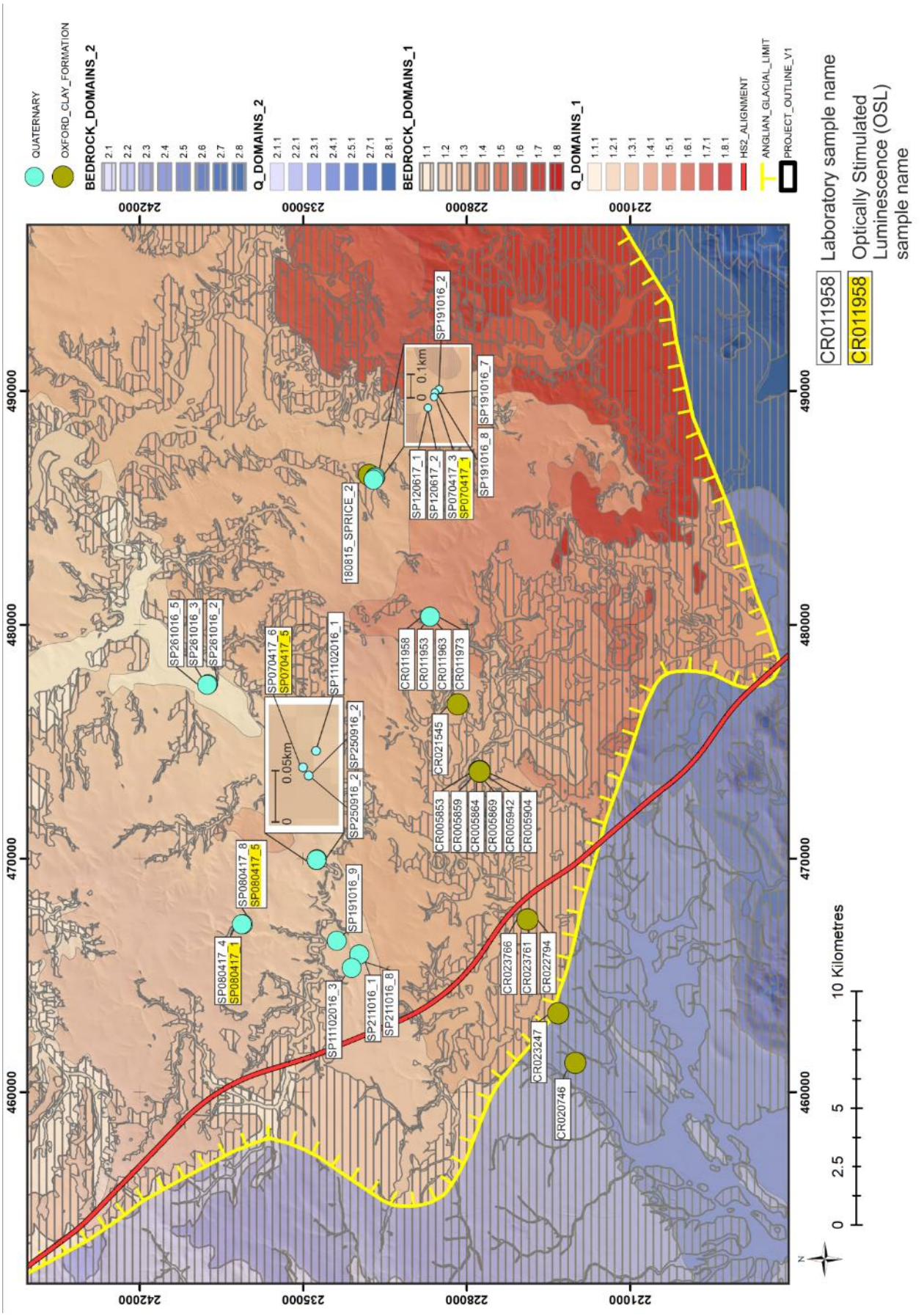

Figure 7-2 Location of geological and geotechnical samples (coloured circles).

7.3 Geological field methodology

After field site selection, localities were inspected, and exposed sections were described by sedimentological logging. Levelling was undertaken using a Leica SmartRover at Bletchley, Buckingham Sand Pit and Home Farm, Stowe Park to give a positional and altitudinal accuracy of ~1 mm. A hand-held Garmin GPS device and OS landform contours were used to determine the position and elevation of section logs at other sites. Measurements of dipping surfaces were recorded in degrees using the convention of dip magnitude and dip azimuth (e.g. 17/090). All elevations were measured relative to Ordnance Datum (OD) and grid references were recorded as easting and northing relative to the British National Grid (BNG). Additionally, samples collected for numerical dating using OSL were converted to latitude and longitude as this was needed as part of the methodology to estimate radiation dose at the site-scale.

During field logging, a compromise was attempted between describing sediments as engineering soils and conventional geological descriptions which are in common usage, especially for the study of glacial sediments. In general, sediment descriptions followed those recommended by British Standards BS5930:1999 incorporating amendment 2, 2010 (British Standards Institution, 1999; Norbury, 2012) except where geological terms were used for clarity or to avoid confusion. All descriptions of clay, silt, sand, gravel, cobbles and boulders are consistent with the meaning defined in British Standards. The engineering descriptions were supplemented with lithofacies codes as recommended by Benn & Evans (2004) based on previous lithofacies schemes including that of Eyles *et al*. (1983)

A simplified series of names for colour was used, following the pragmatic recommendation of Norbury (Norbury, 2012). The term mottled is used to denote the presence of two or more colours which my be banded or irregularly intermixed.

7.4 Geological laboratory methodology

Geological laboratory analysis comprised loss-on-ignition (LOI) and qualitative X-Ray Diffractometry of clay minerals (XRD) for Oxford Clay and tills. Additional Quaternary samples were analysed including sediments from river terrace deposits, glaciolacustrine deposits and solifluction ‘head’. Numerical dating of glacigenic sediments was undertaken using Optically Stimulated Luminescence. LOI and sample preparation for clay mineralogy XRD was undertaken at the University of Cambridge’s Department of Geography Science Laboratories. Clay mineral XRD analysis was undertaken at the University of Cambridge’s Department of Earth Sciences by Dr Giulio Lampronti.

7.4.1 Loss-on-ignition (LOI)

Samples were prepared to measure the percentage of organic material, carbonate content and silicate residue. Gravimetric water content (GWC) was only measured for those samples whose GWC had not been measured during geotechnical sample preparation for Atterberg limit determination.

1cm^3 sub-samples were taken using a metal spatula and placed into 0.6 cm^3 glass vials and sealed with a plastic stopper ready for analysis. The analytical steps are summarised in Table 7-2.

Step number	Description of procedure
1.0	Clean and dried ceramic crucibles weighed.
2.0	Wet sample removed from glass vial, placed into crucible and weighed.
3.0	Samples placed into oven overnight at 105ºC. Samples removed from oven, cooled in a desiccator and the weight recorded for those samples where GWC had not been measured previously.
4.0	Samples in crucibles placed onto trays and then into a muffle furnace overnight at 550ºC.
5.0	Samples cooled to 100ºC then removed from muffle furnace, cooled in a desiccator, weighed and returned to the muffle furnace overnight at 950ºC.
6.0	Samples cooled to 100ºC then removed from muffle furnace, cooled in a desiccator and weighed.

Table 7-2 Loss-on-ignition procedure.

7.4.2 Clay mineral X-Ray Diffractometry (XRD)

The aim of this step was to qualify the type of clay minerals within each sample and to relate this to their geotechnical behaviour described in terms of undrained shear strength, stiffness and compressibility. In addition, this step aimed to establish the extent to which the clay mineralogy of glacigenic sediments reflects that of their sediment source areas especially related to Middle and Late Jurassic mudrocks of the Oxford Clay.

Approximately 10-20g of sediment was sub-sampled and used to prepare them for XRD analysis. Sub-samples were either taken from <425µm sub-samples prepared for Atterberg analysis or directly from unprepared bulk samples. The XRD sub-samples and their sources are given in Table 7-3.

Sample name	Geology	Sub-sample source	Previous sub-sample preparation
CR023247	OXC_PET	Atterberg	Atterberg method 1
CR011958	TILL	Atterberg	Atterberg method 2

SP250916_3	TILL	Atterberg	Atterberg method 2
SP261016_5	TILL	Atterberg	Atterberg method 2
SP11102016_1	TILL	Atterberg	Atterberg method 2
SP211016_8	TILL	Atterberg	Atterberg method 2
SP191016_2	TILL	Atterberg	Atterberg method 2
CR005853	OXC_STW	Atterberg	Atterberg method 1
SP211016_1	TILL	Atterberg	Atterberg method 2
CR022794	OXC_STW	Atterberg	Atterberg method 1
180815_SPRICE_2	OXC_PET	Atterberg	Atterberg method 1
CR023247	OXC_PET	Bulk	None
CR021545	OXC_WEY	Bulk	None
CR023761	OXC_PET	Bulk	None
CR005942	OXC_PET	Atterberg & bulk	Atterberg method 1
CR011953	TILL	Atterberg	Atterberg method 2
CR011981	TILL	Atterberg	Atterberg method 2
CR011976	TILL	Atterberg	Atterberg method 2
CR020746	OXC_PET	Atterberg	Atterberg method 1
CR011963	TILL	Atterberg	Atterberg method 2
CR005904	OXC_STW	Atterberg	Atterberg method 1
CR011973	TILL	Atterberg	Atterberg method 2
CR005864	OXC_PET	Atterberg	Atterberg method 1
CR011961	TILL	Atterberg	Atterberg method 2
CR011966	TILL	Atterberg	Atterberg method 2
CR011971	TILL	Atterberg	Atterberg method 2
CR023766	OXC_PET	Bulk	None
CR005859	OXC_PET	Bulk	None
CR005869	OXC_PET	Bulk	None

Table 7-3 Sub-sample sources for clay mineral XRD analysis. Atterberg method 1 requires sample maturation in a sealed polythene bag for at least 24 hours with no prior wet-sieving. Atterberg method 2 requires sample maturation in a sealed polythene bag for at least 24 hours after wet-sieving to separate <425µm fraction.

The methodology described is based on that described by Moore & Reynolds (1997) and adapted following the procedures developed by Dr Chris Jeans at the University of Cambridge. The aim was to prepare orientated aggregate sample mounts of the <2 µm fraction to enhance the (00l) crystal reflections and reduce those form (hkl). The sample preparation steps are given in Table 7-4.

Step number	**Description of procedure**

1.0	Transfer 10-20g of sample into washed and dried glass bottles.
2.0	**Removal of carbonate** Add 100mL, 1M concentration glacial acetic acid to sample in glass bottle and add rubber stopper. Samples in bottles placed on bottle holders and left overnight.
3.0	Manually shake each bottle with sample and place into ultrasonic water-bath for at least 60 seconds. Add a further mL glacial acetic acid to sample. Replace stopper.
4.0	Continue to manually end-over-end shake bottles with samples at intervals of ~2 hours for 3 days, settling overnight.
5.0	**Washing to remove acetic acid (1)** De-ionised water added to each bottle to a level ~two thirds of the bottle volume and shaken manually end-over-end before leaving overnight.
5.1	**Washing to remove acetic acid (2)** Supernatant liquid decanted using a vacuum. Fresh de-ionised water added and manual end-over-end shaking repeated before leaving for six hours.
5.2	**Washing to remove acetic acid (3)** Supernatant liquid decanted using vacuum. Fresh de-ionised water added and manual end-over-end shaking repeated. Samples with visible aggregates of sediment were added to the ultrasonic water-bath for at least 60 seconds.
5.3	**Washing to remove acetic acid (4)** Supernatant liquid decanted using vacuum. Fresh de-ionised water added and manual end-over-end shaking repeated. Samples left overnight.
5.4	**Final washing to remove acetic acid (5)** Supernatant liquid removed using vacuum.
6.0	**Extraction of clay fraction** Extracted by pipette based on settling velocities according to Stoke's Law (see text). 4.4% concentration Na-hexametaphosphate was added sufficient to cover the sample and then manually shaken, end-over-end. Each sample, still within a glass bottle was placed in a bottle holder. Dried and washed centrifuge tubes with 2-3 drops of $CaCl_2$ added were set aside.
6.1	After end-over-end shaking, each sample was left to settle for 3 hours 54 minutes to allow <2 µm fraction to settle to a depth of 50mm. Once the time had elapsed, the rubber stoppers of each sample were removed and the time recorded. The first sample was extracted by glass pipette and transferred to the centrifuge tubes. Each subsequent sample was taken by pipette and transferred to the centrifuge tube at 90 second intervals, rinsing the pipette in de-ionised water after each sample transfer.
6.2	**Centrifuge** Each sample plus CaCl2 solution was balanced and centrifuged at 2600rpm for 20

	minutes. On completion, the resulting supernatant was poured off and the samples within the centrifuge tubes placed upside-down in test tube holders.
7.0	**Slide mounting** Custom-made, square, glass slide mounts were placed onto a rectangular glass slide. The sample was removed from the centrifuge tubes using a metal spatula and placed onto the slide mount before gentle smearing across the slide to create an even coating. This was repeated twice for each sample. Using forceps, the glass smear mount was placed onto a ceramic tile. All samples were then transferred to a desiccator and placed above a container with calcium nitrate.

Table 7-4 Sample preparation procedures for clay mineralogy XRD after Moore & Reynolds (1997) and proprietary method developed by Dr Chris Jeans, University of Cambridge.

Step 6 required the separation of the <2 µm equivalent spherical diameter fraction. This is based on Stoke's formula which assumes that particles are spheres. Clays are platy and the method relies on the assumption that 1 µm of clay mineral crystallite settles at the same velocity as a 1 µm sphere of equal density. The <2 µm fraction was separated based on the time taken for those particles to settle over 50 mm within a measured time interval. The terminal velocity of a particle (V_T) is proportional to the gravitational force (g in cm/sec^2) acting on it and inversely proportional to the viscosity of the fluid (η). It is also directly proportional to the diameter of the particle (D^2) and the difference in density between the particle and the liquid (ρ_p-ρ_l). The equation for Stoke's formula is:

$$V_T = \frac{g(\rho_p\text{-}\rho_l)D^2}{18\eta}$$

Equation 7-1

This can be rearranged using the relationship V=h/t where h is distance/height and t is time.

$$t = \frac{18\eta h}{g(\rho_p\text{-}\rho_l)D^2}$$

Equation 7-2

From equation 7-2, the time (t) taken for a particle of a given diameter to settle over a given distance can be calculated.

The samples were placed on plastic analysis mounts and presented for analysis using a Bruker D5000 diffractometer with Cu Kα radiation. Each clay mineral assemblage was subjected to four analyses of two-hour duration; air dried (untreated), heating to 400ºC, heating to 550ºC

and glycolation. X-ray powder diffractograms in the 2θ range 2 to 40° (step size 0.04, 5 seconds per step) were collected after each treatment in Bragg-Brentano geometry.

7.4.3 Optically-Stimulated Luminescence (OSL)

Four samples were collected in the field with the assistance of Dr Chris Rolfe from the University of Cambridge's Geography Science Laboratories. Samples were transported to the Sheffield Luminescence Laboratory (SLL) at the University of Sheffield where sample preparation and analysis was undertaken by Professor Mark Bateman. The laboratory methodology described here is an edited version of that provided by Professor Bateman in a summary laboratory methodology and results report.

7.4.3.1 Field sample collection

Samples were collected from three field sites; Bletchley [SP 869 322], Buckingham Sand Pit [SP 700 344] and Home Farm, Stowe [SP 671 376]. The sample sites at each location are shown in Figure 7-3.

At each site, an open-ended aluminium or black plastic cylindrical tube was dynamically pushed into the sampling horizon in a horizontal position. Once fully inserted, the outward facing end was packed with tissue paper and taped using silver Duck-tape. The tube was gently extracted and the inward facing also packed with tissue and taped. The sample was then labelled including the relative positions of the inward and outward-facing ends. During excavation, approximately 400g of loose material was collected in sealable polythene bags for particle-size and moisture content analysis. Field samples were observed to be variably silty fine- to coarse-sand. Their field setting and geological interpretation are described in Sections 8.2.1 and 8.4.1.

The hole was further excavated and enlarged using a trenching tool to allow insertion of the University of Sheffield's Micronomad gamma spectrometer to derive field estimates of radiation dose rate. The gamma spectrometer was inserted into the excavated hole and set to record for 60 minutes. After completion of background gamma radiation recording, two duplicates OSL samples were taken either side of the primary hole.

A Leica SmartRover Global Navigation Satellite System (GNSS) was used to locate and level each sample site relative to height above Ordnance Datum (OD) and to within 1 mm horizontal accuracy within the British National Grid (BNG) coordinate system.

The samples were submitted for luminescence dating to the SLL. The samples were assumed not to have been exposed to sunlight during sampling or transportation. On arrival at SLL, the

samples were allocated Sheffield laboratory numbers (Table 7-5), which are used throughout this section.

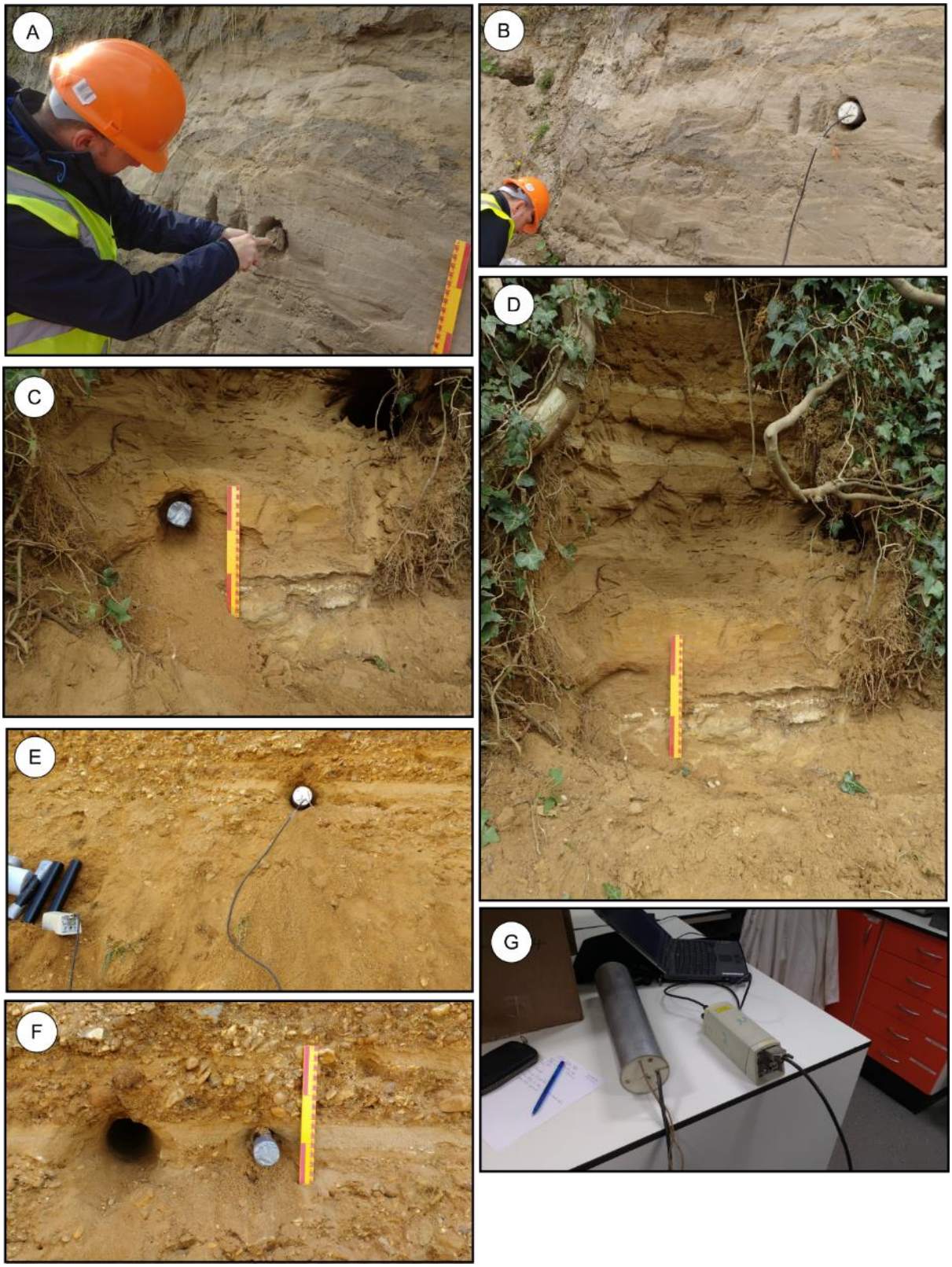

Figure 7-3 OSL field-sample collection. A) and B) Bletchley with gamma spectrometer in-place. C) and D) Buckingham Sand Pit, with primary OSL sample in-place with outward face taped. E) and F) Home Farm, Stowe

with gamma spectrometer in-place, location 1 and taped duplicate sample location 2. G) Laboratory calibration of gamma spectrometer before fieldwork, University of Sheffield.

Lab No.	Field Reference	Latitude (° N)	Longitude (° W)	Altitude (m)	Sampling Depth (m below present-day surface)
Shfd17085	SP070417-1	51°58'	0° 44'	80.9	5.3
Shfd17086	SP070417-5	52°00'	0° 59'	89.4	4.0
Shfd17087	SP080417-1	52°02'	1° 01'	121	9.9
Shfd17088	SP080417-5	52°02'	1° 01'	126	5.5

Table 7-5 OSL sample descriptive data. Sample locations expressed in Latitude and Longitude to cross-check radiation dose.

To derive an OSL age both the palaeodose (D_e - the amount of absorbed dose since the sample was buried) and the dose rate (the estimated radiation flux for the sedimentary bodies) must be determined. Aitken (1998) gives a detailed explanation of both these parameters. To calculate an age, the palaeodose (expressed in Grays, Gy where 1 Gy = $1J/kg^{-1}$) is divided by the annual dose rate (Gy/yr). An inherent assumption in these age calculations is that the sediment was fully reset or 'bleached' by exposure to sunlight during the last transport event or whilst *in situ* before burial and that no post-depositional sediment disturbance has occurred.

As part of this analysis, efforts have been taken to establish whether the sediments have been bleached prior to burial. As the OSL signal measured at the single aliquot level is an average of ~2000 grains, the true distribution of D_e values may be masked. This is of significance in sediment samples that have been poorly reset by bleaching. In these cases, grains with a high D_e signal will dominate the signal at the expense of grains containing a true burial D_e. The samples in this study underwent OSL dating both at the small aliquot (approx. 500 grains per aliquot) and at the single-grain level.

7.4.3.2 Dose Rate Analysis

Naturally occurring potassium (K), thorium (Th) and uranium (U) are the main contributors of radioactive dose to sedimentary quartz. The concentrations of these elements were determined in the field using both a Micronomad field gamma spectrometer and in the laboratory using inductively coupled plasma (ICP) spectroscopy (Table 7-6). Elemental concentrations were converted to annual dose rates using data from Adamiec and Aitken (1998), Marsh *et al.* (2002), and Aitken (1998). Calculations accounted for attenuation factors relating to sediment grain sizes used, density and palaeo-moisture. Attenuation of dose by an estimated gravimetric moisture content of 15% compared to measured values, was interpreted to account for historical lowering of the groundwater by quarry activity with a ± 5 % error to

incorporate fluctuations through time. The combined dose rate used the gamma spectrometer data for the gamma dose and the ICP data for the beta dose.

Lab Code	**Method**	**U** (ppm)	**Th** (ppm)	**K** (%)	**D_{cosmic}**$^{+}$ ($\mu Gy/a^{-1}$)	**Moisture** (%)	**Combined Dose rate**† ($\mu Gy/a^{-1}$)
Shfd17085	Gamspec	1.52	5.42	0.99	107 ± 5	15	1698 ± 88
	ICP	1.43	5.4	1.2			
Shfd17086	Gamspec	1.46	5.40	0.99	126 ± 5	15	1815 ± 93
	ICP	2.01	7.4	1.2			
Shfd17087	Gamspec	0.96	3.16	0.56	100 ± 5	15	1008 ± 50
	ICP	1.56	2.90	0.60			
Shfd17088	Gamspec	0.92	3.12	0.55	101 ± 5	15	1387 ± 80
	ICP	1.04	4.1	1.2	±		

Table 7-6 Summary of dosimetry related data. $^{+}$ Cosmic dose is calculated as a linear decay curve at depths below 50 cm. Above this depth, errors in calculation may lead to an underestimation of the cosmic dose contribution.† Total dose is attenuated for grain size, density and moisture.

The contribution to dose rates from cosmic sources was calculated using the expression published in Prescott and Hutton (1994; Table 2). The calculated dose rates are based on analyses of the sediment sampled at the present day. This assumption is only valid if no movement and/or reprecipitation of the four key elements has taken place since sediment burial and the adjacent sediments to those sampled had similar dose rates. Further analysis, for example field gamma spectroscopy, would have to be undertaken to establish whether the latter is true and if radioactive disequilibrium is present in the dose rate.

7.4.3.3 Palaeodose (D_e) determination

Samples were prepared under subdued red lighting to extract and clean quartz grains following the procedures outlined in Bateman and Catt (1996). Material for dating was taken from prepared quartz isolated to a size range of 125-250 μm. The samples underwent measurement using a Risø DA-20 luminescence reader with radiation doses administered using a calibrated ^{90}strontium beta source. For the small aliquot measurement, quartz grains were mounted as a ~5 mm diameter monolayer on 9.6 mm diameter stainless steel using silkospray. An array of blue/green LEDs provided the stimulation and luminescence detection was through a Hoya U-340 filter. Samples were analysed using the single aliquot regenerative (SAR) approach (Murray & Wintle, 2000, 2003) in which an interpolative

growth curve is constructed using data derived from repeated measurements of a single aliquot which has been given various laboratory irradiations (Figure 7-4 A, B). Five regeneration points were used to characterise growth curves, with the first regeneration point being identical to the last to check if sensitivity changes caused by repeated measurement of the same grains are correctly monitored and corrected for by the SAR protocol (known as the "recycling ratio"). The most appropriate preheat temperature for measurement was selected using a dose recovery preheat plateau test conducted on sample Shfd17086. This test resulted in the selection of a preheat temperature of 180°C for 10 seconds. This was applied to each sample prior to OSL measurement to remove any unstable signal generated by laboratory irradiation. D_e values from individual aliquots were thus only accepted if they exhibited an OSL signal measurable above background, good growth with dose, recycling values within ± 10 % of unity, and a signal greater than 3 times background level. While the aliquot shown in Figure 7-4 shows good growth with laboratory dose some aliquots, whilst not saturated, were on the flat part of the exponential curve.

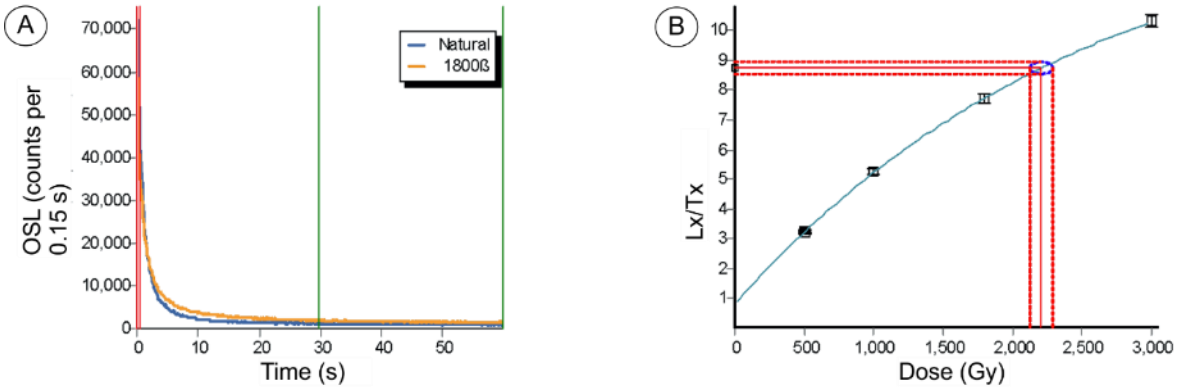

Figure 7-4 Example OSL laboratory decay curve at single aliquot level (A) and Single Aliquot Regenerative (SAR) growth curve (B) used to determine equivalent dose, D_e for sample Shfd17085. In A, red lines denote integration limits for signal measurement, green lines represent background measurement once the signal has been zeroed. In B the luminescence response (Lx) to a series of known laboratory doses is normalised by small test doses (Tx). The natural dose in B is extrapolated to intersect the growth curve to determine D_e from the x-axis.

7.4.3.4 Sedimentary bleaching behaviour and sample saturation

The effects of incomplete bleaching of the sediment during the last period of transport or exposure *in situ* can be profound. Typically, poorly bleached sediments retain a significant level of residual signal from previous phases of sedimentary cycling, leading to inherent inaccuracies in the calculation of a palaeodose value. By plotting the replicate D_e data for the sample as a probability density function some assessment of whether older or younger

material has been included in the sample measurements can be made (although of less significance for older samples). In principle, a well-bleached sample that has not been subjected to post-depositional disturbance should have replicate D_e data which are normally distributed and highly reproducible (Bateman *et al.*, 2003; Figure 3; Bateman *et al.*, 2007 a). Where post-depositional disturbance or incomplete bleaching prior to sample burial has occurred, skewing of this distribution may occur and/or replicate reproducibility may be lower (Bateman *et al.*, 2007 b; Bateman *et al.*, 2007 a). In the case of poorly bleached material, skewness should be evident with a high D_e tail (e.g. Olley *et al.*, 2004). High D_e tails may also be indicative of saturated samples and interpolation of the D_e values from the upper, low gradient part of the growth curve (Murray & Funder, 2003).

The D_e distributions of all samples are generally normally distributed although broad with some outliers (Figure 7-5). D_e replicate scatter (OD) is consistently around 24-27%. Given the antiquity of the samples, partial bleaching if it existed, should constitute only a small proportion of the burial dose.

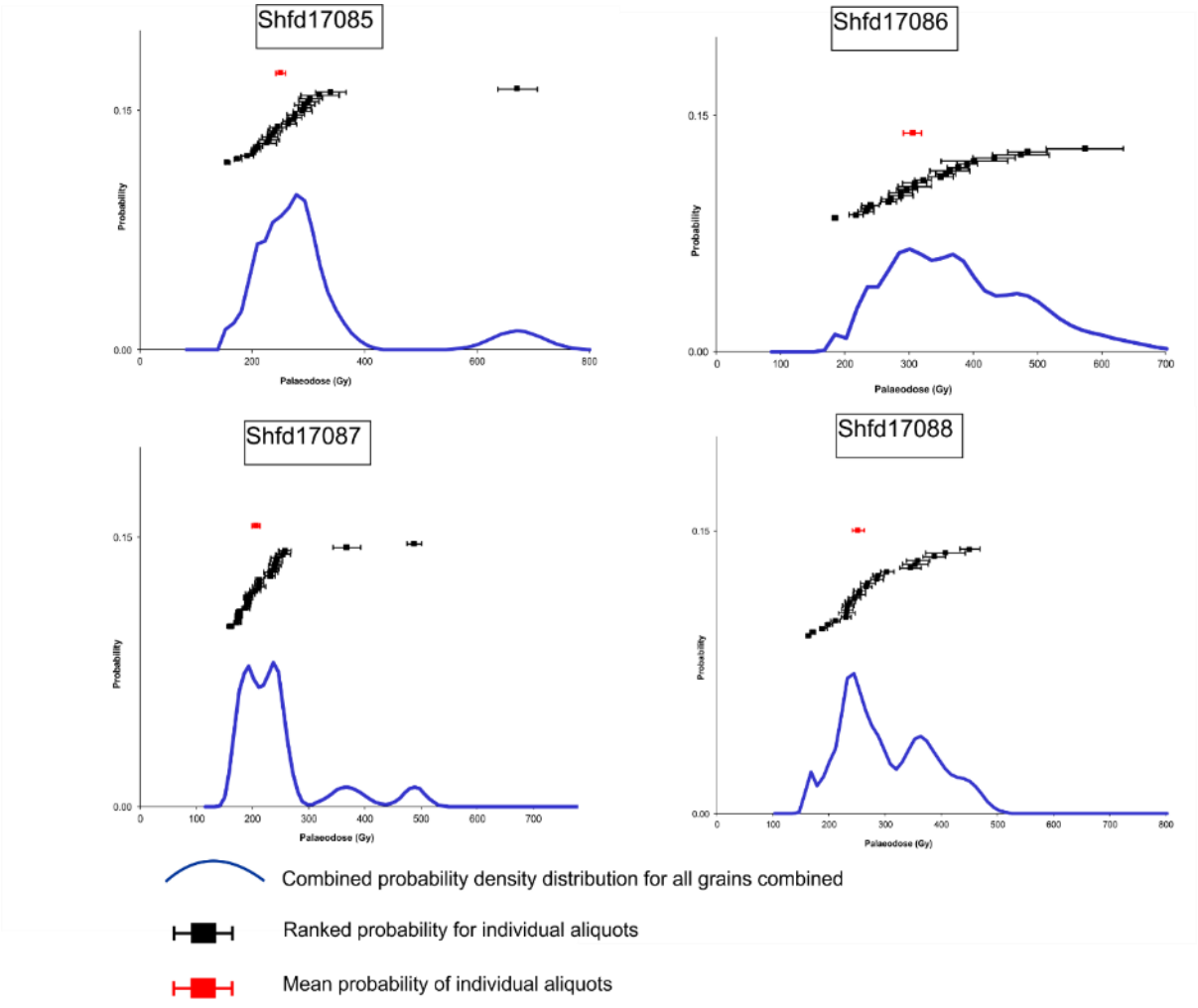

Figure 7-5 Probability distribution functions for OSL palaeodose (D_e).

7.5 Geotechnical laboratory methodology

The objectives of the geotechnical laboratory programme were to determine key geotechnical properties and behaviour of Oxford Clay and Quaternary sediments and compare the results to regional spatial patterns of property variability and Quaternary Domains defined in Section 5.2.1. Where possible, intact UT100 samples were chosen from the EWR sample collection or bulk samples collected in the field to provide a representative sample distribution in terms of spatial extent and depth relative to the Middle Pleistocene Anglian glacial limit.

The measurement and variability of geotechnical behaviour in terms of compressibility, undrained shear strength, stress-strain and small-strain stiffness was selected to be representative of the types of behaviour most relevant to the strategic location of the study area. Engineering soils comprising till and Oxford Clay have been classified according to soil quality classes applied to earthworks and trackbed design for railways and are summarised in Table 7-7. QS0 soils are considered as engineering soils which do not form a suitable subgrade and therefore require ground improvement. QS3 soils are classified as good engineering soils typically comprising well-graded soils containing <5% clay and silt.

Bedrock	**Quaternary sediments over bedrock (Y/N/type)**	**Earthwork Type**	**Soil Quality Class for earthwork type**
Oxford Clay	N	At grade	QS0
Oxford Clay	N	Cutting	QS0
Oxford Clay	N	Embankment	QS3
Oxford Clay	Y/Alluvium	Embankment	QS3
Oxford Clay	Y/Alluvium	At grade	QS0
Oxford Clay	Y/River Terrace Deposits	At grade	QS0
Oxford Clay	Y/River Terrace Deposits	Embankment	QS3
Oxford Clay	Y/Till	Cutting	QS0

Table 7-7 Engineering soil classification for railway earthworks after (2008).

The most important criteria determining the pre-failure deformation of railtrack geometry is the stiffness of the ballast and blanket layer combined with the subgrade, which is characterised by its bearing capacity (Union Internationale Des Chemin de Fer, 2008). Subgrade beneath ballast can provide upto 50% of trackbed stiffness (Huille & Hunt, 2000). The variability in track subgrade stiffness has been shown to cause reduced train speeds and higher track maintenance costs. Subgrade stiffness is provided by a combination of natural, *in situ* bedrock and/or Quaternary deposits and engineered materials. Estimates of subgrade

stiffness in natural geological materials can be based on small-strain shear modulus with the initial shear modulus G_0, being recognised as a fundamental soil property (Gunn *et al.*, 2003).

The thickness of ballast and blanket layers for ballasted track can be determined by the subgrade soil quality class and its related bearing capacity. Geological subgrade therefore influences the design thickness of prepared subgrade, blanket layer and ballast thickness where higher quality bearing capacity classes result in thinner ballast and blanket layers.

Desk study based estimates of shear modulus in natural geological materials can be derived from relationships between lithology (soil class), shear wave velocity, density and moisture content (Gunn *et al.*, 2003). The relationship can be defined in terms of effective stress so that depth-density profiles can be modelled. The voids ratio and stress history-dependent relationship between shear wave velocity and effective stress can be used to calculate shear wave velocity with depth for known engineering soil types.

Whilst soft trackbed foundations will produce greater bending stresses in the rail and high ballast strains, a stiff foundation can increase dynamic impact loads. Both effects may result in rail wear and deformation of track geometry (Hunt, 2005). This had led to the development of the concept of optimal stiffness in railway design. The variability in stiffness between soft and stiff ground is therefore a key factor in linear earthwork design.

This experimental design therefore aimed to characterise the stress-strain behaviour, effective stress strength parameters of cohesion and angle of shearing resistance and small-strain stiffness for till and Oxford Clay by conducting single and multi-stage, isotropically-consolidated triaxial experiments. Hall effect sensors in triaxial experiments were used to measure small-strain stiffness to derive estimates of initial shear modulus. Compressibility in 1D was measured using 1D consolidation apparatus. In addition to measuring compressibility, the results of 1D consolidation experiments were used to infer the influence of glacial and/or periglacial stress history by estimating the ratio between preconsolidation pressure (past maximum effective stress) and present-day stress. Index properties were determined in terms of particle-size analysis (PSA), particle density (specific gravity) and Atterberg limits (plasticity) including measurement of gravimetric moisture content. Samples of Oxford Clay and till were selected for determination of index properties, compressibility, undrained shear strength, stress-strain and small-strain stiffness. Index properties including Atterberg limits and PSA were determined for other Quaternary sediments including ‘head’, River Terrace Deposits and Alluvium.

Particle density, Atterberg limits, moisture content, 1D consolidation and multi-stage triaxial experiments were carried-out at the BGS's geotechnical laboratories. PSA was undertaken at the Department of Geography's Science Laboratories.

7.5.1 Particle-Size Analysis (PSA)

The aim of the particle-size analysis was to classify each sample of Oxford Clay and till (including granular interbeds) based on the relative proportion of particle-sizes expressed as percentage passing (or percentage finer) using a cumulative particle-size distribution plot. Particle-size analysis was carried out using two methods. The selection of each method depended on the visual assessment of the range of particle-sizes, the presence of clay and/or silt and soil behaviour. The combined methodologies and workflow are summarised in Figure 7-6.

Samples were selected from four sources (types 1 – 4). Most cohesive, fine-grained (clay and silt-rich) samples of type 1 and 2, were selected from surplus material prepared for Atterberg limit tests. This was done to maximise the use of samples whose original mass was not sufficient for the preparation of multiple sub-samples for different experiments.

Type 1 samples were cohesive, fine-grained samples prepared for Atterberg testing using Atterberg preparation Method 1, described in Section 7.5.3. Type 1 samples were dominantly from the Oxford Clay and consequently sieving was not required for the preparation of samples for PSA. Type 2 samples were derived from both the <0.425 and >0.425 mm size fraction of sieved cohesive soils that contained some granular particles and were prepared using Method 2 for Atterberg testing. Type 2 samples were derived from till and 'head'. Type 3 samples were bulk samples of coarse-grained, granular soils comprising silt, sand and gravel. Type 3 samples were derived from granular glaciofluvial deposits. Type 4 samples were previously untreated bulk samples derived from the Oxford Clay, one of till which had not been previously prepared for Atterberg testing and bulk granular samples from intra-till sand and gravel lenses. A summary of samples selected for PSA and their preparation method is given in Table 7-8.

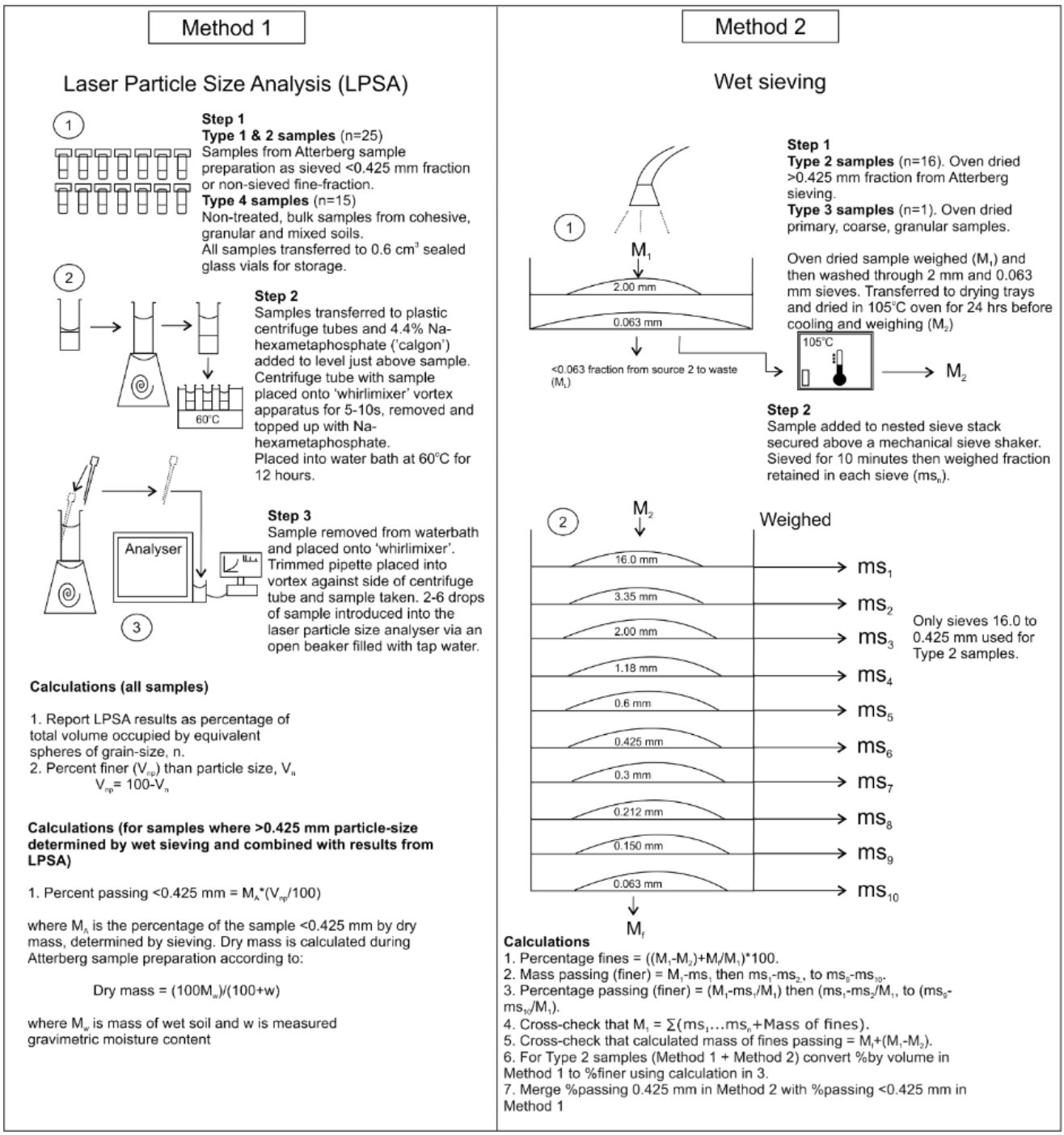

Figure 7-6 Summary of Particle-Size Analysis (PSA) methodologies.

Sample name	Geology	Sample type
CR022794	OXC_STW	1

Sample name	Geology	Sample type
CR023761	OXC_PET	4
CR023766	OXC_PET	4
CR023247	OXC_PET	1
CR020746	OXC_PET	1
CR011958	TILL	2
CR011968	TILL	4
CR011963	TILL	2
CR011961	TILL	2
CR011953	TILL	2
CR011981	TILL	2
CR011973	TILL	2
CR011971	TILL	2
CR011966	TILL	2
CR011976	TILL	2
CR005904	OXC_STW	1
CR005942	OXC_PET	1
CR005869	OXC_PET	4
CR005864	OXC_PET	4
CR005859	OXC_PET	4
CR005853	OXC_STW	1
CR021545	OXC_WEY	4
SP211016_1	TILL	2
SP211016_8	TILL	2
SP191016_7	TILL_SAND	4
SP191016_8	TILL_SAND	4
SP250916_2	TILL_SAND	4
SP250916_3	TILL	2
SP11102016_1	TILL	2
SP191016_2	TILL	2
180815_SPRICE_2	OXC_PET	1
SP261016_5	TILL	2
SP191016_9	'HEAD'	4
SP261016_2	ALLUVIUM	2
SP261016_3	RTD	3
SP120617_1	GLLD	1
SP120617_2	GLLD	1
SP080417_8	GLAC_UNDIFF	4
SP070417_3	GLLD	4
SP070417_6	GLLD	4
SP080417_4	GLAC_UNDIFF	4

Table 7-8 Particle-size analysis samples and types. Refer to Table 7-1 for definition of geological codes.

The results of the PSA are presented as percentage passing (finer) – log particle-size plots for individual samples and ternary plots of clay, silt and sand for samples within each Quaternary

Domain. For Type 2 samples and sample CR011968, the percentage passing – log particle-size plots were constructed by combining the results of wet sieving for the >0.425 mm fraction and the results of LPSA for the <0.425 mm fraction. LPSA results were rounded to one significant figure and converted from % by volume to % finer. Results expressed as % finer were converted to equivalent masses of the sample according to:

$$\text{Equivalent mass} = \frac{M_{\text{L}} \times P_{\text{f}}}{M_1}$$

Equation 7-3

where M_L is dry mass of <0.425 mm fraction, P_f is percent finer than given particle-size and M_1 is sample dry mass. This method assumes that the <0.425 mm sub-sample for LPSA is representative of the whole <0.425 mm fraction. The point corresponding to percentage finer for the 0.425 mm wet sieve fraction was not plotted for combined, wet sieve and LPSA plots to produce a smoother curve between the datasets.

For Type 1 and 4 samples, results of LPSA analysis reported as % by volume were converted to % finer. The results from LPSA analysis assume that all particles can be measured as equivalent spheres. Samples containing platy clay minerals may therefore not meet the conditions of this assumption.

7.5.2 Particle density (specific gravity)

Particle density represents the average mass per unit volume of a sample of soil. Particle density was measured for those samples subject to 1D consolidation and triaxial compression experiments. The small pyknometer method was used following the procedures described in Head (2006) and which are summarised in Table 7-9. This test is suitable for fine-grained soils with a grain-size of <2 mm. Where the sediment sample contained particles >2 mm, they were ground down to a size that passed a 2 mm sized sieve.

Step	Description
1	**Preparation of density bottles**

Step	Description
	Each density bottle and stopper was washed and rinsed with acetone or an alcohol-ether mixture and dry by blowing warm air through them. Each labelled bottle was cooled and weighed to the nearest 0.001 g (m_1).
2	**Preparation of test specimen** A sample of 50–100 g was obtained by quartering the original dry sample. Where gravel-sized particles were present a representative proportion was included but were ground with pestle and mortar to pass a 2 mm British Standard (BS) sieve. The sample was riffled to obtain a test specimen of about 30 g, oven dried at 105°C, and cooled in a desiccator.
3	**Placing in bottles** The dried specimen was divided into two approximately equal parts using a riffle box and placed into a density bottle by pouring from a folded sheet of paper while wearing nitrile gloves. Each bottle with soil was weighed to 0.001 g (m_2).
4	**Adding liquid and applying vacuum** De-aired water was carefully added to each bottle by pouring down the sides to minimize sample disturbance, so that the soil was just covered and the bottles were no more than half full. Ten bottles at a time, without stoppers, into a vacuum desiccator. The pressure was gradually reduced to about 2 kPa and leave under vacuum for at least one hour. Bubbles were seen to leave the sample and the vacuum was maintained until no further loss of air could be seen.
5	**Removal of air** After one hour and when no bubble could be seen to emerge from the sample, the vacuum was slowly released, and the desiccator lid removed. The soil in the bottle was carefully stirred with a Chattaway spatula. Soil particles adhering to the blade back were carefully washed back into the bottle with a little of the de-aired liquid. The desiccator lid was replaced, and the vacuum applied again until no further loss of air could be seen.
6	**Transfer to constant-temperature bath** Each bottle was removed in-turn from the desiccator and de-aired water added until full. Stoppers were added to the bottles and each placed in a constant-temperature bath at 24.7ºC so that they were immersed up to their necks. The samples were left immersed for at least one hour.
7	**Weighing**

Step	Description
	The stoppered bottles were removed from the bath and wiped it dry with blue-roll, avoiding prolonged contact with hands. The bottle + stopper + soil + liquid was weighed and recorded to 0.001 g (m_3).
8	**Weighing bottle with liquid** Each bottle was then rinsed, cleaned and filled completely with de-aired water. The stopper was inserted and immersed in the constant-temperature bath as before. The bottle and stopper was removed from the bath and wiped dry avoiding prolonged contact with hands. The bottle + stopper + liquid was weighed to 0.001 g (m_4).
9	**Calculations** The particle density, ρ_s, of the soil in each bottle was calculated from: $$\rho_s = \frac{\rho_L(m_2 - m_1)}{(m_4 - m_1) - (m_3 - m_2)}$$ **Equation 7-4** Where ρ_L = density of liquid used, m_1= mass of empty bottle, m_2=mass of bottle + soil, m_3=mass of bottle+soil+liquid and m_4=mass of bottle + liquid The average of the two measured values was calculated. In some cases the average for any one value differed by more than 0.03Mg/m^3 which indicates that the test should be repeated according to Head (2006). Because of time constraints this was not repeated for this research. Where average values differ by more than 0.03Mg/m^3, it is indicated as such. The average values were reported to the nearest 0.01Mg/m^3 as the soil's particle density.

Table 7-9 Procedures for the measurement of particle density using the small pyknometer method after Head (2006).

7.5.3 Atterberg limits (plasticity) and moisture content

Moisture content (ω), Liquid Limit (W_L) and Plastic Limit (P_L) were determined on the soil fraction passing a 0.425 mm sieve following the sample preparation and experimental procedures described in Head (2006).

Between 350 - 500 g of material was taken from bulk samples or trimmings of samples prepared for 1D consolidation and/or triaxial testing. Each sample was prepared by one of two methods depending on the visual assessment of the presence or absence of particles likely to be retained on a 0.425 mm sieve. The procedures for sample preparation are described below and summarised in Figure 7-7.

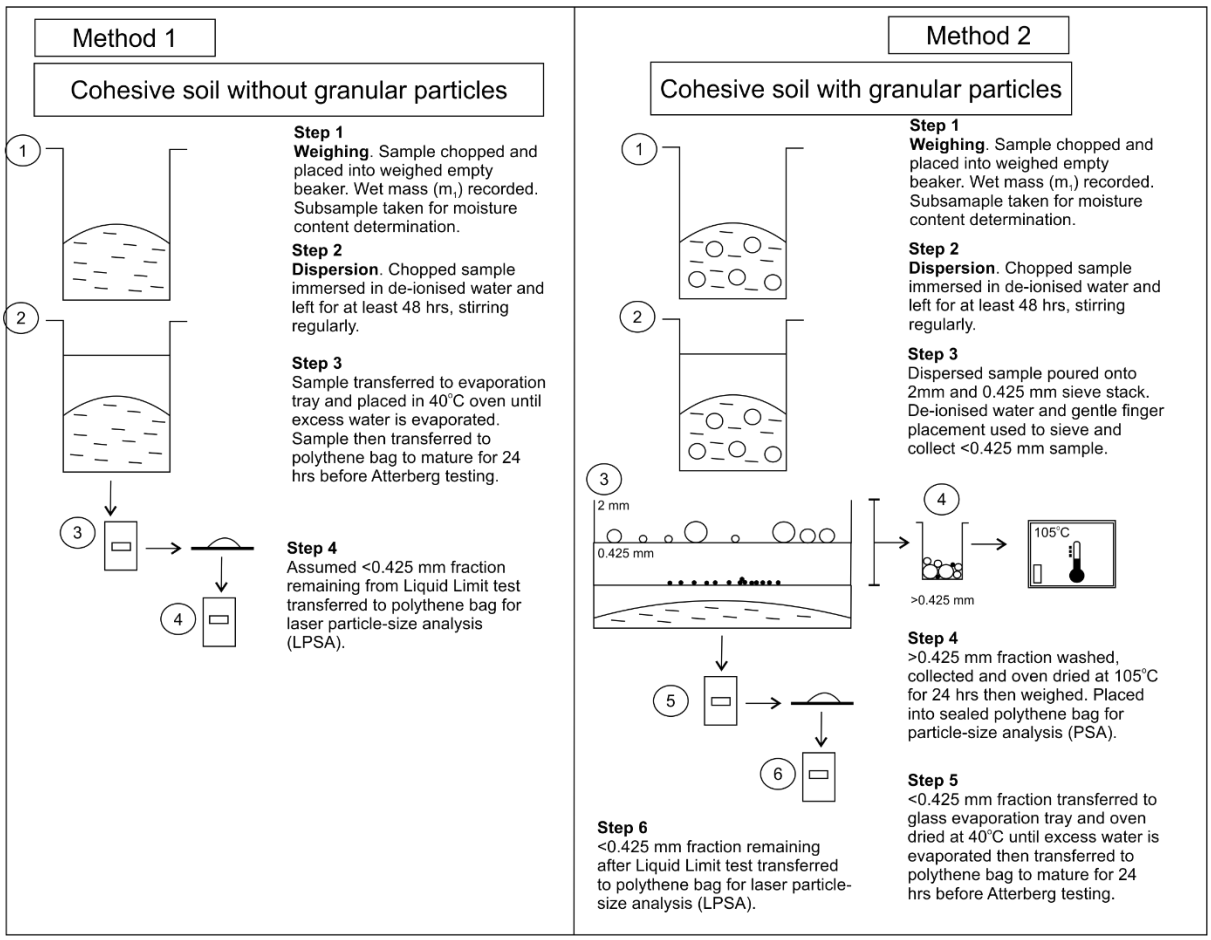

Figure 7-7 Workflow procedures for moisture content and Atterberg limit determinations. Method 1 used generally for Oxford Clay samples. Method 2 used for poorly-graded till.

7.5.3.1 Sample preparation Method 1 (little or no material retained on a 0.425 mm sieve)

A representative sample of about 500 g of soil was taken and chopped into small pieces using a large kitchen knife. The sample was mixed with de-ionised water on a glass plate using two palette knives. Coarse particles were removed by hand or with tweezers. The water was thoroughly into the soil for at least 10 minutes, until a thick homogeneous paste was formed, and the paste had absorbed all the water with no surplus water visible. The mixed soil was placed in a sealed polythene bag and left to mature for at least 24 hours.

7.5.3.2 Sample preparation method 2 (material retained on a 0.425 mm sieve)

Where the samples contained material likely to be retained on the 0.425 mm sieve, or where coarser particles would be difficult to remove by hand, a representative sample of the soil at its natural moisture content was taken to give at least 350 g of material passing the 0.425 *m*m sieve. The sample was chopped into small pieces using a large kitchen knife and placed into

an empty, weighed, glass beaker. The mass of the wet soil, *m* (g) was determined by subtraction.

A similar representative sample was taken and its gravimetric moisture content, ω (%) determined by:

$$Gravimetric\ moisture\ content\ (\%)\ =\ \frac{m_2\ -\ m_3}{m_3} \times 100$$

Equation 7-5

where, m_2 is mass of the wet soil, m_3 is the mass of soil dried overnight at 105ºC and m_1 is the mass of an empty container.

The dry mass of soil in the test sample, m_D (g), can then be calculated from:

$$\text{Dry mass } (m\text{D})\ =\ \frac{100m}{100 + \omega}$$

Equation 7-6

where, *m* is the mass of the wet soil.

De-ionised water was added to the beaker to submerge the soil and the soil pieces broken with a spatula, taking not to crush larger particles and stirred until the mixture formed a slurry. The sample was left, stirring regularly for at least 24 hours. A 0.425 mm sieve on a base receiver was placed under a 2 mm guard sieve. The slurry was poured through the sieves a little at a time and washed with de-ionised water, collecting all the washings in the receiver. All the washings passing the sieves were transferred to a glass drying tray, taking care not to lose any soil particles. The sample was dried back in a low temperature (40ºC) oven to remove excess moisture and taking care to prevent complete drying.

The washed material retained on the sieves was dried in a 105ºC oven, cooled in a desiccator and weighed to determine the dry mass, m_R (g). The percentage, by dry mass, of soil in the original sample passing the 0.425 mm sieve (p_a) was calculated using:

$$P_a\ =\ \frac{m_D\ -\ m_R}{m_D} \times 100$$

Equation 7-7

7.5.3.3 Liquid limit determination

The method described in Table 7-10 is the cone penetrometer method and is taken from Head (2006). The test is based on the measurement of the amount of penetration into the sample, of a cone of known mass and dimensions. The sample's liquid limit is defined as the moisture content which allows 20 mm penetration.

Step	Description
1	**Checking apparatus** The cone penetrometer was visually checked for defects and cleaned.
2	**Mixing and working** The soil paste was mixed on a glass plate with two spatulas for at least 10 minutes (Figure 7-8). After a test penetration, a little more de-ionised water was added if needed to give a cone penetration of about 15 mm, then mixed well. The soil was kept together near the middle of the glass plate to minimise drying-out due to exposure to air. The sample was covered with polythene when not mixing.
3	**Placing in cup** Using a spatula, the sample was pressed against the side of the cup, to avoid trapping air then more paste smeared well into the bottom of the cup, without creating an airpocket. The middle of the cup was then filled and pressed well down while the cup was manually rotated. Finally, the top surface was finally smoothed off level with the rim using the straightedge of a spatula (Figure 7-8B).
4	**Adjustment of cone** The cone and shaft unit was lowered so that the tip of the cone was within a few millimetres of the surface of the soil in the cup. With the cone held by hand, the release button was pressed and adjusted so that the tip just touched the soil surface.
5	**Adjustment of dial gauge** The stem of the dial gauge was lowered to contact the top of the cone shaft and the pointer adjusted to read zero ($R_1 = 0$).
6	**Measuring cone penetration** The cone was allowed to fall by pressing the button, which was held in the pressed position without jerking the stand for 5 seconds, timed with a digital timer. After 5 seconds, the button was released and automatically clamped to the cone shaft. The dial gauge stem was lowered to make contact with the top of the cone shaft, without allowing the pointer sleeve to rotate relative to the stem adjustment knob. The dial reading was recorded to the nearest 0.1 mm to give the depth of penetration (R_2).
7	**Repeat penetration**

Step	Description
	The cone was lifted upwards and cleaned carefully with blue towel, avoiding touching the sliding stem. A little more wet soil was added to the cup, without entrapping air, smoothed off with the spatula and stages 4– 6 repeated. If the second cone penetration did not differ from the first by any more than 0.5 mm, the average value was recorded, and the moisture content was measured (Step 8). If the second penetration was between 0.5–1 mm different from the first, a third test was carried out, and provided the overall range did not exceed 1 mm, the average of the three penetrations was recorded and the moisture content measured (Step 8). If the overall range exceeds 1 mm, the soil was removed from the cup, the cup cleaned and dried, the soil remixed, and the test repeated from stage 2.
8	**Moisture content measurement** A moisture content sample of about 10 g was taken from the area penetrated by the cone, using the tip of a small spatula. This was placed in a numbered moisture content container, which is weighed, oven dried and weighed as in the standard moisture content procedure. The moisture content sample was dropped cleanly into the container by tapping the spatula on another spatula held close to the container rim.
9	**Remixing** The soil remaining in the cup was remixed with the rest of the sample on the glass plate together with a little more de-ionised water, until a uniform softer consistency was obtained. The cup was scraped out with a spatula, wiped clean and dried, and stages 3-8 repeated at least three more times (four in total), with further increments of de-ionised water. Each repeat step aimed for range of penetration values from about 15 mm to 25 mm giving a uniformly distribution of values.

Table 7-10 Procedures for the determination of Liquid Limit, modified after Head (2006).

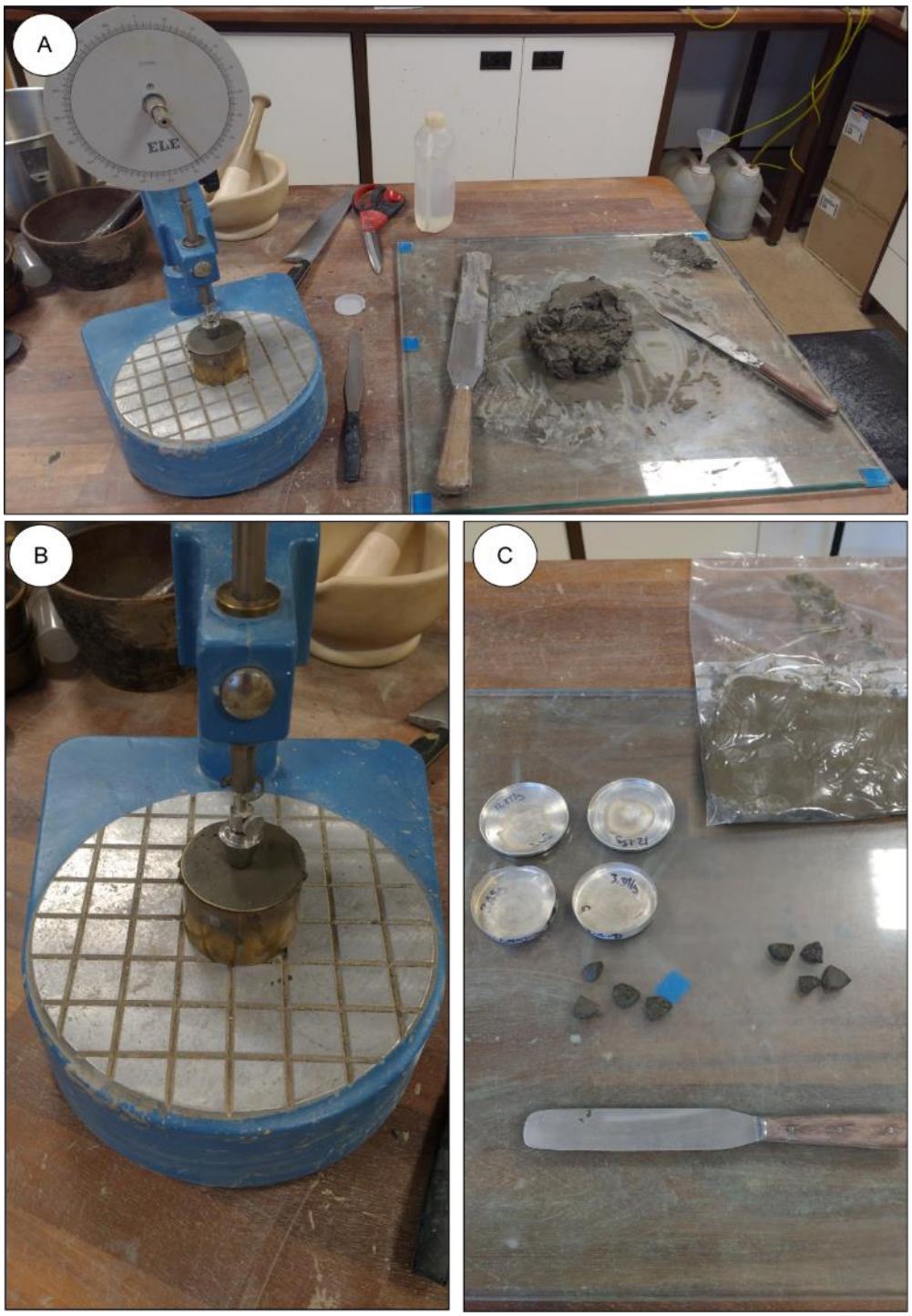

Figure 7-8 Atterberg limit testing at the BGS's geotechnical laboratories. A) Liquid limit, cone penetrometer method. Partial penetration after first test. B) Close-up of A showing sample in cup. C) Plastic limit with duplicate sub-samples before rolling into a thread.

7.5.3.4 Plastic limit determination

Determination of the Plastic Limit is defined on the percentage of a sample passing the 0.425 mm sieve. The test is designed to determine the moisture content at which the sample behaviour changes from plastic to solid. The procedure used is based on that described by Head (2006) and summarised in Table 7-11 and shown in Figure 7-8C.

Step	Description
1	**Rolling into a ball** A portion of sample was set aside on a glass plate at the start of the Liquid Limit determination and allowed to partially air dry. When the soil was plastic enough, it was well-kneaded and then shaped into a ball. The ball was moulded between the fingers and rolled between the palms of the hands so that the warmth of the hands slowly dried it. When slight cracks began to appear on the surface, the ball was divided into two portions each of about 10 g. This further divided each into four equal parts, but each set of four parts was kept together (Figure 7-8C).
2	**Rolling into threads** One of the parts was kneaded using the fingers to equalize the distribution of moisture, and then formed into a thread about 6 mm diameter using the first finger and thumb of each hand. The thread remained intact and homogeneous. Using a steady pressure, the thread was rolled between the fingers of one hand and the surface of the glass plate. Uniform hand pressure was applied to reduce the diameter of the thread from 6 mm to about 3 mm after between 10-15 back-and-forth movements of the hand. The soil was dried further by moulding between the fingers again. The sample was formed into a thread and rolled out again as before. This procedure was repeated until the thread crumbled when it had been rolled to 3 mm diameter. A metal rod was used as a reference for gauging this diameter. Crumbling of the thread occurred in different ways including falling apart in small pieces, breaking into a number of short pieces tapered towards the ends and longitudinal splitting from the ends towards the middle and then falling apart.
3	**Moisture content measurement** As soon as the crumbling stage was reached, the crumbled threads were collected and placed into a weighed moisture content container and the lid replaced immediately.
5	**Repeat tests** Step 2 was repeated for the other three pieces of soil, and each placed in the same container. The container and soil was weighed as soon as possible, dried in the oven overnight, cooled and weighed, as in the standard moisture content procedure.

Step	Description
	Steps 2–5 were repeated for the other set of four portions of the soil using a second moisture content container. To give about 6 g of soil in each container.
6	**Calculations** The moisture content of the soil in each of the two containers was calculated. If they differed by more than 0.5%, the test should was repeated. The average of the two results was calculated and rounded to the nearest whole number to give the plastic limit, (W_p). The difference between the liquid limit and plastic limit was calculated to give the plasticity index (I_P) of the soil: $$Ip = W_L - W_P$$ **Equation 7-8**

Table 7-11 Procedures for the determination of Plastic Limit, modified after Head (2006).

7.5.4 1D consolidation

The compressibility characteristics of undisturbed (intact) samples of Oxford Clay and till were measured in 1D using a GDS 1D automated oedometer at the BGS's Geotechnical Laboratories. The objective was to experimentally derive estimates of the consolidation parameters; coefficient of consolidation (c_v) and coefficient of volume compressibility (m_v) for given values of stress for at least nine load-unload stages following one determination of swelling pressure. A second objective was to calculate overconsolidation ratio (OCR) using estimates of preconsolidation pressure derived from the void ratio – log stress increment (e-logσ_v) results of the experiments.

The specimens selected are listed in Table 7-1 according to the sample handling procedures described in Section 7.2. All specimens were prepared by manually cutting and trimming from UT100 samples (Figure 7-9). The experimental procedure is based on that given in Head & Epps (2011) and where the specimen is allowed to drain freely from its top and base.

The configuration of the 1D automated oedometer is shown in Figure 7-10 and the sample preparation and experimental procedure is given in Table 7-12.

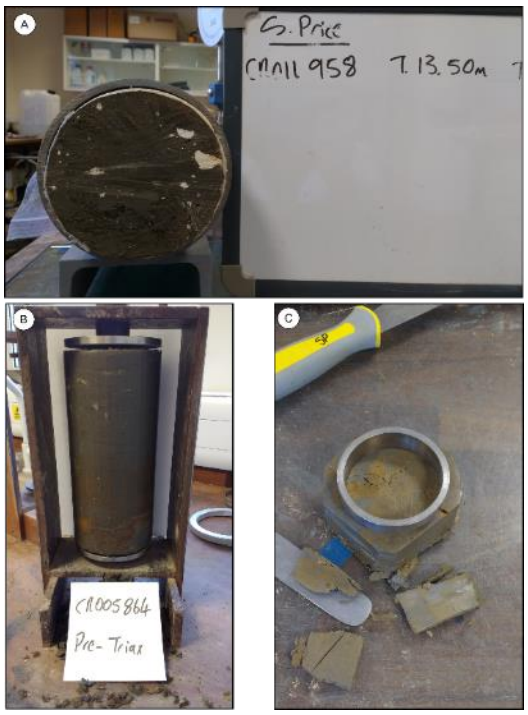

Figure 7-9 1D oedometer and triaxial sample preparation. A) Horizontal, end-on view of UT100 sample cut from transport tube. B) UT100 triaxial sample preparation in 100 mm diameter soil lathe. C) 1D oedometer sample during trimming.

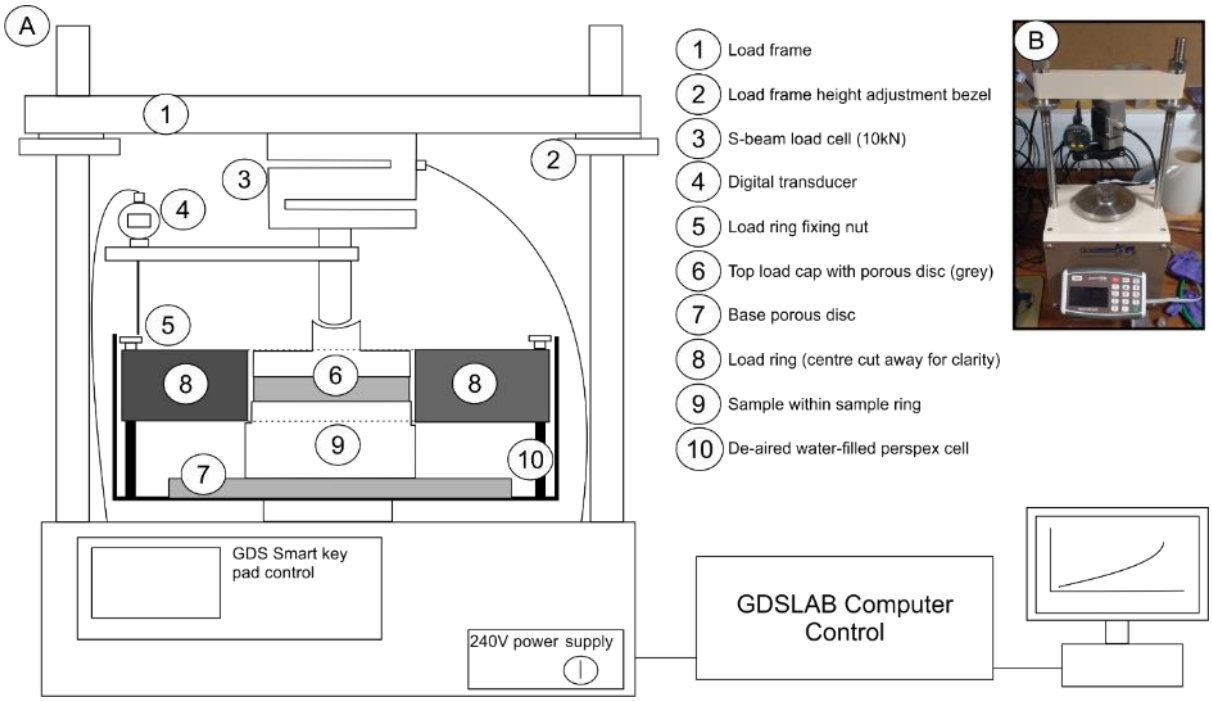

Figure 7-10 A) Schematic illustration of GDS automated oedometer configuration. Not to scale. B) Apparatus *in situ*. Oedometer cell not shown in B.

Step	Description
1.0	**General** 1.0 The sample ring was visually checked for defects, cleaned dried and weighed (m_R). The internal diameter of the ring was measured using Vernier calipers at least three times, with each measurement at 90º to the previous one and recorded to an accuracy of 0.1 mm and the mean diameter, D (mm), calculated. The height of the sample ring was measured in the same way to an accuracy of 0.01 mm to obtain the mean initial height, H_0 (mm). The mass of a weighing tray was also recorded (m_T).
2.0	**Apparatus checks** 2.1 The fit of the sample ring in the oedometer cell was checked before selection for sample preparation. 2.2 The consolidation cell, digital transducer and wiring were visually checked for defects.
3.0	**Specimen preparation** 3.1 A sub-sample was taken for moisture content determination. A rough cut of the specimen was prepared from the extruded UT100 sample to ~twice height of sample ring by cutting the specimen in a horizontal position. Cutting and trimming tools were chosen including a kitchen knife, palette knife and craft knives and the specimen placed on flat glass plate. 3.2 The oedometer ring was placed onto the top of the specimen with a little even hand pressure. Beginning at the base, the specimen was trimmed, always angle cutting slowly and evenly outwards to prevent undercutting. 3.2 The specimen was gradually trimmed, turning it evenly with each cut, keeping the knife at a shallow angle. Trimming was continued in this way until a flat metal palette knife could be used where it contacted each edge of the sample ring. If the specimen was accidentally scraped so that small fragments or coarse-grains were dislodged, the gaps were carefully filled with the cuttings. 3.3 The specimen was turned over and the procedure repeated.

Step	Description
	3.4 The trimmings were collected and used for liquid and plastic limit determination. 3.5 After trimming and smoothing, the wet weight of the specimen in the sample ring on the weighing tray (m_1) was recorded to the nearest 0.01 g and the mass of the wet specimen (m_o) calculated from: $$m_o = m_1 - (m_R + m_T)$$ **Equation 7-9** where m_R and m_T were measured in Step 1.
4.0	**Automated oedometer preparation** 4.1 The top and base porous discs were placed in de-ionised water (the top porous disc forms part of the top load platen). 4.2 The base porous disc was placed onto the 1D oedometer cell base. The specimen in the sample ring was placed centrally onto the base porous disc. The upper cell ring was placed centrally over the specimen and the shoulder of the sample ring and secured using two fixing nuts. The top porous disc and load platen were carefully placed onto the specimen ensuring that the specimen and top disc fitted evenly through the cell ring. 4.3 The cell assembly was then lifted by hand into the load frame and onto the base pad of the oedometer. The cell was adjusted so that the digital axial transducer needle was in contact with one of the fixing nuts. 4.4 De-aired water was prepared and set to one side.
5.0	**Experimental programme** 5.1 Using the GDSLAB PC control system procedure, the experimental programme was set and the recoding interval set to record using square-root time. 5.2 The specimen details including diameter, height and mass were manually entered and bulk density (ρ_B) was calculated. 5.3 Each loading stage was run using the BS1377 Oedometer Logging module which preceded with a swell stage programmed using the Oedometer Swelling module.

Step	Description
	Subsequent loading and unloading stages were selected based on doubling the load to an axial stress of 3000kPa load/unload stages. Each experiment programme included axial stress intervals (after swelling) of 62.5kPa, 125kPa, 250kPa, 500kPa, 1000kPa, 2000kPa, 3000kPa, 1500kPa and 62.5kPa. If the sample swelling pressure was seen to exceed the first load stage stress interval, the first loading stage was omitted. Programme termination criteria were set to equal 1440 minutes. 5.4 Using GDS manual keypad control, the base platen was raised to line up within 2-3 mm of the base of the load cell. 5.5 Using GDSLAB PC control a docking (seating) load equivalent to 1kPa stress was calculated and set to 0.003kN and the base platen raised to achieve it. A manual check was made to ensure that the axial displacement transducer was in contact with the cell fixing nut. 5.6 Selecting the axial displacement control on GDSLAB system, soft zero offset was selected to set base level against which the axial displacement would be measured. 5.7 A final check for sample seating, displacement gauge contact and programme setting was undertaken before starting the experiment.
6.0	**Experiment start and run** 6.1 Within 60 seconds of starting the experiment, the cell container was filled with de-ionised water. Top covers were placed over the cell to reduce water evaporation. 6.2 The experiment was monitored at intervals of ~2 hours during the working day as each swell, load and unload stage was applied. Each subsequent 24-hour stage was manually started after checking for stage completion. Water was topped-up as necessary.
7.0	**End of experiment** 7.1 The axial displacement (mm) was recorded using the digital transducer gauge and GDSLABS control system. 7.2 A tube was inserted between the edge of the cell and the upper cell ring and lowered to the cell base. Axial displacement values were recorded again. A plastic

Step	Description
	syringe was attached, and the cell water was then syphoned off and the apparatus left in-place for 30 minutes. The displacement values were recorded once again, and any differences noted. 7.3 The base platen was lowered using the GDS key pad control on the oedometer. 7.4 An empty drying tray was weighed, the oedometer cell dismantled and the wet specimen placed on the drying tray. Any soil remaining on the porous discs were transferred back to the specimen and the combined mass recorded to the nearest 0.01g (m_2). The specimen, ring and tray were then transferred to a 105ºC oven and left to dry overnight before cooling and weighing ($_{m3}$). The final mass of the specimen (m_F) was calculated from: $$m_F = m_2 - (m_R + m_T)$$ **Equation 7-10** And the dry mass (m_d) calculated from: $$m_d = m_3 - (m_R + m_T)$$ **Equation 7-11** Where m_R and m_T were measured in Step 1.
8.0	**Calculation of moisture contents** The calculated initial moisture content ω_i was calculated from*:* $$\omega_i = \frac{m_o - m_d}{m_d} \times 100$$ **Equation 7-12** which provides a check against the moisture content, ω_o obtained from the trimmings (Step 3). The final moisture content, ω_f was calculated from: $$\omega_f = \frac{m_f - m_d}{m_d} \times 100$$ **Equation 7-13**
9.0	**Calculations**

Step	Description
	The analytical calculations were based on those described in Head & Epps (2011) and comprised: ***Initial Conditions*** Area of specimen, $A = \frac{\pi D^2}{4}\ mm^2$ **Equation 7-14** Initial Volume, $V_o = \frac{AH_0}{1000}\ cm^3$ **Equation 7-15** Initial Mass, $m_o = m_1 - (m_R + m_T)g$ **Equation 7-16** Dry mass (remains constant), $m_d = m_3 - (m_R + m_T)g$ **Equation 7-17** Moisture content, $\omega_0 = \frac{m_0 - m_d}{m_d}\ (\%)$ **Equation 7-18** Bulk density, $\rho_B = \frac{m_0}{v_0} Mg/m^3$ **Equation 7-19** Dry Density, $\rho_D = \rho_B \times \frac{100}{100 \times w_0} Mg/m^3$ **Equation 7-20** Voids Ratio, $e_o = \frac{\rho_s}{\rho_d} - 1$ **Equation 7-21** Degree of Saturation, $Sr_o = \frac{\omega_o \rho_s}{e_o}\ (\%)$ **Equation 7-22** Equivalent height of solid particles, $H_s = \frac{H_o}{1+e_o}\ mm$ **Equation 7-23** ***Final Conditions*** Mass, $m_f = m_2 - (m_R + m_T)g$ **Equation 7-24** Moisture content, $\omega_f = \frac{m_f - m_d}{m_d} \times 100$

Step	Description
	Equation 7-25 Height of specimen, $H_{f=} H_o - (\Delta H)_f$ mm **Equation 7-26** Bulk Density, $\rho_{Bf} = \frac{m_f}{AH_f} \times 1000\ Mg/m^3$ **Equation 7-27** Dry density, $\rho_{Df} = \rho_f \times \frac{100}{100 \times \omega_f} Mg/m^3$ **Equation 7-28** Voids ratio, $e_{f=} e_o - (\Delta e)_f$ **Equation 7-29** Degree of Saturation, $Sr_f = \frac{\omega_f \rho_s}{e_f}$ (%) ***End of each loading stage*** Voids ratio change (cumulative), $\Delta_e = \frac{\Delta H}{H_s}$ **Equation 7-30** Voids ratio after increment, $e = e_0 - \Delta e$ **Equation 7-31** Voids ratio change during an increment, $\delta e = e_1 - e_2$ **Equation 7-32** Coefficient of volume compressibility for an increment, $m_v = \frac{\delta_e}{\delta_p} \times \frac{1000}{1+e_1}$ m²/MN **Equation 7-33** where p = pressure increment for stage (kPa). Coefficient of consolidation during an increment, $c_v = \frac{0.026 \times (H^2)}{t_{50}}$ m²/year **Equation 7-34** where t50 is the time (s) at which 50% consolidation is complete. It is derived from manual interpretation of a log-time consolidation plot. Time factor 0.026 for two-way drainage from Head & Epps (2011). Coefficient of secondary compression measured over one log-cycle of compression, $C_{sec} = \frac{(\Delta H)_s}{H_o}$ **Equation 7-35**

Step	Description
	Voids ratios were calculated for the unloading as well as the loading stages. Calculations of m_v, c_v and k were made for the loading stages only.

Table 7-12 Experimental methodology and analytical calculations for 1D consolidation using 1D automated oedometer. Modified after Head & Epps (2011).

7.5.5 Isotropically consolidated-undrained (CIU) triaxial

The undrained shear strength and small-strain stiffness of undisturbed (intact) samples of Oxford Clay and till were measured using multi-stage isotropically consolidated, undrained triaxial methods. Multi-stage triaxial experiments with measurement of small-strain stiffness were undertaken at the BGS's Geotechnical Laboratories using a Bishop & Wesley type stress path triaxial testing system (SPTTS). The BGS's Geotechnical Laboratory was temperature controlled to ~20ºC but the Schofield Centre triaxial room was not.

The objectives were to experimentally derive measurements of undrained shear-strength (c_u) and to derive estimates for secant angle of friction, $ø_{crit}$. In addition, Hall effect sensors were used to measure small-strain (<1%) stiffness during shear. The total and effective stress conditions within a triaxial cell are shown in Figure 7-11.

The specimens selected are listed in Table 7-1 according to the sample handling procedures described in Section 7.2. All specimens were prepared by manually cutting and trimming from UT100 samples (Figure 7-9B). The experimental procedure was modified from that given for effective stress triaxial tests given in Head & Epps (2014).

The triaxial appartus configurations are shown in Figures 7-12 and 7-13. The sample preparation and experimental procedure is given in Table 7-13.

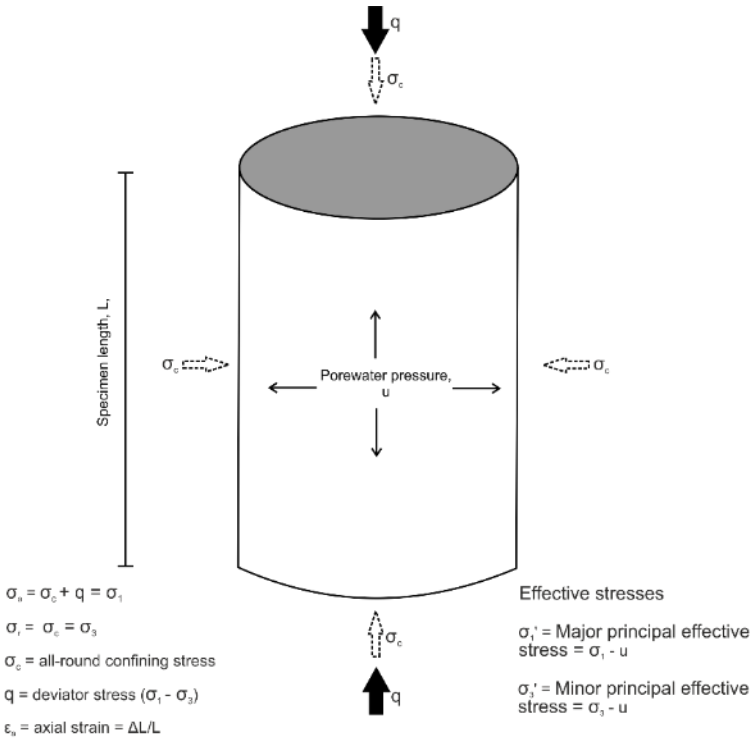

Figure 7-11 Schematic illustration of total and effective stresses within a triaxial cell surrounding a cylindrical soil specimen. Not to scale.

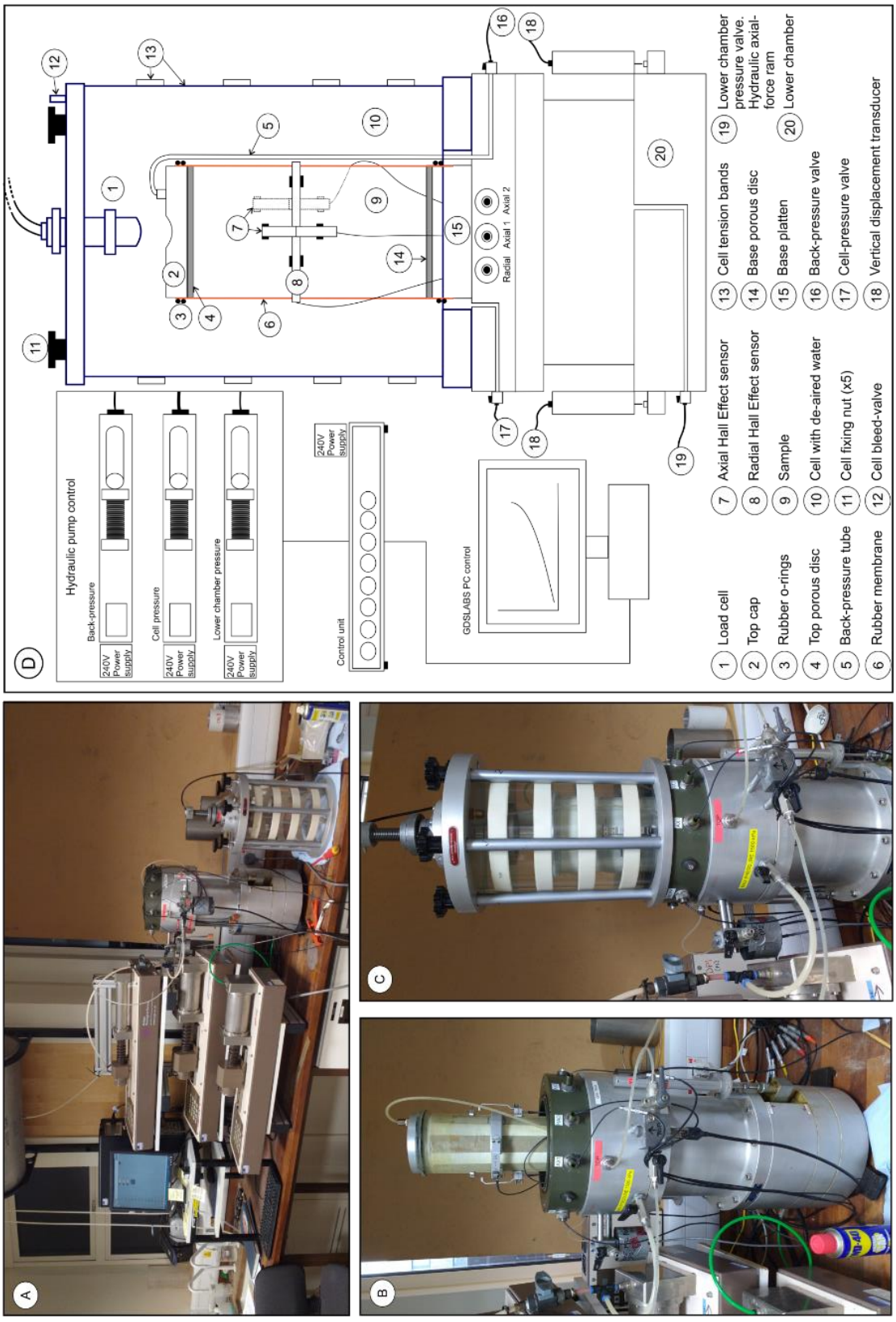

Figure 7-12 SPTTS triaxial configuration, BGS. A) Cell, hydraulic pumps and PC control, cell base and cell removed. B) Close-up of cell base with sample mounted and instrumented with axial and radial Hall effect sensors. C) Cell attached and filled. D) Schematic diagram (not to scale).

Step	Description
1	**Preparation of apparatus** 1.1 All elements of the SPTTS including cell, connector pipes, valves and cell base were checked visually for defects and wiped clean with a dry cloth. A small amount of light grease was applied to rubber o-ring between the cell and cell base, the side of the base platen and the side and seating recess of the top cap. 1.2 The distance between the tip of the load cell and the top of the base platen of the cell was measured and the load cell adjusted to ensure that there was sufficient clearance for a ~200 mm long sample plus porous discs to fit. 1.3 The capacity of the hydraulic pumps was checked and filled with pre-prepared de-aired water if needed. Each test was started with each pump set within its maximum and minimum extension to allow for pump movement during each experiment phase. De-aired water was briefly expelled from each pump before fitting connectors to the cell and placing the sample, until no air bubbles were seen. 1.4 The base and top porous discs were visually checked before placing into de-aired water. Once removed, circular filter-paper drains were placed on the porous discs which were then placed with the filter paper in contact with the specimen when placed onto the base platen and the top cap fitted. 1.5 In preparation for fitting of the sample, the base platen was raised to facilitate sample fitting and Hall effect instrumentation.
2	**Specimen preparation** 2.1 The extruded specimen was placed horizontally onto the laboratory bench, unwrapped and removed from its protective packaging. The orientation of the top of the sample was noted and marked. 2.2 It was carefully placed horizontally and cut with a knife, piano wire or saw to retrieve a 220 mm length. A sub-sample was taken for moisture content determination. The sample was then transferred and placed vertically in a 100 mm soil lathe (Figure 7-9B). A wire saw was used to trim the specimen by gently moving the blade downwards and slowly rotating the soil lathe and attempting to maintain verticality in the specimen. On completion, a 100 mm diameter split sample former was placed around the specimen and lifted from the

	soil lathe onto a glass plate. The base and top of the specimen were trimmed to the horizontal until a flat palette knife blade could easily be moved across the specimen and the edge of the split former. Samples were trimmed to 195 mm to provide additional strain and ensure that the sample could be fitted with sufficient clearance into the apparatus. The trimmings were collected and placed in a polythene bag for Atterberg determination. 2.3 The split former was removed, and the specimen was transferred by hand, vertically, to a glass plate where its height and diameter were measured three times each to the nearest 0.5 mm using Vernier calipers and the mean of each calculated. After placing onto a dry and weighed tray, the wet mass of the sample was measured to the nearest 1 g and the bulk density, ρ_B, calculated. 2.4 For multi-stage tests, pre-cut side and top filter-paper drains were placed on the specimen and fixed with a little de-aired water applied with a brush. A 100 mm rubber membrane was placed inside an aluminum membrane stretcher, suction applied and carefully lifted over and onto the specimen with side drains before releasing the suction and removing the membrane stretcher. The top of the membrane was gently folded and used to gently lift the specimen onto the base platen onto which were already placed the base porous disc and filter paper drain.
3	**Assembling the specimen in the cell** 3.1 Once the specimen had been transferred to the cell and placed on the base platen and porous disc with filter paper, the base of the membrane was gently rolled downwards, over the base platen. Two rubber o-rings were placed onto an o-ring fitter, lowered over the specimen and gently pushed off the fitter onto the base platen and membrane. Where possible, the membrane was then rolled up and over the o-rings. Two more o-rings were placed onto the o-ring fitter and lowered over the specimen and rested at the base. The top filter drain, top porous disc and top cap were placed onto the top of the specimen and the rubber membrane rolled up and over the top cap assembly. The o-ring fitted was gently lifted and the o-rings pushed off it onto the top cap assembly before lifting off and away from the specimen. 3.2 The sample was measured and marked with a permanent marker to attach two axial and one radial Hall effect sensor to the specimen and rubber membrane at its mid-height. A small negative pressure (-10 kPa) was applied to the specimen using the back-pressure pump to ensure that the membrane and specimen were in close contact. The top to base length of each radial sensor was measured and recorded. After marking the seating positions of each sensor,

	the pads of each were cleaned and then gently roughened with sand paper. *Loctitie* general purpose glue was applied in a thin coating to the pad and the pad position on the specimen. After 30 s drying, each pad was gently pressed and held for between 2 and 5 minutes and left to dry for at least 30 minutes. After drying, each senor magnet was adjusted and fixed in-place with fixing screws.
4	**Assembling and pressurising the cell** 4.1 After specimen fitting and Hall effect gluing, the base platen was lowered to accommodate the cell. The cell was lifted carefully and with help, over the sample to engage the cell base taking extreme care to prevent knocking the specimen or dislodging the Hall effect sensors. The relative position of the load cell and top cap recess was checked visually to ensure correct seating. The load cell was manually adjusted to ~3 mm from the top cap recess. Once the top and base parts of the cell were engaged, the cell and cell base were fixed using the cell tie rods which were tightened using a diagonal pairs pattern. 4.2 With all valves including the cell bleed valve open, the cell was filled with de-aired water. Using the SPTTS, just before the cell was full, the cell pressure inlet valve was partially closed to slow the rate of filling. The bleed valve was closed when water emerged. After closing the bleed valve, the cell pressure valve was fully opened again. 4.3 After filling the cell, the back pressure, cell pressure and lower chamber valves were closed and the connection tubes removed. In turn, water was expelled from each pump to remove air. With help, the pump tubes were held together at a height equal to half that of the sample and the pressure reading in each pump was manually zeroed. A soft-zero setting was applied to the load cell and Hall effect sensors. 4.4 A final check was made to ensure that the cell pressure, back pressure and lower chamber valves connecting the cell to the hydraulic pumps remained open. The secondary pore pressure valve was left in the closed position.
5	**Experimental programme** The GDSLAB PC control system was used to design and set the experimental parameters. After inputting the specimen details and data saving location a correction for side and top drains was applied. For single and multi-stage effective stress triaxial tests, saturation-consolidation-shear procedures were followed with three consolidation-shear stages for multi-stage tests.

5.1 **Saturation**. With the specimen in the undocked position, the saturation stage was undertaken to ensure that all voids were filled with water and that the pore pressure transducer and drainage lines were de-aired. Using the GDSLABS PC control, all samples were initially saturated under a constant effective (differential) stress of at least 20 kPa using the Sat Con module and illustrated below.

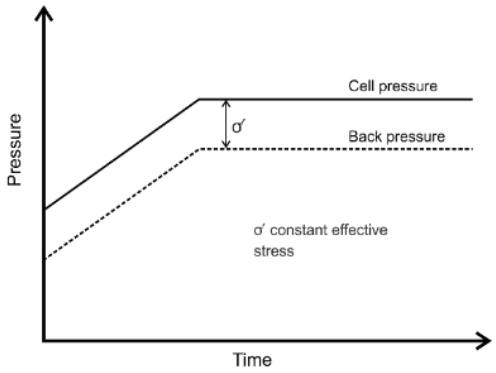

Depending on the initial behaviour of the specimen, determined by measuring the swell pressure in 1D consolidation, saturation was only achieved after increasing the back pressure but whilst maintain a constant effective stress.

5.2 **B-value test.** To determine the degree of specimen saturation, the Skempton B-value test was performed by raising the cell pressure by 50 kPa and measuring the pore pressure response with the specimen in the undocked position. The B-value is specific to the type and state of the soil, but a value of ≥0.95 is usually indicative of sample saturation. ε

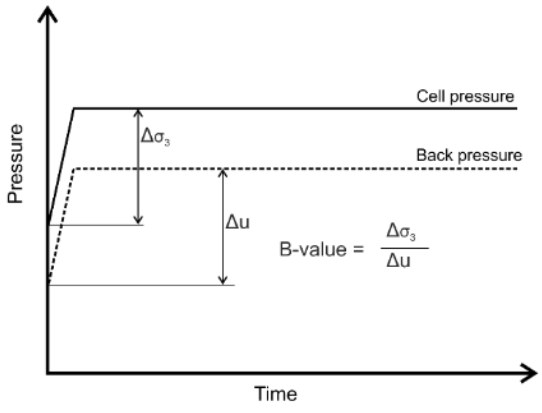

5.3 **Consolidation**. The consolidation stage was used to bring the specimen to its calculated *in situ* condition and set the effective stress level for the first of three shear stages in the SPTTS configuration. *In situ* vertical effective stress, σ_v', was calculated from:

$$\sigma_{v'} = ((\rho_B * g) * z) - u$$

Equation 7-36

where ρ_B is bulk density, g gravitational acceleration, z is depth below ground level and u is pore pressure assuming groundwater level approximates the ground surface.

Consolidation was complete when there was no observed reduction in volume, ΔV which approximated a reduction in V ≈ <5 mm^3/5min. The consolidation step is illustrated below.

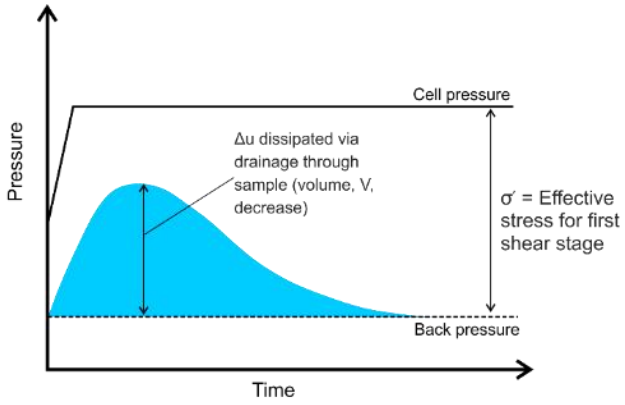

5.4 Shear (single- or multi-stage) load and unload

The GDS Standard Triaxial, Consolidated-Undrained module was used to perform the shearing single or multi-stage shearing step. With the drainage line closed, the shear stage was programmed and the sample docking criteria set. Typical parameters used were:

Docking velocity:	0.2 mm/min
Docking detection force:	0.1 kN
Compression (shearing) velocity:	0.2 mm/min
Unload (multistage):	-0.2 mm/min

The parameters determining the termination of the shear stage depended on the triaxial configuration. For the DYNTTS single-stage shear configuration, termination conditions were set to ~10% strain (~20 mm). The termination of the first and second of three shear stages was determined subjectively by monitoring the stress-strain, effective stress-ratio and deviator stress-mean effective principal stress plots. The typical conditions at which shearing was stopped during the first and second shear stages is shown schematically, below.

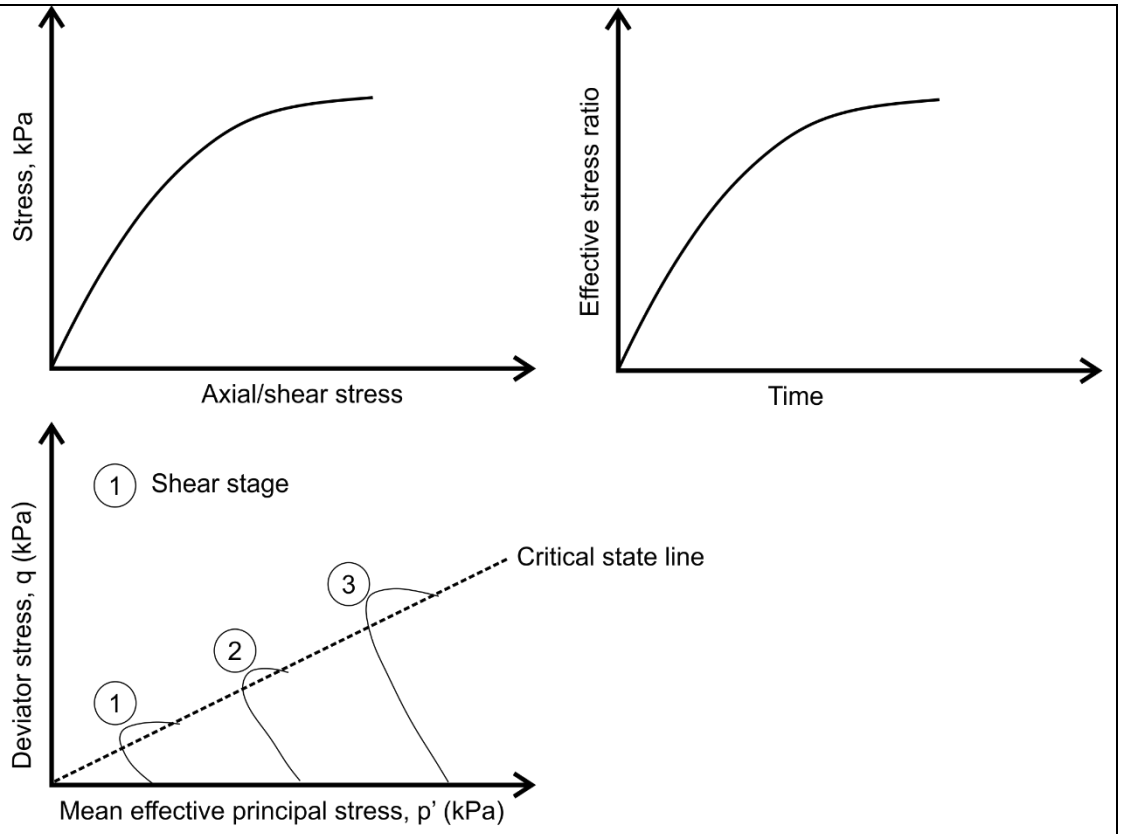

6 **Dismantling cell and removing specimen**

6.1 Following completion of the final shear stage unloading, the cell pressure and back pressure were reduced to 0 kPa and the cell drained. The tie rods were undone, and the cell lifted from the cell base, taking care to prevent knocking the sample. The post-test sample was photographed *in situ* before removal of the Hall effect sensors then the top cap assembly. The o-rings fitted to the base platen were pushed downwards and the sample lifted from the cell after removing gently sideways to remove suction.

6.2 The specimen was carefully transferred to a flat glass plate and the rubber membrane, side and top filter drains removed before weighing after placing on a dry and weighed tray. The post-test mass was compared against the pre-test mass. A sub-sample (~15 g) was taken for moisture content determination before photographing and sketching the sample. As a secondary moisture content measure, the specimen was dried whole in a 105ºC oven before slicing.

7 **Cleaning equipment**

The base platen, top cap assembly, o-rings and cell base and cell were wiped clean with a damp cloth. Excess glue was removed the Hall effect sensors and their condition visually inspected. The rubber membrane was thrown away and not re-used. Porous discs were

	cleaned with a jet of water and placed back into de-aired water to soak.
8	**Calculations** The value of the major principal stress at failure, σ_{1f}, is calculated from: $$\sigma_{1f} = (\sigma_1 - \sigma_3)_f + \sigma_3$$ **Equation 7-37** where σ_3 is the cell confining pressure which remains constant throughout the test. The undrained shear strength (c_u) is given by: $$c_u = \frac{1}{2}(\sigma_1 - \sigma_3)_f$$ **Equation 7-38**

Table 7-13 Sample preparation and experimental procedure for triaxial compression using DYNTTS and PSTTS triaxial configurations. Modified after Head & Epps (2014).

8 Field and laboratory results

The results of the field and laboratory investigations described in Sections 7.3 to 7.5 are presented here. The results are divided into Sections according to the location of the samples

and/or field sites, relative to the Quaternary Domains defined in Section 5.2.1. Samples are further divided based on their geology. Bedrock samples are derived from the Oxford Clay only. Quaternary samples include matrix-supported, sandy and gravelly clay and silt (interpreted as till or solifluction 'head'), river terrace deposits and alluvium. The focus of the investigation was to characterise the geotechnical properties and behaviour of Oxford Clay and till, but additional Quaternary samples were investigated where exposures allowed or where specimens were available as bulk samples from the EWR ground investigation. Clay mineralogy, moisture content, organic content, carbonate content, particle density, particle-size and Atterberg limits were determined for representative specimens for each type of geology within each Domain where it possible to do so. Triaxial effective stress and 1D consolidation tests were carried out only on specimens of till or Oxford Clay. The results of four OSL numerical age estimates were performed on specimens of glacigenic sand within two Domains only because of the limitation of budget and limited exposures of Quaternary sediments.

A summary of the Quaternary Domains and related field sites is given in Table 8-1. As samples were collected either from pits, quarries or surplus material from the EWR ground investigation, not all Domains have equal numbers of samples selected for laboratory analysis as discussed in Section 7.2.

Domain description	**Domain Code**			
	Bedrock Glaciated - Periglaciated	**Bedrock_Quaternary Glaciated-Periglaciated**	**Bedrock Periglaciated**	**Bedrock_Quaternary Periglaciated**
Late Jurassic mudrocks (West Walton, Ampthill and Kimmeridge Clay formations)	1.4	**1.4.1** **No field sites**	2.4	2.4.1
Middle-Late Jurassic mudrocks, sandstones (Kellaways and Oxford Clay formations)	**1.3** **Field site: Calvert**	**1.3.1** **Field site: Bletchley (Newton Longville)**	**2.3** **No field sites**	2.3.1
Middle to Late Jurassic limestones, sandstones and mudrocks (Inferior and	1.2	**1.2.1** **Field sites:** **1. Home Farm, Stowe** **2. Tingewick**	2.2	2.2.1

Domain description	Domain Code			
	Bedrock Glaciated - Periglaciated	**Bedrock_Quaternary Glaciated-Periglaciated**	**Bedrock Periglaciated**	**Bedrock_Quaternary Periglaciated**
Great Oolite Groups)		**3. Buckingham Sand Pit**		
Early to Middle Jurassic mudrocks (Lias Group)	1.1	**1.1.1 Field site: Passenham**	2.1	2.1.1

Table 8-1 Quaternary Domains descriptions. Shading indicates Domains for which laboratory specimens were taken and analysed. Domain locations of field sites highlighted.

Each section presents the results of field investigation first, followed by the laboratory of specimens collected from the field sites and from other locations within the Domain.

In defining the scope of the field and laboratory research, the following limitations are important:

- The number of field sites found does not represent the full complexity of the probable geological sequence in north Buckinghamshire. This is compounded by the fact that not all domains have representative field sites;
- The collection of bulk samples from field sites was complimented by the collection of undisturbed UT100 samples from the East West Rail ground investigation. The selection of samples to use was determined by those that were not needed for the ground investigation. Consequently, not all domains have representative samples for each type of geology, on which to carry out effective stress tests;
- Every care was taken to transport, extrude and prepare specimens for testing from each sample. Only UT100 samples that were sealed with soft wax and intact were selected. However, some disturbance from the combined effects from each phase of transportation cannot be discounted.

8.1 Quaternary Domain 1.1.1

Quaternary Domain 1.1.1 comprises Early to Middle Jurassic mudrocks overlain by glacigenic deposits. Bedrock in this domain is fine-grained and is therefore similar to to Domains 1.3 and 1.4. The Domain is interpreted to have been glaciated on at least one occasion and influenced by multiple phases of glacial and periglacial activity.

Laboratory results are presented for loss-on-ignition (LOI) and particle-size analysis (PSA) for specimens of till and alluvium, clay mineralogy for till and particle-size analysis only for river terrace deposits.

8.1.1 Field locality: Passenham

Temporary exposures were described in a shallow quarry where sand and gravel are extracted for aggregate. The location of the site and sections are shown in Figure 8-1.

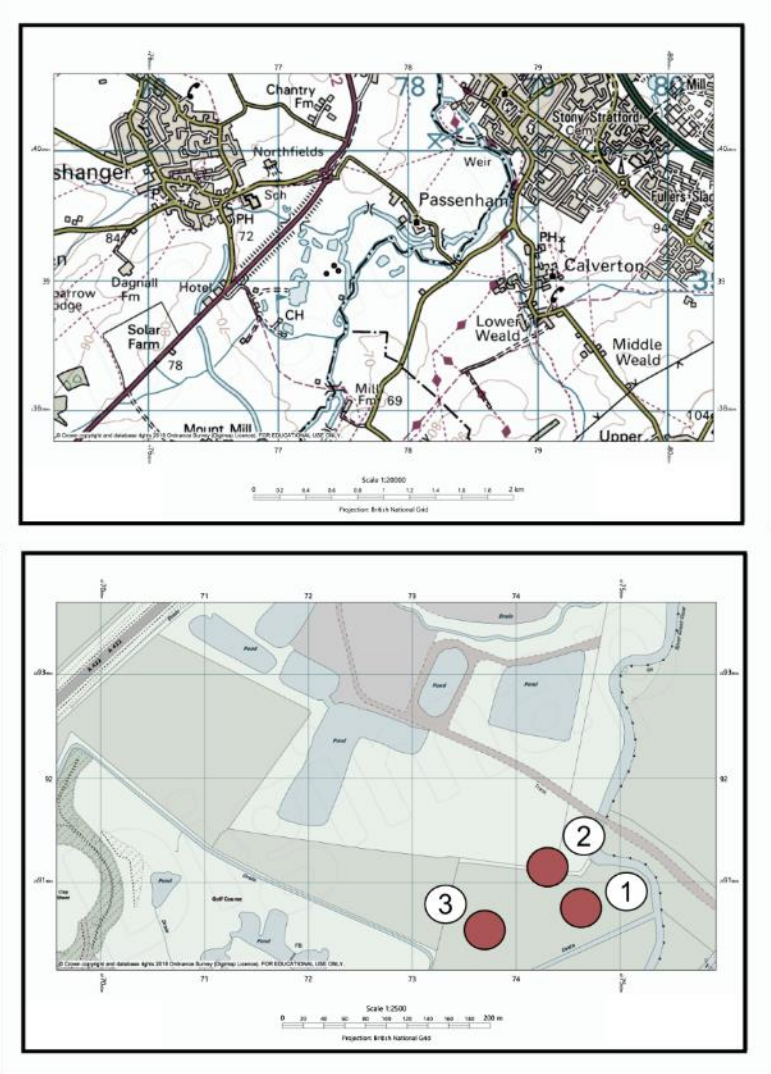

Figure 8-1 Location of sedimentary sections, Passenham field site, Quaternary Domain 1.1.1.

The sediments exposed at Passenham are not known to have been previously described in the literature but the 1:50 000 scale geological map shows the site is underlain by river terrace deposits. The site is <1 km from the BGS Deanshanger borehole (described in section 3.3.4.2) which encountered glacigenic sediments to at least 63 mbgl.

8.1.1.1 Section descriptions

Three sections were described and are shown in Figures 8-2 and 8-3. Measured sedimentary structures are presented as equal-area stereograms in Figure 8-4. The legend for sedimentological logs is given in Appendix 13.1. Sediments were grouped into lithofacies associations and assigned codes following the recommendations of Benn & Evans (2004). Lithofacies codes were the same for each section. As a result, not all lithofacies observed in the project area, were observed in all sections.

Lithofacies 2 (LF2)

Lithofacies 2 occurs at the base of the quarry and comprises greyish-brown, very sandy, gravelly silt and clay. The gravel is angular grey flint, grey sandstone and rounded white and grey chalk. It is conformably overlain by LF6 and LF5a.

Lithofacies 5a (LF5a)

Lithofacies 5a comprises multi-coloured, massive- to thinly-, horizontally- and cross-bedded, variably sandy gravel. The gravel clasts are dominated by sub-rounded to rounded, low sphericity, quartzite, red sandstone, micritic limestone, sub-angular flint, convex-up *Gryphaea* shells and rare igneous lithologies including prophyry. In places, the clasts appear to be frost shattered. Gravel beds are commonly clast supported and the sand is coarse-grained. In places, the gravel beds fine upwards to medium to coarse sand. Oxidation along the bedding planes is common.

Ball-shaped involutions are present where the unit overlies clayey LF2. Angular, wedge-shaped structures are seen to taper downwards.

Lithofacies 6 (LF6)

Lithofacies 6 is dominated by reddish-brown, brown and greyish-brown, massive, moderately- to poorly-sorted, sandy to very sandy gravel. The gravel clasts are low sphericity, angular grey flint, rounded yellowish-grey limestone, red quartzite and light brown sandstone. The sand beds comprise well-sorted, coarse sand which contain apparent slump structures in medium to coarse sand at the base.

Lithofacies 7 (LF7a and b)

Lithofacies 7 is the youngest lithofacies. It is seen to unconformably overlie older lithofacies. This passes into LF7a which comprises matrix-supported fine to coarse gravel of chalk and flint in a grey and dark grey matrix of clay and silt with rootlets. LF7a grades upwards into

LF7b which is characterised by dark and light grey, prismatic-weathering clay and silt, grading upwards into reddish-brown, oxidised clay and silt with rare gravel of flint.

Representative images of each lithofacies and the sections at Passenham are shown in Figures 8-5 and 8-6.

Note that LF1, LF3 and LF4 were not observed at this location.

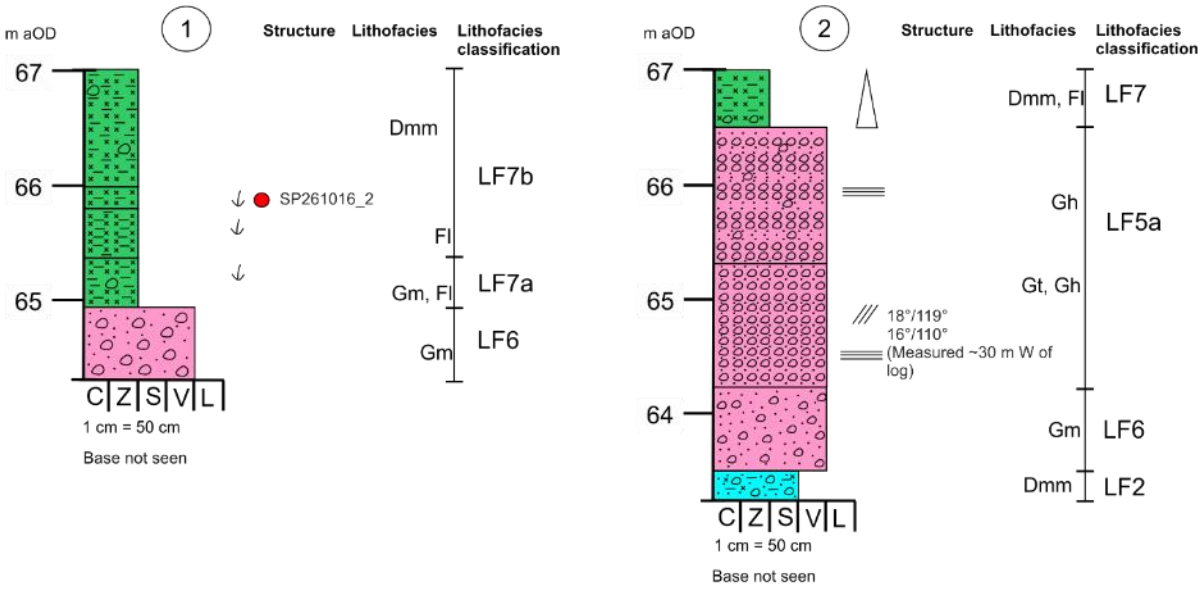

Figure 8-2 Sedimentary graphical logs 1 and 2, Passenham. Refer to Appendix 13.1 for legend.

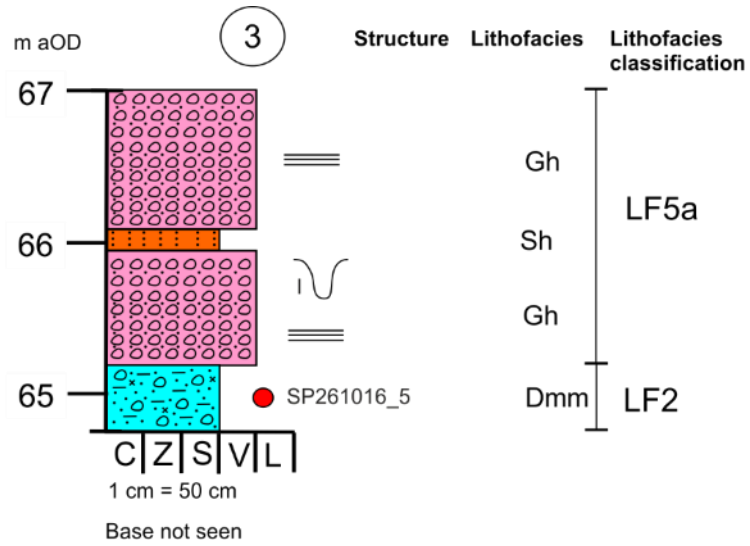

Figure 8-3 Sedimentary graphical log 3, Passenham. Refer to Appendix 13.1 for legend.

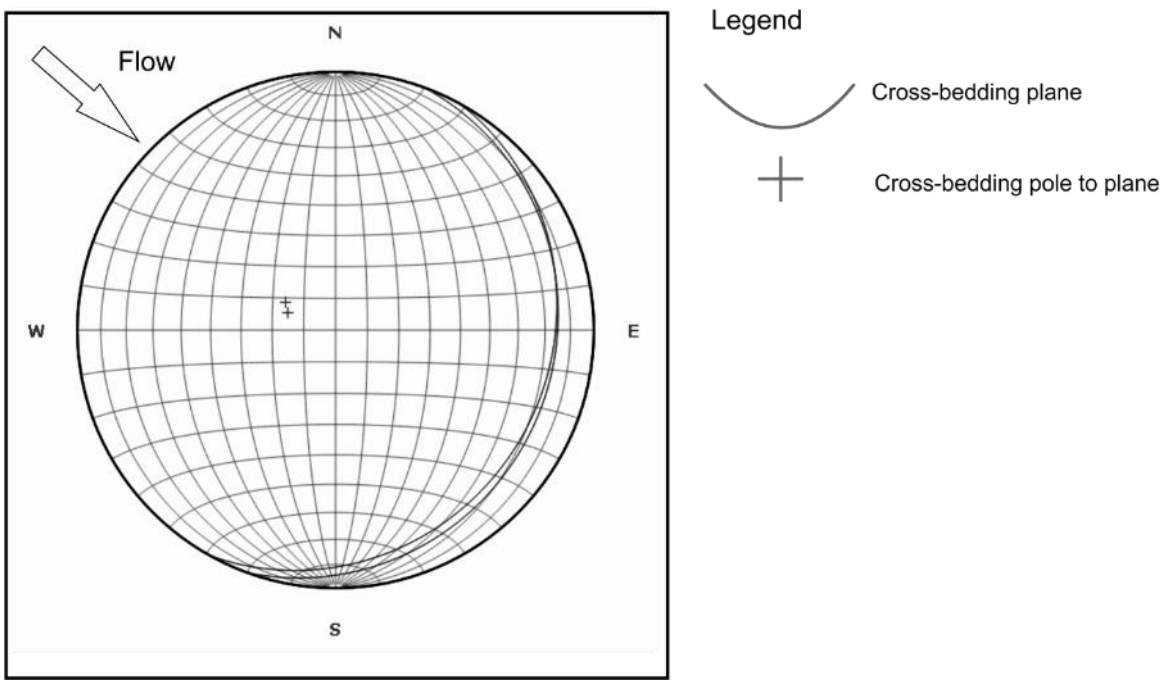

Figure 8-4 Equal area stereogram of cross-bedding, Passenham.

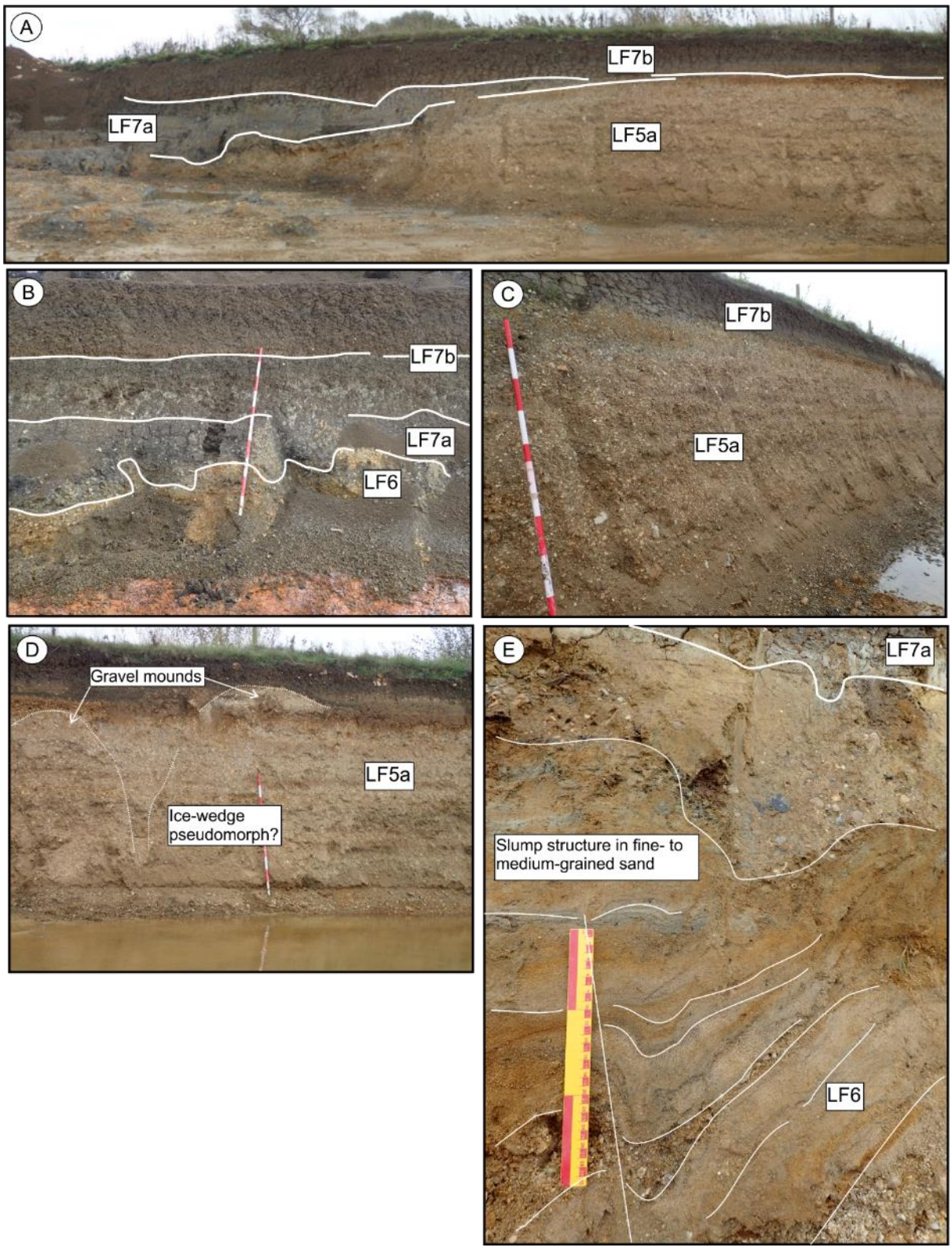

Figure 8-5 Passenham lithofacies associations. A) Erosional, contact between LF5a and LF7. B) Fining-upwards sequence. C) Onlap of LF7b onto LF5a. D) Gravel mounds interpreted as the flanks of ice-wedge pseudomorphs. E) Slump structure (ice-wedge pseudomorph?) with thickening into centre of feature.

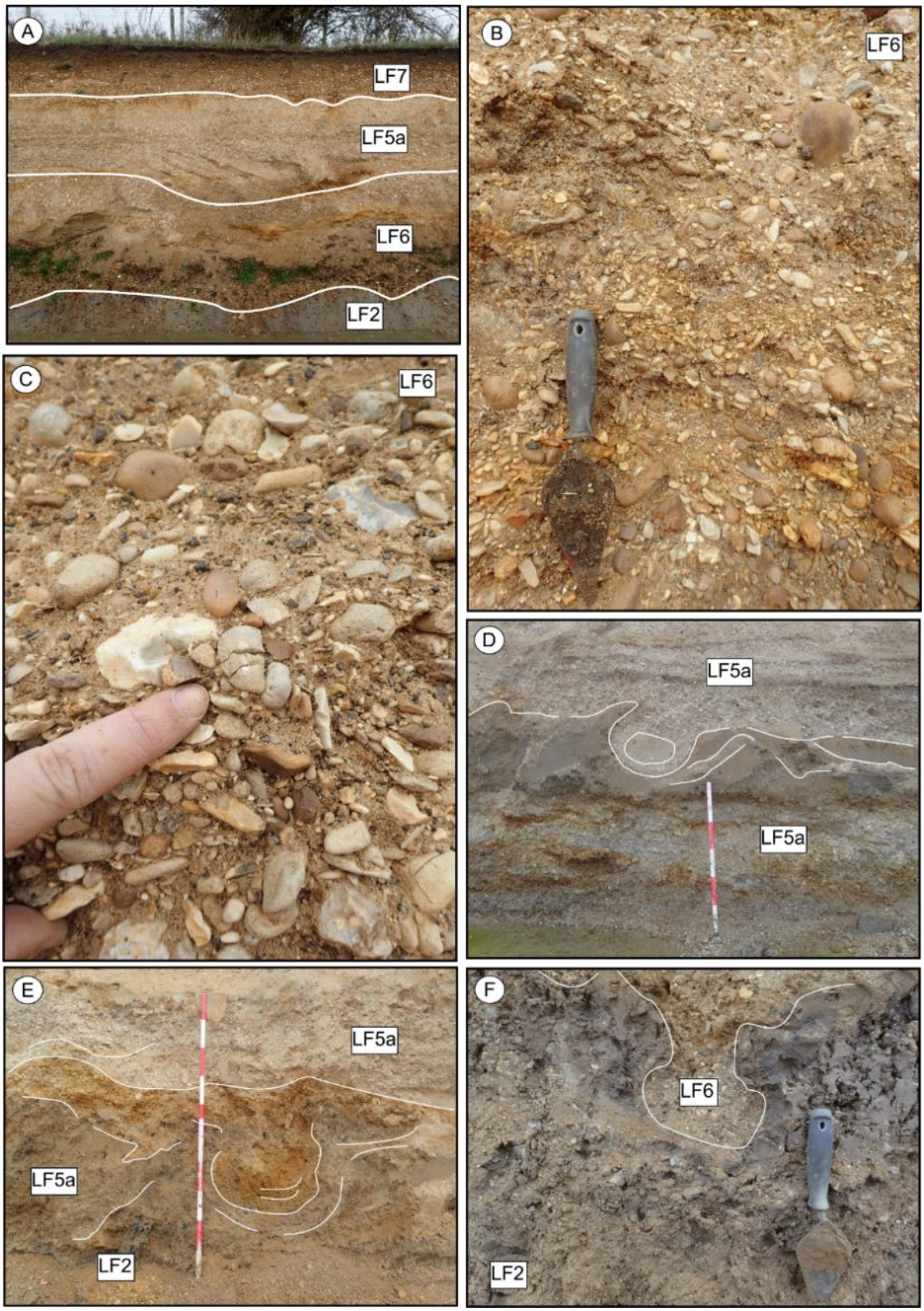

Figure 8-6 A) Lithofacies stratigraphical relationships looking north. B) Massive, clast-supported gravel. C) Possible evidence of clast frost-wedging. D), E) and F) Involutions at the boundary between LF2 and overlying LF6/LF5a.

8.1.1.2 Interpretation

The sequence exposed at Passenham is interpreted as a fining-upwards sequence of (glacio)fluvial river terrace gravels grading upwards into fine-grained alluvium (LF7). Both units are interpreted to overlie a unit of chalk-rich, matrix-supported till (LF2). Because of the proximity of the Deanshanger borehole, the sequence exposed at Passenham is interpreted to overlie the Deanshanger buried valley. LF2 may correlate with chalk-rich tills overlying glaciolacustrine silt and clay in the Deanshanger borehole.

The chalk-rich, matrix-supported till of LF2 is here referred to as the Milton Keynes Till Member. Based on lithology and clast content, it is correlated with similar exposures of till in Tingewick, Buckingham Sand Pit and Bletchley (see Sections 8.2.2, 8.2.3 and 8.4.1 respectively for descriptions).

8.1.2 Laboratory results

8.1.2.1 Loss-on-ignition (alluvium, till)

Results for loss-on-ignition for one sample of till and one sample interpreted as alluvium are shown in Table 8-2. Both samples are slightly organic, and the till is calcareous.

Sample	Geology	% water	%organic	%$CaCO_3$	% silicate residue
SP261016_2	ALV	N/A	5.7	5.9	88.4
SP261016_5	TILL	N/A	3.9	26	70.1

Table 8-2 Loss-on-ignition (LOI), Domain 1.1.1. N/A denotes gravimetric water content measured as part of Atterberg, 1D consolidation or triaxial analysis.

8.1.2.2 Clay mineral XRD (till, Oxford Clay)

Diffractograms from the analysis of orientated, aggregate specimens are presented in Figure 8-7. The identification of clay minerals followed the recommendations described in Moore & Reynolds (1997). Atomic spacing, d, in Ångstroms (Å) was derived with reference to the published tables in Brown (1980) which use Bragg's formula:

$$2d\sin\theta = n\lambda$$

Equation 8-1

Rearranged in terms of d for reported results for 2θ:

$$d = \frac{n\lambda}{\sin\theta}$$

Equation 8-2

Where, θ is the angle between the refraction plane and the reflected X-ray path, λ is radiation wavelength and n is number of wavelengths which can be any whole number which for a first-order X-Ray reflection is 1, second-order, 2 and nth order n. The value for λ using Cu Kα radiation was taken as 1.541838 after Brown (1980).

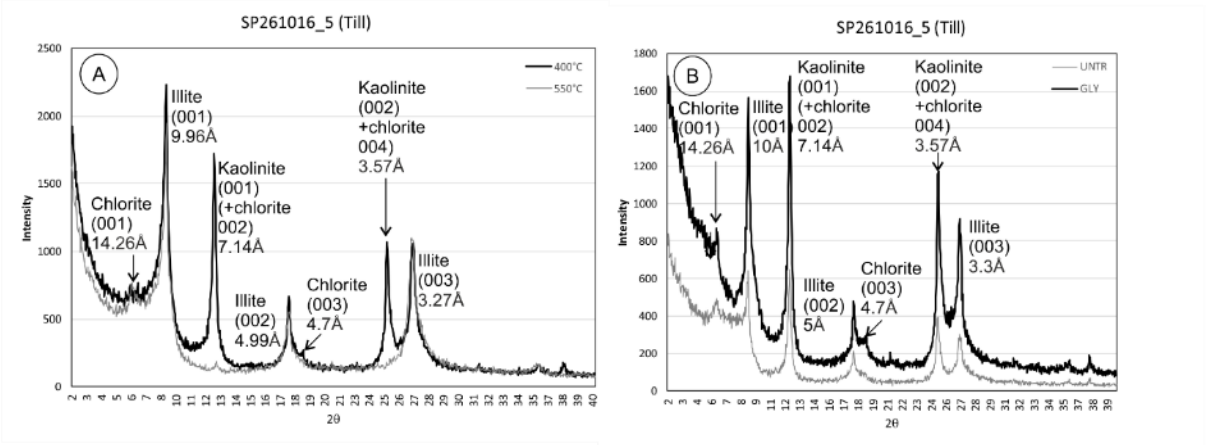

Figure 8-7 Clay mineral XRD for till, Quaternary Domain 1.1.1. A) Heat treated at 400ºC and 550ºC. B) Air dried, untreated (untr) and glycolated (gly).

For specimens of till, strong, narrow peaks are seen in the diffractogram associated with a detrital clay mineral assemblage of illite (mica), kaolinite (with minor or trace amounts of chlorite) and chlorite. The enhanced 10Å peak on heating to 400°C indicates the presence of collapsible minerals associated with illite. The composition of the collapsible mineral assemblage is unknown. Kaolinite is characterised by peak intensity reduction or loss-on-heating to 550ºC. Non-clay minerals are poorly defined but probably include quartz (4.35Å) and gypsum.

8.1.2.3 Particle-size analysis (PSA), (till, river terrace deposits, alluvium)

The results of particle-size analysis are plotted as percentage passing (finer) – log particle-size plots for specimens of alluvium, river terrace deposits and till (Figures 8-8 and 8-9). The grading characteristics and classification of each specimen is summarised in Table 8-3. The coefficient of uniformity (C_u) was calculated from:

$$C_u = \frac{D_{60}}{D_{10}}$$

Equation 8-3

Where D_{10} and D_{60} are the particle-sizes at which 10% and 60% of the sample passes. The coefficient of curvature (C_z) was calculated from:

$$C_z = \frac{D^2_{30}}{D_{60}D_{10}}$$

Equation 8-4

where D_{30} is the particle-size at which 30% of the sample passes.

Sample grading terms are geotechnical rather than geological. Broadly equivalent geological terms for poorly-graded, uniformly-graded and well-graded are moderately-sorted, well-sorted and poorly-sorted, respectively.

Sample	Geology	Method[1]	Lithological Description[2]	Sample grading[3]	C_u	C_z
SP261016_2	ALV	LPSA	Slightly clayey, slightly sandy SILT	Well-graded	9.0	1.0
SP261016_3	RTD	WS	Slightly clayey/silty, very sandy, GRAVEL	Well-graded	35.0	2.579
SP261016_5	TILL	LPSA + WS	Slightly clayey, slightly gravelly, slightly sandy SILT	Poorly-graded	40.0	0.9

Table 8-3 PSA summary for geological units in Domain 1.1.1. [1]LPSA – Laser Particle-Size Analysis, WS – wet sieving. [2]Based on proportions by mass from PSA following conventions in British Standards BS5930:1999 with Amendment 2 (British Standards Institution, 1999). [3]Geotechnical terminology.

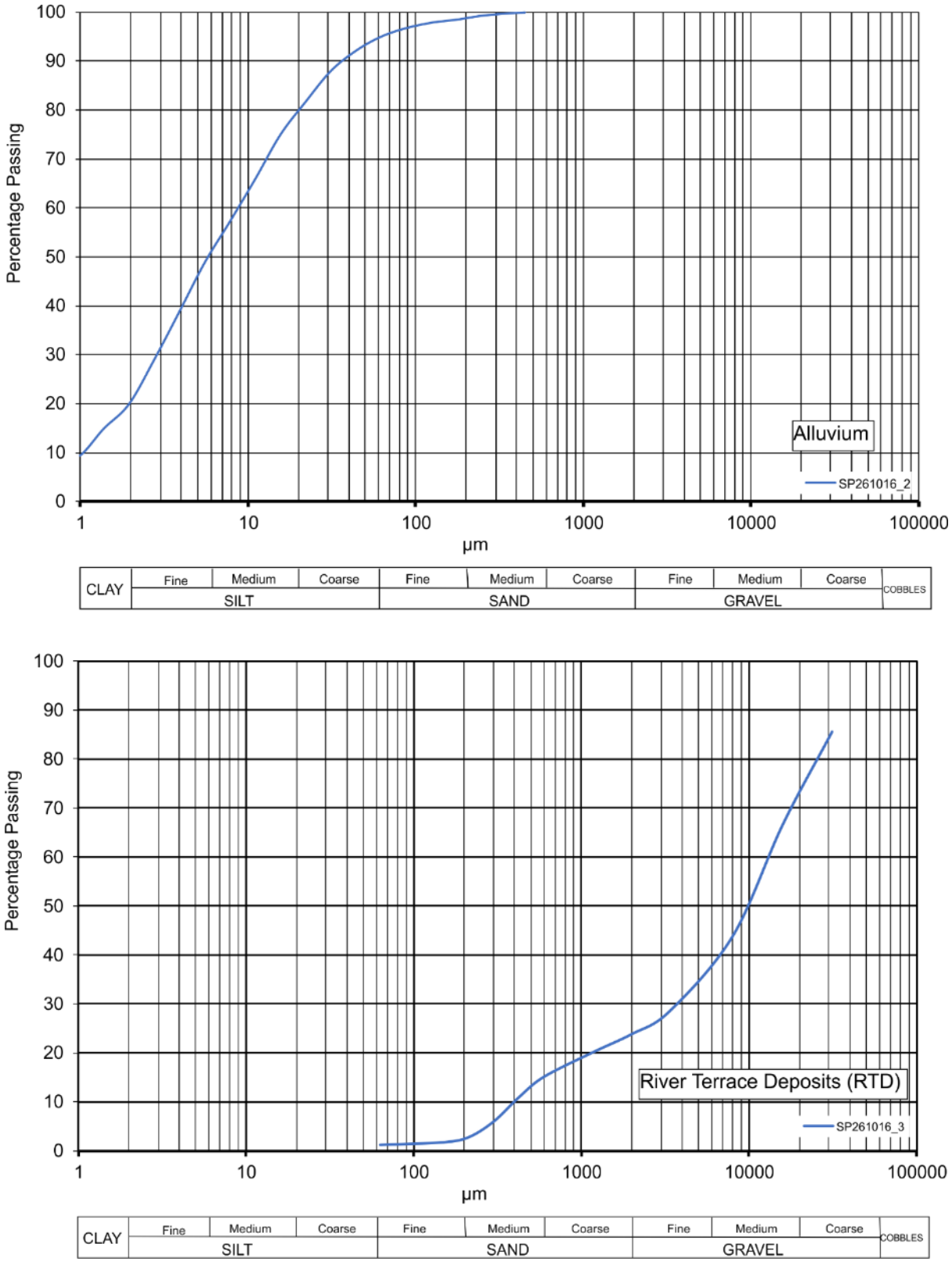

Figure 8-8 Particle-size grading curves Quaternary Domain 1.1.1, alluvium and river terrace deposits.

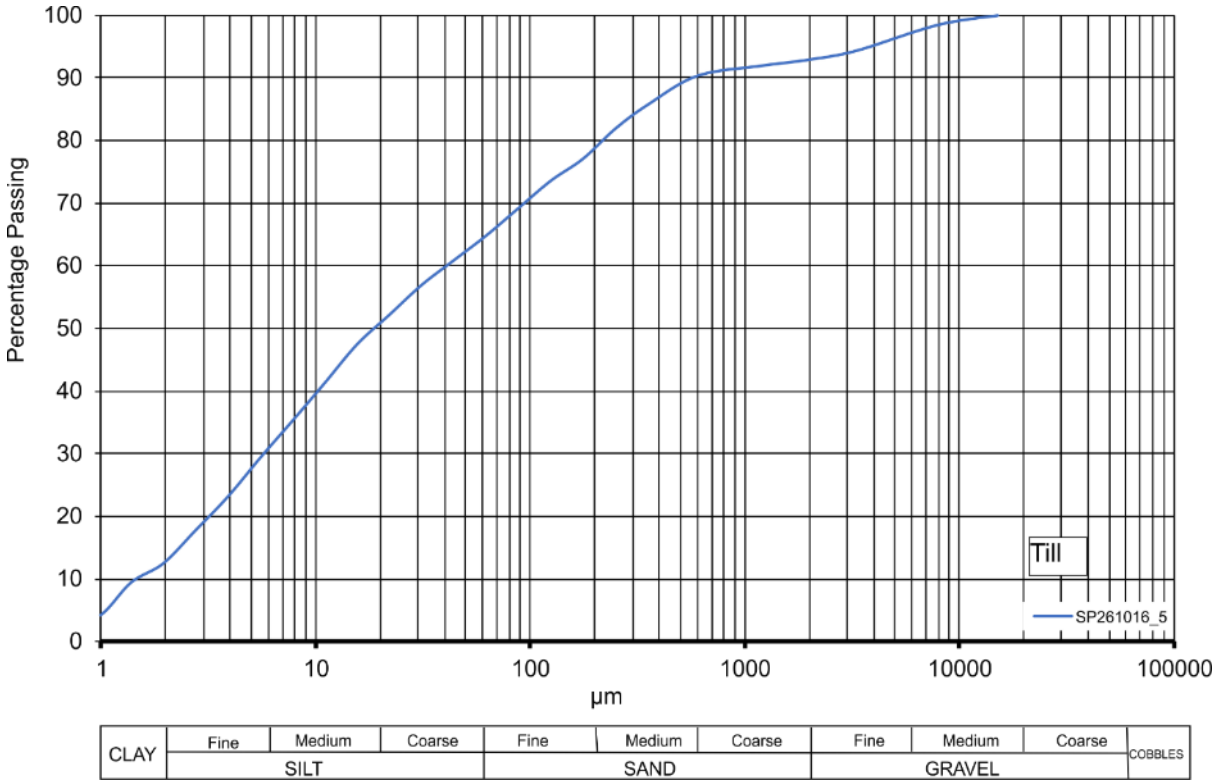

Figure 8-9 Particle-size grading curves Quaternary Domain 1.1.1, till.

8.1.2.4 Atterberg limits and moisture content (till, alluvium)

The results of Atterberg limit determinations for till and alluvium, including moisture content, are shown in Table 4. The results are plotted on a conventional liquid limit-plasticity index chart in Figures 8-10 and 8-11. Supporting data for the calculation of liquid limit, plastic limit and moisture content is given in Appendix 13.2.

Sample	Geology	Liquid Limit (W_L)	Plastic Limit (W_P)	Plasticity Index (I_p)	Moisture content (%)	Liquidity Index (LI)[1]	Activity[2]
SP261016_2	ALV	95	32	63	51	0.3	3.15(A)
SP261016_5	TILL	39	16	23	19	0.17	1.3(A)

Table 8-4 Atterberg limits, moisture content and activity, Quaternary Domain 1.1.1. [1]Calculated from (ω-W_P/I_p). [2]Calculated based on I_p/%clay fraction (0.002mm), where %clay was determined by LPSA. Activity classes I (inactive), N (normal) and A (active) after Skempton (1953). Geological abbreviations defined in Table 7-1.

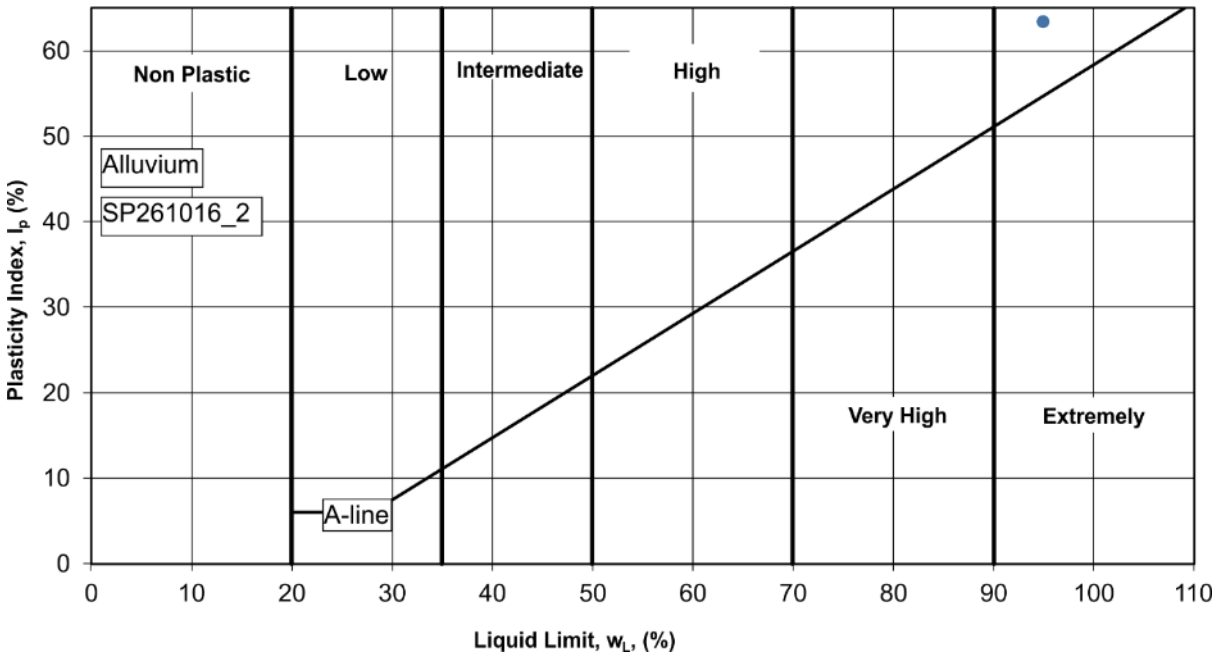

Figure 8-10 Plasticity plot for alluvium, Quaternary Domain 1.1.1.

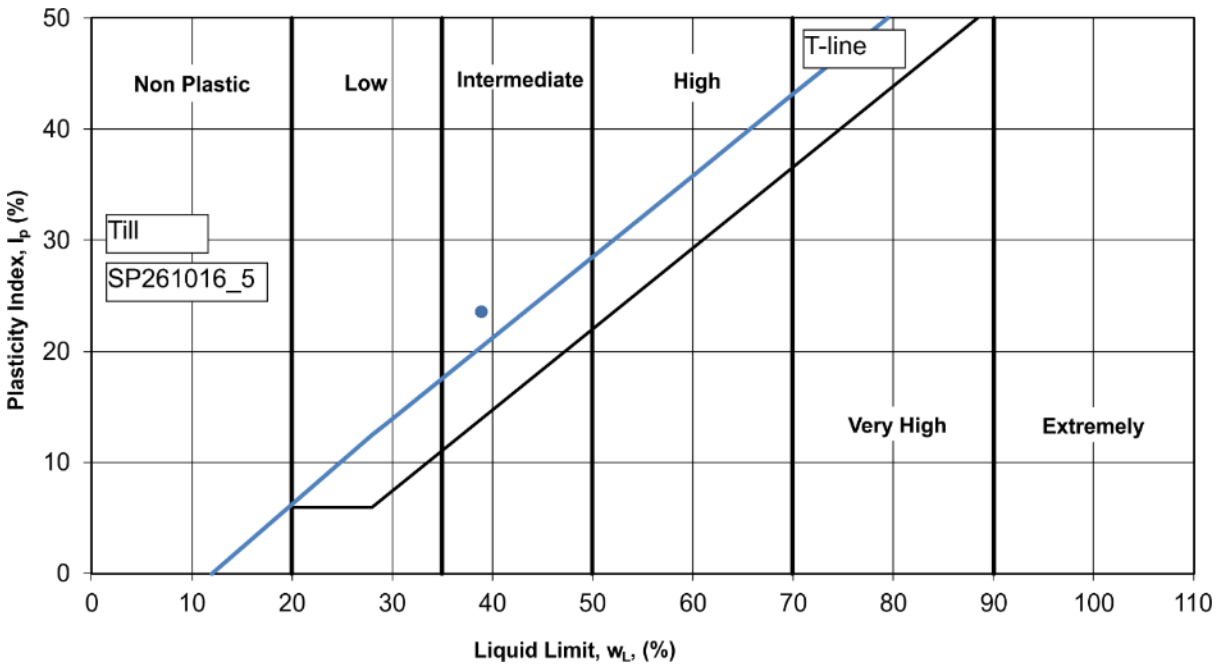

Figure 8-11 Plasticity plot for till, Quaternary Domain 1.1.1. T-line for tills from Boulton & Paul (1976).

Plasticity between the sediments is seen to be variable. Alluvium has extremely high plasticity whilst the plasticity of till is intermediate.

8.1.3 Summary

The specimen interpreted from field evidence as alluvium at Passenham comprises extremely high plasticity, well-graded (poorly-sorted), slightly sandy, slightly clayey silt. It is classified as active with a value greater than 2. The value of activity is interpreted to be the result of I_p

from mixed sources of silt and clay and the low proportion of clay. ω is high compared to the W_p so the value of LI is >0.

The specimen of till at Passenham comprises intermediate plasticity, poorly-graded, calcareous, slightly clayey, slightly gravelly, slightly sandy silt. It is classified as active, with an activity between 1.2 and 2. The value of activity is interpreted to be the result of I_p from silt and clay and the low proportion of clay. The clay mineral assemblage is illite, kaolinite and chlorite with minor non-clay minerals including quartz. ω is high compared to W_p and so the value of LI is >0.

The river terrace deposits comprise well-graded, slightly clayey/silty, very sandy, gravel.

8.2 Quaternary Domain 1.2.1

Quaternary Domain 1.2.1 comprises Middle to Late Jurassic limestone, sandstone and mudrocks of the Inferior and Great Oolite Groups, overlain by glacigenic and periglacial deposits. Bedrock in this Domain is granular compared to those underlain by Middle- to Late-Jurassic mudrocks. The Domain is interpreted to have been glaciated on at least one occasion and influenced by multiple phases of pre- and post-glacial periglacial activity.

Laboratory results are presented for loss-on-ignition (LOI) and particle-size analysis (PSA) for specimens of till (including sandy facies), glaciolacustrine deposits and sediments interpreted as solifluction 'head'. Results for clay mineralogy and plasticity for till are also presented.

8.2.1 Field locality: Home Farm, Stowe

The site at Home Farm, Stowe is a former gravel pit. It is partially infilled, but Sumbler (2002) described 18 m of poorly-sorted gravel containing cobbles and boulders up to 0.7 m in diameter. He interpreted the sequence as occurring within the main body of chalk-rich till which he mapped throughout the Buckingham area.

The location of Home Farm and the sedimentary graphical logs are shown in Figure 8-12. Two OSL samples (SP080417_1 and SP080417_5) were collected from this site and are shown on the logs (see Section 8.7 for results).

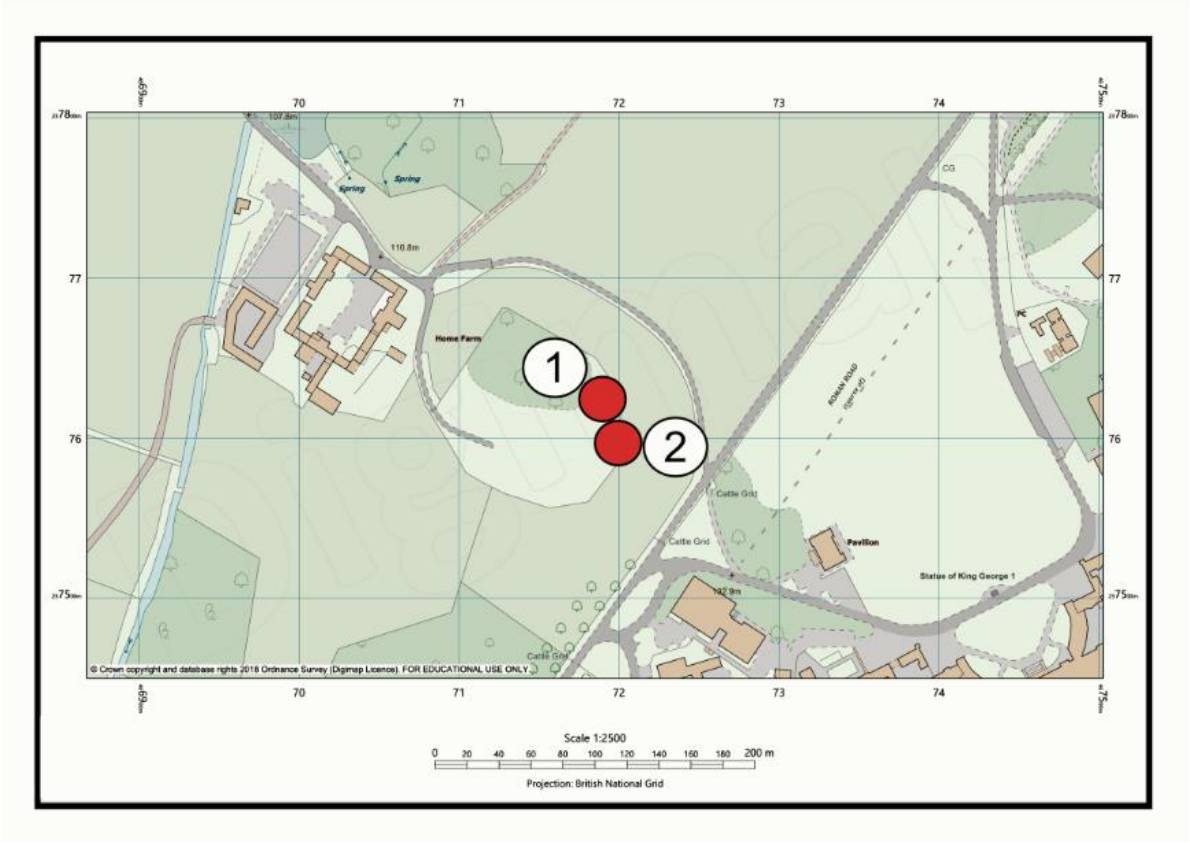

Figure 8-12 Location of Home Farm, Stowe and sedimentological logs, Quaternary Domain 1.2.1.

8.2.1.1 Section descriptions

Two sections were described from the eastern face of the pit (Figure 8-13). Sedimentary structural data is presented in Figure 8-14. The base of the exposure is partially obscured by talus and fill. Representative images of lithofacies are shown in Figures 8-15 to 8-17.

The exposed sequence comprises at least 5 m of massive- to thinly-interbedded sand, gravelly sand and sandy gravel. Rounded clasts of brown till are common. The sequence has been divided into two lithofacies associations.

Lithofacies 5a (LF5a)

Lithofacies 5a consists of reddish-brown and brown, massive to sub-horizontally-bedded, clast-supported, imbricated in places, gravel, cobbles and sandy gravel. Layers of gravel are thinly-interbedded with brown and reddish-brown planar cross-bedded/laminated medium to coarse sand with gravel. Sand beds commonly fine upwards. The bedding dip was recorded as 14°/137°.

The gravel is poorly- to moderately-sorted and clast lithology includes limestone, quartzite, grey flint and white chalk at the base which becomes rare upwards. Gravel is fine to coarse, sub-angular to well-rounded and low sphericity. Gravelly sand lenses are poorly-sorted.

Erosional channel forms are present in places marked by laterally impersistant, <0.5 m wide erosive bases with imbricated coarse gravel and cobbles. Brown, matrix-supported clay and silt with chalk and sandstone clasts is common as rounded, coarse gravel-sized clasts.

Approximately 18 m below the base of the logged exposures, at the edge of the lake, several springs issue. A small section there exposes a matrix-supported sandy clay and silt (LF2b) dominated by quartzite and flint gravel (Figure 8-17 E and F).

Lithofacies 5b (LF5b)

Lithofacies 5b consists of dark reddish-brown, dense, gravelly, silty sand with cobbles. The sediment is associated with rounded, steep-sided funnels and wedges which taper downwards from the ground surface. The sand is >70% reddened, sub-rounded, moderately-sorted quartz. The gravel and cobble clasts consist of quartzite, flint, grey sandstone and ironstone. Chalk and limestone clasts are rare. Within 100 mm of the sides of the wedges, clasts are steeply inclined.

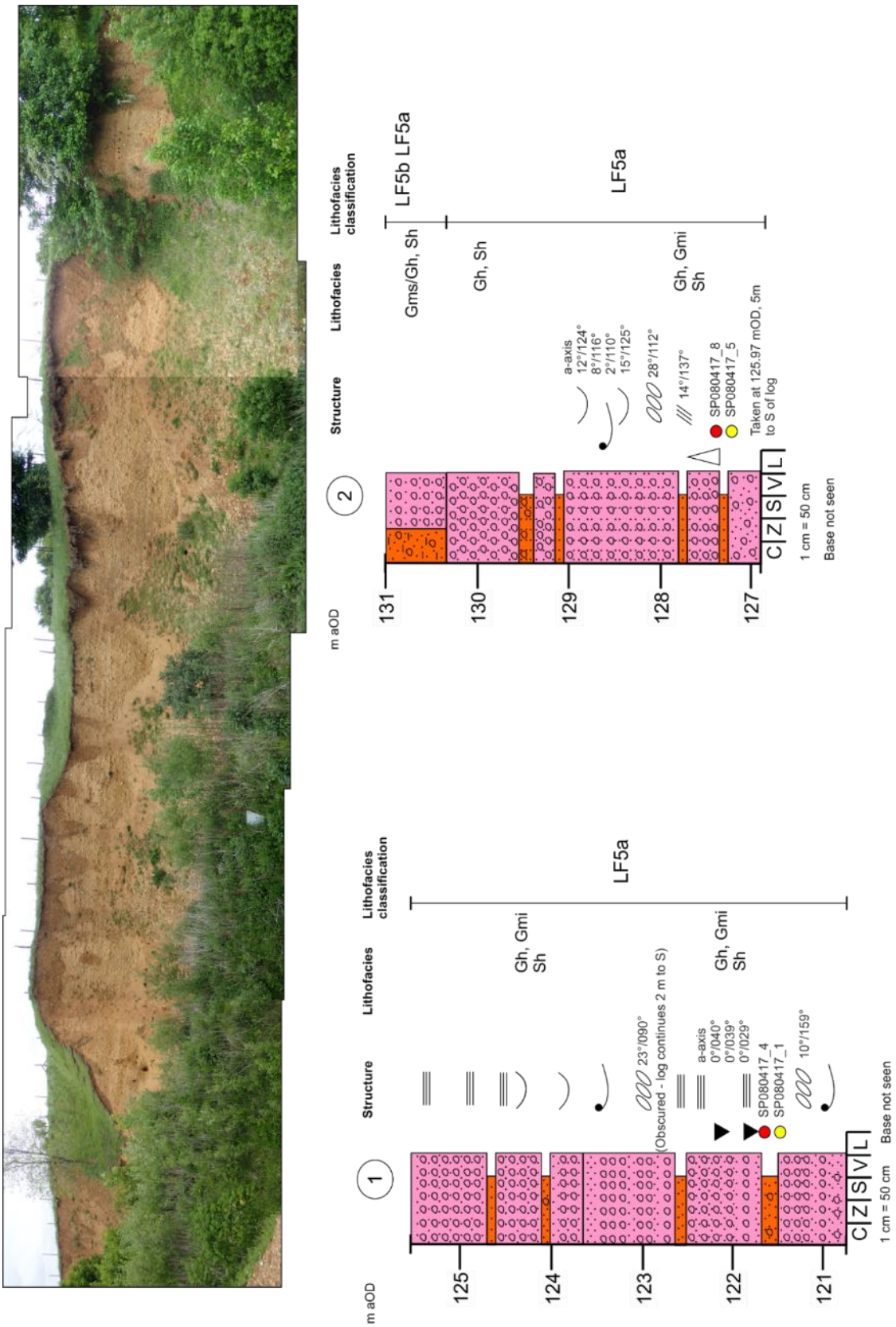

Figure 8-13 Section view and sedimentary graphical logs, Home Farm, Stowe. Refer to Appendix 13.1 for legend.

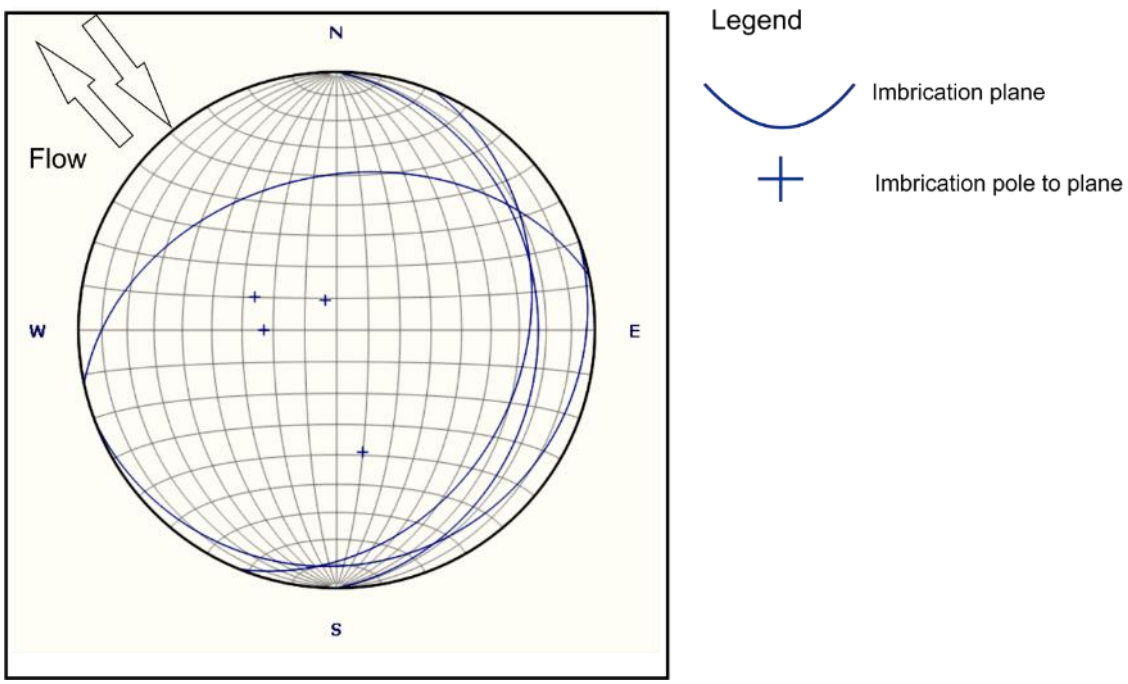

Figure 8-14 Equal are plot of imbrication, Home Farm, Stowe.

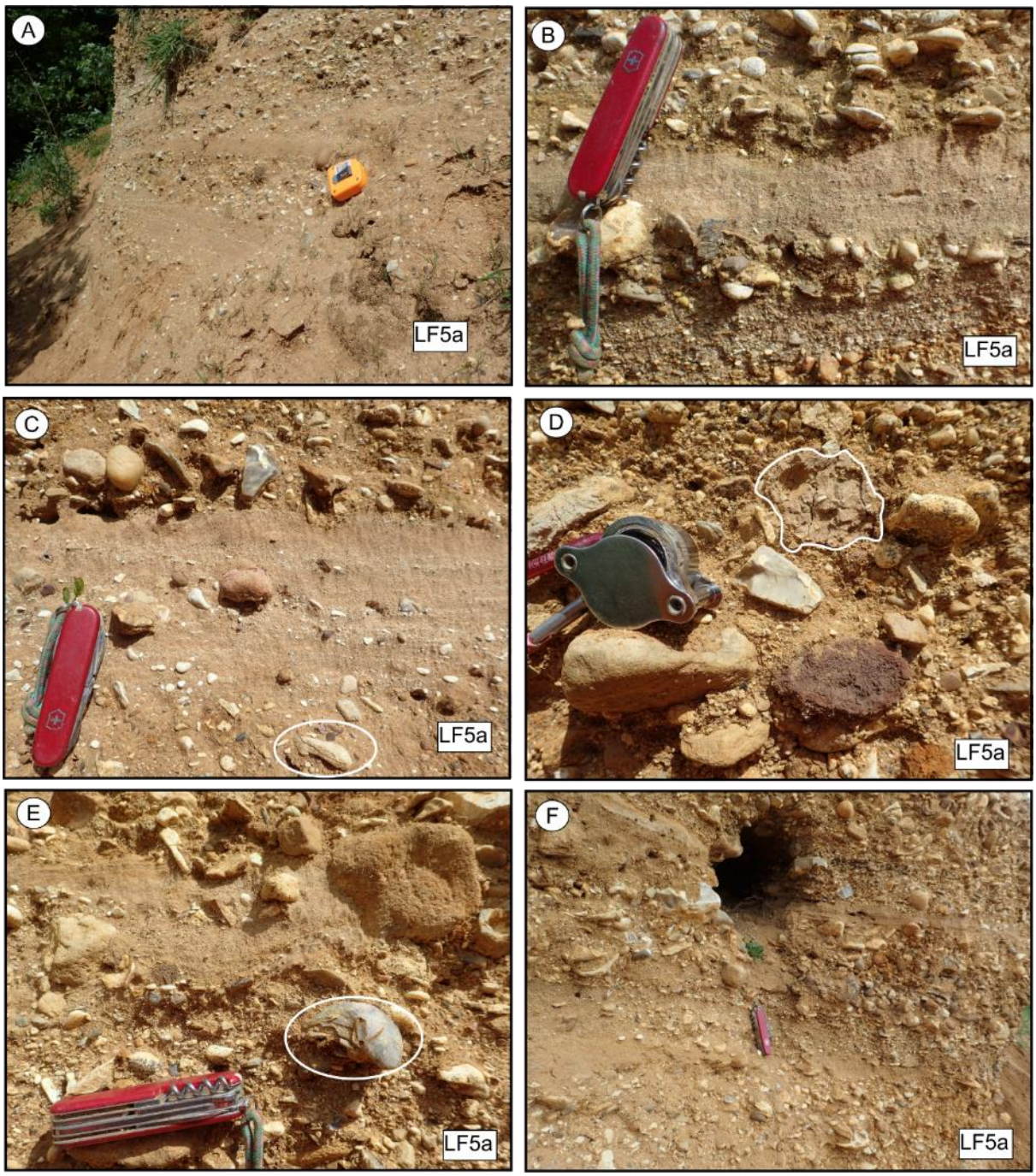

Figure 8-15 Lithofacies 5a, Home Farm, Stowe, 1. A) and B) Interbedded gravelly sand and sandy gravel, base of exposure. C) As A and B with clast showing possible frost-wedging. D) Sub-rounded till clast (highlighted). E) Deformed bedding with convex-up thick-shelled *Gryphaea*. F) Poorly-sorted gravel with interbeds of sand.

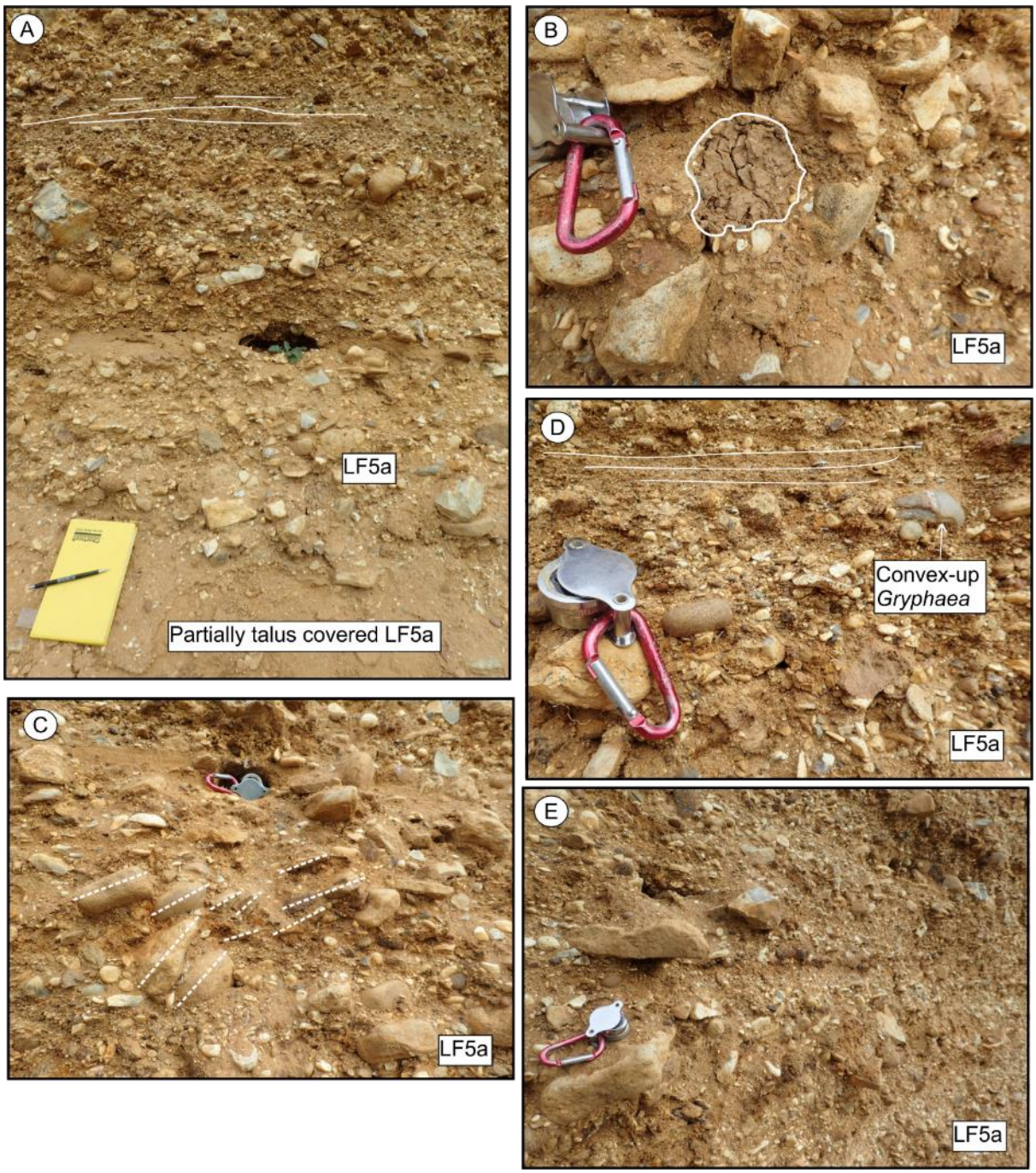

Figure 8-16 Lithofacies 5a, Home Farm, Stowe, 2. A) Poorly-sorted, massive to weakly cross-bedded sandy gravel and gravel. B) Rounded clast of till. C) Imbricated coarse gravel and cobbles within an erosional channel base. D) Massive, poorly-sorted sandy gravel and interbedded, planar-bedded coarse sand. E) Weakly planar-bedded gravel with platy cobbles and coarse gravel.

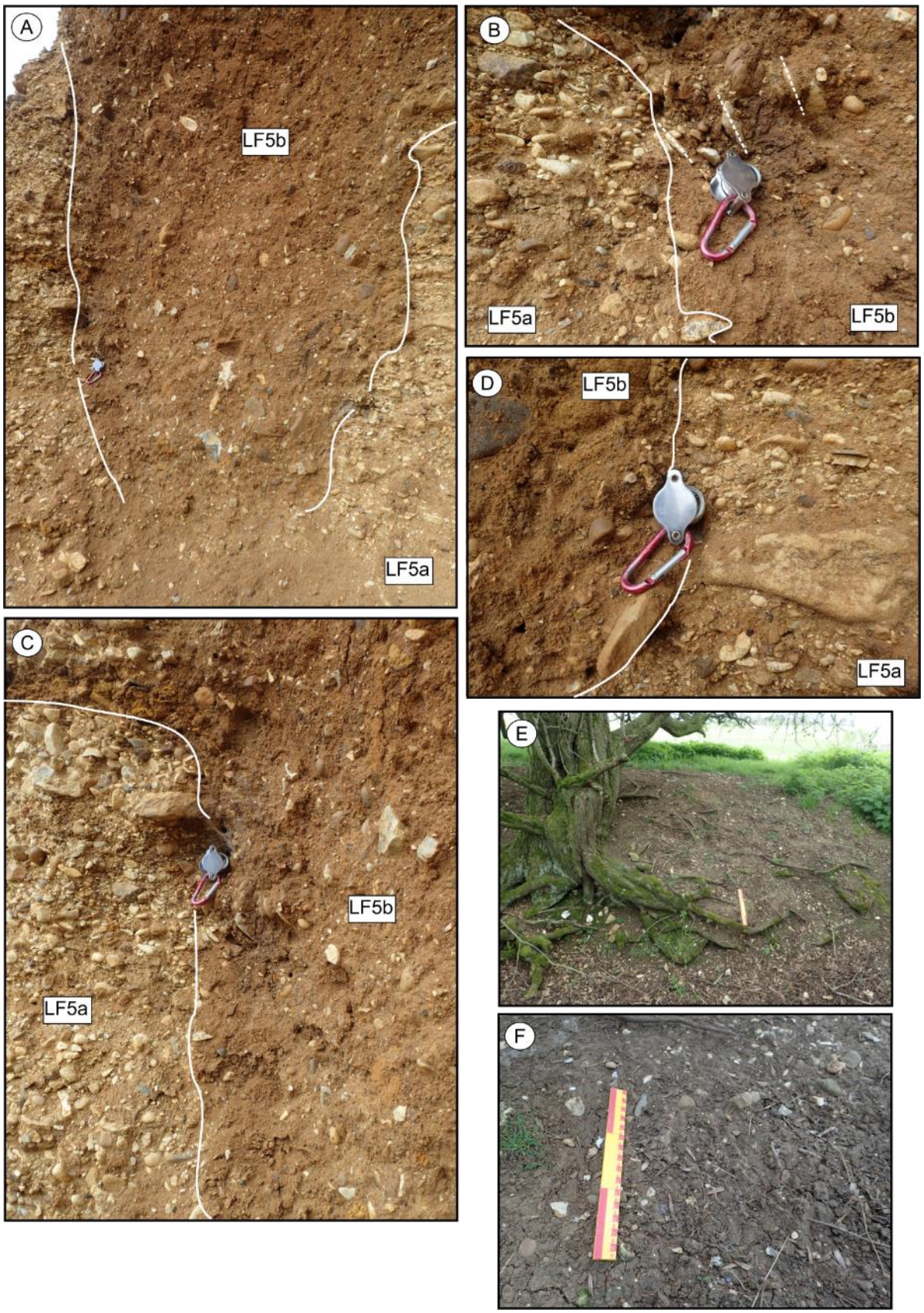

Figure 8-17 Lithofacies 5a, 5b and 2b, Home Farm, Stowe. A) Steeply inclined funnel, Weak bedding visible continuing from surrounding outcrop. B) Edge of funnel with side-parallel orientated clasts. C) Apparently vertical edge of funnel. D) Chalk and limestone-rich LF5a and chalk and limestone poor LF5b. E) and F) Quartzite-rich till.

8.2.1.2 Interpretation

The alternating sequence of massive to weakly-bedded gravel, cobbles and sandy gravels, interbedded with laminated medium to coarse sand with gravel are referred to as gravel rhythmites and are interpreted as part of a terminoglacial fan. Terminoglacial fans (Zielinski & Van Loon, 2000) are characteristic of deposition from sediment-laden meltwaters, proximal to a retreating ice-margin. Evidence for proximity to an ice-margin is present in the form of rounded clasts of matrix-supported till and rapidly alternating massive to crudely-bedded gravel and cobbles interbedded with laminated sand. Massive, weakly-bedded, gravel-rich beds here are interpreted to represent deposits that were deposited by fluvial activity into a shallow, ice-proximal waterbody. It is interpreted that the alternating sequence of planar and cross-bedded sediments form gravel bar and bedform elements using the definition of Giles et al. (2017). Evidence of channelised river flow is provided by erosional channel bases infilled with coarse gravel and cobbles. The latter are interpreted as palimpsest deposits indicating reworking of older sediment by high-energy flows which deposit coarse-gravel, cobbles and occasional boulders. Planar bedding at the outcrop-scale bedding suggests flow towards the southeast. In contrast, imbrication directions indicate flow to the northwest and southeast.

The source of the deposits is interpreted to be from ice-proximal debris flows from an ice-margin retreating to the northwest. The alternation between gravel and laminated sand deposition is interpreted to result from temporal variations in sediment supply from the former ice-front. If this interpretation is correct, it is significant since it implies the spatial location of a former margin of the BIS.

The dark reddish-brown balls and tapering funnels are interpreted to result from preferential weathering and dissolution of carbonate in the upper part of the sequence. Further, dissolution and the creation of small voids are interpreted to account for tilting of clasts at the margins of the structures.

The sediments comprising LF5a and 5b are here named the Home Farm Member. They are correlated with unit C in the section observed by Green (1864) and reviewed in Section 3.3.4. The valley section exposing sediments of LF2b is correlated with the Buckingham Till Member exposed in Buckingham Sand Pit (Section 8.2.3) and unit C of the section observed by Green (1864), described in Section 3.3.4.

8.2.2 Field locality: Tingewick

Small exposures or temporary excavations were present in and around the village of Tingewick, 3 km west of Buckingham. Their locations are shown in Figure 8-18 and described in Section 8.2.2.1.

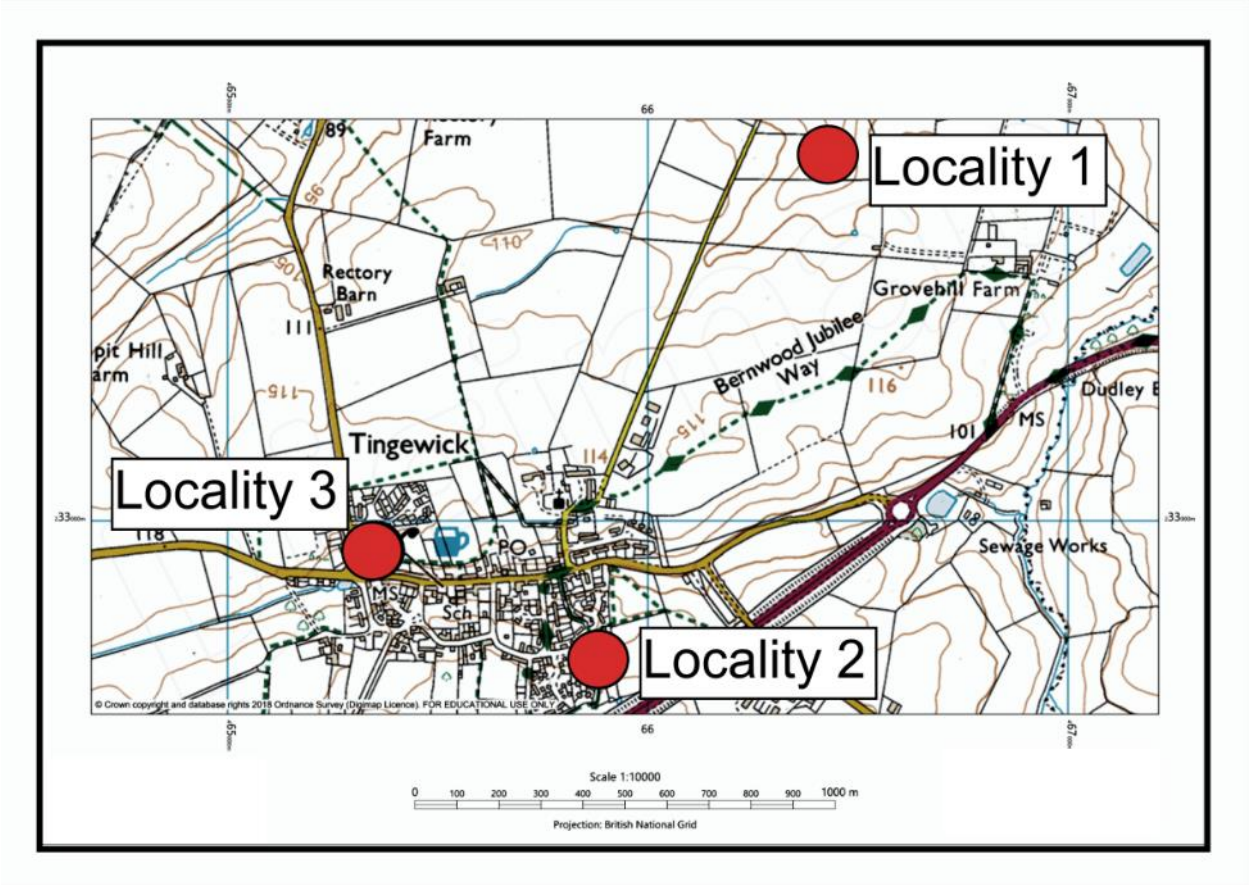

Figure 8-18 Location of temporary exposures in Tingewick, Quaternary Domain 1.2.1.

8.2.2.1 Description of temporary exposures

Representative images of the temporary exposures observed in Tingewick are shown in Figure 8-19.

Locality 1

A temporary excavation for the construction of a local farm house was observed and shown in Figure 8-19B, C and D. Here, approximately 1.0 m of thinly-bedded, 'flaggy' limestone of the Cornbrash Formation is exposed and overlain by 0.6 m of brown, matrix-supported clay and silt with angular fragments of limestone. The thin beds of limestone are seen to be folded into small amplitude upright folds. The folds are interpreted to be involutions and therefore indicative of the former presence of permafrost. The overlying material is interpreted to represent solifluction material, locally-derived from the underlying Cornbrash Formation.

Locality 2

Figure 8-19A shows bluish-grey and brown matrix-supported, rounded, chalk and flint gravel in a matrix of clay and silt. The material was observed as spoil discarded from a temporary borehole excavation in advance of housing development. It is interpreted as till and equated with lithofacies LF2 observed in the exposures at Buckingham Sand Pit and Bletchley.

Locality 3

Locality 3 is an overgrown gravel pit, formerly used as a local refuse site. It is poorly-exposed but is interpreted to be the site of the former exposure described by Green (1864) and discussed in Section 3.3.4.6.

Well-rounded fine to coarse gravel is partially exposed comprising rounded to well-rounded chalk, limestone, flint and quartzite.

The sediments are interpreted as glaciofluvial in origin on the basis of clast roundness and the interbedded and cross-bedded nature of the sediments formerly exposed in Tingewick (Section 3.3.4).

Figure 8-19 Temporary exposures observed in Tingewick. A) Discarded core of chalk-rich till from borehole drilling. B) 'Head' overlying limestone of the Cornbrash Formation. C) and D) involutions in thinly-bedded limestone of the Cornbrash Formation.

8.2.3 Field locality: Buckingham Sand Pit

The location of Buckingham sand Pit, and the locations of the sections described, are shown in Figure 8-20. Exposures are good but intermittent because of extensive vegetation and talus. Despite the small size of the quarry, tracing the lateral continuity of each lithofacies, and determining the nature of their stratigraphical or tectonic boundaries, proved difficult.

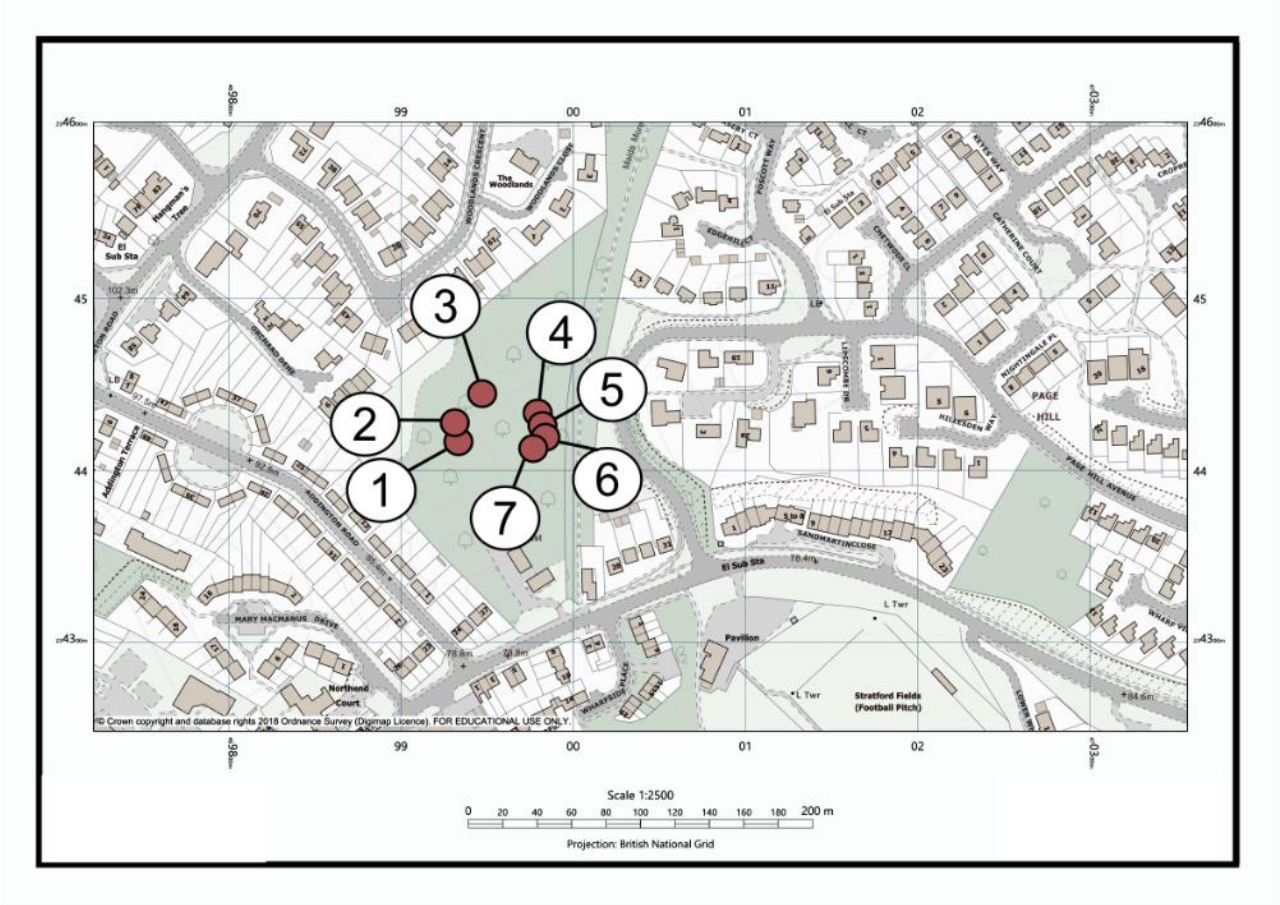

Figure 8-20 Location of sections, Buckingham Sand Pit, Quaternary Domain 1.2.1.

One sample (SP070417_5) was collected from this site for OSL analysis (Section 8.7).

8.2.3.1 Description of sections

Seven sedimentary logs were recorded from observation of sections on the western, northern and eastern faces of the former quarry. Starting from the west, a summary field sketch is provided in Figure 8-21.

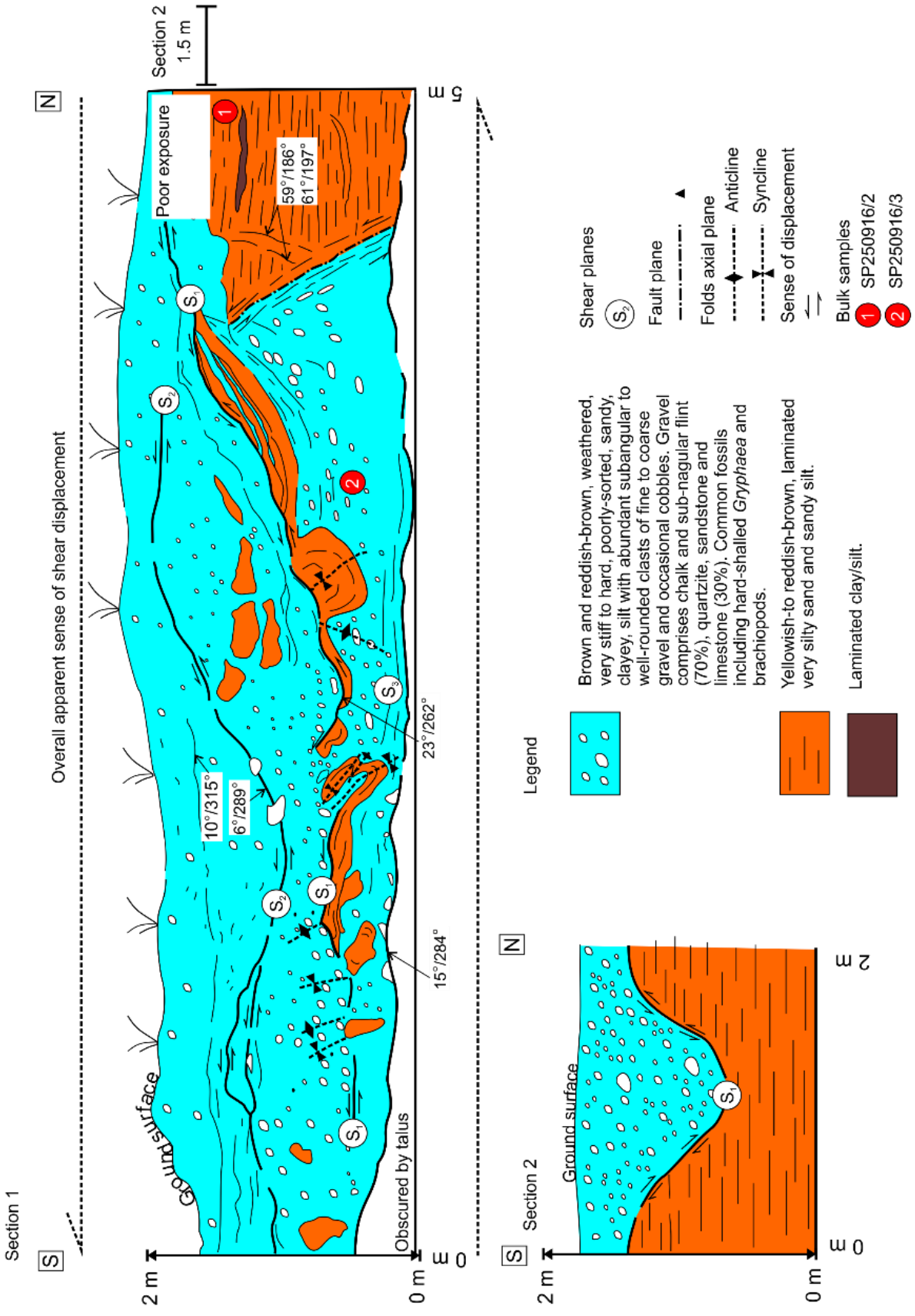

Figure 8-21 Field sketch, western face of Buckingham Sand Pit showing stratigraphical and structural relationships between till (LF2a) and laminated, silty sand (LF1c).

Sedimentary logs are shown in Figures 8-22 to 8-25 and the lithofacies associations are described below and illustrated in Figure 8-27 to 8-30.

Lithofacies 1c (LF1c)

Lithofacies 1c occurs throughout the quarry and is at least 5.6 m thick. It is interpreted to underlie and be partially re-worked and deformed within LF2. Its contact elsewhere with LF 2 is interpreted to be steeply-inclined and faulted or sheared. It comprises an overall coarsening-upwards sequence of reddish-brown and brown, calcareous parallel- and cross-bedded/laminated, very silty sand with some evidence of erosion and channeling. Wisps of chalk are common. Thinly-cross-bedded, clast supported beds of gravel (gravel rythmite) are common towards the top. Thin beds of calcareous silt occur, which in Log 2, overlies gravel and has been brecciated. The gravel is fine to medium, rounded to well-rounded flint, quartzite and chalk.

The orientation of cross-bedding is shown in Figure 8-26.

Folded and overturned lenses of LF1c are associated with LF2a in the area of Logs 1 and 2 where separate units of this intermixed assemblage can be seen to be separated by shear planes, inclined towards the west.

Lithofacies 2 a, b (LF2a, b)

In contrast to exposures of LF2 in Passenham, in Buckingham Sand Pit, LF2 has been subdivided into LF2a and LF2b.

LF2a comprises very stiff to hard, bluish-grey, weathering brown, massive, matrix-supported, poorly-sorted, sandy, gravelly silt and clay. Closely-spaced, sub-horizontal discontinuities are present throughout. Gravel consists of abundant well-rounded chalk and pink quartzite with grey angular flint. In places, lenses of chalk particles are deformed either into low-amplitude, open folds or aligned parallel to inclined discontinuities (Figure 8-21). It is interpreted to be the youngest unit exposed.

Lithofacies 2b is interpreted to be the oldest unit exposed where it crops out in the area of Log 7. Here, it comprises massive, matrix-supported, mottled brownish red, brown and light grey, very stiff to hard, very sandy, gravelly silt and clay. The gravel comprises rounded to well-rounded pink and red quartzite, grey flint and rare chalk and is fine- to coarse-grained. The azimuth of the a-axis of suitable clasts was recorded and presented in Figure 8-26.

LF2a and LF2b are interpreted to crop-out together in Log 7 where they are separated by sand and silty sand of LF1c.

Lithofacies 4 (LF4)

LF4 is interpreted to conformably underlie LF1c. It comprises clast-supported, cobbles and boulders of limestone with some matrix material of sandy, gravelly, silt. In Log 2, it is steeply inclined 48°/049° where it is interpreted to be in reverse-faulted contact with LF2a. In Log 5, LF4 appears to occupy a channel where it cuts out by erosion, underlying lenses of silt. To the south, near Log 6, it rests unconformably on an inclined planar surface overlying LF2b.

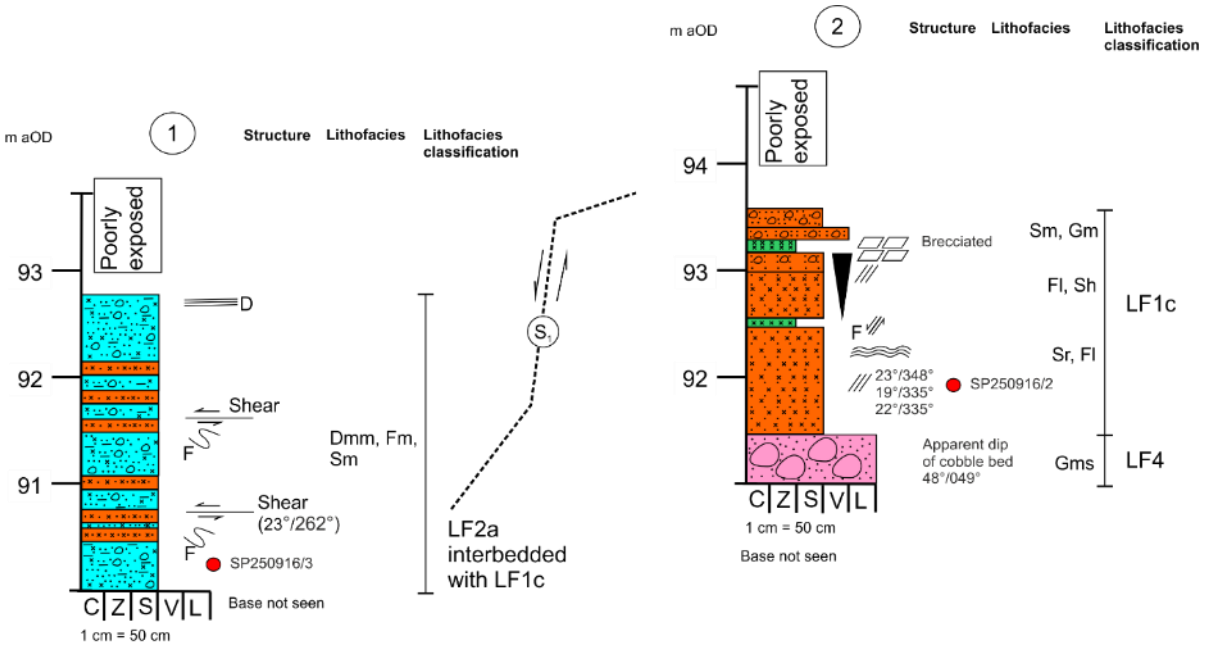

Figure 8-22 Sedimentary graphical logs 1 and 2, Buckingham Sand Pit. Refer to Appendix 13.1 for legend.

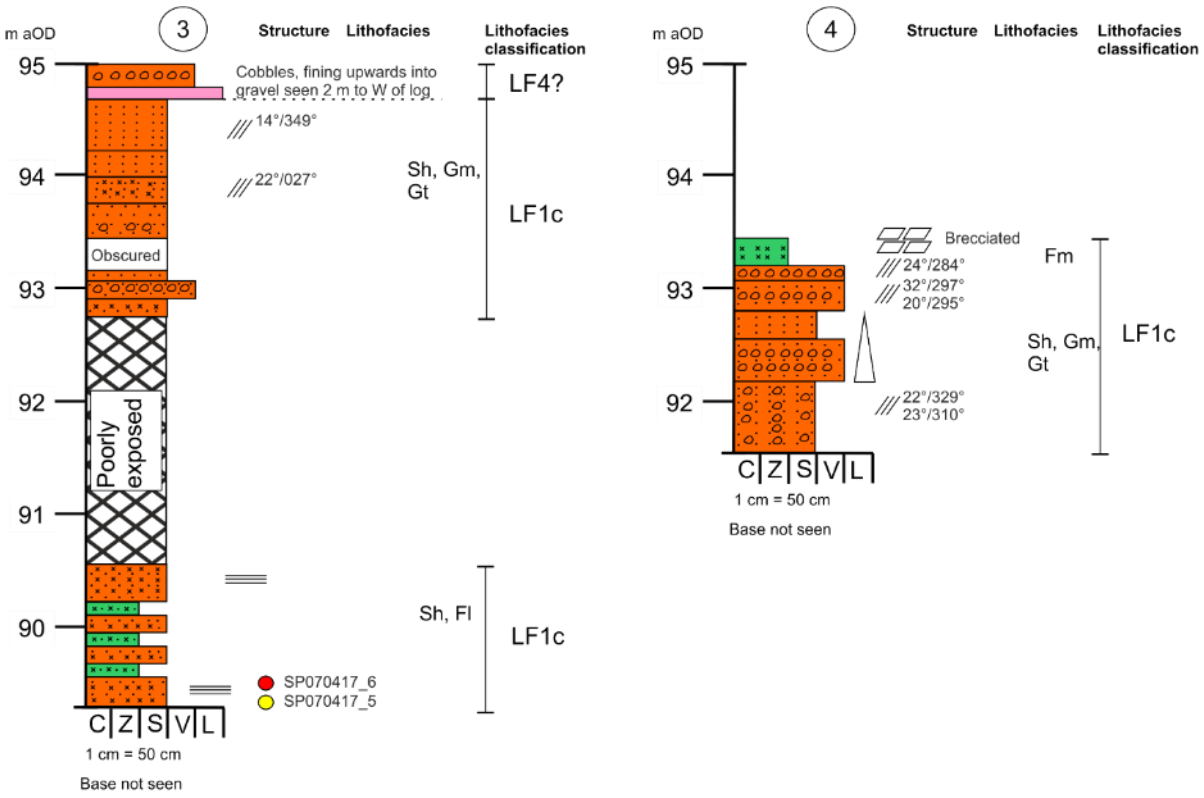

Figure 8-23 Sedimentary graphical logs 3 and 4, Buckingham Sand Pit. Refer to Appendix 13.1 for legend.

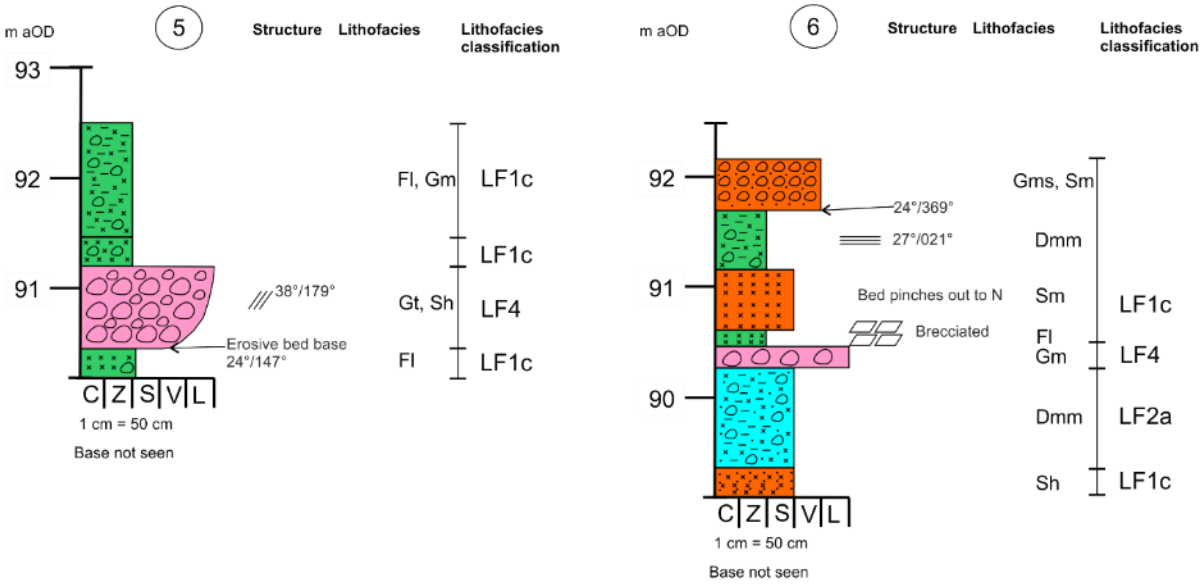

Figure 8-24 Sedimentary graphical logs 5 and 6, Buckingham Sand Pit. Refer to Appendix 13.1 for legend.

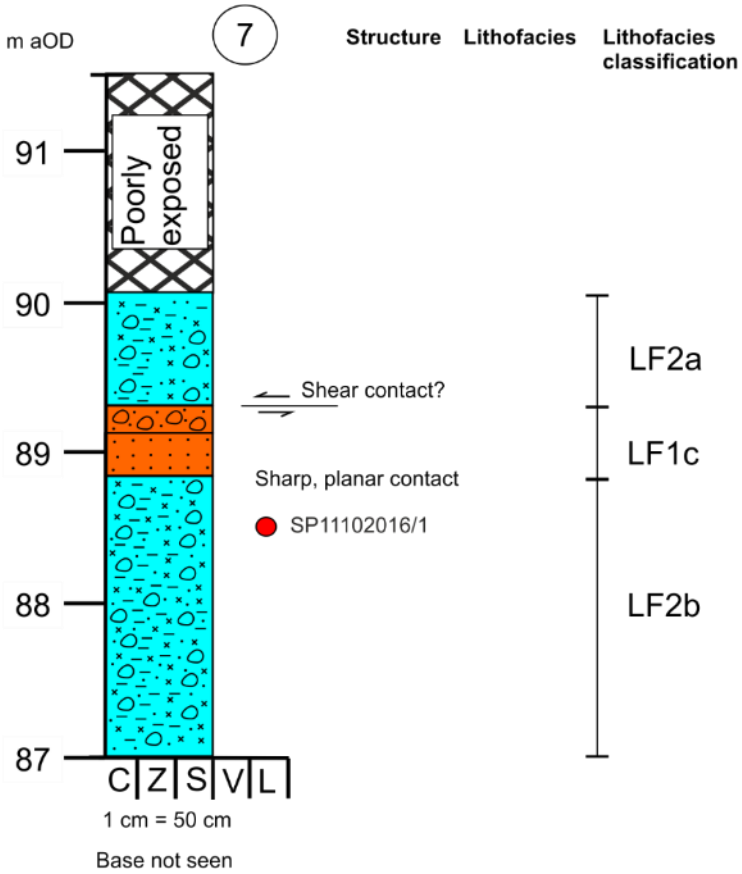

Figure 8-25 Sedimentary graphical log 7, Buckingham Sand Pit. Refer to Appendix 13.1 for legend.

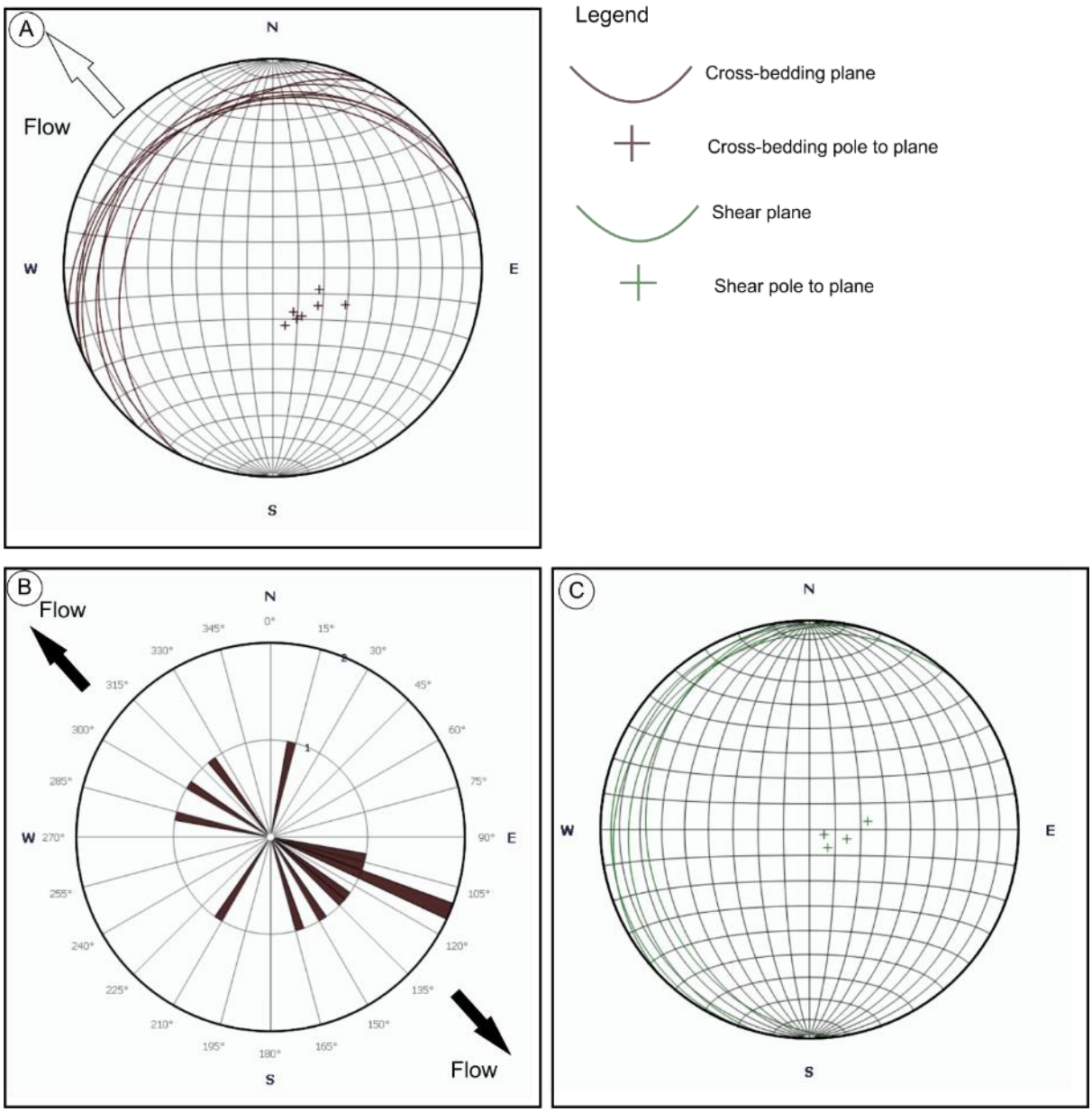

Figure 8-26 Sedimentary fabric measurement, Buckingham Sand Pit. A) LF1c, cross-bedding/lamination. B) Long-axis orientation of fine to coarse gravel (up to 60 mm) in LF2b. C) Orientation of shear planes,

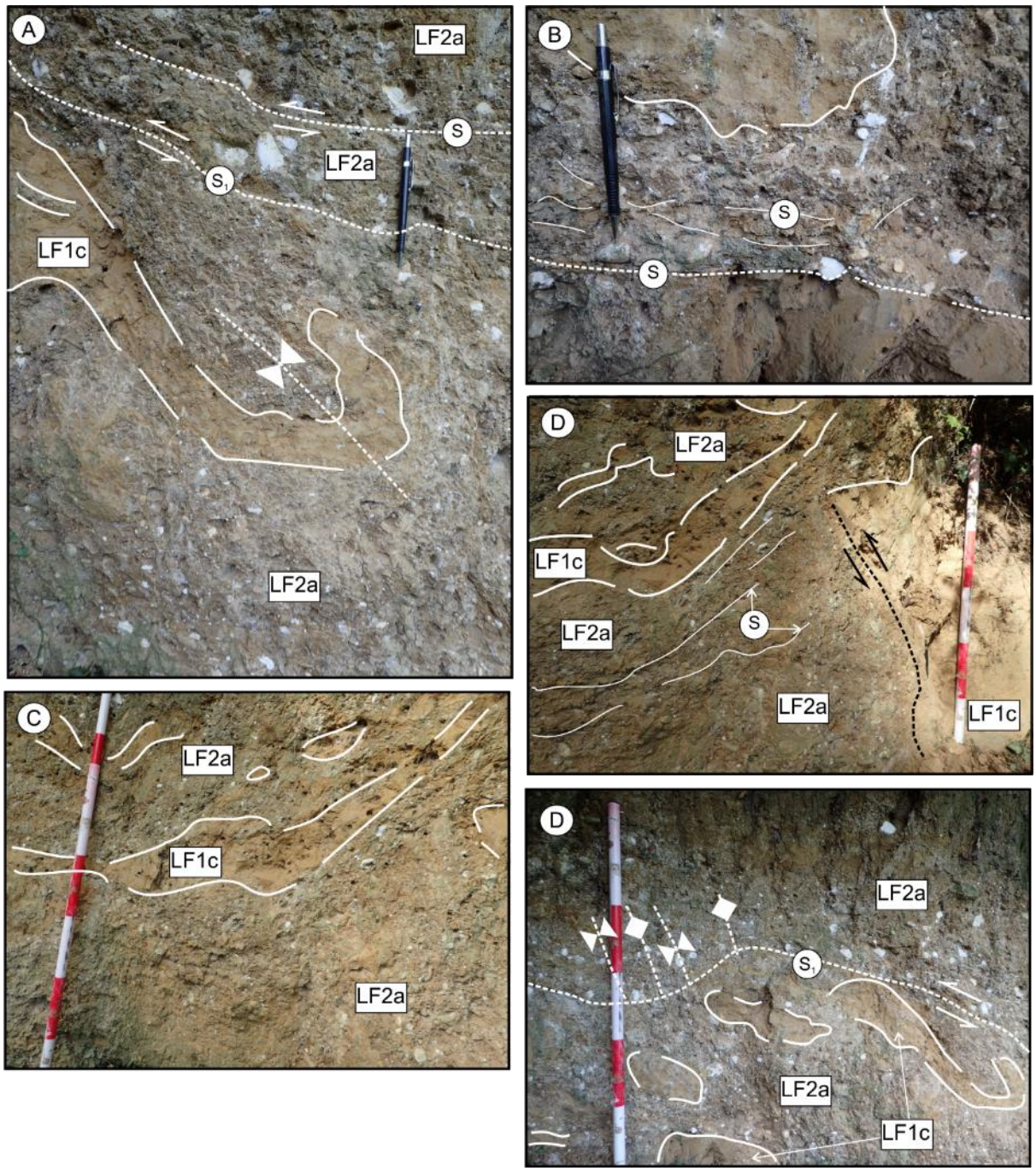

Figure 8-27 Lithofacies associations 1, Buckingham Sand Pit. A), B) and C) LF2a till incorporating folded and sheared lenses of LF1c. D) Open folding in LF2a above apparent shear zone. 25 cm bands on measuring rod.

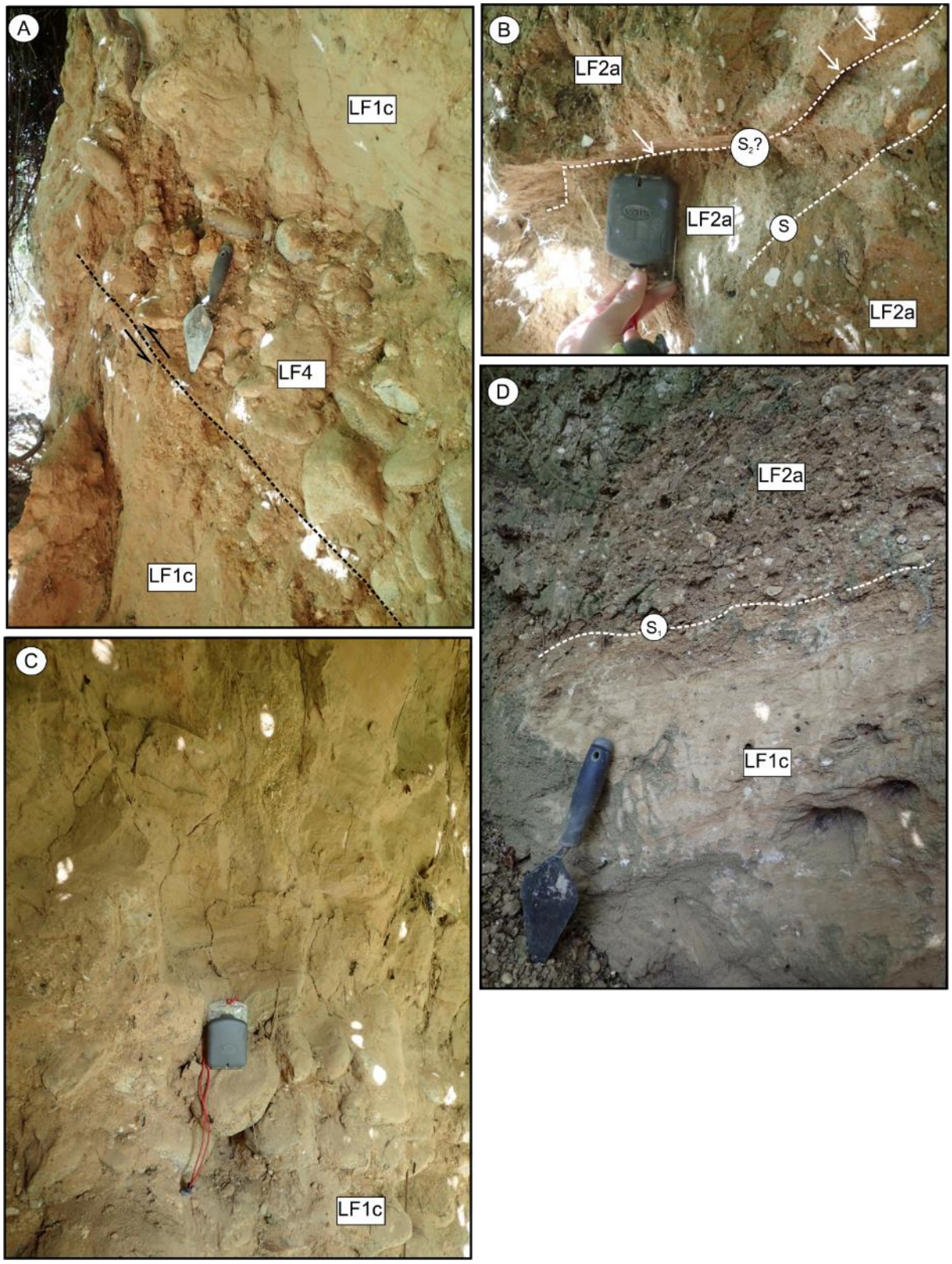

Figure 8-28 Lithofacies associations 2, Buckingham Sand Pit. A) Steeply inclined (reverse-faulted) boulders in LF4. B) Shear surfaces in LF2a till.

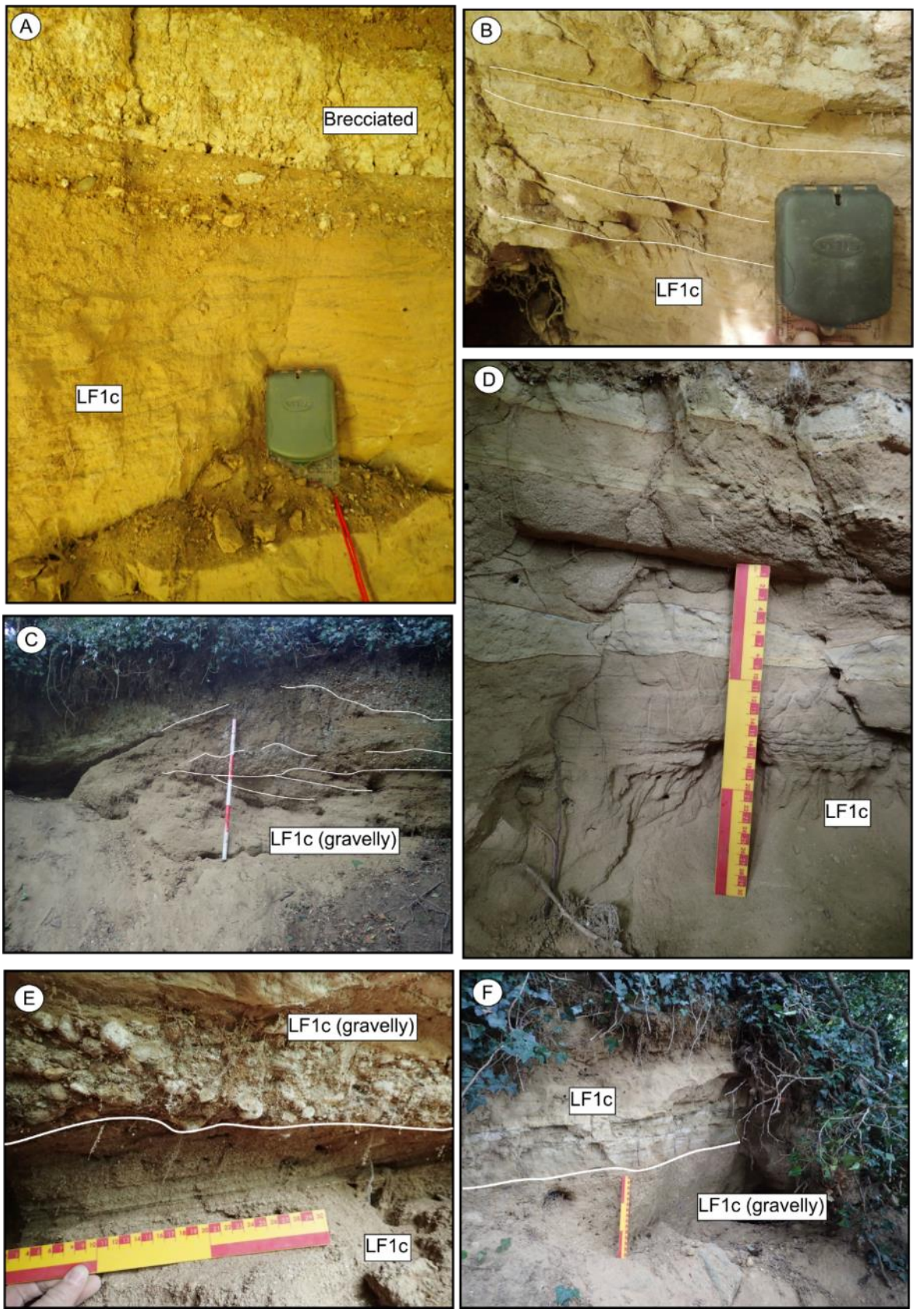

Figure 8-29 Lithofacies associations 3, Buckingham Sand Pit. A) Coarsening-upwards sequence into gravel and brecciated? silt. B) to F) cross-bedded and parallel laminated silty sand and clast-supported chalk-rich gravel.

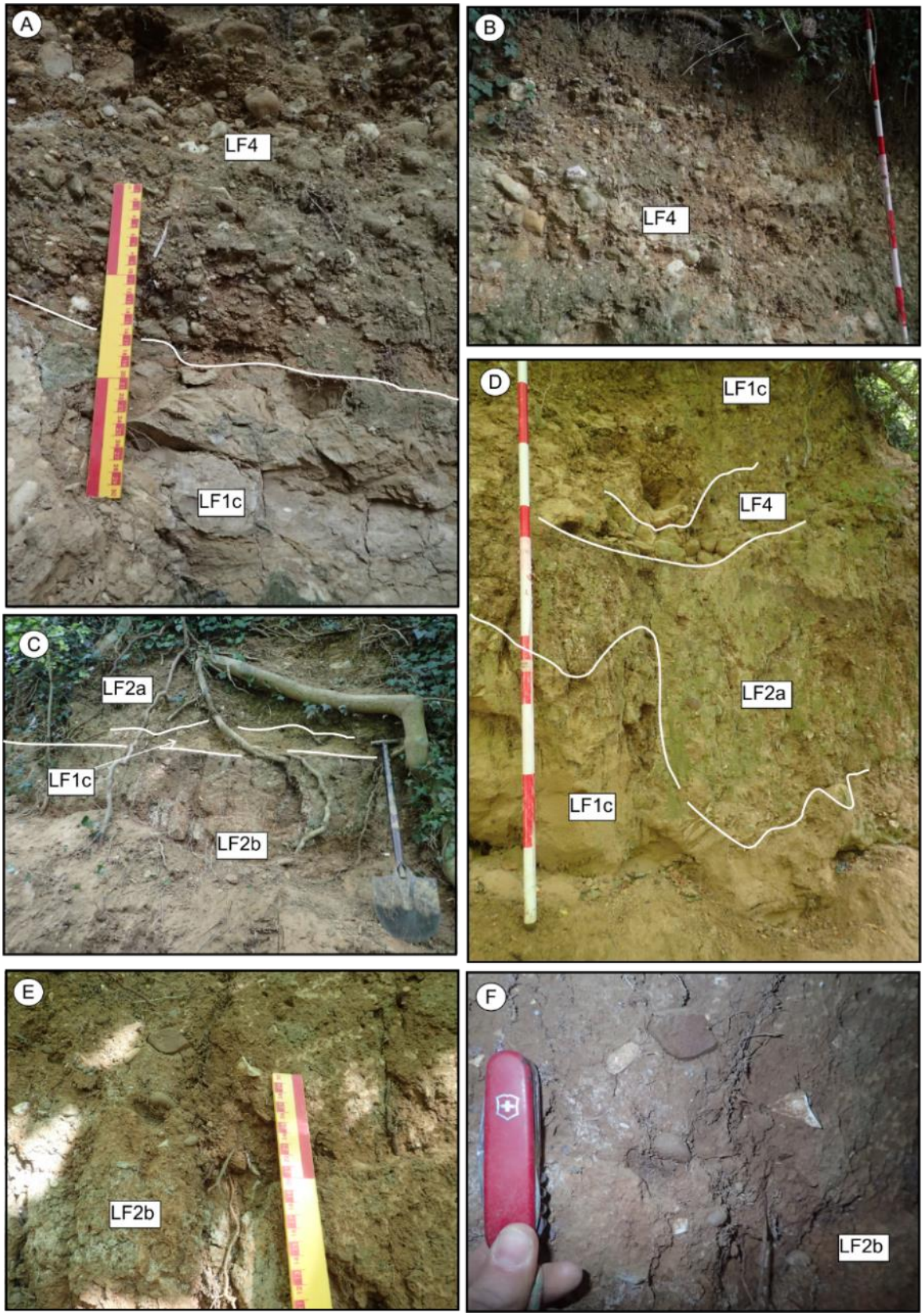

Figure 8-30 Lithofacies associations 4, Buckingham Sand Pit. A) Poorly-sorted gravel and cobbles incised into underlying silt within a channel. B) Poorly-sorted, crudely-bedded gravel and cobbles. C) Planar contact between LF2b and LF1c. D) Erosive contact between LF4 and LF2b. E) and F) quartzite-dominated till of LF2b.

8.2.3.2 Interpretation

The sequence exposed in Buckingham Sand Pit is interpreted as a tripartite sequence of sub-glacially deformed glacigenic sediments. The oldest unit is LF2b which is interpreted to be a till whose Triassic-derived, quartzite-dominant clast composition reflects a glacier-source to the northwest of the area. This unit is in turn overlain by cobbles and boulders of LF4 which are interpreted as high-energy, subaqueous debris flows which flowed into a standing body of water, possibly a proglacial lake and partially eroded into the underlying till of LF2b. Evidence of the formation of a glaciolacustrine environment of deposition is provided by the accumulation of silty sand and silt in LF1c, including periodic input of calcareous silt. Evidence from cross-bedding indicates that the dominant sediment flow direction into the lake was to the northwest.

The presence of shear planes inclined towards the northwest, folded and overturned lenses of LF1c incorporated within chalk-rich till of LF2a, indicates that the LF1c may have been overridden by a subsequent glacier advance. The incorporation of folded LF1c into an assemblage with LF2a separated by shear planes is interpreted as evidence of subglacial, basal shearing.

LF2b is referred to here, for the first time, as the Buckingham Till Member. It has not been named previously. It is interpreted to correlate with the basal sediments recorded by Green (1864) west of Buckingham and referred to unit as G in Section 3.3.4. LF4 is named here the Page Hill Member. It has not been named previously. It is interpreted to correlate with unit F of the section described by Green (1864). LF1c is named here as the Deanshanger Glaciolacustrine Member and interpreted to correlate with the sequence of laminated silt and sandy silt with matrix-supported, sandy, gravely silt and cay with common chalk clasts, recorded in the BGS Deanshanger borehole described in Section 3.3.4.2. It is further correlated with laminated silt, clay, sand and till exposed in Bletchley, described in Section 8.4.1.

The chalk-rich till comprising LF2a is here referred to as the Milton Keynes Till Member. It is interpreted to correlate with other exposures of chalk-rich, matrix-supported till exposed at Bletchley (Section 8.4.1) and seen as exaction debris in Tingewick (Section 8.2.2).

8.2.4 Laboratory results

8.2.4.1 Loss-on-ignition (till, glaciolacustrine, undifferentiated glacigenic deposits and 'head')

Results for loss-on-ignition are shown in Table 8-5. Samples of till, including its sandy facies, are calcareous (n=5), comprising between 8% and 27% calcareous material. Sample SP11102016_1 is markedly less calcareous than other samples of till. Undifferentiated glacigenic and glaciolacustrine deposits (n=3) are comprise between 14% and 26% material which exceeds that of the specimen interpreted as 'head' which contains 13%.

Sample	Geology	% water	%organic	%$CaCO_3$	% silicate residue
SP250916_2	GLLD	0.7	1.3	21.7	77
SP250916_3	TILL	N/A	4.6	18.17	77.3
SP11102016_1	TILL	N/A	2.9	5.2	92
SP211016_1	TILL	N/A	3.8	23	73.3
SP211016_8	TILL	N/A	4.3	18	77.7
SP191016_9	'HEAD'	13.5	4.5	8.9	86.7
SP080417_8	GLAC_UNDIFF	4.5	0.9	24.7	74.4
SP070417_6	GLLD	3.8	1.4	19.4	79.2
SP080417_4	GLAC_UNDIFF	5.7	0.8	13	86.3

Table 8-5 Loss-on-ignition (LOI), all geology, Domain 1.2.1. N/A denotes gravimetric water content measured as part of Atterberg, 1D consolidation or triaxial analysis.

8.2.4.2 Clay mineral XRD (till)

Diffractograms from the analysis of orientated, aggregate specimens are presented in Figure 8-31. The identification of clay minerals followed the procedure described in Section 8.1.2.2.

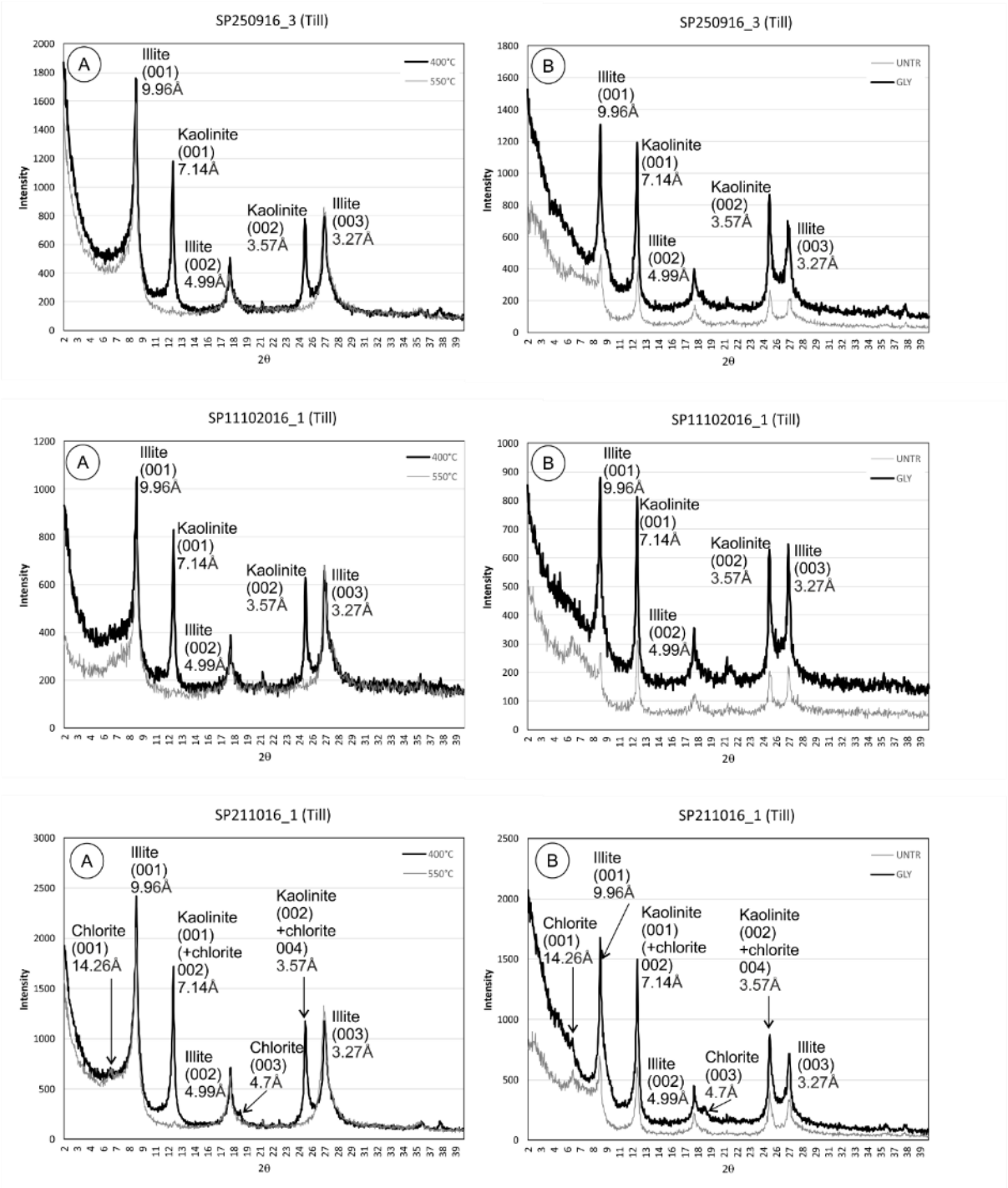

Figure 8-31 Clay mineral XRD for till, Quaternary Domain 1.2.1. A) Heat treated at 400ºC and 550ºC. B) Air dried, untreated (untr) and glycolated (gly).

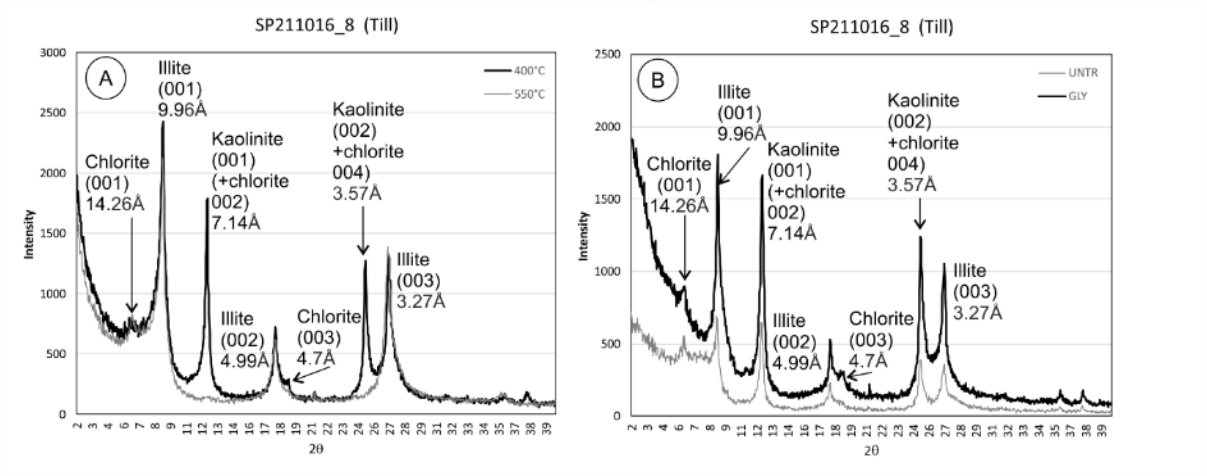

Figure 8-31 continued. Clay mineral XRD for till, Quaternary Domain 1.2.1. A) Heat treated at 400ºC and 550ºC. B) Air dried, untreated (untr) and glycolated (gly).

Strong, narrow peaks are seen in the diffractograms associated with a clay mineral assemblage that includes illite (mica) and kaolinite (with minor or trace amounts of chlorite) in samples SP250916_3 and SP11102016_1. In contrast, samples SP211016_1 and SP211016_8 include chlorite as a separate phase and in association with kaolinite. Illite forms a mixed layer assemblage with collapsible clay minerals of unknown composition. Kaolinite is characterised by peak intensity reduction or loss-on-heating to 550ºC. Non-clay minerals are poorly defined but probably include quartz (4.35 Å) and gypsum. The intensity of the quartz peak is higher in sample SP11102016_1.

8.2.4.3 Particle-size analysis (PSA), (till, glaciolacustrine, undifferentiated glacigenic deposits and 'head')

The results of particle-size analysis are plotted as percentage passing (finer) – log particle-size plots (Figures 8-32 and 8-33) for specimens of till, undifferentiated glacigenic deposits, glaciolacustrine deposits and 'head'. The grading characteristics and classification of each specimen are summarised in Table 8-6. Coefficient of uniformity and coefficient of curvature were calculated using the method described in Section 8.1.4.

Sample	Geology	Method[1]	Lithological Description[2]	Sample grading[3]	C_u	C_z
SP250916_2	GLLD	LPSA	Slightly clayey, very silty, SAND	Well-graded	13.0	1.923
SP250916_3	TILL	LPSA + WS	Clayey, gravelly, very silty, SAND	Well-graded	65.0	2.6
SP11102016_1	TILL	LPSA + WS	Slightly gravelly, slightly clayey, slightly sandy, SILT	Poorly-graded	13.0	0.942
SP211016_1	TILL	LPSA + WS	Slightly gravelly, slightly clayey,	Well-graded	16.0	1.563

			slightly sandy, SILT			
SP211016_8	TILL	LPSA + WS	Slightly gravelly, slightly clayey, slightly sandy, SILT	Well-graded	16.0	1.0
SP191016_9	'HEAD'	WS	Slightly gravelly, slightly sandy, CLAY/SILT	N/A	N/A	N/A
SP080417_8	GLAC_UNDIFF	LPSA	Very silty, SAND	Well-graded	40.0	8.1
SP070417_6	GLLD	LPSA	Very silty, SAND	Well-graded	9.231	1.801
SP080417_4	GLAC_UNDIFF	LPSA	Silty, SAND	Well-graded	18.5	6.541

Table 8-6 PSA summary for all geological units in Domain 1.2.1. [1]LPSA – Laser Particle-Size Analysis, WS – wet sieving**.** [2]Based on proportions by mass from PSA following conventions in British Standards BS5930:1999 with Amendment 2 (British Standards Institution, 1999). [3]Geotechnical terminology.

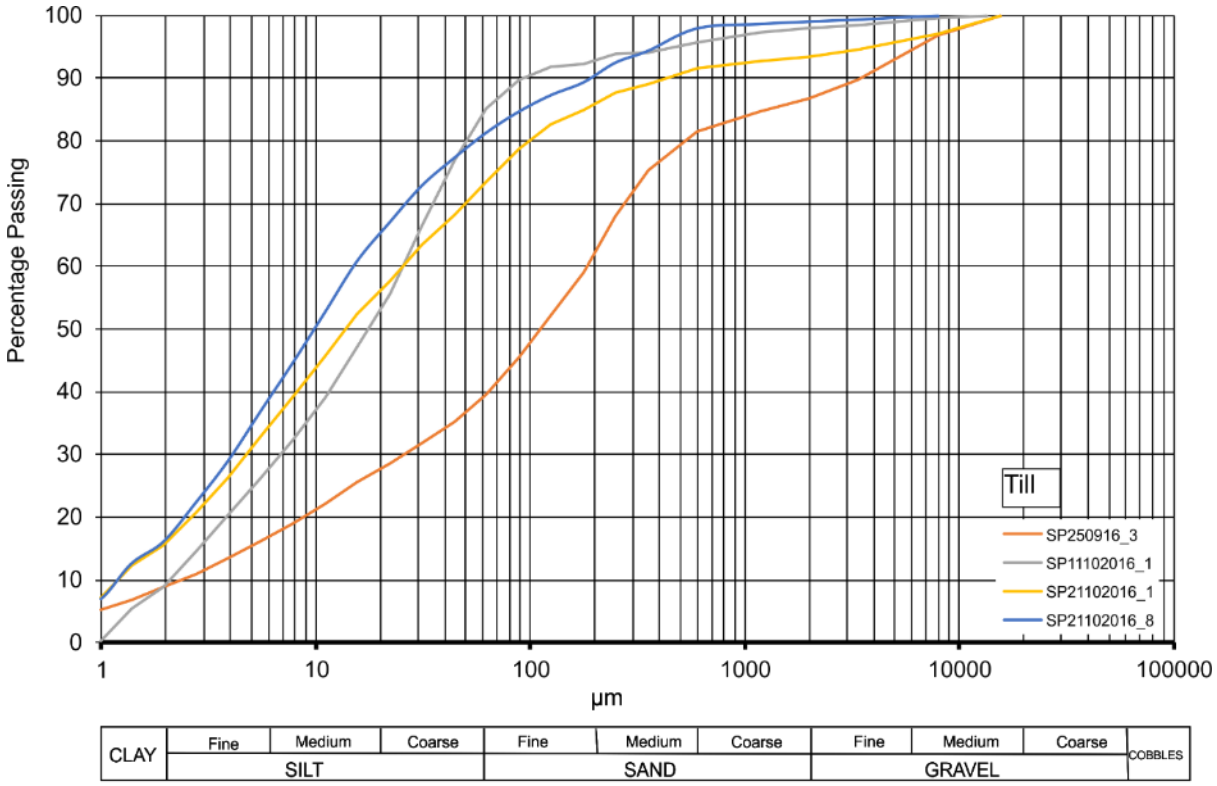

Figure 8-32 Particle-size grading curves Quaternary Domain 1.2.1, till.

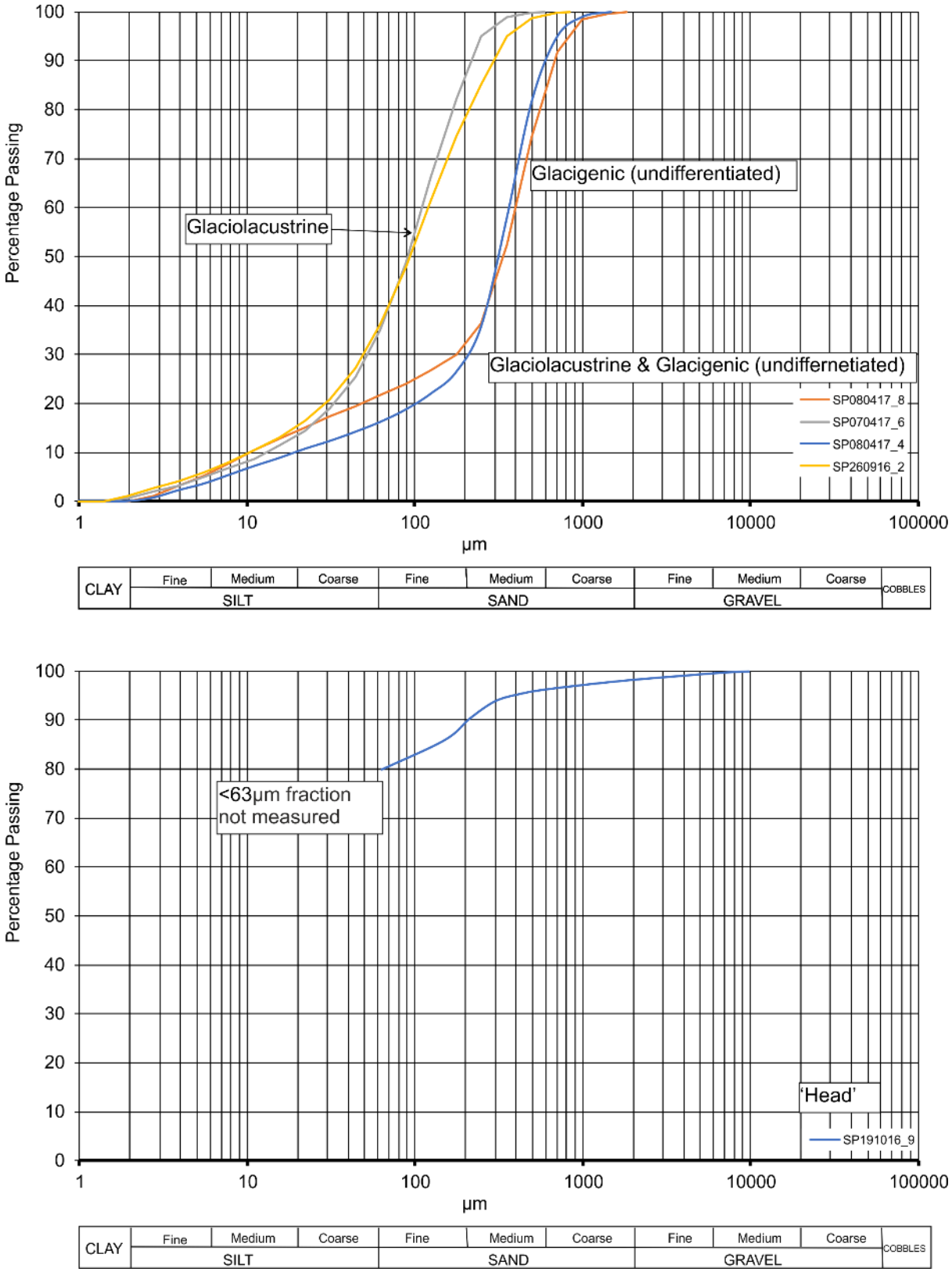

Figure 8-33 Particle-size grading curves Quaternary Domain 1.2.1, glaciolacustrine deposits, glacigenic (undifferentiated) and 'head'.

Specimens interpreted as till from Buckingham Sand Pit and Tingewick are well- to poorly-graded comprising at least 60% particles finer than fine sand. In contrast, glaciolacustrine or undifferentiated glacigenic sediments are well-graded and are dominantly silty sands. Based on particle-size, the undifferentiated glacigenic sediments are likely to be glaciolacustrine in origin.

8.2.4.4 Atterberg limits and moisture content (till)

The results of Atterberg limit determinations, including moisture content, for till are shown in Table 8-7. The results are plotted on a conventional liquid limit-plasticity index chart in Figure 8-34. Supporting data for the calculation of liquid limit, plastic limit and moisture content is given in Appendix 13.2.

Sample	Geology	Liquid Limit (W_L)	Plastic Limit (W_P)	Plasticity Index (I_p)	Moisture content (%)	Liquidity Index (LI)[1]	Activity[2]
SP250916_3	TILL	32	15	17	4	-0.65	1.7 (A)
SP11102016_1	TILL	37	18	19	8	-0.53	2.1(A)
SP211016_1	TILL	45	17	28	21	0.14	1.9(A)
SP211016_8	TILL	49	18	31	16	-0.06	1.9(A)

Table 8-7 Atterberg limits, moisture content and activity for till, Quaternary Domain 1.2.1. [1]Calculated from (ω-W_P/I_p). [2]Calculated based on I_p/%clay fraction (0.002mm), where %clay was determined by LPSA. Activity classes I (inactive), N (normal) and A (active) after (Skempton, 1953).

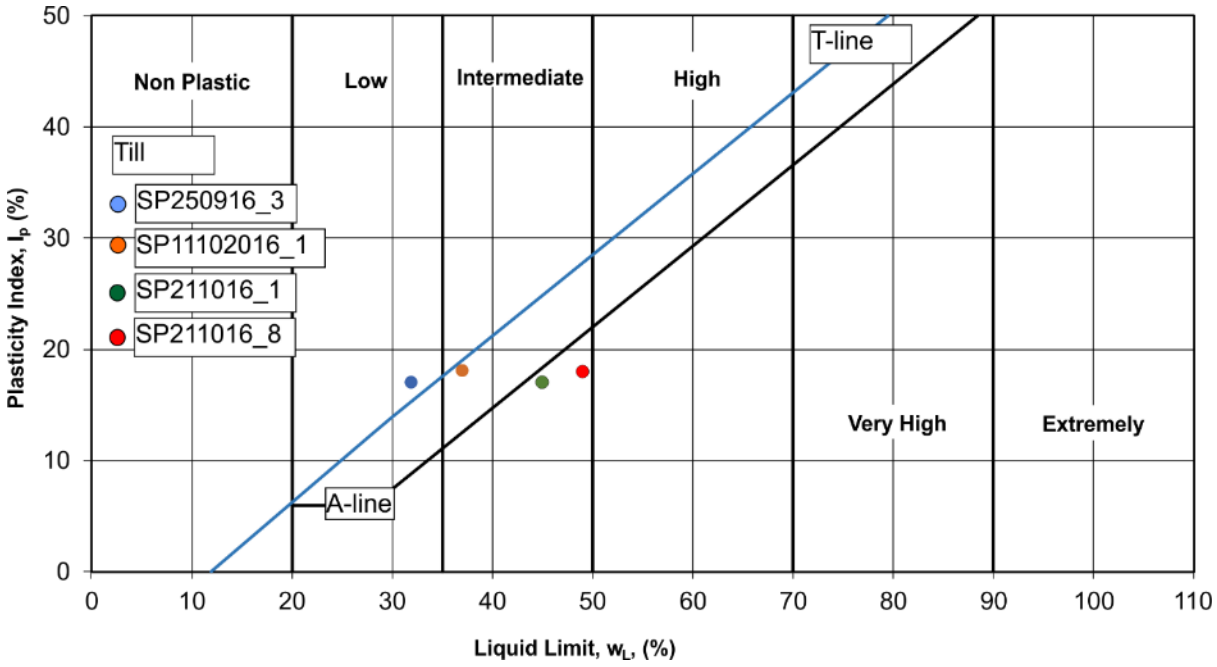

Figure 8-34 Plasticity plot for till, Quaternary Domain 1.2.1. T-line for tills from Boulton & Paul (1976).

Specimens SP250916_3 and SP11102016_ plot close to the T-line of Boulton & Paul (1976) but samples SP211016_1 and SP211016_8, for similar values of I_p, plot closer to the A-line.

The higher liquid limits of SP211016_1 and SP211016_8 may be explained by their greater proportion of clay-grade particles as determined by particle-size analysis.

8.2.5 Summary

Sediments, interpreted as till, at Buckingham Sand Pit and Tingewick, Domain 1.2.1, are low to intermediate plasticity, active, well-graded, calcareous, slightly clayey, slightly gravelly, slightly sandy silt. Sample SP11102016_1 is notably poorly-graded and less calcareous. Except for sample SP250916_3, tills comprise 80 to 90% particles finer than fine-sand. The tills are classified as active and normally active with activity values between 1.2 and 2. Sample SP11102016_1 is active with an activity value >2. The value of activity is interpreted to be the result of I_p derived from silt and clay and the low proportion of clay. The clay-mineral assemblage includes illite, kaolinite and chlorite with minor non-clay minerals including quartz. Chlorite appears to be absent in samples SP11102016_1 and SP250916_3 and both are associated with lower plasticity. The peak intensities for all clay minerals in sample SP11102016_3 are lower than other till samples. Intra-till sand beds are well-graded and comprise slightly clayey, very silty, fine-medium-grained sand. The glaciolacustrine deposits comprise well-graded, very-silty fine-medium-grained sand.

Exposures at Buckingham Sand Pit demonstrate that a stratigraphically-older, reddish-brown till is overlain by laminated glaciolacustrine sediments that have subsequently been deformed, and possibly overridden, by glacier ice, depositing a second and younger chalk-rich till. Evidence of periglaciation in the temporary exposure near Tingewick is seen where involutions in thinly-bedded limestone were seen.

8.3 Quaternary Domain 1.3

Quaternary Domain 1.3 comprises Middle to Late Jurassic mudrocks of the Oxford Clay underlain by mudrocks and sandstone of the Kellaways Formation. Glacigenic deposits were either not deposited or removed by erosion in this Domain. Periglacial solifluction ('head') deposits may be present but are not shown on published 1:50 000 scale geological maps. The Domain is interpreted to have been glaciated on at least one occasion and influenced by multiple phases of pre- and post-glacial periglacial activity.

Laboratory results are presented for loss-on-ignition (LOI), particle-size analysis (PSA), clay mineralogy and plasticity for specimens of Oxford Clay taken from the East West Rail ground investigation. One-dimensional (1D) consolidation (n=5) and multi-stage triaxial experiments with measurement of small-strain stiffness (n=4) were undertaken for variably weathered specimens of Oxford Clay at different depths below ground level and in different locations relative to maximum extent of glaciation. All specimens for 1D consolidation and triaxial testing were prepared from UT100 sample tubes.

8.3.1 Field locality: Calvert

The landfill and recycling centre at Calvert is currently operated by FCC Environment. The pit was formerly worked for brick-making and the exposures of the Peterborough and Stewartby members of the Oxford Clay were previously described by Callomon (1968).

The exposures at Calvert are coincident with the northwest-southeast trending ridge of Oxford Clay which is overlain by till that has previously been interpreted as the maximum extent of glacier ice during the Anglian stage glaciation. The exposures therefore provided the opportunity to investigate the possible presence of glacigenic sediments and possible evidence for subglacial bedrock deformation at the margin of the BIS. The location of the site and the sedimentary sections is shown in Figure 8-35.

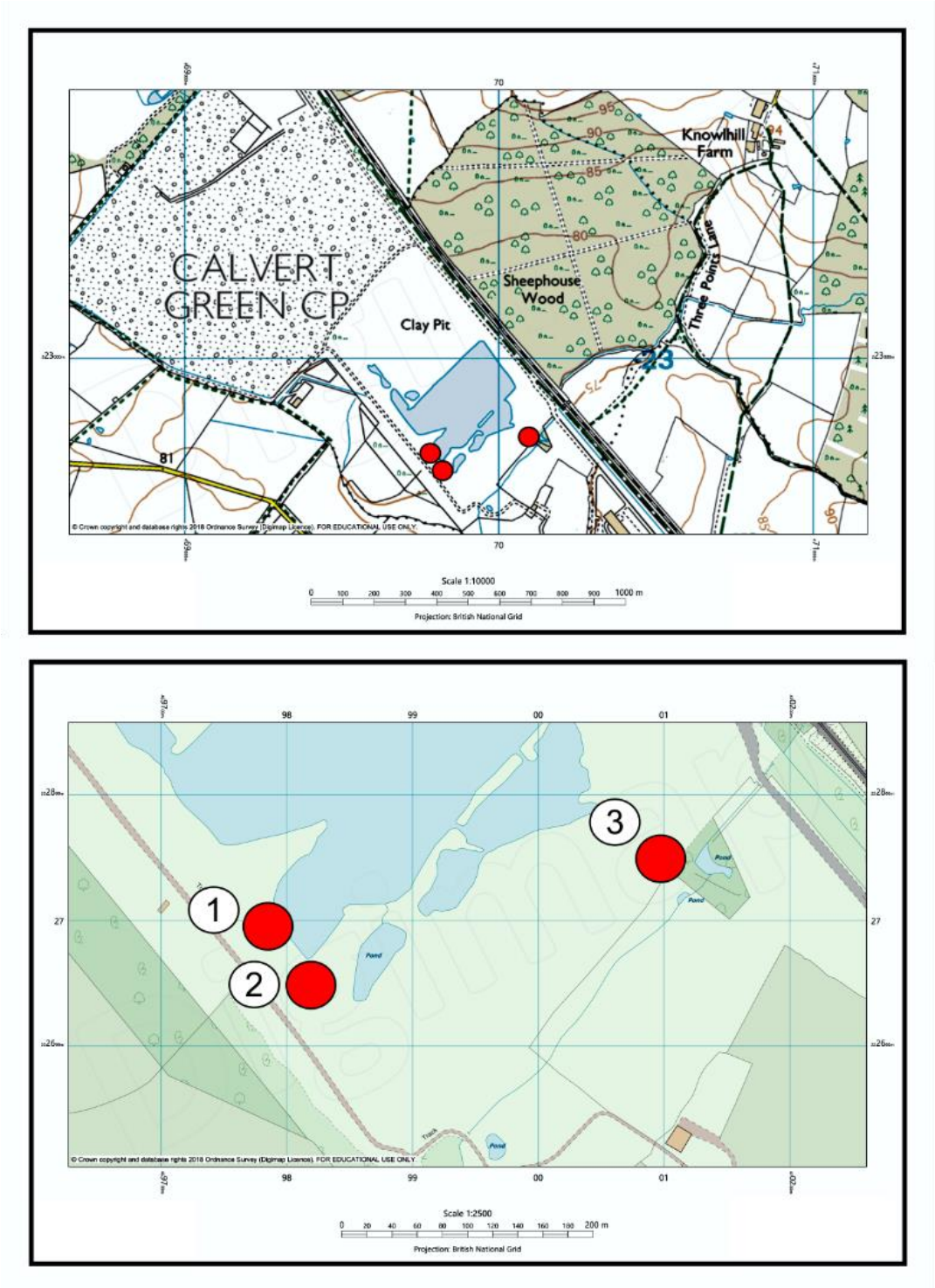

Figure 8-35 Site and section location, Calvert, Quaternary Domain 1.3.

8.3.1.1 Section descriptions

Three sections were examined and the logs are shown in Figures 8-36 and 8-37. Exposures of Oxford Clay and lithofacies 7 are illustrated Figures 8-38 and 8-39.

The Oxford Clay consists of grey and dark grey, fissile, jointed, weak mudstone to very stiff clay, becoming soft at the top of the exposure. Joints are subvertical and closely-spaced.

Hand-dug pits at ground level exposure soft, mottled brown and grey silt and clay with common rounded, fine to coarse quartzite gravel.

Brecciated and oxidised clay surrounds zones of pyritized and intact ammonite shells.

The micritic limestone of the *Acutistriatum* Band is brecciated with bedding parallel and subvertical joints. Except for one normal fault identified by steepening of bedding in mudstone, no other structural features were observed.

Weathered, soft clay of the Oxford Clay is overlain by sandy gravel and gravelly silt (lithofacies 7).

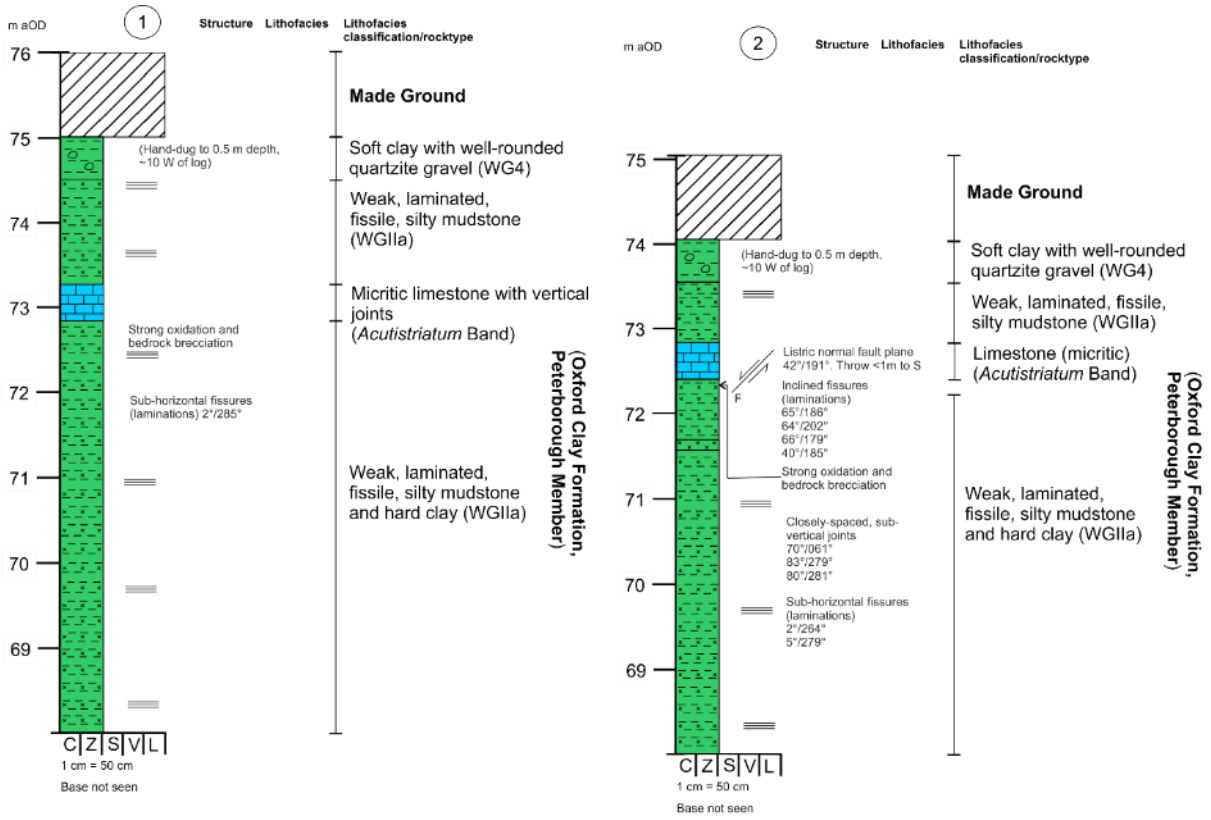

Figure 8-36 Sedimentary logs 1 and 2, Calvert. Refer to Appendix 13.1 for legend.

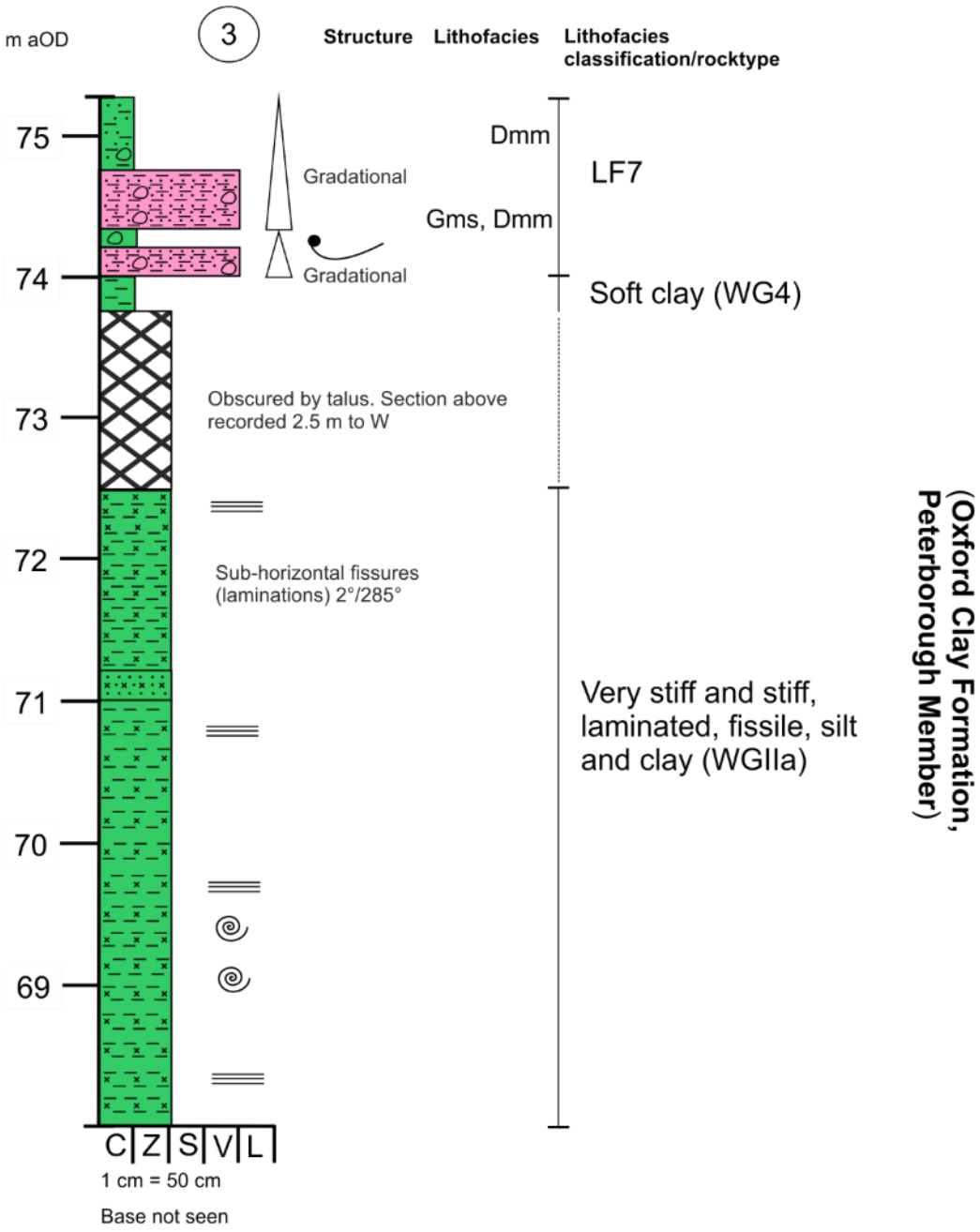

Figure 8-37 Sedimentary log 3, Calvert. Refer to Appendix 13.1 for legend.

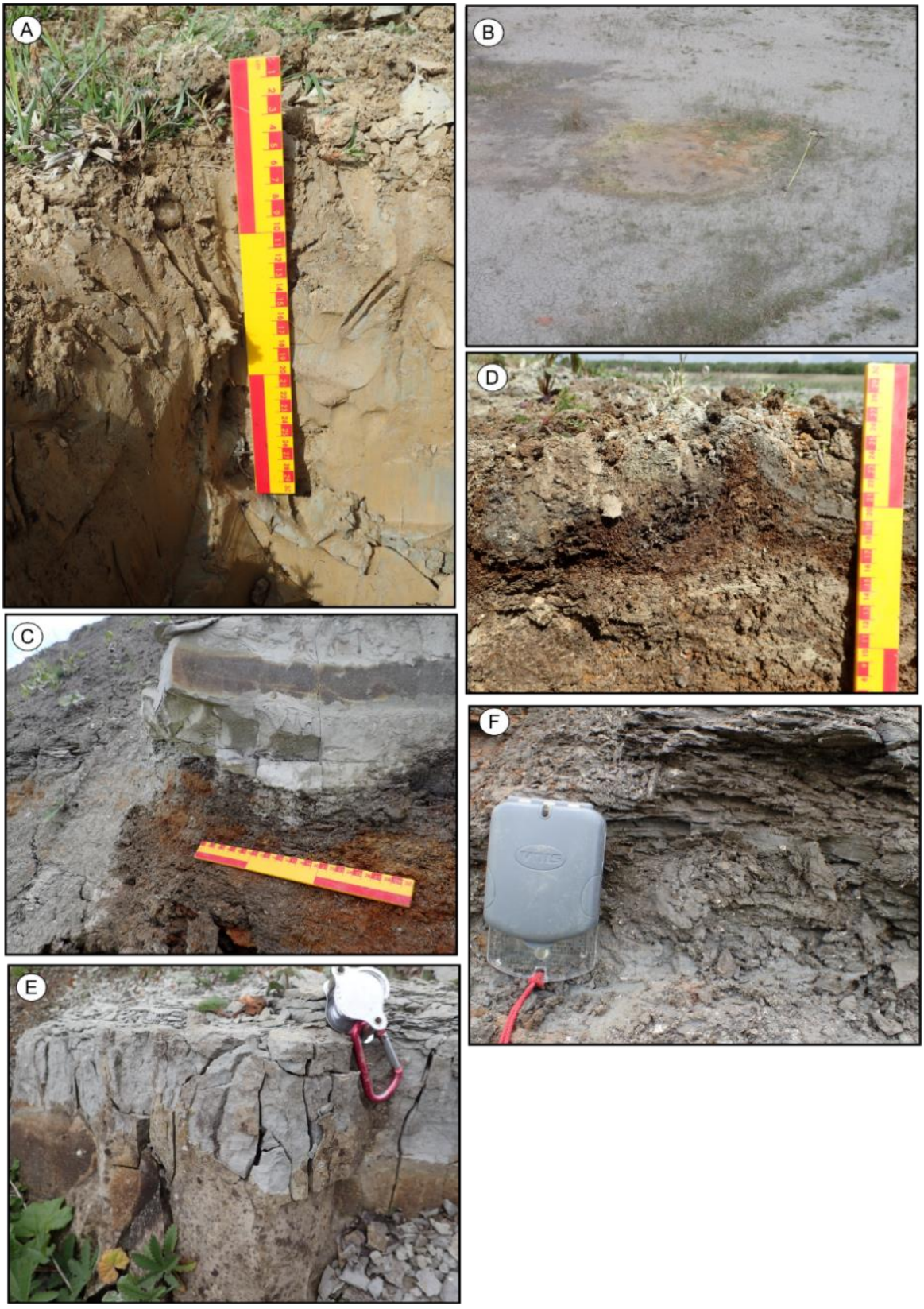

Figure 8-38 Oxford Clay, Calvert. A) Hand-dug pit revealing weathered, soft clay and quartzite gravel. B) Oxidised and sand-rimmed zone exposed in bench of quarry. C) Brecciation and oxidation beneath micritic limestone of the *Acutistriatum* Band. D) Apparent flame structure at the edge of sand-rim in B). E) Brecciated micritic limestone of the *Acutistriatum* Band.

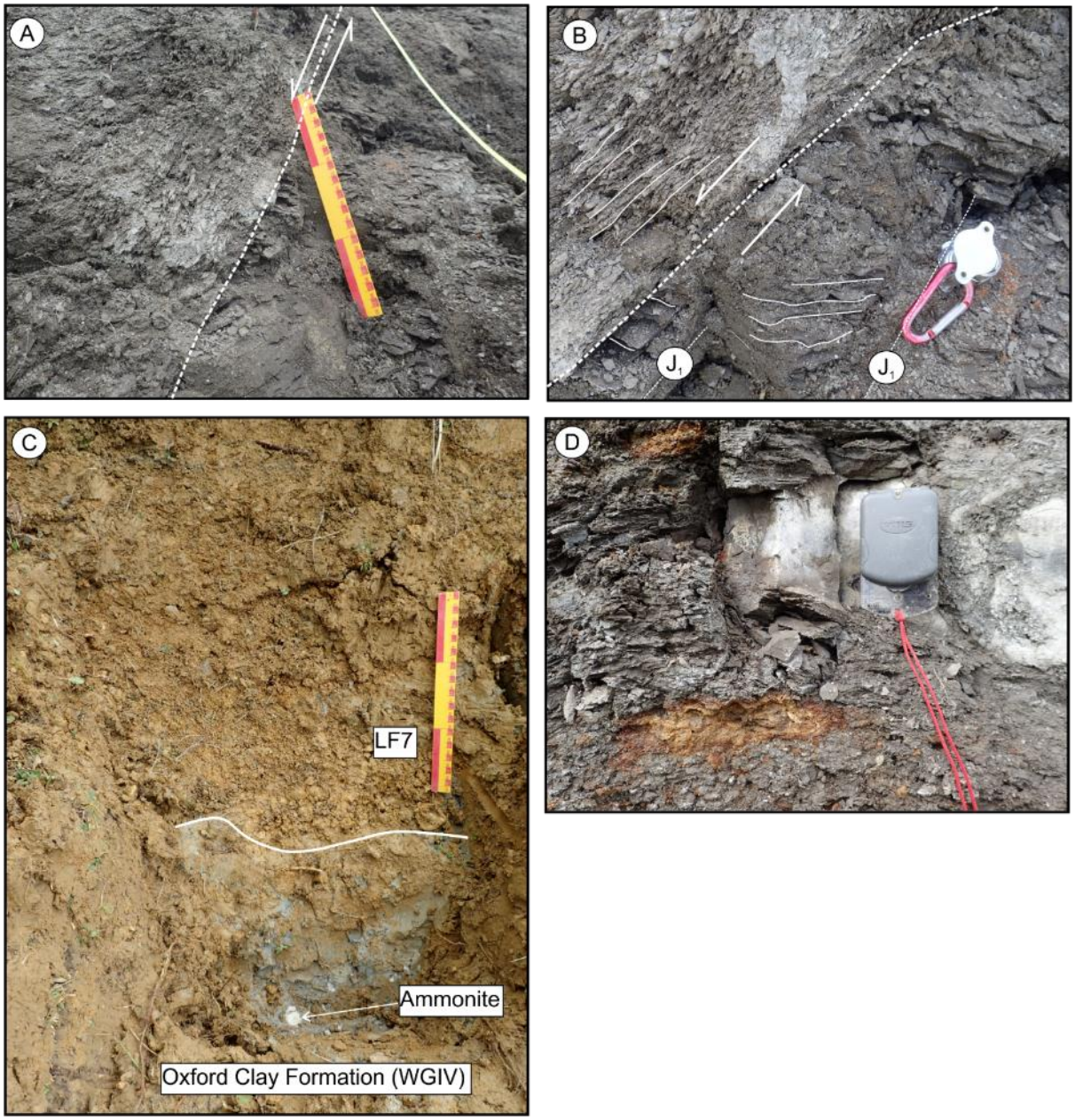

Figure 8-39 Oxford Clay, Calvert. A) and B) Normal fault down-throwing to the south. C) Sandy gravel and gravelly silt overlying grey weathered clay of the Oxford Clay. D) Oxidised and brecciated mudstone and *Acutistriatum* Band limestone.

8.3.1.2 Interpretation

No evidence is seen of subglacial deformation associated with the margin of the BIS. Either deformation did not occur, or it occurred above the depth of exposure and has subsequently been removed erosion. Ground ice formation may account for brecciation in the micritic limestone of the *Acutistriatum* Band but no clear evidence of lithorelics in mudstone were seen. Weathered, mottled brown and grey clay with rare, rounded quartzite clasts exposed in hand-dug pits is interpreted as a periglacial, solifluction deposit.

The origin of the dip-slip faults is unknown. They may be tectonic in origin or may represent faulting resulting from the melting of former permafrost in the style observed in the London Clay Formation by Spink (1991).

LF7 is interpreted as a fining-upwards alluvial deposit.

8.3.2 Laboratory results

8.3.2.1 Loss-on-ignition (Oxford Clay)

Results for loss-on-ignition are shown in Table 8-8. Oxford Clay samples (n=9) are variably calcareous and organic with upto 27% calcareous matter in the Stewartby Member. Much of the variability in the percentage of calcareous material is interpreted to be derived from fossil remains within each specimen.

Sample	Geology	% water	%organic	%$CaCO_3$	% silicate residue
CR022794	OXC_STW	N/A	14.1	11.2	74.7
CR023761	OXC_PET	N/A	8.3	8.8	82.9
CR023766	OXC_PET	N/A	6.1	7.4	86.5
CR005904	OXC-STW	N/A	3.9	27.3	68.8
CR005942	OXC_PET	N/A	9.3	8.9	81.9
CR005869	OXC_PET	N/A	14.5	16.9	68.6
CR005864	OXC_PET	N/A	5.5	12.5	82.1
CR005859	OXC_PET	N/A	7	16.6	76.3
CR005853	OXC_STW	N/A	5	20.2	74.8

Table 8-8 Loss-on-ignition (LOI), Domain 1.3. N/A denotes gravimetric water content measured as part of Atterberg, 1D consolidation or triaxial analysis.

8.3.2.2 Clay mineral XRD (Oxford Clay)

Diffractograms from the analysis of orientated, aggregate specimens are presented in Figure 8-40. The identification of clay minerals followed the procedure described in Section 8.1.2.2.

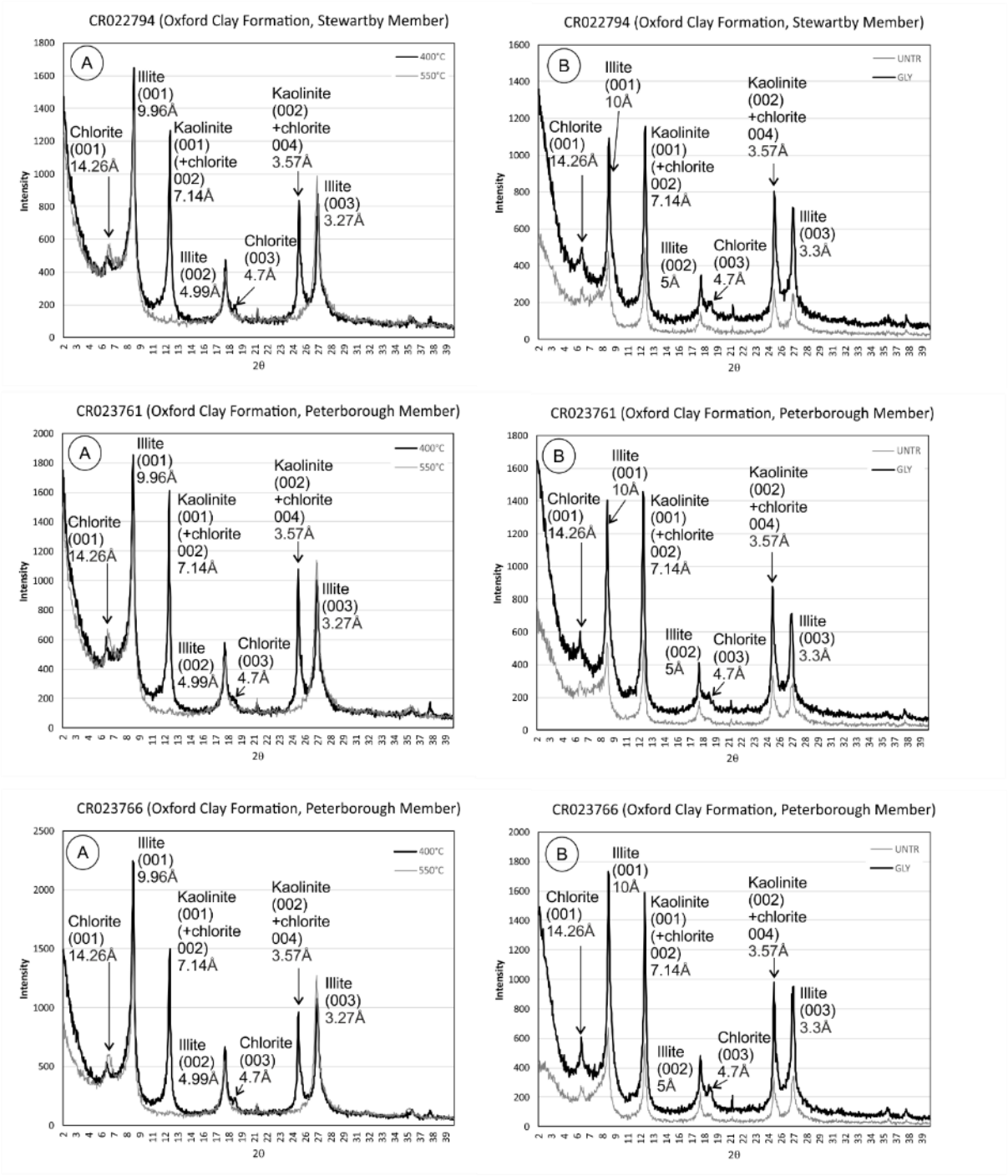

Figure 8-40 Clay mineral XRD for the Oxford Clay, Quaternary Domain 1.3. A) Heat treated at 400ºC and 550ºC. B) Air dried, untreated (untr) and glycolated (gly).

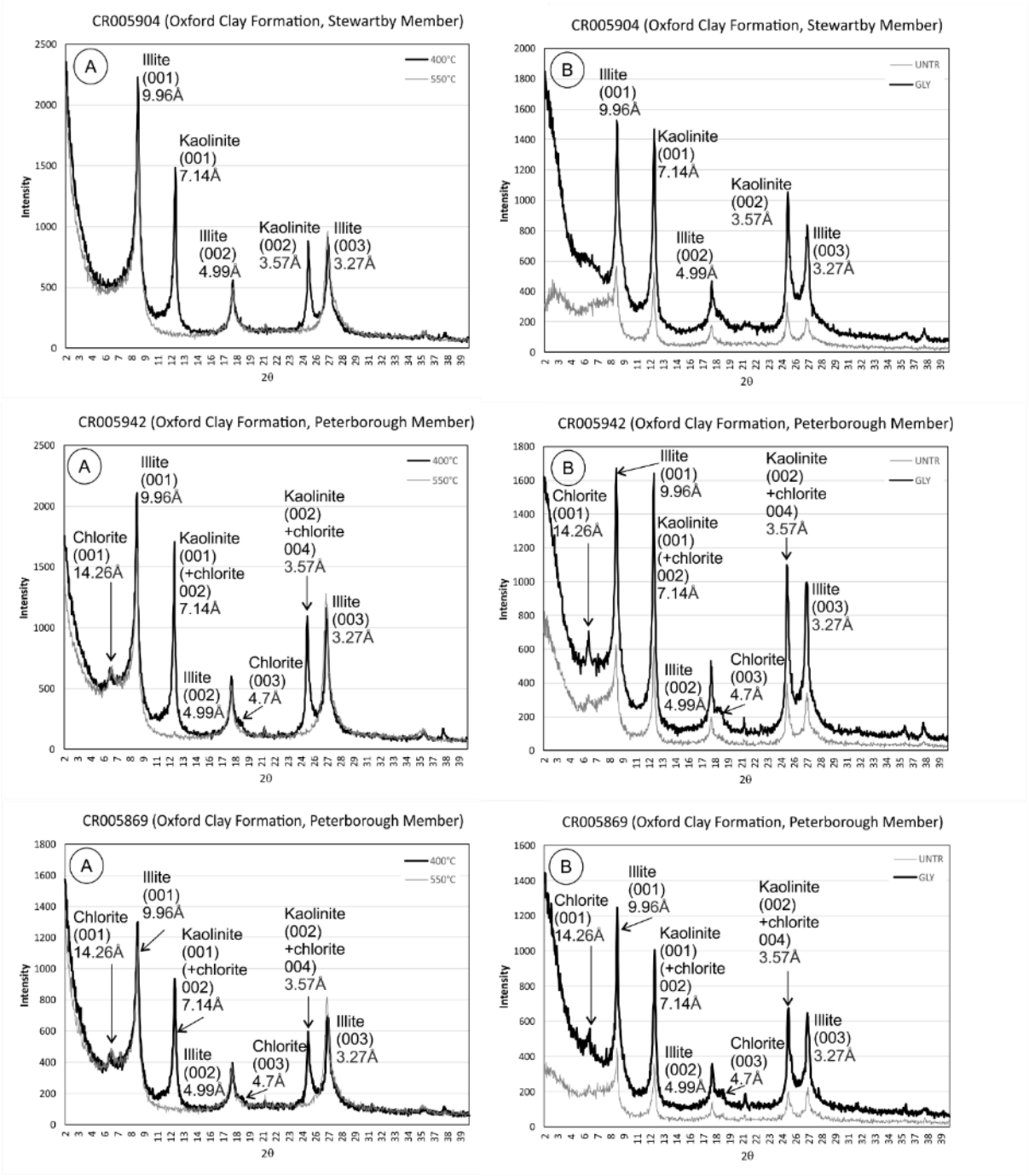

Figure 8- 40 continued. Clay mineral XRD for the Oxford Clay, Quaternary Domain 1.3. A) Heat treated at 400ºC and 550ºC. B) Air dried, untreated (untr) and glycolated (gly).

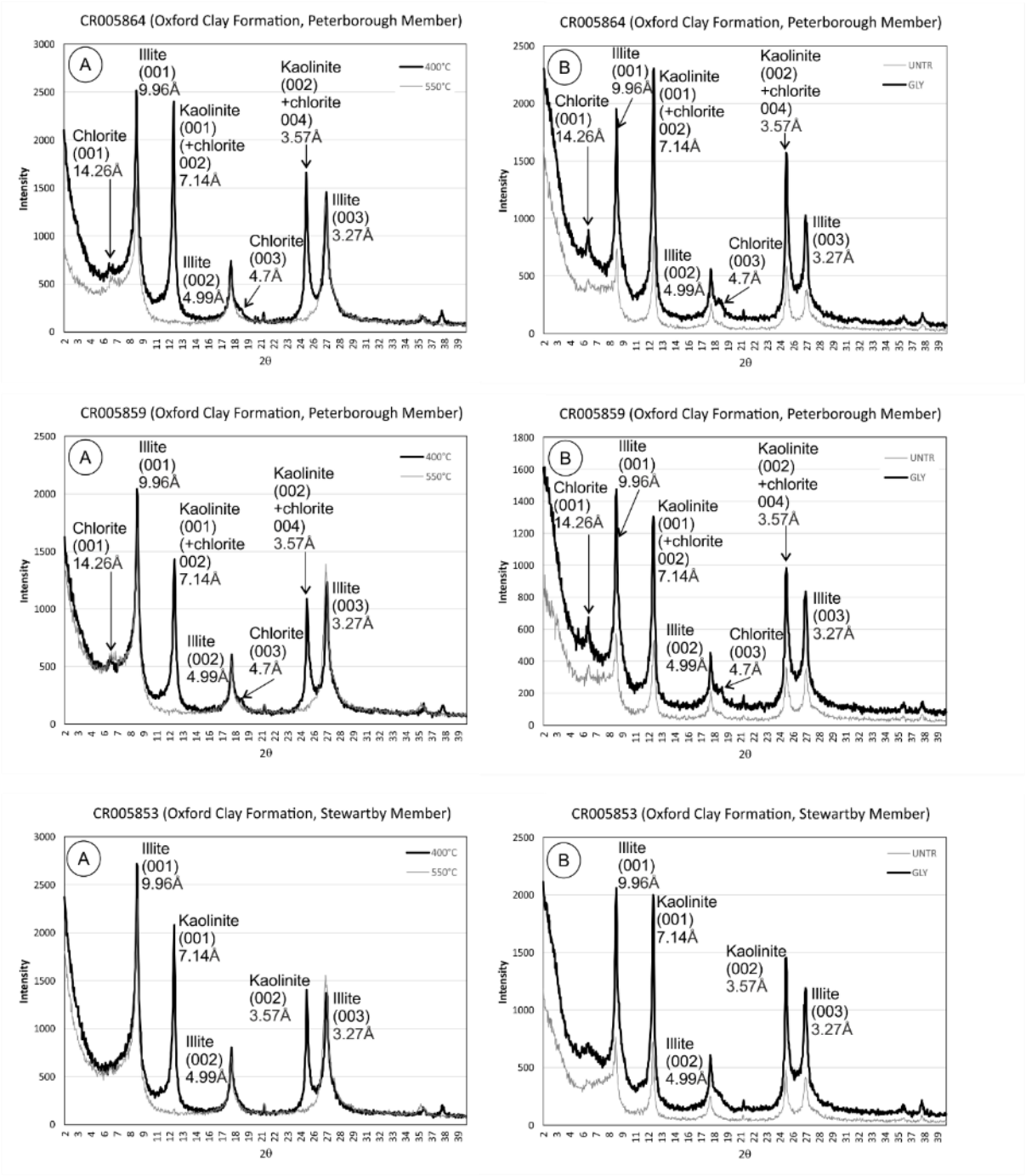

Figure 8- 40 continued. Clay mineral XRD for the Oxford Clay, Quaternary Domain 1.3. A) Heat treated at 400ºC and 550ºC. B) Air dried, untreated (untr) and glycolated (gly).

Strong, narrow peaks are seen in the diffractograms associated with clay minerals characterised by illite (mica) and kaolinite. Kaolinite (with minor or trace amounts of chlorite?) are seen in the Peterborough Member of the Oxford Clay but, except for sample CR022794, chlorite appears to be absent in the Stewartby Member of the Oxford Clay. Illite forms a mixed layer assemblage with collapsible clay minerals of unknown composition. Kaolinite is characterised by peak intensity reduction or loss-on-heating to 550ºC. Non-clay minerals are poorly defined but probably include quartz (4.35 Å), gypsum and carbonate.

There appears to be no qualitative difference in the clay mineral assemblages from each of the specimens.

8.3.2.3 Particle-size analysis (PSA), (Oxford Clay)

The results of particle-size analysis are plotted as percentage passing (finer) – log particle-size plots (Figure 8-41). The grading characteristics and classification of each specimen is summarised in Table 8-9. Coefficient of uniformity and coefficient of curvature were calculated using the method described in Section 8.1.4.

Sample	Geology[1]	Method[1]	Lithological Description[2]	Sample grading[3]	C_u	C_z
CR022794	OXC_STW	LPSA	Slightly sandy, slightly clayey SILT	Poorly-graded	7.5	0.833
CR023761	OXC_PET	LPSA	Slightly sandy, slightly clayey, SILT	Uniformly-graded	1.286	1.016
CR023766	OXC_PET	LPSA	Slightly sandy, slightly clayey, SILT	Uniformly-graded	1.286	1.016
CR005904	OXC-STW	LPSA	Slightly sandy, slightly clayey, SILT	Well-graded	9.0	1.0
CR005942	OXC_PET	LPSA	Slightly clayey SILT	Well-graded	7.0	1.286
CR005869	OXC_PET	LPSA	Slightly clayey, slightly sandy, SILT	Well-graded	11.0	1.01
CR005864	OXC_PET	LPSA	Slightly sandy, slightly clayey, SILT	Well-graded	7.0	1.286
CR005859	OXC_PET	LPSA	Slightly sandy, slightly clayey SILT	Well-graded	8.0	1.125
CR005853	OXC_STW	LPSA	Slightly sandy, clayey, SILT	Poorly-graded	6.0	0.167

Table 8-9 PSA summary for geological units in Domain 1.3. [1]LPSA – Laser Particle-Size Analysis, WS – wet sieving**.** [2]Based on proportions by mass from PSA following conventions in British Standards BS5930:1999 with Amendment 2 (British Standards Institution, 1999). [3]Geotechnical terminology.

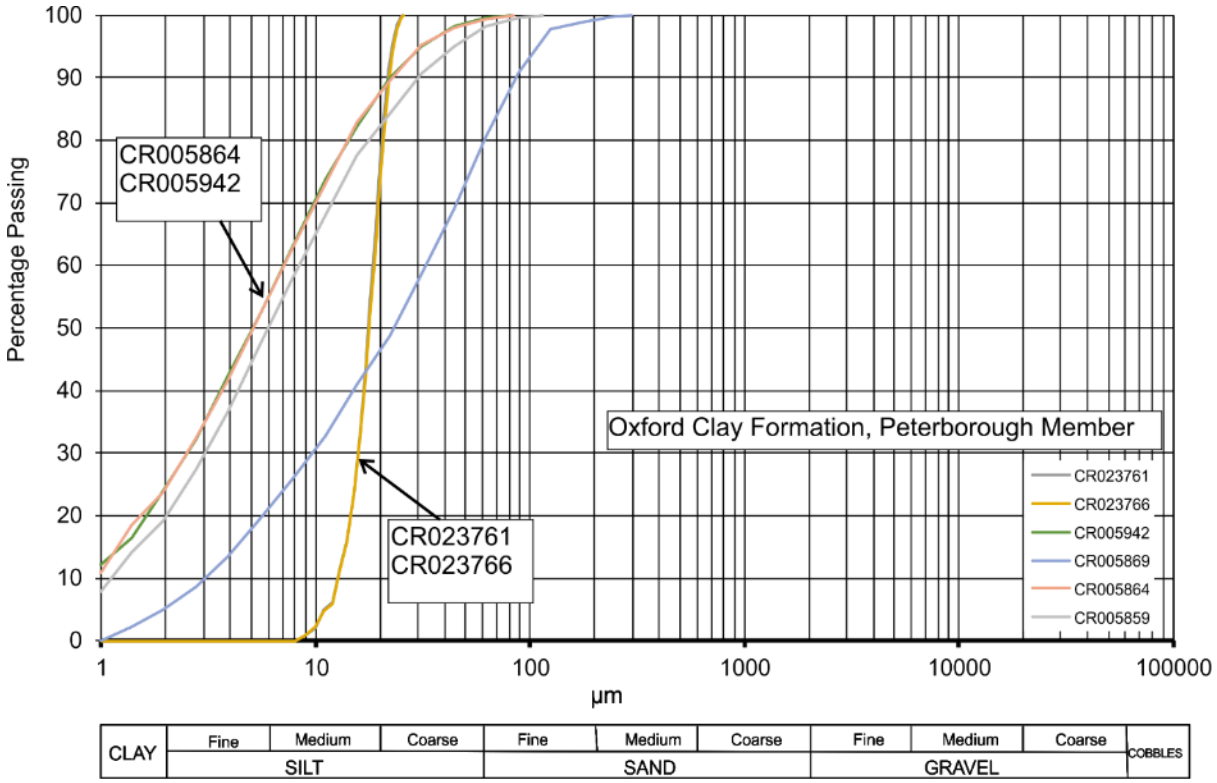

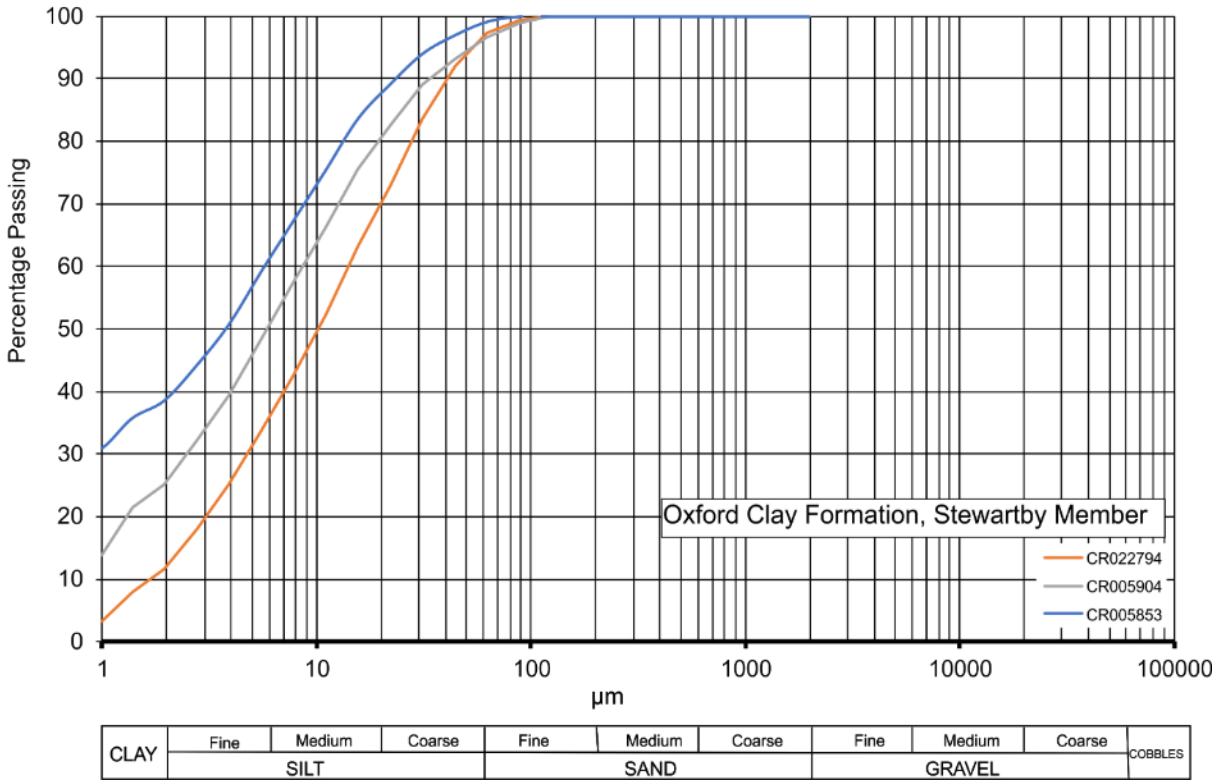

Figure 8-41 Particle-size grading curves Quaternary Domain 1.3, Oxford Clay.

Specimens of Oxford Clay are well- to uniformly-graded. All samples are slightly sandy silt and clay. The proportion of clay-grade particles varies between 38% and 5%, the lowest value associated with the Peterborough Member. Specimens CR023761 and CR023766 are uniformly-graded silts. The presence of a high proportion of silt relative to clay compared to published values in the literature (Section 4.1) may indicate that the measured silt-grade material is in fact agglomerations of clay particles and the dissagregation using sodium-hexmetaphosphate was not adequate to fully separate the particles.

8.3.2.4 Atterberg limits and moisture content (Oxford Clay)

The results of Atterberg limit determinations, including moisture content, are shown in Table 8-10. The results are plotted on a conventional liquid limit-plasticity index chart in Figure 8-42. Supporting data for the calculation of liquid limit, plastic limit and moisture content is given in Appendix 13.2.

Sample	Geology	Liquid Limit (W_L)	Plastic Limit (W_P)	Plasticity Index (I_p)	Moisture content (%)	Liquidity Index (LI)[1]	Activity[2]
CR022794	OXC_STW	63	35	28	32	-0.11	2.3(A)
CR023761	OXC_PET	60	25	35	22	-0.09	2.2(A)
CR005904	OXC-STW	55	23	32	20	-0.09	1.3(A)
CR005942	OXC_PET	72	29	43	30	0.02	1.8(A)
CR005864	OXC_PET	65	23	42	21	-0.05	1.8(A)
CR005853	OXC_STW	58	22	36	14	-0.22	0.9(N)

Table 8-10 Atterberg limits, moisture content and activity, Quaternary Domain 1.3. [1]Calculated from (ω-W_P/I_p). [2]Calculated based on I_p/%clay fraction (0.002mm), where %clay was determined by LPSA. Activity classes I (inactive), N (normal) and A (active) after Skempton (1953).

Specimens have high to very high plasticity. Except for CR022794, all specimens plot above the A-line.

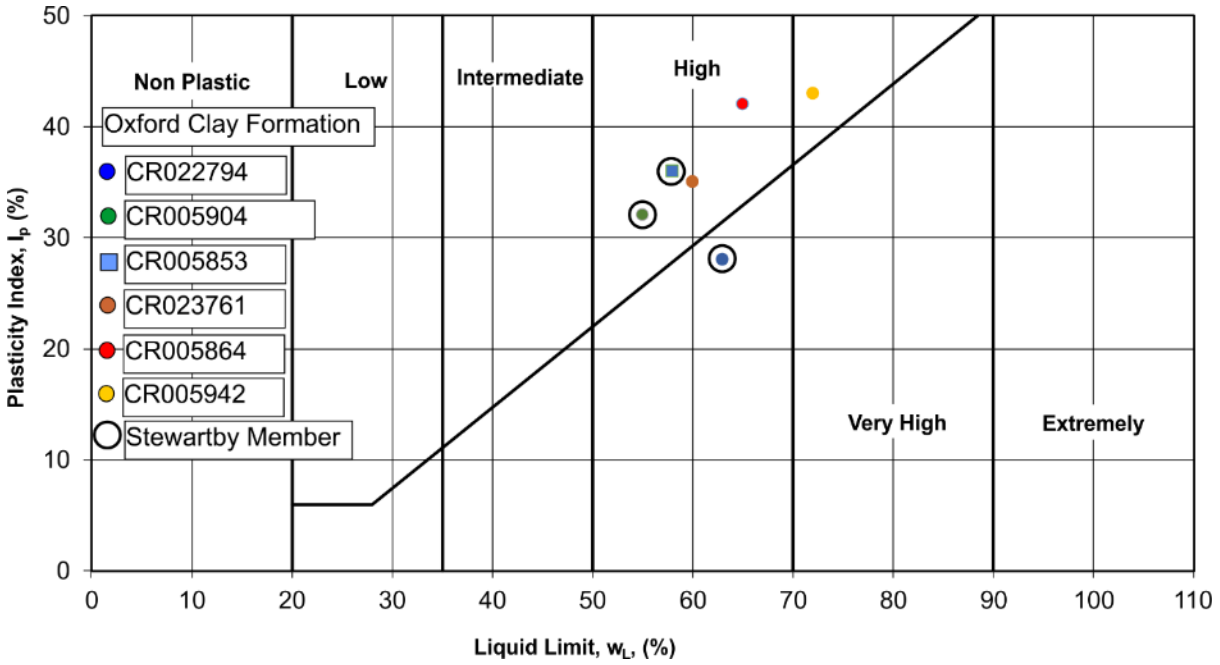

Figure 8-42 Plasticity plot for Oxford Clay, Peterborough and Stewartby (surrounded by open circles) members, Quaternary Domain 1.3.

8.3.2.5 Particle Density (Oxford Clay)

The calculation of particle density analyses using the small pyknometer method described in Section 7.5.2 are given in Appendix 13.4.

Particle density for specimens of the Oxford Clay range between 2.44 and 2.65 Mg/m^3.

8.3.2.6 1D consolidation (Oxford Clay)

The results from 1D consolidation experiments on specimens of Oxford Clay are reported as; specimen parameters describing initial and final conditions, graphically-derived values for initial (r_o), primary (r_p) and secondary (r_s) compression ratios and coefficient of secondary compression (C_{sec}), calculation of coefficient of consolidation (c_v), coefficient of volume compressibility (m_v) and finally as e-logσ_v plots representing change in void ratio *versus* log-σ_v. The graphical curve-fitting procedure to determine values for 50% settlement at time t_{50} and to estimate c_v, m_v, r_o, r_p, r_s and C_{sec} followed the procedures for clayey silts described by Head & Epps (2011) using plots of settlement *versus* log-time.

As the samples behaved as clayey silts, the initial, convex-upwards portion of the consolidation curve was missing (i.e. initial consolidation happened so rapidly that the initial specimen consolidation was passed before recording). In these cases, the theoretical value for 0% consolidation (U=0%) was determined by assuming that the value for U=0% lies between the initial reading for each compression stage and the first recorded reading. This difference was divided graphically into thirds to obtain a maximum and minimum estimate for t_{50}. Two

examples of the graphical methodology applied to each loading stage for all specimens, are shown in Appendix 13.6. The point at which consolidation is assumed to be complete (U=100%) was solved by curve-fitting at the intersection of tangents to the two parts of the curve whose gradient changes at ~75% consolidation. Estimates of preconsolidation pressure and intrinsic properties were made and described by comparison with all tested samples in Section 9.

Experimental results for specimens of Oxford Clay are shown in Figures 8-43 to 8-47. Initial and final conditions for each experiment are given in Appendix 13.4. All calculations are shown in Table 7-12.

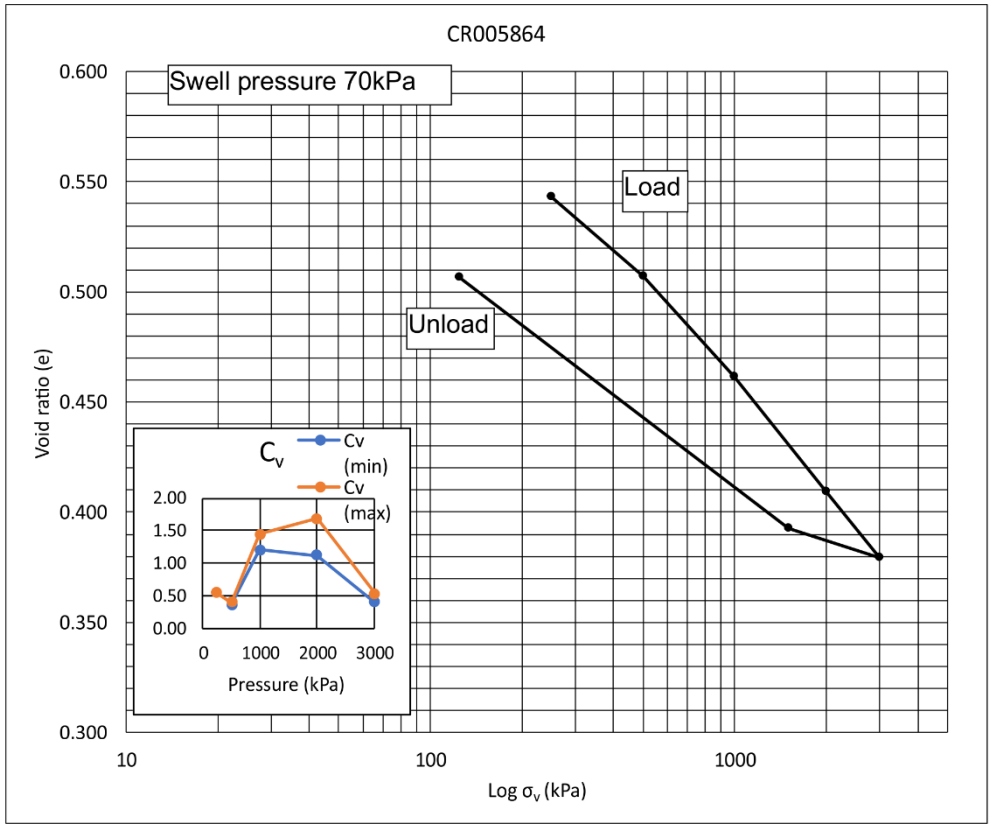

Figure 8-43 1D consolidation results for specimen CR005864, Oxford Clay, Quaternary Domain 1.3.

	Voids ratio				Volume compressibility (m_v)				Coeffecient of consolidation (C_v)						
Stage number	Pressure P, (kPa)	Settlement ΔH (mm)	Δe= ΔH/H_s (H_s=12.56)	e=e_o-Δe (e_o=0.58)	δe (e_1-e_2)	δp (kN/m^2)	1+e_1	m_v= (δe/δp)*((1000)/1+e)) m^2/MN	t_{50} (min) Minimum	t_{50} (max) Maximum	H=H_o-ΔH H_o=19.86 (mm)	$\hat{H}$=(H_1+H_2)/2 (mm)	$\hat{H}^2$ mm^2	Cv=(0.026*$\hat{H}^2$)/t_{50} (m^2/yr) Maximum	Cv=(0.026*$\hat{H}^2$)/t_{50} (m^2/yr) Minimum
2.1	125								NA	NA				NA	NA
2.2	250	0.486	0.0387	0.543	0.039	125	1.582	0.196	18.17	NA	19.37	19.62	385	0.55	NA
2.3	500	0.938	0.0747	0.507	0.036	250	1.543	0.093	23.75	26.25	18.92	19.15	367	0.40	0.36
2.4	1000	1.512	0.1204	0.461	0.046	500	1.507	0.061	6.25	7.50	18.35	18.64	347	1.44	1.20
2.5	2000	2.163	0.1723	0.409	0.052	1000	1.461	0.035	5.00	7.50	17.70	18.02	325	1.69	1.13
2.6	3000	2.541	0.2024	0.379	0.030	1000	1.409	0.021	15.00	20.00	17.32	17.51	307	0.53	0.40
2.7	1500	2.372	0.1889	0.393	-0.013	-1500									
2.8	125	0.944	0.0752	0.507	-0.114	-1375									

c_v and m_v not calculted for load stage 2.1 as sample was incorrectly seated during compression.

Stage number	Voids ratio					Volume compressibility (m_v)				Coeffecient of consolidation (C_v)						
	Pressure P, (kPa)	Settlement ΔH (mm)	$\Delta e = \Delta H/H_s$ (H_s=12.85)	$e = e_o - \Delta e$ (e_o=0.55)	δe (e_1-e_2)	δp (kN/m²)	$1+e_1$	m_v= (δe/δp)*((1000)/1+e)) m²/MN	t_{50} (min) Minimum	t_{50} (max) Maximum	H=H_o-ΔH H_o=19.97 (mm)	$\bar{H}$=(H_1+H_2)/2 (mm)	$\bar{H}^2$ mm²	Cv=(0.026*($\bar{H}$)²)/t_{50} (m²/yr) Maximum	Cv=(0.026*($\bar{H}$)²)/t_{50} (m²/yr) Minimum
2.1	125	0.093	0.0071	0.518	0.007	125	1.525		0.037	8.75	NA	19.88	19.92	397	1.18	NA
2.2	250	0.373	0.0285	0.496	0.021	125	1.518		0.113	12.50	15.00	19.60	19.74	390	0.81	0.68
2.3	500	0.742	0.0567	0.468	0.028	250	1.496		0.075	17.50	52.08	19.23	19.41	377	0.56	0.19
2.4	1000	1.152	0.0880	0.437	0.031	500	1.468		0.043	15.00	17.50	18.82	19.02	362	0.63	0.54
2.5	2000	1.657	0.1265	0.398	0.039	1000	1.437		0.027	12.50	15.00	18.31	18.57	345	0.72	0.60
2.6	3000	2.004	0.1530	0.372	0.026	1000	1.398		0.019	13.75	16.25	17.97	18.14	329	0.62	0.53
2.7	1500	1.824	0.1393	0.386	-0.014	-1500										
2.8	125	0.768	0.0586	0.466	-0.081	-1375										

Figure 8-44 1D consolidation results for specimen CR005904, Oxford Clay, Quaternary Domain 1.3.

Stage number	Voids ratio				Volume compressibility (m_v)				Coeffecient of consolidation (C_v)					
	Pressure P, (kPa)	Settlement ΔH (mm)	Δe= ΔH/H_s (H_s=10.38)	e=e_o-Δe (e_o=0.83)	δe (e_1-e_2)	δp (kN/m^2)	1+e_1	m_v= (δe/δp)*((1000)/1+e)) m^2/MN	t_{50} (min) Minimum	t_{50} (max) Maximum	H=H_t-ΔH H_b=19.04 (mm)	$\hat{H}$=(H_t+H_b)/2 (mm)	$\hat{H}^2$ mm^2	Cv=(0.026*$\hat{H}^2$)/t_{50} (m^2/yr) Maximum	Cv=(0.026*$\hat{H}^2$)/t_{50} (m^2/yr) Minimum
2.1	62.5	0.030	0.0027	0.716	0.003	62.50	1.718	0.025	1.00	2.00	19.01	19.03	362	9.41	4.71
2.2	125	0.231	0.0208	0.697	0.018	62.50	1.716	0.169	1.25	2.25	18.81	18.91	358	7.44	4.13
2.3	250	0.611	0.0551	0.663	0.034	125	1.697	0.162	3.25	4.25	18.43	18.62	347	2.77	2.12
2.4	500	1.106	0.0998	0.618	0.045	250	1.663	0.107	4.75	10.00	17.93	18.18	331	1.81	0.86
2.5	1000	1.660	0.1498	0.568	0.050	500	1.618	0.062	8.33	9.17	17.38	17.66	312	0.97	0.88
2.6	2000	2.204	0.1989	0.519	0.049	1000	1.568	0.031	7.50	10.00	16.84	17.11	293	1.01	0.76
2.7	3000	2.512	0.2267	0.492	0.028	1000	1.519	0.018	10.83	14.17	16.53	16.68	278	0.67	0.51
2.8	1500	2.350	0.2121	0.506	-0.015	-1500									
2.9	125	0.873	0.0788	0.639	-0.133	-1375									

Figure 8-45 1D consolidation results for specimen CR005942, Oxford Clay, Quaternary Domain 1.3.

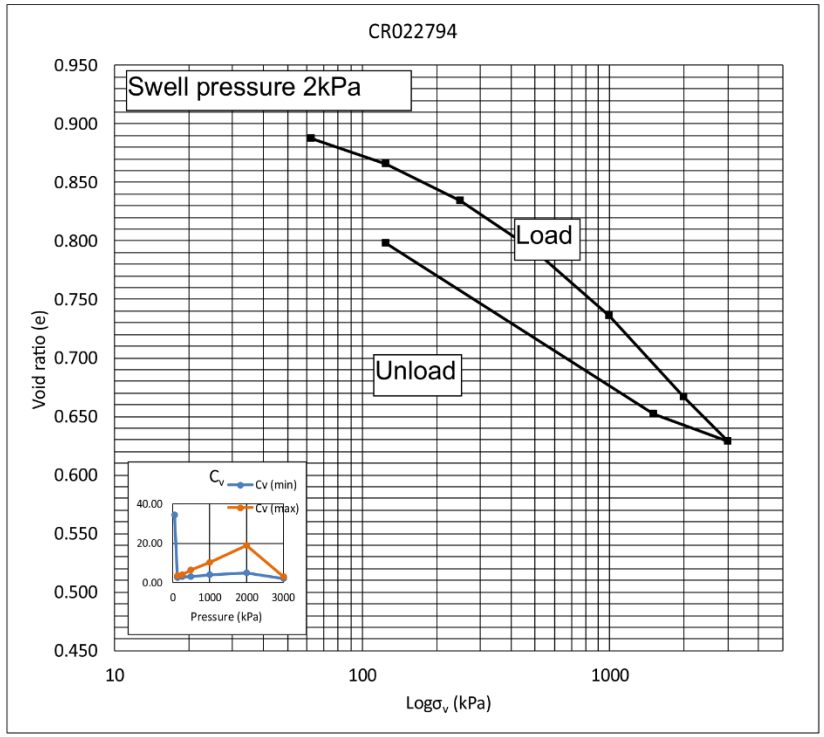

Figure 8-46 1D consolidation results for specimen CR022794, Oxford Clay, Quaternary Domain 1.3.

	Voids ratio				Volume compressibility (m_v)				Coeffecient of consolidation (C_v)						
Stage number	Pressure P, (kPa)	Settlement ΔH (mm)	Δe= ΔH/H_s (H_s=10.41)	e=e_o-Δe (e_o=0.94)	δe (e_1-e_2)	δp (kN/m^2)	1+e_1	m_v= (δe/δp)*((1000)/1+e)) m^2/MN	t_{50} (min) Minimum	t_{50} (max) Maximum	H=H_o-ΔH H_o=20.17 (mm)	$\hat{H}$=(H_1+H_2)/2 (mm)	$\hat{H}^2$ mm^2	Cv=(0.026*$\hat{H}^2$)/t_{50} (m^2/yr) Maximum	Cv=(0.026*$\hat{H}^2$)/t_{50} (m^2/yr) Minimum
2.1	62.5	0.520	0.0499	0.887	0.050	62.50	1.937	0.412	NA	0.30	19.65	19.91	396	NA	34.36
2.2	125	0.745	0.0716	0.866	0.022	62.50	1.887	0.183	2.72	3.75	19.43	19.54	382	3.65	2.65
2.3	250	1.070	0.1028	0.835	0.031	125	1.866	0.134	2.50	3.12	19.10	19.26	371	3.86	3.10
2.4	500	1.521	0.1461	0.791	0.043	250	1.835	0.094	1.45	3.12	18.65	18.87	356	6.39	2.97
2.5	1000	2.101	0.2018	0.736	0.056	500	1.791	0.062	0.83	2.08	18.07	18.36	337	10.52	4.21
2.6	2000	2.819	0.2708	0.667	0.069	1000	1.736	0.040	0.43	1.67	17.35	17.71	314	18.82	4.89
2.7	3000	3.212	0.3085	0.629	0.038	1000	1.667	0.023	2.50	3.75	16.96	17.15	294	3.06	2.04
2.8	1500	2.971	0.2854	0.652	-0.023	-1500									
2.9	125	1.455	0.1398	0.798	-0.146	-1375									

Stage number	Voids ratio					Volume compressibility (m_v)				Coeffecient of consolidation (C_v)						
	Pressure P, (kN/m²)	Settlement ΔH (mm)	Δe= ΔH/H_s (H_s=10.76)	e=e_o-Δe (e_o=0.78)	δe (e_1-e_2)	δp (kN/m²)	1+e_1	m_v= (δe/δp)*((1000)/(1+e)) m²/MN	t_{50} (min) Minimum	t_{50} (min) Maximum	H=H_o-ΔH H_o=19.11 (mm)	$\bar{H}$=(H_1+H_2)/2 (mm)	$\bar{H}^2$ mm²	Cv=(0.026*$\bar{H}^2$)/t_{50} (m²/yr) Maximum	Cv=(0.026*$\bar{H}^2$)/t_{50} (m²/yr) Minimum
2.1	125	0.230	0.0214	0.754	0.021	125.00	1.775	0.096	3.50	5.00	18.88	19.00	361	2.68	1.88
2.2	250	0.634	0.0589	0.716	0.038	125	1.754	0.171	6.25	7.50	18.48	18.68	349	1.45	1.21
2.3	500	1.169	0.1086	0.667	0.050	250	1.716	0.116	6.25	8.75	17.94	18.21	332	1.38	0.99
2.4	1000	1.808	0.1680	0.607	0.059	500	1.667	0.071	7.50	8.75	17.30	17.62	311	1.08	0.92
2.5	2000	2.474	0.2298	0.545	0.062	1000	1.607	0.038	4.88	6.25	16.64	16.97	288	1.54	1.20
2.6	3000	2.841	0.2639	0.511	0.034	1000	1.545	0.022	8.75	10.00	16.27	16.45	271	0.80	0.70
2.7	1500	2.631	0.2444	0.531	-0.020	-1500									
2.8	125	1.369	0.1272	0.648	-0.117	-1375									

Figure 8-47 1D consolidation results for specimen CR023761, Oxford Clay, Quaternary Domain 1.3.

In all cases, the coefficient of volume compressibility (m_v) decreases with increasing applied stress. The maximum value at 62.5 kPa was 0.412 m^2/MN for specimen CR022794. At an applied stress of 500 kPa, values for m_v varied between 0.075 and 0.93 m^2/MN. At an applied stress of 3000 kPa, values ranged between 0.022 and 0.018 m^2/MN. Except for specimen CR022794, the specimens are low to medium compressibility (after Head & Epps, 2011).

The coefficient of compressibility, c_v, is variable. In general, c_v decreases with increasing applied stress. Referring to c_v calculated from the maximum estimated value of consolidation at t_{50}, values for the 500 kPa stress increment vary between 0.4 and 6.39 m^2/yr. Corresponding maximum values of c_v for the stress increment at 3000 kPa vary between 0.53 and 3.06 m^2/yr. These values are within the range typical for high to medium plasticity clays (after Head & Epps, 2011). However, the decrease in c_v with increasing applied stress is not linear. The greatest magnitude decrease in c_v occurs at stress <500 kPa. However, specimens CR005864, CR023761 and CR022794, show an increase in c_v with increasing applied stress above 500 kPa before a decrease at stresses >2000 kPa.

The compression ratios for initial, primary and secondary compression are shown in Tables 8-11 and 8-12 and calculated using the following formulae:

$$r_o = (d_0 - d_c)/(d_f - d_c)$$

Equation 8-5

$$r_p = (d_{100} - d_0)/(d_f - d_c)$$

Equation 8-6

$$r_s = (d_f - d_{100})/(d_f - d_c)$$

Equation 8-7

where d_c is initial gauge reading and equivalent to the corrected gauge reading on the automated oedometer, d_0 is 0% consolidation, d_{100} is 100% consolidation and d_f is the final gauge reading. The values for 0 and 100% consolidation are estimated using the graphical log-time method illustrated in Appendix 13.3.

The compression ratios vary little between specimens with applied stress. Primary consolidation accounts for most of the consolidation (81 – 89%) except for specimen CR005942 where r_o at 62.4 kPa is 57%. The secondary compression ratio is higher at the 3000 kPa stress increment, ranging between 11% and 16%.

	CR023761			CR022794			CR005942		
Stress increment	r_o	r_p	r_s	r_o	r_p	r_s	r_o	r_p	r_s
62.5 (kPa)	NA	NA	NA	0.22	0.75	0.04	0.03	0.57	0.40
125 (kPa)	0.05	0.84	0.11	0.08	0.79	0.13	0.08	0.75	0.17
250 (kPa)	0.05	0.85	0.09	0.09	0.79	0.12	0.08	0.82	0.11
500 (kPa)	0.05	0.87	0.08	0.11	0.79	0.10	0.07	0.82	0.11
1000 (kPa)	0.05	0.87	0.08	0.12	0.77	0.10	0.07	0.86	0.07
2000 (kPa)	0.04	0.86	0.09	0.14	0.78	0.08	0.06	0.86	0.08
3000 (kPa)	0.02	0.82	0.16	0.09	0.81	0.11	0.03	0.82	0.14

Table 8-11 Estimated initial, primary and secondary compression ratios for the Oxford Clay specimens CR023761, CR022794 and CR005942, Domain 1.3.

	CR005904			CR005864		
Stress increment	r_o	r_p	r_s	r_o	r_p	r_s
62.5 (kPa)	NA	NA	NA	NA	NA	NA
125 (kPa)	0.03	0.88	0.09	NR	NR	NR
250 (kPa)	0.05	0.88	0.08	0.01	0.94	0.06
500 (kPa)	0.04	0.89	0.08	0.04	0.89	0.07
1000 (kPa)	0.03	0.88	0.09	0.05	0.84	0.11
2000 (kPa)	0.03	0.86	0.11	0.05	0.87	0.08
3000 (kPa)	0.03	0.81	0.16	0.03	0.84	0.13

Table 8-12 Estimated initial, primary and secondary compression ratios for Oxford Clay CR005904 and CR005864, Domain 1.3.

To investigate the potential effects of secondary consolidation, the coefficient of consolidation, C_{sec}, was calculated from Equation 7-35 and the results presented in Table 8-13.

	Stress increment						
Specimen	**62.5 (kPa)**	**125 (kPa)**	**250 (kPa)**	**500 (kPa)**	**1000 (kPa)**	**2000 (kPa)**	**3000 (kPa)**
CR023761	NA	0.0010	0.0016	0.0021	0.0021	0.0027	0.0025
CR022794	0.0008	0.0011	0.0008	0.0013	0.0019	0.0034	0.0015
CR005942	0.0004	0.0016	0.0016	0.0024	0.0025	0.0028	0.0024
CR005904	NA	0.0005	0.0014	0.0017	0.0018	0.0024	0.0027
CR005864	NA	NR	0.0018	0.0019	0.0021	0.0019	0.0025

Table 8-13 Coefficient of secondary consolidation for Oxford Clay, Domain 1.3. NA – stage not recorded as swell pressure exceeded stress increment. NR- not recorded, platen not seated correctly.

Generally, C_{sec} increases with applied stress reaching a maximum at 3000 kPa between 0.0015 and 0.0027. These values are consistent with values for overconsolidated clays (after Head & Epps, 2011).

The combined results for all samples of Oxford Clay, plotted as e-logσ_v, are shown in Figure 8-48.

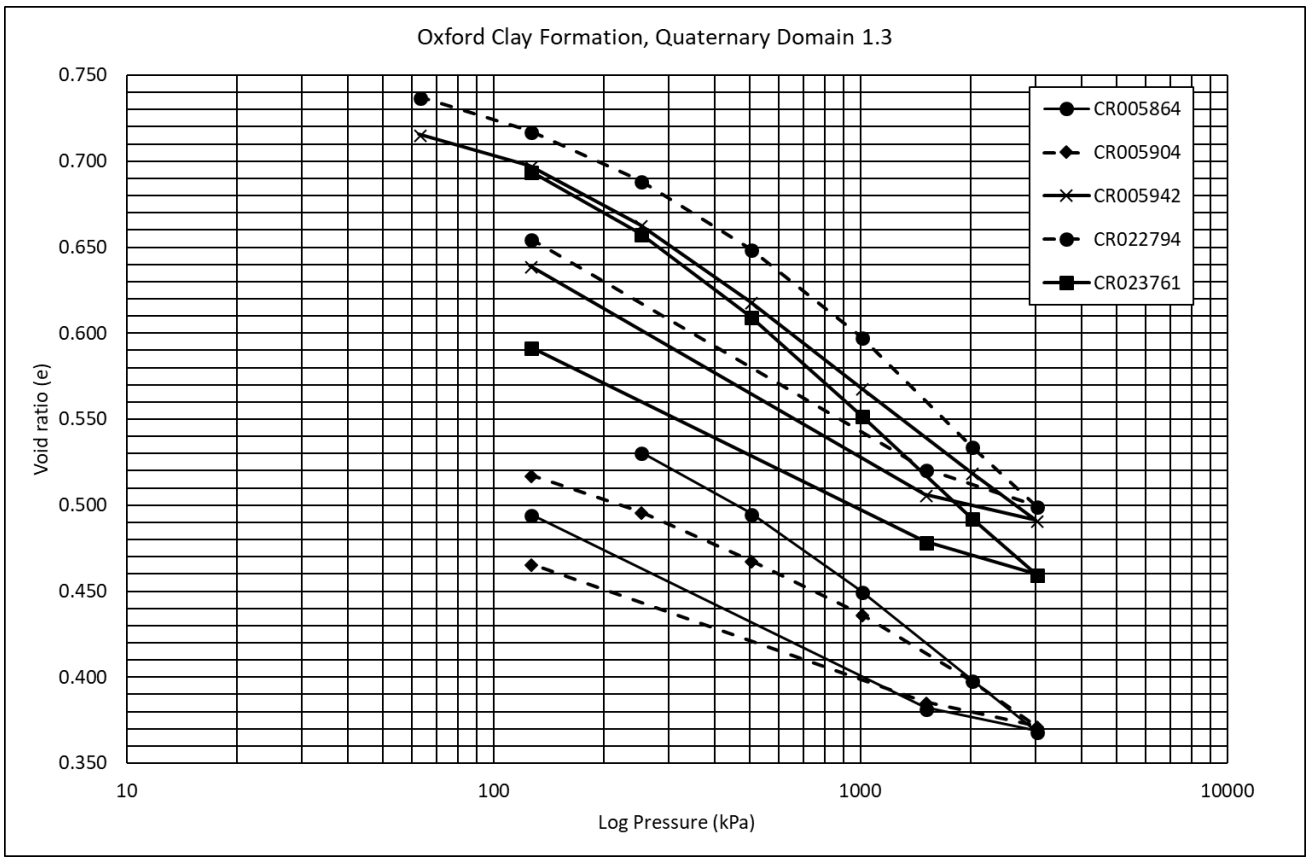

Figure 8-48 Combined e-logσ_v plot for all Oxford Clay specimens in Quaternary Domain 1.3.

Specimens within Quaternary Domain 1.3, form two groups, whose densities (expressed as void ratio) and compressibility characteristics are different. Specimens CR005904 and CR005864 (Group 1) are denser and slightly less compressible than specimens CR023761, CR022794 and CR005942 (Group 2).

To compare the load and unload characteristics of each specimen, cumulative displacement plots are shown in Figures 8-49 and 8-50.

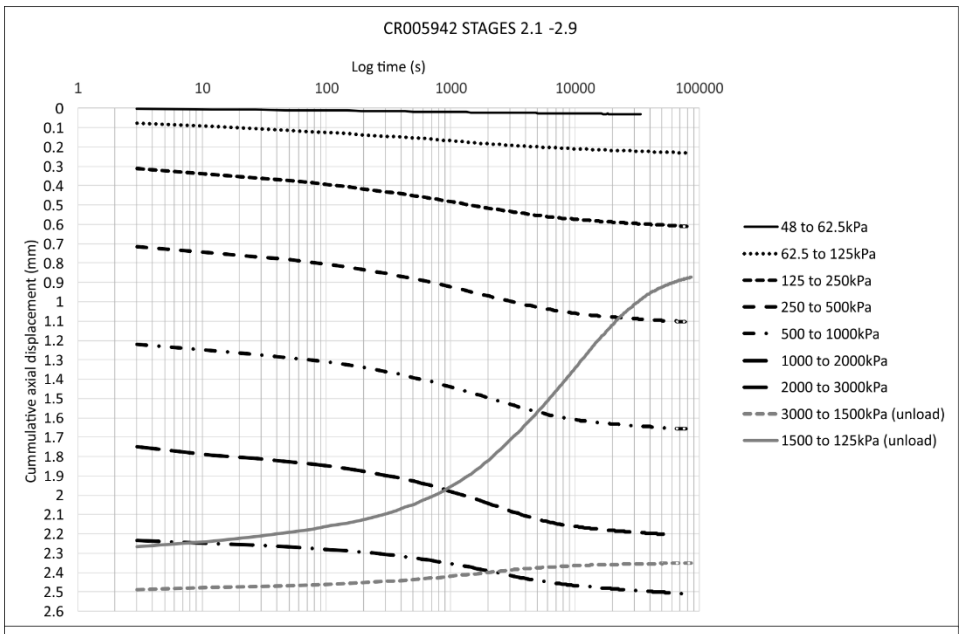
CR005942 STAGES 2.1 -2.9
Log time (s)
1
10
100
1000
10000
100000
Cummulative axial displacement (mm)
0
0.1
0.2
0.3
0.4
0.5
0.6
0.7
0.8
0.9
1
1.1
1.2
1.3
1.4
1.5
1.6
1.7
1.8
1.9
2
2.1
2.2
2.3
2.4
2.5
2.6
48 to 62.5kPa
62.5 to 125kPa
125 to 250kPa
250 to 500kPa
500 to 1000kPa
1000 to 2000kPa
2000 to 3000kPa
3000 to 1500kPa (unload)
1500 to 125kPa (unload)

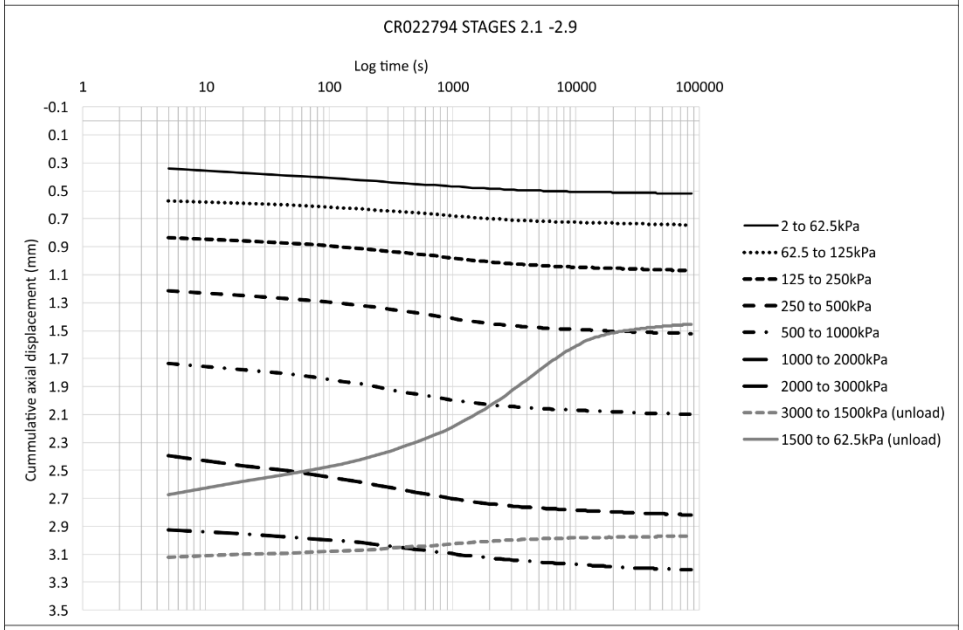
CR022794 STAGES 2.1 -2.9
Log time (s)
1
10
100
1000
10000
100000
Cummulative axial displacement (mm)
-0.1
0.1
0.3
0.5
0.7
0.9
1.1
1.3
1.5
1.7
1.9
2.1
2.3
2.5
2.7
2.9
3.1
3.3
3.5
2 to 62.5kPa
62.5 to 125kPa
125 to 250kPa
250 to 500kPa
500 to 1000kPa
1000 to 2000kPa
2000 to 3000kPa
3000 to 1500kPa (unload)
1500 to 62.5kPa (unload)

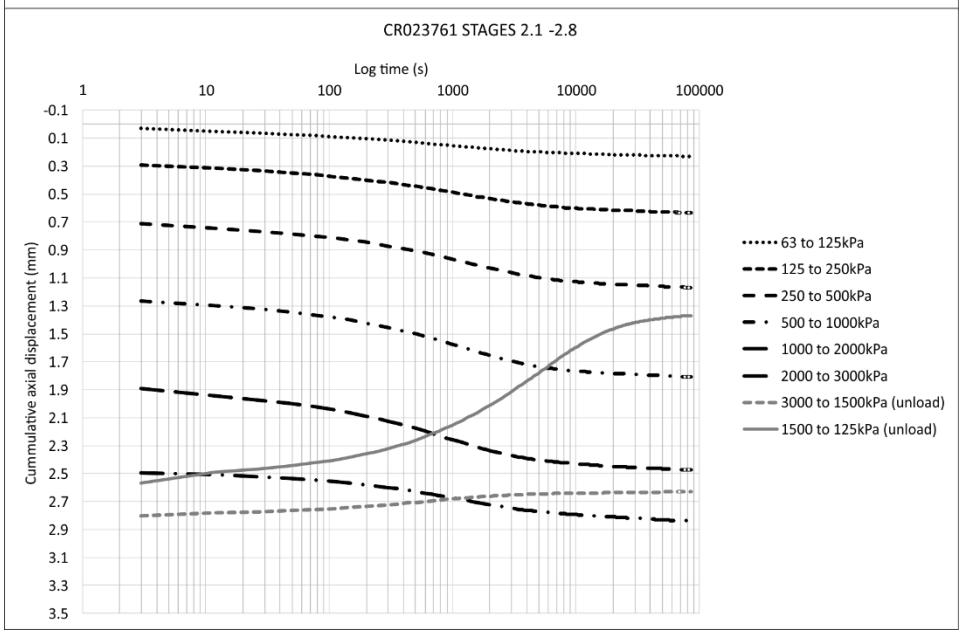
CR023761 STAGES 2.1 -2.8
Log time (s)
1
10
100
1000
10000
100000
Cummulative axial displacement (mm)
-0.1
0.1
0.3
0.5
0.7
0.9
1.1
1.3
1.5
1.7
1.9
2.1
2.3
2.5
2.7
2.9
3.1
3.3
3.5
63 to 125kPa
125 to 250kPa
250 to 500kPa
500 to 1000kPa
1000 to 2000kPa
2000 to 3000kPa
3000 to 1500kPa (unload)
1500 to 125kPa (unload)

Figure 8-49 Cumulative displacement, Oxford Clay, Quaternary Domain 1.3.

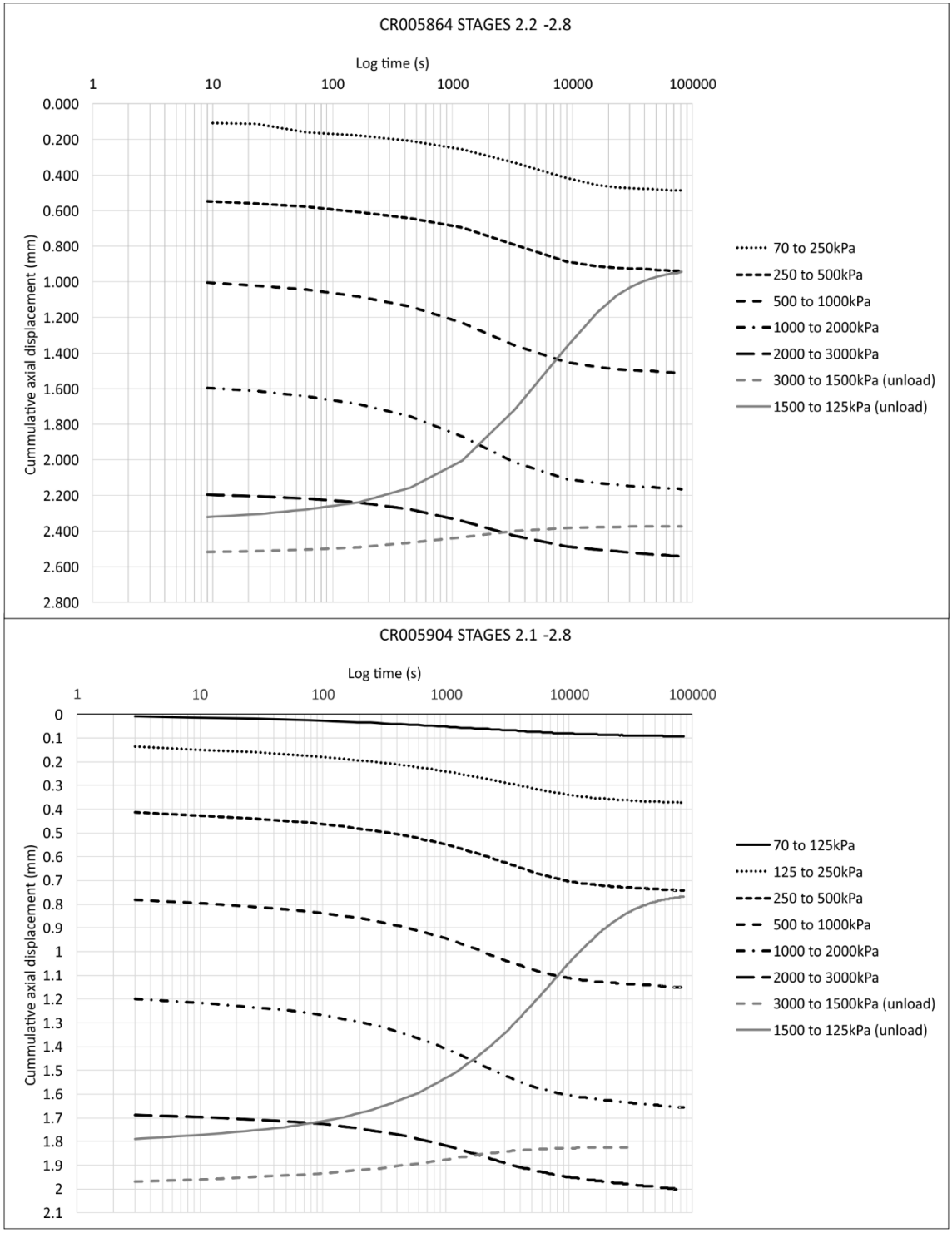

Figure 8-50 Cumulative displacement, Oxford Clay, Quaternary Domain 1.3.

8.3.2.7 Triaxial undrained shear strength (Oxford Clay)

Isotropically consolidated, undrained, multi-stage triaxial experiments with measurement of small-strain stiffness using Hall effect sensors were carried out using specimens from samples CR005864, CR005904, CR005942 and CR023761 from Quaternary Domain 1.3. The experiments were undertaken in the BGS SPTTS configuration.

The results of the triaxial experiments are presented and analysed according to their stress-strain behaviour, undrained shear strength, effective stress paths using the stress invariants p′-q, isotropic consolidation, secant stiffness and small-strain stiffness in terms of undrained Young's modulus, E'. The latter was estimated where results from strain analysis using Hall effect sensors provided the data to so. For the stress-path analysis of each specimen, the Cambridge parameters for mean effective stress, p′ and deviator stress, q were used, where:

$$p = (\sigma_1 + 2\sigma_3)/3$$

Equation 8-8

$$p' = p - u$$

Equation 8-9

$$q = \sigma_1 - \sigma_3$$

Equation 8-10

where p′ represents the mean effective stress at failure and accounts for changes in specimen volume and q represents deviator stress and accounts for changes in specimen shape. Values for p′ and q are derived from measured values of principal stresses, σ_1 and σ_3 and corresponding pore pressure, u, for failure of the specimen at maximum deviator stress, q_{max} interpreted from the experimental results using GDSLAB software.

Multi-stage procedures for 100 mm specimens were chosen in preference to sub-sampling three, 38 mm specimens, to use the maximum specimen size possible that was most representative of the geological layer under investigation. Three stages of shearing were undertaken so that failure conditions were only allowed to develop during the third and final stage. For each stage, the confining stress was twice that of the previous stage. Stages 1 and 2 could approach, but not exceed, a failure condition. To estimate at which point to stop shearing during stages 1 and 2, pore pressure, effective stress ratio and axial stress-strain were continuously monitored but choosing the point at which to stop was subjective.

Accepting that stages 1 and 2 in a multi-stage triaxial test do not take the specimen to shear failure, analysis using Mohr-circles to derive effective stress shear strength parameters (angle of shearing resistance (ø′) and cohesion (c′)), do not give a meaningful estimate of their values. As an alternative, a critical state framework (Schofield & Wroth, 1968) was used. The analytical framework requires all samples to have reached their post-peak, critical states. As this was not consistently the case for the specimens tested here, alternative shear strength parameters were defined to enable comparison between specimens. One of the points along a specimens' effective stress path defines a critical stress ratio at which a phase transformation takes place. At this stress ratio, pore-pressure change is almost zero and the specimen remains at a constant volume. The state beyond this point reflects either dilation or compression of the specimen as deviatoric stress increases. This stress ratio is defined here as:

$$\eta_{trans} = \frac{q}{p'}$$

Equation 8-11

where η_{trans} is the stress ratio at constant volume which was given the symbol M by Schofiled & Worth (1969) such that it is assumed here that:

$$\eta_{trans} = M$$

Equation 8-12

The state parameter η_{trans} can be used to estimate the effective friction angle $ø'_{trans}$. To compare the frictional strength parameters between stages in a multi-stage experiment for values < η_{trans}, a value of strain was chosen common to all specimens, prior to peak deviator stress being reached. The value chosen was 0.4% strain so that the parameter $\eta_{0.4\%}$ is defined as the ratio between q and p′ corresponding to an axial strain value of 0.4%. Therefore, η_{trans}=M at the transformation stress ratio , η_{max}>M at the maximum stress ratio and $\eta_{0.4\%}$<M.

To derive values for $ø'_{trans}$ and $ø'_{0.4\%}$ corresponding to η_{trans} and $\eta_{0.4\%}$, respectively, the derivation from Bolton (1979), following Schofiled & Wroth (1968) is used here. The derivation established the link between the angle of shearing resistance and the critical state frictional parameter, M.

The relationship is defined as the ratio between the deviator stress and the average principal effective stress at the critical state, expressed for conditions in a triaxial experiment:

$$M = \frac{(\sigma'_1 - \sigma'_3)_c}{(\sigma'_1 + \sigma'_3)_c/3}$$

Equation 8-13

where the subscript c denotes conditions at the critical state.

In relation to a Mohr-circle of effective stresses, the angle of shearing resistance at the critical state, $ø'_c$, is:

$$\sin ø'_c = \frac{\text{radius of circle}}{\text{origin of circle}} = \frac{(\sigma'_1 - \sigma'_3)/2}{(\sigma'_1 + \sigma'_3)/2}$$

Equation 8-14

Using equations 8-14 and 8-15, a value for $\sin ø'_c$ can be derived. In the following definition, the ratio σ'_1/σ'_3 is denoted by K'_c.

Equation 8-14 is re-written:

$$M = \frac{(K'_c - 1)3}{(K'_c + 2)}$$

Equation 8-15

Equation 8-15 is re-written:

$$\sin ø'_c = \frac{K'_c - 1}{K'_c + 1}$$

Equation 8-16

Inverting equations 8-14 and 8-15 gives:

$$K'_c = \frac{2M + 3}{3 - M} = \frac{1 + \sin ø'_c}{1 - \sin ø'_c}$$

Equation 8-17

giving:

$$\sin ø'_c = \frac{3M}{M + 6}$$

Equation 8-18

and in relation to the strength parameter η defined here:

$$\sin ø' = \frac{3\eta}{\eta + 6}$$

Equation 8-19

Equation 8-19 is used in the stress-path analysis here to derive values for $ø'_{trans}$ and $ø'_{0.4\%}$.

Undrained shear strength, c_u, corresponding to maximum deviator stress, is defined in Section 7.5.5 as:

$$c_u = \frac{1}{2}(\sigma'_1 - \sigma'_3)_f$$

This is accepted here but redefined in terms of Mobilised Strength Design (MSD) parameters following Vardanega & Bolton (2012). Vardanega & Bolton (2012) used an approach that related factors of safety (FOS) in geotechnical design to mobilised shear strength and its corresponding value of shear strain. They defined mobilised shear strength, $\tau_{mob,}$ as:

$$\tau_{mob} = 0.5q$$

Equation 8-20

Vardanega and Bolton (2012) also identified a reference strain $\gamma_{M=2}$. This reference strain represents the magnitude of shear strain corresponding to $q = 0.5_{qmax}$ and was referred to by Vardenega & Bolton (2012) as a mobilisation factor.

Following this principle, a new reference strain parameter, equivalent to a value of mobilised strain at $0.5q_{max}$, and therefore equivalent to a FOS of 2, is defined here as $\varepsilon_{F=2}$. Therefore,

$$\varepsilon_{F=2} = \frac{q_{max}}{2}$$

The initial and final conditions for specimens of the Oxford Clay CR005864, CR005904, CR005942 and CR023761 are given, along with the experimental design and stress conditions, in Appendix 13.5. Photographic images of the pre- and post-experiment specimen are shown in Figures 8-51 to 8-54.

The experimental conditions for each specimen are summarised in Table 8-14 and further details are given in Appendix 13.5.

Specimen name	**Stage**	**Cell pressure (kPa)**	**Back pressure (kPa)**	**Differential (effective) pressure, σ'_o (kPa)**
CR005864	Consolidation stage 1	980	880	100
CR005864	Shear stage 1	980	880	100
CR005864	Consolidation stage 2	1080	880	200
CR005864	Shear stage 2	1080	880	200
CR005864	Consolidation stage 3	1180	880	300

CR005864	Shear stage 3	1180	880	300
CR005904	Consolidation stage 1	440	370	70
CR005904	Shear stage 1	440	370	70
CR005904	Consolidation stage 2	510	370	140
CR005904	Shear stage 2	510	370	140
CR005904	Consolidation stage 3	570	370	200
CR005904	Shear stage 3	570	370	200
CR005942	Consolidation stage 1	950	600	350
CR005942	Shear stage 1	950	600	350
CR005942	Consolidation stage 2	1125	600	525
CR005942	Shear stage 2	1125	600	525
CR005942	Consolidation stage 3	1300	600	700
CR005942	Shear stage 3	1300	600	700
CR023761	Consolidation stage 1	790	670	120
CR023761	Shear stage 1	790	670	120
CR023761	Consolidation stage 2	910	670	240
CR023761	Shear stage 2	910	670	240
CR023761	Consolidation stage 3	1030	670	360
CR023761	Shear stage 3	1030	670	360

Table 8-14 Summary of triaxial experiment conditions, Oxford Clay, Quaternary Domain 1.3.

Photographs of pre- and post-experiment specimens are shown in Figures 8-51 to 8-54.

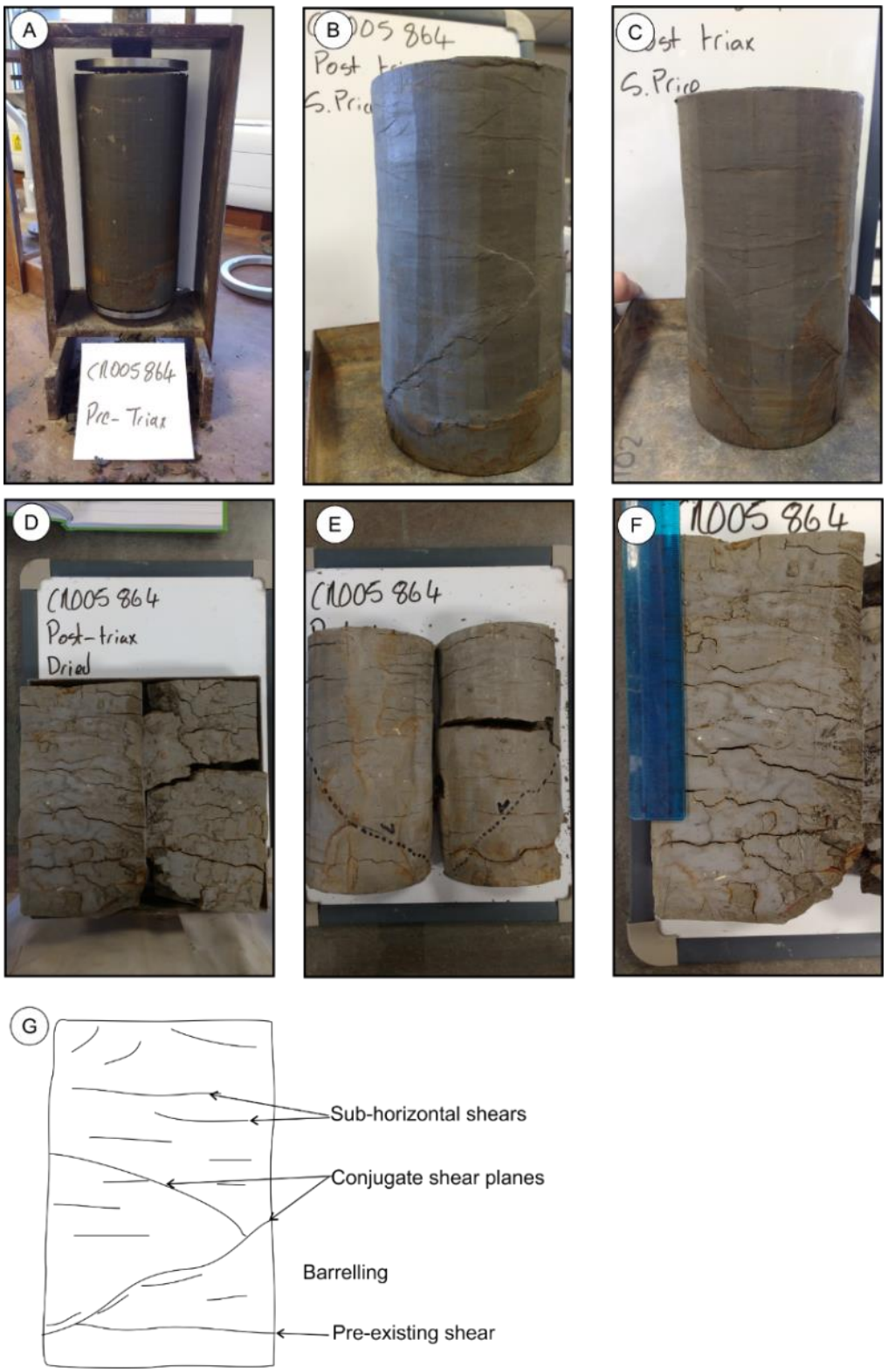

Figure 8-51 Pre- and post-triaxial specimen conditions, CR005864, Oxford Clay. A) Pre-experiment after preparation with soil lathe. B) and C) Post-experiment showing conjugate primary shear planes. D), E) and F) Oven-dried, post-triaxial specimen showing splitting along sub-horizontal planes; primary shear plane annotated. G) Hand sketch interpretation.

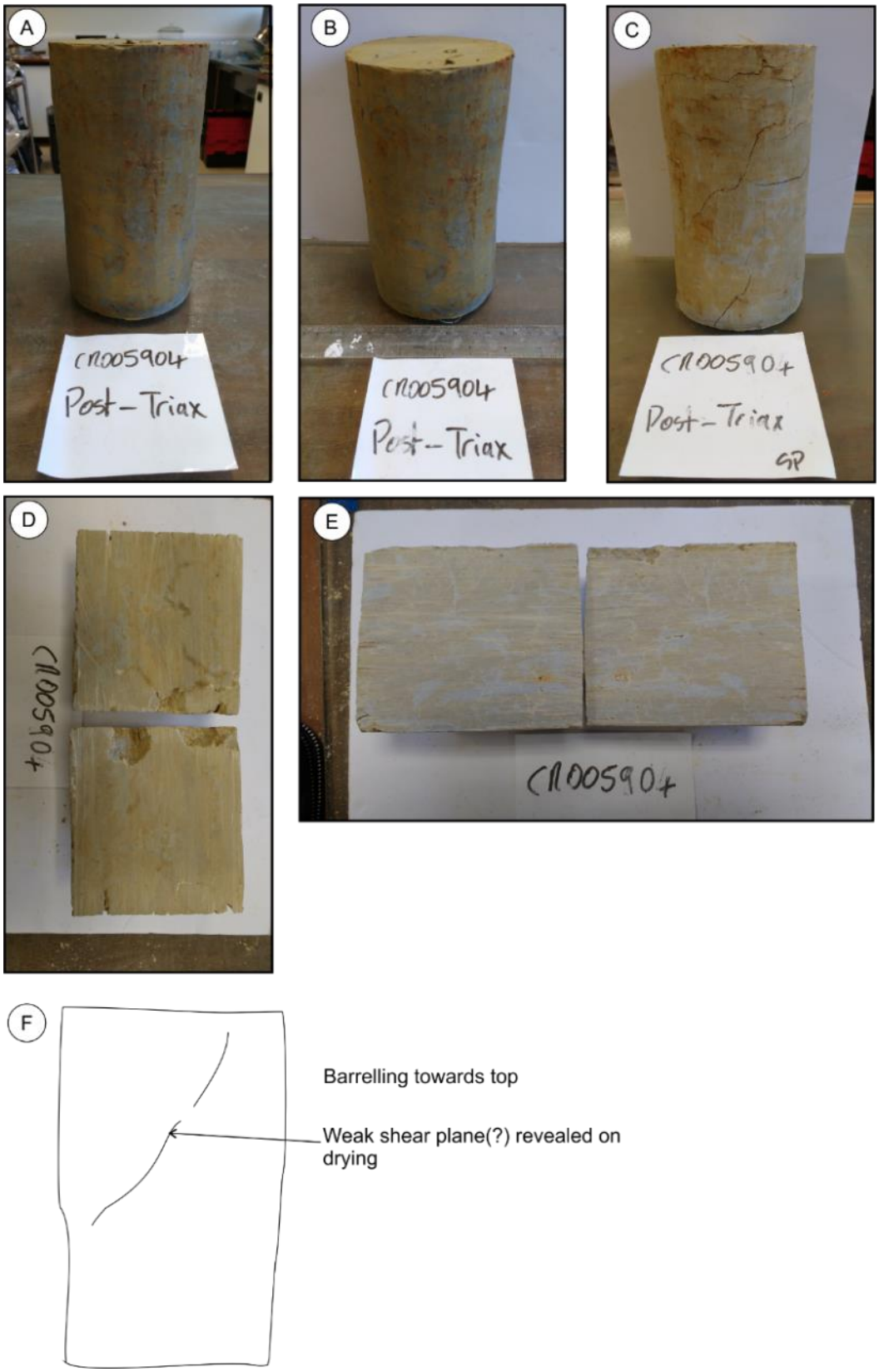

Figure 8-52 Pre- and post-triaxial specimen conditions, CR005904, Oxford Clay. A) and B) Post-experiment showing pervasive oxidation throughout. C) Oven-dried post-experiment specimen splitting along possible planar shear plane. D) and E) Oven-dried and axial-parallel sliced post-triaxial specimen revealing strong internal oxidation. F) Hand sketch interpretation.

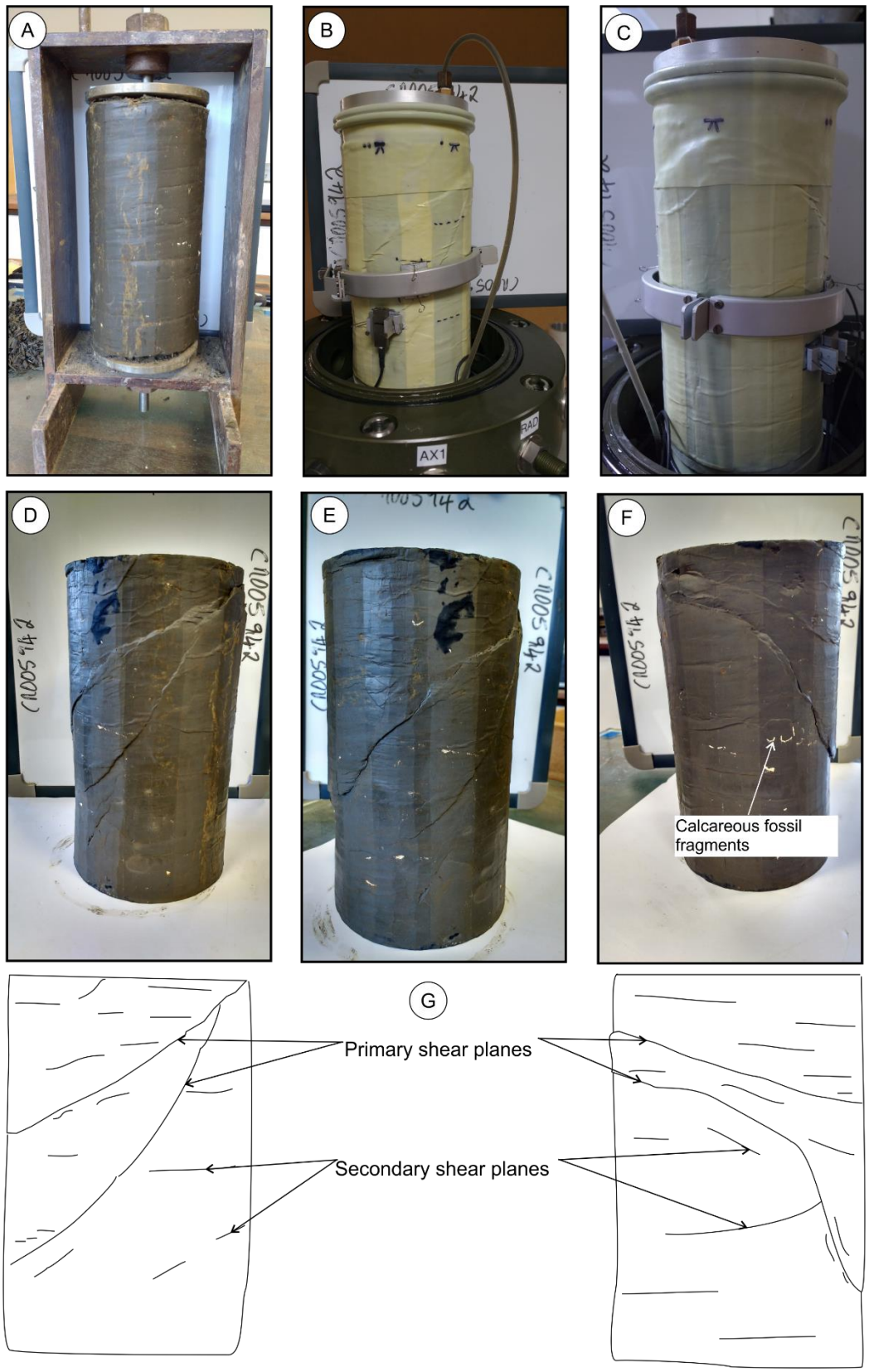

Figure 8-53 Pre- and post-triaxial specimen conditions, CR005942, Oxford Clay. A) Pre-experiment after preparation with soil lathe, sub-vertical, oxidised fractures. B) and C) Post-experiment specimen within triaxial apparatus showing evidence of shear plane displacement. D), E) and F) Post-triaxial specimen with membrane removed showing inclined planar shear planes. G) Hand sketch interpretation.

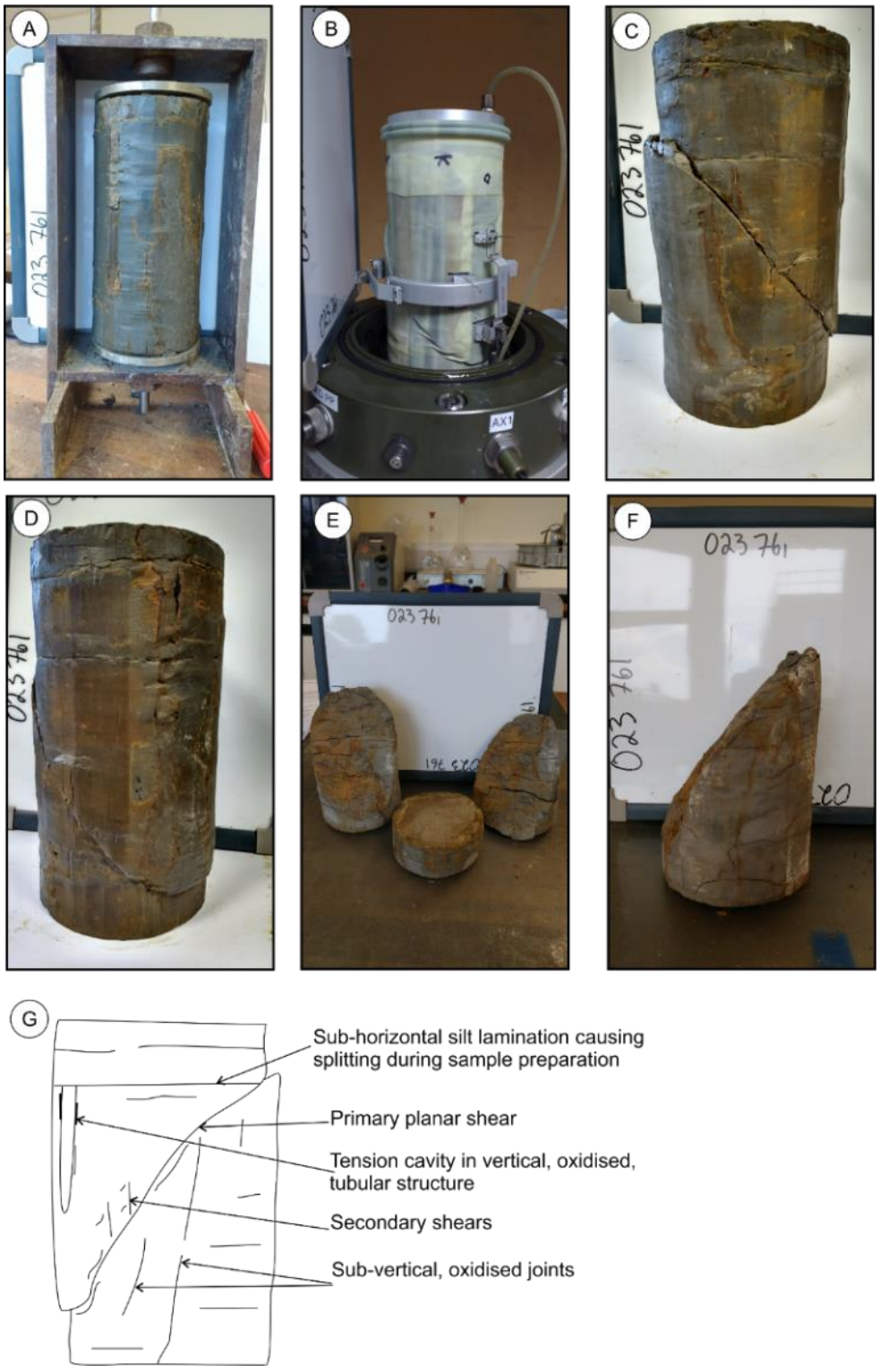

Figure 8-54 Pre- and post-triaxial specimen conditions, CR023761, Oxford Clay. A) Pre-experiment after preparation with soil lathe. Oxidised vertical fractures. B) Post-experiment specimen within triaxial apparatus showing position of Hall effect sensor relative to shear plane. C) and D) post-triaxial specimen with membrane removed showing dilated, planar shear plane. E) and F) Oven-dried, post-experiment specimen, split along primary shear plane. G) Hand sketch interpretation.

8.3.2.8 Stress-strain and mobilised shear strength (Oxford Clay)

The results are plotted as deviator stress, q, *versus* axial strain, ε_a, in Figures 8-55 to 8-58. The plots correspond to a starting deviator stress interpreted as the point at which the specimen was engaged and fully docked. Values of strain, starting from 0%, were taken from this point. The experimental parameters and conditions in the triaxial cell are given in Section 7.5.5.

Referring to the behaviour during the final stage of shearing, stage 3, all specimens exhibit an increase in axial stress with increasing strain. Specimens CR005864, CR005942 and CR023761 reach a peak value of deviator stress which then decreases with increasing strain (strain softening) suggesting that the critical state of the specimens has been reached. Specimen CR005904 softened with increasing strain but did not reach a peak value of deviator stress when the final shear stage was stopped.

Estimates of peak undrained shear strength, q_{max}, mobilised strength equal to $0.5q_{max}$ and mobilised strain equal to 0.5_{qmax}, are shown in Table 8-15.

						Mobilised strength		**Mobilised strain (%)**
Specimen	**Geology**	**Specimen depth (mbgl)**	**Stage 3 cell pressure (σ_3)**	**Stage 3 back pressure (kPa)**	**Differential (effective) stress, σ'_o (kPa)**	**q_{max} (kPa)**	**$0.5q_{max}$ (kPa)**	**$\varepsilon_{F=2}$**
CR005864	OXC	9-9.45	1180	880	300	265	133	0.35
CR005904	OXC	1.5-1.95	570	370	200	196	98	1.27
CR005942	OXC	24-24.45	1300	600	700	439	220	1.15
CR023761	OXC	11.5-11.95	1030	670	360	324	162	0.17

Table 8-15 Undrained, mobilised shear strength parameters for the Oxford Clay, Quaternary Domain 1.3. mbgl (metres below ground level).

The results show that there is an increase in undrained shear strength with increasing depth below ground level. The maximum value of q_{max} was reached in specimen CR005942 and the minimum value reached in CR005904. The value of mobilised shear strain, at 0.5_{qmax}, decreases with increasing depth below ground level; ranging from 0.12 at 24.95 mbgl to 0.45 at 1.95 mbgl. All specimens, except for CR005904, fail along one or more inclined shear planes (Figures 8-51, 8-53 and 8-54). Specimen CR005904 fails dominantly by barrelling (Figure 8-52).

The results show that there is an inverse relationship between mobilised strain and depth below ground level where a ~73% increase in $\varepsilon_{F=2}$ with decreasing depth below ground level is seen. The depth below which mobilised strain increases is ~10 mbgl.

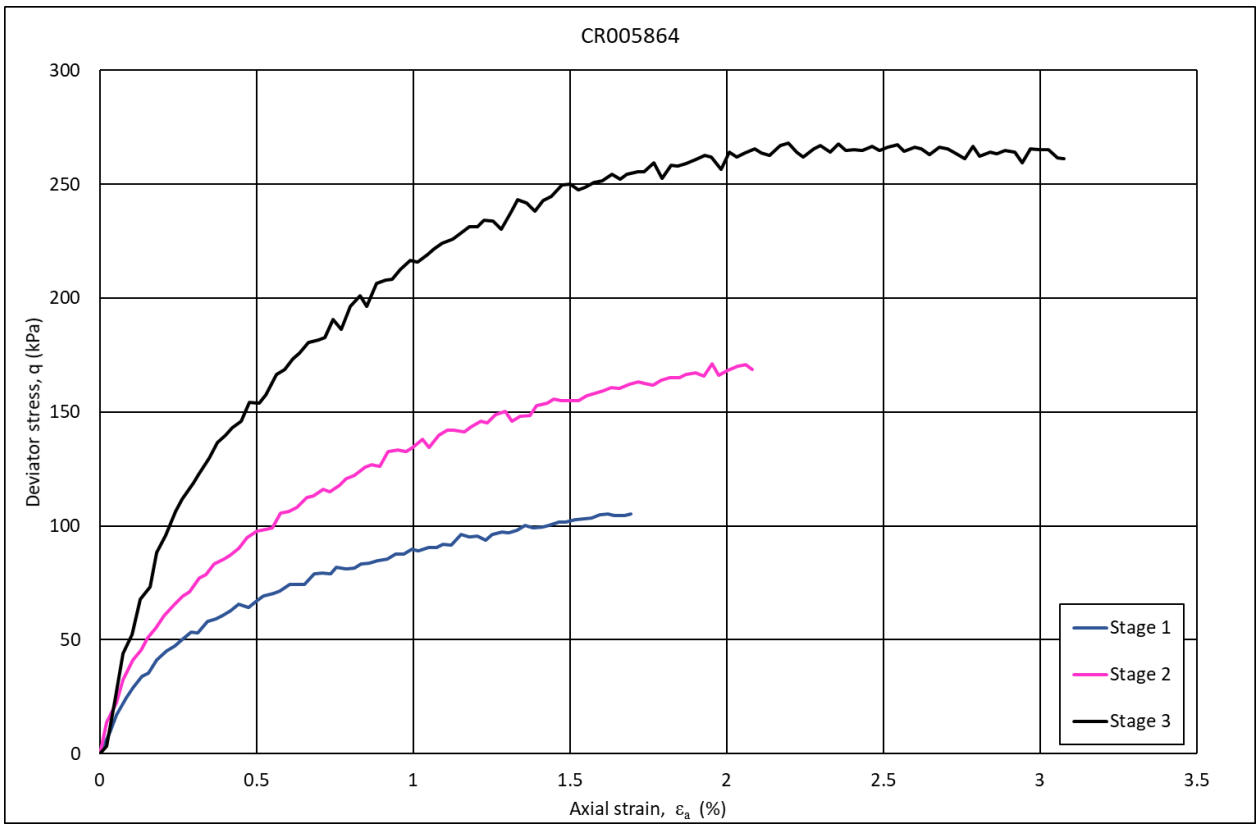

Figure 8-55 Stress-axial strain behaviour for specimen CR005864, Quaternary Domain 1.3.

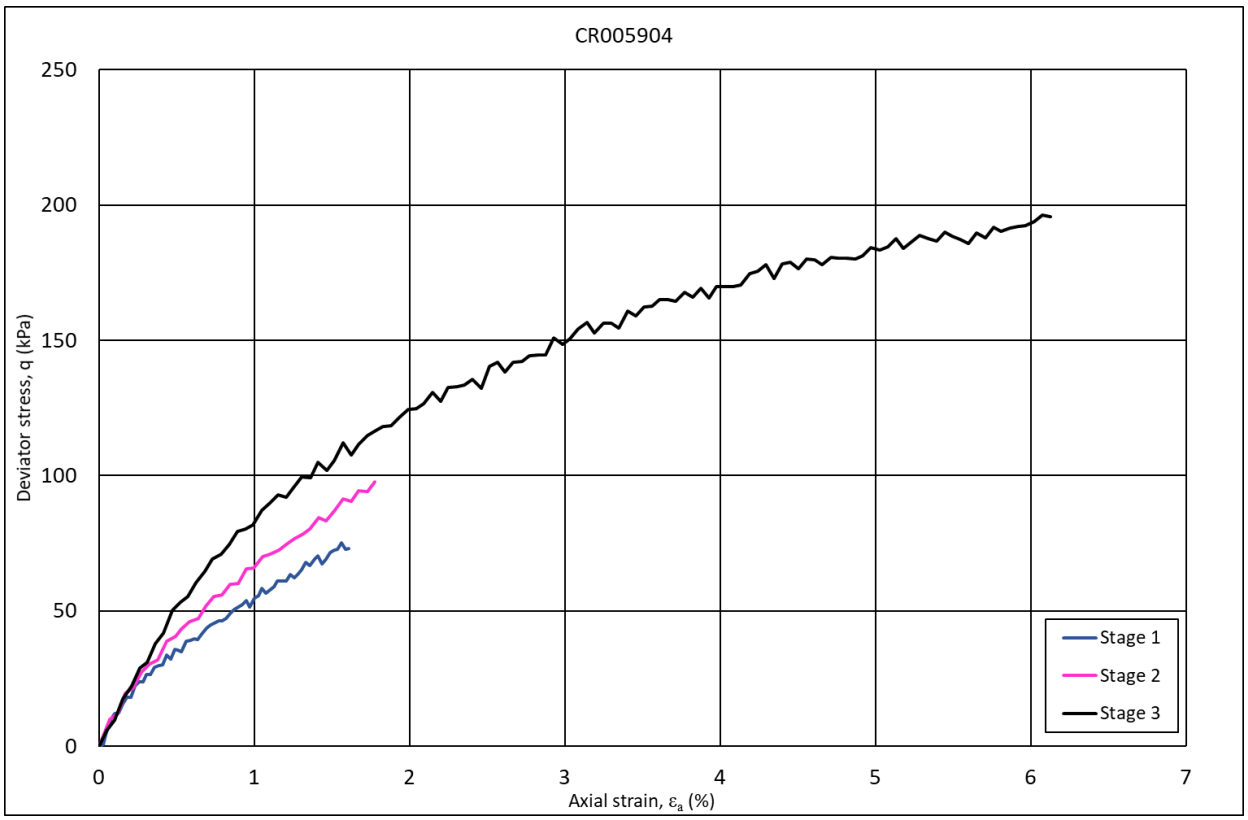

Figure 8-56 Stress-axial strain behaviour for specimen CR005904, Quaternary Domain 1.3.

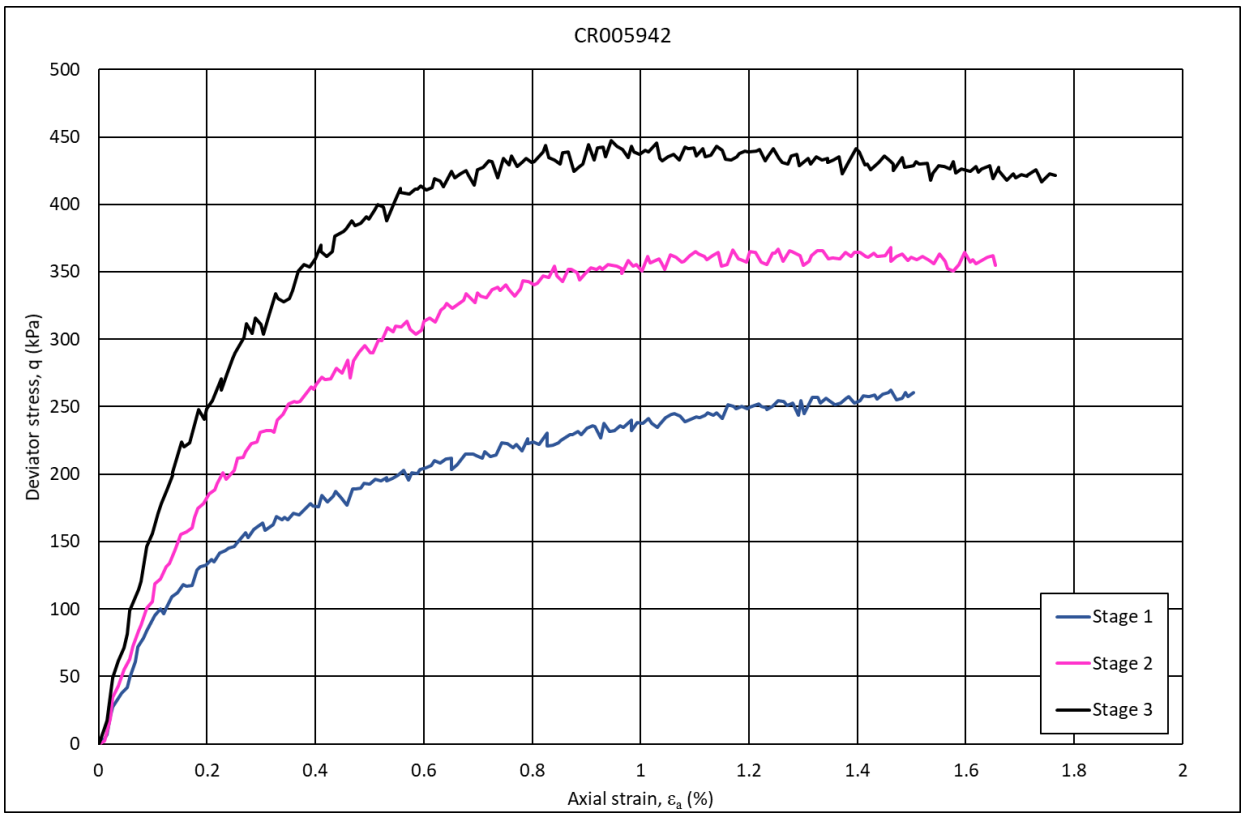

Figure 8-57 Stress-axial strain behaviour for specimen CR005942, Quaternary Domain 1.3.

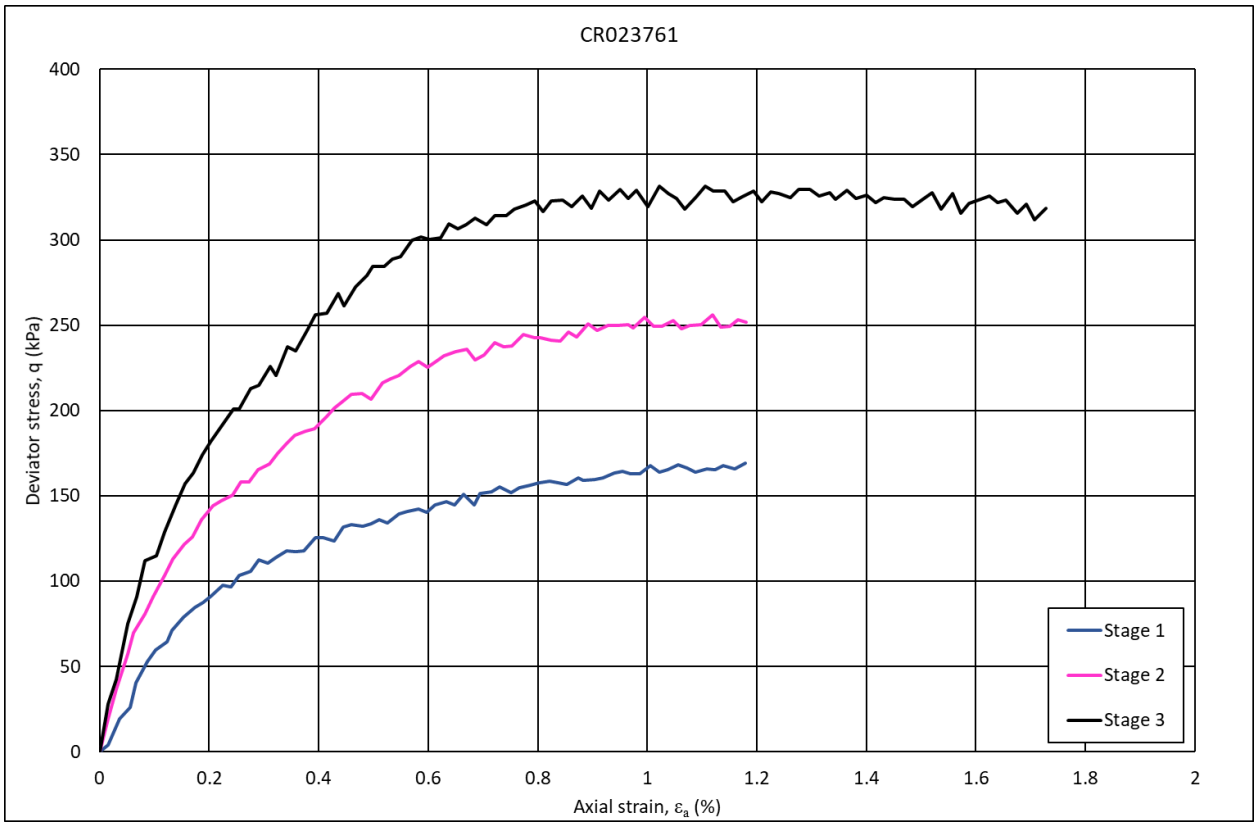

Figure 8-58 Stress-axial strain behaviour for specimen CR023761, Quaternary Domain 1.3.

8.3.2.9 Undrained stress path analyses (Oxford Clay)

The results of stress path analyses during shearing are shown in Figures 8-59 to 8-62 where deviator stress, q, is plotted against mean effective stress, p′, as described in Section 8.3.2.7.

The parameters describing the effective angle of friction, $ø'_{trans}$ and $ø'_{0.4\%}$ are presented here using Equation 8-19. Both values represent undrained strength conditions such that $ø'_{crit}$ will lie between them according to the friction parameter η, and its relationship to the critical state friction parameter M, as described in Section 8.3.2.7.

During the initial stages of shearing, the specimens, except for CR005942, follow an effective stress path (ESP) that deviates to the left, towards the critical state line. The ESP approaching the critical state line is characterised by decreasing effective mean stress, p′, as deviators stress, q, increases. The reduction in p′ is interpreted to result from increasing pore pressure, u. Before reaching the critical state line corresponding to $ø'_{crit}$, a transitional state is reached where q continues to increase but p′ remains almost constant, defining the stress ratio η_{trans}. After reaching the critical stress ratio, the ESP for all specimens except CR005942, deviates upwards and to the right as p′ increases because of pore pressure reduction and specimen dilation. This behaviour is characteristic of overconsolidated soils. In contrast, the ESP for specimen CR005942, on reaching the critical state line, deviates steeply to the left as p′ increases and q, decreases. The latter behaviour is characteristic of normally consolidated soils as the specimen decreases in volume during shearing.

With continued shearing, the ESP for specimens CR005864 and CR023761 gradually falls back down to the critical state line as q decreases. Specimen CR005904 does not show this behaviour and so q did not decreases before the shearing stage was terminated. This implies that dilation continued, and the ultimate peak deviator stress was not reached.

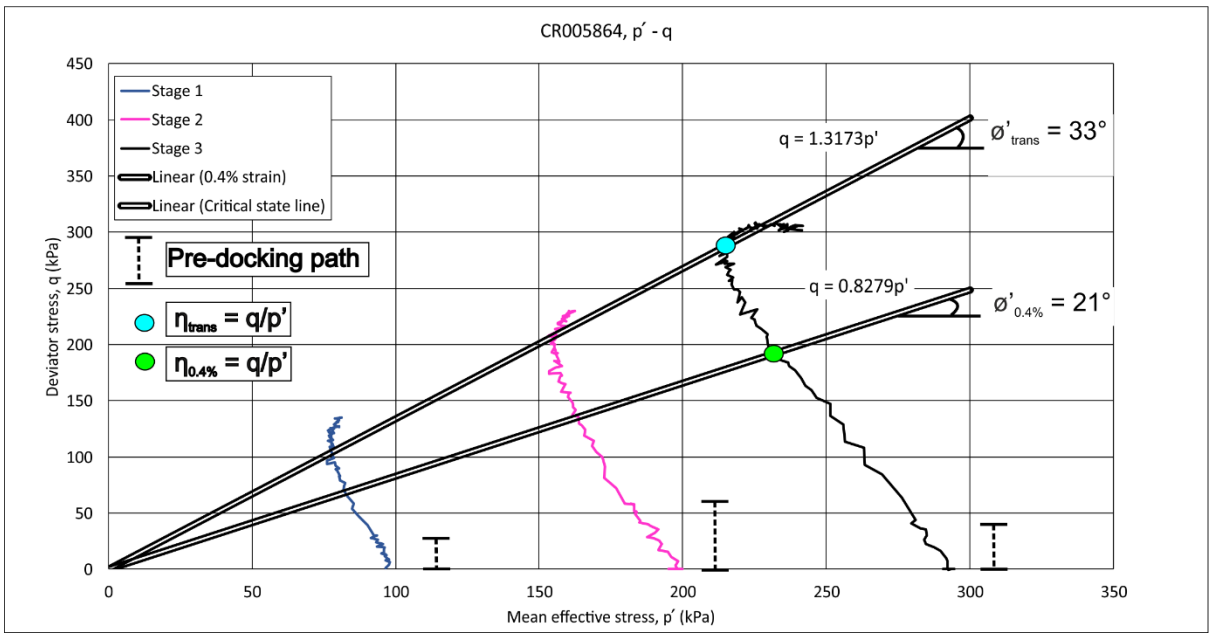

Figure 8-59 Effective stress path analysis for specimen CR005864, Oxford Clay, Quaternary Domain 1.3.

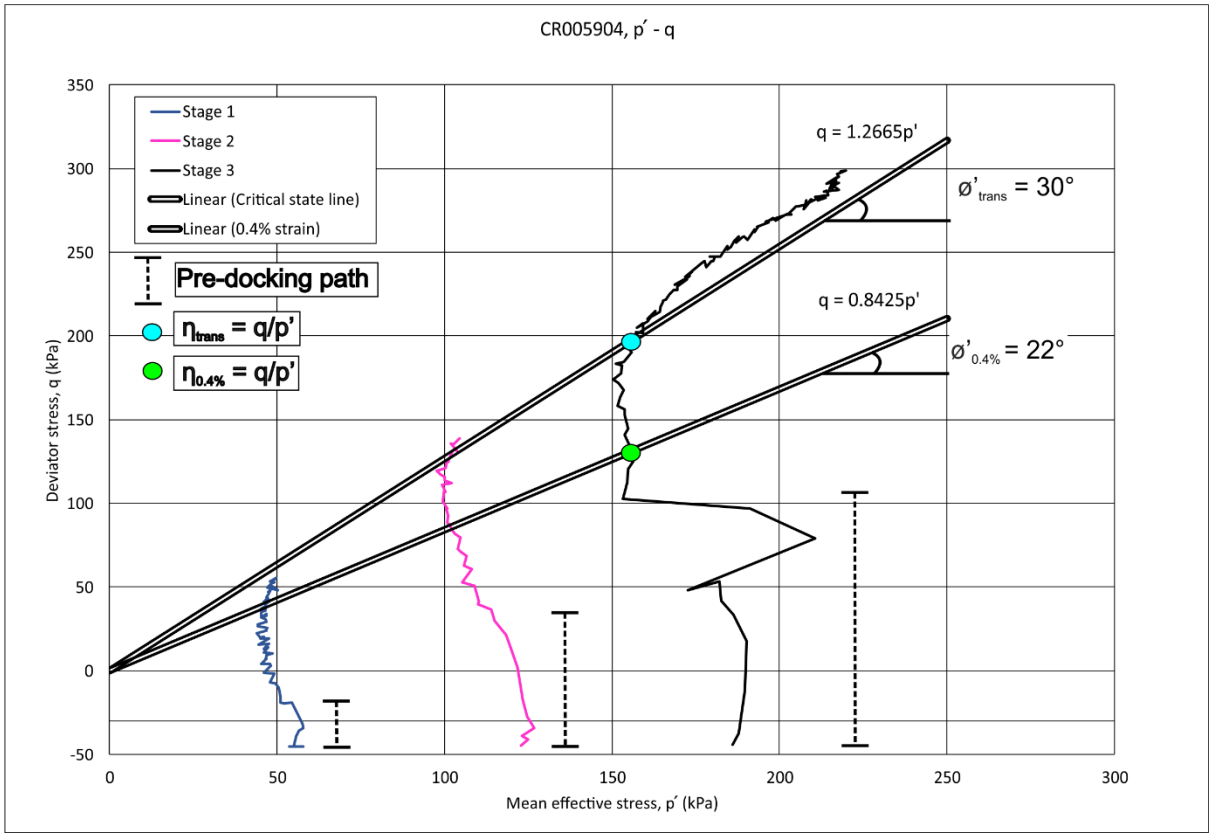

Figure 8-60 Effective stress path analysis for specimen CR005904, Oxford Clay, Quaternary Domain 1.3.

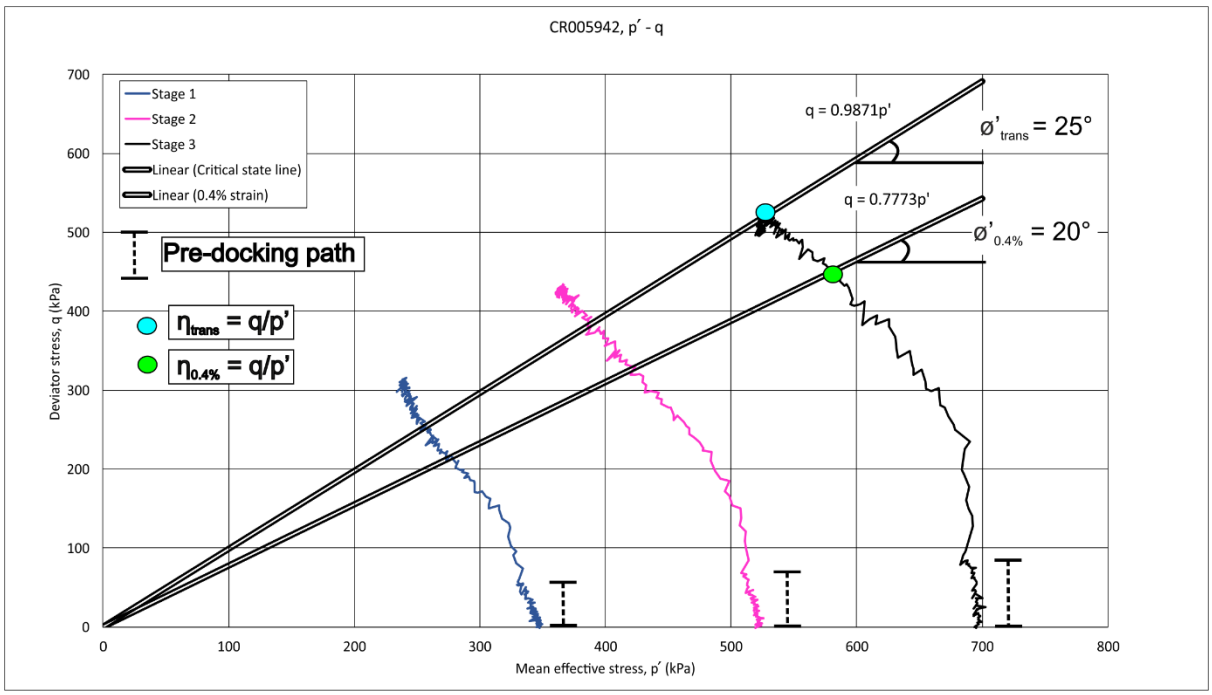

Figure 8-61 Effective stress path analyses for specimen CR005942, Oxford Clay, Quaternary Domain 1.3.

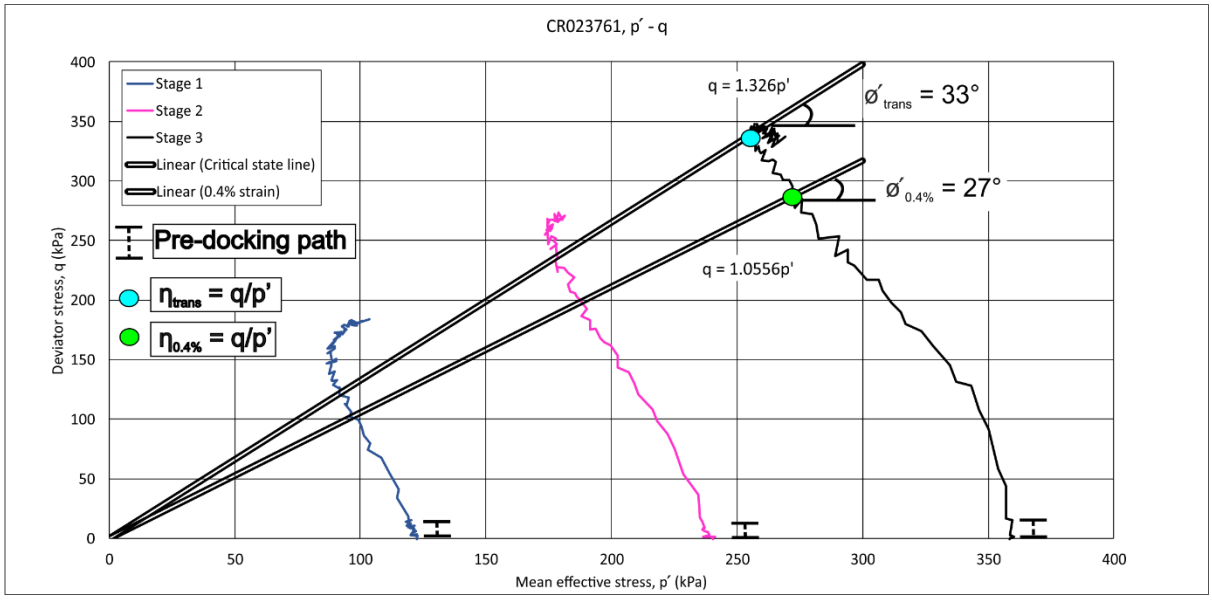

Figure 8-62 Effective tress path analyses for specimen CR023761, Oxford Clay, Quaternary Domain 1.3.

8.3.2.10 Isotropic consolidation (Oxford Clay)

Plots of isotropic consolidation before each shearing stage are shown in Figures 8-63 to 8-66 as change in volume (ΔV) *versus* square-root time in seconds. From each plot, estimates were made of the isotropic coefficient of compressibility (c_{vi}).

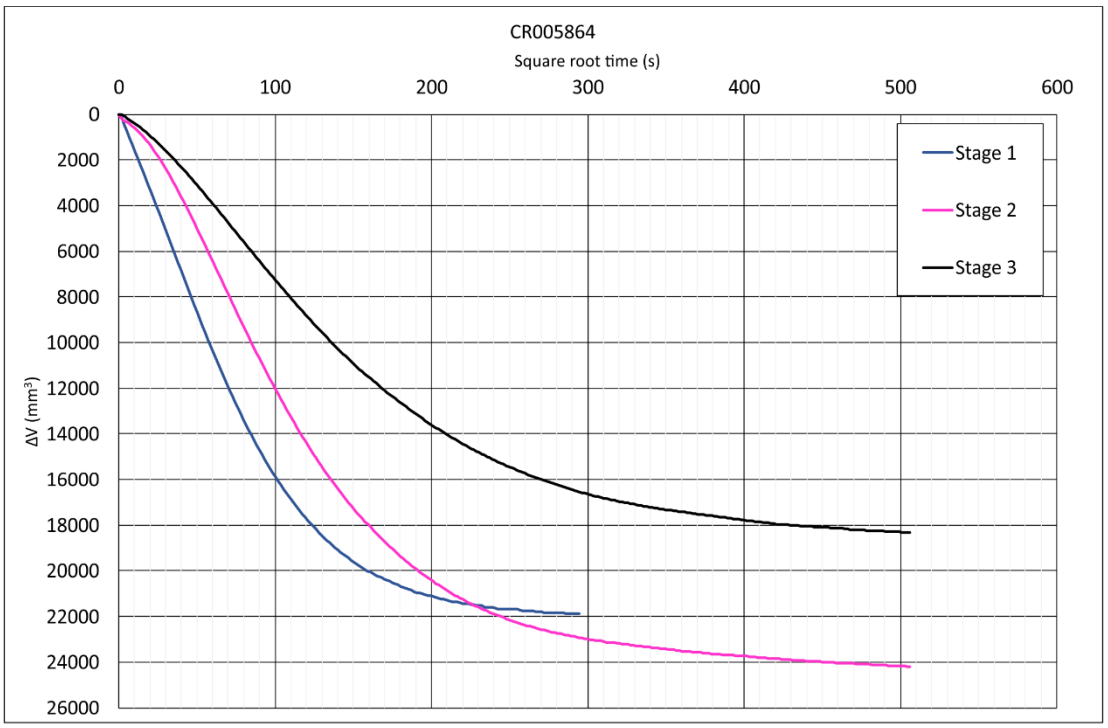

Initial		
Height (mm)	H_o	191.76
Diameter (mm)	D_o	99.43
Mass (g)	M_o	2999.01
Volume	cm^3	1489
Volume	mm^3	1489085
Area	mm^2	7765

Isotropic consolidation

	Stage 1	Stage 2	Stage 3
c_{vi} m^2/yr	28	11	10
t_{90}(min)	2	5	6
Side-drain correction applied (λ=80)			

End consolidation 1		
Height (mm)	H_1	**190.82**
Diameter (mm)	D_1	**98.94**
Volume (mm^3)	V_1	**1467194**
Area (mm^2)	A_1	**7689**

Change	
Δ_H	**0.94**
Δ_D	**0.49**
Δ_V	**21891**
Δ_A	**76**

End shear 1		
Height (mm)	H_2	**187.57**
Diameter (mm)	D_2	**99.80**
Volume (mm^3)	V_2	**1467194**
Area (mm^2)	A_2	**7822**

Change	
Δ_H	**3.25**
Δ_D	**-0.85**
Δ_V	**0**
Δ_A	**-133**

End consolidation 2		
Height (mm)	H_3	**186.54**
Diameter (mm)	D_3	**99.24**
Volume (mm^3)	V_3	**1442996**
Area (mm^2)	A_3	**7736**

Change	
Δ_H	**1.03**
Δ_D	**0.55**
Δ_V	**24198**
Δ_A	**86**

End shear 2		
Height (mm)	H_4	**182.60**
Diameter (mm)	D_4	**100.31**
Volume (mm^3)	V_4	**1442996**
Area (mm^2)	A_4	**7902**

Change	
Δ_H	**3.94**
Δ_D	**-1.06**
Δ_V	**0**
Δ_A	**-166**

End consolidation 3		
Height (mm)	H_3	**181.83**
Diameter (mm)	D_3	**99.88**
Volume (mm^3)	V_3	**1424675**
Area (mm^2)	A_3	**7836**

Change	
Δ_H	**0.77**
Δ_D	**0.43**
Δ_V	**18321**
Δ_A	**67**

End shear 3		
Height (mm)	H_4	**176.09**
Diameter (mm)	D_4	**101.50**
Volume (mm^3)	V_4	**1424675**
Area (mm^2)	A_4	**8091**

Change	
Δ_H	**5.74**
Δ_D	**-1.61**
Δ_V	**0**
Δ_A	**-255**

Figure 8-63 Isotropic consolidation and estimated coefficient of isotropic consolidation (c_{vi}), specimen CR005864, Oxford Clay, Quaternary Domain 1.3.

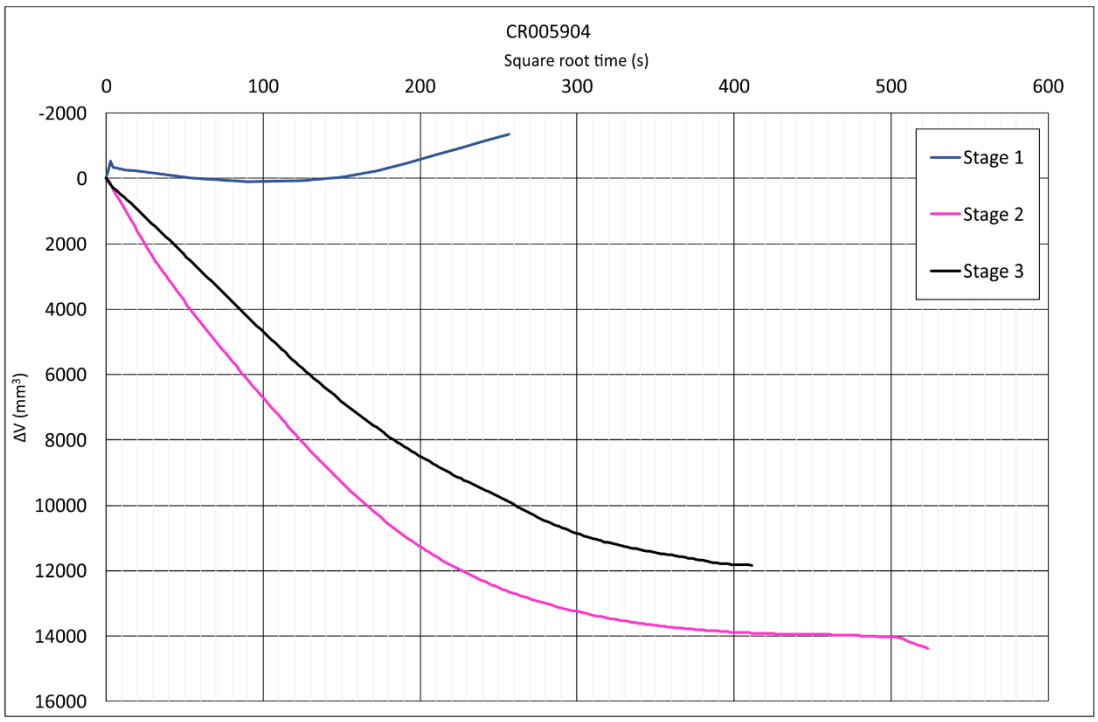

Initial		
Height (mm)	H_o	195.27
Diameter (mm)	D_o	99.45
Mass (g)	M_o	3274.4
Volume	cm^3	1517
Volume	mm^3	1516823
Area	mm^2	7768

Isotropic consolidation

	Stage 1	Stage 2	Stage 3
c_{vi} m^2/yr	NA	11	9
t_{90}(min)	NA	5	6
Side-drain correction applied (λ=80)			

End consolidation 1	(Swelling)	
Height (mm)	H_1	**195.33**
Diameter (mm)	D_1	**99.48**
Volume (mm^3)	V_1	**1518184**
Area (mm^2)	A_1	**7772**

Change	
Δ_H	**-0.06**
Δ_D	**-0.03**
Δ_V	**-1361**
Δ_A	**-5**

End shear 1		
Height (mm)	H_2	**192.19**
Diameter (mm)	D_2	**100.29**
Volume (mm^3)	V_2	**1518184**
Area (mm^2)	A_2	**7899**

Change	
Δ_H	**3.14**
Δ_D	**-0.81**
Δ_V	**0**
Δ_A	**-127**

End consolidation 2		
Height (mm)	H_3	**191.58**
Diameter (mm)	D_3	**99.97**
Volume (mm^3)	V_3	**1503809**
Area (mm^2)	A_3	**7850**

Change	
Δ_H	**0.61**
Δ_D	**0.32**
Δ_V	**14375**
Δ_A	**50**

End shear 2		
Height (mm)	H_4	**188.15**
Diameter (mm)	D_4	**100.88**
Volume (mm^3)	V_4	**1503809**
Area (mm^2)	A_4	**7993**

Change	
Δ_H	**3.43**
Δ_D	**-0.91**
Δ_V	**0**
Δ_A	**-143**

End consolidation 3		
Height (mm)	H_3	**187.66**
Diameter (mm)	D_3	**100.61**
Volume (mm^3)	V_3	**1491969**
Area (mm^2)	A_3	**7951**

Change	
Δ_H	**0.49**
Δ_D	**0.27**
Δ_V	**11840**
Δ_A	**42**

End shear 3		
Height (mm)	H_4	**184.30**
Diameter (mm)	D_4	**101.53**
Volume (mm^3)	V_4	**1491969**
Area (mm^2)	A_4	**8095**

Change	
Δ_H	**3.36**
Δ_D	**-0.91**
Δ_V	**0**
Δ_A	**-145**

Figure 8-64 Isotropic consolidation and estimated coefficient of isotropic consolidation (c_{vi}), specimen CR005904, Oxford Clay, Quaternary Domain 1.3. c_{vi} not interpreted in stage 1 due to swelling.

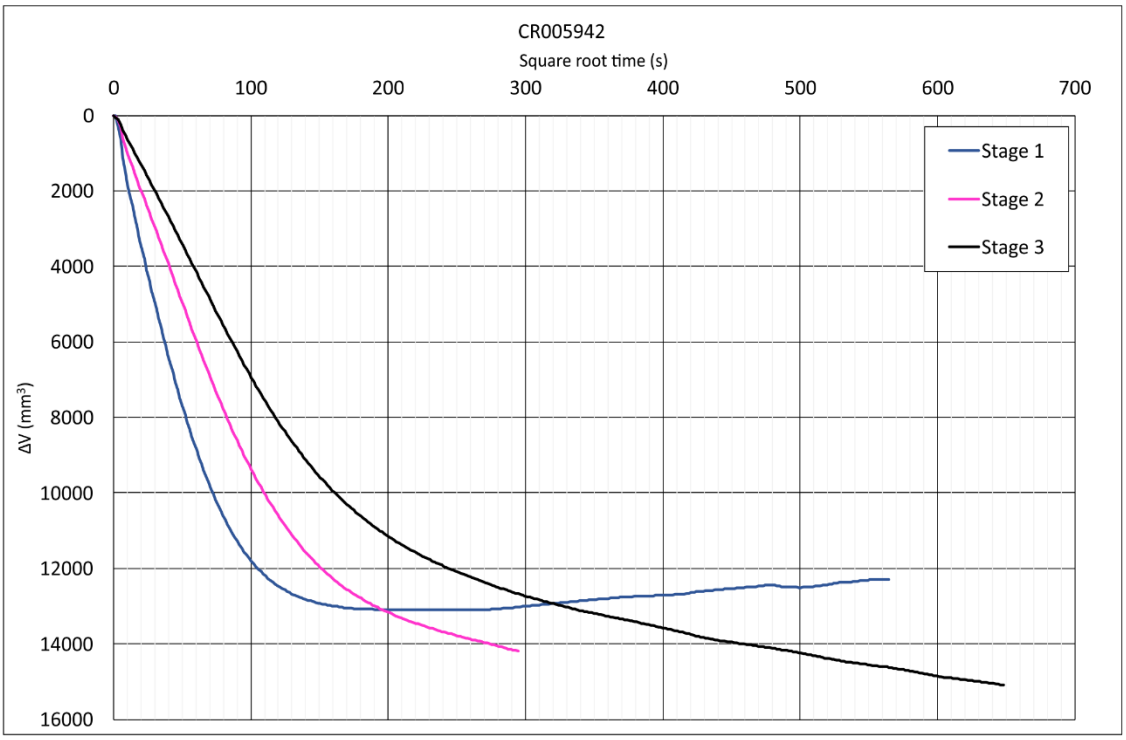

Initial		
Height (mm)	H_o	192.15
Diameter (mm)	D_o	99.34
Mass (g)	M_o	2841.04
Volume	cm^3	1489
Volume	mm^3	1489162
Area	mm^2	7750

Isotropic consolidation

	Stage 1	Stage 2	Stage 3
c_{vi} m^2/yr	27	16	13
t_{90}(min)	2	4	4
Side-drain correction applied (λ=80)			

End consolidation 1		
Height (mm)	H_1	**191.62**
Diameter (mm)	D_1	**99.06**
Volume (mm^3)	V_1	**1476862**
Area (mm^2)	A_1	**7707**

Change	
Δ_H	**0.53**
Δ_D	**0.27**
Δ_V	**12300**
Δ_A	**43**

End shear 1		
Height (mm)	H_2	**188.73**
Diameter (mm)	D_2	**99.82**
Volume (mm^3)	V_2	**1476862**
Area (mm^2)	A_2	**7825**

Change	
Δ_H	**2.89**
Δ_D	**-0.76**
Δ_V	**0**
Δ_A	**-118**

End consolidation 2		
Height (mm)	H_3	**188.12**
Diameter (mm)	D_3	**99.50**
Volume (mm^3)	V_3	**1462672**
Area (mm^2)	A_3	**7775**

Change	
Δ_H	**0.60**
Δ_D	**0.32**
Δ_V	**14190**
Δ_A	**50**

End shear 2		
Height (mm)	H_4	**184.95**
Diameter (mm)	D_4	**100.35**
Volume (mm^3)	V_4	**1462672**
Area (mm^2)	A_4	**7908**

Change	
Δ_H	**3.17**
Δ_D	**-0.85**
Δ_V	**0**
Δ_A	**-133**

End consolidation 3		
Height (mm)	H_3	**184.32**
Diameter (mm)	D_3	**100.00**
Volume (mm^3)	V_3	**1447589**
Area (mm^2)	A_3	**7854**

Change	
Δ_H	**0.64**
Δ_D	**0.35**
Δ_V	**15083**
Δ_A	**54**

End shear 3		
Height (mm)	H_4	**180.96**
Diameter (mm)	D_4	**100.92**
Volume (mm^3)	V_4	**1447589**
Area (mm^2)	A_4	**8000**

Change	
Δ_H	**3.36**
Δ_D	**-0.92**
Δ_V	**0**
Δ_A	**-146**

Figure 8-65 Isotropic consolidation and estimated coefficient of isotropic consolidation (c_{vi}), specimen CR005942, Oxford Clay, Quaternary Domain 1.3. Note swelling observed at the end of primary consolidation in stage 1.

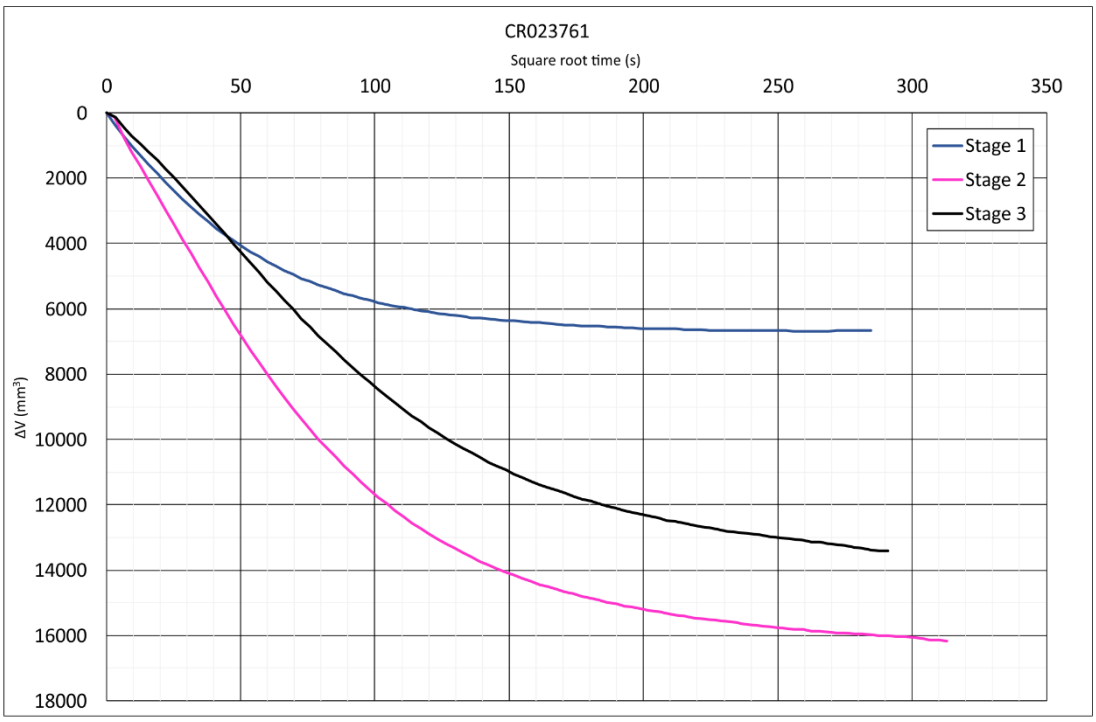

Initial		
Height (mm)	H_o	195.80
Diameter (mm)	D_o	100.07
Mass (g)	M_o	3126.9
Volume	cm^3	1540
Volume	mm^3	1540066
Area	mm^2	7866

Isotropic consolidation

	Stage 1	Stage 2	Stage 3
c_{vi} m^2/yr	33	22	15
t_{90}(min)	2	3	4
Side-drain correction applied (λ=80)			

End consolidation 1		
Height (mm)	H_1	**195.52**
Diameter (mm)	D_1	**99.93**
Volume (mm^3)	V_1	**1533393**
Area (mm^2)	A_1	**7843**

Change	
Δ_H	**0.28**
Δ_D	**0.14**
Δ_V	**6673**
Δ_A	**23**

End shear 1		
Height (mm)	H_2	**193.21**
Diameter (mm)	D_2	**100.52**
Volume (mm^3)	V_2	**1533393**
Area (mm^2)	A_2	**7937**

Change	
Δ_H	**2.31**
Δ_D	**-0.60**
Δ_V	**0**
Δ_A	**-94**

End consolidation 2		
Height (mm)	H_3	**192.53**
Diameter (mm)	D_3	**100.17**
Volume (mm^3)	V_3	**1517235**
Area (mm^2)	A_3	**7881**

Change	
Δ_H	**0.68**
Δ_D	**0.35**
Δ_V	**16158**
Δ_A	**56**

End shear 2		
Height (mm)	H_4	**190.24**
Diameter (mm)	D_4	**100.77**
Volume (mm^3)	V_4	**1517235**
Area (mm^2)	A_4	**7975**

Change	
Δ_H	**2.29**
Δ_D	**-0.60**
Δ_V	**0**
Δ_A	**-95**

End consolidation 3		
Height (mm)	H_3	**189.68**
Diameter (mm)	D_3	**100.47**
Volume (mm^3)	V_3	**1503815**
Area (mm^2)	A_3	**7928**

Change	
Δ_H	**0.56**
Δ_D	**0.30**
Δ_V	**13420**
Δ_A	**47**

End shear 3		
Height (mm)	H_4	**186.35**
Diameter (mm)	D_4	**101.37**
Volume (mm^3)	V_4	**1503815**
Area (mm^2)	A_4	**8070**

Change	
Δ_H	**3.33**
Δ_D	**-0.89**
Δ_V	**0**
Δ_A	**-142**

Figure 8-66 Isotropic consolidation and estimated coefficient of isotropic consolidation (c_{vi}), specimen CR023761, Oxford Clay, Quaternary Domain 1.3.

All samples show a trend for decreasing rate of isotropic consolidation with increasing confining and effective stress. The maximum value for c_{vi} was $33m^2/yr$ at an effective stress of 120 kPa. The lowest was $9m^2/yr$ at an effective stress of 200 kPa. Using Equation 4-3 to estimate permeability, the difference in rates of consolidation may be explained by differences in permeability. Specimen CR005904 has the lowest permeability of all Oxford Clay specimens tested at $4.52x10^{-14}$ m/s and correspondingly has the lowest values of c_{vi}. Specimen

CR023761 has a calculated permeability of $3.64x10^{-13}$ m/s and correspondingly has the highest value of c_{vi}.

8.3.2.11 Stiffness (Oxford Clay)

Stiffness is not a unique property of soil. Triaxial tests conducted in this research are undrained, where drainage during compression is not allowed and so no change in volume occurs, volumetric strains are zero and only changes in shape of the soil specimen occur. For a cylindrical triaxial soil specimen experiencing effective normal stresses, then:

$\sigma'_a = \sigma'_1$ and $\sigma'_r = \sigma'_2 = \sigma'_3$

where σ'_n are effective principal stresses.

The resulting changes in axial and radial strain are given by $\delta\varepsilon_a = \delta\varepsilon_1$ and $\delta\varepsilon_r = \delta\varepsilon_2 = \delta\varepsilon_3$ so that the total work input (Muir Wood, 1991) to the sample is:

$$\delta W_v = \sigma'_a \delta\varepsilon_a + 2\,\sigma'_r \delta\varepsilon_r$$

Equation 8-21

and the increment of volumetric strain, $\delta\varepsilon_p$, in an undrained triaxial experiment is:

$$\delta\varepsilon_p = \delta\varepsilon_a + 2\delta\varepsilon_r = 0$$

Equation 8-22

and $\delta\varepsilon_p = 0$ implies that:

$$\delta\varepsilon_a = -2\delta\varepsilon_r$$

Equation 8-23

It can be shown (Muir Wood, 1991)that the distortional strain increment quantity, $\delta\varepsilon_q$ equals $\delta\varepsilon_a$.

In terms of soil elasticity expressed as Young's modulus, E and Poisson's ratio, ν the response of a soil specimen to a triaxial change of effective stress is given by (Muir Wood, 1991):

$$\begin{vmatrix}\delta\varepsilon_a\\ \delta\varepsilon_r\end{vmatrix} = \frac{1}{E'}\begin{bmatrix}1 & -2\nu'\\ -\nu' & 1-\nu'\end{bmatrix}\begin{vmatrix}\delta\sigma'_a\\ \delta\sigma'_r\end{vmatrix}$$

Equation 8-24

The elastic response of a triaxial soil specimen in terms of the stress invariants p' and q, defined in Section 8.3.2.7, can be related to changes in size (bulk modulus, K) and changes in shape (shear modulus, G) by:

$$\begin{bmatrix}\delta\varepsilon_p\\ \delta\varepsilon_q\end{bmatrix} = \begin{bmatrix}1/K' & 0\\ 0 & 1/3G'\end{bmatrix}\begin{bmatrix}\delta p'\\ \delta q\end{bmatrix}$$

Equation 8-25

Therefore, assuming elastic and undrained behaviour,

$$\delta\varepsilon_q = \frac{1}{3G'}\ \delta q$$

Equation 8-26

and

$$G' = \frac{1}{3}\ \frac{\delta q}{\delta\varepsilon_q} = \frac{1}{3}\ \frac{\delta\sigma_a - \delta\sigma_r}{\delta\varepsilon_a}$$

Equation 8-27

In this research, triaxial elasticity is expressed as the relationship between deviator stress, $\delta\varepsilon_q$ and axial strain, $\delta\varepsilon_a$ to estimate undrained Young's modulus, E'. The relationship between elastic moduli is;

$$G = \frac{E}{2(1+\nu)}$$

Equation 8-28

Stiffness may be measured as tangent or secant stiffness. Secant stiffness is approximately twice that of tangent stiffness. Secant stiffness at strains >0.1% were estimated here as Young's modulus, E, corresponding to $0.5q_{max}$ as described in Section 8.3.8.1. For each sample, two estimates of E were made; one from the plot of deviator stress *versus* axial strain recorded by the axial displacement transducers within the triaxial apparatus, and a second from the recording of change in mean axial local strain recorded using two Hall effect sensors attached to the specimen as described in Section 7.5.5. A third estimate was made from the results of mean axial local strain recorded by the Hall effect sensors at 0.1% strain and referred to as $E_{0.1\%}$. In each case, the estimate was made from the final shear stage, 3, where failure of the specimen was allowed. The results are shown in Table 8-16 and Figures 8-67 and 8-68.

	Triaxial apparatus	Hall effect	
	E (MPa), $0.5q_{max}$	E (MPa), $0.5q_{max}$	$E_{0.1\%}$ (MPa)
Specimen			
CR005864	0.379	NA	NA
CR005904	0.08	0.13	0.17
CR005942	1.44	NA	NA
CR023761	0.95	1.45	1.57

Table 8-16 Estimates of secant stiffness for specimens of Oxford Clay, Quaternary Domain 1.3 derived from shear stage 3 results. NA – error in axial Hall effect recordings for CR005864 and no measurement for stage 3 from specimen CR005942 because of sensor detachment during shearing.

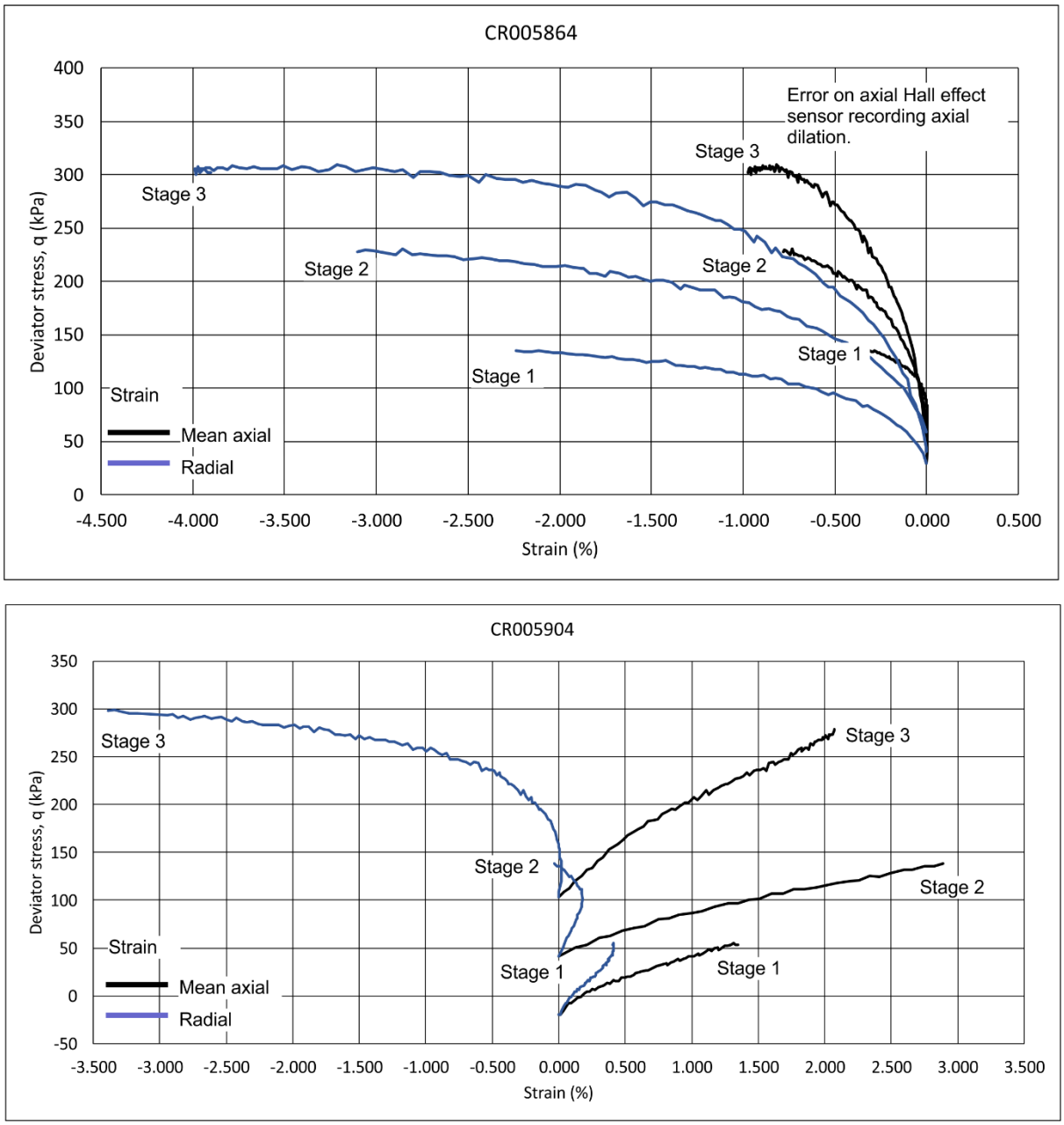

Figure 8-67 Small-strain stiffness measured using Hall effect sensors, Oxford Clay specimens CR005864 and CR005904, Quaternary Domain 1.3. Note, specimen CR005904 swelled during Stage 1 before consolidation.

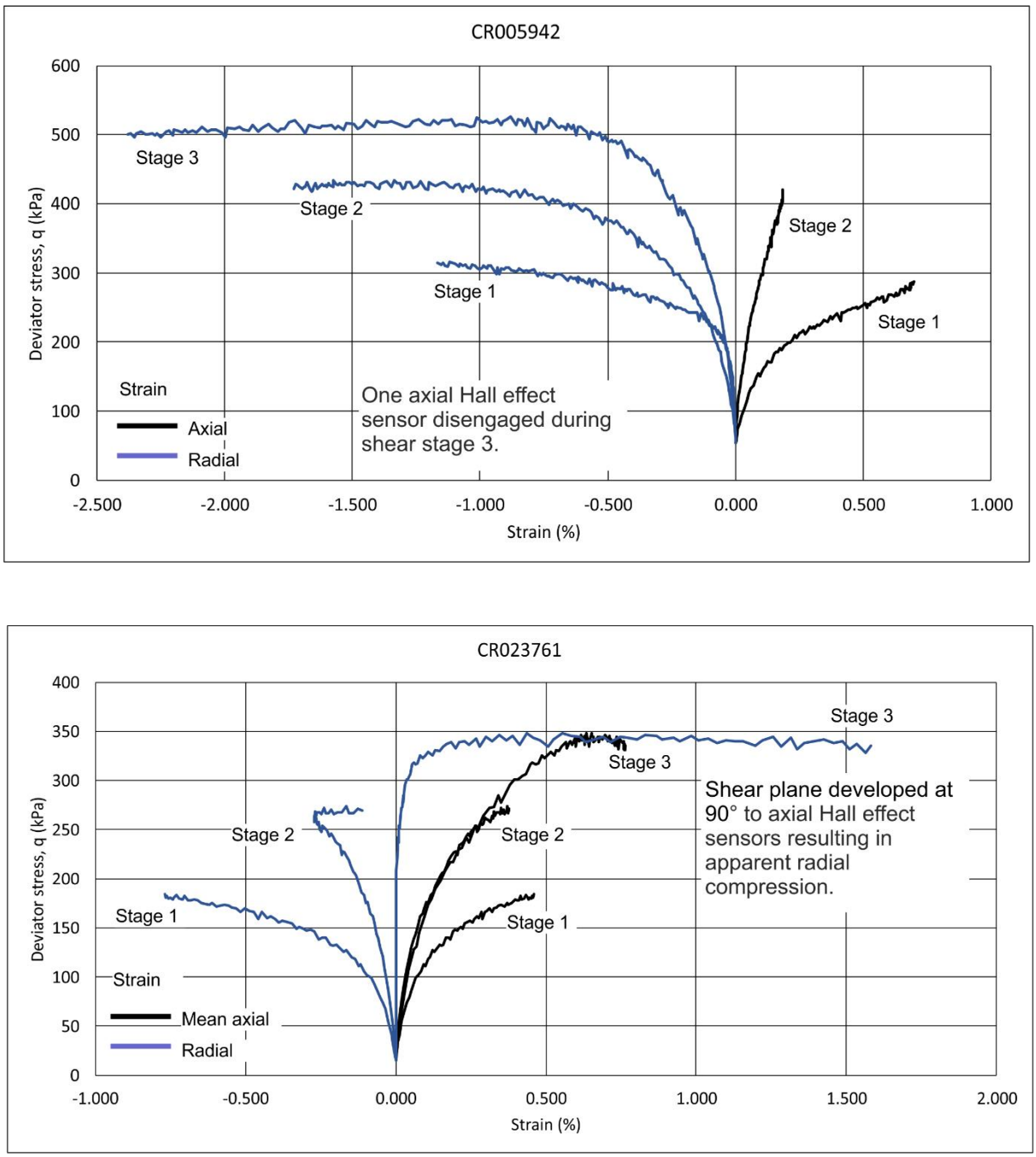

Figure 8-68 Small-strain stiffness measured using Hall effect sensors, Oxford Clay specimens CR005942 and CR023761, Quaternary Domain 1.3. Note Hall effect sensor Ax1, disengaged from sample CR005942 during shear stage 3.

The variability in secant shear modulus at 0.5_{qmax}, is seen to be related to increasing depth below ground level where specimen CR005904 (1.95 mbgl) is the least stiff and specimen CR005942 (24.45 mbgl) is the stiffest, ~7 times greater than CR005904. Depth-dependent variation in shear modulus for the Oxford Clay approximates to 0.05 MPa $^{m-1}$. Because of errors in the Hall effect sensor readings, or detachment of the sensors, comparison between shear modulus values measured using the triaxial cell axial displacement transducers and Hall effect sensors difficult. Young's modulus at 0.5_{qmax} measured using the Hall effect sensors is

greater for specimen CR023761 than for CR005904; deeper and shallower specimens respectively. Shear modulus at 0.1% shear strain is higher for both specimens but the magnitude of difference varies from 30% in CR005904 to 8% in CR023761.

8.3.3 Summary

Except for specimens CR023761 and CR023766, the Peterborough Member of the Oxford Clay is a well-graded, variably organic and calcareous, slightly sandy, slightly clayey silt. Specimens CR023761 and CR023761 are uniformly-graded, slightly sandy, slightly clayey silts. The Stewartby Member shares the same lithology but is well- to poorly-graded, being poorly-graded where the C_z <1. The clay mineral assemblage is characterised by illite, kaolinite (with minor or trace chlorite) and chlorite. Chlorite is absent from samples CR005853 (Stewartby Member) and CR005904 (Peterborough member) and they have lower plasticity compared to other samples. The activity classes of the samples range from normal to active.

At outcrop, the Oxford Clay comprises stiff, laminated and thinly bedded silt and clay with common fossils which are oxidised around their margins. Hand dug pits at ground level demonstrate the Oxford Clay is weathered to a soft clay with common gravel of quartz and quartzite which is interpreted here as solifluction 'head'. This part of the Oxford Clay is likely to have been periglacially sheared although none were seen in the hand-dug pits.

Despite their lithological characterisation as silts, the samples have high to very high plasticity; the Stewartby Member having lower plasticity compared to the Peterborough Member. It is interpreted that much of the silt determined using particle-size analysis is in fact agglomerations of clay particles and so disaggregation was not sufficient. The Stewartby Member sample, CR022794 behaves as a silt. The activity of the Peterborough and Stewartby members is classed as active with values between 1.3 and 2.3. The Stewartby Member sample, CR005853 has normal activity with a value of 0.9. The value of activity is interpreted to be the result of I_p derived from silt and clay and the low proportion of clay. Measured moisture content values are generally less than that of the values for W_P and so values for LI are < 0 or ~0.

The plasticity results indicate that silt-size particles within samples of the Oxford Clay are agglomerations of clay. This may reflect the limited effectiveness of the sample preparation in breaking down agglomerations using sodium hexametaphosphate.

The Oxford Clay has low to medium compressibility with values of m_v for the 500 kPa stress increment between 0.075 and 0.93m^2/MN. The coefficient of compressibility, c_v, is variable but in general, decreases with increasing applied stress. Calculated values for the 500 kPa stress increment vary between 0.4 and 6.39 m^2/yr. Between 81% to 89% compression is complete within the primary compression phase except for specimen CR005942 where only 57% is complete, most consolidation taking place in the secondary phase.

Mobilised shear strength at $0.5q_{max}$ ranges between 98 and 220kPa with corresponding mobilised strain, $\varepsilon_{F=2}$ ranging between 0.17 and 1.27%. The variability is related to *in situ* effective stress where there is a positive correlation between increasing depth below ground level and increasing undrained shear strength. The lowest strength and greatest mobilised strain at $0.5q_{max}$ is associated with specimen CR005904. The effective stress paths for all samples except CR005942 behave as overconsolidated clays. The effective stress path for CR005942 appears to behave as a normally consolidated clay, indicating that the degree of overconsolidation in its stress history has been partially or wholly removed. It is suggested here that it may result from sub-glacial shearing.

In terms of secant shear strength parameter $ø'_{trans}$, except for specimen CR005942, values range between 30 and 33°, reducing to $ø'_{0.4\%}$ values between 21 and 27°. Values for $ø'_{trans}$ and $ø'_{0.4\%}$ are 25 and 20° respectively for specimen CR005942. The measured reduction in undrained shear strength parameter values, as well as the stress path behaviour, may support the interpretation of a zone of sub-glacial deformation at ~25 mbgl within the Oxford Clay in Quaternary Domain 1.3.

Young's modulus, E, values measured using the axial displacement transducers of the triaxial apparatus are between 0.08 and 1.44 MPa. Values of G measured using Hall effect sensors for specimens CR005904 and CR023761 are 0.13 and 1.45 respectively. The latter values of G are between 23 and 28% higher than those measured using the displacement transducers of the triaxial apparatus.

The clay mineralogy of the tills is characterised by illite, kaolinite, mixed layer illite and collapsible minerals, and chlorite. Till sample SP11012016_1 is characterised by less intense peaks compared to other samples. Sample SP11102016_1 contains less carbonate than other till samples and contains a greater proportion of silicate material (92% compared to 73 – 77%).

8.4 Quaternary Domain 1.3.1

Quaternary Domain 1.3.1 comprises Middle to Late Jurassic mudrocks of the Oxford Clay and mudrocks and sandstone, weathered to sand of the Kellaways Formation, overlain by glacigenic, glaciolacustrine and/or periglacial deposits. This Domain is interpreted to have been glaciated on at least one occasion and influenced by multiple phases of pre- and post-glacial periglacial activity.

Laboratory results are presented for loss-on-ignition (LOI) and particle-size analysis (PSA) for till (including sandy facies), glaciolacustrine deposits and the Oxford Clay. Analyses for clay mineralogy are presented for till and the Oxford Clay. Plasticity results are presented for glacigenic and glaciolacustrine deposits, till and the Oxford Clay.

Samples for laboratory analysis were collected as bulk samples from field sites. 1D consolidation and multi-stage triaxial experiments, with measurement of small-strain stiffness, were undertaken for one specimen of Oxford Clay which was prepared from a UT100 sample.

8.4.1 Field locality: Bletchley (Newton Longville)

Glacigenic sediments and Oxford Clay bedrock are exposed in the domestic refuse landfill and recycling site at Bletchley. Exposures of the Oxford Clay were previously described by Horton *et al*. (1974) and Callomon (1968). Horton *et al*. (1974) observed large wavelength, open folds, in the *Acutistriatum* Band interpreted as evidence of valley-bulging. The face in which these structures were observed is no longer accessible but a new section, to the south of the operating landfill site was examined as it exposed previously unrecorded glacigenic sediments. Glaciolacustrine sediments comprising laminated silt and clay, occur in the nearby valley of the River Ouzel.

The location of the site and the sedimentary logs are shown in Figure 8-69.

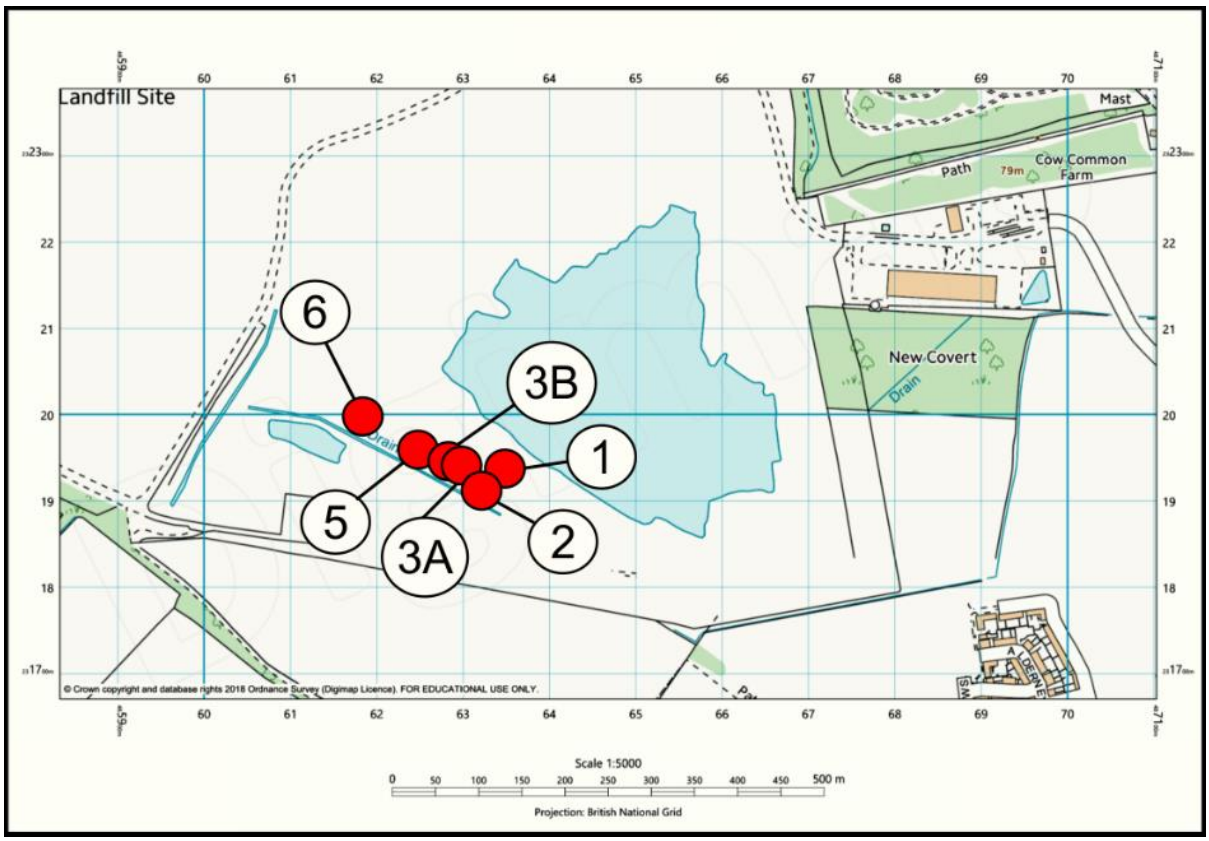

Figure 8-69 Site and section location, Bletchley (Newton Longville), Quaternary Domain 1.3.1.

8.4.1.1 Description of sections

Six sedimentary sections were logged and are shown in Figures 8-70 to 8-73. The orientation of cross-bedding is plotted on an equal-area stereogram in Figure 8-74. Four lithofacies were identified and are summarised below. They are illustrated in Figures 8-75 to 8-80.

Lithofacies 1 (LF1)

This lithofacies comprises sandy gravel and gravelly sand. It is sub-divided into lithofacies a, b and c. LF1a is dominated by dark and reddish-brown, grey, poorly-sorted, weakly-bedded, fine- to coarse- sand with well-rounded gravel. The gravel is fine- to coarse-grained, well-rounded and includes chalk, chatter-marked flint and quartzite.

LF1b comprises light grey, light brown and brown, thinly-interbedded and thickly-interlaminated clay/silt and fine to coarse sand with beds of gravel. Ripple laminations are common. Sand grains are dominated by quartz and white chalk. The gravel includes chalk and grey chatter-marked flint.

LF1c comprises brown and grey, moderately- to well-sorted, silty, fine- to medium-sand which becomes coarse with some gravel towards the top. Through field inspection the sand is 70% grey and pink quartz, 20% white and grey chalk and 10% other lithic grains.

Lithofacies 2 (LF2)

Lithofacies 2 comprises bluish-grey and brown, firm to very stiff, sandy, gravelly clay and silt with occasional cobbles. Gravel is fine to coarse, sub-angular to well-rounded and includes white and grey chalk, grey and pink chatter-marked flint, grey sandstone, grey, weathered yellow limestone, ironstone, purple sandstone and quartzite. Jurassic fossils are common and include thick-shelled *Gryphaea dilatata* and occasional serpulid worms including *Pentacrinus*. Chalk gravel is seen to split easily into multiple sections, splitting along wavy planes of weakness.

Lithofacies 3 (LF3)

Lithofacies 3 comprises variably interbedded and interlaminated sand, silt and clay with rare gravel. It is divided into two sub-facies LF3a and LF3b. LF3a comprises light brown and grey, thickly-interlaminated and cross-laminated very silty, fine sand becoming clayey towards the top. The sand is 70% grey quartz, 20% white chalk and 10% lithics.

LF3b comprises grey, brown and greyish-brown, stiff to very stiff, thickly-interlaminated and interbedded to massive clay, silt and sandy silt with interbedded fine sand and some lenses of gravel. Silt and clay tends to be grey and sand tends to be brown or greyish- and reddish-brown. Where the LF3b includes interbeds of sand, repeated couplets of sand grading upwards into silt and sandy silt are common. Micro-scale normal and reverse are common with throws upto 50 mm. In places, sandy silt beds are brecciated forming micro-scale ‘boudins’. This facies passes westwards into interlaminated clay/silt and sandy silt with fine sand. Thin beds and lenses of bluish-grey till with common fine gravel and coarse sand of chalk are common.

LF4 and LF5 as observed in Buckingham Sand Pit and Stowe respectively, were not observed here.

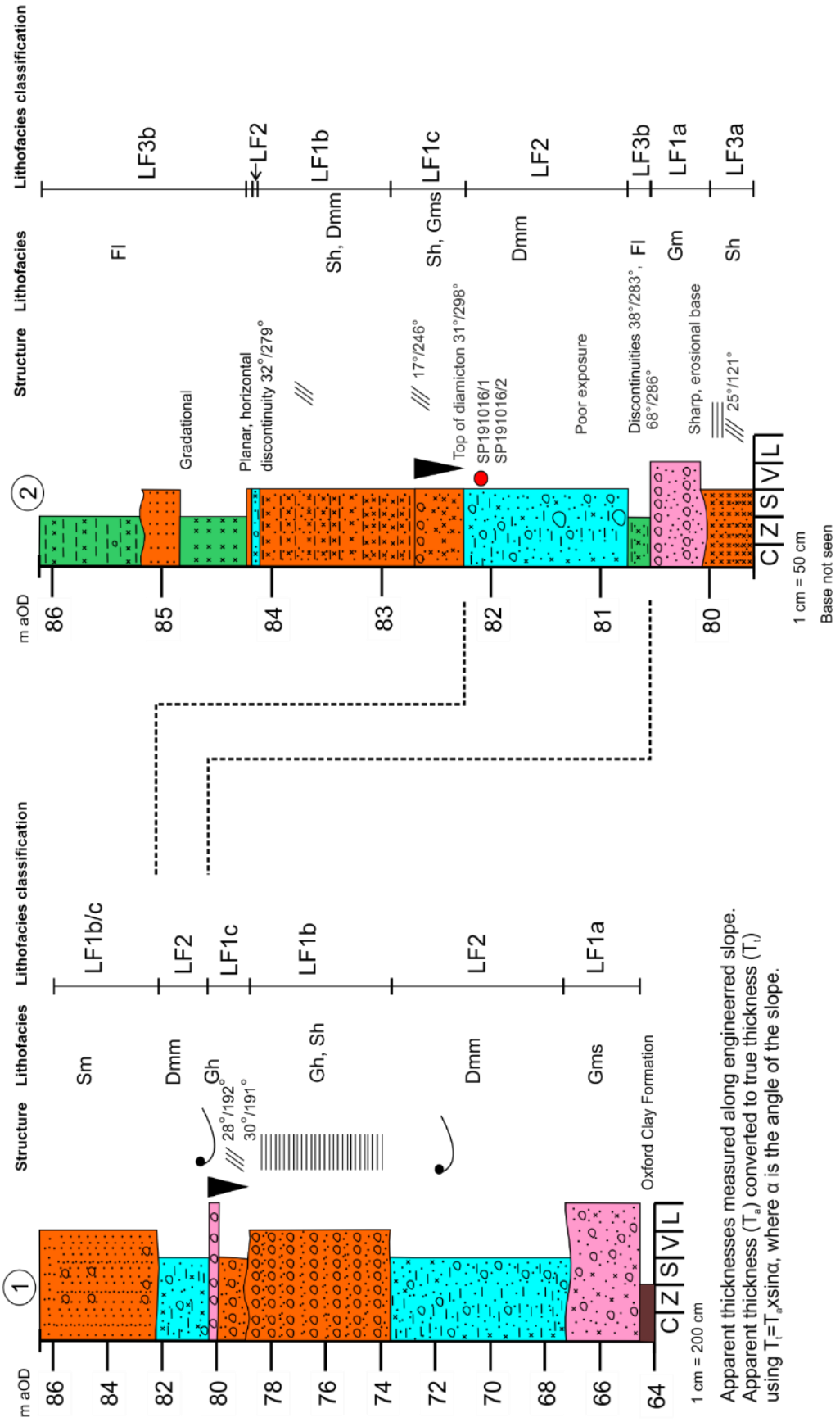

Figure 8-70 Sedimentary graphical logs 1 and 2, Bletchley. Refer to Appendix 13.1 for legend.

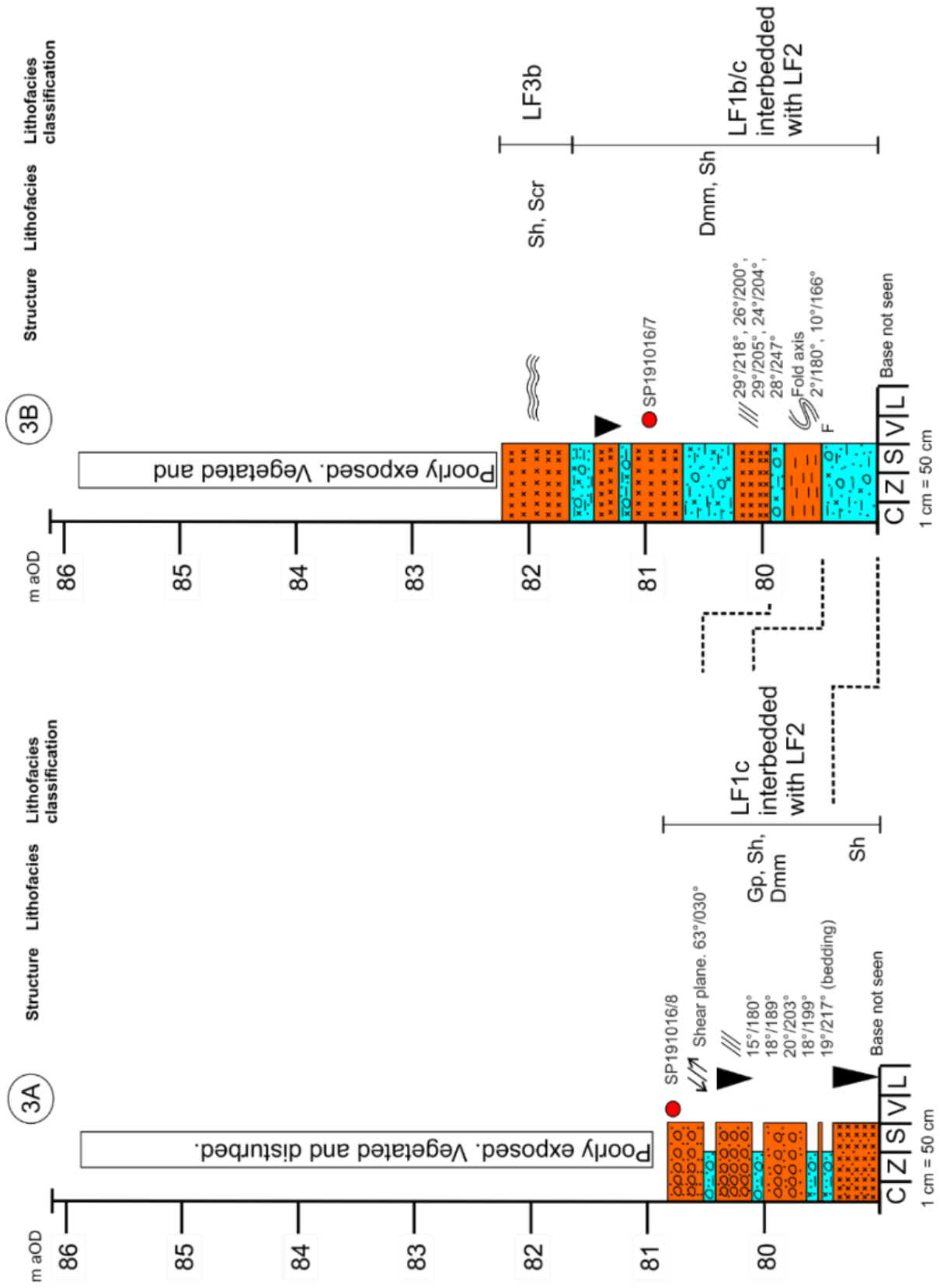

Figure 8-71 Sedimentary graphical logs 3A and 3B, Bletchley. Refer to Appendix 13.1 for legend.

Figure 8-72 Sedimentary graphical logs 4 and 5, Bletchley. Refer to Appendix 13.1 for legend.

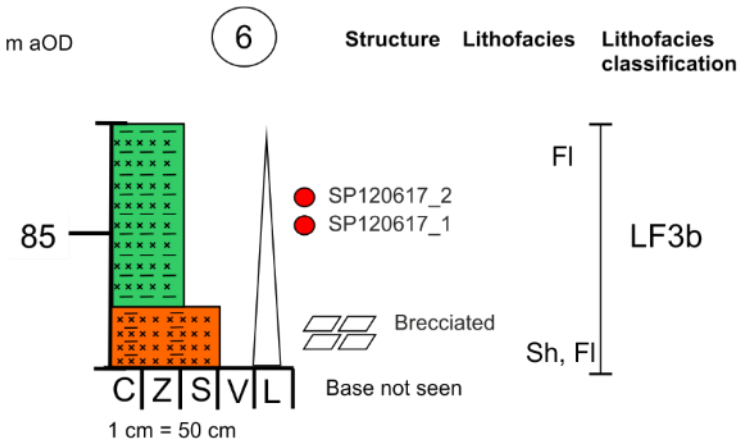

Figure 8-73 Sedimentary log 6, Bletchley. Refer to Appendix 13.1 for legend.

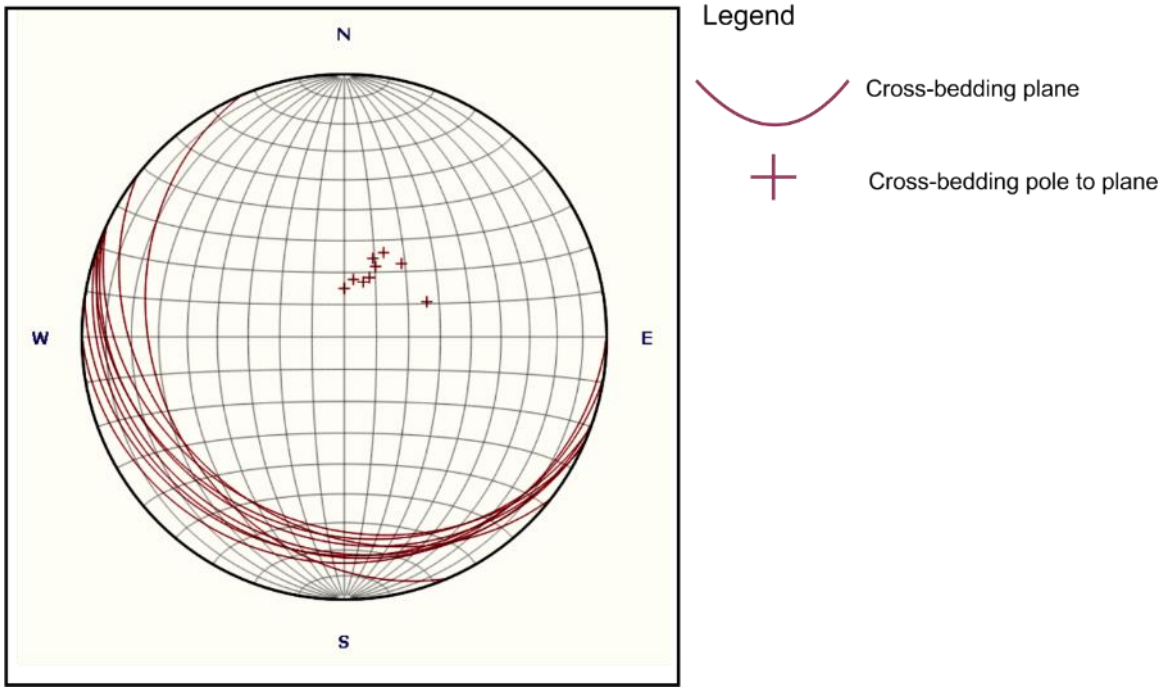

Figure 8-74 Orientation of cross-bedding, LF1b/c, Bletchley.

Figure 8-75 Lithofacies associations 1, Bletchley. A), B) and C) Hand-dug boundary between weathered Oxford Clay and LF1a on engineered landfill slope. D) Laminated and cross-laminated sand overlain by gravel and till.

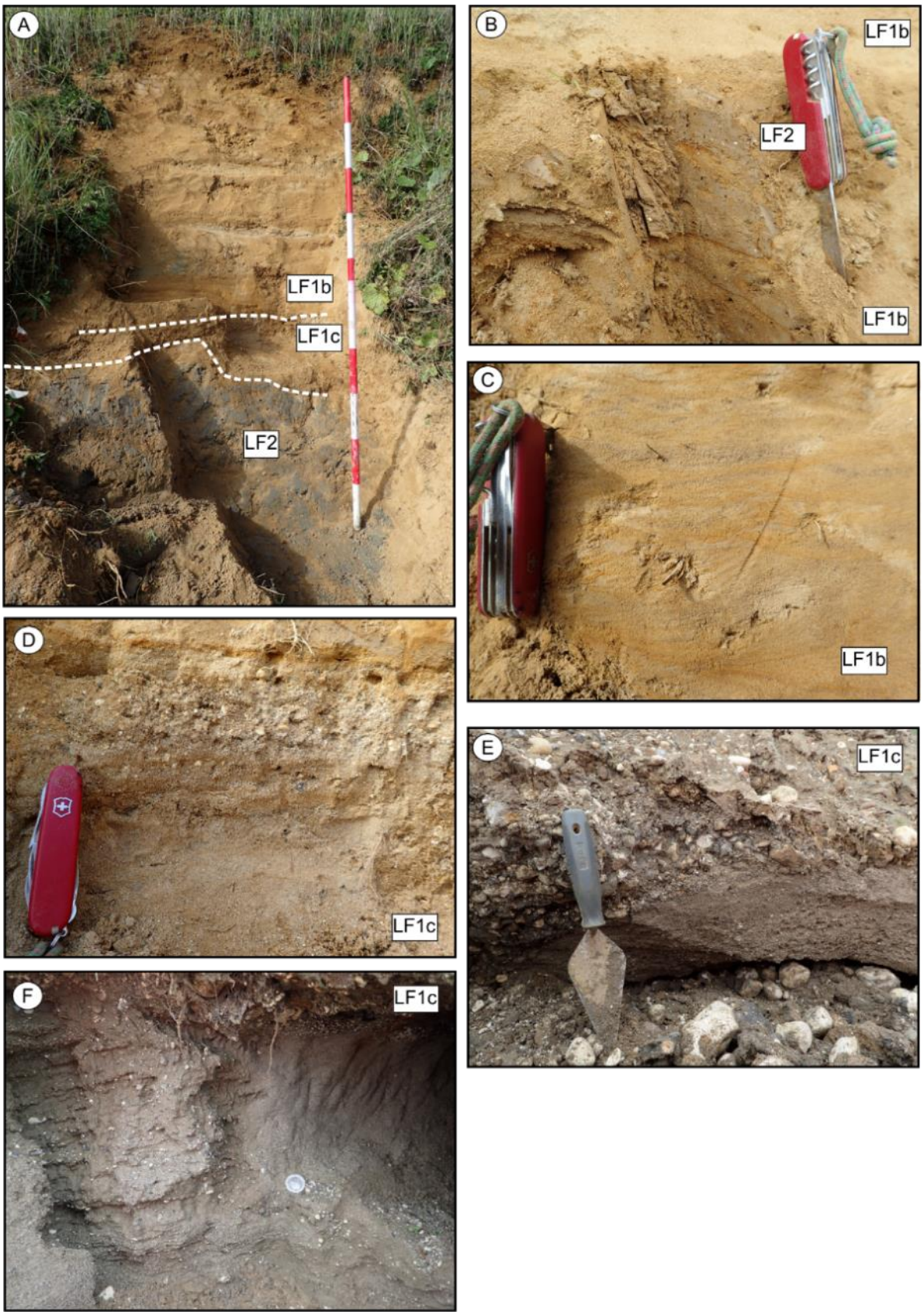

Figure 8-76 Lithofacies associations 2, Bletchley. A) and B) Stratified and interbedded grey till and laminated sand. C) Ripple-laminated sand. D) Thinly- cross-bedded coarse sand. E) and F) Cross-bedded coarse sand and sandy gravel.

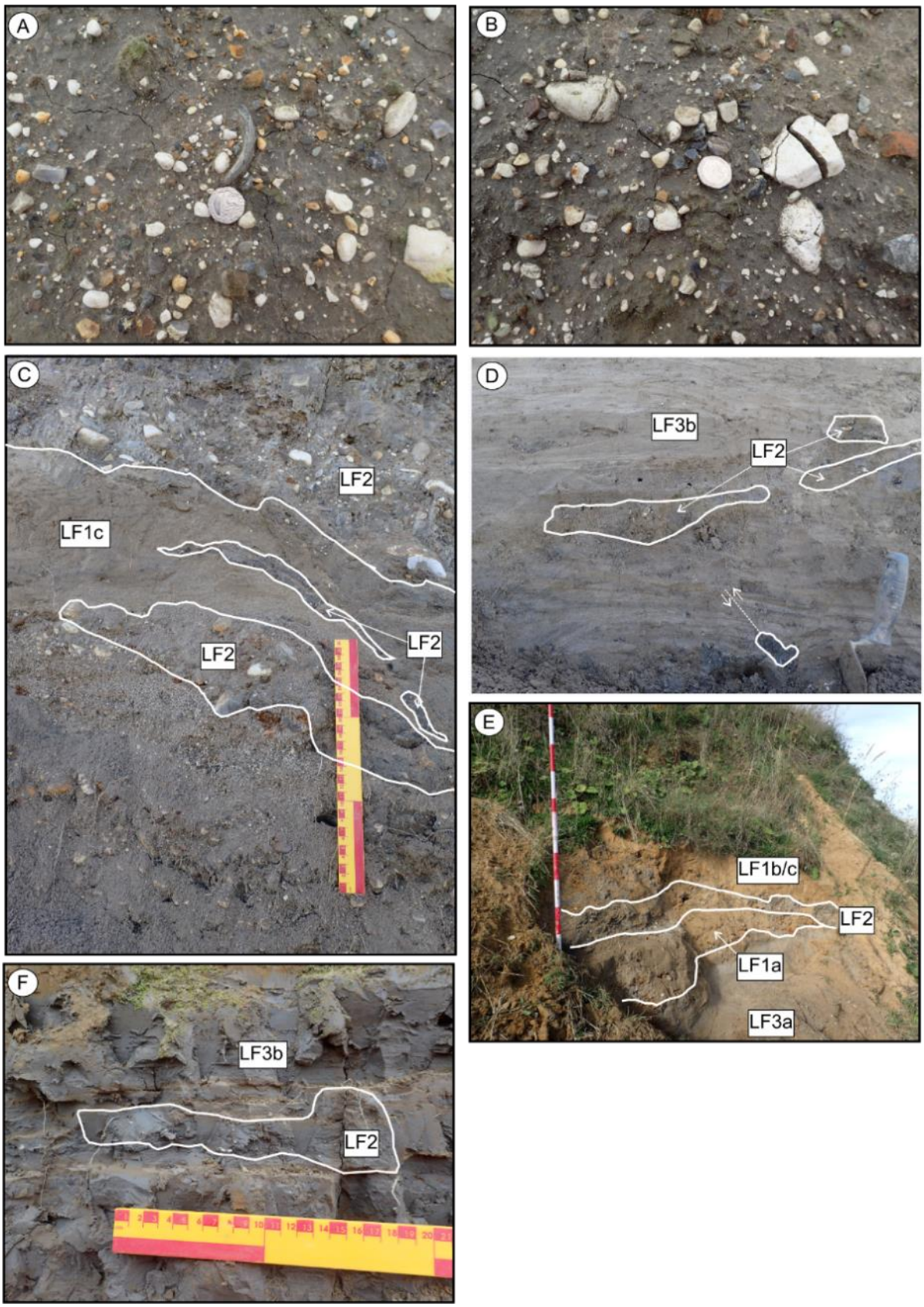

Figure 8-77 Lithofacies associations 3, Bletchley. A) Thick-shelled *Grpyphaea*. B) Frost-wedging in rounded chalk clasts. C) and D) Stratified till and sandy gravel becoming less persistent upwards to F) with laminated silt and clay. E) stratified till overlain by medium to coarse sand.

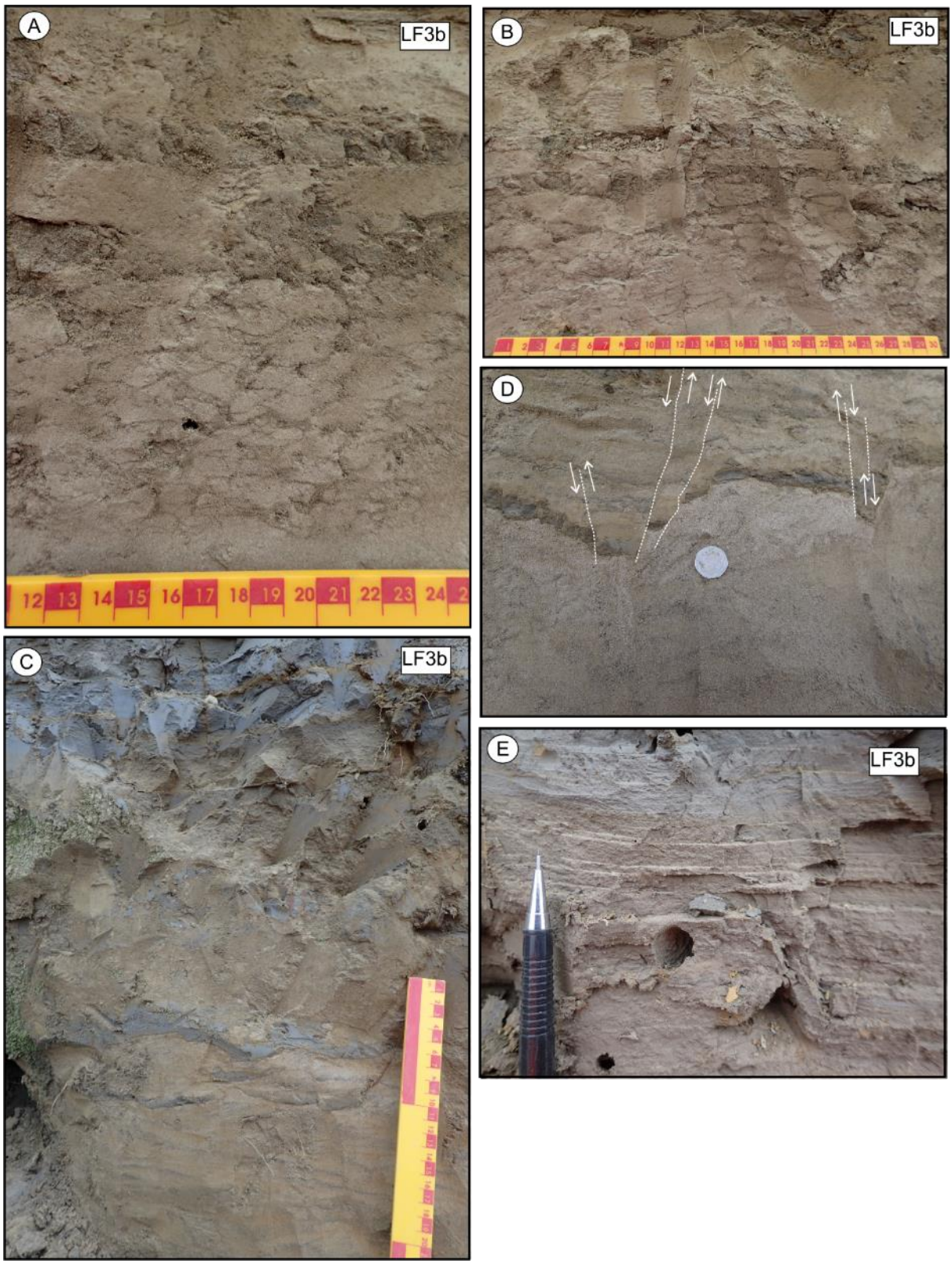

Figure 8-78 Lithofacies associations 4, Bletchley. A) and B) Brecciated silty sand. C) Fining-upwards sequence from sand with folded lenses (involutions?) of silt to laminated silt and clay. D) Micro-faulted silt lens. E) Laminated silt.

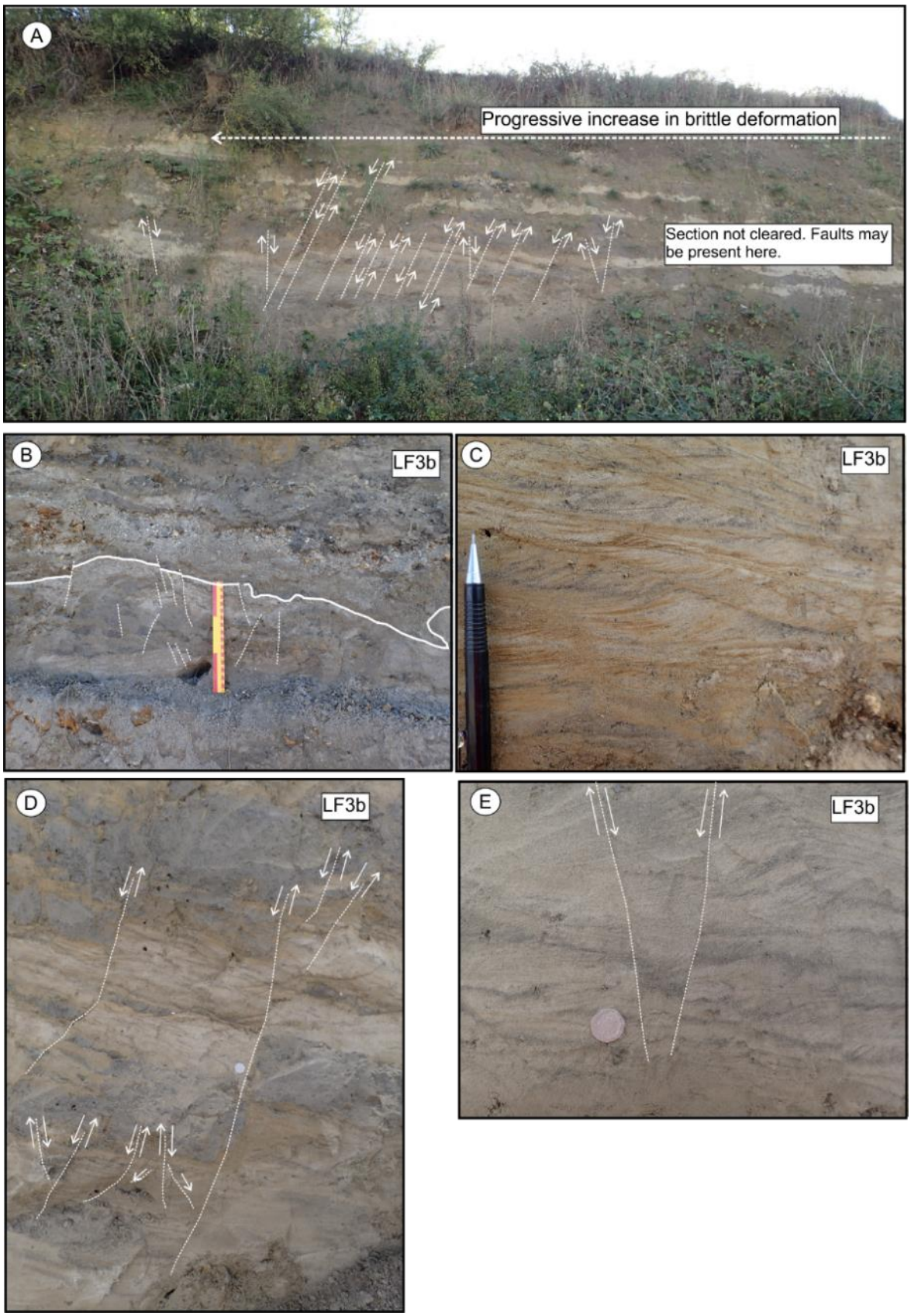

Figure 8-79 Lithofacies associations 5, Bletchley. A) Outcrop view of micro-faulting. Fault dipping towards the east. B) Stratified silt and sand with lenses of till and gravel. C) Climbing ripples. D) and E) Normal micro-faults.

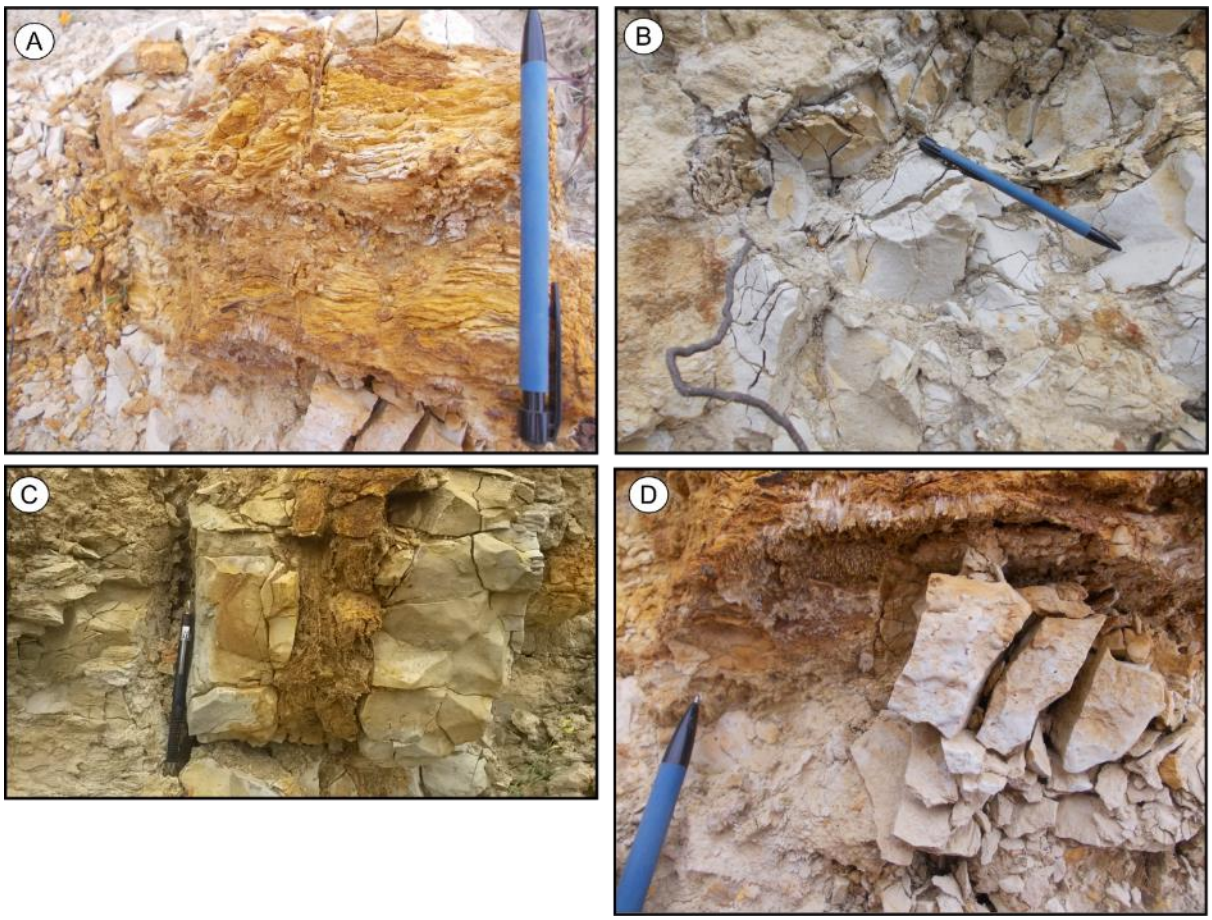

Figure 8-80 Interpreted periglacial features within the Oxford Clay, Bletchley. A) Laminated silty-sand joint infill with micro-cracking. B) Brecciation of *Acutistriatum* Band micritic limestone. C) Vertical joint infill of laminated sand. D) Brecciation of *Acutistriatum* Band micritic limestone with calcite efflorescence?

8.4.1.2 Interpretation

The sequence overlying weathered Oxford Clay is interpreted to represent a glacigenic succession of outwash and glacier ice-proximal, stratified glaciolacustrine sediments including subaquatic tills (undermelt till).

Immediately overlying the Oxford Clay, sandy gravel may represent pre-glacial fluvial outwash or glaciofluvial outwash associated with a glacial event that deposited till between 68 and 74 m aOD. This lower till is overlain by sand and stratified till and interbedded clast-supported, massive to planar cross-bedded gravel and sandy gravel. Evidence from cross-bedding suggests that flow was towards the southeast. Ripple lamination indicates periods of depositions in shallow water. Till becomes more common towards the top of the latter sequence. The presence of stratified till becoming more persistent upwards is taken as evidence of deposition in an ice-proximal position into a pro-glacial lake followed by subsequent overriding by glacier ice. The till is interpreted to be undermelt till (Giles *et al.*,

2017), deposited from melting ice which may have floated locally on the lake forming an ice-shelf.

The sequence fines upwards so that stratified undermelt till becomes less common and laminated silt and clay with thin sand beds (rhythmites) dominate. Laterally impersistant lenses of chalk-rich till occur and indicate proximity of the proglacial lake to a probably, northward-retreating ice-margin.

Evidence of subsequent periglacial weathering is present in the form of frost-wedging of chalk clasts within till, brecciated silty, glaciolacustrine sand and limestone bedrock and laminated sand infill of joint within limestone.

Micro-faulting, which increases in intensity from west to east is interpreted to be the result of extension during post-depositional degradation of ground ice.

LF2 is interpreted to be equivalent to the chalk-rich, matrix-supported till Milton Keynes Till Member observed in Passenham and Buckingham Sand Pit (Sections 8.1.1 and 8.2.3 respectively), although the mechanism of deposition differs. LF1 is correlated with the Deanshanger Glaciolacustrine Member. Sediments within LF3 are considered to have been deposited within a glaciolacustrine environment but which post-dates the main phase of glaciation associated with deposition of the Milton Keynes Till Member. This sequence is here named the Bletchley Glaciolacustrine Member. The stratigraphical relationships within the Buckinghamshire Glacigenic Formation remain uncertain however.

8.4.2 Laboratory results

8.4.2.1 Loss-on-ignition (till, Oxford Clay)

Results for loss-on-ignition analysis are shown in Table 8-17. Samples of till and sandy facies within till (n=3) and glaciolacustrine deposits (n=3) are calcareous including values exceeding 30%. The Oxford Clay (n=2) is organic and calcareous with highest values associate with the Weymouth Member.

Sample	Geology	% water	%organic	%$CaCO_3$	% silicate residue
SP191016_7	TILL_SAND	9	1.5	24.6	73.8
SP191016_8	TILL_SAND	4	1.5	33	66.5
SP191016_2	TILL	N/A	3	32.6	64.4
SP120617_1	GLLD	N/A	3.4	36.6	60
SP120617_2	GLLD	N/A	3.4	35.8	60.8
SP070417_3	GLLD	7	2	24.7	73.2
CR021545	OXC_WEY	N/A	5.2	21	73.9

180815_SPRICE_2	OXC_PET	N/A	10.4	10.9	78.7

Table 8-17 Loss-on-ignition (LOI), all specimens, Quaternary Domain 1.3.1. N/A denotes gravimetric water content measured as part of Atterberg, 1D consolidation or triaxial analysis. Definitions of geological abbreviations given in Table 7-2.

8.4.2.2 Clay mineral XRD (till, Oxford Clay)

Diffractograms from the analysis of orientated, aggregate specimens are presented in Figure 8-81 for till and the Oxford Clay. The identification of clay minerals followed the procedure described in Section 8.1.2.2.

Strong, narrow peaks are seen in the diffractograms associated with clay minerals characterised by illite (mica), kaolinite (with minor or trace amounts of chlorite?) and chlorite for till and Oxford Clay specimens. Illite forms a mixed layer assemblage with collapsible clay minerals of unknown composition. Kaolinite is characterised by peak intensity reduction or loss on heating to 550ºC. Non-clay minerals are poorly defined but probably include quartz (4.35 Å), gypsum and carbonate.

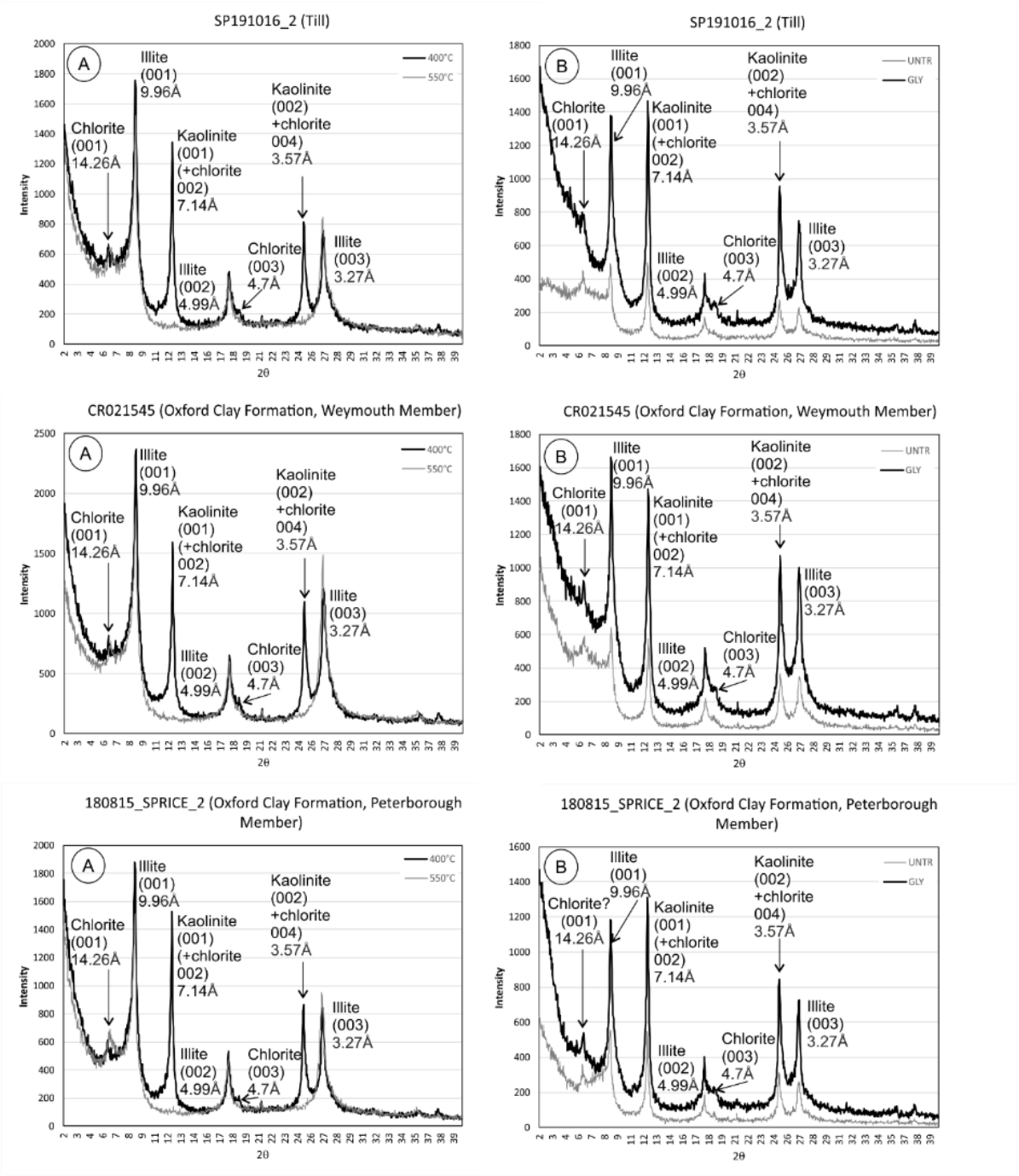

Figure 8-81 Clay mineral XRD, till (SP191016_2) and Oxford Clay, Quaternary Domain 1.3.1. A) Heat treated at 400ºC and 550ºC. B) Air dried, untreated (untr) and glycolated (gly).

8.4.2.3 Particle-size analysis (PSA), (till, Oxford Clay)

The results of particle-size analysis are plotted as percentage passing (finer) – log particle-size plots (Figure 8-82 and 8-83) for specimens of till, glaciolacustrine deposits and Oxford Clay. The grading characteristics and classification of each specimen are summarised in Table 8-18. The coefficient of uniformity and the coefficient of curvature were calculated using the method described in Section 8.1.4.

Sample	Geology	Method[1]	Lithological Description[2]	Sample grading[3]	C_u	C_z
SP191016_7	TILL_SAND	WS	Very clayey/silty, SAND	N/A	N/A	N/A
SP191016_8	TILL_SAND	WS	Slightly clayey/silty, gravelly, SAND	Poorly-graded	3.444	0.806
SP191016_2	TILL	LPSA + WS	Slightly gravelly, slightly clayey, slightly sandy, SILT	Poorly-graded	11.5	0.783
SP120617_1	GLLD	LPSA	Slightly clayey, slightly sandy, SILT	Well-graded	6.667	1.350
SP120617_2	GLLD	LPSA	Slightly sandy, slightly clayey SILT	Well-graded	8.0	1.531
SP070417_3	GLLD	LPSA	Silty, SAND	Well-graded	4.0	1.563
CR021545	OXC_WEY	LPSA	Slightly clayey, SILT	Poorly-graded	5.0	0..8
180815_SPRICE_2	OXC_PET	LPSA	Slightly sandy, slightly clayey, SILT	Well-graded	15.0	1.667

Table 8-18 PSA summary for all geological units in Quaternary Domain 1.3.1. [1]LPSA – Laser Particle-Size Analysis, WS – wet sieving**.** [2]Based on proportions by mass from PSA following conventions in British Standards BS5930:1999 with Amendment 2 (British Standards Institution, 1999). [3]Geotechnical terminology.

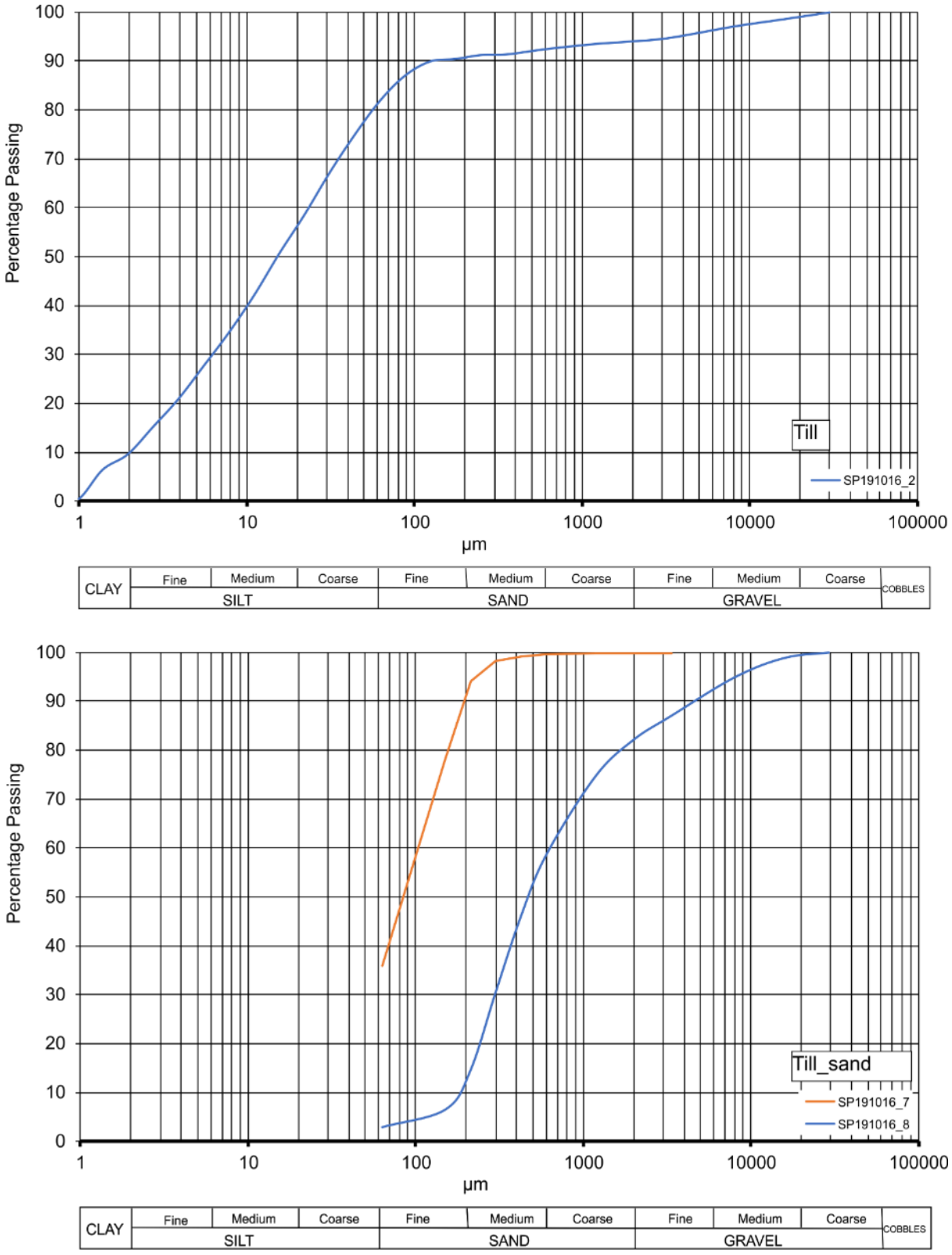

Figure 8-82 Particle-size grading curves Quaternary Domain 1.3.1, till and sandy facies within till (Till_sand).

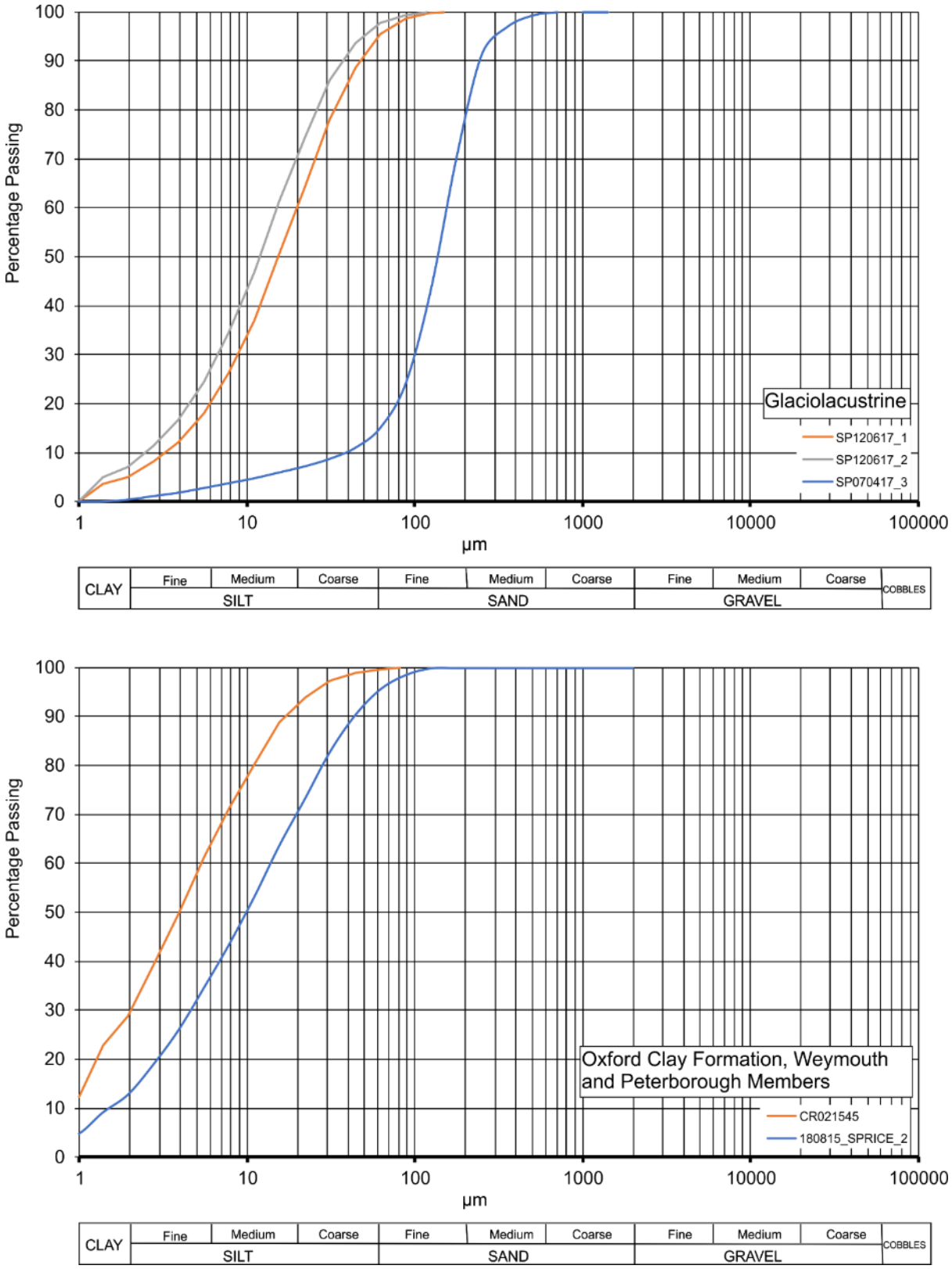

Figure 8-83 Particle-size grading curves Quaternary Domain 1.3.1, Oxford Clay and glaciolacustrine deposits.

Till is poorly-graded and comprises ~90% particles finer than fine sand. Glaciolacustrine sediments are well-graded and are clayey, sandy silts and silty sands. Sandy facies within till is gravelly sand. The Oxford Clay is a slightly sandy, clayey silt.

8.4.2.4 Atterberg limits and moisture content (till, Oxford Clay)

The results of Atterberg limit determinations, including moisture content, are shown in Table 8-19 for till, glaciolacustrine deposits and specimens of Oxford Clay. The results are plotted on a conventional liquid limit-plasticity index chart in Figures 8-84 and 8-85. Supporting data for the calculation of liquid limit, plastic limit and moisture content is given in Appendix 13.2.

Sample	Geology	Liquid Limit (W_L)	Plastic Limit (W_P)	Plasticity Index (I_p)	Moisture content (%)	Liquidity Index (LI)[1]	Activity[2]
SP191016_2	TILL	29	16	13	15	-0.07	1.3(A)
SP120617_1	GLLD	F	NP	N/A	28	N/A	N/A
SP120617_2	GLLD	34	NP	N/A	27	N/A	N/A
CR021545	OXC_WEY	63	22	41	23	0.02	1.4(A)
180815_SPRICE_2	OXC_PET	68	28	33	20	-0.24	2.5(A)

Table 8-19 Atterberg limits, moisture content and activity, Quaternary Domain 1.3.1. [1]Calculated from (ω-W_P/I_p). [2]Calculated based on I_p/%clay fraction (0.002mm), where %clay was determined by LPSA. Activity classes I (inactive), N (normal) and A (active) after Skempton (1953). F – failed to successfully measure liquid limit because of strong dilatancy in sample preparation. NP – not plastic.

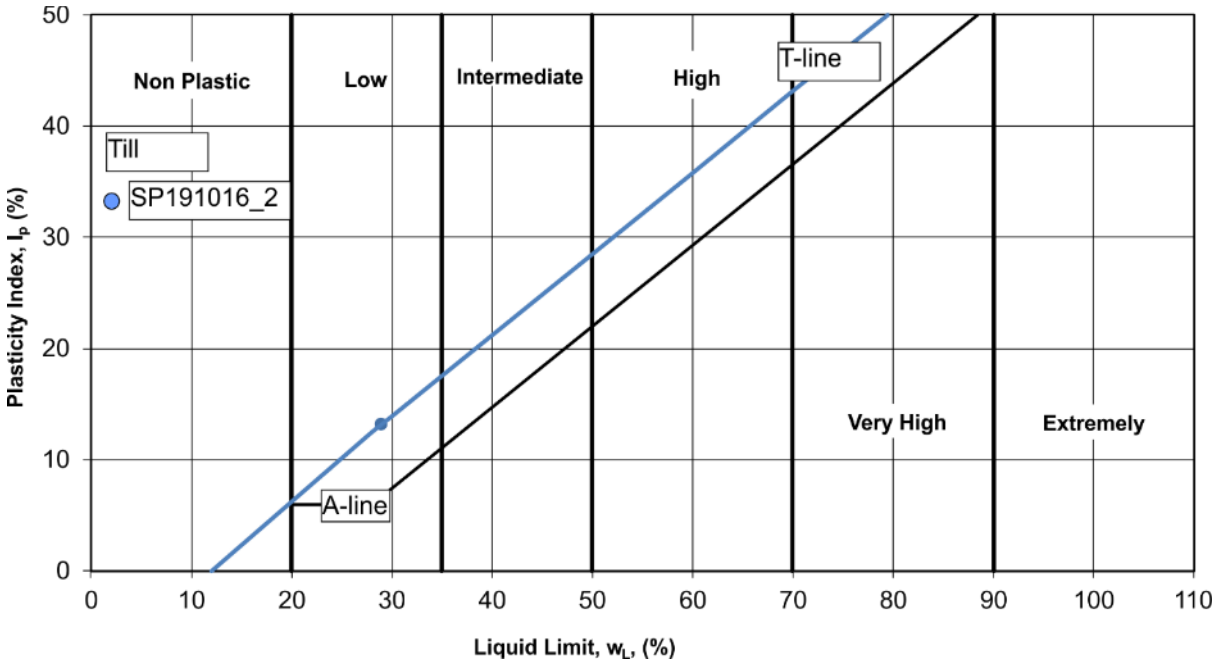

Figure 8-84 Plasticity plot for till, Quaternary Domain 1.3.1. T-line for tills from Boulton & Paul (1976).

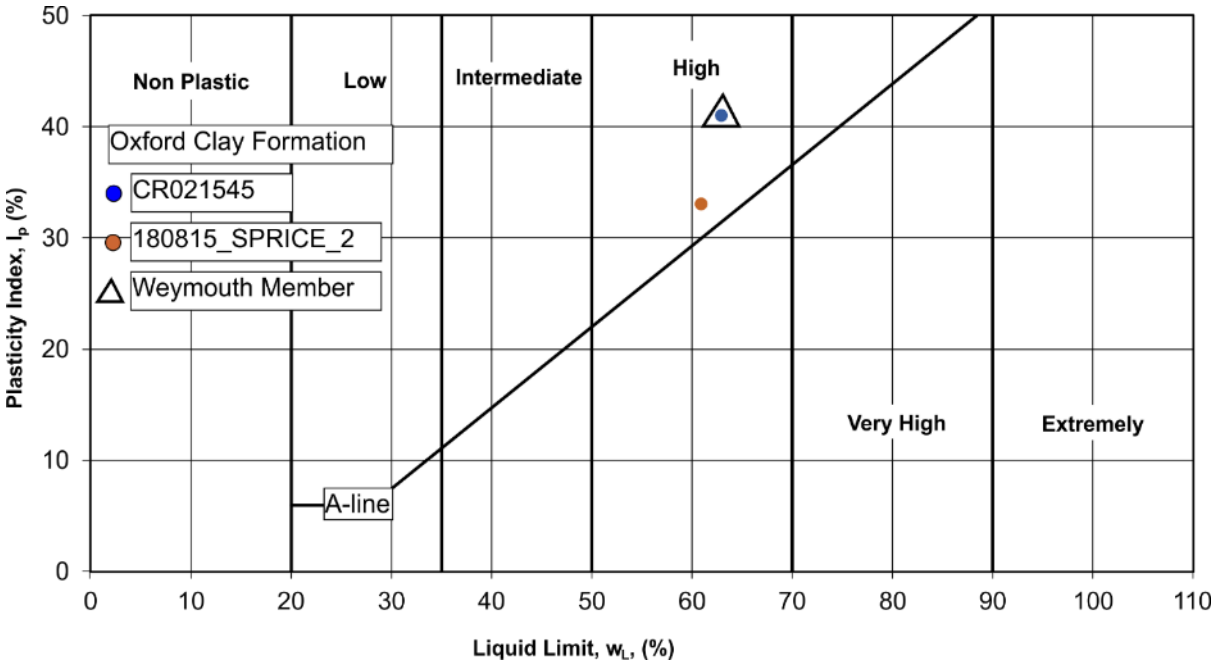

Figure 8-85 Plasticity plot for Oxford Clay, Peterborough and Weymouth (open triangle) members. Quaternary Domain 1.3.1.

In common with till in Domain 1.2.1, its plasticity is low, plotting on the T-line of Boulton & Paul (1976). The Oxford Clay is high plasticity in common with specimens from Domain 1.3. Measured moisture content values are at or below the plastic limit, giving values for LI at or below 0.

8.4.2.5 Particle density (Oxford Clay)

The results of the small pyknometer determination of particle density are given in Appendix 13.3. The value determined for specimens from the Oxford Clay is 2.63 Mg/m^3. This value is within the range determined for equivalent specimens in Domain 1.3.

8.4.2.6 1D consolidation (Oxford Clay)

The experimental results for 1D consolidation of Oxford Clay specimen CR021545 are shown in Figure 8-86 and the initial and final specimen conditions given in Appendix 13.4. There were no specimens of till available for 1D consolidation analysis for this Domain. The calculation of compressibility parameters follows that given in Section 8.3.2.6.

The coefficient of volume compressibility (m_v) decreases from 0.092 to 0.019 m^2/MN with increasing applied stress from 500 kPa. An initial swelling pressure of 116 kPa was recorded before the first loading stage. At an applied stress of 500 kPa, the value for m_v was 0.092 m^2/MN which is within the range for equivalent specimens in Domain 1.3. The specimen is classified as low compressibility (after Head & Epps, 2011).

The coefficient of compressibility, c_v, decreases with increasing applied stress to 1000 kPa where it increases from 1.23 to 1.38 m^2/yr before decreasing again to 0.66m^2/yr at 300 kPa. Referring to c_v calculated from the maximum estimated value of consolidation at t_{50}, the value at the 500 kPa stress increment is 1.55 m^2/yr which is within the range for specimens of Oxford Clay in Domain 1.3. 1.55m^2/yr is slightly higher than that expected for high plasticity clays (after Head & Epps, 2011).

The estimated compression ratios for initial, primary and secondary compression are shown in Table 8-20.

	CR021545		
Stress increment	**r_o**	**r_p**	**r_s**
62.5 (kPa)	NA	NA	NA
125 (kPa)	NA	NA	NA
250 (kPa)	0.11	0.84	0.05
500 (kPa)	0.07	0.88	0.06
1000 (kPa)	0.06	0.88	0.07
2000 (kPa)	0.01	0.90	0.09
3000 (kPa)	0.03	0.80	0.17

Table 8-20 Estimated initial, primary and secondary compression ratios for Oxford Clay, Domain 1.3.1.

Between 80% and 90% consolidation is related to the primary phase of consolidation, which is independent of applied stress. The highest value for r_s is at the 3000 kPa stress increment. Values for secondary compression, C_{sec}, are shown in Table 8-21 where values are seen to be comparable with those in Domain 1.3.

	Stress increment						
Specimen	**62.5 (kPa)**	**125 (kPa)**	**250 (kPa)**	**500 (kPa)**	**1000 (kPa)**	**2000 (kPa)**	**3000 (kPa)**
CR021545	NA	NA	0.0009	0.0014	0.0016	0.0024	0.0021

Table 8-21 Coefficient of secondary consolidation for Oxford Clay, Domain 1.3..1. NA – stage not recorded as swell pressure exceeded stress increment.

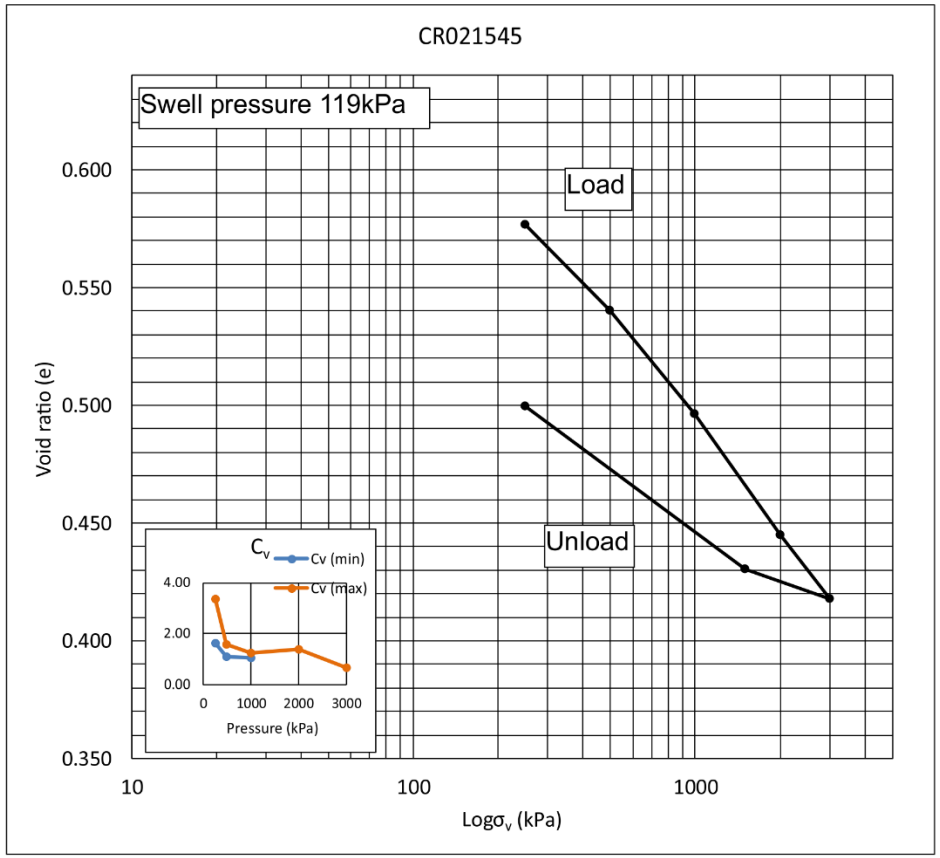

Figure 8-86 1D consolidation results for specimen CR021545, Oxford Clay, Quaternary Domain 1.3.1.

Final moisture content determined after removal from drying oven and consolidation ring. Final dry mass calculated from dry weight of sample and calculated soil mass lost (initial dry weight - final dry weight).

t_{50} maximum not determined graphically for load stages 2.4 and 2.5 as t_{50} max ≈ t_{50} min.

	Voids ratio				Volume compressibility (m_v)				Coeffecient of consolidation (C_v)						
Stage number	Pressure P, (kN/m²)	Settlement ΔH (mm)	Δe= ΔH/H_s (H_s=12.40)	e=e_o.Δe (e_o=0.60)	δe (e_1-e_2)	δp (kN/m²)	1+e_1	m_v= (δe/δp)*((1000)/1+e)) m²/MN	t_{50} (min) Minimum	t_{50} (max) Maximum	H=H_o-ΔH H_o=19.87 (mm)	$\hat{H}$=(H_1+H_2)/2 (mm)	$\hat{H}^2$ mm²	Cv=(0.026*$\hat{H}^2$)/t_{50} (m²/yr) Maximum	Cv=(0.026*$\hat{H}^2$)/t_{50} (m²/yr) Minimum
2.1	250	0.323	0.0261	0.577	0.03	250.0	1.603	0.065	3.00	6.25	19.55	19.71	388	3.37	1.62
2.2	500	0.771	0.0622	0.540	0.04	250	1.577	0.092	6.25	8.75	19.10	19.32	373	1.55	1.11
2.3	1000	1.321	0.1065	0.496	0.04	500	1.540	0.058	7.50	8.75	18.55	18.82	354	1.23	1.05
2.4	2000	1.955	0.1577	0.445	0.05	1000	1.496	0.034	6.25	NA	17.92	18.23	332	1.38	NA
2.5	3000	2.292	0.1849	0.418	0.03	1000	1.445	0.019	12.50	NA	17.58	17.75	315	0.66	NA
2.6	1500	2.134	0.1721	0.430	-0.01	-1500									
2.7	250	1.276	0.1029	0.500	-0.07	-1250									

Oxford Clay specimen CR021545 was added to the e-logσ_v plot for Oxford Clay specimens in Quaternary Domain 1.3 and is seen to plot closet to the densest specimens identified in Domain 1.3.

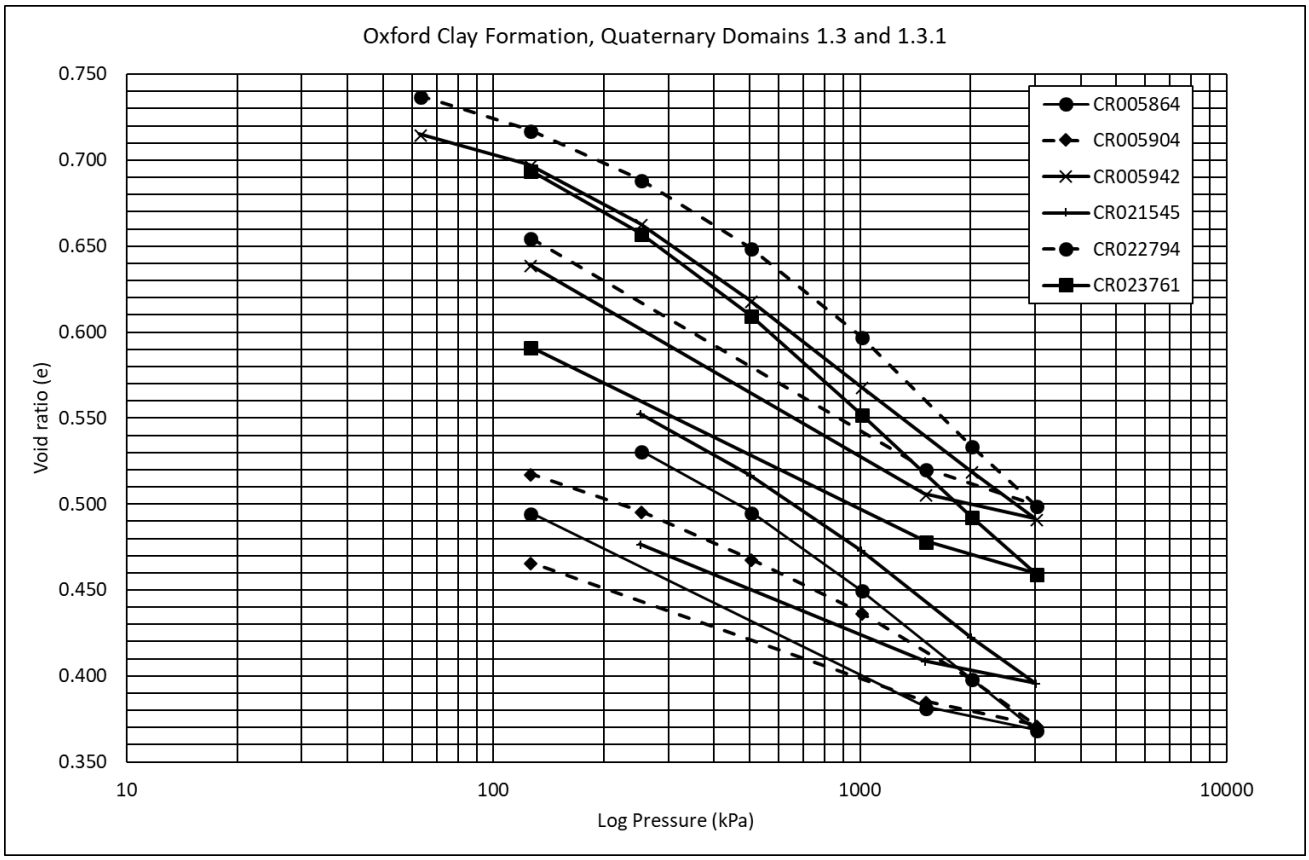

Figure 8-87 Comparison of compressibility for Oxford Clay for all specimens, Domains 1.3 and 1.3.1.

8.4.2.7 Triaxial undrained shear strength and stiffness (Oxford Clay)

One, isotropically consolidated, undrained, multi-stage triaxial tests with measurement of small-strain stiffness using Hall effect sensors was carried out for Oxford Clay specimen CR0121545. The experiment was undertaken in the BGS SPTTS configuration. The results are divided into stress-strain, undrained and mobilised shear strength, effective stress paths in p′-q space, isotropic consolidation behaviour and stiffness.

The experimental stress conditions are given in Table 8-22. The initial and final specimen conditions are given Appendix 13.5. Photographic images of the pre- and post-experiment specimen are shown in Figure 8-88.

Specimen	Stage	Cell	Back	Differential

name		pressure (kPa)	pressure (kPa)	(effective) pressure, σ'_o (kPa)
CR021545	Consolidation stage 1	770	570	200
CR021545	Shear stage 1	770	570	200
CR021545	Consolidation stage 2	870	570	300
CR021545	Shear stage 2	870	570	300
CR021545	Consolidation stage 3	970	570	400
CR021545	Shear stage 3	970	570	400

Table 8-22 Summary of triaxial experiment conditions, Oxford Clay, Quaternary Domain 1.3.1.

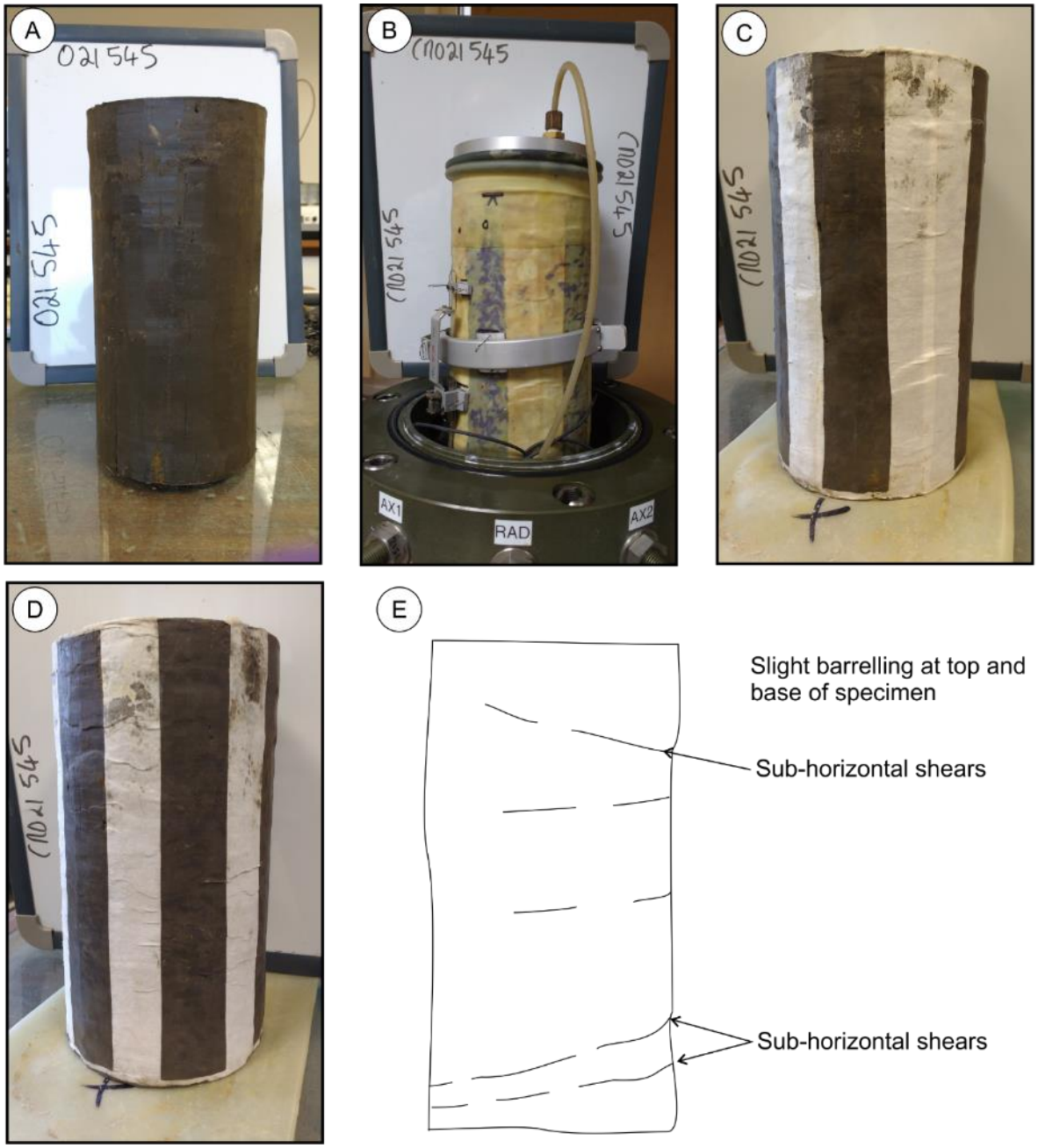

Figure 8-88 Pre- and post-triaxial specimen conditions, specimen CR021545, Oxford Clay, Quaternary Domain 1.3.1. A) Pre-experiment after preparation with soil lathe. B) Post-experiment specimen within triaxial apparatus. C) and D) post-triaxial specimen with membrane removed. Side, top and base drains stuck to specimen. E) Hand sketch interpretation.

8.4.2.8 Stress-strain and mobilised shear strength (Oxford Clay)

The results are plotted as deviator stress *versus* shear strain in Figure 8-89. The experimental parameters and conditions in the triaxial cell are given in Section 7.5.5.

During the final stage of shearing, during which failure was permitted, the specimen exhibits an increase in axial stress with increasing strain. At ~2.5% shear strain, peak deviator stress is reached before strain continues to increase without a further increase in deviator stress.

Estimates of peak undrained shear strength, q_{max} and mobilised strength equal to $0.5q_{max}$ have been estimated following the procedure described in Section 8.3.2.7 and the results are shown in Table 8-23.

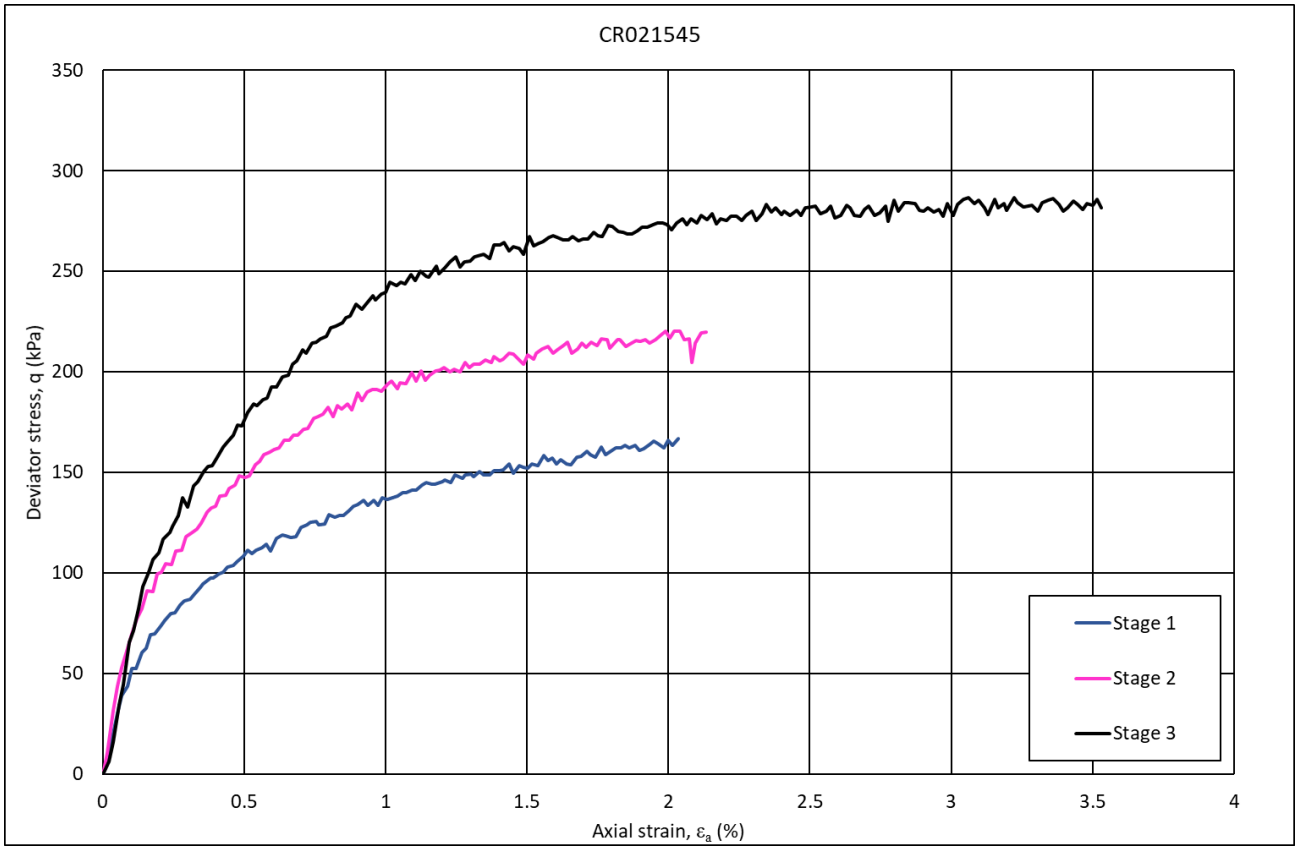

Figure 8-89 Stress-shear strain behaviour for specimen CR021545, Oxford Clay, Quaternary Domain 1.3.1.

						Mobilised strength		Mobilised strain (%)
Specimen	**Geology**	**Specimen**	**Stage 3**	**Stage 3**	**Differential**	**q_{max}**	**$0.5q_{max}$**	**$\varepsilon_{F=2}$**

		depth (mbgl)	cell pressure (σ_3)	back pressure (kPa)	(effective) stress, σ'_o (kPa)	(kPa)	(kPa)	
CR021545	OXC	9.25	970	570	400	282	141	0.32

Table 8-23 Mobilised strength parameters for specimen CR021545, Oxford Clay, Quaternary Domain 1.3.1.

8.4.2.9 Undrained stress path analyses (Oxford Clay)

The results of stress path analyses are shown in Figure 8-90 where deviator stress, q, is plotted against mean effective stress, p′, as described in Section 8.3.8.

The parameters for the effective angle of shearing resistance, ø′, corresponding to two conditions: $ø'_{trans}$ and $ø'_{0.4\%}$ are presented as described in Section 8.3.8.2. Both values represent two conditions so that the critical state value of secant effective angle of shearing resistance will lie between them according to the friction parameter η, and its relationship to the critical state friction parameter M, as described in Section 8.3.2.7.

The ESP for specimen CR021545 deviates to the left, towards the critical state line during the early stages of shearing as pore pressure increases and p′ decreases. On reaching and passing the critical stress ratio, Equation 8-11, Section 8.3.2.7, the ESPs for stages 1, 2 and 3 all show a subsequent deviation to the right, parallel to the critical state line as p′ increases with increasing q. This effect is interpreted to be the result of dilation of the specimen. During stage 3, q is seen to decrease slightly as p′ increases indicating that peak q was reached and that the ESP approached the critical state line.

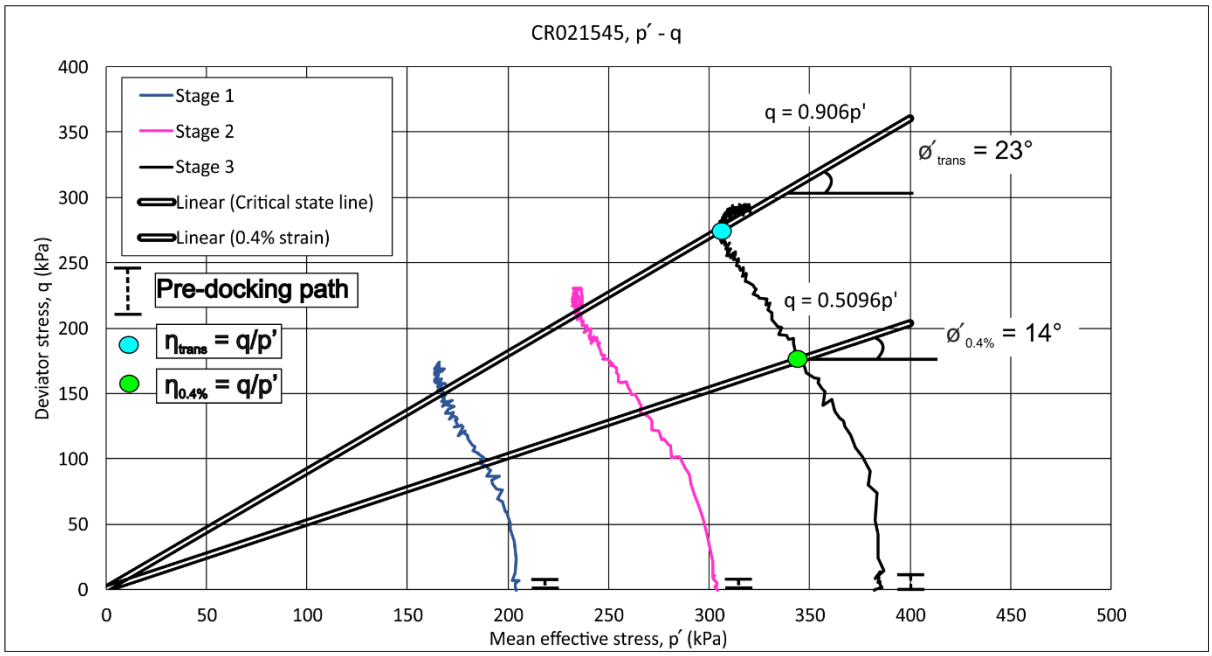

Figure 8-90 Effective tress path analyses for specimen CR021545, Oxford Clay, Quaternary Domain 1.3.1.

8.4.2.10 Isotropic consolidation (Oxford Clay)

The plot of isotropic consolidation before each shearing stage is shown in Figure 8-91 for specimen CR021545 as change in volume (ΔV) *versus* square-root time in seconds. From each plot, estimates were made of the isotropic coefficient of compressibility (c_{vi}).

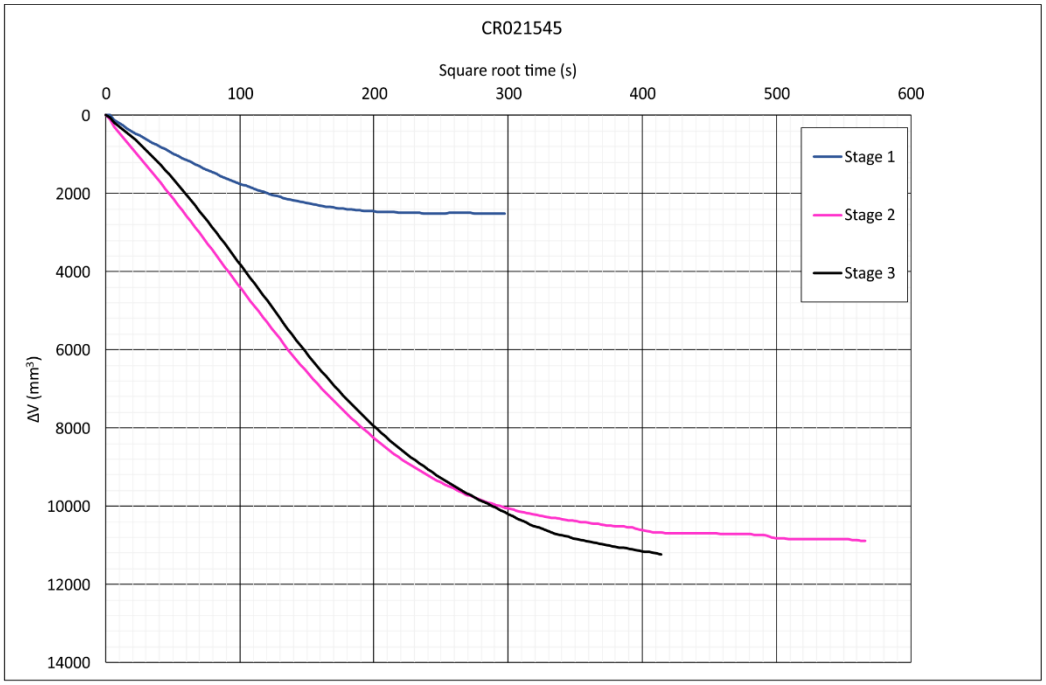

Initial		
Height (mm)	H_o	195.04
Diameter (mm)	D_o	99.05
Mass (g)	M_o	3065.34
Volume	cm^3	1503
Volume	mm^3	1502949
Area	mm^2	7706

Isotropic consolidation

	Stage 1	Stage 2	Stage 3
c_{vi} m^2/yr	16	10	9
t_{90}(min)	3	6	6
Side-drain correction applied (λ=80)			

End consolidation 1		
Height (mm)	H_1	194.93
Diameter (mm)	D_1	99.00
Volume (mm^3)	V_1	1500436
Area (mm^2)	A_1	7697

Change	
Δ_H	0.11
Δ_D	0.06
Δ_V	2513
Δ_A	9

End shear 1		
Height (mm)	H_2	190.96
Diameter (mm)	D_2	100.02
Volume (mm^3)	V_2	1500436
Area (mm^2)	A_2	7857

Change	
Δ_H	3.97
Δ_D	-1.02
Δ_V	0
Δ_A	160

End consolidation 2		
Height (mm)	H_3	190.50
Diameter (mm)	D_3	99.78
Volume (mm^3)	V_3	1489560
Area (mm^2)	A_3	7819

Change	
Δ_H	0.46
Δ_D	0.24
Δ_V	10876
Δ_A	38

End shear 2		
Height (mm)	H_4	186.38
Diameter (mm)	D_4	101.64
Volume (mm^3)	V_4	1489560
Area (mm^2)	A_4	8114

Change	
Δ_H	4.12
Δ_D	-1.86
Δ_V	0
Δ_A	294

End consolidation 3		
Height (mm)	H_5	185.91
Diameter (mm)	D_5	100.62
Volume (mm^3)	V_5	1478315
Area (mm^2)	A_5	8073

Change	
Δ_H	0.47
Δ_D	1.02
Δ_V	11245
Δ_A	41

End shear 3		
Height (mm)	H_5	179.17
Diameter (mm)	D_5	102.50
Volume (mm^3)	V_5	1478315
Area (mm^2)	A_5	8251

Change	
Δ_H	6.74
Δ_D	-1.88
Δ_V	0
Δ_A	178

Figure 8-91 Isotropic consolidation and estimated coefficient of isotropic consolidation (c_{vi}), specimen CR021545, Oxford Clay, Quaternary Domain 1.3.1.

In isotropic consolidation, the magnitude of volume change is low during stage 1 but the coefficient of compressibility is high compared to values at higher effective stresses. At

higher effective stresses, the coefficient of isotropic consolidation decreases but ΔV per increment of time is high compared to the low effective stresses in stage 1. This could be a result of incomplete consolidation during stage 1 or the effects of dilation during shear stage 1.

Values for isotropic coefficient of consolidation (c_{vi}) are upto 10 times larger than values c_v derived from 1D consolidation at effective stresses <200 kPa and ~8 times higher for effective stresses >500 kPa.

8.4.2.11 Stiffness (Oxford Clay)

Estimates of secant stiffness, expressed as Young's modulus derived from axial displacement measurements from the axial displacement transducers of the triaxial apparatus and the mean axial strain from the Hall effect sensors, are summarised in Table 8-24 and shown in Figure 8-92.

	Triaxial apparatus	Hall effect	
	E (MPa), $0.5q_{max}$	E (MPa), $0.5q_{max}$	$E_{0.1\%}$ (MPa)
Specimen			
CR021545	0.44	0.69	1.00

Table 8-24 Estimates of secant stiffness for specimen CR021545, Oxford Clay, Quaternary Domain 1.3.1.

Secant stiffness values compare well with specimens of Oxford Clay in Domain 1.3. at ~9 mbgl where values of 0.46 MPa and 0.43 MPa are estimated for Domains 1.3.1 and 1.3 respectively. This suggests that variation in stiffness may be due to depth-related differences in effective stress.

During shearing, the specimen responded in a similar way in each stage for deviator stresses <300 kPa where stiffness is seen to increase with increasing effective stress. At values of q <170 kPa, in stage 1, the axial strain increases, and the sample shortens parallel to σ_a. At the same time, the sample undergoes an increase in radial strain and dilation parallel to σ_h. Similar behaviour is seen during stage 2 where stiffness increases compared to stage 1 except in the initial part of radial strain <-0.3% where stiffness is greater in the elastic region of specimen shearing, at lower effective stresses.

During stage 3, at q >250 kPa, radial strain becomes increasingly negative indicating that the specimen is dilating in shear with strain exceeding 5%. These results agree with those from the p′-q stress-path results which indicate increasing, followed by decreasing, pore pressure which results in increasing effective stress and dilation at post-peak q failure of the specimen.

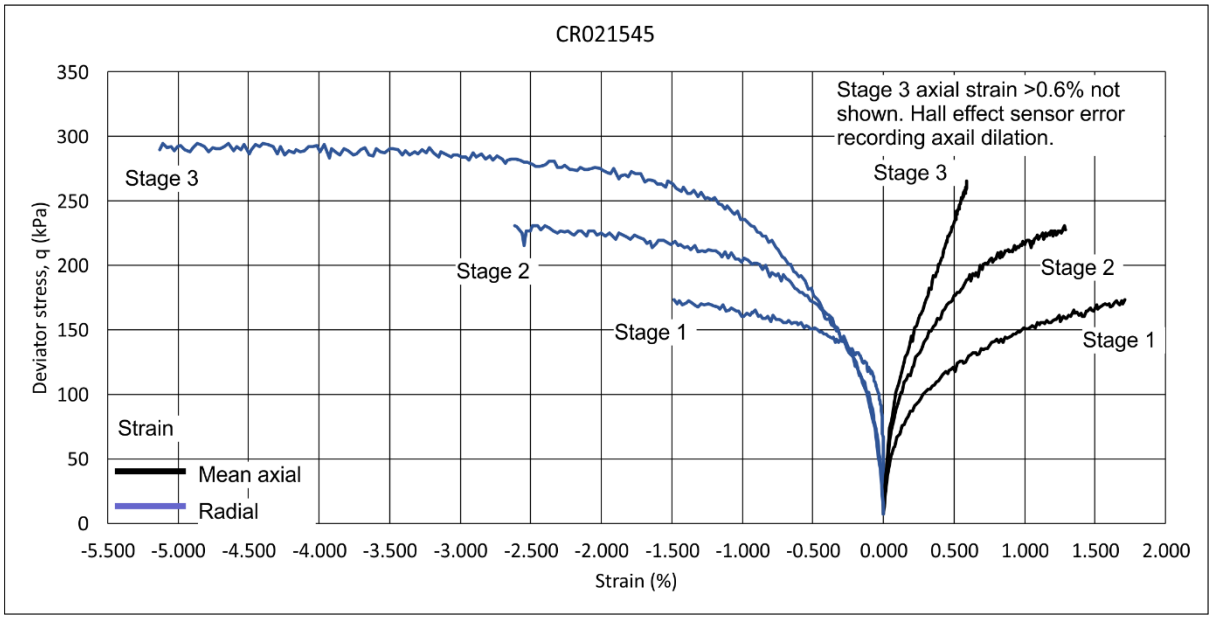

Figure 8-92 Small-strain stiffness measured using Hall effect sensors, specimen CR021545, Oxford Clay, Quaternary Domain 1.3.1.

8.4.3 Summary

Till in Bletchley and surrounding areas in Quaternary Domain 1.3.1 is poorly-graded, calcareous slightly gravelly, slightly clayey, slightly sandy, silt with low plasticity and is active with a value of 1.3. The clay mineral assemblage for till comprises illite, kaolinite (with minor or trace chlorite) and chlorite. ω values are < W_P so LI values are < 0. Sand beds within till comprise poorly-graded, slightly clayey/silty, gravelly, sand and very clayey, silty sand. Glaciolacustrine deposits are well-graded, silty sands which fine up-sequence into well-graded, slightly sandy, slightly clayey silts. The silts are non-plastic. Their clay mineralogy was not measured.

The Peterborough Member was measured as a well-graded, high plasticity, slightly sandy, slightly clayey, silt. However, it is likely that silt-size particles are present as agglomerations of clay as discussed in Section 8.3.9. Sand-size particles may originate from crushed aggregates of aragonite-rich fossil fragments. It is active with a value of 2.5 reflecting its I_p and ~10% clay content. Its clay mineral assemblage includes illite, kaolinite (with minor or trace amounts of chlorite) and chlorite. ω values are <W_P so LI values are <0.

In contrast, the Weymouth Member is a slightly clayey, silt of high plasticity and greater I_p. Its clay mineral assemblage is the same as for the Peterborough Member. It is active a value of 1.4. the lower activity value compared to that for the Peterborough Member is interpreted to be the result of a higher I_p, which compensates for the higher percentage, ~30% of clay-size particles.

The Oxford Clay has low compressibility with values of m_v between 0.092 and 0.019 m^2/MN. Specimen CR021545 groups with the densest specimens from Domain 1.3 when plotted as e *versus* logp.

The mobilised shear strength at $0.5q_{max}$ is 141 kPa with a corresponding mobilised strain, $\varepsilon_{F=2}$ of 0.32. Both values are within the range of values determined for Oxford Clay specimens in Domain 1.3. Values of $ø'_{trans}$ and $ø'_{0.4\%}$ are 23 and 14° respectively. Both values are low in comparison to specimens in Quaternary Domain 1.3, except for specimen CR005942. The effective stress path for specimen CR021545 behaves as an overconsolidated clay. Its reduction in secant strength parameters $ø'_{trans}$ and $ø'_{0.4\%}$ are comparable to specimen CR005842 and it is suggested here that the reduction may be a result of the presence of a sub-glacial shear zone at ~9 mbgl.

Young's modulus, E, at $0.5q_{max}$, measured using the triaxial apparatus axial displacement transducers is 0.44 MPa, within the range of values for specimens in Domain 1.3. E, is 33% higher when measured using Hall effect sensors with a value of 0.69 MPa.

8.5 Quaternary Domain 2.3

Quaternary Domain 2.3 comprises Middle to Late Jurassic mudrocks of the Oxford Clay and mudrocks and sandstone of the Kellaways Formation. This Domain is interpreted to have remained free of glacier ice during Middle Pleistocene glaciations and its Quaternary history is therefore influenced only by multiple phases of periglacial activity. Periglacial deposits in the form of 'head' may be present but are not shown on published 1:50 000 scale geological maps and have not been mapped as part f this research.

Laboratory results are presented for loss-on-ignition (LOI), clay mineralogy, particle-size analysis (PSA), particle density and plasticity for Oxford Clay specimens. 1D consolidation (n=2) and one multi-stage triaxial with measurement of small-strain stiffness were undertaken. Specimens were prepared from UT100 samples taken from the East West rail ground investigation. No field sites were examined in this Domain.

8.5.1 Laboratory results

8.5.1.1 Loss-on-ignition (Oxford Clay)

Results for two specimens from the Oxford Clay are shown in Table 8-25.

Sample	Geology	% water	%organic	%$CaCO_3$	% silicate residue
CR023247	OXC_PET	N/A	4.3	5.9	89.9
CR020746	OXC_PET	N/A	5	6	89

Table 8-25 Loss-on-ignition (LOI), Oxford Clay, Domain 2.3. N/A denotes gravimetric water content measured as part of Atterberg, 1D consolidation or triaxial analysis.

Both samples are slightly organic and calcareous. The percentage of carbonate is low compared to equivalent specimens in Domains 1.3 and 1.3.1.

8.5.1.2 Clay mineral XRD (Oxford Clay)

Diffractograms from the analysis of orientated, aggregate specimens are presented in Figure 8-93. The identification of clay minerals followed the procedure described in Section 8.1.2.2.

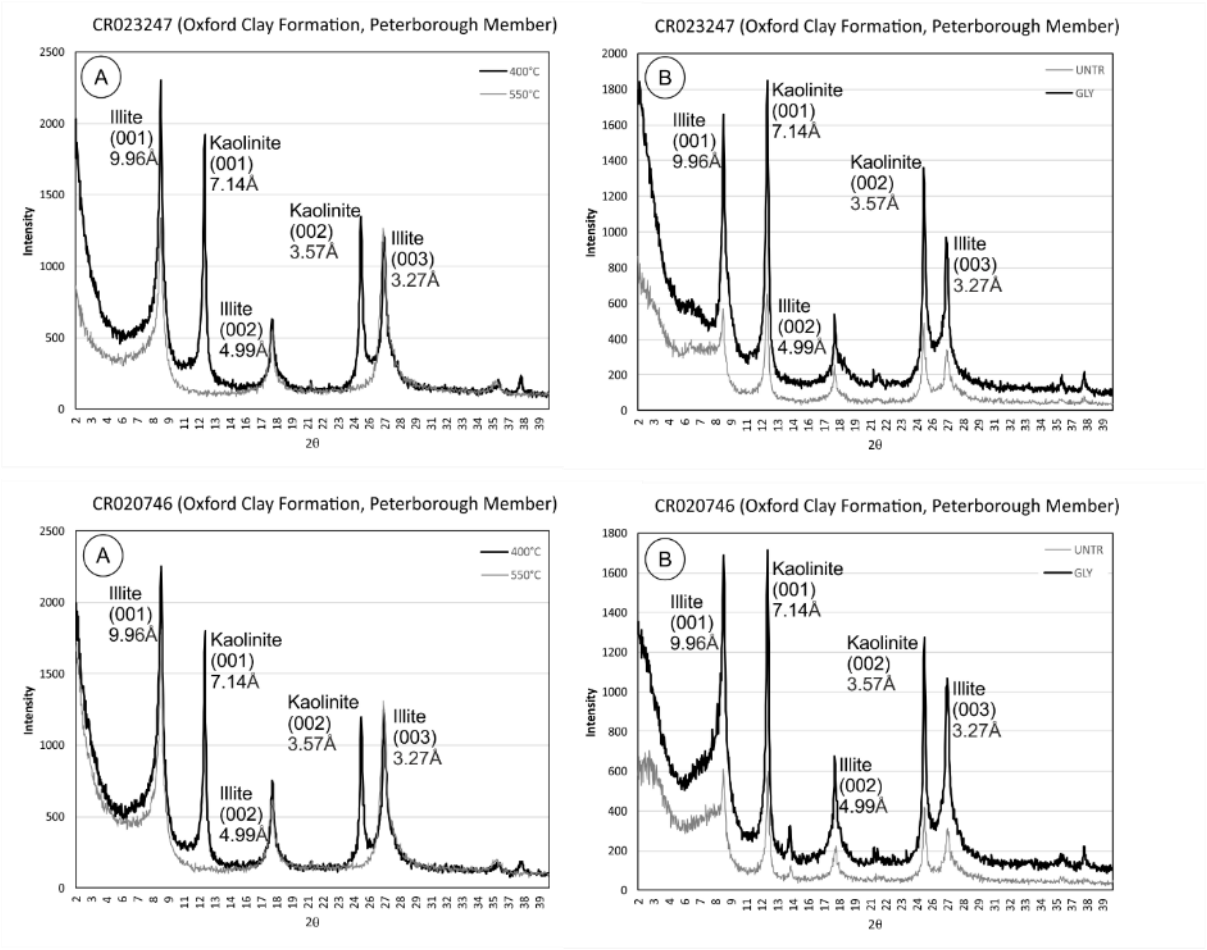

Figure 8-93 Clay mineral XRD for the Oxford Clay, Quaternary Domain 2.3. A) Heat treated at 400ºC and 550ºC. B) Air dried, untreated (untr) and glycolated (gly).

Strong, narrow peaks are seen in the diffractograms associated with clay minerals characterised by illite (mica) and kaolinite (with minor or trace amounts of chlorite?). Illite forms a mixed layer assemblage with collapsible clay minerals of unknown composition. Kaolinite is characterised by peak intensity reduction or loss on heating to 550ºC. Non-clay minerals are poorly defined but probably include quartz (4.35 Å), gypsum and carbonate.

8.5.1.3 Particle-size analysis (PSA), (Oxford Clay)

The results of particle-size analysis are plotted as percentage passing (finer) – log particle-size plots (Figure 8-94). The grading characteristics and classification of each specimen is summarised in Table 8-26. Coefficient of uniformity and coefficient of curvature were calculated using the method described in Section 8.1.4.

Sample	Geology	Method[1]	Lithological	Sample grading[3]	C_u	C_z

			Description[2]			
CR023247	OXC_PET	LPSA	Slightly clayey, SILT	Uniformly-graded	1.8	1.250
CR020746	OXC_PET	LPSA	Clayey SILT	Poorly-graded	3.0	0.333

Table 8-26 PSA summary for Oxford Clay, Domain 2.3. [1]LPSA – Laser Particle-Size Analysis, WS – wet sieving. [2]Based on proportions by mass from PSA following conventions in British Standards BS5930:1999 with Amendment 2 (British Standards Institution, 1999). [3]Geotechnical terminology

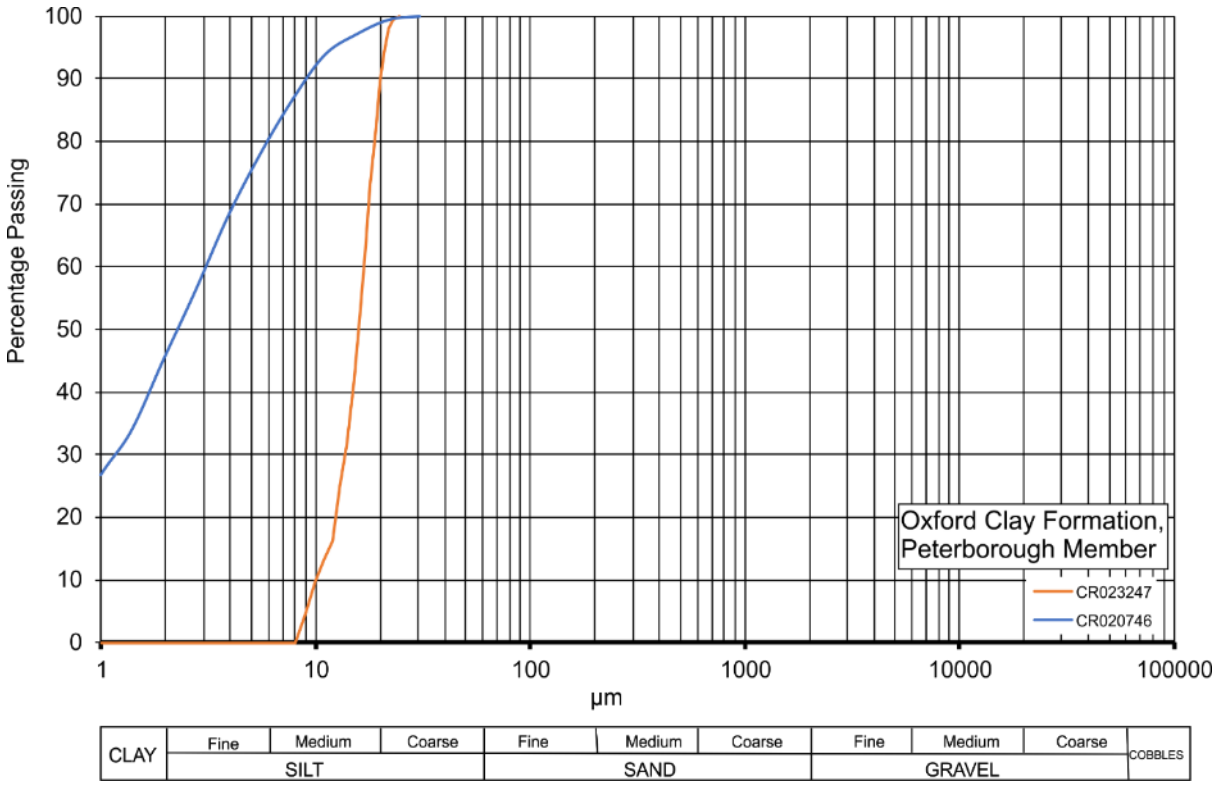

Figure 8-94 Particle-size grading curves Quaternary Domain 2.3, Oxford Clay, Peterborough Member.

Specimens from the Oxford Clay are poorly- to uniformly-graded clayey silt and silt. Clay appears to be absent in specimen CR023247, but it is possible that this reflects silt-grade agglomerations of clay particles as discussed in Section 8.3.4.

8.5.1.4 Atterberg limits and moisture content (Oxford Clay)

The results of Atterberg limit determinations, including moisture content, are shown in Table 8-27. The results are plotted on a conventional liquid limit-plasticity index chart in Figure 8-95. Supporting data for the calculation of liquid limit, plastic limit and moisture content is given in Appendix 13.2.

Sample	Geology	Liquid	Plastic	Plasticity	Moisture	Liquidity	Activity[2]

		Limit (W_L)	Limit (W_P)	Index (I_p)	content (%)	Index (LI)[1]	
CR023247	OXC_PET	60	28	32	43	0.47	1.0(N)
CR020746	OXC_PET	79	28	51	34	0.12	1.1(N)

Table 8-27 Atterberg limits, moisture content and activity, Oxford Clay, Quaternary Domain 2.3. [1]Calculated from (ω-W_P/I_p). [2]Calculated based on I_p/%clay fraction (0.002mm), where %clay was determined by LPSA. Activity classes I (inactive), N (normal) and A (active) after Skempton (1953).

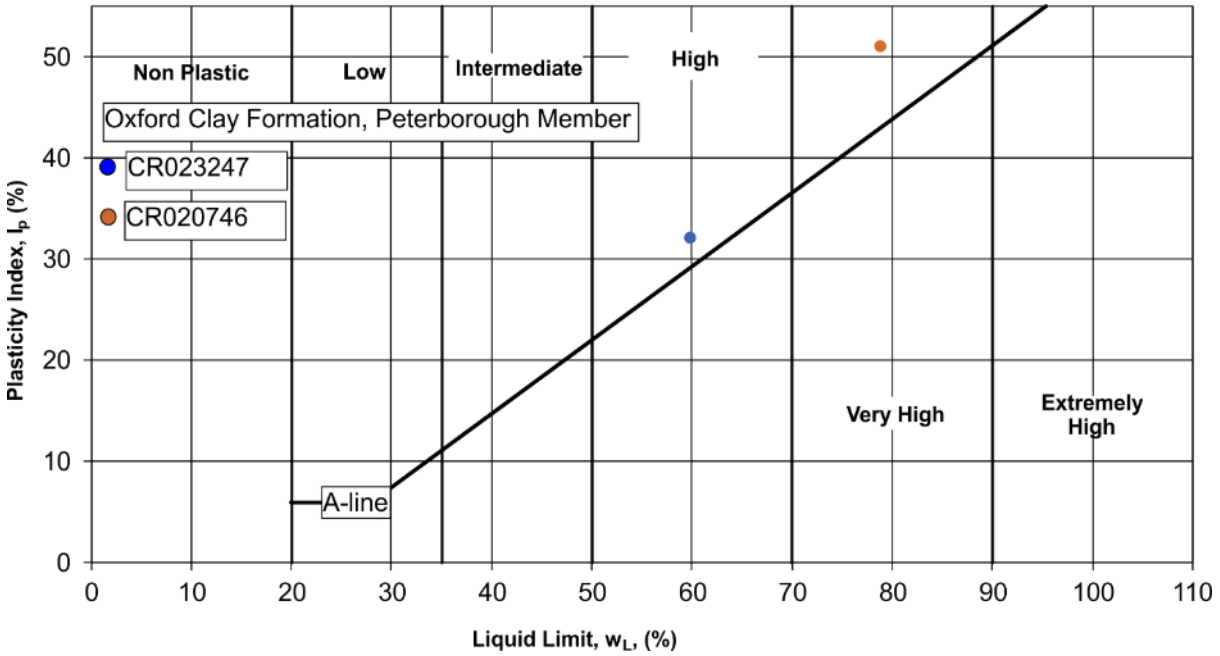

Figure 8-95 Plasticity plot for Oxford Clay, Peterborough Member. Quaternary Domain 2.3.

Both specimens have high to very high plasticity which is comparable with equivalent specimens from the Oxford Clay in Domains 1.3 and 1.3.1.

8.5.1.5 Particle Density (Oxford Clay)

The results from particle density determination using the small pyknometer method are given in Appendix 13.3. Both samples are within the specified tolerance and show a particle density of 2.78 Mg/m^3 which is denser than equivalent samples in Domains 1.3 and 1.3.1.

8.5.1.6 1D consolidation (Oxford Clay)

The methodology described in Section 8.3.2.6 for the analysis of the results from 1D consolidation experiments could not be applied to the results from specimen CR023247. The loading curves plotted as log- and square-root-time did not show prominent consolidation curves relating to initial and primary compression. Therefore, values corresponding to 0% and 100% consolidation and estimates of stress-dependent values of c_v, could not be determined. An example of axial displacement *versus* log-time and square-root time for loading stage increment 500 kPa is shown in Figure 8-96.

From Figure 8-96A it can be seen that there is no clear primary consolidation line and from 8-96B that there is no clear linear portion of the consolidation curve. The curves in Figure 8-96 are interpreted to represent a secondary compression curve and the curve appears to be typical of silt and reference to the particle-size grading curve in Figure 8-94 confirms that the sample is 100% silt. It is interpreted that the initial and primary consolidation parts of the curve were passed before the first reading in the experiment, and before log 0.1 seconds. For the sample thickness of 19.04 mm, the coefficient of consolidation can be approximated as $0.026*19.04^2/0.1 = >90 m^2/yr$.

The equivalent e-logσ_v plot is plotted and shown in Figure 8-97. The coefficient of volume compressibility (m_v) decreases from 0.847 to 0.027 m^2/MN with increasing applied stress starting from 125 kPa. An initial swelling pressure <1 kPa was recorded before the first loading stage. At an applied stress of 500 kPa, the value for m_v was 0.126 m^2/MN which is exceeds that for Oxford Clay specimens in Domains 1.3 and 1.3.1. The specimen is classified as medium compressibility (after Head & Epps, 2011).

All specimens of Oxford Clay from glaciated-periglaciated Domains 1.3 and 1.3.1 and periglaciated-only Domain 2.3, are shown as e-logσ_v plots in Figure 8-98. Comparing initial and final void ratios, specimen CR023247 is the most compressible specimen tested. All specimens appear to lie along a void ratio transition from those in the densest state (CR005864, CR005904, Domain 1.3 and CR021545, Domain 1.3.1) to the least dense, CR023247 in Domain 2.3. Specimen CR005942, Domain 1.3, despite being taken from the greatest depth below ground level, also plots with those samples transitional between the least and most dense states.

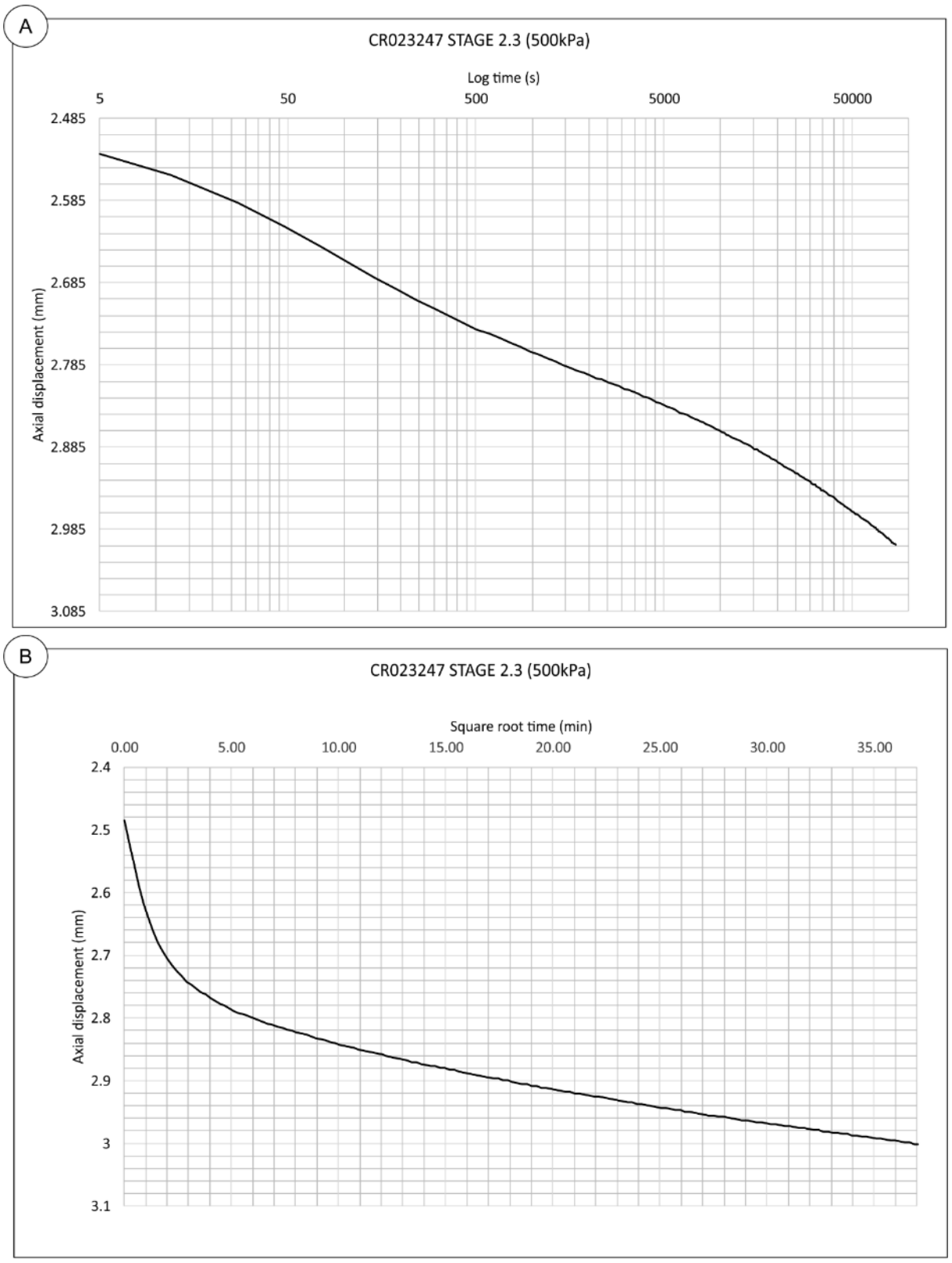

Figure 8-96 Example consolidation curves for specimen CR023247, Oxford Clay, Quaternary Domain 2.3. A) Log-time. B) Square-root time.

Stage number	Voids ratio					Volume compressibility (m_v)				Coeffecient of consolidation (C_v)					
	Pressure P, (kN/m^2)	Settlement ΔH (mm)	$\Delta e = \Delta H/H_s$ (H_s=8.7)	$e=e_o-\Delta e$ (e_o=1.19)	δe (e_1-e_2)	δp (kN/m^2)	$1+e_1$	m_v= (δe/δp)*((1000)/1+e)) m^2/MN	t_{50} (min) Minimum	t_{50} (min) Maximum	H=H_o-ΔH H_o=19.04 (mm)	$\bar{H}$=(H_1+H_2)/2 (mm)	$\bar{H}^2$ mm^2	Cv=(0.026*$(\bar{H})^2$)/t_{50} (m^2/yr) Maximum	Cv=(0.026*$(\bar{H})^2$)/t_{50} (m^2/yr) Minimum
2.1	125	2.017	0.2319	0.958	0.232	125	2.189	0.847	Not calculated.						
2.2	250	2.484	0.2856	0.904	0.054	125	1.958	0.219							
2.3	500	3.004	0.3454	0.844	0.060	250	1.904	0.126							
2.4	1000	3.614	0.4156	0.774	0.070	500	1.844	0.076							
2.5	2000	4.335	0.4985	0.691	0.083	1000	1.774	0.047							
2.6	3000	4.729	0.5438	0.646	0.045	1000	1.691	0.027							
2.7	1500	4.623	0.5316	0.658	-0.012	-1500									
2.8	125	3.828	0.4402	0.749	-0.091	-1375									

Figure 8-97 1D consolidation results for specimen CR023247, Oxford Clay, Quaternary Domain 2.3.

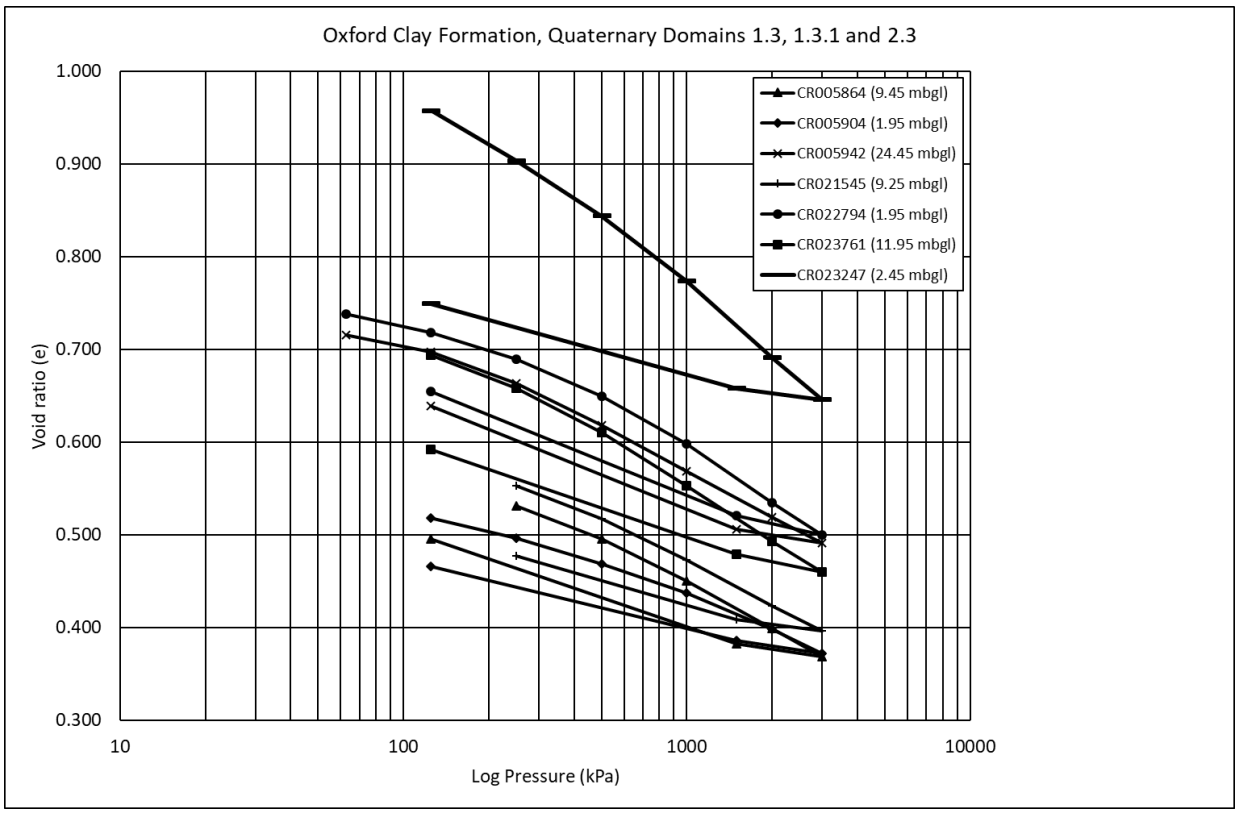

Figure 8-98 1D consolidation results for all Oxford Clay specimens in Quaternary Domains 1.3, 1.3.1 and 2.3.

8.5.1.7 Triaxial undrained shear strength and stiffness (Oxford Clay)

One, isotropically consolidated, multi-stage, undrained triaxial test with measurement of small-strain stiffness using Hall effect sensors was carried out for specimen CR023247 in the BGS SPTTS. The results are divided into stress-strain behaviour, undrained shear strength, effective stress paths in p′-q space, isotropic consolidation behaviour and small-strain stiffness and follow the calculations and procedures given in Section 8.3.2.7.

The experimental conditions are shown in Table 8-28. The initial and final specimen conditions are given Appendix 13.5. Photographic images of the pre- and post-experiment specimen are shown in Figure 8-99.

Specimen name	**Stage**	**Cell pressure (kPa)**	**Back pressure (kPa)**	**Differential (effective) pressure, σ'_o (kPa)**
CR023247	Consolidation stage 1	540	470	70
CR023247	Shear stage 1	540	470	70
CR023247	Consolidation stage 2	690	550	140
CR023247	Shear stage 2	690	550	140
CR023247	Consolidation stage 3	760	550	210
CR023247	Shear stage 3	760	550	210

Table 8-28 Multi-stage triaxial experimental conditions for Oxford Clay specimen CR023247, Domain 2.3.

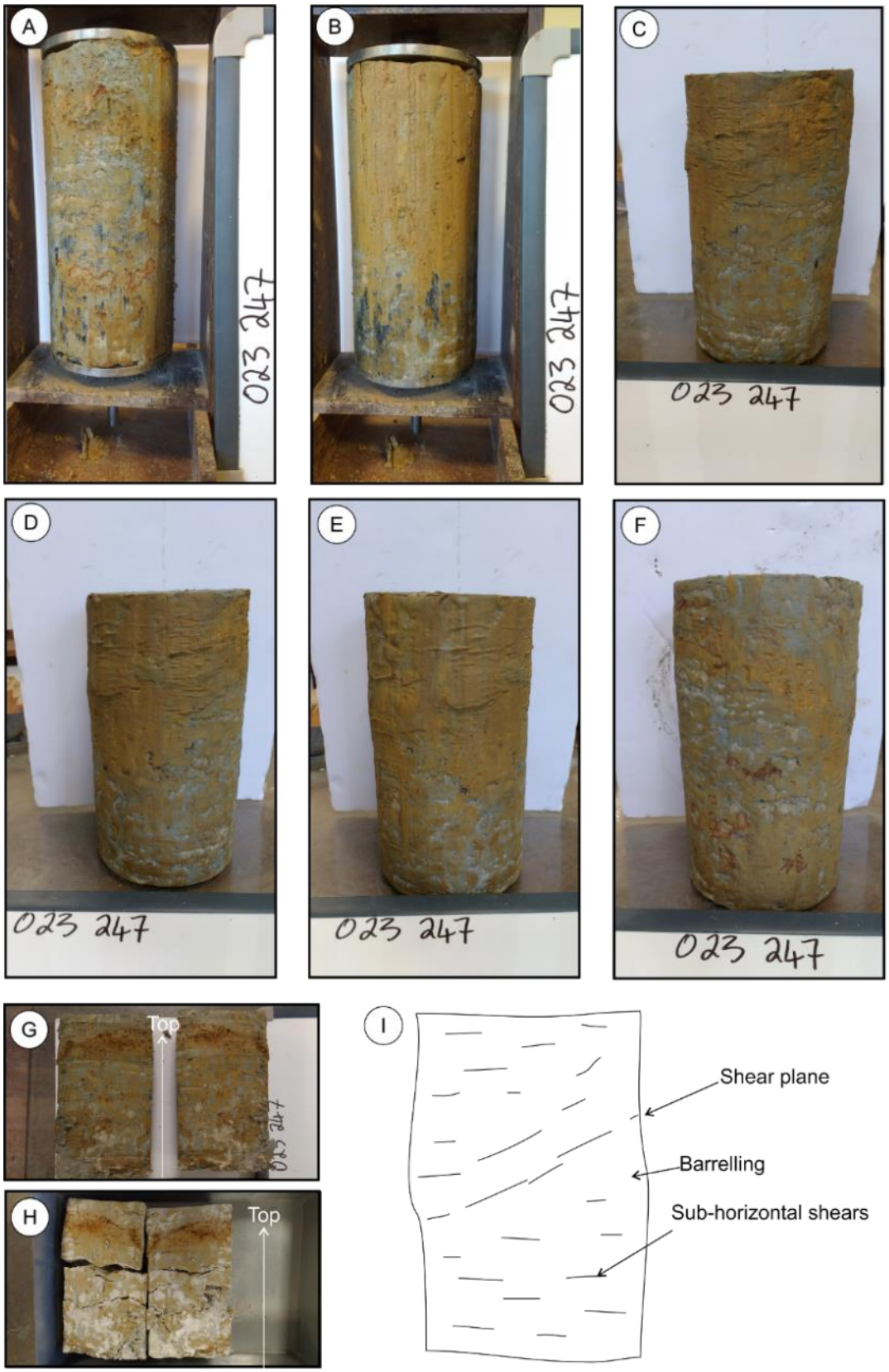

Figure 8-99 Pre- and post-triaxial conditions for sample CR023247, Oxford Clay, Quaternary Domain 2.3. A) and B) Initial condition in soil lathe. Note gleying resulting in grey and orange mottling. Gypsiferous silt lenses. C) to F) post-failure condition. G) Specimen sliced axially showing lamination, mottling and failure surface. H) Strong efflorescence (interpreted as gypsum) after drying. I) Hand sketch of failure condition.

8.5.1.8 Stress-strain and mobilised shear strength (Oxford Clay)

The results from the triaxial experiment are plotted as deviator stress *versus* shear strain and shown in Figures 8-100. The experimental parameters and conditions in the triaxial cell are given in Section 7.5.5.

During the final stage of shearing, during which failure was permitted, the specimen exhibits an increase in shear strain with increasing deviator stress. At ~3% shear strain, peak deviator stress is reached before strain continues to increase without a further increase in deviator stress.

Estimates of peak undrained shear strength, q_{max} and mobilised strength equal to $0.5q_{max}$ have been estimated and the results shown in Table 8-29.

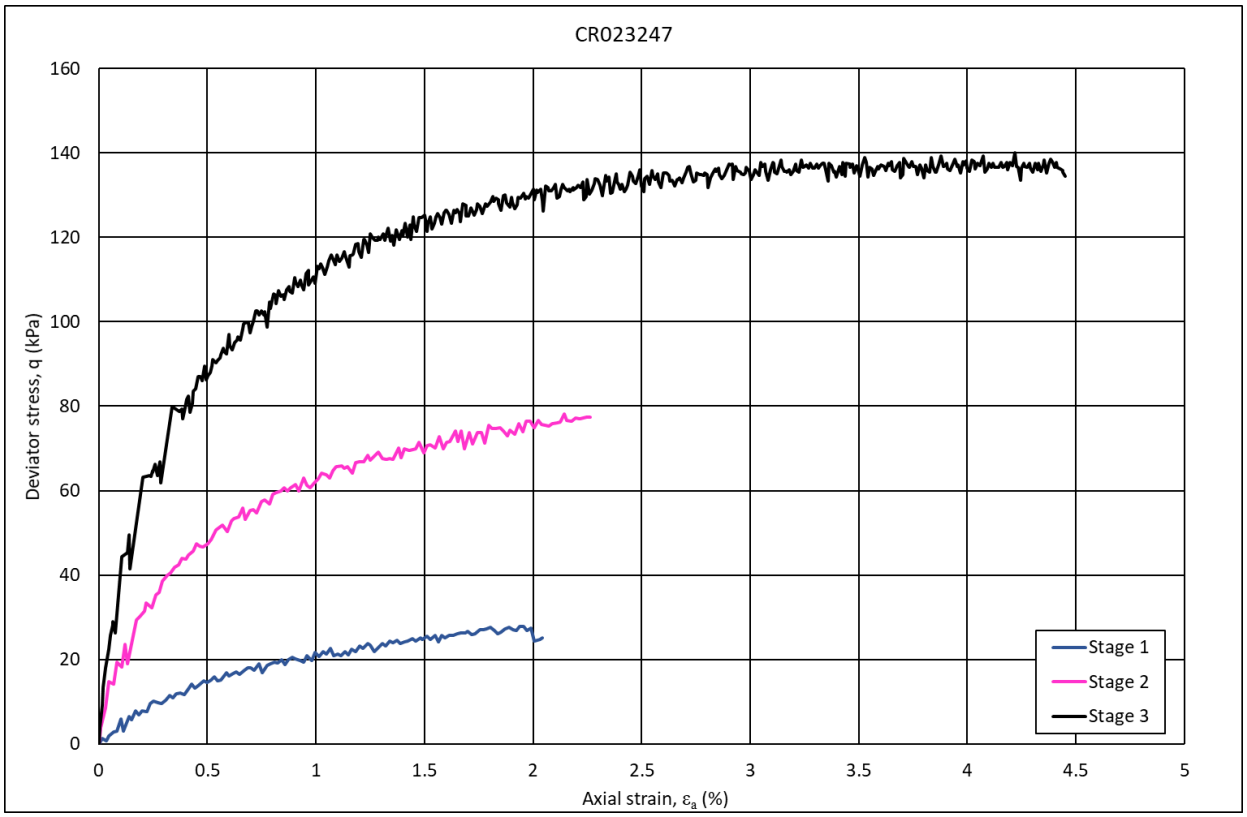

Figure 8-100 Stress-strain behaviour specimen CR023247, Oxford Clay, Quaternary Domain 2.3.

						Mobilised strength		Mobilised strain (%)
Specimen	**Geology**	**Specimen depth (mbgl)**	**Stage 3 cell pressure (σ_3)**	**Stage 3 back pressure (kPa)**	**Differential (effective) stress, σ'_o (kPa)**	**q_{max} (kPa)**	**$0.5q_{max}$ (kPa)**	**$\varepsilon_{F=2}$**
CR023247	OXC	2.45	760	550	210	136	68	0.31

Table 8-29 Mobilised strength parameters for specimens CR023247, Oxford Clay, Quaternary Domain 2.3.

Values for $0.5q_{max}$ are between 30% and 68% less than the lowest value for specimens of the Oxford at equivalent depths below ground level in Quaternary Domains 1.3 and 1.3.1.

8.5.1.9 Undrained shear strength, stress path analyses (Oxford Clay)

The results of stress path analyses are shown in Figures 8-101 for specimen CR023247. Deviator stress, q, is plotted against mean effective stress, p′. The parameters for the effective angle of shearing resistance, ø′, corresponding to two conditions of $ø'_{trans}$ and $ø'_{0.4\%}$ are presented as described in Section 8.3.2.7.

The ESP for specimen CR023247 deviates to the left from its initial effective stress, towards the critical state line during the early stages of shearing as pore pressure increases. Stages 2 and 3 then show a deviation to the right, parallel to the critical state line as p′ increases with increasing q. This effect is interpreted to be the result of dilation of the specimen. During stages 2 and 3, q is seen to decrease slightly as p′ increases indicating that peak q was reached and that the ESP approached the critical state line.

For specimen CR023247, the values for $ø'_{trans}$ and $ø'_{0.4\%}$ are the lowest for specimens of Oxford Clay when compared to those in Quaternary Domains 1.3 and 1.3.1.

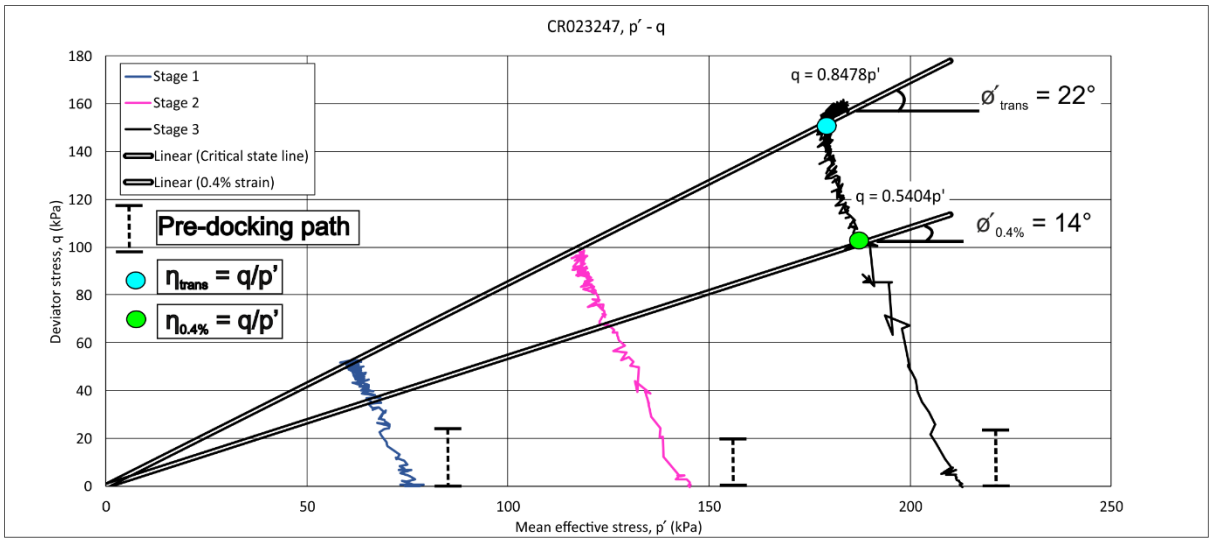

Figure 8-101 Effective tress path analyses for specimen CR023247, Oxford Clay, Quaternary Domain 2.3.

8.5.1.10 Isotropic consolidation

The plot of isotropic consolidation before each shearing stage for specimen CR023247 is shown in Figure 8-102 as change in volume (ΔV) *versus* square-root time in seconds. From each plot, estimates were made of the isotropic coefficient of compressibility (c_{vi}).

The magnitude of volume change in isotropic consolidation is seen to decrease with increasing effective stress. For specimen CR023247, the magnitude of volume change decreases by about 50% from an effective stress of 70 to 210 kPa. The magnitude of volume change is comparable to specimen CR023761 in Domain 1.3 but values of c_{vi} are greater than for other specimens in Domains 1.3 and 1.3.1.

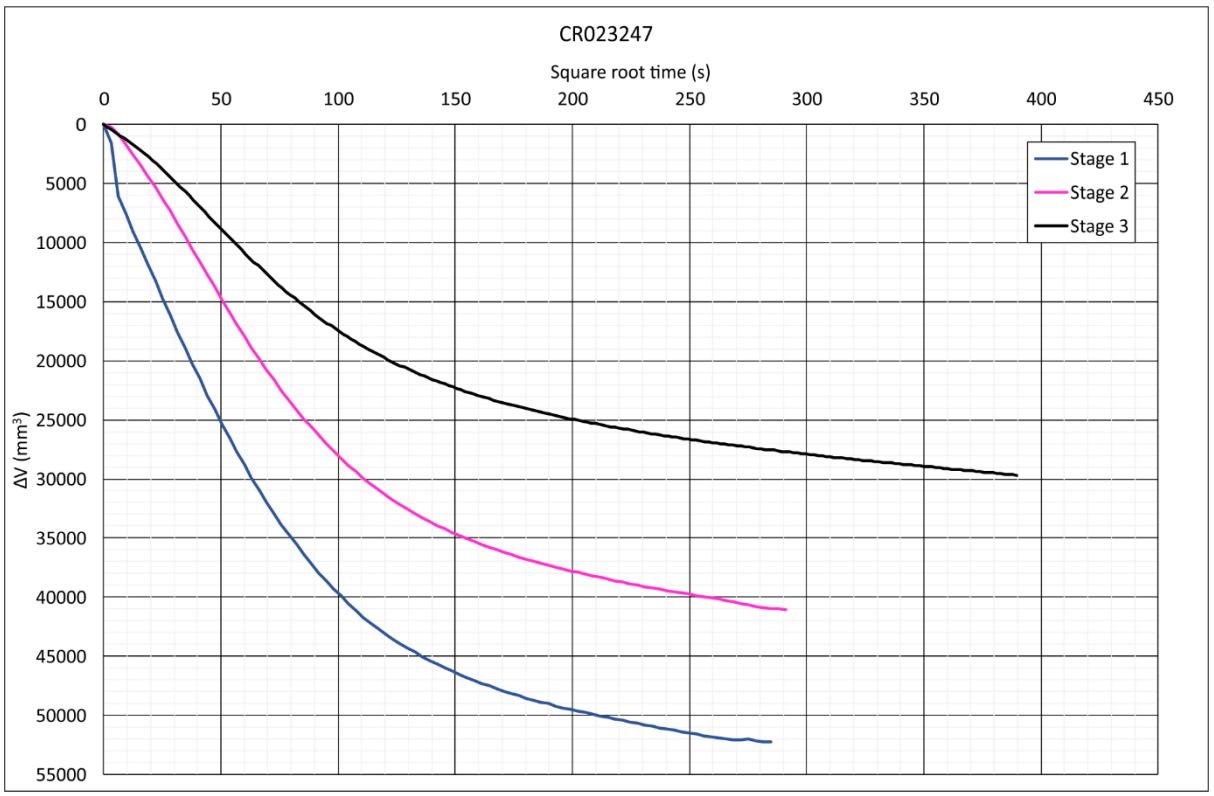

Initial		
Height (mm)	H_o	193.87
Diameter (mm)	D_o	100.25
Mass (g)	M_o	2805.7
Volume	cm^3	1530
Volume	mm^3	1530172
Area	mm^2	7893

Isotropic consolidation

	Stage 1	Stage 2	Stage 3
c_{vi} m^2/yr	21	18	17
t_{90}(min)	3	3	3
Side-drain correction applied (λ=80)			

End consolidation 1		
Height (mm)	H_1	191.66
Diameter (mm)	D_1	99.09
Volume (mm^3)	V_1	1477920
Area (mm^2)	A_1	7134

Change	
Δ_H	2.21
Δ_D	1.16
Δ_V	52252
Δ_A	52252

End shear 1		
Height (mm)	H_2	187.70
Diameter (mm)	D_2	100.13
Volume (mm^3)	V_2	1477920
Area (mm^2)	A_2	7874

Change	
Δ_H	3.96
Δ_D	-1.04
Δ_V	0
Δ_A	739

End consolidation 2		
Height (mm)	H_3	185.96
Diameter (mm)	D_3	99.18
Volume (mm^3)	V_3	1436845
Area (mm^2)	A_3	7728

Change	
Δ_H	1.74
Δ_D	0.94
Δ_V	41075
Δ_A	146

End shear 2		
Height (mm)	H_4	181.63
Diameter (mm)	D_4	100.36
Volume (mm^3)	V_4	1436845
Area (mm^2)	A_4	7911

Change	
Δ_H	4.33
Δ_D	-1.18
Δ_V	0
Δ_A	183

End consolidation 3		
Height (mm)	H_3	180.38
Diameter (mm)	D_3	99.66
Volume (mm^3)	V_3	1407164
Area (mm^2)	A_3	7802

Change	
Δ_H	1.25
Δ_D	0.70
Δ_V	29681
Δ_A	109

End shear 3		
Height (mm)	H_4	171.99
Diameter (mm)	D_4	102.06
Volume (mm^3)	V_4	1407164
Area (mm^2)	A_4	8181

Change	
Δ_H	8.39
Δ_D	-2.40
Δ_V	0
Δ_A	380

Figure 8-102 Isotropic consolidation and estimated coefficient of isotropic consolidation (c_{vi}), specimen CR023247, Oxford Clay, Quaternary Domain 2.3.

8.5.1.11 Small-strain stiffness

Estimates of secant stiffness, expressed as Young's modulus E, derived from axial transducer measurements from the triaxial apparatus and the mean strain from the local Hall effect sensors, are summarised in Table 8-30 and shown in Figures 8-103.

	Triaxial apparatus	Hall effect	
	E (MPa), $0.5q_{max}$	E (MPa), $0.5q_{max}$	$E_{0.1\%}$ (MPa)
Specimen			
CR023247	0.219	NA	NA

Table 8-30 Estimates of secant stiffness, specimens CR023247, Oxford Clay, Quaternary Domain 2.3. NA – shear modulus not calculated for stage 3 as one axial Hall effect sensor became displaced during shearing.

Values for E at $0.5q_{max}$ compare with the least stiff values derived for Oxford Clay specimens at equivalent depths below ground level in Domains 1.3 and 1.3.1. Deviator stress *versus* axial and radial strain using Hall effect sensors is plotted in Figure 8-112. Stiffness increases with increasing effective stress between shear stage 1 and 2. Increasing negative radial strain from stage 1 to 3 is interpreted to be the result of specimen dilation. Increasing negative axial strain above q ~40 kPa is considered an error in sensor recording as axial dilation is not possible in triaxial compression.

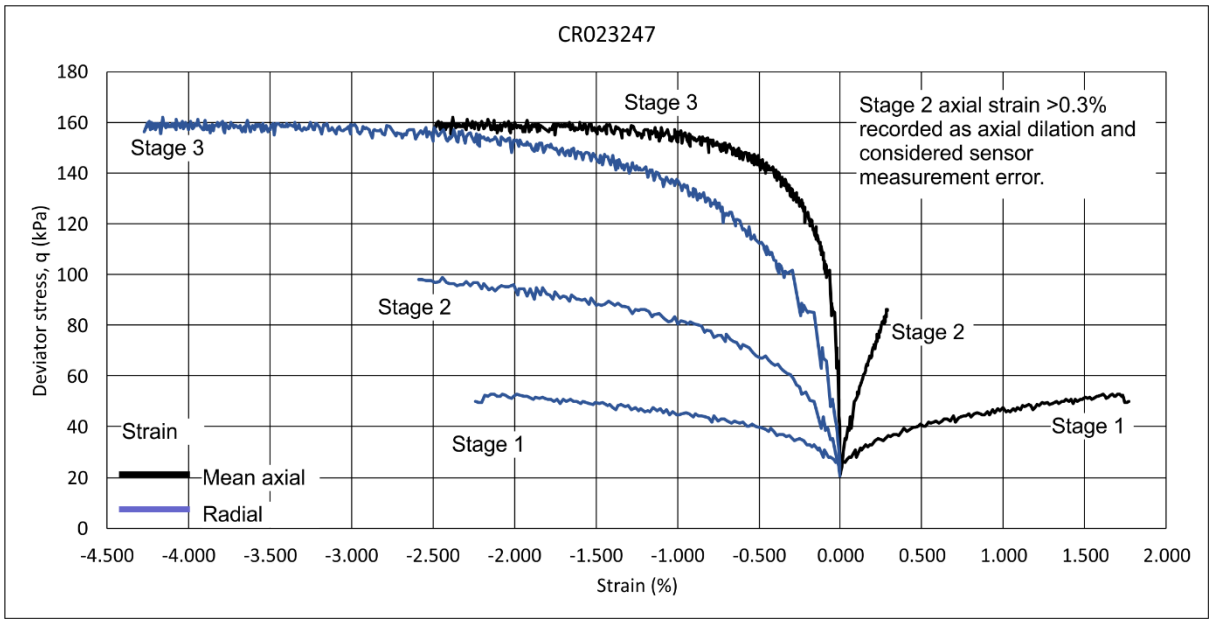

Figure 8-103 Small-strain stiffness using Hall effect sensors, specimen CR023247, Oxford Clay, Quaternary Domain 2.3.

8.5.2 Summary

The Oxford Clay comprises calcareous, high to very high plasticity, poorly- and uniformly-graded, slightly clayey silt and silt. It has normal activity, with values between 1 and 1.1. Activity is interpreted to be the result of agglomeration of silt-grade clay particles as

described in Section 8.3.4. Its clay mineral assemblage includes illite and kaolinite. Chlorite is absent from the clay mineral assemblage compared to the glaciated Domains. Moisture content values are > W_P and so values of LI are > 0, in contrast to the Oxford Clay in Glaciated-Periglaciated Domains 1.3 and 1.3.1. Given the high values of moisture content and LI in sample CR020746, it is interpreted that this sample is a solifluction deposit derived from the Peterborough Member of the Oxford Clay.

The coefficient of compressibility for specimen CR023247, was estimated to be >90 m^2/yr which exceeds the measured values for equivalent specimens in Domains 1.3. and 1.3.1. This along with a value of 0.26 m^2/MN at 500 kPa, is interpreted to reflect the greater compressibility of the Oxford Clay in non-glaciated Domain 2.3, compared to those specimens in glaciated-periglaciated Domains 1.3 and 1.3.1.

The mobilised shear strength of specimen CR023247, at $0.5q_{max}$ is 68 kPa with an equivalent value for mobilised strain, $\varepsilon_{F=2}$ of 0.31. The value of 0.5_{qmax} is 47% less than the lowest values measured in Domains 1.3 and 1.3.1. In terms of secant strength parameters $ø'_{trans}$ and $ø'_{0.4\%,}$ estimated values are 22 and 14° respectively. The latter values compare well with the lower-bound values for specimens CR005942 and CR021545 in Quaternary Domains 1.3 and 1.3.1 respectively. The reduction in secant strength parameter values at <2 mbgl and increase in compressibility, is interpreted here to reflect the presence of one or more solifluction shear zones within weathered Oxford Clay. The net effect of periglacial shearing appears to have been to de-structure the Oxford Clay so that it approaches its residual strength values with a corresponding decrease in its *in situ* state of consolidation and increase in compressibility.

8.6 Quaternary Domain 1.4.1

Quaternary Domain 1.4.1 comprises Late Jurassic mudrocks of the West Walton, Ampthill and Kimmeridge Clay formations overlain by glacigenic and periglacial deposits, the latter comprising 'head'. This Domain is interpreted to have been glaciated on at least one occasion with multiple phases of pre- and post-glacial periglaciation. Chalk of the Chalk Group crops out ~10km to the southeast of the domain. The outcrop trends northeast-southwest. It is interpreted (Section 3.2) that the lobe of the BIS that deposited glacigenic sediments in this area, crossed the Chalk outcrop in the present-day Wash area, or to the northeast in Lincolnshire.

Laboratory results are presented for loss-on-ignition (LOI), clay mineralogy, particle-size analysis (PSA), particle density and plasticity for till collected as bulk or UT100 samples from the East West Rail ground investigation. 1D consolidation (n=1), single-stage triaxial (n=3) and multi-stage triaxial experiments with measurement of small-strain stiffness (n=1) were undertaken. No field sites were identified in this Domain.

8.6.1 Laboratory results

8.6.1.1 Loss-on-ignition

Results for loss-on-ignition for samples of till are shown in Table 8-34. All samples are very calcareous, containing between 27% and 54% carbonate. Their organic content is low, <5%.

Sample	Geology	% water	%organic	%$CaCO_3$	% silicate residue
CR011958	TILL	N/A	4	32.7	63.4
CR011968	TILL	N/A	4	30.6	65.4
CR011963	TILL	N/A	4.2	29.6	66.2
CR011961	TILL	N/A	4	30.3	65.6
CR011953	TILL	N/A	3	54	42.9
CR011981	TILL	N/A	3.9	27.1	69
CR011973	TILL	N/A	3.8	30.8	65.4
CR011971	TILL	N/A	3.9	31	65.1
CR011966	TILL	N/A	4.5	28.9	66.5
CR011976	TILL	N/A	3.7	31.2	65.1

Table 8-31 Loss-on-ignition (LOI), till Domain 1.4.1. N/A denotes gravimetric water content measured as part of Atterberg, 1D consolidation or triaxial analysis.

8.6.1.2 Clay mineral XRD (till)

Diffractograms from the analysis of orientated, aggregate specimens are presented in Figure 8-104. The identification of clay minerals followed the procedure described in Section 8.1.3.

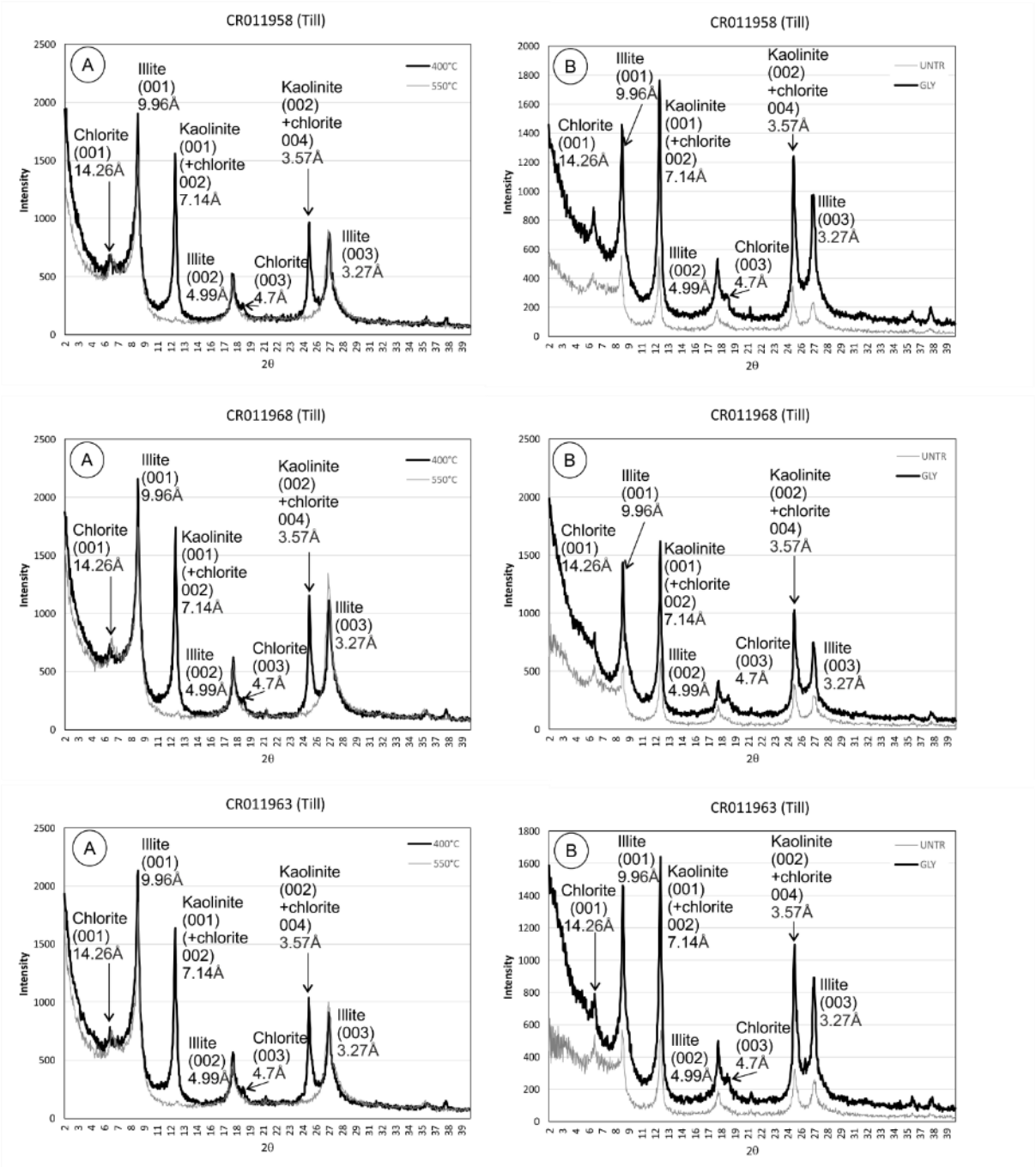

Figure 8-104 Clay mineral XRD for till, Quaternary Domain 1.4.1. A) Heat treated at 400ºC and 550ºC. B) Air dried, untreated (untr) and glycolated (gly).

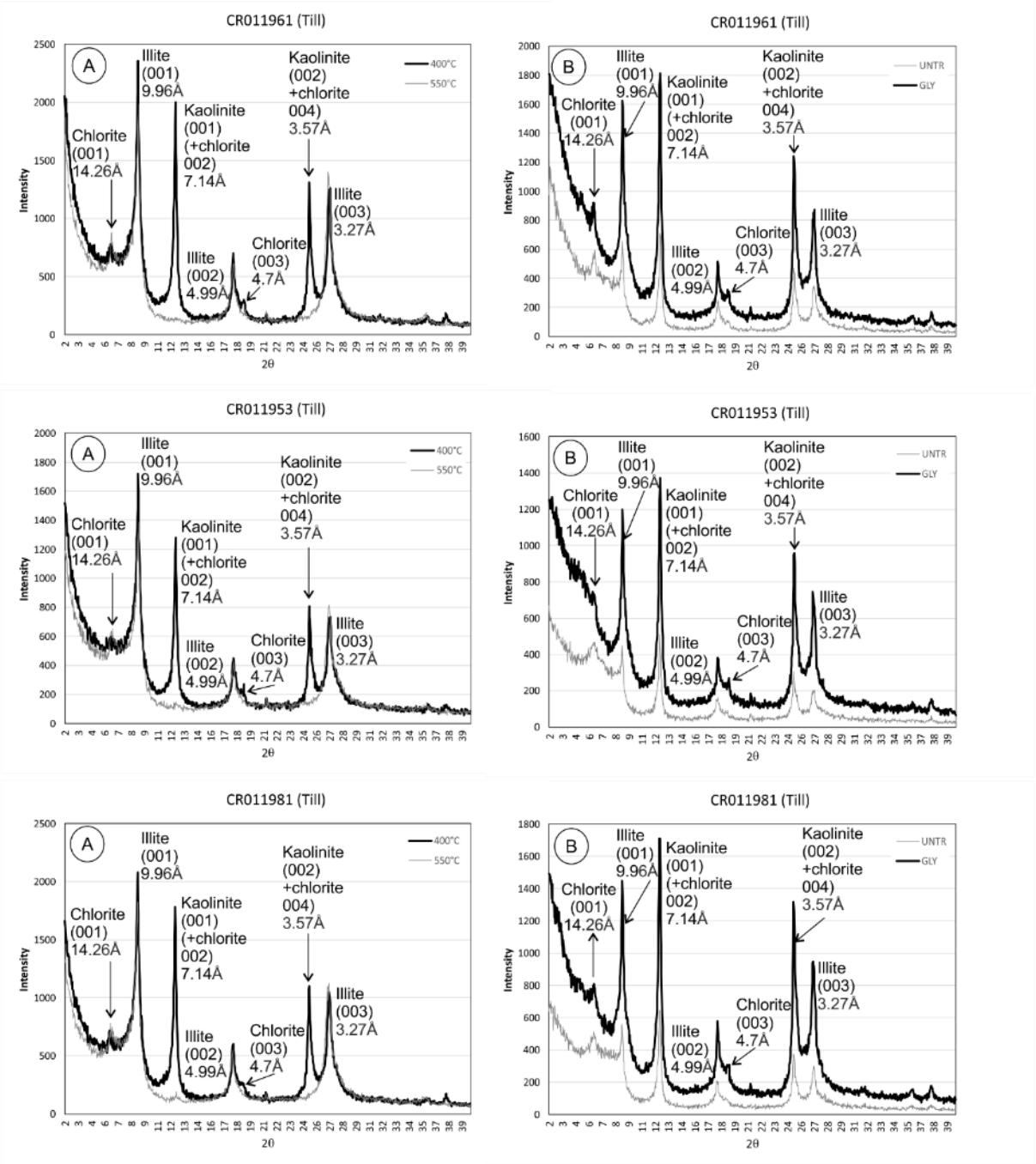

Figure 8-104 continued. Clay mineral XRD for till, Quaternary Domain 1.4.1. A) Heat treated at 400ºC and 550ºC. B) Air dried, untreated (untr) and glycolated (gly).

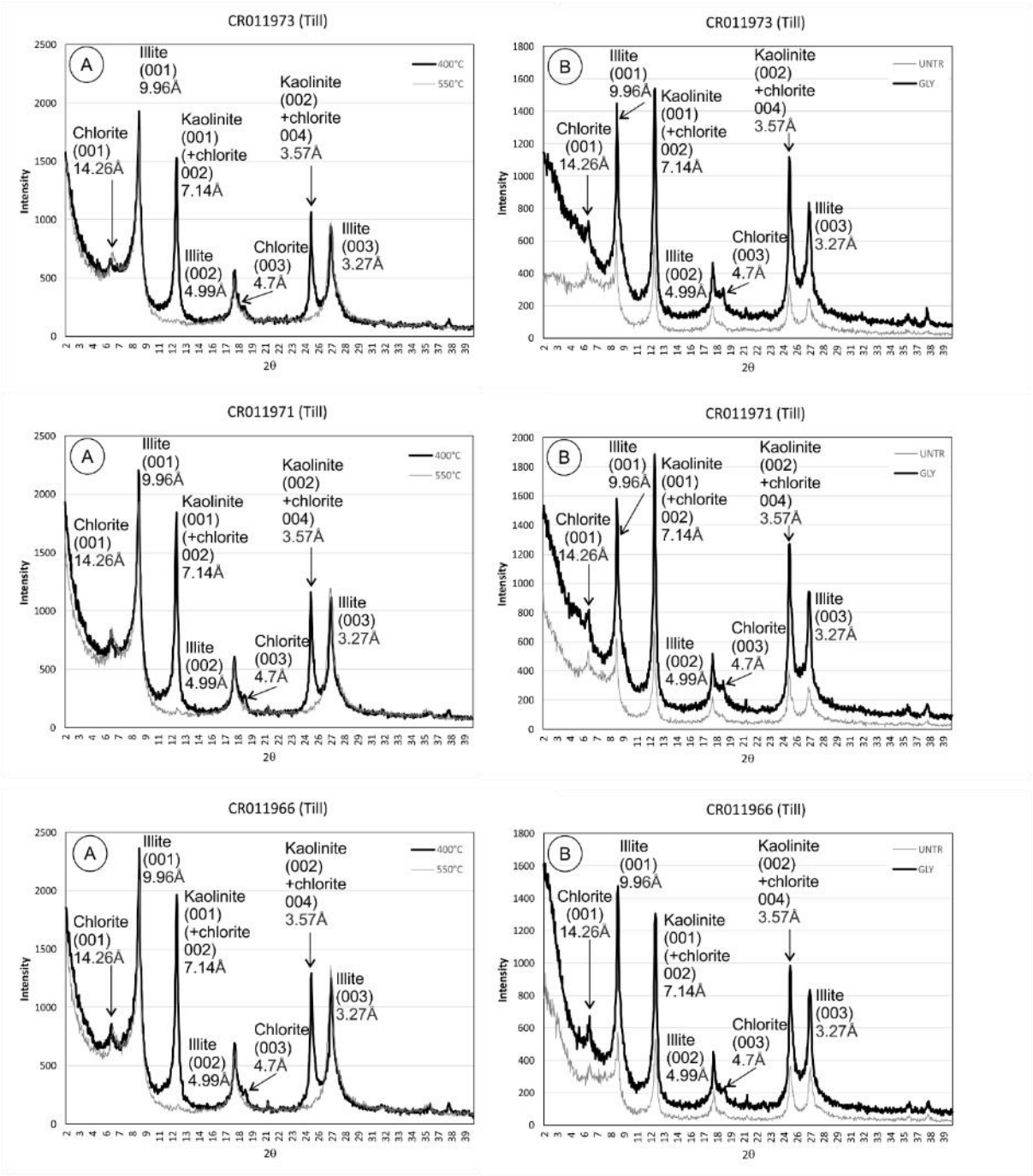

Figure 8-104 continued. Clay mineral XRD for till, Quaternary Domain 1.4.1. A) Heat treated at 400ºC and 550ºC. B) Air dried, untreated (untr) and glycolated (gly).

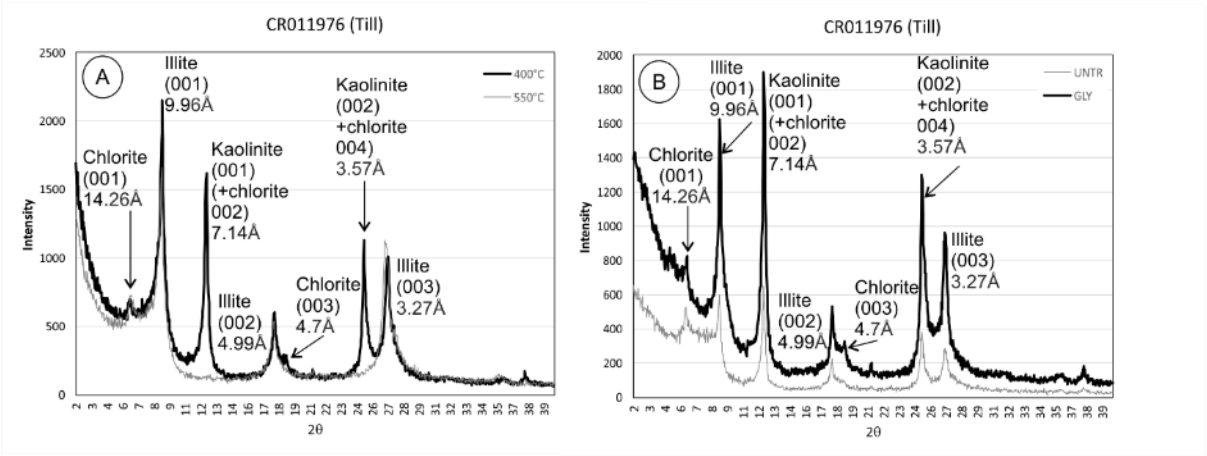

Figure 8-104 continued. Clay mineral XRD Quaternary Domain 1.4.1. A) Heat treated at 400ºC and 550ºC. B) Air dried, untreated (untr) and glycolated (gly).

Strong, narrow peaks are seen in the diffractograms associated with clay minerals characterised by illite (mica), kaolinite (with minor or trace amounts of chlorite?) and chlorite. Illite forms a mixed layer assemblage with collapsible clay minerals of unknown composition and Kaolinite is characterised by peak intensity reduction or loss on heating to 550ºC. Non-clay minerals are poorly defined but probably include quartz (4.35 Å), gypsum and carbonate.

8.6.1.3 Particle-size analysis (PSA), (till)

The results of particle-size analysis are plotted as percentage passing (finer) – log particle-size plots (Figure 8-105). The grading characteristics and classification of each specimen is summarised in Table 8-35. Coefficient of uniformity and coefficient of curvature were calculated using the method described in Section 8.1.4.

Sample	Geology	Method[1]	Lithological Description[1]	Sample grading[2]	C_u	C_z
CR011958	TILL	LPSA + WS	Slightly gravelly, slightly sandy, slightly clayey SILT	Poorly-graded	14.0	0.643
CR011968	TILL	LPSA + WS	Slightly gravelly, slightly clayey, slightly sandy SILT	Poorly- to well-graded	15.0	1.067
CR011963	TILL	LPSA + WS	Slightly gravelly, slightly clayey, slightly sandy SILT	Poorly-graded	25.0	0.810
CR011961	TILL	LPSA + WS	Slightly gravelly, slightly sandy, slightly clayey, SILT	Well-graded	15.0	1.067
CR011953	TILL	LPSA + WS	Slightly gravelly, slightly sandy, slightly clayey, SILT	Poorly-graded	10.0	0.9
CR011981	TILL	LPSA + WS	Slightly gravelly, slightly clayey, slightly sandy SILT	Well-graded	30.0	1.2
CR011973	TILL	LPSA + WS	Slightly gravelly, slightly sandy, slightly clayey, SILT	Poorly-graded	10.0	0.9
CR011971	TILL	LPSA + WS	Slightly gravelly, slightly sandy, slightly clayey, SILT	Well-graded	15.0	1.0
CR011966	TILL	LPSA +	Slightly gravelly, slightly sandy,	Poorly-graded	13.0	0.692

		WS	slightly clayey, SILT			
CR011976	TILL	LPSA + WS	Slightly gravelly, slightly sandy, slightly clayey, silt	Well-graded	13.0	1.231

Table 8-32 PSA summary for till in Domain 1.4.1. [1]LPSA – Laser Particle-Size Analysis, WS – wet sieving. [2]Based on proportions by mass from PSA following conventions in British Standards BS5930:1999 with Amendment 2 (British Standards Institution, 1999). [3]Geotechnical terminology

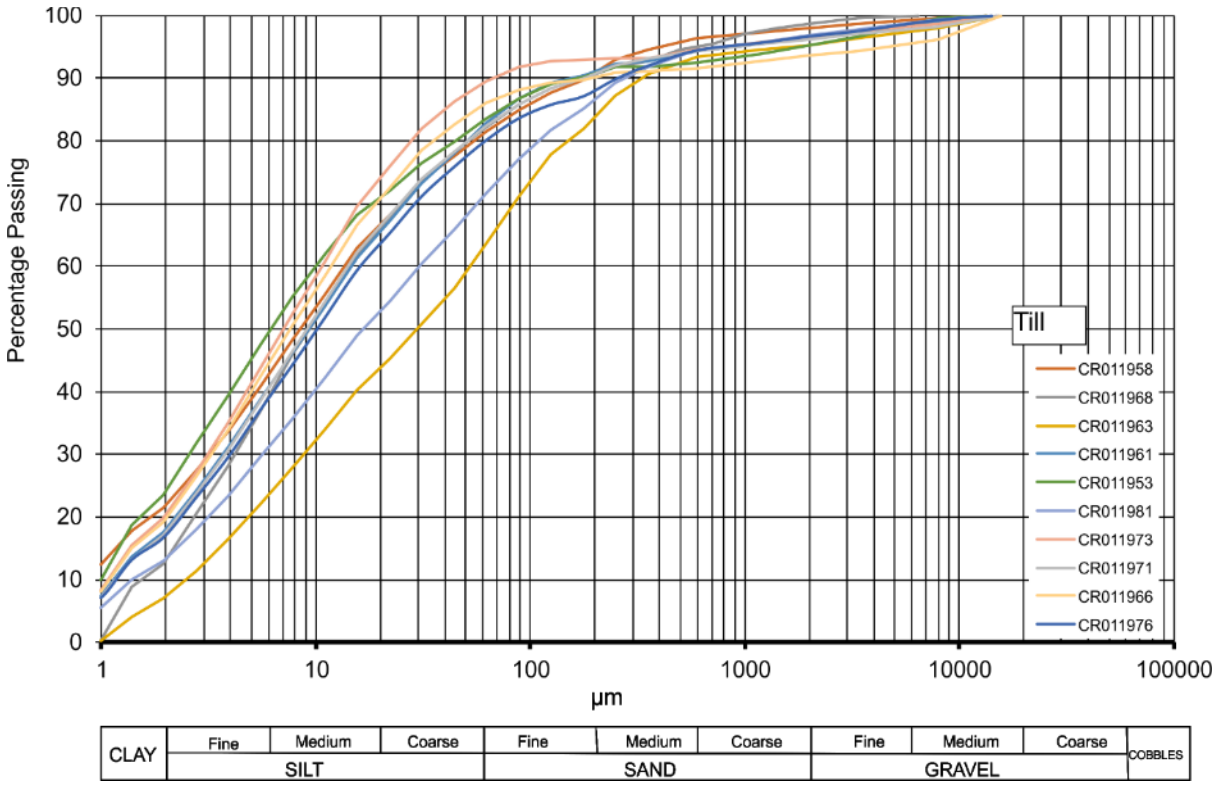

Figure 8-105 Particle-size grading curves, till, Quaternary Domain 1.4.1.

All samples are poorly- to well-graded, variably gravelly, sandy silts and clays. Samples are more closely represent poorly-graded soils where the proportion of silt is > about 80%. The gravel is fine to medium and comprises rounded and well-rounded chalk, angular flint, limestone, sandstone and fossil debris.

8.6.1.4 Atterberg limits and moisture content (till)

The results of Atterberg limit determinations, including moisture content, are shown in Table 8-36. The results are plotted on a conventional liquid limit-plasticity index chart in Figure 8-106 and shown *versus* depth below ground level in Figure 8-107. Supporting data for the calculation of liquid limit, plastic limit and moisture content is given in Appendix 13.2.

Sample	Geology	Liquid Limit (W_L)	Plastic Limit	Plasticity Index (I_p)	Moisture content	Liquidity Index	Activity[2]

			(W_P)		(%)	(LI)[1]	
CR011958	TILL	39	17	22	14	-0.14	1.0(N)
CR011963	TILL	41	18	23	13	-0.22	3.3(A)
CR011961	TILL	41	18	23	15	-0.13	1.3(A)
CR011953	TILL	32	15	17	15	0	0.7(I)
CR011981	TILL	40	18	22	13	-0.23	1.7(N)
CR011973	TILL	42	18	24	12	-0.25	1.2(N)
CR011971	TILL	41	18	23	14	-0.17	1.4(A)
CR011966	TILL	41	18	23	15	-0.13	1.2(N)
CR011976	TILL	41	17	24	15	-0.08	1.4(A)

Table 8-33 Atterberg limits, moisture content and activity, till, Quaternary Domain 1.4.1. [1]Calculated from (ω-W_P/I_p). [2]Calculated based on I_p/%clay fraction (0.002mm), where %clay was determined by LPSA. Activity classes I (inactive), N (normal) and A (active) after Skempton (1953).

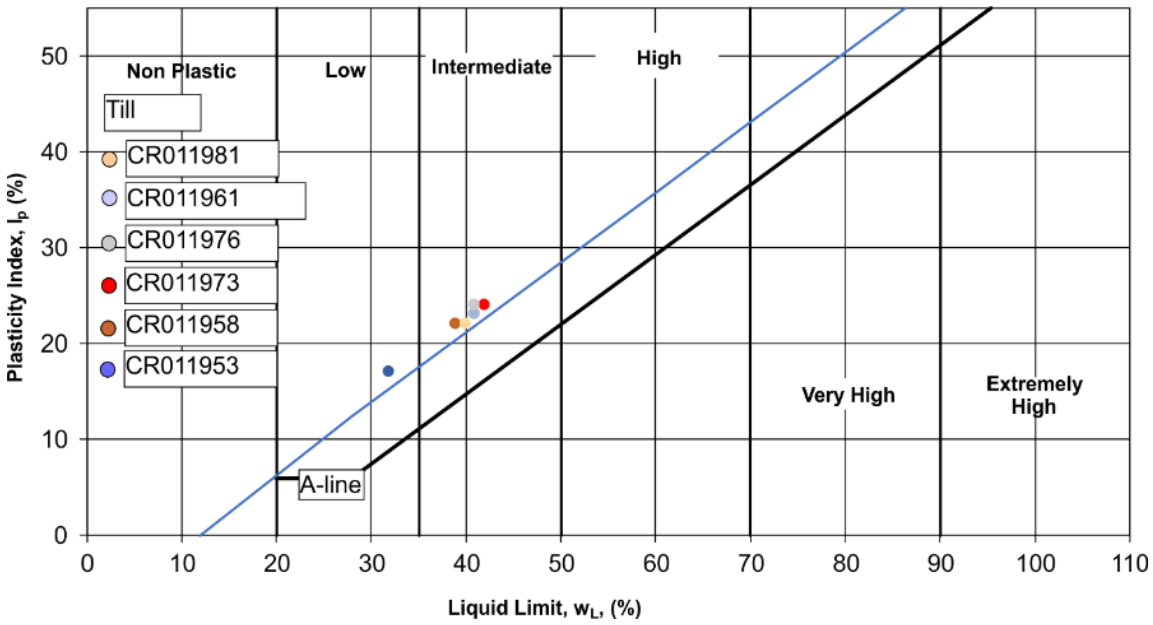

Figure 8-106 Plasticity plot for till, Quaternary Domain 1.4.1. T-line for tills from Boulton & Paul (1976).

In common with other till specimens in Domains 1.1.1, 1.2.1 and 1.3.1, their plasticity is low to intermediate. All samples plot close to the T-line of Boulton & Paul (1976). Differences in I_p probably reflect variation in the proportion of granular particles rather than clay mineralogy. There is no qualitative difference in clay mineralogy between the samples (Section 8.6.2). There is little variation with depth in values for liquid limit, plastic limit or moisture content. Moisture content values plot below the plastic limit so that values for liquidity index are close to 0. The increase in activity at 17 mbgl appears to be related to a decrease in clay content.

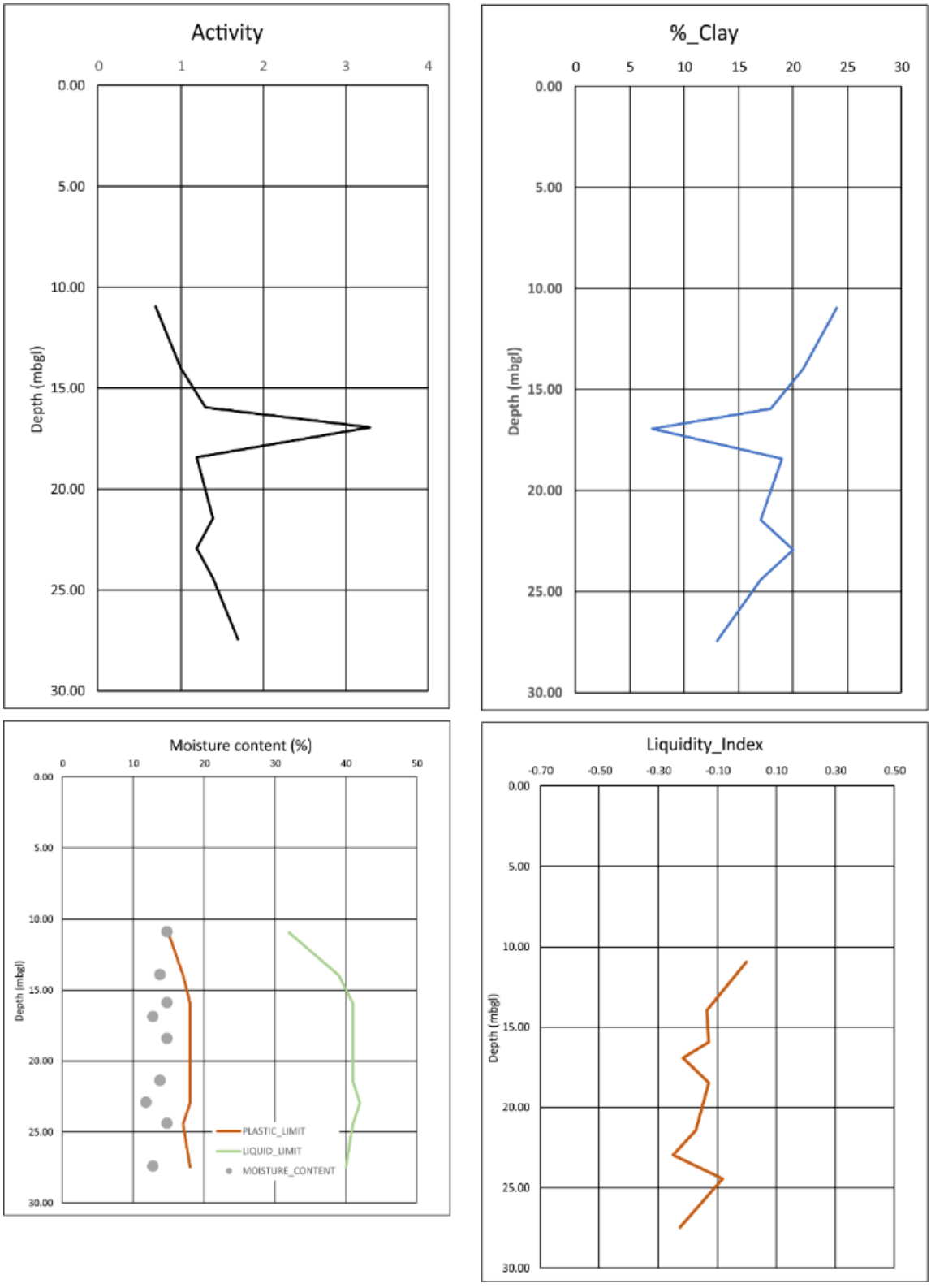

Figure 8-107 Atterberg limit-, activity-, % clay- and liquidity index-depth profile for till, Quaternary Domain 1.4.1.

8.6.1.5 Particle density (till)

The results of the particle density determination using the small pyknometer method are shown in Appendix 13.3. For specimens within 0.03g tolerance, the measured particle density

is between 2.64 and 2.69 Mg/m^3. Differences in particle density are interpreted to be the result of variation in the proportion of chalk particles, where particle density is reduced with increasing chalk content.

8.6.1.6 1D consolidation (till)

The experimental results for till specimen CR011958 are shown in Figure 8-108 and the initial and final specimen conditions given in Appendix 13.4. The methodology for the interpretation of the experimental results is described in Section 8.3.7.

Stage number	Voids ratio					Volume compressibility (m_v)			Coeffecient of consolidation (C_v)						
	Pressure P, (kPa)	Settlement ΔH (mm)	Δe= ΔH/H_s (H_s=13.34)	e=e_o - Δe (e_o=0.50)	δe (e_1-e_2)	δp (kN/m^2)	$1+e_1$	m_v= (δe/δp)*((1000)/1+e)) m^2/MN	t_{50} (min) Minimum	t_{50} (max) Maximum	H=H_o-ΔH H_o=19.99 (mm)	$\hat{H}$=(H_1+H_2)/2 (mm)	$\hat{H}^2$ mm^2	Cv=(0.026*$\hat{H}^2$)/t_{50} (m^2/yr) Maximum	Cv=(0.026*$\hat{H}^2$)/t_{50} (m^2/yr) Minimum
2.1	125	0.510	0.0382	0.461	0.04	125.0	1.499	0.204	0.35	1.88	19.48	19.74	389	28.93	5.38
2.2	250	0.907	0.0680	0.431	0.03	125	1.461	0.163	2.38	3.50	19.08	19.28	372	4.06	2.76
2.3	500	1.388	0.1041	0.395	0.04	250	1.431	0.101	3.23	4.88	18.60	18.84	355	2.85	1.89
2.4	1000	1.910	0.1432	0.356	0.04	500	1.395	0.056	4.75	6.25	18.08	18.34	336	1.84	1.40
2.5	2000	2.423	0.1817	0.317	0.04	1000	1.356	0.028	5.00	6.25	17.57	17.82	318	1.65	1.32
2.6	3000	2.696	0.2021	0.297	0.02	1000	1.317	0.016	6.25	7.50	17.29	17.43	304	1.26	1.05
2.7	1500	2.624	0.1967	0.302	-0.01	-1500									
2.8	125	1.954	0.1465	0.352	-0.05	-1375									

Figure 8-108 1D consolidation results for specimen CR011958, till, Quaternary Domain 1.4.1.

The coefficient of volume compressibility (m_v) is stress dependent; decreasing from 0.204 to 0.01 m^2/MN with increasing applied stress. An initial swelling pressure of 43 kPa was recorded before the first loading stage. At an applied stress of 500 kPa, the value for m_v was 0.101 m^2/MN. Specimen CR011958 is classified as low compressibility (after Head & Epps, 2011).

The coefficient of compressibility, c_v, decreases with increasing applied stress from 28.93 to 1.26 m^2/yr. Referring to c_v calculated from the maximum estimated value of consolidation at t_{50}, the value at the 500 kPa stress increment is 2.85 m^2/yr. The latter value exceeds that for the Oxford Clay reflecting the greater proportion of granular particles including silt and fine sand in the specimen of till. The value of 2.85m^2/yr is typical of low to medium plasticity clays (after Head & Epps, 2011).

The estimated compression ratios for initial, primary and secondary compression are shown in Table 8-34.

	CR011958		
Stress increment	r_o	r_p	r_s
62.5 (kPa)			
125 (kPa)	0.17	0.79	0.04
250 (kPa)	0.01	0.84	0.01
500 (kPa)	0.07	0.83	0.10
1000 (kPa)	0.06	0.81	0.13
2000 (kPa)	0.05	0.83	0.13
3000 (kPa)	0.02	0.73	0.25

Table 8-34 Estimated initial, primary and secondary compression ratios for till, Quaternary Domain 1.4.1.

Between 73% and 84% of consolidation occurs during the primary compression phase, independent of applied stress. Secondary compression becomes apparent at the 3000 kPa stress increment where is increases by 92% from the value of r_s at 2000 kPa. Estimated values for the coefficient of secondary compression, C_{sec}, are shown in Table 8-35.

	Stress increment						
Specimen	**62.5 (kPa)**	**125 (kPa)**	**250 (kPa)**	**500 (kPa)**	**1000 (kPa)**	**2000 (kPa)**	**3000 (kPa)**
CR011958	NA	0.0012	0.0016	0.0019	0.0024	0.0015	0.0024

Table 8-35 Estimated initial, primary and secondary compression ratios for till, Quaternary Domain 1.4.1.

Values generally increase with increasing applied stress to a maximum of 0.0024 but the value is seen to decrease to 0.0015 at the 2000 kPa stress increment.

8.6.1.7 Triaxial undrained shear strength and stiffness (till)

One, isotropically consolidated, undrained, multi-stage triaxial test with measurement of small-strain stiffness using Hall effect sensors was carried out for specimen CR011958 in the BGS SPTTS configuration.

The experimental conditions are given in Table 8-36 and the initial and final specimen conditions are given in Appendix 13.5. Photographic images of the pre- and post-experiment specimens are shown in Figure 8-109.

Specimen name	**Stage**	**Cell pressure (kPa)**	**Back pressure (kPa)**	**Differential (effective) pressure, σ'_0 (kPa)**
CR011958	Consolidation stage 1	800	600	200
CR011958	Shear stage 1	800	600	200
CR011958	Consolidation stage 2	1000	600	400
CR011958	Shear stage 2	1000	600	400
CR011958	Consolidation stage 3	1200	600	600
CR011958	Shear stage 3	1200	600	600

Table 8-36 Triaxial experimental conditions, specimen CR011958, till, Domain 1.4.1.

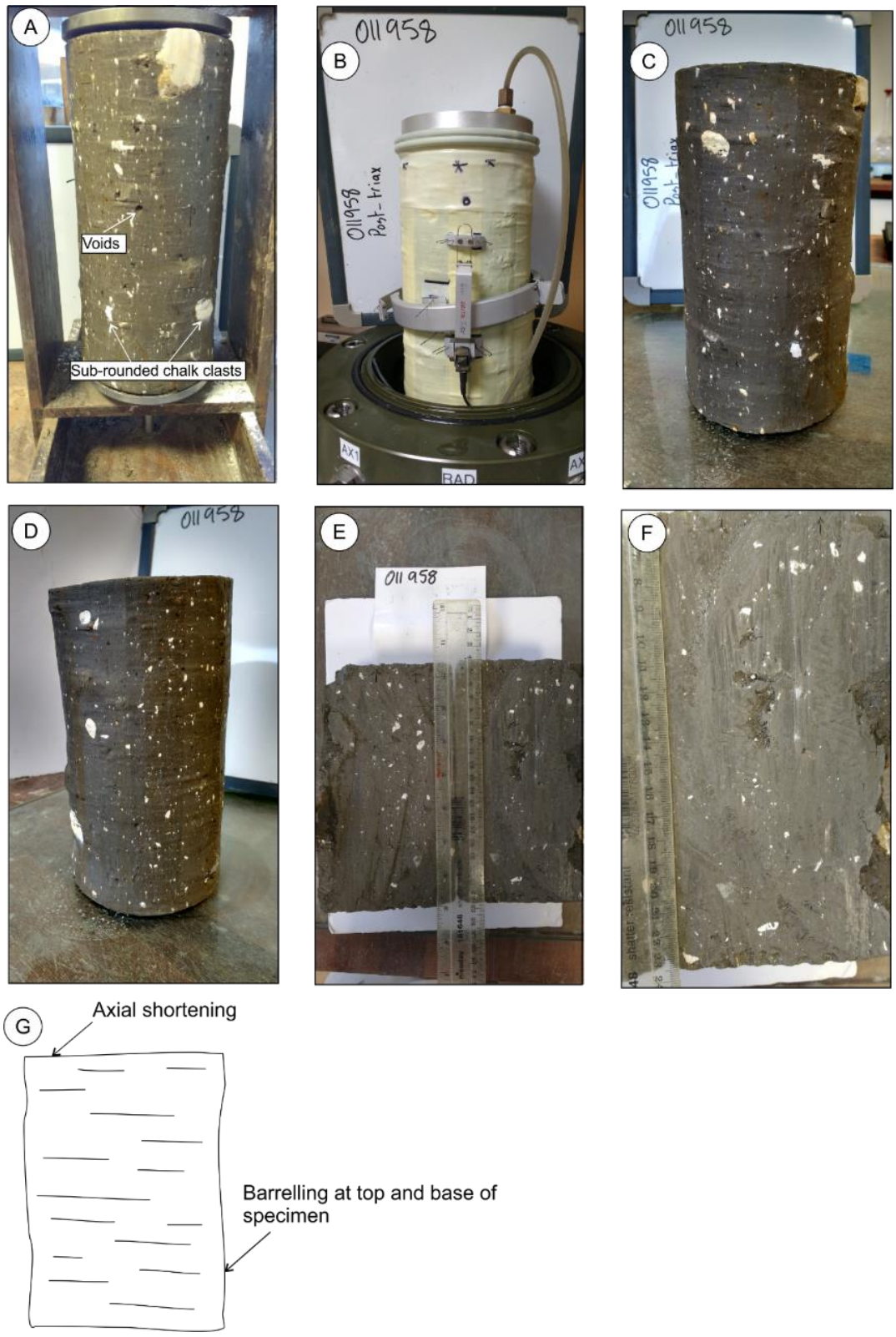

Figure 8-109 Pre- and post-triaxial test conditions, specimen CR011958, till Quaternary Domain 1.4.1. A) Pre-experiment. Voids carefully filled with specimen shavings. B) Post-experiment, side drains visible through membrane. C) and D) post-experiment, membrane, side-drains, top and base drains removed. E) Post-experiment specimen sliced parallel to long axis. F) Close-up view of one specimen side seen in E. G) Simplified hand sketch of failure conditions.

8.6.1.8 Stress-strain and mobilised shear strength (till)

The results are plotted as deviator stress *versus* shear strain in Figure 8-110. The experimental parameters and conditions in the triaxial cell are given in Section 7.5.5.

During the final stage of shearing, during which failure was permitted, the specimen shows an increase in shear strain with increasing deviator. Specimen CR011958 appears not to show a decrease in deviator stress with increasing strain indicating that peak deviator stress was not reached. Strength values presented here are therefore a minimum estimate.

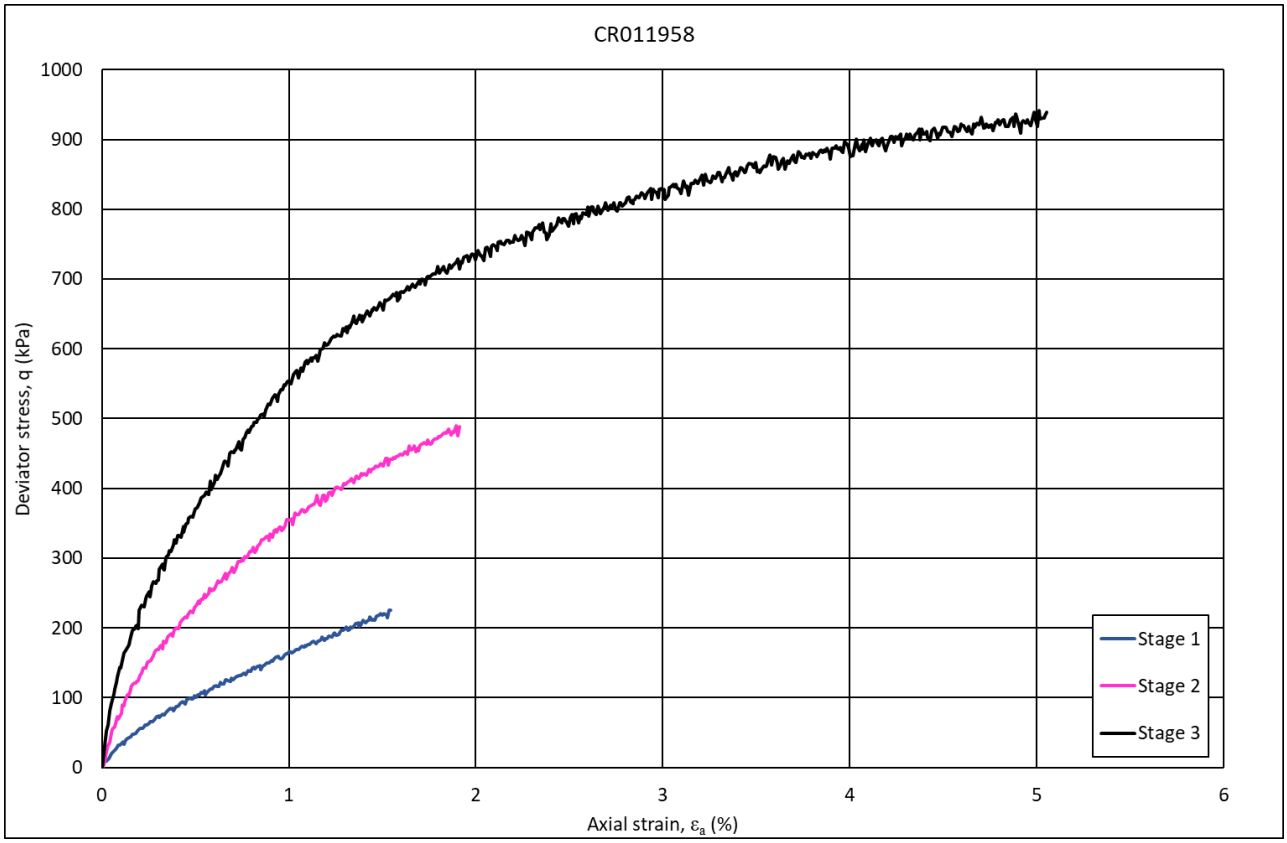

Figure 8-110 Stress-strain behaviour specimen CR011958, till, Quaternary Domain 1.4.1.

Estimates of peak undrained shear strength, q_{max} and mobilised strength equal to $0.5q_{max}$ were made and the results shown in Table 8-37.

The mobilised shear strength of till is up to 46% greater than the geologically-underlying Oxford Clay. The corresponding value of mobilised shear strain is 81% greater than any value recorded for Oxford Clay.

						Mobilised strength		Mobilised strain (%)
Specimen	**Geology**	**Specimen depth (mbgl)**	**Stage 3 cell pressure (σ_3)**	**Stage 3 back pressure (kPa)**	**Differential (effective) stress, σ'_o (kPa)**	**q_{max} (kPa)**	**$0.5q_{max}$ (kPa)**	**$\varepsilon_{F=2}$**
CR011958	TILL	13.95	1200	600	600	917	459	0.72

Table 8-37 Mobilised shear strength parameters for till, Quaternary Domain 1.4.1.

8.6.1.9 Undrained shear strength, stress path analyses (till)

The results of stress path analyses are shown in Figures 8-111 where deviator stress, q, is plotted against mean effective stress, p′, as described in Section 8.3.8. The parameters for the effective angle of shearing resistance, ø′, corresponding to two conditions of $ø'_{trans}$ and $ø'_{0.4}$ are presented as described in Section 8.3.2.7.

The ESP for all stages for specimen CR011958 initially follows a path to the right as p′ increases as a result of an initial decrease in pore pressure. With increasing deviator stress, the stress path moves to the left reflecting increasing pore pressure and a consequent decrease in p′. On approaching the critical state line, the stress path moves to the right and parallel to it, reflecting increasing p′ because of a reduction in pore pressure associated with dilation of the sample. As shearing progresses in Stage 3, q ultimately decreases slightly so that the ESP drops towards the critical state line, indicating that peak deviator stress was reached.

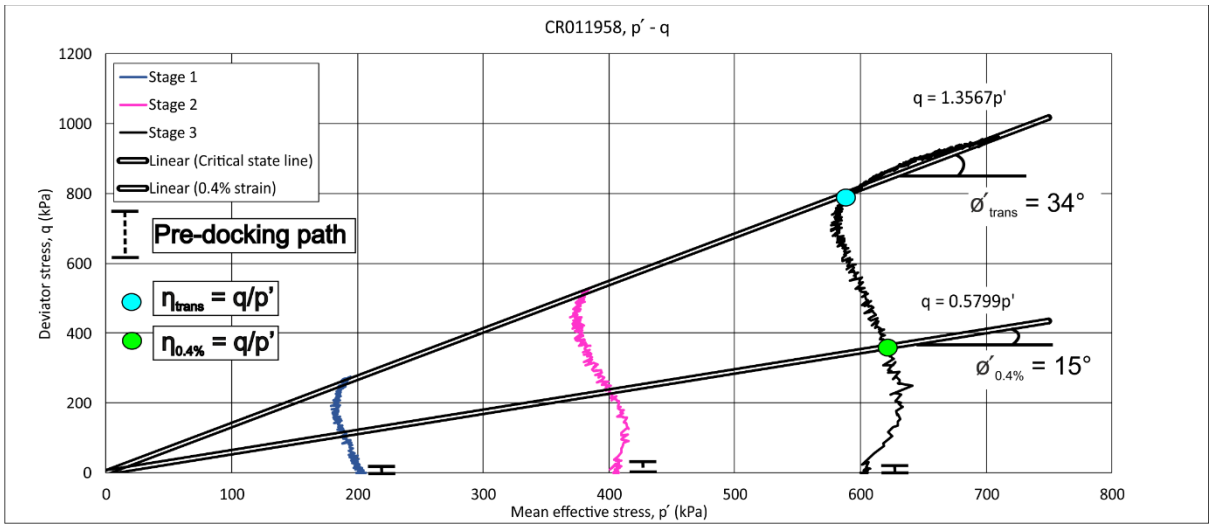

Figure 8-111 Effective tress path analyses for specimen CR011958, till, Quaternary Domain 1.4.1.

Values of η_{trans} and $\eta_{0.4\%}$ for specimen CR011958 give equivalent secant strength parameter values of $ø'_{trans}$ 34° and $ø'_{0.4\%}$ of 15°.

8.6.1.10 Isotropic consolidation (till)

The plot of isotropic consolidation before each shearing stage is shown in Figure 8-112 as change in volume (ΔV) *versus* square-root time in seconds. From each plot, estimates were made of the isotropic coefficient of compressibility (c_{vi}).

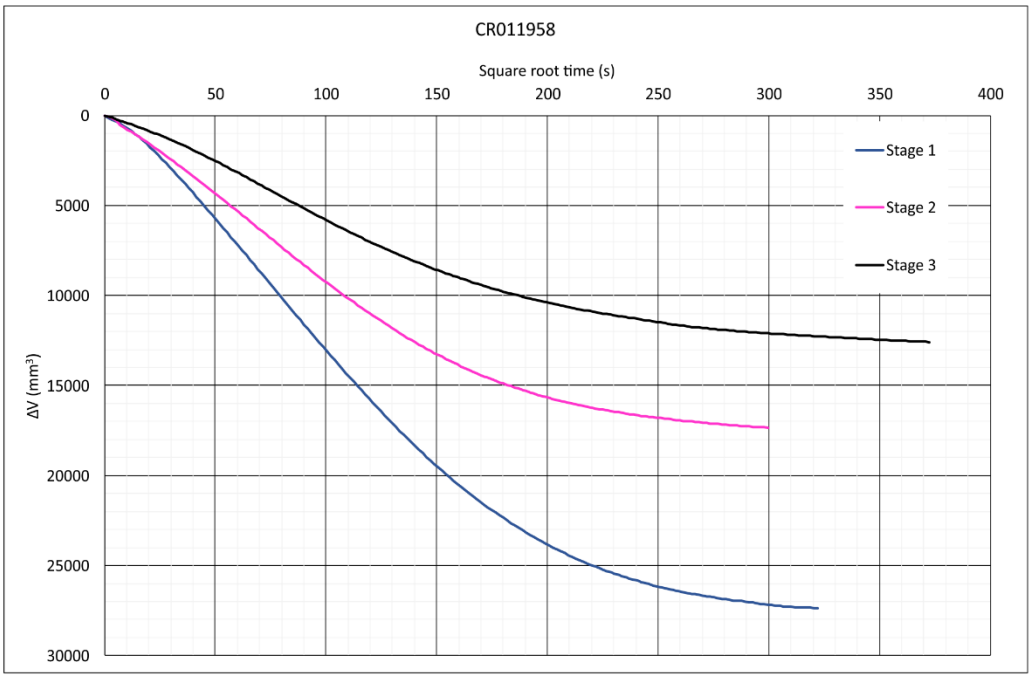

Isotropic consolidation

Initial		
Height (mm)	H_o	195.22
Diameter (mm)	D_o	99.18
Mass (g)	M_o	3331.68
Volume	cm^3	1508
Volume	mm^3	1508136
Area	mm^2	7725

	Stage 1	Stage 2	Stage 3
c_{vi} m^2/yr	11	12	11
t_{90}(min)	5	5	5
Side-drain correction applied (λ=80)			

End consolidation 1		Calculated
Height (mm)	H_1	**194.04**
Diameter (mm)	D_1	**98.57**
Volume (mm^3)	V_1	**1480767**
Area (mm^2)	A_1	**7632**

Change	Calculated
Δ_H	**1.18**
Δ_D	**0.61**
Δ_V	**27369**
Δ_A	**93**

End shear 1		
Height (mm)	H_2	**191.02**
Diameter (mm)	D_2	**99.35**
Volume (mm^3)	V_2	**1480767**
Area (mm^2)	A_2	**7752**

Change	
Δ_H	**3.02**
Δ_D	**-0.78**
Δ_V	**0**
Δ_A	**120**

End consolidation 2		
Height (mm)	H_3	**190.28**
Diameter (mm)	D_3	**98.96**
Volume (mm^3)	V_3	**1463429**
Area (mm^2)	A_3	**7691**

Change	
Δ_H	**0.75**
Δ_D	**0.39**
Δ_V	**17338**
Δ_A	**61**

End shear 2		
Height (mm)	H_4	**186.58**
Diameter (mm)	D_4	**99.93**
Volume (mm^3)	V_4	**1463429**
Area (mm^2)	A_4	**7844**

Change	
Δ_H	**3.7**
Δ_D	**-0.98**
Δ_V	**0**
Δ_A	**152**

End consolidation 3		
Height (mm)	H_5	**186.04**
Diameter (mm)	D_5	**99.65**
Volume (mm^3)	V_5	**1450844**
Area (mm^2)	A_5	**7799**

Change	
Δ_H	**0.54**
Δ_D	**0.29**
Δ_V	**12585**
Δ_A	**45**

End shear 3		
Height (mm)	H_5	**176.36**
Diameter (mm)	D_5	**102.35**
Volume (mm^3)	V_5	**1450844**
Area (mm^2)	A_5	**8227**

Change	
Δ_H	**9.68**
Δ_D	**-2.70**
Δ_V	**0**
Δ_A	**428**

Figure 8-112 Isotropic consolidation and estimated coefficient of isotropic consolidation (c_{vi}), specimen CR011958, till, Quaternary Domain 1.4.1.

Referring to specimen CR011958, in isotropic consolidation the magnitude of volume change deceases with increasing effective stress. Values for isotropic coefficient of consolidation (c_{vi})

are much larger than those for p′ >125 kPa in 1D consolidation (Section 8.6.7). At a confining stress of 1000 kPa, c_{vi} is 12 m^2/yr compared to c_v from 1D consolidation of 1.84 m^2/yr.

8.6.1.11 Stiffness (till)

Estimates of secant stiffness, expressed as Young's modulus, derived from axial transducer displacement measurements from the triaxial apparatus and the mean strain from the Hall effect sensors, are summarised in Table 8-39.

	Triaxial apparatus	Hall effect	
	E (MPa), $0.5q_{max}$	E (MPa), $0.5q_{max}$	$E_{0.1\%}$ (MPa)
Specimen			
CR011958	0.64	1.94	2.68

Table 8-38 Estimates of secant stiffness for till, Quaternary Domain 1.4.1.

The results of small-strain measurement using Hall effect sensors is shown in Figure 8-113 for specimen CR011958. During shear stages 1, 2 and 3, the specimen responds in a similar way for deviator stresses, q <600 kPa. At values of q <600 kPa, in stage 1, the axial strain increases and the sample shortens parallel to σ_a.

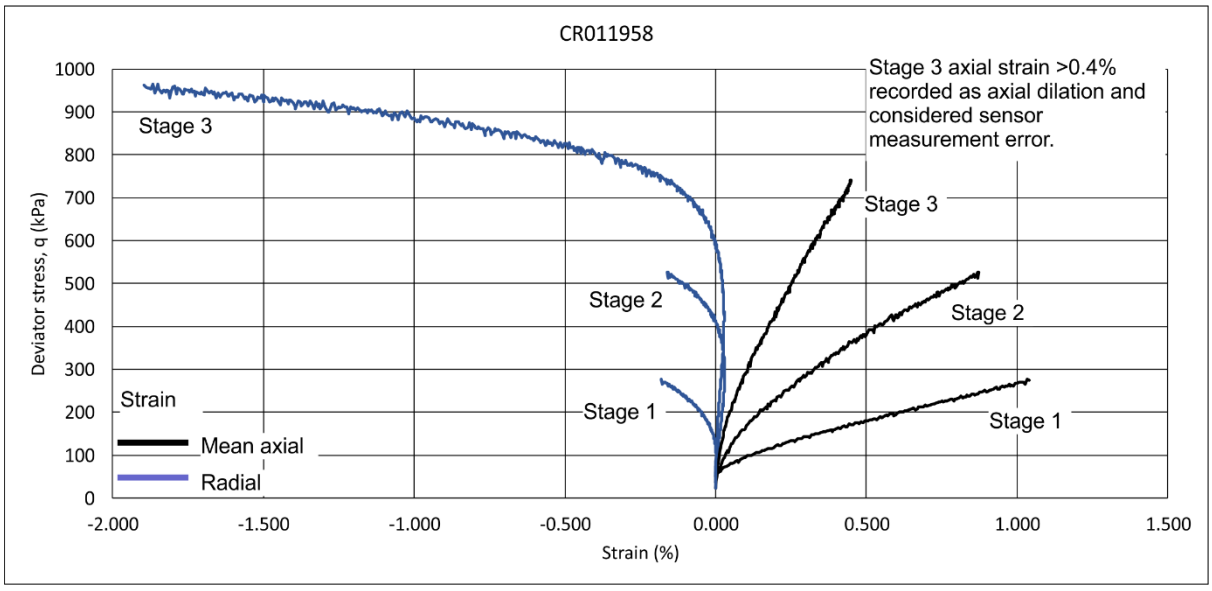

Figure 8-113 Small-strain stiffness using Hall effect sensors, specimen CR011958, till, Quaternary Domain 1.4.1.

At the same time, the sample undergoes an increase in radial strain and so dilates parallel to σ_h. The same behaviour is seen in stage 2 except that the magnitude of axial strain decreases relative to stage 1. In stage 3, for values of q <700 kPa, the same behaviour is seen and the magnitude of axial strain is less than that in stage 2. At values of q >600 kPa, radial strain becomes increasingly negative indicating that the specimen is dilating during shear. These

results agree with those from the p′-q stress-path results which indicate decreasing pore pressure, increasing effective stress and dilation and are indicative of heavily overconsolidated clay.

8.6.2 Summary

Tills from the East West Rail ground investigation in Quaternary Domain 1.4.1, are low to intermediate plasticity, calcareous, well- to poorly-graded, slightly gravelly, slightly clayey, slightly sandy silt and whose clay content varies between ~8 and 24%. Except for sample CR011953 which is inactive, all samples are normal to active with values ranging from 1.2 to 3.3. The clay mineral assemblage is homogenous comprising illite, kaolinite (with minor or trace chlorite) and chlorite. Samples, except for CR011953, have $\omega < W_p$ values so values for LI are ≤ 0. Sample CR011953 has the greatest proportion of clay for all samples (24%) and a lower I_p because of a lower value of W_L. Correspondingly, it has a lower activity and higher value of LI.

Till has low compressibility with values of m_v between 0.101and 0.016 m^2/MN for stress increments 500 and 3000 kPa respectively. Values of c_v, decreases with increasing applied stress with the greatest rate of compression between 125 and 500 kPa.

Mobilised strength at $0.5q_{max}$ for specimen CR011958 is 459kPa with a corresponding mobilised strain, $\varepsilon_{F=2}$ of 0.72%. Young's modulus, at $0.5q_{max}$ is 1.94 MPa and 0.64 MPa measured using Hall effect sensors and with axial displacement transducers on the triaxial cell respectively. In common with measurements for Oxford Clay, shear modulus values are higher when measured using Hall effect sensors than with the axial cell transducers. This effect is interpreted to result from the dampening effect of the apparatus including the top and base platens and the porous discs. The effective stress path for specimen CR011958 is typical of overconsolidated clay.

8.7 Optically-Stimulated Luminescence (OSL)

The single aliquot results presented in Table 8-24 are based on the minimum age model of (Galbraith & Green, 1990) once outliers have been excluded.

Unlike Pawley *et al*. (2008) where the dose-rates are very low allowing ages >400 ka to be determined, the dose rates for samples in this study are average for sedimentary sequences. This limits how quickly the quartz OSL traps are filled and how quickly the samples go into saturation. Saturated samples will underestimate burial ages. Only one sample (Shfd17086) had any aliquots in saturation but all samples had some aliquots near saturation. Given this and the magnitude of the D_e from the quartz a possibility exists that the resultant D_e values are under-estimates as has been reported elsewhere (Murray *et al.*, 2008). Consequently, the ages reported here are conservatively reported as a minimum.

The samples are assumed to have reset prior to burial but may be under-estimates due to saturation. Ages are quoted as minimums in years from the present day (2017) and are presented with one sigma confidence intervals which incorporate systematic uncertainties with the dosimetry data, uncertainties with the palaeomoisture content and errors associated with the D_e determination. Table 8-23 shows the final OSL age estimates which range from >145 ± 10 to >205 ± 13 ka. Samples from site SP080417 do appear older than those from SP070417. Ages are within error of each other, so it cannot be confirmed whether they are in stratigraphical order.

Lab Code	**Field Sample ID**	**Depth (m)**	**MAM D_e** (Gy)	**Dose rate** ($\mu Gy/a^{-1}$)	**Age** (ka)
Shfd17085	SP070417-1	5.3	245 ± 10.1	1698 ± 88	**>145 ± 10**
Shfd17086	SP070417-5	4.0	304 ± 15.7	1815 ± 93	**>168 ± 12**
Shfd17087	SP080417-1	9.9	207 ± 6.07	1008 ± 50	**>178 ± 17**
Shfd17088	SP080417-5	5.5	247 ± 11.4	1387 ± 80	**>205 ± 13**

Table 8-39 Summary of calculated ages using Minimum Age Model (MAM).

9 Synthesis and discussion

The results of the research are synthesised here and related back to the research hypotheses and previous literature where relevant for discussion. This chapter is divided into a geological and geotechnical discussion. The former relates to the Middle Pleistocene geological evolution of the project. The latter relates to the variability in geotechnical properties and behaviour of till and Oxford Clay within and between Quaternary Domains.

9.1 Middle to Late Pleistocene geological evolution

To address the research objective which aimed to determine the extent, timing and style of glaciation in north Buckinghamshire, the field and laboratory results are synthesised into a Quaternary event stratigraphy. With reference to field evidence, published 1:50 000 scale geological maps, the ground model developed in Section 5 and the Quaternary geology literature review, an event stratigraphy has been established for north Buckinghamshire. It is described below, summarised in Table 9-1 and illustrated in Figure 9-2.

9.1.1 Event 1, Pre-glacial

No direct evidence of this event has been observed as part of this research. It is interpreted from outcrops of quartz, quartzite and limestone-rich gravel in the Buckingham area observed by Sumbler (2002). The sediments are interpreted here to represent fluvial or glaciofluvial outwash deposited in southwestward flowing streams, parallel to the regional dip of the underlying bedrock (Figure 9-2A). It is possible that the continuation of their course southeast of Buckingham, was via the Princes Risborough and Tring Gaps in the Chiltern escarpment. Possible evidence for this interpretation comes from the presence of northwest-southeast aligned remnants of Jurassic bedrock that span the otherwise low-lying vales, floored by Jurassic mudrocks. It is therefore possible that these present-day bedrock remnants were previously partially protected from erosion, by fluvial deposits, relative to their neighbouring areas and thus preserve the former courses of the pre-glacial streams expressed as topographic inversion as observed elsewhere in Southern Britain (e.g. Ehlers *et al.*, 1991; Clark, P L Gibbard, *et al.*, 2004; Rose, 2009). If this interpretation is correct, the pre-glacial network of streams may be equivalent to the Milton and Letchworth formations in Bedfordshire and Hertfordshire and therefore form part of a left-bank drainage system of the ancestral River Thames as suggested by Belshaw *et al*. (2014). The latter also noted the presence of gravel-filled cols beneath glacigenic deposits in the Chiltern Hills.

9.1.2 Event 2, Glacial 1

This event is interpreted from the presence of the Buckingham Till Member of a newly named Tingewick Formation. It is exposed at the base of the sequence within Buckingham Sand Pit

and in a small section at Home Farm, Stowe, (LF2b). Advance of glacier ice from the north or northwest is interpreted from the presence of well-rounded erratics of 'Bunter' (Sherwood Sandstone Group) quartzite and sandstone and the rare occurrence of chalk erratics relative to the chalk-rich Milton Keynes Till Member. Limited macro-fabric data recorded in Buckingham Sand Pit indicates deposition from glacier ice from the northwest (Figure 9-2B).

The maximum extent of this advance is unknown. Existing ground investigation boreholes in the Buckingham area demonstrate the presence of the Buckingham Till and Milton Keynes Till members, separated by laminated sand, silty sand and gravel (see also Section 5 for cross-sections). This sequence was also observed in 1998 during ground investigation works for the Tingewick By-pass, in the area of SP 664 328 (Phil Gibbard, Pers. Comm.). The presence of lower and upper tills is also indicated by the outcrop pattern of till and sand and gravel where they are mapped in valleys on the Buckingham 1:50 000 geological maps. Lower and upper till units are shown to be separated by sand and gravel, although the latter is undifferentiated on the map. This outcrop pattern has been used to interpret the southern extent of glacier ice during event 2, although its extent has not been observed or proved as part of this research.

It is interpreted that an ice lobe of the BIS entered the area via a breach in the Middle-Jurassic escarpment which marks the northwest boundary of the project area, around Brackley [SP 582 368]. Here, deep incision into bedrock has resulted in a northwest-southeast-trending probable buried valley. The valley breaches sandstone and limestone of the Great Oolite Group and erodes down to Early Jurassic, Lias Group mudstone. A similar valley feature exposing Lias Group mudstone at subcrop beneath Quaternary deposits exists around Towecster [SP 693 486]. Here, the Lias Group-floored valley trends northwest-southeast where it exists to the north of the project area around Stony Stratford [SP 793 402]. At this point it may join the buried valley proved at Deanshanger (Figure 9-1).

Evidence for an ice lobe of the BIS entering the area from the northwest is inferred from palynomorphs preserved within a sample of till collected south of Buckingham (Riding 2008). Within this research area, the till samples are dominated by Middle and late Jurassic palynomorphs, derived principally from the underlying Oxford Clay.

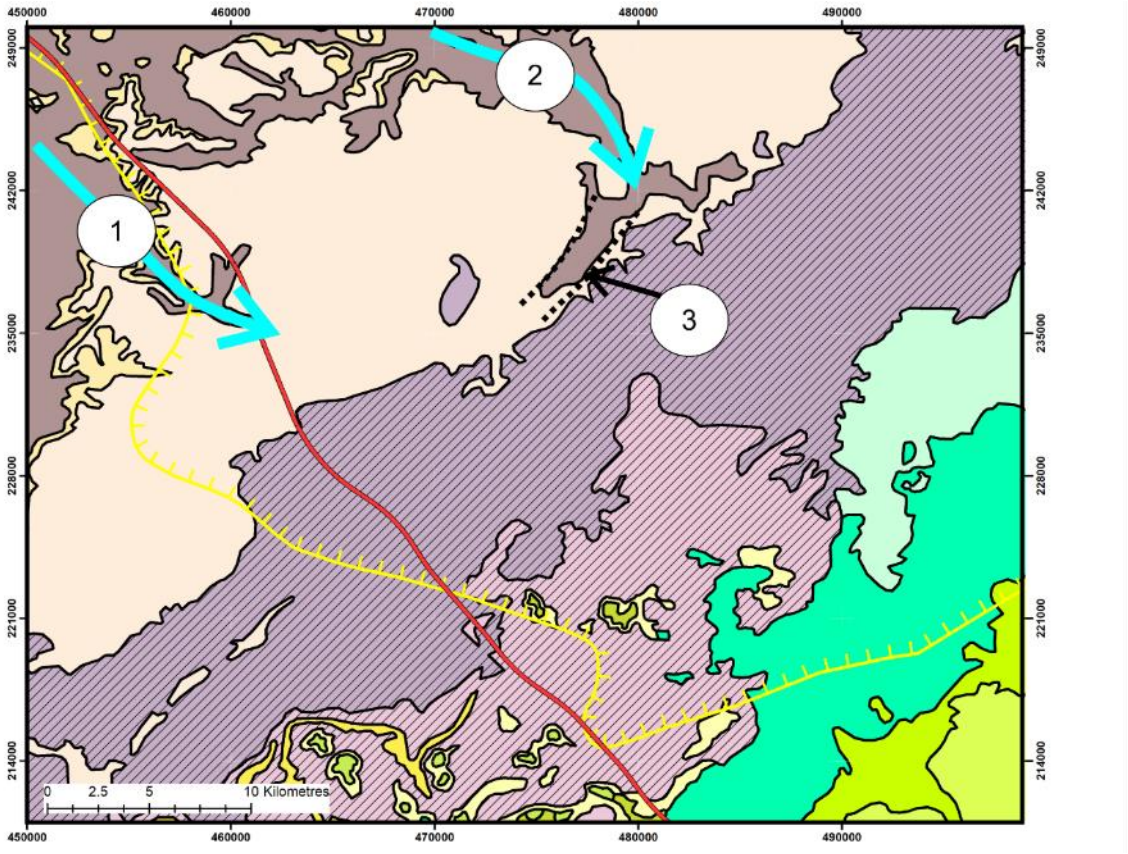

Figure 9-1 Possible entry points for glacier advance from the northwest, into the project area via breaches in the Middle Jurassic escarpment around Brackley (1) and Towcester (2). Breaches are indicated by northwest-southeast orientated erosional valley features that expose Lias Group mudrocks at their base. 3) Deanshanger buried valley. Legend as for Figure 3-1.

Of the allochthonous non-local material, Carboniferous palynomorphs were recorded in all samples. Late Triassic palynomorphs are relatively common but Early Jurassic and Cretaceous palynomorphs are rare. Only one sample, MPA56147, preserves Early Jurassic palynomorphs. This is interpreted as evidence that a lobe of the BIS entered from a main stream that was present to the northwest of the area. This main ice stream may have entered Central England to the north of the northwest-southeast trending Middle Jurassic escarpment so that it overrode Lower Jurassic mudrocks in the west and east Midlands.

The presence of an 'older' glacial phase represented by till of different lithology to the regionally extensive 'chalky till', supports earlier suggestions of at least two glacial events in Bedfordshire, Northamptonshire and Milton Keynes (Hollingworth & Taylor, 1946; Horton *et al.*, 1974; Barron *et al.*, 2006, 2010). The interpretation of differences in lithology between chalk-rich and chalk-poor tills as the effect of weathering (Sumbler, 2002) is not supported here. The pattern of valley-controlled glaciation is also similar in style to that interpreted in the Vale of St Albans (Gibbard, 1977).

9.1.3 Event 3, deglaciation 1

Following glacier advance and deposition of the Buckingham Till Member, deglaciation towards the northwest is implied (Figure 9-2C). Glaciofluvial outwash is assumed and is interpreted to have initiated or re-worked northeast-southwest trending valleys cut into the Oxford Clay. The latter orientation is interpreted to reflect a combination of two dominant processes; northeastward tilting resulting from glacier loading and relative ease of erosion and glaciofluvial incision into underlying mudrocks of the Oxford Clay. The focus of drainage is interpreted to be the stratigraphical boundary between the Oxford Clay and the underlying sand and sandstone of the Kellaways Formation. The softer sediments of the Kellaways Formation may have provided a preferential route for glaciofluvial erosion after bedrock dip-parallel drainage over the underlying Cornbrash and Forest Marble formations. This drainage pattern is observed today where southeastward-directed drainage over the Cornbrash Formation is directed southwestward along the Kellaways-Oxford Clay boundary around the River Ray. Northeastward tilting is interpreted to result from the early onset of a second phase of glacier ice advance, this time from the northeast.

Exposures of coarse gravel and limestone boulders (Page Hill Member) in Buckingham Sand Pit, (LF4) are interpreted to have been deposited at this time as outwash, which partially infilled incised valleys to the west of the project area and were sourced from the northwest-directed retreating glacier margin. Alternatively, they may have been deposited as part of a proximal, glaciolacustrine deltaic sequence with a sediment source from the area of Ockley Brook [SP 545 314]. The breach in the Cornbrash Formation limestone in the centre of Buckingham, and through which the River Great Ouse now flows, is interpreted to have formed at this time.

The timing of onset of glaciolacustrine conditions is unknown. It is interpreted here to occur during this first phase of deglaciation resulting in the deposition of interbedded and interlaminated glaciolacustrine sediments comprising silt, clay and sand (Deanshanger Glaciolacustrine Member, LF1b and LF1c of Section 8.4). It is likely that glaciolacustrine deposition took place within pro-glacial lakes, dammed to the northeast by glacier ice and to the southwest by bedrock topography, in part controlled by its southeast regional dip (Figure 9-2D).

9.1.4 Event 4, glaciation 2

The presence of exposures of stratified till, interbedded with lenses of gravel and sandy gravel in Bletchley (LF2/LF1c), are interpreted as evidence for deposition beneath a local ice-shelf

floating on the lake that developed during Event 3. The timing of onset and the interaction and behaviour of the retreating and subsequently advancing ice-margin, is uncertain. The advance of glacier ice provided a source of chalk-rich till that was either released directly from the melting ice-shelf or by subaquatic debris flows (undermelt till). Cross-bedding measured in outcrops in Bletchley indicate that gravel-laden streams, sourced from the retreating ice-front and rich in chalk, entered the lake form the north and flowed towards the southwest. The position of the ice-front is unknown but is interpreted to be proximal to Deanshanger and Bletchley to deposit interbedded till and glaciolacustrine sediments. The number of oscillations of the ice lobe at this position is unknown although Horton *et al*. (1974) interpreted at least three, based on the number of thick till layers within the Deanshanger borehole sequence.

The spatial extent of the pro-glacial(s) lake is uncertain. Its sediments are preserved within the BGS Deanshanger borehole where they occupy a buried valley. The lowermost sediments were interpreted as 'fluviatile' by Horton *et al*. (1974) and may have been sourced from the advancing ice front to the north.

The preservation of glaciolacustrine deposits has also been observed in the River Ouzel by Horton (1970). Glaciolacustrine sediments (LF1c) were observed in Bletchley but it is not known if they occupy a buried valley in this area. Considering the outcrop pattern of glaciolacustrine sediments recorded on the 1:50 000 geological map, it is probable that the pro-glacial lake extended beyond the buried valleys either during this stage or Event 3, during deglaciation. It is possible, but not known, that sediment was sourced from the west, from streams entering the lake via the channel at Ockley Brook.

9.1.5 Event 5, glaciation 2

Beds of chalk-rich, matrix-supported clay and silt, interpreted as subaquatic (undermelt) tills (LF2/LF1c) become more common towards the top of the Deanshanger Glaciolacustrine Member, the lower part of which was deposited during Event 4. This, together with deformation structures, including overturned folds, faults and shear planes observed in the equivalent unit in the BGS Deanshanger borehole and at outcrop in Buckingham Sand Pit, are interpreted to indicate the progressive advance and ultimate overriding of glaciolacustrine sediments, by glacier ice advancing from the north or northeast (Figure 9-2E). The observed deformation structures are interpreted to similar in style, and to correlate with, those observed by Green (1864) where upright and overturned folds, steeply and dipping beds in sand and gravel and 'blue clay' near Foscott [SP 716 358], east of Buckingham.

This advance deposited chalk-rick till interpreted as sub-glacial traction till (Milton Keynes Till Member). Its maximum extent is not known with certainty but is inferred from the distribution of till and interbedded sand and gravel shown on 1:50 000 scale geological maps and geomorphological evidence. The latter takes the form of a roughly arcuate, till and sand and gravel-capped ridge that extends northwest-southeast, across the otherwise low-lying Jurassic mudrocks of the Vale of Aylesbury and its equivalents. This bedrock cored ridge in around the village of Poundon [SP 644 252] probably formed a geomorphological barrier to further glacier advance towards the southwest, and so is interpreted to mark the maximum extent of glacier ice in the region.

The direction of the glacier advance that deposited chalk-rich till, is supported regionally by micropalaeontological and palynological evidence. Based on evidence of microfossils within chalk erratics and till-matrix material, Fish & Whiteman (2001) concluded that the direction of glacier flow into southern Britain was initially through eastern England before fanning into East Anglia and moving southwestwards into the north Buckinghamshire area. Based on analysis of till palynomorphs, including those derived from Westphalian Coal Measures, Riding (2008) concluded that chalk-rich till in Buckingham was derived from an ice source to the north or northeast. It is interpreted here that the till deposited during Events 4 and 5 was derived from an ice lobe of the BIS entering the area from the northeast. This allowed a lobe to advance to the south of the Middle Jurassic escarpment that had previously acted as a breached barrier during Event 2 and occupy a broad valley, underlain by Middle and Late Jurassic mudrocks, including the Oxford Clay. This is tentatively correlated with the eastward shift in the BIS, inferred by Fish & Whiteman (2001) because of confinement of the BIS by the Scandinavian Ice Sheet in the southern North Sea.

Preserved, evidence of pro-glacial outwash associated with this glacial advance is lacking. It is possible that southwestward-directed outwash entered the valley of the River Ray and/or the River Thame, before entering the Upper Thames catchment. There is some support for this where erratics in the basal sequence at Marsworth have been suggested as being transported there by outwash from a glacier margin to the north of the locality (Murton *et al*., 2015).

Alternatively, because of the presence of the bedrock ridge at its terminus, subglacial drainage could have been facilitated within the pre-existing, sand-filled, buried valleys excavated into Jurassic mudrocks. There is no field evidence, but this style of subglacial drainage may have controlled the dynamics of the lobe of the BIS at its terminus. Excess pore pressure that may

have otherwise built up beneath the lobe where it advanced over low permeability mudrocks may have been allowed to dissipate and so effectively reduce the degree of basal sliding.

9.1.6 Events 6 & 7, deglaciation 2

It is assumed that glacier retreat occurred towards the northeast (Figure 9-2F) although there is no geomorphological evidence to support this. Deglaciation is characterised in the study area by a second phase of glaciolacustrine deposition resulting in the deposition of the Bletchley Glaciolacustrine Member.

At Bletchley, stratified till and sand and gravel, grades upwards into laminated silt and clay with sand beds (LF3b of Section 8.4) within the Bletchley Glaciolacustrine Member. Some sand beds form lithorelics and are interpreted as brecciation resulting from seasonal freezing or permafrost development. This evidence indicates that sandy facies within the lake were deposited sub-aerially or at the shallow margins of the lake, allowing ground-ice to develop. The brecciated zone at Bletchley is overlain by laminated silt and clay marking a return to deeper water, glaciolacustrine deposition. Its upper part becomes gravelly and cross-bedded indicating unidirectional stream flow towards the north as the former, active ice-front retreated.

The sequence of interbedded sands and gravels with cobbles, representing a sub-aerial terminoglacial fan exposed at Home Farm, Stowe, and named the Home Farm Member, could have also been deposited at this time (Figure 9-2G).

At an unknown time, following deglaciation, the post-glacial drainage system of the River Great Ouse and its tributaries were established on a northeastward-tilted landscape. Notably, this post-glacial, bedrock-strike orientated, drainage direction is perpendicular to that interpreted prior to glaciation during Event 1. This pre- and post-glacial drainage pattern is consistent with drainage development patterns recognised elsewhere in previously glaciated landscapes of lowland Britain (e.g. Belshaw *et al.*, 2014).

9.1.7 Event 8, periglacial

Although presented here as the last of a sequence of Middle Pleistocene events, it is probable that the periglacial processes, deposits and landforms that are present within the study area operated during any cool period during the Quaternary (Figure 9-2H).

Frost wedging was widely observed in till erratics along with brecciation of fine-grained (micritic) limestone within the Oxford Clay. These features are taken as evidence of post-depositional ground-freezing either as permafrost or seasonally frozen ground. Involutions

were observed in river terrace gravels of the River Great Ouse in Passenham and in thinly-bedded limestone near Passenham and Tingewick. Involutions, in the form of gravel-filled balls and pillows, were also previously observed in river terrace gravels and underlying mudrocks of the Oxford Clay at Bletchley (Horton *et al*., 1974). There is insufficient evidence to unequivocally interpret these features resulting from permafrost development or seasonal freezing. Ice-wedge pseudomorphs identified in sediments from Marsworth, near Aylesbury [SP 918 144] demonstrate the presence the potential for permafrost in the area.

Matrix-supported silt and clay with angular clasts, interpreted as 'head', are widespread and are often best developed on the flanks of the main drainage systems of the River Great Ouse. This observation provides evidence of post-glacial solifluction. In some areas including Ot Moor, the River Great Ouse tributaries of Padbury Brook and Claydon Brook, thermokarst lakes may have developed; the present drainage courses potentially taken by routeways following thermokarst lake drainage. No direct evidence for their presence was observed but their development overlying frost-susceptible Jurassic and early Cretaceous mudrocks might be expected as highlighted by West (1991) and Burton (1976) who identified similar features in Cambridgeshire. Deposits of 'head' shown on the 1:50 000 scale geological map in areas including Stewartby [TL 022 422], Whaddon [SP 803 344] and alluvium and 'head' in Ot Moor, may be related to slumping and thaw erosion before drainage of these potential lakes.

Geological unit		**Sedimentology**	**Palaeoenvironmental interpretation**	**Relative event chronology (1 = oldest)**
Alluvium		Sandy silt and clay with gravel towards the base.	Fluvial.	8
'Head'		Brown, sandy, clayey, gravelly silt and clay.	Periglacial solifluction.	7
River Terrace Deposits		Gravel and sandy gravel.	(Glacio)fluvial, periglacial.	7
Buckinghamshire Glacigenic Formation	Bletchley Glaciolacustrine Member, Home Farm Member	Interbedded and interlaminated silt, sandy silt, chalk-rich till, sand and gravel.	Glaciolacustrine, proglacial. Infills buried valleys.	6
	Milton Keynes Till Member	Bluish-grey, sandy, clayey, gravelly silt with cobbles and occasional boulders. Common well-rounded chalk and sub-	Sub-glacial traction till and sub-aerial terminoglacial fans.	5

		angular flint erratics. Common sand and gravel, beds and lenses of sand.		
	Deanshanger Glaciolacustrine Member	Interbedded and interlaminated silt, sandy and clay with common beds and lenses of chalk-rich till, increasing in abundance upwards.	Glaciolacustrine, proglacial. Infills buried valleys.	4
	Page Hill Member	Sand, gravel and cobbles. Coarse gravel and cobbles in Buckingham Sand Pit?	Glaciofluvial erosion on NE-ward tilting land surface.	3
Tingewick Formation	Buckingham Till Member	Reddish-brown, very sandy, clayey, gravelly silt. Common Triassic-derived 'Bunter' quartz and quartzite and locally derived Jurassic erratics, rare chalk.	Sub-glacial traction till.	2
	'Pre-glacial gravel'	Quartz, quartzite and limestone gravel.	Southeastward-directed, fluvial or glaciofluvial streams. North-bank proto-Thames tributaries?	1

Table 9-1 Relative Quaternary event stratigraphy in North Buckinghamshire, Milton Keynes and Bedfordshire areas interpreted from research results and; Green, 1864; Horton, 1970; Horton *et al.*, 1974; Ambrose & Horton, 1991; Sumbler, 2002; Barron *et al.*, 2006, 2010). Numbers represent the sequence of local events and do not represent Marine Isotope Stages.

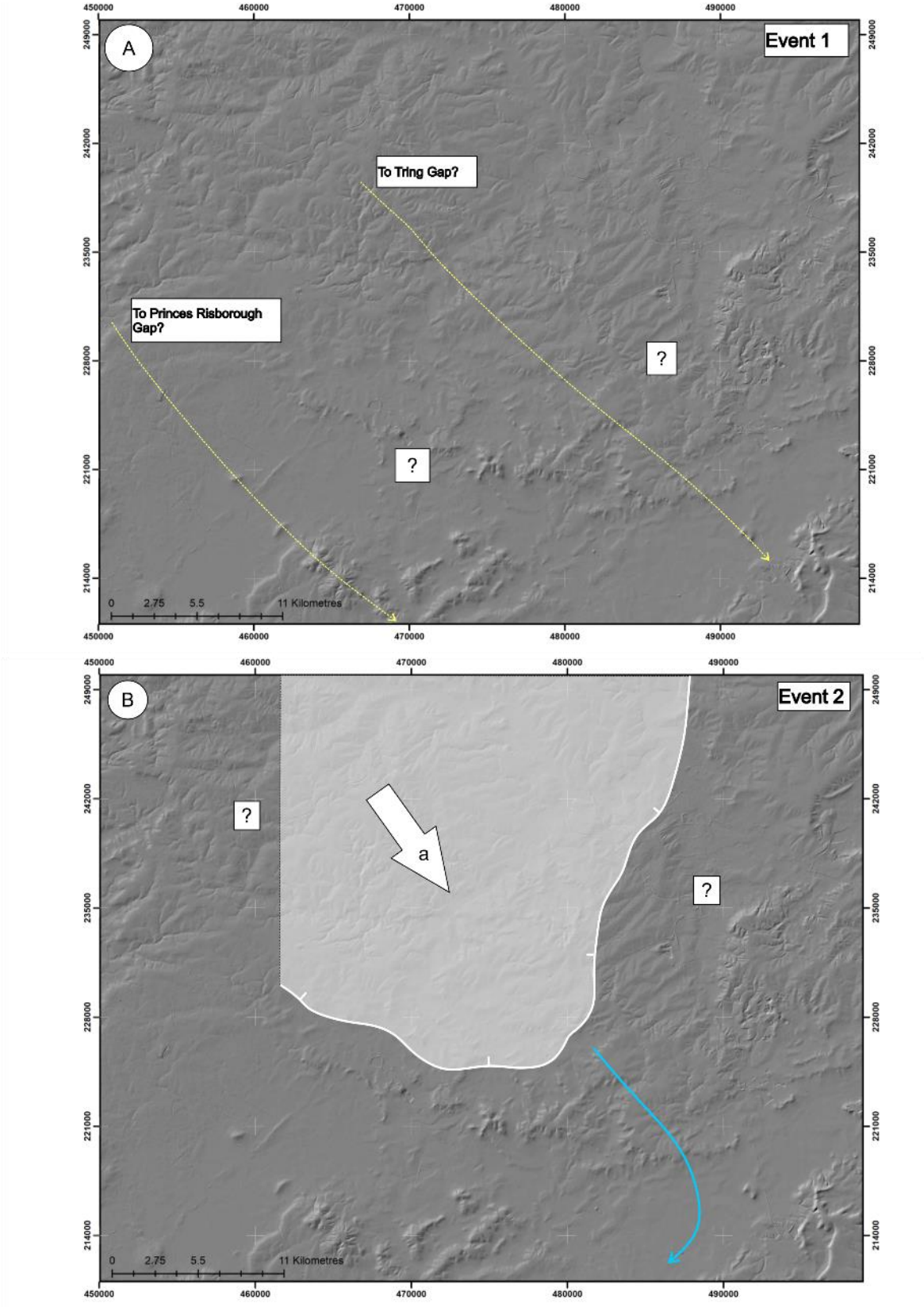

Figure 9-2 Interpreted glacial and periglacial event stratigraphy in north Buckinghamshire. Geographic extent as shown in Figure 1-1. Ordnance Survey data © Crown Copyright and Database Right [2018]. Ordnance Survey (Digimap Licence). Legend shown at the end of the Figure.

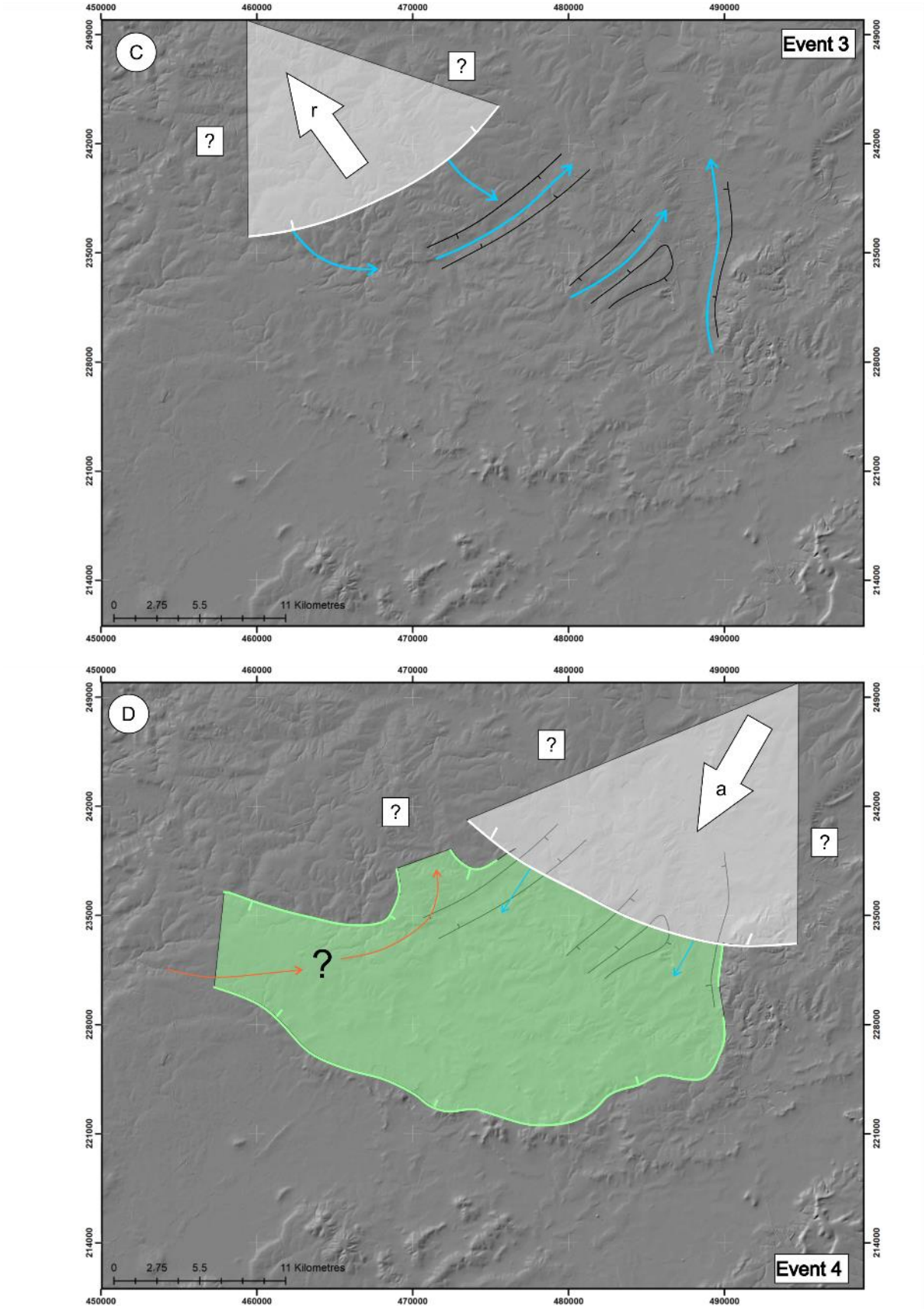

Figure 9-2 continued.

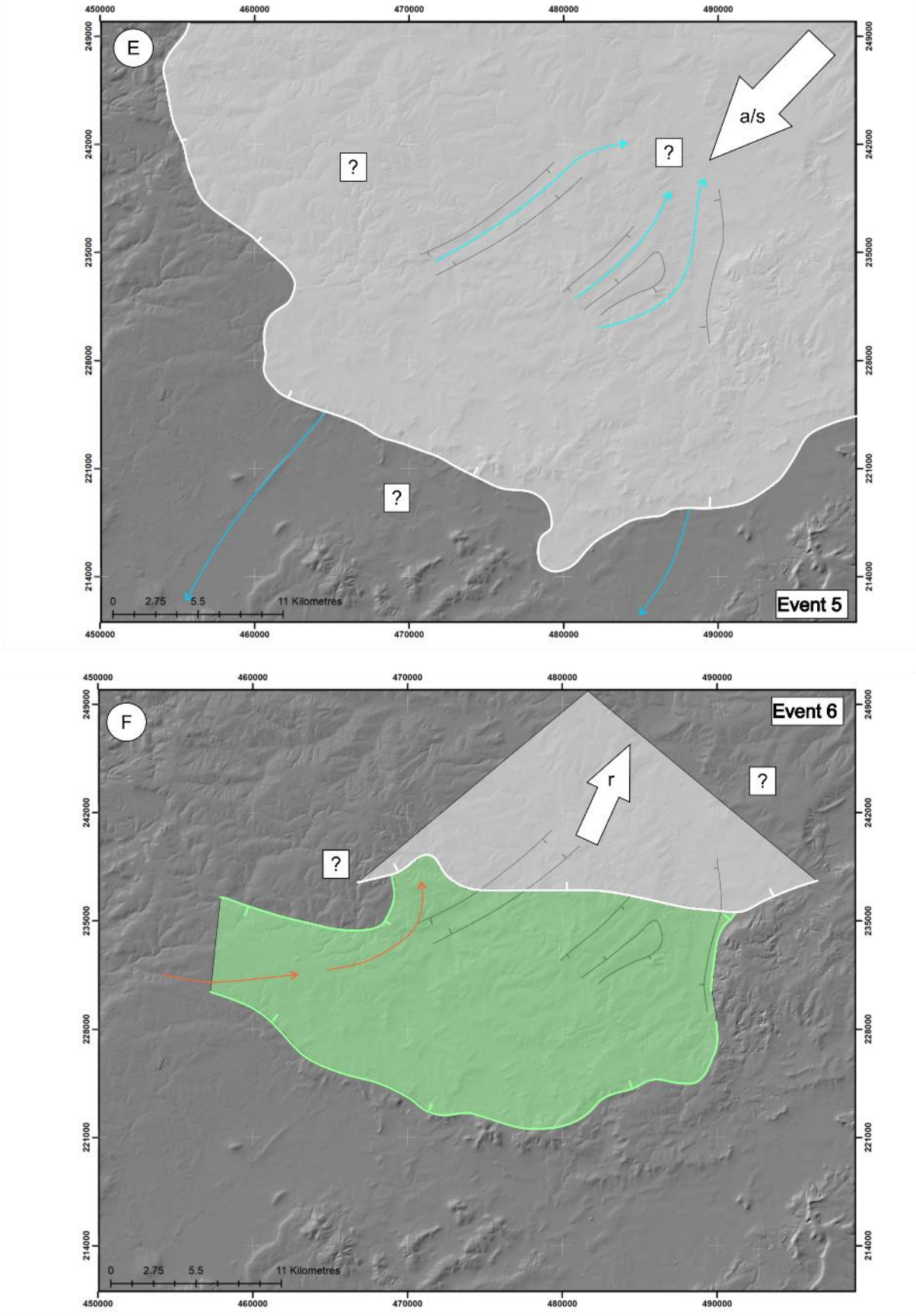

Figure 9-2 continued.

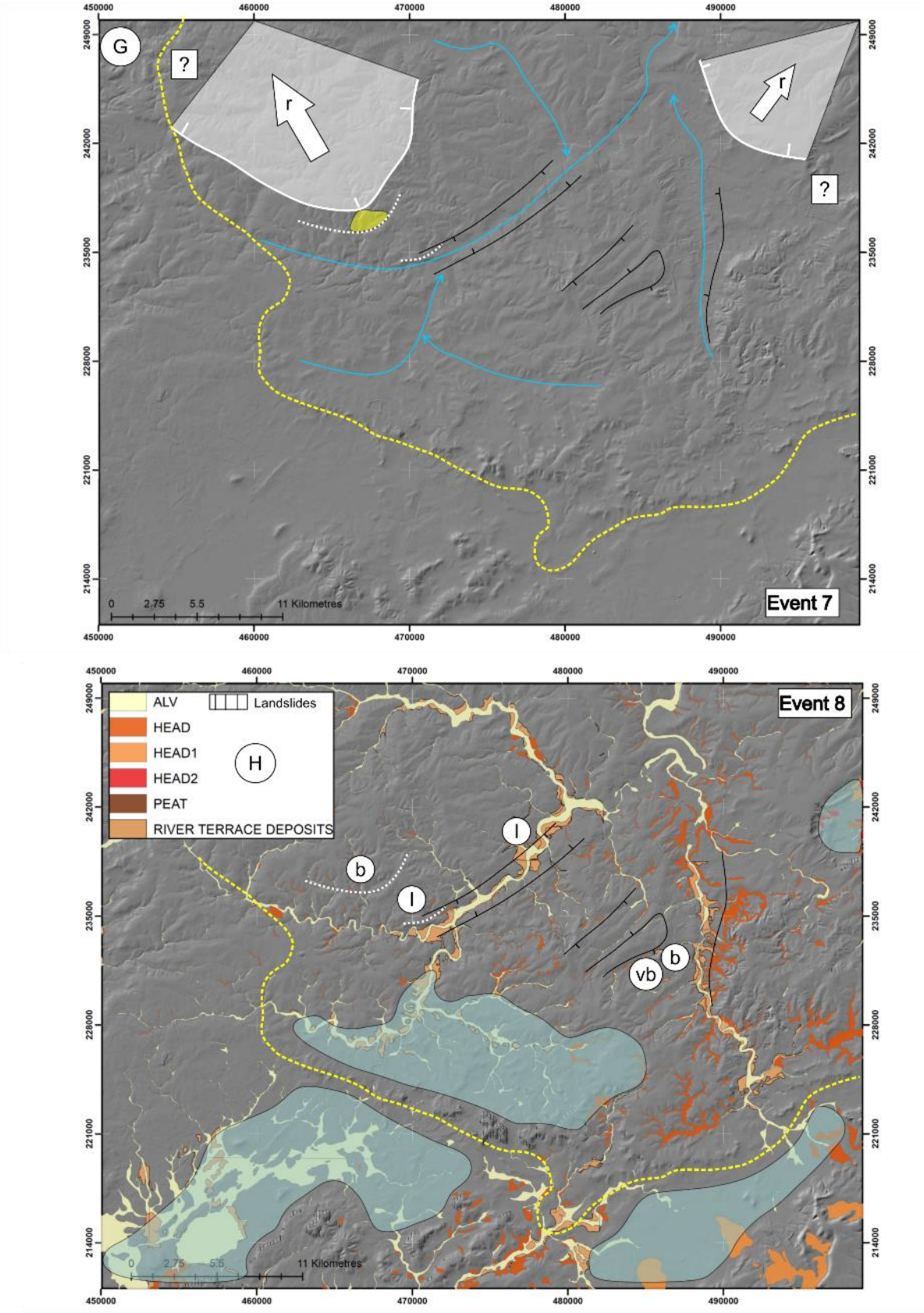

Figure 9-2 continued.

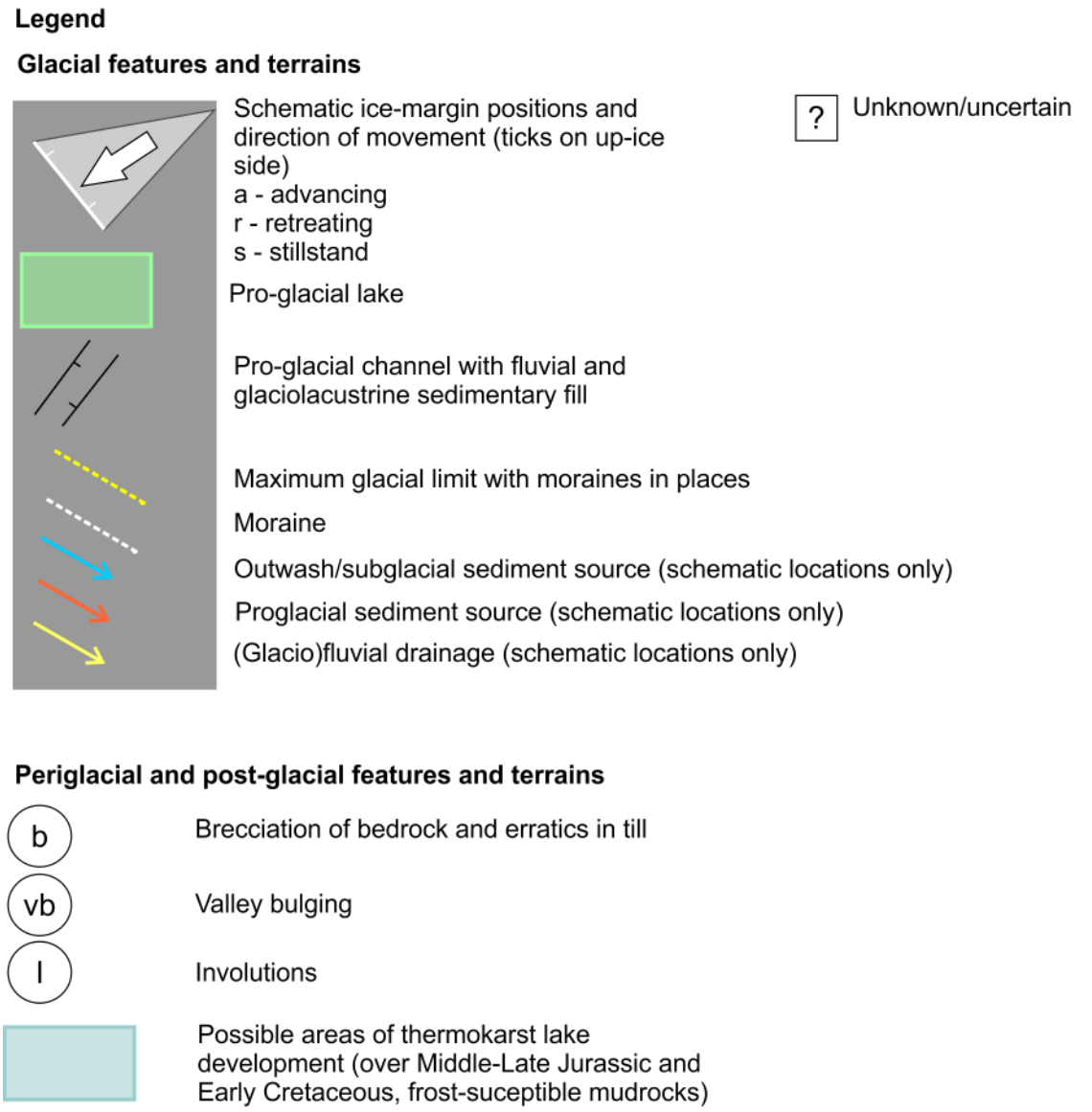

Figure 9-2 continued.

9.1.8 Geochronology

The Quaternary events described in Sections 9.1.1 to 9.1.7 provide a relative event stratigraphy, based on possible, or observed, stratigraphical relationships seen in outcrop, proved in existing boreholes or from previous literature. The two-phase model interpreted here supports earlier models of two-phase glaciation in southern Britain. The model presented here supports advance of glacier ice into the area from the northwest during an older event, and from the north or northwest during a younger event. The direction of advance of the younger event supports that as proposed by Fish & Whiteman (2001) where glacier advance from eastern England is envisaged to enter southern Britain from the north before advancing southwestwards into the north Buckinghamshire area. It is not possible to confirm if this ice-

stream merged with another, North Sea-derived lobe of the BIS, advancing from east, coincident with the A6 event of Lee *et al*. 2017.

As reviewed in Section 3.2.4, the numerical chronology of glacial and periglacial events is poorly known in the English Midlands, including north Buckinghamshire, and remains a topic of debate. The glacigenic sequences of north Buckinghamshire occur geographically between sedimentary sequences unequivocally dated and associated with the Anglian Stage (MIS 12) in East Anglia, and those of the English Midlands. The timing of the glacial events resulting in deposition of the Wolston Formation in the English Midlands remains a topic of intense debate, with the sequence variably equated with both the Anglian and Wolstonian stages (see review in Section 3.3.2.4). By convention, the glacigenic sequences in north Buckinghamshire have been assumed to have been deposited during the Anglian Stage. The latter assumption was tested during this research using OSL dating to attempt to obtain representative numerical ages for different parts of the glacigenic sequence.

Samples, numerically-dated using OSL techniques, revealed minimum ages between >145 ± 10 and >205 ± 13 ka. Although the sediments could be older, they may just as likely equate with the calculated minimum age. Although sediments to the west (Home Farm, Stowe) appear relatively older than those to the east, the numerical-age resolution is insufficient to differentiate individual events. Importantly, each of the four ages calculated for this research are within analytical age overlap and so any conclusions regarding relative stratigraphy between them is uncertain. If the calculated ages are accepted using their minimum age, each of the samples equates with the late Wolstonian (Saalian) Stage, approximately equivalent to MIS 6 (the Warthe or Drente Stadials of mainland Europe; see Section 2.1), a period of intense cold and glaciation.

The most recent, and closest area to the project which used a multi-proxy approach to palaeoenvironmental reconstruction, was Marsworth (Murton *et al*., 2015). Here, sediments infilling a former river channel, were investigated using sedimentology, particle-size analysis, mineralogical analysis, clast lithology analysis, biostratigraphy and OSL and amino-acid dating. The site lies ~10 km to the south of the Anglian glacial limit. Palaeoenvironmental reconstruction at the site identifies indirect evidence for glacier ice during MIS 12 and a further intensely cold-stage dominated by periglacial activity during ~MIS 6, separated by full interglacial conditions during Marine Isotope substages 7 e and 7 c. The latter interpretation was based on fossil evidence from Molluscan and mammals remains. The site therefore

highlights the potential for glacier ice to be locally present in MIS 12 and MIS 6 Sediments interpreted as outwash at Marsworth, were correlated with MIS 12.

A late-Wolstonian age for the sediments in the project area, is not supported by recent work which reveals the extent and timing of glaciation in the Fenland of eastern England (Gibbard *et al.*, 2018). Based on geomorphological and sedimentological evidence, the maximum southern and western extent of glacier advance at this time is taken from a line running approximately from Cambridge in the southeast to Huntingdon in the northwest.

Correlation of river terraces in the Upper Thames and Great Ouse catchments has been used to establish the relative age of glaciation in Buckinghamshire (Gibbard, 1985; Sumbler, 1995, 2001, 2002; Bridgland, 2006; Boreham *et al.*, 2010). Glacigenic deposits comprising till and outwash in the headwaters of the River Thame catchment have been correlated with terraces of the River Thame and Upper Thames (Sumbler 1995). Glacigenic sediments have been altitudinally correlated with the Blackditch (Thame) and Wolvercote (Upper Thames) terraces, the latter terrace being correlated with the Taplow Gravel of the Lower Thames which is considered Late Wolstonian in age (e.g. Gibbard, 1994). The Wolvercote Terrace in the Upper Thames region is considered to be post-Anglian in age and correlated with ~MIS10 to 6 by Sumbler (1995). The oldest terrace in Upper and Middle Great Ouse catchment has been correlated with the Biddenham terrace and correlated with MIS 10-8 (Harding *et al.*, 1992). Thus, terrace aggradations in the Great Ouse and Thame catchments suggest post-Anglian deposition.

The equivocal and conflicting geochronological evidence presented in this research, and consideration of the literature, makes definitive conclusions about the timing of glaciation difficult. The presence of the Buckingham and Milton Keynes members comprising till, separated by glaciolacustrine sediments, indicates two distinct glacial events that could be correlated with glaciation during the Anglian and the late Wolstonian respectively. However, there is no evidence to support this conclusion. Multiple advances of glacier ice could occur within one glaciation. Numerical OSL dating provided minimum ages only and demonstrated that the glacial deposits are pre-Devensian in age. The numerical ages are not sufficient to discriminate between any previous Middle Pleistocene glaciations.

Given the palaeoenvironmental sequence described in the Marsworth area, the glacigenic sequence in the project area is tentatively related to the Anglian Stage where it is represented by at least two glacial events. The period of intense cold during the Late Wolstonian, (MIS 6), recorded in the Marsworth area is interpreted as the major cold period which resulted in

widespread periglacial activity, including the brecciation of erratics within the till and bedrock and the formation of involutions.

Additional, multi-proxy methods for numerical dating are needed to resolve the timing of glaciation at this major margin of the former British Ice Sheet.

9.1.9 Stratigraphical correlation

The potential correlation between the glacigenic sequences identified as part of this research, the English Midlands and East Anglia is considered here (see Section 3.3.2.4 for review).

The presence of two tills, here referred to as the Buckingham Till and Milton Keynes Till members, presents an opportunity for lithostratigraphical correlation with the Central England. It is proposed that the lower, Buckingham Till Member, is correlated with the Bozeat Till Member of the Bedford and Wellingborough areas (Barron *et al.*, 2006, 2010). It is also interpreted to correlate with the 'Lower Boulder Clay' in the Kettering area (Hollingworth & Taylor, 1946). The upper, Milton Keynes Till Member, could be correlated with the chalk-rich and regionally extensive till that has conventionally been assigned to the Oadby Till Member. The latter is consistent with the stratigraphical division of tills on the published 1:50 000 scale geological maps.

The Buckingham Till Member, Milton Keynes Till Member and the Deanshanger Glaciolacustrine Member have been assigned member status as part of a newly formed North Buckinghamshire Glacigenic Formation. The Milton Keynes Till and Buckingham Till members are tentatively correlated with the Oadby Till and Bozeat (Thrussington) Till members of the Wolston Formation of the English Midlands (Shotton, 1953, 1983; Rice & Douglas, 1991). The Deanshanger Glaciolacustrine Member may also correlate with that of the glaciolacustrine, lower Wolston Member. As reviewed in Section 3.2.2.1, the Wolston Formation has been variably associated with glacigenic deposits interpreted to be either Anglian or Wolstonian in age. The lithostratigraphical correlation of the glacigenic sequence in north Buckinghamshire can only be valid if it is established that it is the same age as that in the English Midlands. The same principle applies at any tentative correlation with East Anglia, where the deposits are conventionally associated with glaciation during the Anglian Stage. If the glacigenic sequence in north Buckinghamshire is in fact Anglian in age, the chalk-rich, Milton Keynes Till Member could correlate with the chalk-rich Lowestoft Formation of East Anglia (e.g. Lunkka, 1994; Lee *et al.*, 2017) or the later, tectonostratigraphically-defined 'A6 event of Lee *et al*. (2017). The Bozeat/Thrussington Till Member (e.g. Barron *et al.*, 2010) was previously correlated with the Walcott Till (Lee *et al*.,

2012) of East Anglia and interpreted to be part of a regionally extensive, dissected till sheet deposited by a 'Pennine Ice Lobe' of the British Ice Sheet (e.g. Lee *et al*., 2017). If the Buckingham Till Member is indeed a correlative of the Bozeat/Thrussington Member, in north Buckinghamshire, it is interpreted to be potentially a local event and doesn't support regional correlation into East Anglia.

9.2 Geotechnical properties and behaviour

To address the research objectives that aimed to characterise the geotechnical properties and behaviour of specimens of till and Oxford Clay and compare their behaviour between Quaternary Domains, the results presented in Chapters 6 and 8 are synthesised here. Geotechnical properties and behaviour are each considered in turn describing loss-on-ignition, clay mineralogy, particle-size, plasticity, compressibility, undrained shear strength and stiffness.

9.2.1 Oxford Clay

The Oxford Clay is variably calcareous, with between 9% and 21% carbonate, probably in the form of residues from the remnants of fossils. It is also organic with values ranging between 5% and 15%. For the specimens analysed, there is no appreciable difference between Domains 1.3 and 1.3.1. Specimens in Domain 2.3 contain <6% carbonate which could be a weathering effect related to the dissolution of carbonate and the precipitation of gypsum as selenite in the weathered zone.

The measured particle density varies between 2.52Mg/m^3 to 2.78Mg/m^3, the densest specimens being in Domain 2.3 reflecting the lower proportion of carbonate compared to Domains 1.3 and 1.3.1.

There is no difference in the clay mineral assemblages between specimens and domains, based on qualitative clay mineral XRD analysis. Specimens comprise an assemblage of illite, kaolinite, mixed-layer collapsible minerals with illite and minor amount of chlorite plus non-clay minerals including quartz. These results agree with previous investigations of the clay mineralogy of the Oxford Clay (Jackson & Fookes, 1974, Jeans, 2006).

9.2.1.1 Particle-size

The Oxford Clay is a slightly sandy, clayey silt and there is no appreciable difference in measured particle-size distributions between Domains. The proportion of clay (0-30%) is in the lower 50th percentile when compared to the regional median value of 40% derived from the statistical analysis in Section 6.2.4. It is possible that this difference reflects the presence

of silt- grade agglomerates of clay particles which were not sufficiently disaggregated in the particle-size specimen preparation procedure.

The presence of rounded clasts as coarse, granular particles within a soft to firm clay matrix in hand-dug pits in the Calvert area, is interpreted as a periglacial solifluction deposit derived from weathered Oxford Clay and incorporating remnants of till. It is likely that this weathered zone persists in Domain 2.3 where the depth of weathering is greater compared to that in glaciated Domains as a result of physical erosion and removal of the weathered zone during glaciation (Cratchley *et al*., 1969). The statistical analysis in Section 6.2.4 demonstrated the presence of granular particles in Oxford Clay specimens taken from <5 mbgl. The observation of granular particles in hand-dug pits in this research, supports the hypothesis that in its upper part (to ~5 mbgl), the Oxford Clay comprises a periglacially modified deposit which may have formed as a result of solifluction.

9.2.1.2 Plasticity

Specimens from the Oxford Clay are high to very high plasticity. Except for one sample, CR022794 in Domain 1.3, all samples plot above the A-line. Values for liquid limit range from 55% to 79%, plastic limit from 22% to 35% and plasticity index from 28% to 51%. Liquid limit values plot between the 50th and 75th percentile, when compared to the regional values derived from the statistical analysis in Section 6, except for the maximum value of 79% which plots in the upper 2.5th percentile range. The upper and lower values for plastic limit plot in the upper and lower 10th percentile range respectively, of regional values. Values for plasticity index plot between the lower 2.5th and upper 2.5th percentiles. Values for liquid and plastic limits and plasticity index agree with those observed by Cratchley *et al*. (1969) and Cripps & Taylor (1997).

Except for specimen CR005942, Domains 1.3 and 1.3.1, moisture content values plot close to the plastic limit, giving values of liquidity index close to, or < 0. This agrees with previous investigations in Bedfordshire, Buckinghamshire and Cambridgeshire (Jackson & Fookes, 1974). In contrast, values for liquidity index are >0 in Domain 2.3 corresponding to moisture contents of 34% and 43%. Similarly, specimen CR005942 in Domain 1.3 has a liquidity index >0, a liquid limit of 72% and a corresponding moisture content of 30%.

To investigate potential changes in plasticity with depth, values of activity, clay content, plastic limit, liquid limit, plasticity index and liquidity index derived from laboratory investigations carried out for this research are shown in Figure 9-3. In Domains 1.3 and 1.3.1, both the liquid limit and plastic limit increase slightly with increasing depth. Moisture content

decreases with depth in Domain 1.3, before increasing again below 10 mbgl. Correspondingly, values of liquidity index decrease but increase again below 10 mbgl. This agrees with decreasing moisture content with depth previously observed for the Oxford Clay in Bedfordshire (Parry, 1972, Burland *et al*., 1977, Jackson & Fookes, 1979). It is not possible to identify depth trends in Domains 1.3.1 and 2.3 as they are limited by the number of data points. The latter authors argued that higher moisture contents were present in the weathered zone of the Oxford Clay and that view is supported here. The effect is greatest in the non-glaciated Domain 2.3 where moisture content is greater than plastic limit which in turn increases the values of liquidity index above 0 so that these samples are more plastic than those in the glaciated Domains 1.3 and 1.3.1.

The high liquid limit and moisture content in specimen CR005942 is anomalous compared to specimens in the same Domain, examined for this research. Weathering is unlikely to be a factor as the specimen was prepared from a sample taken at 24.45 mbgl. A possible explanation is that the sample was previously sheared. Assuming the specimen was overconsolidated at the time of shearing, shear-induced dilation may have resulted in negative porewater pressure thus drawing pore water towards the shear plane. The subsequent reduction in overconsolidation through shearing may also account for the anomalous stress-path behaviour of the sample which is discussed further in Section 9.2.1.4. The increased moisture content and liquid limit measured for specimens CR023247 and CR020746 may also be explained by the mechanism described for specimen CR005942.

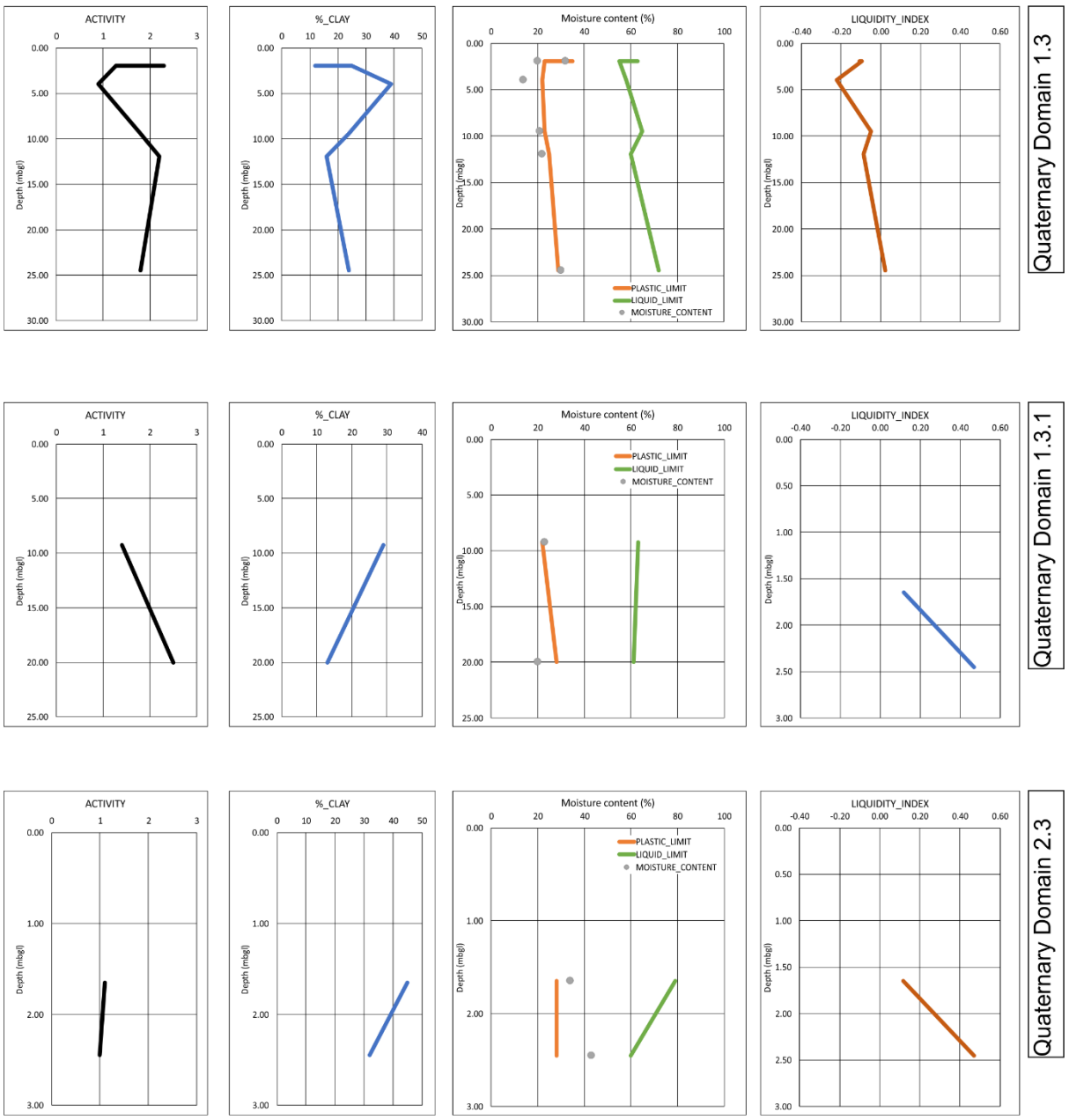

Figure 9-3 Comparison of activity, clay content, Atterberg limits, moisture content and activity for selected laboratory specimens, plotted as depth below ground level between Domains.

Activity (plotted using equation 4-1) is shown in Figure 9-4. Activity values appear to be highest (>2) for specimens from Domains 1.3 and 1.3.1 compared to 2.3. However, it is probable that these activity values are misleading. Values upto 0.8 were measured by Jackson & Fookes (1974) with little variation with depth. It is probable that clay particles, contributing to the plasticity of the samples, are in fact agglomerations of silt-grade particles which were not fully dispersed during sample preparation. This effect was also noted by Jackson & Fookes (1974) who suggested that carbonate may act as a cementing agent between clay particles. The apparent decrease in activity values with decreasing clay content for a given

value of plasticity index, is therefore interpreted to be the result of plasticity being maintained in the silt-grade portion of the specimens.

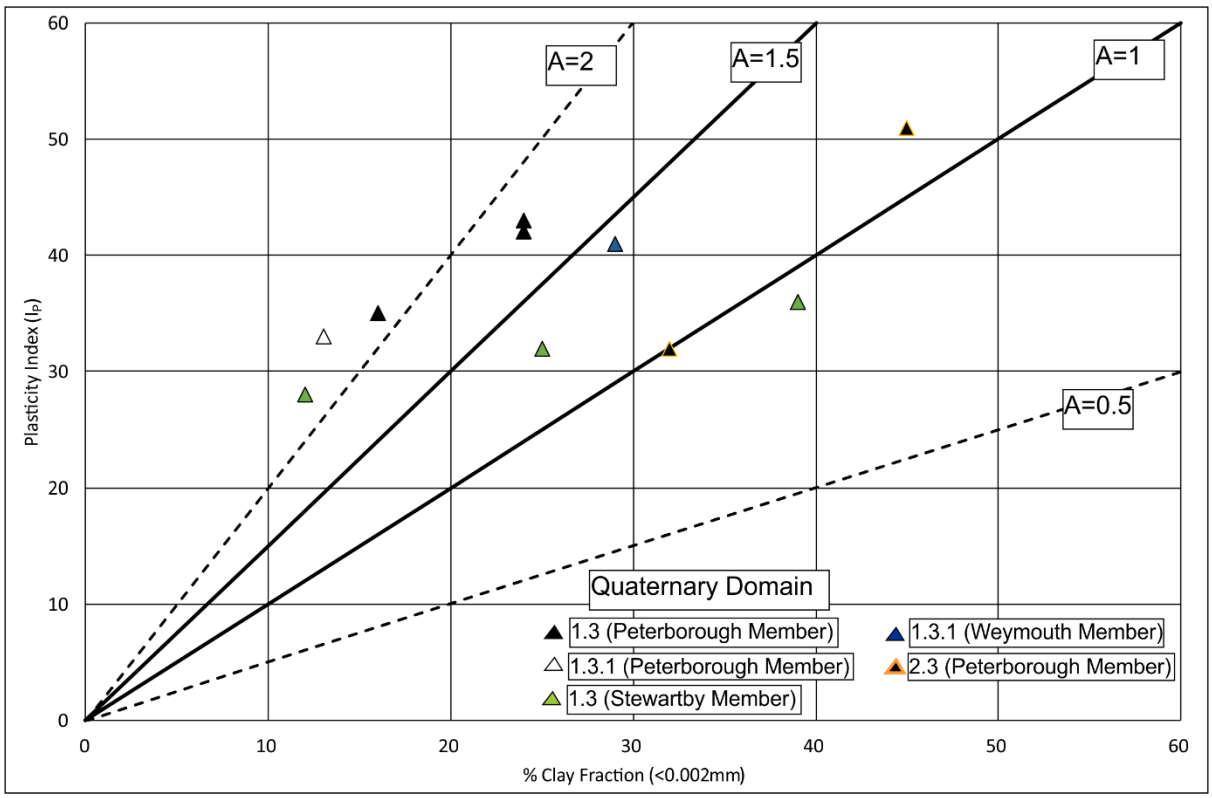

Figure 9-4 Apparent activity for specimens of Oxford Clay, all Domains.

9.2.1.3 Compressibility

All Oxford Clay specimens in Domains 1.3 and 1.3.1 are classed as low compressibility and that in Domain 2.3, medium compressibility, based on their estimated values for the coefficient of volume compressibility, m_v using the classification of Head & Epps (2011). To compare the *in situ* void ratio and 1D consolidation curves between specimens and Domains, each specimen was plotted together on an e-logσ' plot (Figure 9-5A). Accepting that the data are limited by the number of experiments undertaken for the research, each specimen has been placed into one of three groups. Those in Group 1 are within Domain 1.3 and Domain 1.3.1 and their sampling depth ranges between 1.95 and 9.45 mbgl. Those in Group 2 are within Domains 1.3 and their sampling depths range between 1.95 and 24.45 mbgl. Specimen CR023247 is the only specimen in Group 3 sampled from a depth of 2.45 mbgl. The variation in initial void ratio does not appear to relate to depth as specimens from similar sampling depths in different Domains, have different initial void ratios. Assuming minimum sampling disturbance, the change in void ratio appears to be related to the proximity of the specimens to the former Middle

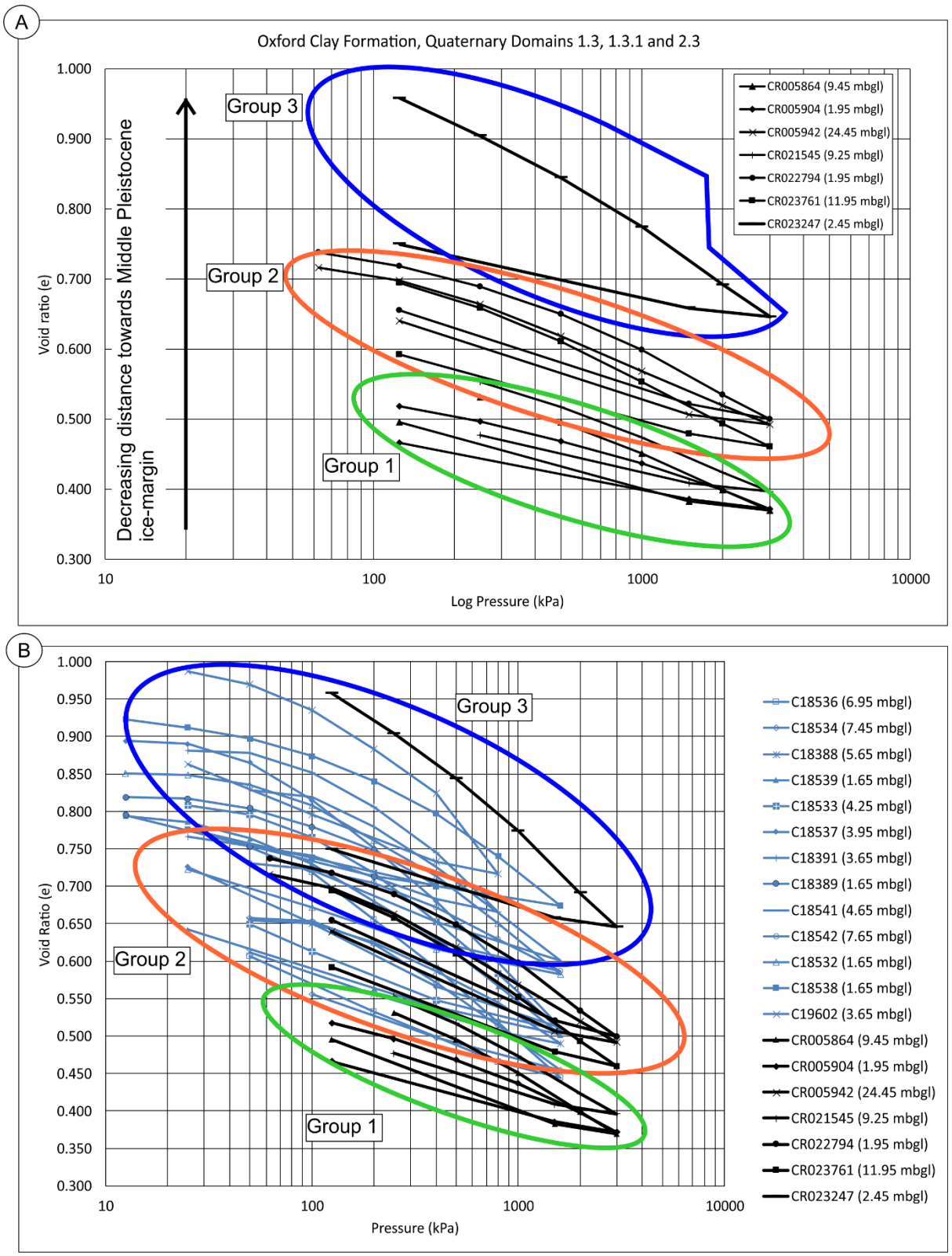

Figure 9-5 Comparison of initial void ratio and 1D consolidation curves, Oxford Clay, all Domains. A) Specimens investigated for this research only. B) Specimens for this research and those from the Energy from Waste ground investigation, Calvert.

Pleistocene ice-margin. Those specimens furthest away in the ‘up-ice’ direction have the densest initial void ratio. The initial void ratio increases, and specimens become less dense with decreasing distance to the former ice-margin (Figure 9-6). This is accompanied by a ‘down-ice’ increase in compressibility.

To compare the compressibility of the Oxford Clay at the former ice-margin with those specimens in glaciated ‘up-ice’ locations, additional data were obtained. Ground investigation data for Calvert’s Energy from Waste scheme were examined. All data were part of the same ground investigation and tested in the same laboratory. The results are shown in Figure 9-5B. Although there is overlap in the plots of initial void ratio and the consolidation curves, all specimens plot within Groups 2 and 3. This comparison suggests that the pattern of increasing void ratio and compressibility towards the former Middle Pleistocene ice-margin observed within the experimental results presented here, are valid.

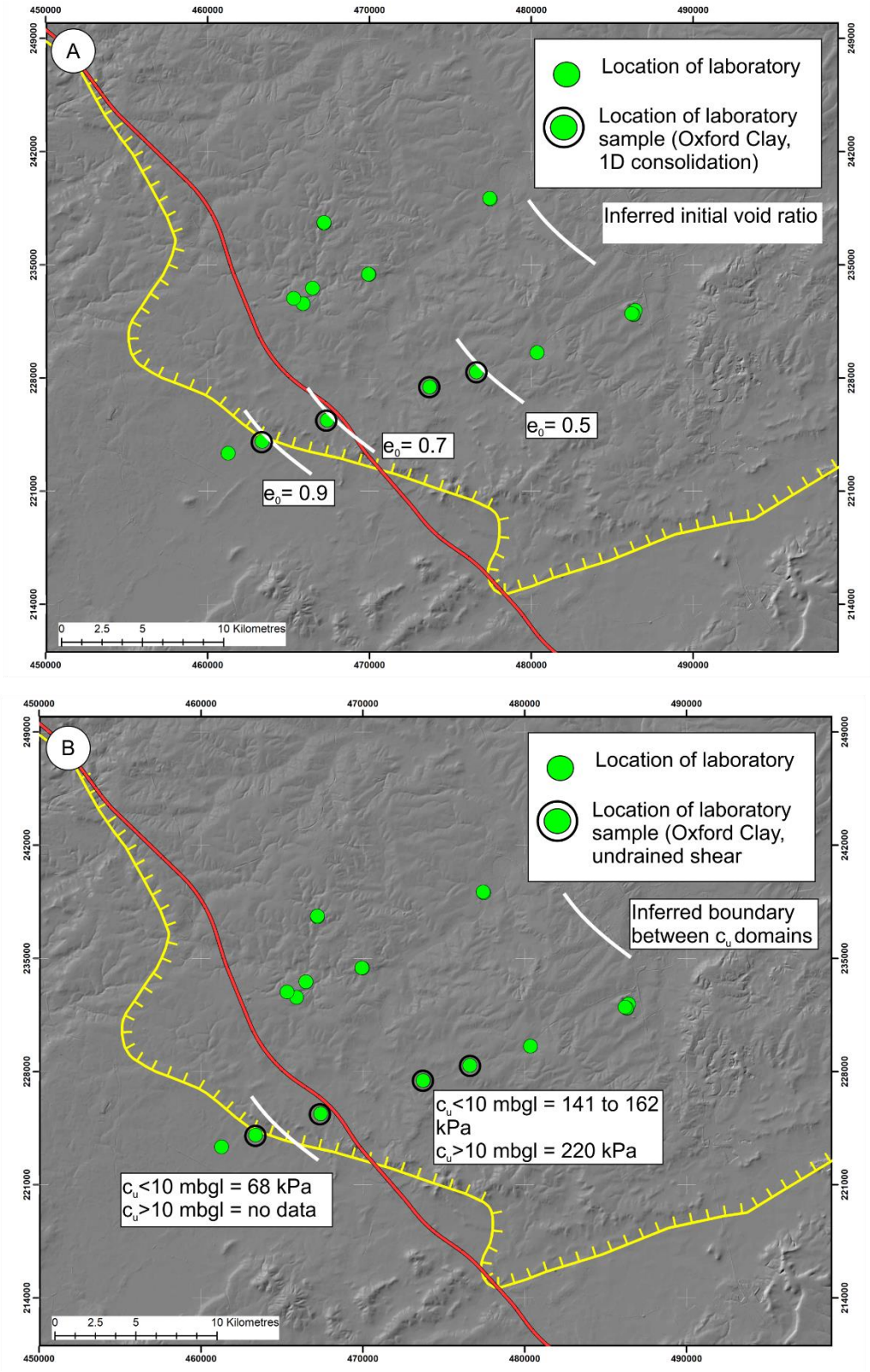

Figure 9-6 Inferred spatial variability in initial void ratio and c_u (as 0.5_{qmax}), this research. Legend for map as Figure 1-1. Mbgl = metres below ground level. Geographical location with reference to Ordnance Survey Landform Profile 50 m resolution Digital Terrain Model (DTM) © Crown Copyright and Database Right [2018]. Ordnance Survey (Digimap Licence).

The void ratio signature in Figure 9-5A could be explained on the assumption that the Oxford Clay was over-ridden by glacier ice in Domains 1.3 and 1.3.1 on at least one occasion in the Middle Pleistocene. Boulton & Dobbie (1993) demonstrated the consolidation effects of glacier loading on glacial sediments in a modern glacier setting. The effect was to increase the density of sediment in the direction of glacier advance. The reverse is seen in this research when the geological bedrock that formed the basal glacier deforming layer is considered. Oxford Clay becomes less dense within glaciated Domains as the former glacier margin is approached. Initial void ratio, and hence compressibility is highest at the former glacier margin and beyond into the ice-proximal and non-glaciated Domain 2.3. This may reflect the greater thickness of weathered Oxford Clay in Domain 2.3 which is likely to have been partially or wholly removed by glacier erosion in Domains 1.3 and 1.3.1.

To estimate the possible degree and spatial variability in overconsolidation ratio, the e-logσ_v plots in Figure 9-5 were examined. To attempt to use the Casagrande curve fitting method to estimate overconsolidation (e.g. Holtz *et al.*, 2011), a distinct yield point in the consolidation curve needs to be identified. For the specimens tested here, the yield points examined are weak. This suggests that the yield point may not have been reached using the pressures tested or that the effects of sampling have masked the yield point. Accepting these limitations, maximum preconsolidation stress and overconsolidation ratio (OCR) was estimated using Equation 2.3 and the Casagrande curve-fitting method. The results are shown in Figure 9-7 and an example of the curve-fitting method shown in Appendix 13.7. Figure 9-7 also shows an estimate of the modelled preconsolidation from geological loading only using estimates of depth of burial for Oxford Clay in Buckinghamshire. The estimated thickness of previous overburden overlying the Oxford Clay ranges between 811 m and 472 m (Jackson & Fookes, 1974). Using a generalised unit weight of 20 Mg/m^3, this gives maximum preconsolidation pressures at the top of the Oxford Clay between 8.11 and 4.72 MPa.

Referring to Figure 9-7, the OCR for all Oxford Clay specimens is lower than that predicted by geostatic loading alone. There are many factors which may influence the post-depositional consolidation state of a clay soil including groundwater rise or lowering, formation of cement between particles and mechanical disturbance during sampling and transport. If the assumptions about overburden thickness are correct, this suggests that one or more mechanisms have acted to reduce the OCR. A trend is seen which suggests that across all Domains, the magnitude of OCR decreases with depth. The estimated preconsolidation pressures increases with depth to ~10 mbgl before decreasing. Both trends appear to be

anomalous; the magnitude of preconsolidation and OCR might be expected to increase with depth.

Lower than expected values of preconsolidation pressure might be explained by weakening or 'de-structuring' of the Oxford Clay because of the loss of inter-particle bonding or cementation for example.

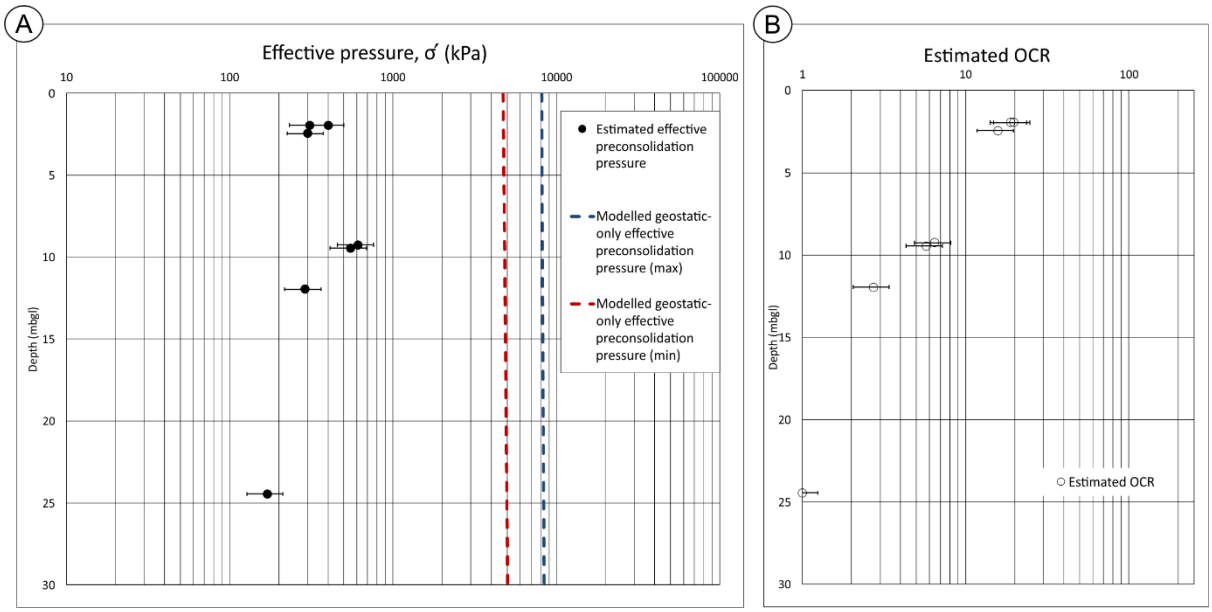

Figure 9-7 Estimation of preconsolidation pressure and OCR, Oxford Clay, all Domains. Error bars represent +/-25%.

A further set of complex processes in geographic areas affected by previous glacial and periglacial activity is sub-glacial drainage, glacial deformation (basal shearing) and periglaciation, the latter including the formation of ground ice in frost-susceptible sediments such as silt and clay. As a result, the soil structure may become less dense compared to its original geostatic-only state, even if thaw consolidation results in subsequent densification.

It is therefore possible that the preconsolidation and OCR signature of clayey and silty Oxford Clay specimens reflects the previous presence of ground ice either in the form of ice-rich permafrost or seasonally frozen ground. High preconsolidation pressures may be associated with suction pressures upto 1MPa induced by ground freezing (Section 2.2.1). Depending on the extent to which drainage is permitted during thawing of ground ice, thaw consolidation may then occur. The magnitude of the overconsolidation that results, reflects the maximum preconsolidation pressure experienced by the soil even if subsequent events occur which do not exceed it.

De-structuring might explain the anomalous results here. Sample disturbance is interpreted to be low (see Section 7) and so another mechanism is needed to explain the apparent anomaly. It is proposed here that de-structuring and loss of inter-particle bonding may be the result of repeated Middle Pleistocene freeze-thaw cycles which resulted in the cyclical growth and decay of segregated ground ice. This interpretation supports that of Jackson & Fookes (1974) who also attributed observed experimentally-derived decreasing OCR with depth and lower than expected values for preconsolidation.

Because of the inherent uncertainty associated with applying the curve-fitting Casagrande method to specimens with a weak yield point derived from 1D compression curves, an alternative method was used here with reference to the intrinsic properties of clays (Burland, 1990; Chandler, 2010).

The intrinsic properties of a clay soil are independent of its depositional and post-depositional fabric and structure, and were defined by Burland (1990) by comparing the behaviour of intact specimens and those that had been reconstituted to ~1.25 times their liquid limit. The intrinsic property framework has been used here to compare *in situ* results with intrinsic properties to estimate preconsolidation pressure and OCR and compare them with the results obtained using the Casagrande curve fitting method. Using additional data from the Calvert Energy from Waste ground investigation, results are compared, and a intrinsic-property ground profile is modelled.

To compare *in situ* and intrinsic properties, the void ratios, *e*, derived from the 1D consolidation experiments described in Section 8, were converted to the normalizing parameter, void index, I_v, using the relationship defined by Burland (1990):

$$I_v = \frac{(e_0 - e_{*100})}{C_{*c}}$$

Equation 9-1

where e_0 is the *in situ* void ratio, e^*_{100} is the void ratio at an effective vertical stress of 100 kPa, measured from a reconstituted sample consolidated in one dimension, and C^*_c is the intrinsic compression index, defining the difference between intrinsic void ratios corresponding to 100 kPa and 1000 kPa.

The empirically-derived curve relating void index to log-effective stress, is defined by Burland (1990) as:

$$I_v = 2.45 - 1.285(\log\sigma'_v) + 0.015(\log\sigma'^3_v)$$

Equation 9-2

where σ'_v is effective stress in kPa. Burland (1990) referred to this as the Intrinsic Compression Line (ICL) and is independent of a soil's stress history or fabric.

Normalising Skempton's sedimentation curves (Skempton, 1970) for normally consolidated natural clays using I_v, Burland derived a relationship between I_v and log-effective stress which he referred to as the sedimentation compression line (SCL). Notably, the SCL provides an estimate of the normal consolidation behaviour of a clay soil in 1D compression which is inclusive of its fabric and structure. By comparison with the ICL, between the values of σ'_v = 10 kPa and σ'_v = 1000 kPa, for a given value of I_v, a natural soil carries ~5 times the overburden pressure of a reconstituted specimen (Burland, 1990).

The parameters e*100 and C*c were not directly measured from 1D consolidation experiments on reconstituted specimens for this research, but they were estimated from their empirical relationship to their Atterberg limits expressed as void ratio at the liquid limit, e_L:

$$e_L = \frac{V_v}{V_s}$$

Equation 9-3

where V_v is volume of voids and V_s is volume of solid particles at the liquid limit calculated here using measured values of bulk density, particle density and moisture content at the liquid limit according to the soil model shown in Figure 2-9, Section 2.2.4. The parameters e*100 and C*c were then calculated from the empirically-derived definition given by Chandler (2010) modified from Burland (1990):

$$e*_{100} = 0.114 + 0.581 e_L$$

Equation 9-4

and

$$C*_c = 0.256 e_L - 0.04$$

Equation 9-5

Skempton (1944) measured values for the Oxford Clay of e_L = 1.362, $e*_{100}$ = 0.96 and $C*_c$ = 0.30 for specimens with W_L = 53, W_P = 27 and G_s = 2.57. The results of normalization of void ratio to normalized to intrinsic void ratio for specimens analysed for this research are shown in Figure 9-8 for Oxford Clay and include *in situ* estimates of vertical effective stress (σ'_v).

The same groupings are seen when compared to those defined on the e-logσ_v plot in Figure 9-5. Specimens closer to the former Middle Pleistocene glacier margin are seen to be less dense than those to the northeast, in the 'up-ice' direction. The exception is specimen CR005942 which appears to be less dense, despite being in the 'up-ice' direction. The *in situ* effective stresses for each sample lie well to the left of the ICL indicating that all the samples are variably overconsolidated. With increasing vertical effective stress, specimens CR023761, CR022794 and CR005942 cross the ICL between 100 kPa and 1000 kPa before continuing parallel to it. In contrast, specimens CR021545, CR005864 and CR005904 parallel but do not cross the ICL.

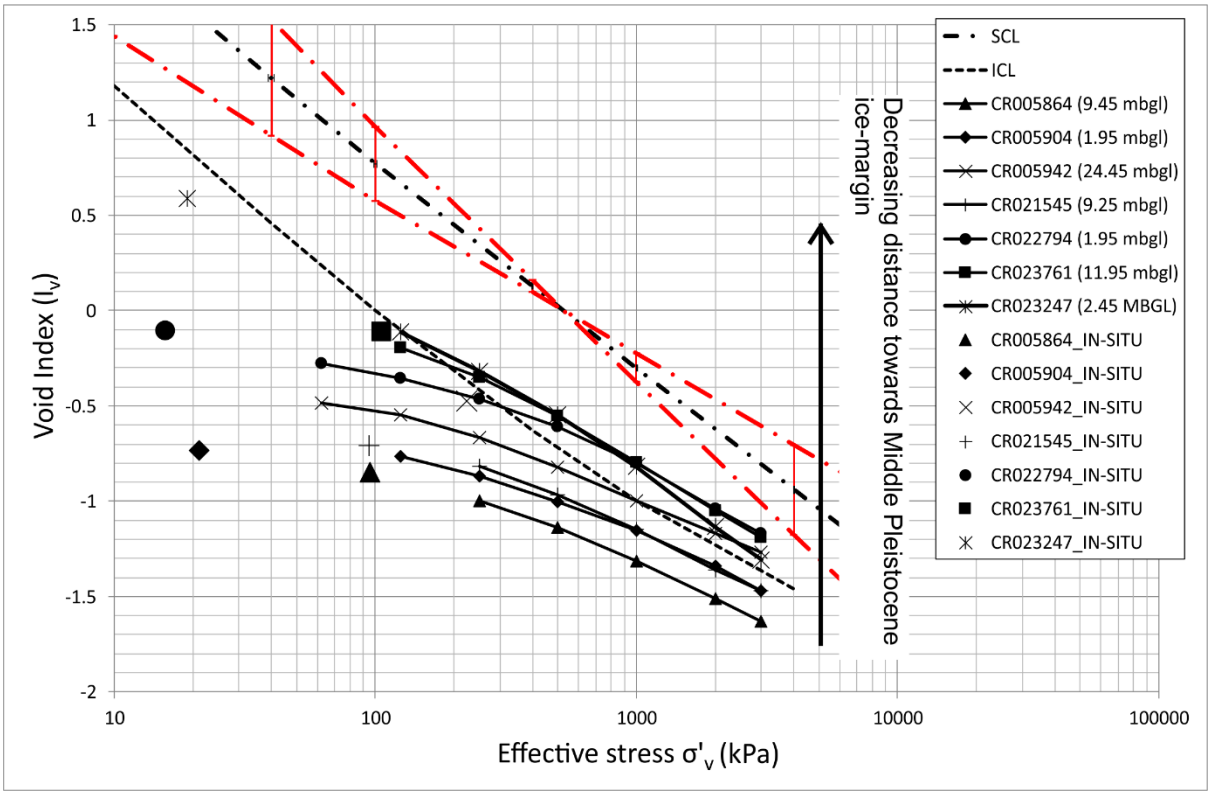

Figure 9-8 Compression characteristics of Oxford Clay specimens expressed as void index, Domains 1.3 and 1.3.1. Red dashed lines denote envelope of uncertainty on the SCL (+/-25%).

Using the intrinsic property framework, it is possible to estimate the yield stress ratio (YSR) of each specimen and compare it to the estimate of OCR using the Casagrande curve-fitting methodology.

Yield stress ratio, after Chandler (2010), is defined as:

$$YSR = \frac{\sigma'_{vy}}{\sigma'_{vo}}$$

Equation 9-6

where σ'_{vy} is the effective yield stress estimated from the plot of I_v versus σ'_v and σ'_{vo} is the *in situ* vertical effective stress. The results are shown in Figure 9-9.

According to Chandler (2010), the yield stress is a function of the soil structure (its fabric and interparticle bonding) and its geological history. Because of the complexities of a natural soils' loading and unloading history, Chandler argues that in general, there is no unique relationship between the maximum previous geological overburden stress and the yield stress; hence the definition of YSR.

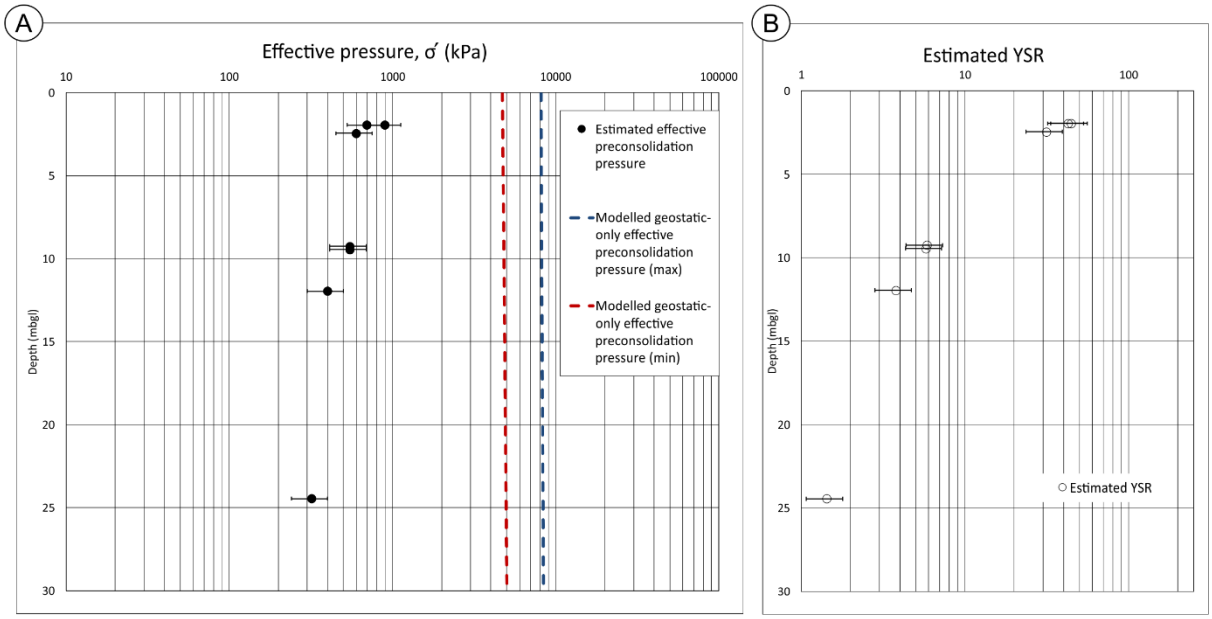

Figure 9-9 Estimated preconsolidation pressure (A) and yield stress ratio (B) following the methodology of Chandler (2010).

A comparison of estimated OCR and YSR for specimens of Oxford Clay tested here is shown in Figure 9-10. From this relationship, the YSR is approximately twice that of the OCR.

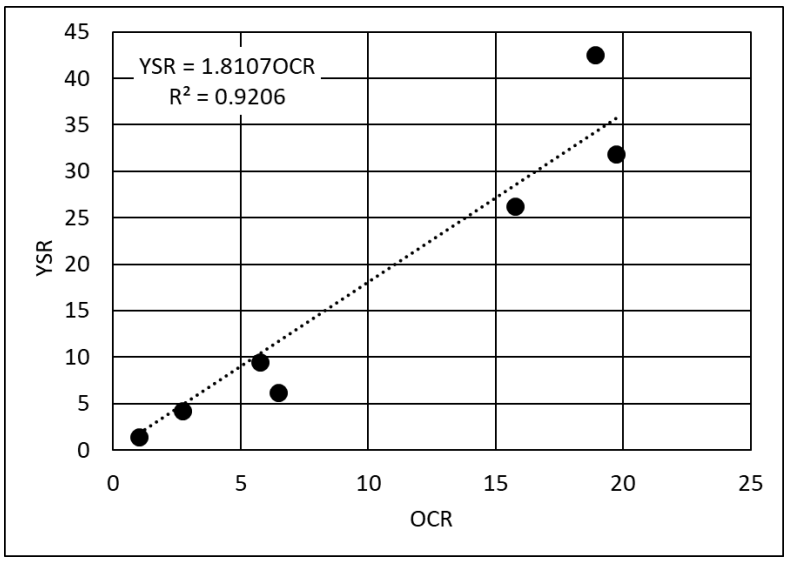

Figure 9-10 The relationship between estimated values of OCR and YSR for Oxford Clay.

Although the magnitude of preconsolidation pressure, OCR and YSR are different between the two methods shown in Figures 9-7 and 9-10, a similar pattern with increasing depth below ground level is seen. In Figure 9-9, again estimates of preconsolidation pressure are less than those estimated form geological overburden removal alone. Preconsolidation pressure decreases with increasing depth below ground level in Figure 9-9; the increase at ~10 mbgl seen in Figure 9-7 is absent. YSR is seen to decrease with depth.

Again, it is suggested here that lower than expected values of preconsolidation pressure might be explained by weakening or 'de-structuring' of the Oxford Clay because of the loss of inter-particle bonding may be the result of repeated Middle Pleistocene freeze-thaw cycles which resulted in the cyclical growth and decay of segregated ground ice and physical breakage of interparticle bonds.

That the relative preconsolidation pressures decrease with depth may be explained by decreasing depth of formation of segregated ground ice during Pleistocene cold periods. At shallower depths, where segregated ice may form within permafrost, freezing-induced suction may generate increased effective stresses compared to deeper depths. The depth of freezing is governed by palaeoclimate and geothermal gradient as discussed in Section 2.2.1. With reference to Figure 2-2, models of the extent and depth of permafrost during the Devensian, suggest that the project area lay within zones of continuous and discontinuous permafrost. The depth of permafrost is estimated to vary between 20 and 70 mbgl. These depths exceed those for which the trends in Figures 9-7 and 9-9 are seen, suggesting that the full depth examined here was, on multiple occasions in the Pleistocene, within the zone of permafrost development.

9.2.1.4 Undrained shear strength and stiffness

Figure 9-11 summarises the undrained shear strength ($0.5q_{max}$), secant stiffness and secant effective angle of friction for Oxford Clay specimens in all Domains. Undrained shear strength shows a clear positive relationship with depth below ground level, undrained strength increases with increasing effective stress (Figure 9-11A). The lowest undrained shear strength is seen in the non-glaciated Domain 2.3. Notably, there is a change in strength gradient below ~10 mbgl but there are too few data to interpret its significance. A similar trend is seen for secant Young's modulus, E (Figure 9-11B). Mobilised shear strain equivalent to 0.5_{qmax} ($\varepsilon_{F=2}$) ranges from 0.17 to 1.27. The highest valued is associated with specimen CR005904 in glaciated Domain 1.3.

The depth-dependant (effective stress) trend in undrained shear strength does not appear to show any correlation with spatial proximity to the Middle Pleistocene ice-margin. However, examination of the variability in secant effective angle of shearing resistance highlights spatial patterns that may be spatially correlated with the former ice-margin (Figure 9-11 C and D).

Specimens CR005864, CR005904 and CR023761 in the glaciated Domain 1.3 show values for $ø'_{trans}$ between 30° and 33°. These values are consistent with the peak effective angle of shearing resistance measured by Parry (1972), Jackson & Fookes (1974) and Burland *et al*. (1977) for specimens from shear box tests, sheared parallel to bedding/lamination. Specimens CR005942 (glaciated Domain 1.3), CR021545 (glaciated Domain 1.3.1) and CR023247 (non-glaciated Domain 2.3) appear to show a reduction in effective stress, strength parameter $ø'_{trans.}$ The magnitude of reduction in $ø'_{trans}$ approaches or exceeds the residual values of effective angle of shearing resistance measured by Jackson & Fookes (1974) and Parry (1972). This seems to be anomalous, especially so as CR005942, at 24.45 mbgl, is the deepest specimen tested.

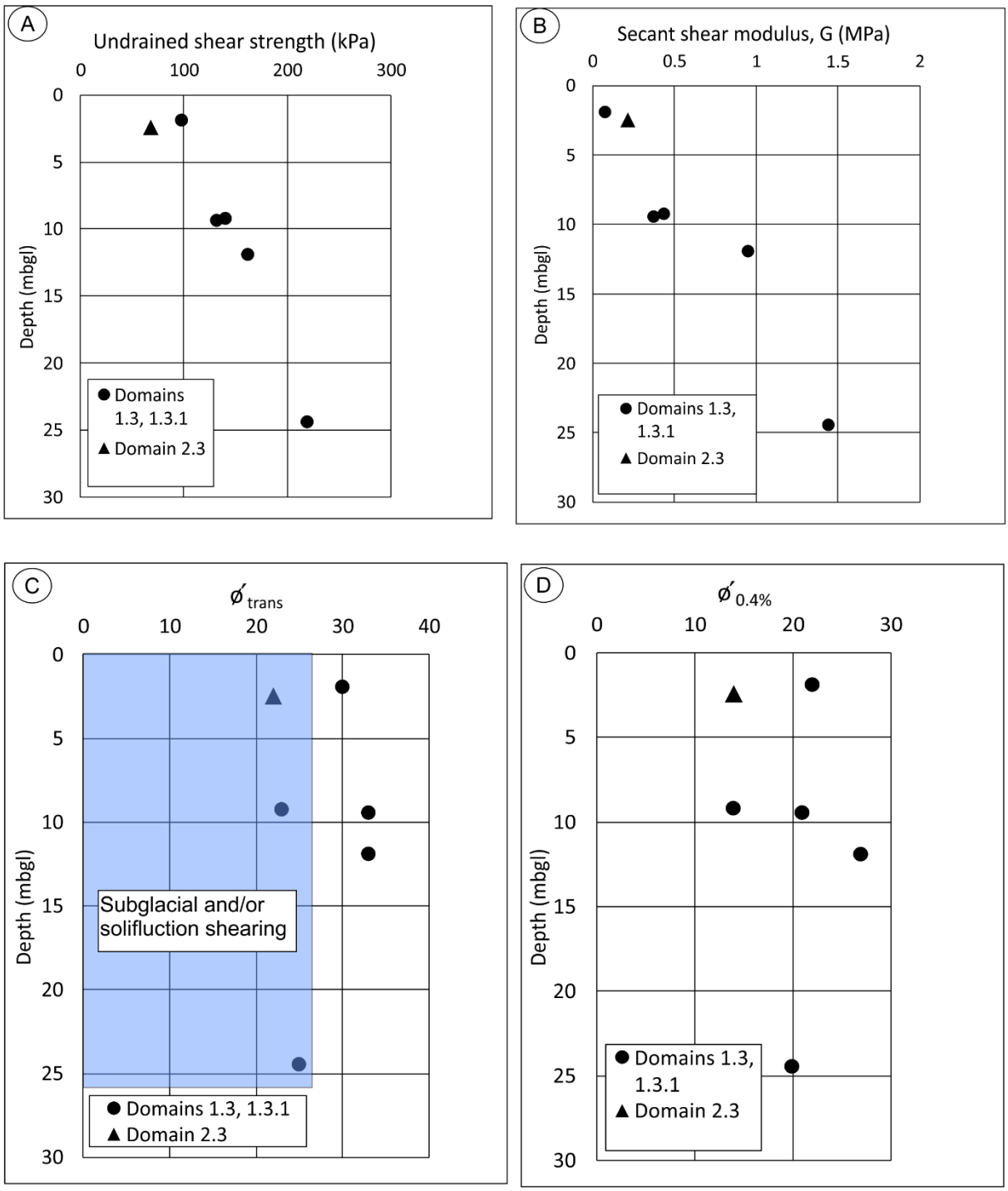

Figure 9-11 Summary undrained strength and stiffness parameters, Oxford Clay, all Domains. A) Undrained shear strength (0.5_{qmax}). B) Secant shear modulus, G. C) Secant strength parameters $ø'_{trans}$ and D) secant strength parameter $ø'_{0.4\%}$.

Assuming minimum sample disturbance during collection, transport and preparation, a mechanism needs to be sought to explain this anomaly which is consistent with the variability in compressibility, discussed in Section 9.2.1.3. It is suggested here that two mechanisms may explain the anomalies observed. For specimens in the glaciated Domains 1.3 and 1.3.1, mechanical de-structuring and weakening of the Oxford Clay measured in specimens

CR021545 and CR005942, is considered to be a result of subglacial shearing. This is also consistent with their transition towards a less dense state in terms of their initial void ratio, as discussed in Section 9.2.1.3. In addition, the stress-path for specimen CR005942 is characteristic of a normally consolidated clay. If its consolidation history has been removed by mechanical disturbance through shearing, this may account for this apparent anomalous behaviour.

Assuming that the Oxford Clay formed part of a deformable glacier bed (Boulton & Hindmarsh, 1987; Benn & Evans, 1998) during glaciation, subglacial shearing or tectonic deformation may occur. Depending on subglacial drainage conditions and availability of basal meltwater, porewater pressures may be elevated such that the Oxford Clay behaves plastically and deforms under glacier-induced stress. Observations of Oxford Clay at Calvert and Bletchley did not reveal evidence that could support this hypothesis and further investigation is needed to validate this interpretation,

Secondly, de-structuring and weakening in specimen CR023247 in non-glaciated Domain 2.3, is also interpreted to be a result of shearing but in response to periglacial solifluction in the style described by Hutchinson (1974) and Skempton & Weeks (1976). The mechanism envisaged is that of shearing induced by gravity and elevated porewater pressure during freezing and thawing of segregated ground ice in frost susceptible Oxford Clay. This interpretation is also consistent with the observation of increasing initial void ratio as the Middle Pleistocene ice-margin is approached from the 'up-ice' direction.

The above interpretation of shear strength variability in the Oxford Clay is also supported by the variability in compressibility described in Section 9.2.1.3. In general, a trend of decreasing effective angle of shearing resistance is accompanied by an increase in initial void ratio which in turn is related to 1) proximity to the Middle Pleistocene ice-margin and 2) the interpreted presence of subglacial and periglacial shear zones. This trend is also interpreted to be a function of depth of weathering. Although it was not specifically investigated as part of this research, it can be expected that subglacial erosion in the glaciated Domains will act to remove some or all the pre-glaciation weathering profile in the Oxford Clay. In contrast, in the non-glaciated, periglacial Domain, a thicker weathering profile is likely to be preserved.

9.2.2 Till

Specimens of till in Domains 1.1.1, 1.2.1 and 1.3.1 are calcareous; containing between 27% and 54% carbonate. Specimen SP11102016_1, taken from the Buckingham Till Member,

contains only 5% and supports its interpretation as a deposit of till, distinct from the Milton Keynes Till Member, from which all other samples were taken. All specimens contain <5% organic matter.

There is no apparent variability in clay mineralogy between the glaciated Domains. The clay mineral assemblage in all samples is qualitatively the same except for specimen SP11102016_1 which shows less intense diffraction peaks. The clay mineral assemblage is dominated illite (mica), kaolinite and mixed layer, collapsible clays associated with illite. Non-clay minerals in the <2 μm include quartz.

9.2.2.1 Particle-size

Specimens of till are slightly gravelly, sandy silt and clay and are poorly- to well-graded (poorly-sorted) with values for coefficient of curvature (C_z) between 0.6 and 1.5. They are matrix-supported with between 54% to 90% particles finer than silt and 8% to 24% clay. The proportion of clay may be underestimated, and the proportion of silt overestimated, if the disaggregation procedure in specimen preparation was insufficient to remove silt-grade agglomerations of clay particles. The particle-size distribution compares well with lowland British tills investigated by Bell (1991) and Paul & Little (1991).

The particle-sizes of till compare with the 50^{th} percentile of equivalent specimens in the project area when compared with values derived from the project geotechnical database (Section 6).

9.2.2.2 Plasticity

All specimens are low to intermediate plasticity and plot on or close to the T-line of Boulton & Paul (1976) with no observable difference between glaciated Domains except for three specimens in Domain 1.2.1 that plot close to, or below the T-line. This contrasts with he regional assessment of the plasticity of till Described in Section 6.2.1 where tills in Domain 1.2.1 plot above the T-line. Because of the similarity in the assemblages of clay minerals between samples, differences in plasticity are attributed to differences in the proportion of granular particles. Specimens plotting below the T-line are interpreted to result from a decrease in the proportion of granular particles which subsequently increases the plastic limit and liquid limit. This supports the observation of ‘granular particle dilution’ suggested by Boulton & Paul (1976) for tills.

The liquid limit varies between 29% and 49%, the plastic limit between 15% and 18% and plasticity index between 17% and 34%. The maximum values for liquid limit plot between the

50th and 75th percentile for regional statistical analysis, while those for plastic limit and plasticity index plot close to the median and greater than the 75th percentile respectively (Section 6.21). The slightly higher median value for plastic limit seen in the regional values for till in Domain 1.4.1, is supported from specimens analysed here.

The granular particle dilution effect appears to have a greater effect on the liquid limit compared to the plastic limit. As moisture content values are close to the plastic limit, varying between 4% (dry) and 19%, the values of liquidity index are close to, or below, 0. This agrees well with the median values from regional statistical analysis in Domains 1.4.1 and 1.3.1. Values below 0 measured in Domain 1.2.1, contrast with the median value of 0.05 from regional analysis. No significant difference is seen between Domains when the specimens are plotted against depth (Figure 9-12).

The activity (A) of till samples was calculated from equation 4-1and plotted in Figure 9-12 where activity appears to increase with decreasing clay content for a given value of plasticity index. Except for one specimen, all activity values exceed 1. Activity values for till are typically 0.58 to 0.72 for lowland British tills (Little & Atkinson, 1988) and so the values measured here appear anomalous. It is likely that the proportion of clay is underestimated in the values measured for this research and thus the values for activity appear to be >1. The proportion of clay is likely to be underestimated because silt-grade agglomerations of clay particle were not completely disaggregated during particle-size sample preparation.

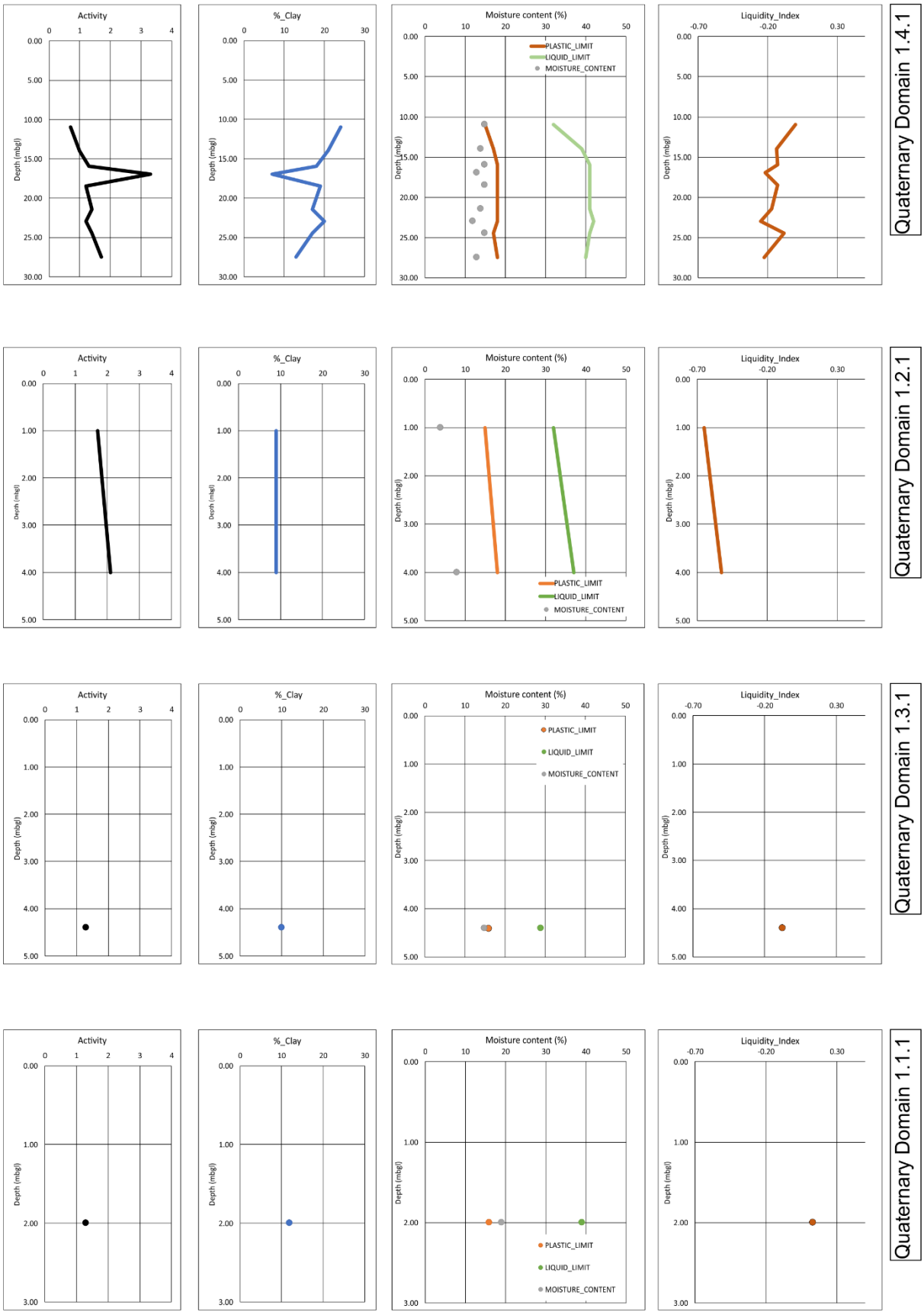

Figure 9-12 Domain comparison of activity, clay content, Atterberg limits, moisture content and activity for selected laboratory specimens, plotted as depth below ground level.

9.2.2.3 Compressibility

The intrinsic property methodology and the Casagrande curve-fitting methodology, described in Section 9.2.1.3, was applied to specimen CR011958 from glaciated Domain 1.4.1. The results are shown in Figures 9-13 and 9-14.

In terms of void index, Iv, specimen CR011958 parallels but does not cross the ICL. Its yield point is diffuse and difficult to define accurately. In contrast to Oxford Clay, estimates of preconsolidation pressure are similar using the Casagrande curve-fitting method and the intrinsic property framework. Both estimates give an OCR of 2.1 and YSR of 2.2.

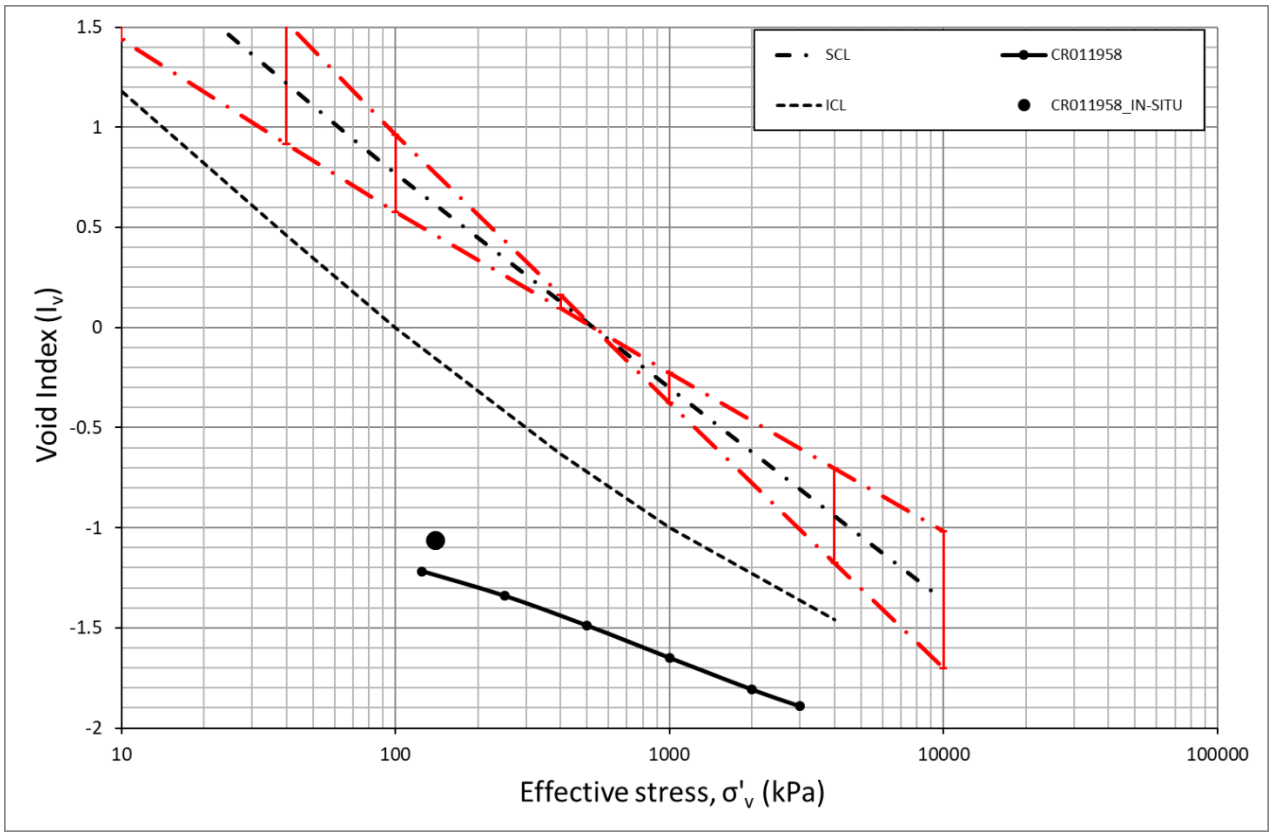

Figure 9-13 Void index, till, Quaternary Domain 1.4.1.

The estimated preconsolidation pressure for the till is between 290 and 300 kPa. These values are almost 10 times lower than that expected from effective stresses induced by ice-loading at Middle Pleistocene ice margin in lowland Britain (Little 1988). This reduction in preconsolidation pressure suggests that post-depositional processes have acted to remove the consolidation memory of the soil. It is not possible to unequivocally determine the process responsible but is likely to include de-structing and reduction of interparticle bonding through periglacial freeze-thaw and post-glacial weathering.

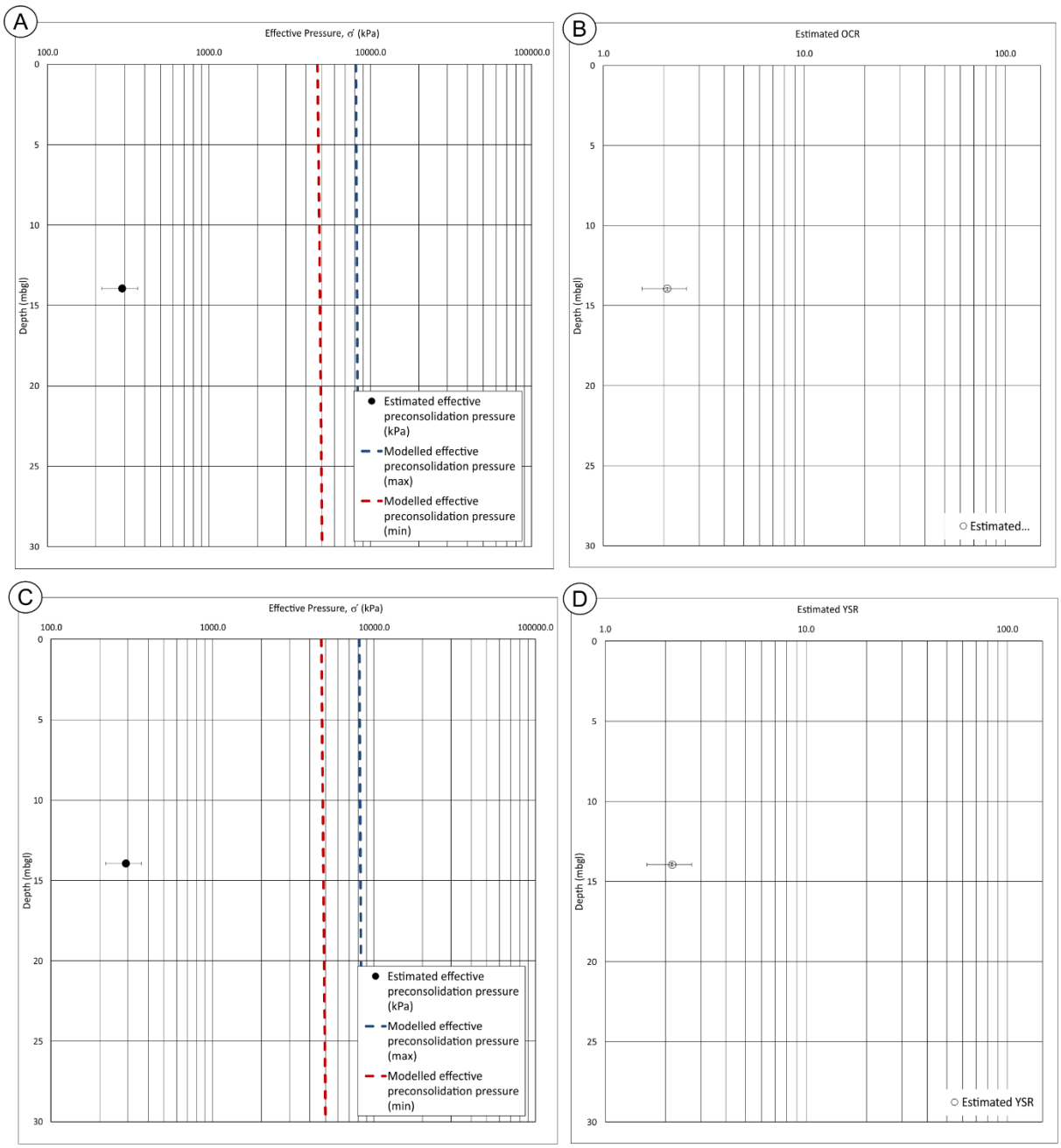

Figure 9-14 Estimated preconsolidation pressure and corresponding OCR and YSR for till, this research, Quaternary Domain 1.4.1. Geostatic model of effective preconsolidation stress used for Oxford Clay shown for reference.

9.2.2.4 Undrained shear strength and stiffness

Till specimen CR011958 behaves as an overconsolidated clay when its effective stress path is examined (Section 8.6.1.9). This implies that the processes that have acted to reduce the OCR and YSR described above, were insufficient to completely remove the stress history memory from the soil. This is confirmed when the undrained strength (0.5_{qmax}) and secant effective strength parameters are examined. The undrained shear strength of 459 kPa (without reaching the maximum value of deviator stress) is almost twice that of the maximum mobilised

undrained shear strength of the Oxford Clay. The value of 34° for $ø'_{trans}$ exceeds that for Oxford Clay, reflecting the presence of granular particles which add frictional strength. The value of undrained shear strength compares well with equivalent 'chalk-rich' tills in the Vale of St Albans (Paul & Little, 1991) which ranged between 400 and 500 kPa. Investigation of the Vale of St Albans tills by Paul & Little may also explain the apparent anomaly of the till measured for this research which suggests a reduction in OCR but high undrained strength and $ø'_{trans}$. They pointed to the presence of carbonate, derived from chalk particles within the till, acting as a cementing agent and thus increasing the effective secant angle of shearing resistance. Specimen CR011958 contains 32.7% carbonate (see also Figure 8-109) and it is therefore possible that re-distribution of carbonate as cement may result in the undrained strength measured here.

9.3 Implications for ground engineering

This research has shown that there are no simple patterns of geotechnical variability in the Oxford Clay or till, that can be unequivocally explained by past glacial and periglacial processes. The research is further limited by the small number of geotechnical experiments. Further work is required to map in detail, spatial patterns of variability between site and regional scale. Geotechnical design at the former margin of the Middle Pleistocene British Ice Sheet, must consider depth and spatial variability in undrained shear strength, secant strength parameters, compressibility, particle-size and lithological layering within Quaternary deposits. The presence of weak zones associated with subglacial and periglacial shearing within Oxford Clay must also be considered.

Some general observations relating to geotechnical variability in glaciated and non-glaciated provinces can be made based on the results of geotechnical properties and behaviour investigated as part of this research. They are summarised schematically in Figure 9-15 with reference to the schematic ground model that was developed in Section 5.

The clay mineralogy of the Oxford Clay and till is seen to vary little based on qualitative analysis. Differences in geotechnical behaviour are therefore unlikely to result from difference in clay mineralogy.

In tills, the undrained shear strength and secant effective strength parameters are increased by the presence of granular particles and carbonate cement. Tills whose glacial source area crossed granular bedrock (Domain 1.4.1) contain more granular particles and are therefore likely to be stiffer and stronger than those tills sourced dominantly from fine-grained mudrocks.

The compressibility of the Oxford Clay increases from northeast to southwest with an associated reduction in secant effective angle of shearing. Secant strength parameters may be reduced to their residual values. Undrained shear strength is dependent on depth (effective stress) as is secant shear modulus, G.

The research suggests that undrained shear strength is not a reliable soil characteristic with which to investigate spatial variability. Effective stress-path analysis and the derivation of secant strength parameters using the stress invariants q and p' demonstrate fundamental differences in behaviour that would not otherwise by known. Much geotechnical design in industry focuses on the derivation of undrained shear strength profiles plotted with elevation or depth and from which estimates can be made of side friction in bored piles for example. This research demonstrates that factors that could influence the derivation of design parameters may be apparent from the results of undrained strength tests alone, without additional stress path analysis.

For example, the results of stress path analysis provided the evidence to support the interpretation of subglacial and periglacial shearing within the Oxford Clay. The implications of this are important. It suggests that glacial and periglacial processes are just as likely to influence the geotechnical behaviour of bedrock as well as those associated with Quaternary sediments. Quaternary effects are commonly considered where tills are present and where there is geomorphological expression of periglacial processes (e.g. solifluction lobes). This research shows that the effects may be still be present even where there is no geomorphological expression of the past process.

This raises a potentially significant possibility which, to the author's knowledge, has not yet been realised; could geotechnical properties and behaviour be used as a proxy for the past presence of Quaternary effects including subglacial and periglacial shearing? In relict glacial and periglacial landscapes, including north Buckinghamshire, it may be possible to use the results of geotechnical tests to infer the previous Quaternary geological history of a soil. If sufficient correlations are established and can be unequivocally attributed to past Quaternary processes, it raises the possibility that geotechnical proxies could be used to infer geological history, rather than the reverse which is the common approach to assessing ground variability in previously glaciated and periglaciated landscapes.

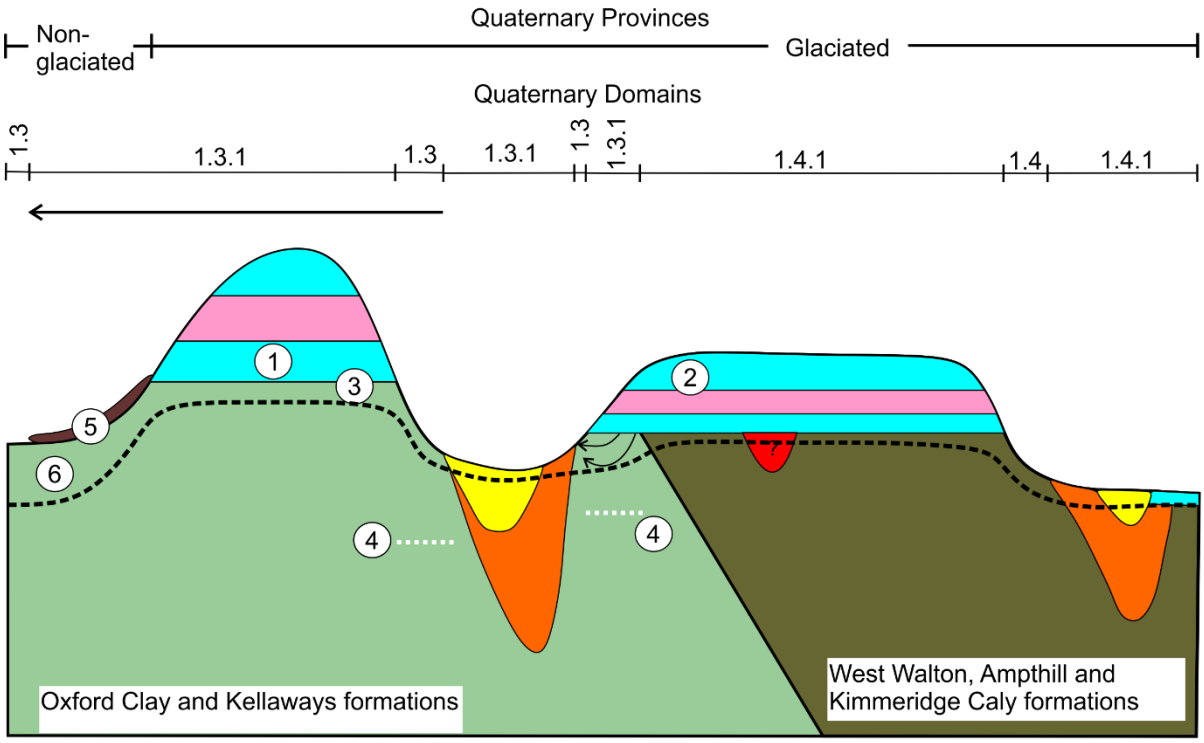

Legend

Post-glacial deposits

Sand, silt and clay (alluvium)

Glacial deposits

Diamicton (till)

Sand and gravel

Buried valley with laminated sand, silt and clay with diamicton (till)

Periglacial deposits and structures

Diamicton ('head')

Possible valley-bulging

Weathering profile

Pre-glacial deposits

Sand and gravel

Implications for ground engineering (excluding hydrogeology)

1. Particle-size of till influenced by geological bedrock. Undrained shear strength and stiffness increased by carbonate cement and granular particles. OCR and YSR reduced by effects of growth and decay of segregated ice.
2. Presence of interbedded granular and fine-grained lithologies in glacial sequence.
3. Magnitude of contrast in undrained shear strength, stiffness and compressibility between glacial deposits and Oxford Clay
4. Reduction in effective stress secant angle of friction and increase in compressibility, as a result of subglacial deformation and shearing.
5. Reduction in effective stress secant angle of friction, undrained shear strength and increase in compressibility as a result of periglacial freeze-thaw.
6. Increase in weathering profile thickness in non-glaciated Domains. Removed or reduced in thickness in glaciated Domains. Increase in compressibility, reduction in undrained and reduction in secant effective angle of friction.

Figure 9-15 Schematic illustration of the implications for ground engineering of past glacial and periglacial processes interpreted as part of this research.

10 Conclusions

The conclusions from this research are summarised below and divided into those that are related to Quaternary geology, and those that are related to geotechnical properties and behaviour.

10.1 Quaternary geology

- The Middle Pleistocene lowland glacial limit of the British Ice Sheet (BIS) in north Buckinghamshire was characterised by at least two advances of glacier ice. The first was limited in extent and possibly sourced from lobes of the BIS that entered the area from the West and East Midlands to the north. Following a period of incision and valley formation, glaciolacustrine conditions were established by the formation of ice- and topographically-dammed lakes prior to a second, and regionally, extensive advance of the BIS from the northeast. The later event resulted in deformation of underlying glaciolacustrine sediments.
- The glaciolacustrine sediments are interpreted to in-part, infill a buried valley system which is likely to be a continuation of the buried valleys identified in parts of Bedfordshire and underlying the present-day drainage course of the River Great Ouse and its tributaries.
- The geochronology of the glacial events is uncertain but it is suggested, on the basis of minimum OSL ages and published river terrace correlations, that the events took place during the late Wolstonian (Saalian of mainland Europe). There is no evidence to suggest the length of time between the two advances of the BIS. If the geochronology is correct, it suggests that the British lowland glacial limit in north Buckinghamshire, previously assumed to have been Anglian in age, is questionable. Glacigenic sediments in north Buckinghamshire may be correlated with the glacigenic sequences of the English Midlands, which are considered by some researchers to be late Wolstonian in age.
- Evidence of periglaciation is present in the form of involutions, possible ice-wedge psuedomorphs, frost-wedging and sub-horizontal shears within Quaternary sediments and bedrock and the presence of solifluction sediments in the form of ‘head’. The formation of thermokarst lakes overlying Mesozoic mudrocks is inferred from the presence of coalesced, arcuate erosional basins.

10.2 Geotechnical

There is no simple spatial pattern of variability in the geotechnical properties and behaviour of Oxford Clay and till that be unequivocally explained solely by past glacial and periglacial processes. However, the following general conclusions can be made.

- There is no qualitative difference in the assemblage of clay minerals in samples of Oxford Clay and the matrix of tills. Any differences in geotechnical behaviour are therefore unlikely to be a result of differences in clay mineralogy.
- The plasticity of till is influenced by the proportion of granular particles within its matrix which is dependent on the lithology of the bedrock source. For a given value of liquid limit, tills in Domain 1.2.1, overlying sandstone and limestone bedrock, have a higher plasticity index compared to tills in Domain 1.3.1 and 1.1.1 which are underlain by mudrocks.
- For tills, the undrained shear strength and values of $ø'_{trans}$ are increased by the increased proportion of granular particles and, potentially, by the presence of carbonate which may act as a cementing agent. Other cementing agents including iron, derived from the chemical weathering of pyrite, may also contribute.
- The Oxford Clay has low to medium compressibility but there is lateral and vertical variability in 1D consolidation behaviour, influenced by proximity to the Middle Pleistocene ice-margin and subglacial and periglacial shearing. The initial void ratio appears to increase towards the former margin of the Middle Pleistocene British Ice Sheet within glaciated Domains 1.3 and 1.3.1, reaching a maximum in non-glaciated Domain 2.3. This behaviour is interpreted to be the result of de-structuring of the microfabric of the Oxford Clay caused by periglacial solifluction shearing in Domain 2.3 and subglacial shearing in Domains 1.3 and 1.3.1. The weathering zone within which high initial void ratios may have developed, is interpreted to have been partially or wholly removed by subglacial erosion in glaciated Domains 1.3 and 1.3.1.
- Undrained shear strength (c_u) and secant shear modulus, G are effective stress dependent and so increase with increasing depth below ground level. Values of mobilised undrained shear strength (0.5_{qmax}) for Oxford Clay are between 79 and 259 kPa. The value of 79 kPa is anomalously low and associated with non-glaciated Domain 2.3. Corresponding values of mobilised strain ($\varepsilon_{F=2}$) range between 0.12 and 0.45.

- Solifluction and subglacial shearing results in partial or whole reversal of the geostatic and periglacial thaw consolidation, overconsolidation signature so that void ratio and compressibility increase, with a corresponding decrease in $ø'_{trans}$, and in the case of specimens in Domain 2.3, a corresponding reduction in c_u.

11 Further Work

Geological

- Investigation of the geomorphology, fill and extent of buried valleys cut into bedrock on the glaciated side of the former margin of the British Ice Sheet and their relationship to other buried valleys in Bedfordshire and Cambridgeshire. Their presence has been known to cause delays in piling for the on-going A14 road extension in Cambridgeshire.
- Validate and refine the geochronology of glacial and periglacial events in north Buckinghamshire using multi-proxy numerical dating techniques.
- Validate the correlation between the glacigenic sediments of north Buckinghamshire with those in the English Midlands and East Anglia.

Geotechnical

- Using physical freeze-thaw experiments on fresh and unweathered Oxford Clay, quantify the changes in compressibility, stiffness and undrained shear strength behaviour, with increasing numbers of free-thaw cycles.
- Quantitative geostatistical analysis of geotechnical property variability in till and the Oxford Clay, adjacent to the former ice margin of the British Ice Sheet.

12 References

Adamiec, G. & Aitken, M. J. (1998) 'Dose-rate conversion factors: update', *Ancient TL*, 16(2), pp. 37–50.

Aitken, M. J. (1998) *An introduction to optical dating: the dating of Quaternary sediments by the use of photon-stimulated luminescence*. Oxford: Oxford University Press.

Allen, P., Cheshire, D. A. & Whiteman, C. A. (1991) 'Glacial deposits of southern East Anglia', in Ehlers, J., Gibbard, P. L., and Rose, J. (eds) *Glacial deposits in Britian and Ireland*. Rotterdam, pp. 225–278.

Ambrose, K. & Horton, A. (1991) 'The origin of Ot Moor, Oxfordshire, England', *Proceedings - Geologists' Association*. The Geologists' Association, 102(4), pp. 265–274. doi: 10.1016/S0016-7878(08)80086-7.

Anonymous (2018) 'Consistency concerns', *Ground Engineering*, March, pp. 22–23.

Antoine, P., Catt, J., Lautridou, J. P. & Sommé, J. (2003) 'The loess and coversands of northern France and southern England', *Journal of Quaternary Science*, 18(3–4), pp. 309–318. doi: 10.1002/jqs.750.

Associaiton of Geotechncial and Geoenvironmental Specilaists (2004) *Electronic transfer of geotechnical and Geoenvironmental data Edition 3.1 including addendum May 2005*. Beckenham, UK.

Association of Geotechnical and Geoenvironmental Specialists (1998) *AGS Guide The Selection of Geotechnical Laboratory Soil Testing*.

Atkinson, J. H. (2007) 'Peak strength of overconsolidated clays', *Géotechnique*, 57(2), pp. 127–135. doi: 10.1680/geot.2007.57.2.127.

Atkinson, J. H. & Little, J. A. (1988) 'Undrained triaxial strength and stress–strain characteristics of a glacial till soil', *Canadian Geotechnical Journal*, 25(3), pp. 428–439. doi: 10.1139/t88-048.

Baden-Powell, D. F. W. (1948) 'The Chalky Boulder Clays of Norfolk and Suffolk', *Geological Magazine*. University of Cambridge Centre of International Studies, 85, pp. 279–296.

Ballantyne, C. K. (2018) *Periglacial geomorphology*. Oxford: Wiley-Blackwell.

Ballantyne, C. K. & Harris, C. (1994) *The periglaciation of Great Britain*. Cambridge: Cambridge University Press.

Banham, P. H. (1968) 'A preliminary note on the Pleistocene stratigraphy of north-east Norfolk', *Proceedings of the Geologists' Assocation*, 79(4), pp. 507–512.

Banham, P. H., Gibbard, P. L., Lunkka, J. P., Parfitt, S. A., Preece, R. C. & Turner, C. (2001) 'A critical assessment of "A New Glacial stratigraphy for Eastern England"', *Quaternary Newsletter*, 93, pp. 5–14.

Banks, V. J., Bricker, S. H., Royse, K. R. & Collins, P. E. F. (2015) 'Anomalous buried hollows in London: development of a hazard susceptibility map', *Quarterly Journal of Engineering Geology and Hydrogeology*, 48(1), pp. 55–70. doi: 10.1144/qjegh2014-037.

Barnes, G. (2010) *Soil Mechanics*. New York: Palgrave Macmillan.

Barron, A. J. M., Sumbler, M. G., Morigi, A. N., Reeves, H. J., Benham, A. J., Entwisle, D. C. & Gale, I. N. (2010) 'Geology of the Bedford district a brief explanation of the geological map Sheet 203 Bedford'. Sheet Explanation of the British Geological Survey 1:50 000 scale Sheet 203 Bedford (England and Wales).

Barron, A. J. M., Morigi, A. N. & Reeves, H. J. (2006) 'Geology of the Wellingborough district a brief explanation of the geological map Sheet 186 Wellingborough'. the British Geological Survey 1:50 000 Sheet 186 Wellingborough (England and Wales).

Bateman, M. D., Frederick, C. D., Jaiswal, M. K. & Singhvi, A. K. (2003) 'Investigations into the potential effects of pedoturbation on luminescence dating', *Quaternary Science Reviews*, 22, pp. 1169–1176. doi: 10.1016/S0277-3791(03)00019-2.

Bateman, M. D., Boulter, C. H., Carr, A. S., Frederick, C. D., Peter, D. & Wilder, M. (2007) 'Detecting post-depositional sediment disturbance in sandy deposits using optical luminescence', *Quaternary Geochronology*, 2(1–4), pp. 57–64. doi: 10.1016/j.quageo.2006.05.004.

Bateman, M. D., Boulter, C. H., Carr, A. S., Frederick, C. D., Peter, D. & Wilder, M. (2007) 'Preserving the palaeoenvironmental record in Drylands : Bioturbation and its significance for luminescence-derived chronologies', *Sedim*, 195(1–2), pp. 5–19. doi: 10.1016/j.sedgeo.2006.07.003.

Bateman, M. D. & Catt, J. A. (1996) 'An absolute chronology for the raised beach and associated deposits at Sewerby, East Yorkshire, England.', *Journal of Quaternary Science*, 11(5), pp. 389–395. doi: 10.1002/(SICI)1099-1417(199609/10)11:5<389::AID-JQS260>3.0.CO;2-K.

de Beer, J., Price, S. J. & Ford, J. R. (2012) '3D modelling of geological and anthropogenic deposits at the World Heritage Site of Bryggen in Bergen, Norway', *Quaternary International*, 251. doi: 10.1016/j.quaint.2011.06.015.

Bell, F. G. (1991) 'A survey of the geotechnical properties of some till deposits on the north coast of Norfolk', in Forster, A. et al. (eds) *Quaternary Engineering Geology. Proceedings of the 25th Annual Conference of the Engineering Group of the Geological Society, Heriot -Watt University, Edinburgh, 10th - 14th September, 1989*. Geological Society of London, pp. 103–110. doi: 10.1144/GSL.ENG.1991.007.01.06.

Bell, F. G. (1992) *Engineering properties of soils and rocks*. Third Edit. Oxford: Butterworth-Heinemann.

Belshaw, R. K., Gibbard, P. L., Murton, J. B. & Murton, D. K. (2014) 'Early Middle Pleistocene drainage in southern central England', *Netherlands Journal of Geosciences - Geologie en Mijnbouw*, 93(04), pp. 135–145. doi: 10.1017/njg.2014.25.

Benn, D. I. (1995) 'Fabric signature of subglacial till deformation, Breidamerkurjökull, Iceland', *Sedimentology*, 42(5), pp. 735–747. doi: 10.1111/j.1365-3091.1995.tb00406.x.

Benn, D. I. & Evans, D. J. A. (1998) *Glaciers and glaciation*. London: Arnold.

Berry, F. G. (1979) 'Late Quaternary scour-hollows and related features in central London', *Quarterly Journal of Engineering Geology and Hydrogeology*, 12(1), pp. 9–29. doi: 10.1144/GSL.QJEG.1979.012.01.03.

Bishop, W. W. (1958) ‘The Pleistocene geology and geomorphology of three gaps in the Midland Jurassic escarpments’, *Philosophical Transactions of the Royal Society of London B Biological Sciences*, 68(2), pp. 255–306.

Bolton, M. D. (1979) *A guide to Soil Mechanics*. Cambridge: Macmillan Education.

Bolton, M. D. (1986) ‘The strength and dilatancy of sands’, *Geotechnique*, 36(1), pp. 65–78.

Boon, D. (2007) *The engineering geology of tills in Milton Keynes and the South Midlands, UK*. Britsih Geological Survey Internal Report, IR/00/00. Nottingham, UK.

Booth, S., Merritt, J. & Rose, J. (2015) ‘Quaternary Provinces and Domains – a quantitative and qualitative description of British landscape types’, *Proceedings of the Geologists’ Association*. The Geologists’ Association., 126(2), pp. 163–187. doi: 10.1016/j.pgeola.2014.11.002.

Boreham, S. (1996) ‘Thermokarst landforms in the Cambridge area’, *Nature in Cambridgeshire*, 38, pp. 16–22.

Boreham, S., White, T. S., Bridgland, D. R., Howard, A. J. & White, M. J. (2010) ‘The Quaternary history of the Wash fluvial network, UK’, *Proceedings of the Geologists’ Association*, 121(4), pp. 393–409. doi: 10.1016/j.pgeola.2010.02.003.

Boulton, G. (2010) ‘Drainage pathways beneath ice sheets and their implications for ice sheet form and flow: the example of the British Ice Sheet during the Last Glacial Maximum’, *Journal of Quaternary Science*, 25(4), pp. 483–500. doi: 10.1002/jqs.1407.

Boulton, G. S. (1968a) ‘Flow tills and related deposits on some Vestspitsbergen glaciers’, *Journal of Glaciology*, 7(51), pp. 391–412.

Boulton, G. S. (1968b) ‘On the origin and transport of englacial debris in Svlabard glaciers’, *Journal of Glaciology*, 9(56), pp. 213–229.

Boulton, G. S. (1970) ‘On the deposition of subglacial and melt-out tills at the margins of certain Svalbard glaciers’, *Journal of Glaciology*, 9(56), pp. 231–245.

Boulton, G. S. (1975) ‘The genesis of glacial tills - a framework for geotechncial interpretation’, in *The Engineering Behaviour of Glacial Materials, Symposium of Midlands Society of Soil Mechanics and Foundation Engineering, Birmingham*, pp. 52–59.

Boulton, G. S. (1977) ‘The Development of Geotechnical Properties in Glacial Tills’, in Legget, R. F. (ed.) *Glacial Till. An inter-disciplinary Study*. Ottawa: Royal Society of Canada, pp. 292–303.

Boulton, G. S. & Dobbie, K. E. (1993) ‘Consolidation of sediments by glaciers: relations between sediment geotechnics, soft-bed glacier dynantics and subglacial ground-water flow’, *Journal of Glaciology*, 39(131), pp. 26–44.

Boulton, G. S. & Hindmarsh, R. C. A. (1987) ‘Sediment deformation beneath glaciers: Rheology and geological consequences’, *Journal of Geophysical Research*, 92(B9), p. 9059. doi: 10.1029/JB092iB09p09059.

Boulton, G. S. & Paul, M. A. (1976) ‘The influence of genetic processes on some geotechnical properties of glacial tills’, *Quarterly Journal of Engineering Geology and Hydrogeology*, 9(3), pp. 159–194. doi: 10.1144/GSL.QJEG.1976.009.03.03.

Bowen, D. Q. (1999) *A revised correlation of Quaternary Deposits in the British Isles*. London: Geological Society Special Report No.23.

Bricker, S. H., Lee, J. R., Banks, V. J., Morigi, A. N. & Garcia-Bajo, M. (2012) 'Woodland Revisited: East Anglia' s buried channel network brought to life in 3D', *Geoscientist*, 22(4), pp. 14–19.

Bridge, D. M., Carney, J. N., Lawley, R. S. & Rushton, A. W. A. (1998) 'Geology of the country around Coventry and Nuneaton'. Geological Survey, Sheet 108 (England and Wales).

Bridgland, D. R. (2006) 'The Middle and Upper Pleistocene sequence in the Lower Thames: A record of Milankovitch climatic fluctuation and early human occupation of southern Britain', *Proceedings of the Geologists' Association*. The Geologists' Association, 117(3), pp. 281–305. doi: 10.1016/S0016-7878(06)80036-2.

Briggs, D. J. & Gilbertson, D. D. (1980) 'Quaternary Processes and Environments in the upper Thames Valley', *Transactions of the Institute of British Geographers*, 5(1), pp. 53–65. doi: 10.2307/622098.

British Standards Institution (1999) *Code of practice for site investigations BS5930:1999+A2:2010*.

British Standards Institution (2007) *BS EN 1997-2:2007 - Eurocode 7: Geotechnical design - Part 2: Ground investigation and testing*, *Eurocode 7*. doi: BS EN 1997-2:2007.

British Standards Instiution (1990) *BS 1377-2:1990 Methods of tests for soils for civil engineering purposes - Part 2 classification tests*, *British Standards Institution*.

Brown, G. (1980) 'Appendix: Tables for the determination of d in Å from $2\Theta^{o}$ for the Kα and Kβ radiations of copper, cobalt and iron', in Brindley, G. W. and Brown, G. (eds) *Crystal structures of clay minerals and their X-Ray identification*. London: Mineralogical Society of Great Britain, pp. 439–475.

Burke, H., Phillips, E., Lee, J. R. & Wilkinson, I. P. (2009) 'Imbricate thrust stack model for the formation of glaciotectonic rafts: An example from the Middle Pleistocene of north Norfolk, UK', *Boreas*, 38(3), pp. 620–637. doi: 10.1111/j.1502-3885.2009.00085.x.

Burland, J. B. (1990) 'On the compressibility and shear strength of natural clays', *Geotechnique*, 40(3), pp. 329–378.

Burland, J. B., Longworth, T. I. & Moore, J. F. A. (1977) 'A study of ground movement and progressive failure caused by a deep excavation in Oxford Clay', *Geotechnique*, 27(4), pp. 557–591.

Burton, R. G. O. (1976) 'Possible thermokarst features in cambridgeshire', *East Midland Geographer*, 6, pp. 230–240.

Busby, J. P., Lee, J. R., Kender, S., Williamson, P. & Norris, S. (2016) 'Regional modelling of permafrost thicknesses over the past 130 ka: Implications for permafrost development in Great Britain', *Boreas*, 45(1), pp. 46–60. doi: 10.1111/bor.12136.

Callomon, J. H. (1968) 'The Kellaways beds and the Oxford Clay', in Sylvester-Bradley, P. C. and Ford, T. D. (eds) *The Geology of the East Midlands*. Leicester University Press, pp. 264–290.

Callomon, J. H. (1969) 'International field symposium on the British Jurassic', *Keele*

University Publication, pp. 29–35.

Candy, I. (2009) 'Terrestrial and freshwater carbonates in Hoxnian interglacial deposits, UK: micromorphology, stable isotopic composition and palaeoenvironmental significance', *Proceedings of the Geologists' Association*. The Geologists' Association., 120(1), pp. 49–57. doi: 10.1016/j.pgeola.2009.03.001.

Casagrande, A. (1932) *Research on the Atterberg limits of soils*. Public Roads 13(8).

Catt, J. A. (1991) 'Late Devensian glacial deposits and glaciations in eastern England and the adjoining offshore areas', in Ehlers, J., Gibbard, P. L., and Rose, J. (eds) *Glacial deposits in Britain and Ireland*. Rotterdam: A A Balkema, pp. 61–68.

Chamberlain, E. J. (1981) 'Overconsolidation effects of ground freezing', *Engineering Geology*, 18, pp. 97–110.

Chamberlain, E. J. & Gow, A. J. (1979) 'Effect of freezing and thawing on the permeability and structures of soils', *Engineering Geology*, 13, pp. 73–92.

Chandler, R. J. (1970) 'The degradation of Lias clay slopes in an area of the east Midlands', *Quarterly Journal of Engineering Geology and Hydrogeology*, 2(3), pp. 161–181. doi: 10.1144/GSL.QJEG.1970.002.03.01.

Chandler, R. J. (1972) 'Lias clay: weathering processes and their effect on shear strength', *Geotechnique*, 22(3), pp. 403–431.

Chandler, R. J. (2010) 'Stiff sedimentary clays: geological origins and engineering properties', *Geotechnique*, 60(12), pp. 891–902.

Christoffersen, P. & Tulaczyk, S. (2003) 'Signature of palaeo-ice-stream stagnation: till consolidation induced by basal freeze-on', *Boreas*, 32, pp. 114–129. doi: 10.1111/j.1502-3885.2003.tb01433.x.

Clark, C. D., Gibbard, P. L. & Rose, J. (2004) 'Pleistocene glacial limits in England, Scotland and Wales', in Ehlers, J. and Gibbard, P. L. (eds) *Quaternary Glaciations—Extent and Chronology, Part I: Europe*. Amsterdam: Elsevier, pp. 47–82.

Clark, C. D., Gibbard, P. L. & Rose, J. (2004) 'Pleistocene glacial limits in England , Scotland and Wales', in Ehlers, J. and Gibbard, P. L. (eds) *Quaternary glaciations: extent and chronology*. Elsevier B.V., pp. 47–82.

Clarke, M. R. & Auton, C. A. (1984) 'Ingham sand and gravel', in Allen, P. (ed.) *Field Guide to the Gipping and Waveney Valleys, Suffolk*. Cambridge: Quaternary Research Association, pp. 71–72.

Cocksedge, J. E. & Hight, D. W. (1975) 'tunnelling in glacial materials in the British Isles', in *The Engineering Behaviour of Glacial Materials, Symposium of Midlands Society of Soil Mechanics and Foundation Engineering, Birmingham*, pp. 197–206.

Cohen, K. M. & Gibbard, P. L. (2011) 'Global chronostratigraphical correlation table for the last 2.7 million years', *Subcommission on Quaternary Stratigraphy (International Commission on Stratigraphy), Cambridge, England*.

Cox, B. M., Hudson, J. D. & Martill, D. M. (1992) 'Lithostratigraphic nomenclature of the Oxford Clay (Jurassic)', *Proceedings of the Geologists' Association*. The Geologists' Association, 103(4), pp. 343–345. doi: 10.1016/S0016-7878(08)80130-7.

Cratchley, C. R., McCann, D. M., Denness, B., Conway, B. W. & Hallam, J. R. (1969) *Regional Geotechnical Investigation of the Milton Keynes Area*.

Cripps, J. C. & Taylor, R. K. (1987) 'Engineering characteristics of British over-consolidated clays and mudrocks, II. Mesozoic deposits', *Engineering Geology*, 23(3–4), pp. 213–253. doi: 10.1016/0013-7952(87)90091-3.

Culshaw, M. G., Cripps, J. C., Bell, F. G. & Moon, C. F. (1991) 'Engineering geology of Quaternary soils: I. Processes and properties', in Forster, A. et al. (eds) *Quaternary Engineering Geology. Proceedings of the 25th Annual Conference of the Engineering Group of the Geological Society, Heriot -Watt University, Edinburgh, 10th - 14th September, 1989*. Geological Society of London, pp. 3–38. doi: 10.1144/GSL.ENG.1991.007.01.01.

Culshaw, M. G. (2005) 'From concept towards reality: developing the attributed 3D geological model of the shallow subsurface', *Quarterly Journal of Engineering Geology and Hydrogeology*, 38(3), pp. 231–284. doi: 10.1144/1470-9236/04-072.

Culshaw, M. G., Entwisle, D. C., Giles, D., Berry, T., Collings, A., Banks, V. J. & Donnelly, L. J. (2017) 'Material properties and geohazards', in Griffiths, J. S. and Martin, C. J. (eds) *Periglacial and Glacial Engineering Geology*. Engineering Group of the Geological Society Special Publications No. 28, pp. 599–740.

Czurda, K. A. & Hohmann, M. (1997) 'Freezing effect on shear strength of clayey soils', *Applied Clay Science*, 12, pp. 165–187.

Davies, B. J., Roberts, D. H., Bridgland, D. R., Cofaigh, C. Ó. & Riding, J. B. (2011) 'Provenance and depositional environments of Quaternary sediments from the western North Sea Basin', *Journal of Quaternary Science*, 26(1), pp. 59–75. doi: 10.1002/jqs.1426.

Davis, A. G. (1967) 'The mineralogy and phase equilibrium of Keuper Marl', *Quarterly Journal of Engineering Geology and Hydrogeology*, 1(1), pp. 25–38. doi: 10.1144/GSL.QJEG.1967.001.01.03.

Denness, B. (1974) 'Engineering aspects of the chalky boulder clay at the new town of Milton Keynes in Buckinghamshire', *Quarterly Journal of Engineering Geology and Hydrogeology*, 7(3), pp. 297–309. doi: 10.1144/GSL.QJEG.1974.007.03.03.

Dobbs, M. R., Culshaw, M. G., Northmore, K. J., Reeves, H. J. & Entwisle, D. C. (2012) 'Methodology for creating national engineering geological maps of the UK', *Quarterly Journal of Engineering Geology and Hydrogeology*, 45(3), pp. 335–347. doi: 10.1144/1470-9236/12-003.

Ehlers, J. & Gibbard, P. L. (1991) 'Anglian glacial deposits in Britain and the adjoining offshre areas', in Ehlers, J., Gibbard, P. L., and Rose, J. (eds) *Glacial deposits in Britain and Ireland*. Rotterdam: A A Balkema, pp. 17–24.

Ehlers, J., Gibbard, P. L. & Hughes, P. D. (2011) 'Introduction. Quaternary Glaciations - Extent and Chronology: A Closer Look', in Ehlers, J., Gibbard, P. L., and Hughes, P. D. (eds) *Quaternary Glaciations - Extent and Chronology: A Closer Look*. Elsevier, pp. 1–14.

Ehlers, J., Gibbard, P. L. & Rose, J. (eds) (1991) *Glacial deposits in Great Britain and Ireland*. Rotterdam: A A Balkema.

Entwisle, D. C., Hobbs, P. R. N., Northmore, K. J., Skipper, J., Raines, M. R., Self, S. J., Ellison, R. A. & Jones, L. D. (2013) 'Engineering geology of British Rocks and Soils -

Lambeth Group', *British Geological Survey Open Report, OR/13/006*, p. 316.

Entwisle, D. C. & Wildman, G. (2010) *Creation of the Till thematic layer*.

Evans, D. J. A. (2017) 'Conceptual glacial ground models: British and Irish Case Studies', in Griffiths, J. S. and Martin, C. J. (eds) *Engineering Geology and Geomorphology of Glaciated and Periglaciated Terrains. Engineering Group Working Party Report*. Geological Society of London Engineering Geology Special Publication 28, pp. 369–500.

Evans, D. J. A. & Benn, D. I. (2004) 'Facies descriptions and the logging of sedimentary exposures', in Evans, D. J. . and Benn, D. I. (eds) *A practical guide to the study of glacial sediments*. London: Arnold, p. 266.

Eyles, N. (1983) 'Glacial Geology: A landsystems approach', in Eyles, N. (ed.) *Glacial Geology An Introduction for Engineers and Earth Scientists*. Pergamon Press, pp. 1–18.

Eyles, N. & Dearman, W. R. (1981) 'A glacial terrain map of Britain for engineering purposes', *Bulletin of the Internaional association of Engineering Geology*, pp. 173–184.

Eyles, N., Dearman, W. R. & Douglas, T. D. (1983) 'The Distribution of Glacial Landsystems in Britain and North America', in Eyles, N. (ed.) *Glacial Geology An Introduction for Engineers and Earth Scientists*. Pergamon Press, pp. 213–228.

Eyles, N., Eyles, C. H. & McCabe, A. M. (1989) 'Sedimentation in an ice-contact subaqueous setting: The mid-Pleistocene "North Sea Drifts" of Norfolk, U.K.', *Quaternary Science Reviews*, 8(1), pp. 57–74. doi: 10.1016/0277-3791(89)90021-8.

Eyles, N., Eyles, C. H. & Miall, A. D. (1983) 'Lithofacies types and vertical profile models ; an alternative approach to the description and environmental interpretation of glacial diamict and diamictite sequences', *Sedimentology*, 30, pp. 393–410.

Fish, P. R. & Whiteman, C. A. (2001) 'Chalk micropalaeontology and the provenancing of Middle Pleistocene lowestoft formation till in Eastern England', *Earth Surface Processes and Landforms*, 26(9), pp. 953–970. doi: 10.1002/esp.237.

Fookes, P. G., Hinch, L. W., Huxley, M. A. & Simons, N. E. (1975) 'Some soil properties in glacial terrain - the Taff Valley, South Wales', in *The Engineering Behaviour of Glacial Materials, Symposium of Midlands Society of Soil Mechanics and Foundation Engineering, Birmingham*, pp. 93–116.

Fookes, P. G. (1991) 'Quaternary engineering geology', in Forster, A. et al. (eds) *Quaternary Engineering Geology. Proceedings of the 25th Annual Conference of the Engineering Group of the Geological Society, Heriot -Watt University, Edinburgh, 10th - 14th September, 1989*. Geological Society of London, pp. 73–98. doi: 10.1144/GSL.ENG.1991.007.01.04.

Fookes, P. G. (1997) 'Geology for Engineers: the Geological Model, Prediction and Performance', *Quarterly Journal of Engineering Geology and Hydrogeology*, 30(4), pp. 293–424. doi: 10.1144/GSL.QJEG.1997.030.P4.02.

Fookes, P. G. & Best, R. (1969) 'Consolidation characteristics of some late Pleistocene periglacial metastable soils of East Kent', *Quarterly Journal of Engineering Geology and Hydrogeology*, 2(2), pp. 103–128. doi: 10.1144/GSL.QJEG.1969.002.02.02.

Fookes, P. G., Gordon, D. L. & Higginbottom, I. E. (1975) 'Glacial landforms, their deposits and engineering characteristics', in *The Engineering Behaviour of Glacial Materials, Symposium of Midlands Society of Soil Mechanics and Foundation Engineering, Birmingham*.

Forster, A., Culshaw, M. G., Cripps, J. C., Little, J. A. & Moon, C. F. (1991) 'Quaternary Engineering Geology', in Forster, A. et al. (eds) *Quaternary Engineering Geology. Proceedings of the 25th Annual Conference of the Engineering Group of the Geological Society, Heriott-Watt University, Edinburgh, 10th-14th September 1989*, p. 725.

de Freitas, M. H. (2009) 'Geology; its principles, practice and potential for Geotechnics', *Quarterly Journal of Engineering Geology and Hydrogeology*, 42(4), pp. 397–441. doi: 10.1144/1470-9236/09-014.

French, H. M. (2007) *The periglacial environment*. Third edit. Chichester: John Wiley & Sons, Inc.

Galbraith, R. F. & Green, P. F. (1990) 'Estimating the component ages in a finite mixture', 17(3), pp. 197–206.

Gibbard, P. L. (1977) 'Pleistocene history of the Vale of St Albans', *Philosophical Transactions of the Royal Society, B*, 280, pp. 445–482.

Gibbard, P. L. (1985) *The Pleistocene history of the Middle Thames Valley*. Cambridge: Cambridge : Cambridge University Press, 1985.

Gibbard, P. L., West, R. G., Andrew, R. & Pettit, M. (1992) 'The margin of a Middle Pleistocene ice advance at Tottenhill, Norfolk, England', *Geological Magazine*, 129(1990), pp. 59–76.

Gibbard, P. L. (1994) *Pleistocene History of the Lower Thames Valley*. Cambridge: Cambridge University Press. doi: DOI: 10.1017/CBO9780511565199.

Gibbard, P. L. (1999) 'The Thames Valley, its tributary valleys and their former courses', in *A revised correlation of Quaternary deposits in the British Isles*. Geological Society of London Special Report No23, pp. 45–58.

Gibbard, P. L., Pasanen, A. H., West, R. G., Lunkka, J. P., Boreham, S., Cohen, K. M. & Rolfe, C. (2009) 'Late Middle Pleistocene glaciation in East Anglia, England', *Boreas*, 38(3), pp. 504–528. doi: 10.1111/j.1502-3885.2009.00087.x.

Gibbard, P. L., West, R. G., Boreham, S. & Rolfe, C. J. (2012) 'Late Middle Pleistocene ice-marginal sedimentation in East Anglia, England', *Boreas*, 41(3), pp. 319–336. doi: 10.1111/j.1502-3885.2011.00236.x.

Gibbard, P. L. & Allen, L. G. (1994) 'Drainage evolution in south and east England during the Pleistocene', *Terra Nova*, 6, pp. 444–452.

Gibbard, P. L. & Clark, C. D. (2011) 'Pleistocene glaciation limits in Great Britain', in *Quaternary Glaciations - Extent and Chronology: A Closer Look*. Elsevier (Developments in Quaternary Sciences), pp. 75–93. doi: 10.1016/B978-0-444-53447-7.00007-6.

Gibbard, P. L. & Lewin, J. (2003) 'The history of the major rivers of southern Britain during the Tertiary', *Journal of the Geological Society*, 160(6), pp. 829–845. doi: 10.1144/0016-764902-137.

Gibbard, P. L., Turner, C. & West, R. G. (2013) 'The Bytham river reconsidered', *Quaternary International*. Elsevier Ltd and INQUA, 292, pp. 15–32. doi: 10.1016/j.quaint.2012.08.2053.

Gibbard, P. L., West, R. G. & Hughes, P. D. (2018) 'Pleistocene glaciation of Fenland , England , and its implications for evolution of the region', *Royal Society open Science*, 5, p.

52.

Giles, D. P., Griffiths, J. S., Evans, D. J. A. & Murton, J. B. (2017) ‘Chapter 3 Geomorphological framework: glacial and periglacial sediments, structures and landforms’, in Griffiths, J. S. and Martin, C. J. (eds) *Engineering Geology and Geomorphology of Glaciated and Periglaciated Terrains. Engineering Group Working Party Report*. Geological Society Engineering Geology Special Publication No.28, pp. 59–368. Available at: http://egsp.lyellcollection.org/content/28/1/59.abstract.

Gosling, D. & Baldwin, M. (2010) ‘Development of a thin wall open drive tube sampler’, *Ground Engineering*, pp. 37–39.

Green, A. H. (1864) ‘Geology of the country round Banbury, Woodstock, Bicester and Buckingham’. Sheet 45 of the map of the Geological Survey of Great Britain.

Griffiths, J. S. & Stokes, M. (2008) ‘Engineering geomorphological input to ground models: an approach based on Earth systems’, *Quarterly Journal of Engineering Geology and Hydrogeology*, 41(1), pp. 73–91. doi: 10.1144/1470-9236/07-010.

Gunn, D. A., Jackson, P. D., Entwisle, D. C., Armstrong, R. W. & Culshaw, M. G. (2003) ‘Predicting subgrade shear modulus from existing ground models’, *NDT & E International*, 36(3), pp. 135–144. doi: 10.1016/S0963-8695(02)00052-X.

Hallam, J. R. (1990) *The statistical analysis and summarisation of geotechnical databases*, *British Geological Survey Technical Report*. doi: 10.1017/CBO9781107415324.004.

Hamblin, R. J. O., Moorlock, B. S. P., Rose, J., Lee, J. R., Riding, J. B., Booth, S. J. & Pawley, S. M. (2005) ‘Revised Pre-Devensian glacial stratigraphy in Norfolk, England, based on mapping and till provenance’, *Geologie en Mijnbouw/Netherlands Journal of Geosciences*, 84(2), pp. 77–85. doi: 10.1017/S0016774600022976.

Harding, P., Bridgland, D. R., Keen, D. H. & Rogerson, R. J. (1992) ‘A Palaeolithic site rediscovered at Biddenham, Bedfordshire.’, *Bedfordshire Archaeology*, 19, pp. 87–90.

Harris, C., Arenson, L. U., Christiansen, H. H., Etzelmüller, B., Frauenfelder, R., Gruber, S., Haeberli, W., Hauck, C., Hölzle, M., Humlum, O., Isaksen, K., Kääb, A., Kern-Lütschg, M. a., Lehning, M., Matsuoka, N., Murton, J. B., Nötzli, J., Phillips, M., Ross, N., *et al.* (2009) ‘Permafrost and climate in Europe: Monitoring and modelling thermal, geomorphological and geotechnical responses’, *Earth-Science Reviews*. Elsevier B.V., 92(3–4), pp. 117–171. doi: 10.1016/j.earscirev.2008.12.002.

Hart, J. K. (1990) ‘Proglacial glaciotectonic deformation and the origin of the Cromer Ridge push moraine complex, North Norfolk, England’, *Boreas*, 19(2), pp. 165–180. doi: 10.1111/j.1502-3885.1990.tb00577.x.

Hart, J. K. & Boulton, G. S. (1991) ‘The glacial drifts of Norfolk’, in Ehlers, J., Gibbard, P. L., and Rose, J. (eds) *Glacial Deposits in Great Britain and Ireland*. Rotterdam: Balkema, pp. 233–243.

Hart, J. K., Hindmarsh, R. C. a. & Boulton, G. S. (1990) ‘Styles of subglacial glaciotectonic deformation within the context of the anglian ice-sheet’, *Earth Surface Processes and Landforms*, 15(3), pp. 227–241. doi: 10.1002/esp.3290150305.

Head, K. H. (2006) *Manual of Soil Laboratory Testing. Volume 1 Soil Classification and Compaction Tests. Third Edition*. Caithness: Whittles Publishing.

Head, K. H. & Epps, R. J. (2011) *Manual of Soil and Laboratory Testing. Volume 2 Permeability, Shear Strength and Compressibility Tests. Third Edition*. Caithness: Whittles Publishing.

Head, K. H. & Epps, R. J. (2014) *Manual of Soil Laboratory Testing. Volume 3 Effective Stress Tests. Third Edition*. Caithness: Whittles Publishing.

Hesselbo, S. P. (2012) 'Triassic-Jurassic Boundary and Jurassic: Disintegrating Pangaea', in Woodcock, N. H. and Strachan, R. A. (eds) *Geological History of Britain and Ireland. Second Edition*. Chichester: Wiley-Blackwell, pp. 322–346.

Hey, R. W. (1976) 'Provenance of far-travelled pebbles in the pre-Anglian Pleistocene of East Anglia', *Proceedings of the Geologists' Association*. The Geologists' Association, 87(1), pp. 69–81. doi: 10.1016/S0016-7878(76)80036-3.

Hiemstra, J. F., Evans, D. J. a, Scourse, J. D., McCarroll, D., Furze, M. F. a & Rhodes, E. (2006) 'New evidence for a grounded Irish Sea glaciation of the Isles of Scilly, UK', *Quaternary Science Reviews*, 25(3–4), pp. 299–309. doi: 10.1016/j.quascirev.2005.01.013.

Higginbottom, I. E. & Fookes, P. G. (1970) 'Engineering aspects of periglacial features in Britain', *Quarterly Journal of Engineering Geology and Hydrogeology*, 3(2), pp. 85–117. doi: 10.1144/GSL.QJEG.1970.003.02.02.

Hobbs, P. R. N., Entwisle, D. C., Northmore, K. J., Sumbler, M. G., Jones, L. D., Kemp, S. J., Self, S. J., Barron, A. J. M. & Meakin, J. L. (2012) *Engineering geology of British rocks and soils : Lias Group*.

Hollingworth, S. E. & Taylor, J. H. (1946) 'An outline of the Geology of the Kettering district', *Proceedings of the Geologists' Association*. The Geologists' Association, 57(3), pp. 204-IN9. doi: 10.1016/S0016-7878(46)80007-5.

Holtz, R. D., Kovacs, W. D. & Sheahan, T. C. (2011) *An Introduction to Geotechnical Engineering*. Upper Saddle River: Pearson.

Hopson, P. M. (1995) 'Chalk rafts in Anglian till in north Hertfordshire', *Proceedings of the Geologists' Association*. The Geologists' Association, 106(2), pp. 151–158. doi: 10.1016/S0016-7878(08)80147-2.

Horton, A. (1970) *The drift sequence and subglacial topography in parts of the Ouse and Nene Basin*. Institute of Geological Sciences Report No. 70/9.

Horton, A., Shephard-Thorn, E. R. & Thurrell, R. G. (1974) *The geology of the new town of Milton Keynes. Explanation of 1:25 000 Special Geological Sheet SP83 with parts of SP73, 74, 84, 93 and 94*. Institute of Geological Sciences Report No. 74/16.

Hosseini Kamal, R. (2012) *Experimental study of the geotechnical properties of UK mudrocks*. Imperial College, London.

Huijzer, B. & Vandenberghe, J. (1998) 'Climatic reconstruction of the Weichselian Pleniglacial in northwestern and central Europe', *Journal of Quaternary Science*, 13(5), pp. 391–417. doi: 10.1002/(SICI)1099-1417(1998090)13:5<391::AID-JQS397>3.0.CO;2-6.

Huille, J. P. & Hunt, G. A. (2000) 'Track stiffness - a tool for maintenance', in *Proceedings of the third International Conference on Railway Engineering, London*, p. 8.

Hunt, G. A. (2005) *Review of the effect of track stiffness on track performance*. Rail Safety

and Standards Board Research Project T372.

Hutchinson, J. N. (1974) ‘Periglacial solifluxion: an approximate mechanism for clayey soils’, *Géotechnique*, 24(3), pp. 438–443. doi: 10.1680/geot.1974.24.3.438.

Hutchinson, J. N. (1980) ‘Possible late Quaternary pingo remnants in central London’, *Nature*, 284, pp. 253–255.

Hutchinson, J. N. (1991) ‘Theme lecture: Periglacial and slope processes’, in Forster, A. et al. (eds) *Quaternary Engineering Geology. Proceedings of the 25th Annual Conference of the Engineering Group of the Geological Society, Heriot -Watt University, Edinburgh, 10th - 14th September, 1989*. Geological Society of London, pp. 283–331. doi: 10.1144/GSL.ENG.1991.007.01.27.

Hutchinson, J. N. (1992) ‘John Neville Hutchinson’, *Géotechnique*, 63(15), pp. 1361–1363.

Hutchinson, J. N. (2001) ‘Reading the Ground: Morphology and Geology in Site Appraisal’, pp. 7–50.

Isarin, R. F. B. (1997) ‘Permafrost Distribution and Temperatures in Europe During the Younger Dryas’, *Permafrost and Periglacial Processes*, 8(3), pp. 313–333. doi: 10.1002/(SICI)1099-1530(199709)8:3<313::AID-PPP255>3.0.CO;2-E.

Jackson, J. O. (1973) ‘The Alteration Characteristics of the Lower Oxford Clay’, *Clay Minerals*, 10, pp. 113–126.

Jackson, J. O. & Fookes, P. G. (1974) ‘The relationship of the estimated former burial depth of the Lower Oxford Clay to some soil properties’, *Quarterly Journal of Engineering Geology*, 7, pp. 137–179.

Jeans, C. V (2006) ‘Jurassic clay mineralogy of the British Isles’, *Clay Minerals*, 41, pp. 187–307.

Kazi, A. & Knill, J. K. (1969) ‘The sedimentation and geotechnical properties of the Cromer Till between Happisburgh and Cromer, Norfolk’, *Quaternary Journal of Engenering Geology*, 2, pp. 63–86. doi: 10.1144/GSL.QJEG.1969.002.01.05.

Kearsey, T., Williams, J., Finlayson, A., Williamson, P., Dobbs, M., Marchant, B., Kingdon, A. & Campbell, D. (2015) ‘Testing the application and limitation of stochastic simulations to predict the lithology of glacial and fluvial deposits in Central Glasgow, UK’, *Engineering Geology*. Elsevier B.V., 187, pp. 98–112. doi: 10.1016/j.enggeo.2014.12.017.

Kemp, R. A., Whiteman, C. A. & Rose, J. (1993) ‘Palaeoenvironmental and stratigraphic significance of the Valley Farm and Barham Soils in Eastern England’, *Quaternary Science Reviews*, 12(10), pp. 833–848. doi: 10.1016/0277-3791(93)90022-E.

Knappett, J. A. & Craig, R. F. (2012) *Criag’s Soil Mechanics 8th Edition*. Abingdon, Oxon: Spoon Press.

Konrad, J.-M. & Morgenstern, N. R. (1981) ‘The segregation potential of a freezing soil’, *Canadian Geotechnical Journal*. NRC Research Press, 18(4), pp. 482–491. doi: 10.1139/t81-059.

Lee, J. R., Rose, J., Riding, J. B., Moorlock, B. S. P. & Hamblin, R. J. O. (2002) ‘Testing the case for a Middle Pleistocene Scandinavian glaciation in eastern England: Evidence for a Scottish ice source for tills within the Corton Formation of East Anglia, UK’, *Boreas*, 31(4),

pp. 345–355. doi: 10.1111/j.1502-3885.2002.tb01078.x.

Lee, J. R., Booth, S. J., Hamblin, R. J. O., Jarrow, A. M., Kessler, H., Moorlock, B. S. P., Morigi, A. N., Palmer, A., Pawley, S. M., Riding, J. B. & Rose, J. (2004) 'A new stratigraphy for the glacial deposits around Lowestoft, Great Yarmouth, North Walsham and Cromer, East Anglia, UK', *Bulletin of the Geological Society of Norfolk*, 53, pp. 3–60.

Lee, J. R., Rose, J., Hamblin, R. J. O. & Moorlock, B. S. P. (2004) 'Dating the earliest lowland glaciation of eastern England: A pre-MIS 12 early Middle Pleistocene Happisburgh glaciation', *Quaternary Science Reviews*, 23(14–15), pp. 1551–1566. doi: 10.1016/j.quascirev.2004.02.002.

Lee, J. R., Rose, J., Hamblin, R. J. O., Moorlock, B. S. P., James, B., Lee, J. R. & Riding, J. B. (2011) 'Quaternary Glaciations - Extent and Chronology - A Closer Look'. Elsevier (Developments in Quaternary Sciences), 15, pp. 59–74. doi: 10.1016/B978-0-444-53447-7.00006-4.

Lee, J. R., Phillips, E., Booth, S. J., Rose, J., Jordan, H. M., Pawley, S. M., Warren, M. & Lawley, R. S. (2013) 'A polyphase glacitectonic model for ice-marginal retreat and terminal moraine development: the Middle Pleistocene British Ice Sheet, northern Norfolk, UK', *Proceedings of the Geologists' Association*. The Geologists' Association., 124(5), pp. 753–777. doi: 10.1016/j.pgeola.2013.07.002.

Lee, J. R., Phillips, E., Rose, J. & Vaughan-Hirsch, D. (2017) 'The Middle Pleistocene glacial evolution of northern East Anglia, UK: a dynamic tectonostratigraphic–parasequence approach', *Journal of Quaternary Science*, 32(2), pp. 231–260. doi: 10.1002/jqs.2838.

Lee, J. R., Busschers, F. S. & Sejrup, H. P. (2012) 'Pre-Weichselian Quaternary glaciations of the British Isles, The Netherlands, Norway and adjacent marine areas south of 68°N: implications for long-term ice sheet development in northern Europe', *Quaternary Science Reviews*. NERC, 44, pp. 213–228. doi: 10.1016/j.quascirev.2010.02.027.

Lee, J. R. & Phillips, E. (2013) 'Glacitectonics – a key approach to examining ice dynamics, substrate rheology and ice-bed coupling', *Proceedings of the Geologists' Association*. The Geologists' Association., 124(5), pp. 731–737. doi: 10.1016/j.pgeola.2013.07.006.

Lee, J. R. & Phillips, E. R. (2008) 'Progressive soft sediment deformation within a subglacial shear zone-a hybrid mosaic-pervasive deformation model for Middle Pleistocene glaciotectonised sediments from eastern England', *Quaternary Science Reviews*, 27(13–14), pp. 1350–1362. doi: 10.1016/j.quascirev.2008.03.009.

Lewis, S. G. (1993) *The status of the Wolstonian glaciation in the English Midlands and East Anglia*. Unpublished PhD thesis, University of London.

Lewis, S. G. (1999) 'Eastern England', in Bowen, D. Q. (ed.) *A revised correlation of Quaternary deposits in the British Isles*. Geological Society Special Report No. 23, pp. 10–27.

Lewis, S. G., Rose, J. & Davies, H. (1999) 'Pre-Anglian fluvial and Anglian glaciogenic sediments, Knettishall, Suffolk, England', *Proceedings of the Geologists' Association*. The Geologists' Association, 110(1), pp. 17–32. doi: 10.1016/S0016-7878(99)80003-0.

Lisiecki, L. E. & Raymo, M. E. (2005) 'A Pliocene-Pleistocene stack of 57 globally distributed benthic δ 18 O records', *Paleoceanography*, 20(1), p. n/a-n/a. doi: 10.1029/2004PA001071.

Little, J. A. (1988) ‘Observations on the consolidation characteristics and permeability of Anglian tills’, *Engineering Geology*, 26, pp. 69–88.

Little, J. A. & Atkinson, J. H. (1988) ‘Some geological and engineering characteristics of lodgement tills from the Vale of St Albans , Hertfordshire’, *Quarterly Journal of Engineering Geology*, 21, pp. 183–199.

Lowe, J. & Walker, M. (2015) *Reconstructing Quaternary Environments*. Third Edit. London, New York: Routledge.

Lunkka, J. P. (1994) ‘Sedimentation and Iithostratigraphy of the North Sea Drift and Lowestoft Till Formations in the Coastal cliffs of northeast Norfolk, England’, *Journal of Quaternary Science*, 9(3), pp. 209–233. doi: 10.1002/jqs.3390090303.

Marsh, R. E., Prestwich, W. V, Rink, W. J. & Brennan, B. J. (2002) ‘Monte Carlo determinations of the beta dose rate to tooth enamel’, *Radiation Measurements*, 35, pp. 609–616.

Marsland, A. (1975) ‘In-situ and laboratory tests on glacial clays at Redcar’, in *The Engineering Behaviour of Glacial Materials, Symposium of Midlands Society of Soil Mechanics and Foundation Engineering, Birmingham*, pp. 149–164.

Marsland, A. & Powell, J. J. M. (1991) ‘Field and laboratory investigations of the clay tills at the test bed site at the Building Research Establishment, Garston, Hertfordshire’, *Geological Society, London, Engineering Geology Special Publications*, 7(1), pp. 229–238. doi: 10.1144/GSL.ENG.1991.007.01.21.

McGown, A. (1971) ‘The classification for engineering purposes of tills from moraines and associated landforms’, *Quarterly Journal of Engineering Geology and Hydrogeology*, 4(1951), pp. 115–130. doi: 10.1144/GSL.QJEG.1971.004.02.03.

McGown, A., Anderson, W. F. & Radwan, A. M. (1975) ‘Geotechncial properties of tills in west central Scotland’, in *The Engineering Behaviour of Glacial Materials, Symposium of Midlands Society of Soil Mechanics and Foundation Engineering, Birmingham*, pp. 81–92.

McGown, A. & Derbyshire, E. (1977) ‘Genetic influences on the properties of tills’, *Quarterly Journal of Engineering Geology and Hydrogeology*, 10(4), pp. 389–410. doi: 10.1144/GSL.QJEG.1977.010.04.02.

McMillan, A. A., Heathcote, J. A., Klinck, B. A., Shepley, M. G., Jackson, C. P. & Degnan, P. J. (2000) ‘Hydrogeological characterization of the onshore the concept of domains’, *Quarterly Journal of Engineering Geology and Hydrogeology*, 33, pp. 301–323.

McMillan, A. A., Hamblin, R. J. O. & Merritt, J. W. (2011) *A lithostratigraphical framework for onshore Quaternary and Neogene (Tertiary) superficial deposits of Great Britain and the Isle of Man*. British Geological Survey Research Report, RR/10/03, Nottingham, UK.

McMillan, A. A. & Powell, J. H. (1999) *BGS Rock Classification Scheme Volume 4 Classification of artificial (man-made) ground and natural superficial deposits. Applications to geological maps and datasets in the UK*. British Geological Survey Research Report 99-04, Nottingham, UK.

Van Der Meulen, M. J., Doornenbal, J. C., Gunnink, J. L., Stafleu, J., Schokker, J., Vernes, R. W., Van Geer, F. C., Van Gessel, S. F., Van Heteren, S., Van Leeuwen, R. J. W., Bakker, M. a J., Bogaard, P. J. F., Busschers, F. S., Griffioen, J., Gruijters, S. H. L. L., Kiden, P., Schroot,

B. M., Simmelink, H. J., Van Berkel, W. O., *et al.* (2013) '3D geology in a 2D country: Perspectives for geological surveying in the Netherlands', *Geologie en Mijnbouw/Netherlands Journal of Geosciences*, 92(4), pp. 217–241.

Mitchell, G.F., Penny, L.F., Shotton, F.W., West, R. . (1973) *A Correlation of Quaternary deposits in the British Isles*. Geological Society Special Report 4.

Mitchell, J. K. & Soga, K. (2005) *Fundamentals of soil behaviour*. Third Edit. Hoboken, New Jersey: John Wiley & Sons, Inc.

Moore, D. M. & Reynolds, R. C. (1997) *X-Ray diffraction and the Identification and Analysis of Clay Minerals*. New York: Oxford University Press.

Morgenstern, N. R. & Nixon, J. F. (1971) 'One-dimensional Consolidation of Thawing Soils', *Canadian Geotechnical Journal*. NRC Research Press, 8(4), pp. 558–565. doi: 10.1139/t71-057.

Muir Wood, D. (1991) *Soil behaviour and critical State soil mechanics*. Cambridge: Cambridge University Press.

Murray, A., Buylaert, J., Henriksen, M., Svendsen, J. & Mangerud, J. (2008) 'Testing the reliability of quartz OSL ages beyond the Eemian', *Radiation Measurements*, 43, pp. 776–780. doi: 10.1016/j.radmeas.2008.01.014.

Murray, A. S. & Funder, S. (2003) 'Optically stimulated luminescence dating of a Danish Eemian coastal marine deposit : a test of accuracy', 22, pp. 1177–1183. doi: 10.1016/S0277-3791(03)00048-9.

Murray, A. S. & Wintle, A. G. (2000) 'Luminescence dating of quartz using an improved single- aliquot regenerative-dose protocol', *Radiation Measurements*, 32.

Murray, A. S. & Wintle, A. G. (2003) 'The single aliquot regenerative dose protocol : potential for improvements in reliability', 37, pp. 377–381. doi: 10.1016/S1350-4487(03)00053-2.

Murton, J. (2001) 'Thermokarst sediments and sedimentary structures, Tuktoyaktuk Coastlands, western Arctic Canada', *Global and Planetary Change*, 28(1–4), pp. 175–192. doi: 10.1016/S0921-8181(00)00072-2.

Murton, J. B. (1996) 'Near-Surface Brecciation of Chalk , Isle of Thanet , South-East England a Comparison with Ice-Rich Brecciated Bedrocks in Canada and Spitsbergen', *Permafrost and Periglacial Processes*, 7(January), pp. 153–164.

Murton, J. B., Baker, A., Bowen, D. Q., Caseldine, C. J., Coope, G. R., Currant, A. P., Evans, J. G., Field, M. H., Green, C. P., Hatton, J., Ito, M., Jones, R. L., Keen, D. H., Kerney, M. P., McEwan, R., McGregor, D. F. M., Parish, D., Robinson, J. E., Schreve, D. C., *et al.* (2001) 'A late Middle Pleistocene temperate–periglacial–temperate sequence (Oxygen Isotope Stages 7–5e) near Marsworth, Buckinghamshire, UK', *Quaternary Science Reviews*, 20(18), pp. 1787–1825. doi: 10.1016/S0277-3791(01)00004-X.

Murton, J. B., Bowen, D. Q., Candy, I., Catt, J. A., Currant, A., Evans, J. G., Frogley, M. R., Green, C. P., Keen, D. H., Kerney, M. P., Parish, D., Penkman, K., Schreve, D. C., Taylor, S., Toms, P. S., Worsley, P. & York, L. L. (2015) 'Middle and Late Pleistocene environmental history of the Marsworth area, south-central England', *Proceedings of the Geologists' Association*. The Geologists' Association., 126(1), pp. 18–49. doi:

10.1016/j.pgeola.2014.11.003.

Murton, J. B. & Ballantyne, C. K. (2017) ‘Chapter 5 Periglacial and permafrost ground models for Great Britain’, in Griffiths, J. S. and Martin, C. J. (eds) *Engineering Geology and Geomorphology of Glaciated and Periglaciated Terrains. Engineering Group Working Party Report*. London: Geological Society Engineering Geology Special Publication No.28, pp. 501–597.

Murton, J. B. & French, H. M. (1993) ‘Thermokarst Involutions , Summer Island , Pleistocene Mackenzie Delta , Western Canadian Arctic’, *Permafrost and Periglacial Processes*, 4(September 1992), pp. 217–229.

Murton, J. B., Peterson, R. & Ozouf, J.-C. (2006) ‘Bedrock fracture by ice segregation in cold regions.’, *Science (New York, N.Y.)*, 314(5802), pp. 1127–9. doi: 10.1126/science.1132127.

Murton, J. B., Whiteman, C. A. & Allen, P. (1995) ‘Involutions in the Middle Pleistocene (Anglian) Barham Soil, eastern England: a comparison with thermokarst involutions from arctic Canada’, *Boreas*, 24(3), pp. 269–280. doi: 10.1111/j.1502-3885.1995.tb00779.x.

Nixon, J. F. & Morgenstern, N. R. (1973) ‘The Residual Stress in Thawing Soils’, *Canadian Geotechnical Journal*. NRC Research Press, 10(4), pp. 571–580. doi: 10.1139/t73-053.

Norbury, D. (2012) *Soil and Rock Description in Engineering Practice*. Caithness: Whittles Publishing.

Northmore, K. J., Entwisle, D. C., Reeves, H. J., Hobbs, P. R. N. & Culshaw, M. G. (2011) ‘The relevance of lithostratigraphy in the assessment and investigation of engineering ground conditions in UK mudstones La pertinence du lithostratigraphy dans l ’ évaluation et la recherche sur les conditions au sol de technologie en argilite UK’, in *15th European Conference of Soil Mechanics and Geotechnical Engineering, ECSMGE, Athens, Greeces, 12th-15th September 2011*, p. 7.

Northmore, K. J., Bell, F. G. & Culshaw, M. G. (1996) ‘The engineering properties and behaviour of the brickearth of south Essex’, *Quarterly Journal of Engineering Geology and Hydrogeology*, 29(2), pp. 147–161. doi: 10.1144/GSL.QJEGH.1996.029.P2.04.

Old, R. A., Sumbler, M. G. & Ambrose, K. (1987) ‘Geology of the country around Warwick’. Memoir of the Geological Survey of Great Britain (England and Wales).

Olley, J. M., Deckker, P. De, Roberts, R. G., Fifield, L. K., Yoshida, H. & Hancock, G. (2004) ‘Optical dating of deep-sea sediments using single grains of quartz : a comparison with radiocarbon’, *Sedimentary Geology*, 169, pp. 175–189. doi: 10.1016/j.sedgeo.2004.05.005.

Parks, C. D. (1991) ‘A review of the mechanisms of cambering and valley bulging’, in Forster, A. et al. (eds) *Quaternary Engineering Geology. Proceedings of the 25th Annual Conference of the Engineering Group of the Geological Society, Heriot -Watt University, Edinburgh, 10th - 14th September, 1989*. Geological Society of London, pp. 373–380. doi: 10.1144/GSL.ENG.1991.007.01.33.

Parry, R. H. G. (1972) ‘Some properties of heaviliy overconsolidated Oxford clay at a site near Bedford’, *Geotechnique*, 22(3), pp. 485–507.

Parry, S., Baynes, F. J., Culshaw, M. G., Eggers, M., Keaton, J. F., Lentfer, K., Novotny, J. & Paul, D. (2014) ‘Engineering geological models: an introduction: IAEG commission 25’, *Bulletin of Engineering Geology and the Environment*, 73(3), pp. 689–706. doi:

10.1007/s10064-014-0576-x.

Paul, M. A. & Little, J. A. (1991) ‘Geotechnical properties of glacial deposits in lowland Britain’, in Ehlers, J., Gibbard, P. L., and Rose, J. (eds) *Glacial deposits in Britain and Ireland*. Rotterdam: A A Balkema, pp. 389–404.

Paul, M. A., Pole, E. L. & Gostelow, T. P. (1981) *Soil Mechanics in Quaternary Science*. London: Quaternary Research Association.

Pawley, S. M., Candy, I. & Booth, S. J. (2006) ‘The Late Devensian terminal moraine ridge at Garret Hill, Stiffkey valley, north Norfolk, England’, *Proceedings of the Yorkshire Geological Society*, 56(1960), pp. 31–39. doi: 10.1144/pygs.56.1.31.

Perrin, R. M. S. (1971) *The clay mineralogy of British sediments*. Mineralogical Society of Great Britain.

Perrin, R. M. S., Rose, J. & Davies, H. (1979) ‘The distribution, variation and origins of pre-Devensian tills in eastern England’, *Philosophical Transactions of the Royal Society of London B Biological Sciences*, 287(1024), pp. 535–570.

Phillips, E. ., Evans, D. J. . & Auton, C. . (2002) ‘Polyphase deformation at an oscillating ice margin following the Loch Lomond Readvance, central Scotland, UK’, *Sedimentary Geology*, 149(1–3), pp. 157–182. doi: 10.1016/S0037-0738(01)00250-0.

Phillips, E. & Lee, J. R. (2013) ‘Development of a subglacial drainage system and its effect on glacitectonism within the polydeformed Middle Pleistocene (Anglian) glacigenic sequence of north Norfolk, Eastern England’, *Proceedings of the Geologists’ Association*. The Geologists’ Association., 124(5), pp. 855–875. doi: 10.1016/j.pgeola.2012.07.005.

Preece, R. C., Parfitt, S. A., Russell Coope, G., Penkman, K. E. H., Ponel, P. & Whittaker, J. E. (2009) ‘Biostratigraphic and aminostratigrraphic constraints on the age of the Middle Pleistocene glacial succession iin north Norfolk, UK’, *Journal of Quaternary Science*, 24(6), pp. 557–580. doi: 10.1002/jqs.1245.

Prescott, J. R. & Hutton, J. T. (1994) ‘Cosmic ray contributions to dose rates for luminescence and ESR dating: large dpeths and long-term time variations’, *Radiation Measurements*, 23(2/3), pp. 497–500.

Price, S. J., Burke, H. F., Terrington, R. L., Reeves, H. J., Boon, D. & Scheib, A. J. (2010) ‘The 3D characterisation of the zone of human interaction and the sustainable use of underground space in urban and peri-urban environments : case studies from the UK’, *Zeitschrift der Deutschen Gesellschaft fur Geowissenschaften*, 161(2), pp. 219–235.

Reid, C. (1882) *The geology of the country around Cromer*. Geological Survey of England and Wales, HMSO, London.

Rice, R. J. (1968) ‘The Quaternary deposits of central Leicestershire’, *Philosophical Transactions of the Royal Society A*, 262(1131), pp. 459–508.

Rice, R. J. (1981) ‘The Pleistocene deposits of the area around Croft in south Leicestershire’, *Philosophical Transactions of the Royal Society of London B Biological Sciences*, 293, pp. 385–418.

Rice, R. J. & Douglas, T. J. (1991) ‘Wolstonian glacial deposits and glaciation in Britain’, in Ehlers, J., Gibbard, P. L., and Rose, J. (eds) *Glacial deposits in Britain and Ireland*. Rotterdam: A A Balkema, pp. 25–36.

Riding, J. B. (2008) *A palynological investigation of the tills in the Milton Keynes area*. British Geological Survey Internal Report, IR/08/019, Nottingham, UK.

Rose, J. (1987) 'Status of the Wolstonian glaciation in the British Quaternary', *Quaternary Newsletter*, 53, pp. 1–9.

Rose, J. (1989) 'Tracing the Baginton-Lillington sands and gravels from the West Midlands to East Anglia', in Keen, D. H. (ed.) *West Midlands Field Guide*. Quaternary Research Association, pp. 102–110.

Rose, J. (1992) 'High lodge—regional context and geological background', in *High Lodge: Excavations by G. de G. Sieveking, 1962-8 and J. Cook, 1988*. London: British Museum Press, pp. 13–24.

Rose, J. (1994) 'Major river systems of central and southern Britain during the Early and Middle Pleistocene', *Terra Nova*, 6, pp. 435–443.

Rose, J., Lee, J. A., Candy, I. & Lewis, S. C. (1999) 'Early and middle pleistocene river systems in eastern England: Evidence from Leet Hill, southern Norfolk, England', *Journal of Quaternary Science*, 14(4), pp. 347–360. doi: 10.1002/(SICI)1099-1417(199907)14:4<347::AID-JQS456>3.0.CO;2-A.

Rose, J. (2009) 'Early and Middle Pleistocene landscapes of eastern England', *Proceedings of the Geologists' Association*. The Geologists' Association., 120(1), pp. 3–33. doi: 10.1016/j.pgeola.2009.05.003.

Rose, J. & Allen, P. (1977) 'Middle Pleistocene stratigraphy in south-east Suffolk', *Journal of Geological Society*, 133(1), p. 83. doi: 10.1144/gsjgs.133.1.0083.

Rose, J., Moorlock, B. S. P. & Hamblin, R. J. O. (2001) 'Pre-Anglian fluvial and coastal deposits in Eastern England: Lithostratigraphy and palaeoenvironments', *Quaternary International*, 79, pp. 5–22. doi: 10.1016/S1040-6182(00)00119-1.

Rowe, P. J., Atkinson, T. C. & Turner, C. (1999) 'U-series dating of Hoxnian interglacial deposits at Marks Tey, Essex, England', *Journal of Quaternary Science*, 14(7), pp. 693–702. doi: 10.1002/(SICI)1099-1417(199912)14:7<693::AID-JQS477>3.0.CO;2-X.

Royse, K. R., Rutter, H. K. & Entwisle, D. C. (2009) 'Property attribution of 3D geological models in the Thames Gateway, London: New ways of visualising geoscientific information', *Bulletin of Engineering Geology and the Environment*, 68(1), pp. 1–16. doi: 10.1007/s10064-008-0171-0.

Russell, D. J., Denness, B. & McCann, D. M. (1978) 'Shear-strength anisotropy variations in weathered Oxford Clay', *Engineering Geology*, 12(C), pp. 337–344. doi: 10.1016/0013-7952(78)90017-0.

Russell, D. J. & Parker, A. (1979) 'Geotechnical, mineralogical and chemical interrelationships in weatheirng profiles of an overconsolidated clay', *Quarterly Journal of Engineering Geology*, 12, pp. 107–116.

Sættem, J., Rise, L., Rokoengen, K. & By, T. (1996) 'Soil investigations , offshore mid Norway : A case study of glacial influence on geotechnical properties', *Global and Planetary Change*, 12, pp. 271–285.

Sage, J. D. & D'Andrea, R. D. (1988) *Long term mitigation of frost deterioration of existing roadways*. Final Report, NSF Grant No. ECE 8518813, Worcester, Mass.

Sandford, K. S. (1924) ‘The river-gravels of the Oxford district’, *Quarterly Journal of the Geological Society*, 80(1–4), pp. 113–170.

Scheib, A. J., Lee, J. R., Breward, N. & Riding, J. B. (2011) ‘Reconstructing flow paths of the Middle Pleistocene British Ice Sheet in central-eastern England: The application of regional soil geochemical data’, *Proceedings of the Geologists’ Association*. The Geologists’ Association., 122(3), pp. 432–444. doi: 10.1016/j.pgeola.2011.01.008.

Schofield, A. N. & Wroth, P. (1968) *Critical state soil mechanics*. London, England: McGraw-Hill.

Self, S. J., Entwisle, D. C. & Northmore, K. J. (2012) *The structure and operation of the BGS National Geotechnical Properties Database Version 2*. British Geological Survey Internal Report, IR/12/056, Keyworth, UK.

Shackleton, N. J. & Opdyke, N. D. (1973) ‘Oxygen isotope and palaeomagnetic stratigraphy of Equatorial Pacific core V28-238: Oxygen isotope temperatures and ice volumes on a 105 year and 106 year scale’, *Quaternary Research*, 3(1), pp. 39–55. doi: 10.1016/0033-5894(73)90052-5.

Shackleton, N. J. & Pisias, N. G. (1982) ‘Atmospheric Carbon Dioxide, Orbital Forcing and Climate’, *Geophysical Monograph Series, The Carbon Cycle and Atmospheric CO2: Natural Variations Archean to Present*, 32.

Shotton, F. W. (1953) ‘The Pleistocene deposits of the area between Coventry, Rugby and Leamington and their bearing upon the topographic development of the Midlands’, *Philosophical Transactions of the Royal Society of London B Biological Sciences*, 237, pp. 209–260.

Shotton, F. W. (1976) ‘Amplification of the Wolstonian Stage of the British Pleistocene’, *Geological Magazine*, 113(03), p. 241. doi: 10.1017/S0016756800043223.

Shotton, F. W. (1983) ‘The Wolstonian stage of the british pleistocene in and around its type area of the english midlands’, *Quaternary Science Reviews*, 2(4), pp. 261–280. doi: 10.1016/0277-3791(83)90012-4.

Shukla, S. K. (2014) *Core principles of Soil Mechanics*. London: ICE Publishing.

Skempton, A. W. (1953) ‘The colloidal “activity” of clays’, in *Proceedings of the Third International Conference on Soil Mechanics and Foundation Engineering, Zurich*, pp. 57–60.

Skempton, A. W. (1970) ‘The consolidation of clays by gravitational compaction’, *Quarterly Journal of the Geological Society*, 125, pp. 373–411.

Skempton, A. W. & Norhey, R. D. (1952) ‘The sensitivity of clays’, *Geotechnique*, 3(1), pp. 30–53.

Skempton, A. W. & Weeks, A. G. (1976) ‘The Quaternary History of the Lower Greensand Escarpment and Weald Clay Vale near Sevenoaks, Kent [and Discussion]’, *Philosophical Transactions of the Royal Society A: Mathematical, Physical and Engineering Sciences*, 283(1315), pp. 493–526. doi: 10.1098/rsta.1976.0094.

Sladen, J. A. & Wrigley, W. (1983) ‘Geotechnical properties of Lodgement Till’, in Eyles, N. (ed.) *Glacial Geology An Introduction for Engineers and Earth Scientists*. Pergamon Press, pp. 184–212.

Spink, T. W. (1991) ‘Periglacial discontinuities in Eocene clays near Denham, Buckinghamshire’, *Geological Society, London, Engineering Geology Special Publications*, 7(1), pp. 389–396. doi: 10.1144/GSL.ENG.1991.007.01.35.

Straw, A. (1960) ‘The Limit of the “Last” Glaciation in North Norfolk’, *Proceedings of the Geologists’ Association*. The Geologists’ Association, 71(4), pp. 379–390. doi: 10.1016/S0016-7878(60)80021-1.

Sumbler, M. G. (1983) ‘A new look at the type Wolstonian glacial deposits of Central England’, *Proceedings of the Geologists’ Association*. The Geologists’ Association, 94(1), pp. 23–31. doi: 10.1016/S0016-7878(83)80024-8.

Sumbler, M. G. (1995) ‘The terraces of the rivers Thame and Thames and their bearing on the chronology of glaciation in central and eastern England’, *Proceedings of the Geologists’ Association*. The Geologists’ Association, 106(2), pp. 93–106. doi: 10.1016/S0016-7878(08)80142-3.

Sumbler, M. G. (2001) ‘The Moreton Drift: a further clue to glacial chronology in central England’, *Proceedings of the Geologists’ Association*. The Geologists’ Association, 112(1), pp. 13–27. doi: 10.1016/S0016-7878(01)80045-6.

Sumbler, M. G. (2002) *Geology of the Buckingham district a brief explanation of the geological map Sheet 219 Buckingham*. Sheet Explanation of the British Geological Survey 1:50 000 Sheet 219 Buckingham (England and Wales).

Sumbler, M. G. & Samuel, M. D. A. (1990) *A preliminary study of potential resources of sand and gravel in Buckinghamshire north of the Chilterns*.

Thompson, J. B. (1896) ‘Pre-glacial valleys in Northamptonshire’, *Journal of Northampton Natural History Society*, 9, pp. 47–51.

Trenter, N. A. (1999) *Engineering in glacial till*. CIRIA Report C504: CIRIA, London, UK.

Union Internationale Des Chemin de Fer (2008) *UIC 719 R Earthworks and track bed for railway lines*.

Vardanega, P. J., Lau, B. H., Lam, S. Y., Haigh, S. K., Madabhushi, S. P. G. & Bolton, M. D. (2012) ‘Laboratory measurement of strength mobilisation in kaolin : link to stress history’, *Geotechnique Letters*, 2, pp. 9–15.

Vardanega, P. J. & Bolton, M. D. (2012) ‘Corrigendum: Strength mobilization in clays and silts’, *Canadian Geotechnical Journal*, 49(5), pp. 631–631. doi: 10.1139/t2012-023.

Vardanega, P. J. & Haigh, S. (2014) ‘The undrained strength-liquidity index relationship’, *Canadian Geotechnical Journal*, 200(1), p. 40. doi: 10.1139/cgj-2013-0169.

Vaughan-Hirsch, D. P., Phillips, E., Lee, J. R. & Hart, J. K. (2013) ‘Micromorphological analysis of poly-phase deformation associated with the transport and emplacement of glaciotectonic rafts at West Runton, north Norfolk, UK’, *Boreas*, 42(2), pp. 376–394. doi: 10.1111/j.1502-3885.2012.00268.x.

van der Vegt, P., Janszen, A. & Moscariello, A. (2012) ‘Tunnel valleys: current knowledge and future perspectives’, in Huuse, M. et al. (eds) *Glaciogenic reservoirs and hydrocarbon systems.* Geological Society Special Publication 368, pp. 75–97. doi: 10.1144/SP368.13.

West, R. G. (1991) ‘On the origin of Grunty Fen and other landforms in southern Fenland,

Cambridgeshire', *Geological Magazine*, 128(03), p. 257. doi: 10.1017/S001675680002210X.

West, R. G. & Banham, P. H. (1968) 'Short field meeting on the North Norfolk Coast', *Proceedings of the Geologists' Association*, 79(4), pp. 493–512.

West, R. G. & Donner, J. J. (1956) 'The glaciations of East Anglia and the East Midlands: a differentiation based on stone-orientation measurements of the tills', *Quarterly Journal of the Geological Society*, 112(1–4), pp. 69–91. doi: 10.1144/gsl.jgs.1956.112.01-04.05.

Williams, P. J. & Smith, M. W. (1989) *The frozen Earth. Fundamentals of geocryology*. Cambridge: Cambridge University Press.

Wood, S. V (1880) 'The newer Pliocene period in England', *Quarterly Journal of the Geological Society of London*, 36, pp. 457–528.

Woodland, A. W. (1970) 'The buried tunnel-valleys of East Anglia', *Proceedings of the Yorkshire Geological Society*, 37, pp. 521–578.

Wroth, C. P. & Wood, D. M. (1978) 'The correlation of index properties with some basic engineering properties of soils', *Canadian Geotechnical Journal*, 15(2), pp. 137–145.

Zalasiewicz, J. & Gibbard, P. L. (1988) 'The Pliocene to Early Middle Pleistocene of East Anglia: an overview', in Gibbard, P. L. and Zalasiewicz, J. (eds) *Pliocene-Middle Pleistocene of East Anglia, Field Guide*. Quaternary Research Association, Cambridge, pp. 1–31.

Zielinski, T. & Van Loon, A. J. (2000) 'Subaerial terminoglacial fans III: Overview of sedimentary characteristics and depositional model', *Netherlands Journal of Geosciences*, 79(1), pp. 93–107.

13 Appendices

13.1 Legend for sedimentological logs

Primary lithology	Code	Colour	Texture
Clay	C		
Silt	Z		
Sand	S		
Gravel	V		
Cobbles	L		
Boulders	B		
Other			
Diamicton			

Notes on lithological descriptions and codes:

Lithological descriptions follow those recommended in British Standards Code of Practice for site investigations, BS5930:1999+A2:2010. For sediment mixtures, the text descriptions record increasing dominance of each lithology when read from left to right e.g. sandy, gravelly, clay is a sediment whose dominant lithology is clay, with gravel and sand as secondary and tertiary components respectively. The codes used are after Cooper *et al.*, 2006.

Lithofacies

Lithological descriptions are supplemented by lithofacies codes after Evans & Benn (2004) following the schemes of e.g. Eyles *et al.*, (2003).

Structures and fossils

Cross-bedding/lamination

28°/192° Dip/azimuth

Horizontal bedding/lamination

Ripple lamination

Coarsening upwards

Fining upwards

Involutions

Fold

Fault

F

Shear plane

Shear

Brecciation

D

Sub-horizontal discontinuities

Debris or in-tact Bi-valve or brachiopod debris

Debris or in-tact ammonites casts or moulds

Flame structures

Erosive channel base

Samples

Bulk sample with sample code

SP070417_6

OSL sample with sample code

SP070417_5

13.2 Atterberg limits

		Liquid Limits				Plastic Limits	
		1	2	3	4	I	II
PENETRATION, mm		14.43	15.95	19.47	22.00		
WT. OF CONTAINER, g		4.52	16.38	5.29	5.41	3.41	3.40
WT. OF WET SOIL + CONTAINER, g		22.54	37.91	22.08	24.18	12.51	10.72
WT. OF DRY SOIL + CONTAINER, g		14.22	27.81	13.91	14.92	10.32	8.96
WT. OF MOISTURE, g		8.32	10.10	8.17	9.26	2.19	1.76
WT. OF DRY SOIL, g		9.70	11.43	8.62	9.51	6.91	5.56
MOISTURE CONTENT, %		85.8	88.4	94.8	97.4	31.7	31.7
Preparation method 1 (Head, 2006)							

MC	
WT. OF CONTAINER, g	19.93
WT. OF WET SOIL + CONTAINER, g	57.68
WT. OF DRY SOIL + CONTAINER, g	45
WT. OF MOISTURE, g	12.68
WT. OF DRY SOIL, g	25.07
MOISTURE CONTENT, %	51

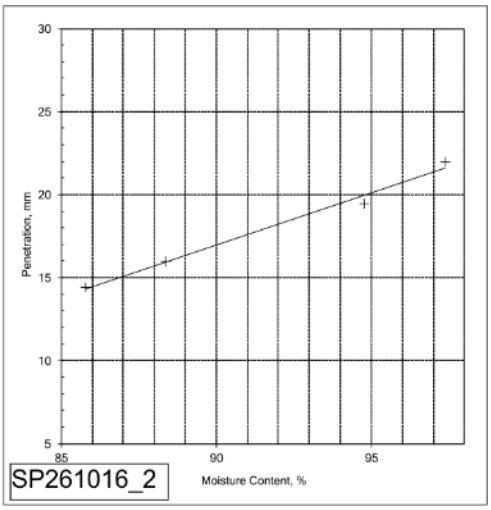

		Liquid Limits				Plastic Limits	
		1	2	3	4	I	II
PENETRATION, mm		13.10	15.60	18.55	21.10		
WT. OF CONTAINER, g		19.36	4.84	4.68	5.80	3.56	3.49
WT. OF WET SOIL + CONTAINER, g		41.20	25.60	27.73	33.91	14.51	14.71
WT. OF DRY SOIL + CONTAINER, g		35.82	20.22	21.41	25.86	13.02	13.22
WT. OF MOISTURE, g		5.38	5.38	6.32	8.05	1.49	1.49
WT. OF DRY SOIL, g		16.46	15.38	16.73	20.06	9.46	9.73
MOISTURE CONTENT, %		32.7	35.0	37.8	40.1	15.8	15.3
Preparation method 2 (Head, 2006)							

MC			DRY_MASS	
WT. OF CONTAINER, g	4.53		WT. CONTAINER, g	451.69
WT. OF WET SOIL + CONTAINER, g	45.41		WT. WET SOIL + CONTAINER, g	1044.38
WT. OF DRY SOIL + CONTAINER, g	38.74		WT. WET SOIL, g	592.69
WT. OF MOISTURE, g	6.67		WT. DRY SOIL >425 microns, g	25.09
WT. OF DRY SOIL, g	34.21		DRY MASS, g	495.99
MOISTURE CONTENT, %	19			

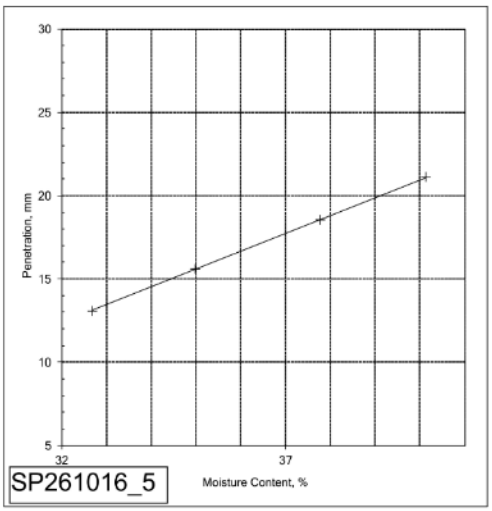

		Liquid Limits				Plastic Limits	
		1	2	3	4	I	II
PENETRATION, mm		14.93	19.80	22.20	26.25		
WT. OF CONTAINER, g		4.58	4.52	5.26	4.81	4.52	5.27
WT. OF WET SOIL + CONTAINER, g		23.95	26.09	23.00	30.73	19.18	18.82
WT. OF DRY SOIL + CONTAINER, g		19.57	20.82	18.51	23.77	17.36	17.14
WT. OF MOISTURE, g		4.38	5.27	4.49	6.96	1.82	1.68
WT. OF DRY SOIL, g		14.99	16.30	13.25	18.96	12.84	11.87
MOISTURE CONTENT, %		29.2	32.3	33.9	36.7	14.2	14.2
Preparation method 2 (Head, 2006)							

MC			DRY_MASS	
WT. OF CONTAINER, g	5.23		WT. CONTAINER, g	526.78
WT. OF WET SOIL + CONTAINER, g	16.34		WT. WET SOIL + CONTAINER, g	1015.81
WT. OF DRY SOIL + CONTAINER, g	15.93		WT. WET SOIL, g	489.03
WT. OF MOISTURE, g	0.41		WT. DRY SOIL >425 microns, g	107.41
WT. OF DRY SOIL, g	10.7		DRY MASS, g	470.98
MOISTURE CONTENT, %	4	DRY		

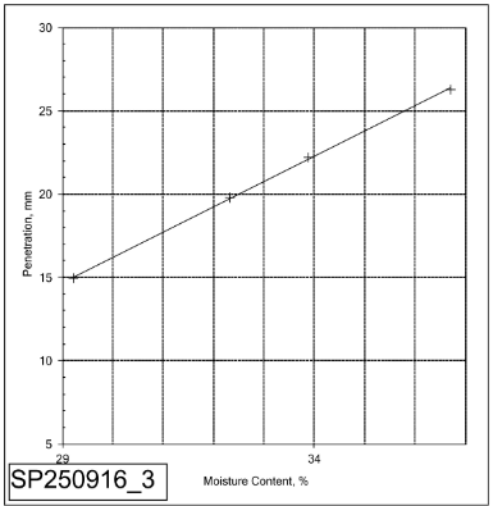

		Liquid Limits				Plastic Limits	
		1	2	3	4	I	II
PENETRATION, mm		17.95	20.17	25.13	26.75		
WT. OF CONTAINER, g		5.27	4.52	4.80	4.58	4.59	5.23
WT. OF WET SOIL + CONTAINER, g		24.15	23.79	21.88	26.06	16.73	16.49
WT. OF DRY SOIL + CONTAINER, g		19.13	18.45	16.95	19.73	14.86	14.73
WT. OF MOISTURE, g		5.02	5.34	4.93	6.33	1.87	1.76
WT. OF DRY SOIL, g		13.86	13.93	12.15	15.15	10.27	9.50
MOISTURE CONTENT, %		**36.2**	**38.3**	**40.6**	**41.8**	18.2	18.5
Preparation method 2 (Head, 2006)							

MC			DRY_MASS	
WT. OF CONTAINER, g	5.81		**WT. CONTAINER, g**	442.8
WT. OF WET SOIL + CONTAINER, g	20.91		**WT. WET SOIL + CONTAINER, g**	896.12
WT. OF DRY SOIL + CONTAINER, g	19.79		**WT. WET SOIL, g**	453.32
WT. OF MOISTURE, g	1.12		**WT. DRY SOIL >425 microns, g**	25.09
WT. OF DRY SOIL, g	13.98		**DRY MASS, g**	419.70
MOISTURE CONTENT, %	8	DRY		

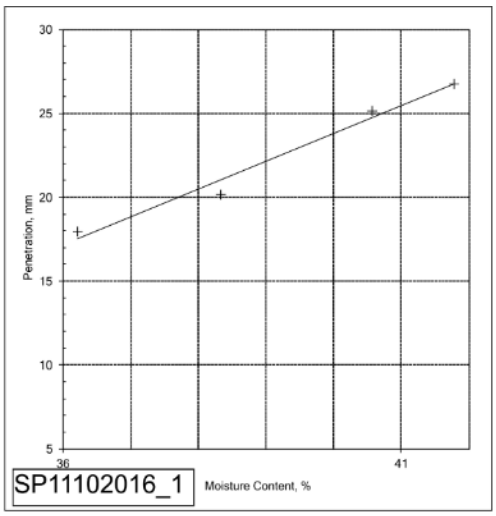

		Liquid Limits				Plastic Limits	
		1	2	3	4	I	II
PENETRATION, mm		16.77	19.35	21.00	23.15		
WT. OF CONTAINER, g		4.59	5.23	4.81	5.47	5.28	4.52
WT. OF WET SOIL + CONTAINER, g		21.99	32.21	31.28	28.52	13.90	10.92
WT. OF DRY SOIL + CONTAINER, g		16.90	23.96	22.93	20.98	12.63	9.96
WT. OF MOISTURE, g		5.09	8.25	8.35	7.54	1.27	0.96
WT. OF DRY SOIL, g		12.31	18.73	18.12	15.51	7.35	5.44
MOISTURE CONTENT, %		**41.3**	**44.0**	**46.1**	**48.6**	17.3	17.6
Preparation method 2 (Head, 2006)							

MC			DRY_MASS	
WT. OF CONTAINER, g	4.67		**WT. CONTAINER, g**	456.17
WT. OF WET SOIL + CONTAINER, g	37.4		**WT. WET SOIL + CONTAINER, g**	1099.84
WT. OF DRY SOIL + CONTAINER, g	31.68		**WT. WET SOIL, g**	643.67
WT. OF MOISTURE, g	5.72		**WT. DRY SOIL >425 microns, g**	50.21
WT. OF DRY SOIL, g	27.01		**DRY MASS, g**	531.18
MOISTURE CONTENT, %	21			

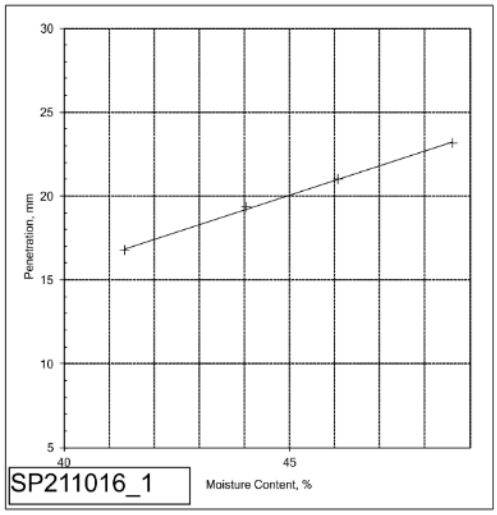

		Liquid Limits				Plastic Limits	
		1	2	3	4	I	II
PENETRATION, mm		15.05	17.65	19.70	22.90		
WT. OF CONTAINER, g		4.67	3.49	3.57	19.35	12.96	3.90
WT. OF WET SOIL + CONTAINER, g		22.38	21.36	28.22	41.74	20.83	11.32
WT. OF DRY SOIL + CONTAINER, g		17.09	15.72	20.15	34.07	19.64	10.18
WT. OF MOISTURE, g		5.29	5.64	8.07	7.67	1.19	1.14
WT. OF DRY SOIL, g		12.42	12.23	16.58	14.72	6.68	6.28
MOISTURE CONTENT, %		**42.6**	**46.1**	**48.7**	**52.1**	17.8	18.2
Preparation method 2 (Head, 2006)							

MC			DRY_MASS	
WT. OF CONTAINER, g	5.47		**WT. CONTAINER, g**	531.92
WT. OF WET SOIL + CONTAINER, g	40.87		**WT. WET SOIL + CONTAINER, g**	1050.11
WT. OF DRY SOIL + CONTAINER, g	36.02		**WT. WET SOIL, g**	518.19
WT. OF MOISTURE, g	4.85		**WT. DRY SOIL >425 microns, g**	11.82
WT. OF DRY SOIL, g	30.55		**DRY MASS, g**	447.20
MOISTURE CONTENT, %	16			

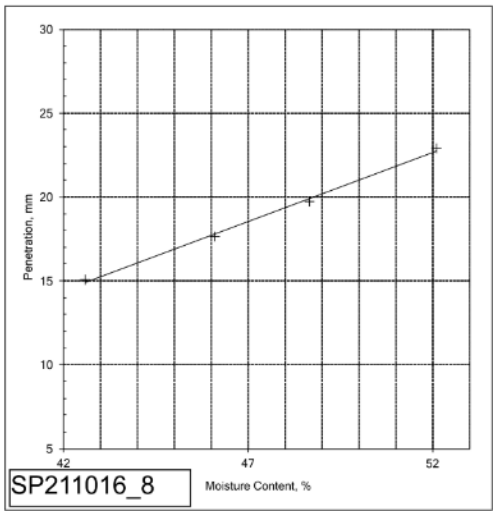

		Liquid Limits				Plastic Limits	
		1	2	3	4	I	II
PENETRATION, mm		17.30	20.10	21.75	22.80		
WT. OF CONTAINER, g		4.82	19.35	16.38	4.59	16.23	12.96
WT. OF WET SOIL + CONTAINER, g		22.86	38.12	37.81	22.96	20.17	18.97
WT. OF DRY SOIL + CONTAINER, g		16.07	30.81	29.31	15.69	19.16	17.42
WT. OF MOISTURE, g		6.79	7.31	8.50	7.27	1.01	1.55
WT. OF DRY SOIL, g		11.25	11.46	12.93	11.10	2.93	4.46
MOISTURE CONTENT, %		**60.4**	**63.8**	**65.7**	**65.5**	34.5	34.8
Preparation method 1 (Head, 2006)							

MC			DRY MASS	
WT. OF CONTAINER, g	5.28		**WT. CONTAINER, g**	456.17
WT. OF WET SOIL + CONTAINER, g	22.89		**WT. WET SOIL + CONTAINER, g**	1099.84
WT. OF DRY SOIL + CONTAINER, g	18.63		**WT. WET SOIL, g**	643.67
WT. OF MOISTURE, g	4.26		**WT. DRY SOIL >425 microns, g**	50.21
WT. OF DRY SOIL, g	13.35		**DRY MASS, g**	487.96
MOISTURE CONTENT, %	32			

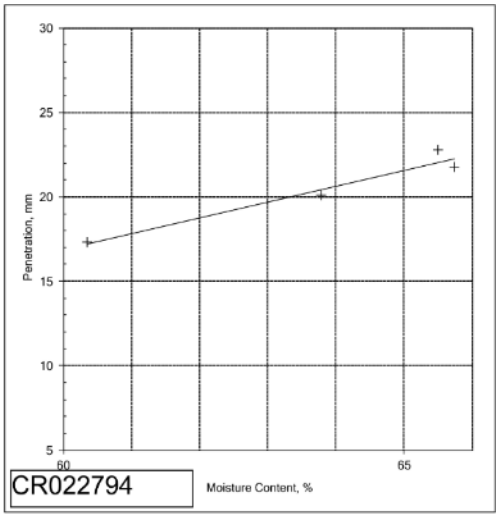

		Liquid Limits				Plastic Limits	
		1	2	3	4	I	II
PENETRATION, mm		16.80	18.65	21.10	24.80		
WT. OF CONTAINER, g		5.40	19.93	5.28	16.38	5.55	19.33
WT. OF WET SOIL + CONTAINER, g		18.39	37.10	23.50	38.86	12.40	26.39
WT. OF DRY SOIL + CONTAINER, g		13.72	30.81	16.55	29.97	11.01	24.98
WT. OF MOISTURE, g		4.67	6.29	6.95	8.89	1.39	1.41
WT. OF DRY SOIL, g		8.32	10.88	11.27	13.59	5.46	5.65
MOISTURE CONTENT, %		**56.1**	**57.8**	**61.7**	**65.4**	25.5	25.0
Preparation method 1 (Head, 2006)							

MC	From 1D consolidation test
WT. OF CONTAINER, g	3.57
WT. OF WET SOIL + CONTAINER, g	16.13
WT. OF DRY SOIL + CONTAINER, g	13.86
WT. OF MOISTURE, g	2.27
WT. OF DRY SOIL, g	10.29
MOISTURE CONTENT, %	22

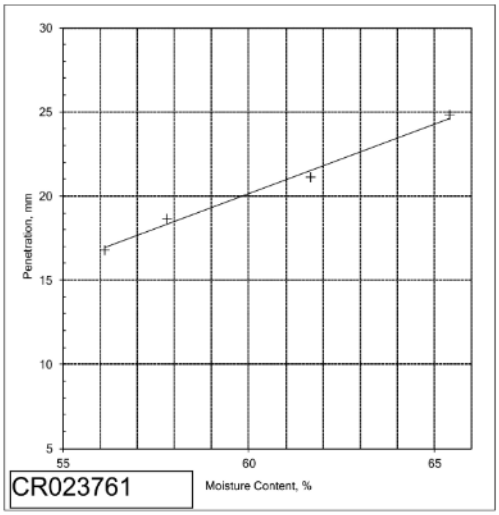

		Liquid Limits				Plastic Limits	
		1	2	3	4	I	II
PENETRATION, mm		15.60	18.15	21.80	24.80		
WT. OF CONTAINER, g		4.52	5.23	5.27	4.58	5.80	4.83
WT. OF WET SOIL + CONTAINER, g		21.65	29.17	27.62	22.75	16.66	14.06
WT. OF DRY SOIL + CONTAINER, g		15.97	20.89	19.47	15.80	14.61	12.31
WT. OF MOISTURE, g		5.68	8.28	8.15	6.95	2.05	1.75
WT. OF DRY SOIL, g		11.45	15.66	14.20	11.22	8.81	7.48
MOISTURE CONTENT, %		**49.6**	**52.9**	**57.4**	**61.9**	23.3	23.4
Preparation method 1 (Head, 2006)							

MC	
WT. OF CONTAINER, g	5.5
WT. OF WET SOIL + CONTAINER, g	22.96
WT. OF DRY SOIL + CONTAINER, g	20.07
WT. OF MOISTURE, g	2.89
WT. OF DRY SOIL, g	14.57
MOISTURE CONTENT, %	20

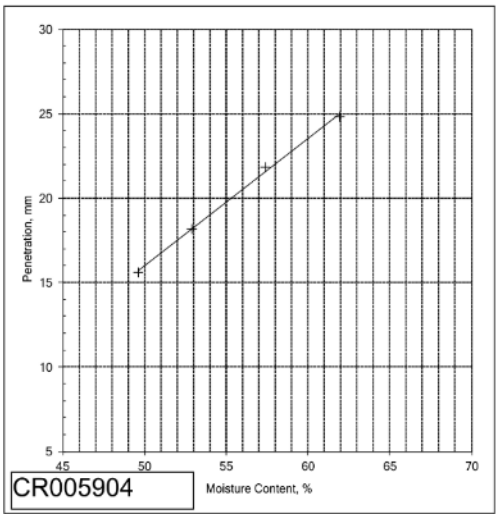

		Liquid Limits				Plastic Limits	
		1	2	3	4	I	II
PENETRATION, mm		16.70	19.35	21.50	22.75		
WT. OF CONTAINER, g		5.47	4.53	4.59	3.56	1.00	0.99
WT. OF WET SOIL + CONTAINER, g		25.04	26.51	27.14	26.85	17.52	17.89
WT. OF DRY SOIL + CONTAINER, g		17.52	17.89	18.09	15.41	13.85	14.12
WT. OF MOISTURE, g		7.52	8.62	9.05	11.44	3.67	3.76
WT. OF DRY SOIL, g		12.05	13.36	13.50	11.85	12.84	13.13
MOISTURE CONTENT, %		**62.4**	**64.5**	**67.0**	**96.5**	28.6	28.7
Preparation method 1 (Head, 2006)							

MC	
WT. OF CONTAINER, g	16.39
WT. OF WET SOIL + CONTAINER, g	39.72
WT. OF DRY SOIL + CONTAINER, g	34.4
WT. OF MOISTURE, g	5.32
WT. OF DRY SOIL, g	18.01
MOISTURE CONTENT, %	30

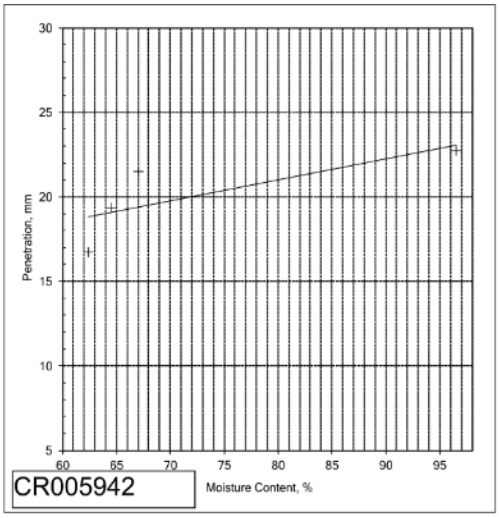

		Liquid Limits				Plastic Limits	
		1	2	3	4	I	II
PENETRATION, mm		16.50	19.75	22.50	23.75		
WT. OF CONTAINER, g		3.54	4.64	3.48	6.37	1.00	1.00
WT. OF WET SOIL + CONTAINER, g		26.08	24.54	29.36	35.11	9.17	10.28
WT. OF DRY SOIL + CONTAINER, g		17.54	16.75	18.80	23.22	7.66	8.56
WT. OF MOISTURE, g		8.54	7.79	10.56	11.89	1.51	1.72
WT. OF DRY SOIL, g		14.00	12.11	15.32	16.85	6.66	7.56
MOISTURE CONTENT, %		**61.0**	**64.3**	**68.9**	**70.6**	22.6	22.8
Preparation method 1 (Head, 2006)							

MC	
WT. OF CONTAINER, g	6.38
WT. OF WET SOIL + CONTAINER, g	21.35
WT. OF DRY SOIL + CONTAINER, g	18.75
WT. OF MOISTURE, g	2.6
WT. OF DRY SOIL, g	12.37
MOISTURE CONTENT, %	21.0

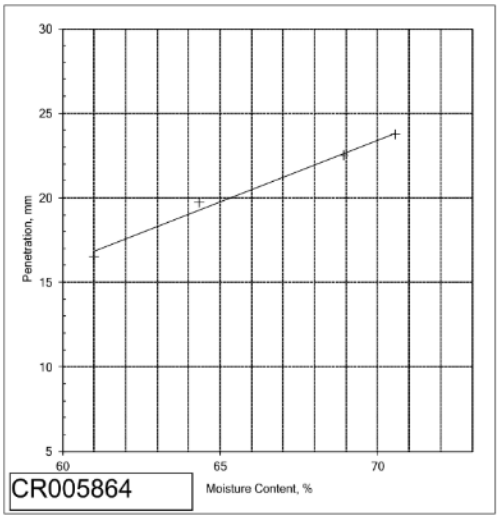

		Liquid Limits				Plastic Limits	
		1	2	3	4	I	II
PENETRATION, mm		16.50	19.23	21.65	24.30		
WT. OF CONTAINER, g		19.35	5.81	5.41	4.59	5.80	4.84
WT. OF WET SOIL + CONTAINER, g		43.21	29.11	33.39	32.28	13.82	11.61
WT. OF DRY SOIL + CONTAINER, g		34.81	20.65	22.85	21.54	12.36	10.36
WT. OF MOISTURE, g		8.40	8.46	10.54	10.74	1.46	1.25
WT. OF DRY SOIL, g		15.46	14.84	17.44	16.95	6.56	5.52
MOISTURE CONTENT, %		**54.3**	**57.0**	**60.4**	**63.4**	22.3	22.6
Preparation method 1 (Head, 2006)							

MC	
WT. OF CONTAINER, g	3.91
WT. OF WET SOIL + CONTAINER, g	19.81
WT. OF DRY SOIL + CONTAINER, g	17.8
WT. OF MOISTURE, g	2.01
WT. OF DRY SOIL, g	13.89
MOISTURE CONTENT, %	14

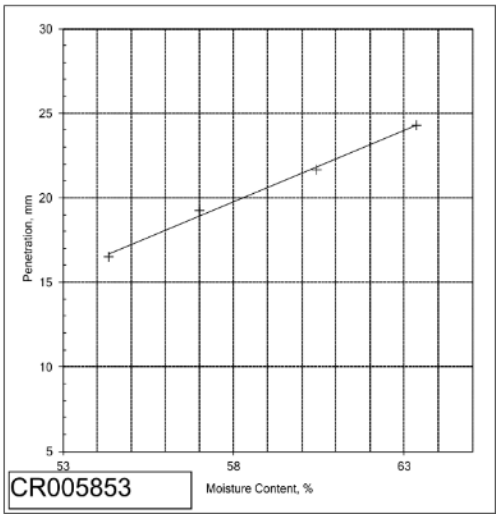

		Liquid Limits				Plastic Limits	
		1	2	3	4	I	II
PENETRATION, mm		16.10	21.65	22.70	25.25		
WT. OF CONTAINER, g		5.46	4.64	3.35	5.41	15.95	16.37
WT. OF WET SOIL + CONTAINER, g		26.16	37.35	30.28	29.23	24.98	24.79
WT. OF DRY SOIL + CONTAINER, g		21.77	29.87	24.03	23.61	23.73	23.65
WT. OF MOISTURE, g		4.39	7.48	6.25	5.62	1.25	1.14
WT. OF DRY SOIL, g		16.31	25.23	20.68	18.20	7.78	7.28
MOISTURE CONTENT, %		26.9	29.6	30.2	30.9	16.1	15.7
Preparation method 2 (Head, 2006)							

MC				
WT. OF CONTAINER, g	4.58		DRY MASS	
WT. OF WET SOIL + CONTAINER, g	24.34		WT. CONTAINER, g	539.1
WT. OF DRY SOIL + CONTAINER, g	21.78		WT. WET SOIL + CONTAINER, g	1085.32
WT. OF MOISTURE, g	2.56		WT. WET SOIL, g	546.22
WT. OF DRY SOIL, g	17.2		WT. DRY SOIL >425 microns, g	42.31
MOISTURE CONTENT, %	15		DRY MASS, g	475.45

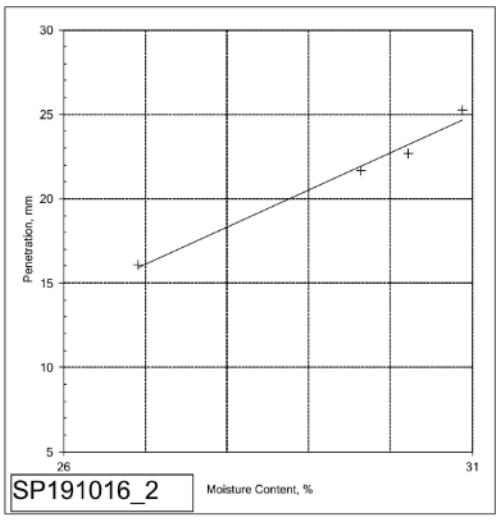

		Liquid Limits				Plastic Limits	
		1	2	3	4	I	II
PENETRATION, mm		13.47	19.10	22.65	N/A		
WT. OF CONTAINER, g		15.96	15.98	4.84		5.23	4.59
WT. OF WET SOIL + CONTAINER, g		34.41	42.49	25.53		14.24	16.66
WT. OF DRY SOIL + CONTAINER, g		30.17	36.11	21.90		12.66	14.48
WT. OF MOISTURE, g		4.24	6.38	3.63	0.00	1.58	2.18
WT. OF DRY SOIL, g		14.21	20.13	17.06	0.00	7.43	9.89
MOISTURE CONTENT, %		29.8	31.7	21.3	#####	NP	NP
Preparation method 1 (Head, 2006)							

Penetration measurement 4 failed after 5 attempts

MC	
WT. OF CONTAINER, g	5.4
WT. OF WET SOIL + CONTAINER, g	33.31
WT. OF DRY SOIL + CONTAINER, g	27.28
WT. OF MOISTURE, g	6.03
WT. OF DRY SOIL, g	21.88
MOISTURE CONTENT, %	28

SP120617_1

		Liquid Limits				Plastic Limits	
		1	2	3	4	I	II
PENETRATION, mm		12.60	16.20	21.05	22.83		
WT. OF CONTAINER, g		4.67	16.04	15.95	12.81	5.25	19.93
WT. OF WET SOIL + CONTAINER, g		22.80	43.79	43.31	41.58	18.80	31.81
WT. OF DRY SOIL + CONTAINER, g		18.59	36.99	36.33	34.17	16.48	29.84
WT. OF MOISTURE, g		4.21	6.80	6.98	7.41	2.32	1.97
WT. OF DRY SOIL, g		13.92	20.95	20.38	21.36	11.23	9.91
MOISTURE CONTENT, %		30.2	32.5	34.2	34.7	NP	NP
Preparation method 1 (Head, 2006)							

MC	
WT. OF CONTAINER, g	5.29
WT. OF WET SOIL + CONTAINER, g	33.31
WT. OF DRY SOIL + CONTAINER, g	27.28
WT. OF MOISTURE, g	6.03
WT. OF DRY SOIL, g	21.99
MOISTURE CONTENT, %	27

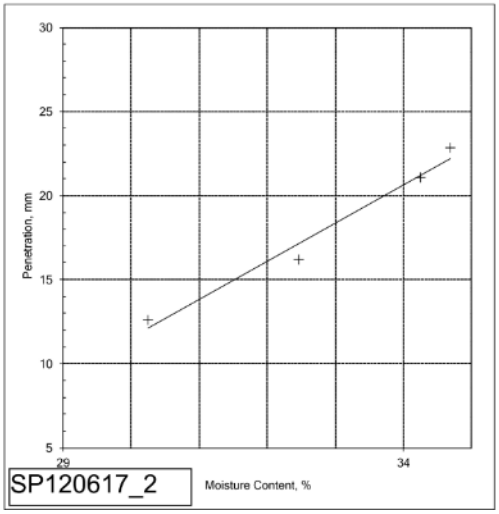

		Liquid Limits				Plastic Limits	
		1	2	3	4	I	II
PENETRATION, mm		15.87	19.85	22.30	23.65		
(or other M.C. test if stated)							
WT. OF CONTAINER, g		12.82	5.23	16.03	15.95	4.52	4.72
WT. OF WET SOIL + CONTAINER, g		31.32	27.49	36.80	41.45	8.18	10.03
WT. OF DRY SOIL + CONTAINER, g		24.64	18.97	28.56	31.12	7.53	9.09
WT. OF MOISTURE, g		6.68	8.52	8.24	10.33	0.65	0.94
WT. OF DRY SOIL, g		11.82	13.74	12.53	15.17	3.01	4.37
MOISTURE CONTENT, %		**56.5**	**62.0**	**65.8**	**68.1**	21.6	21.5
Preparation method 1 (Head, 2006)							

MC	From triaxial test
WT. OF CONTAINER, g	8.42
WT. OF WET SOIL + CONTAINER, g	19.36
WT. OF DRY SOIL + CONTAINER, g	17.28
WT. OF MOISTURE, g	2.08
WT. OF DRY SOIL, g	8.86
MOISTURE CONTENT, %	23

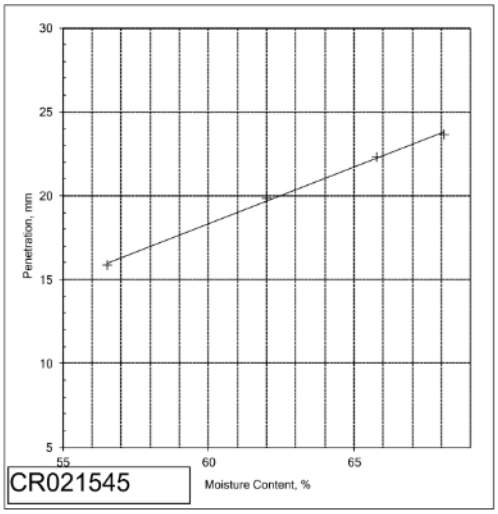

		Liquid Limits				Plastic Limits	
		1	2	3	4	I	II
PENETRATION, mm		16.10	17.40	20.85	23.35		
WT. OF CONTAINER, g		5.27	5.40	4.67	3.57	4.58	4.64
WT. OF WET SOIL + CONTAINER, g		25.47	24.00	29.72	32.04	15.41	14.93
WT. OF DRY SOIL + CONTAINER, g		18.28	17.03	20.20	20.97	13.02	12.69
WT. OF MOISTURE, g		7.19	6.97	9.52	11.07	2.39	2.24
WT. OF DRY SOIL, g		13.01	11.63	15.53	17.40	8.44	8.05
MOISTURE CONTENT, %		**55.3**	**59.9**	**61.3**	**63.6**	28.3	27.8
Preparation method 1 (Head, 2006)							

MC	
WT. OF CONTAINER, g	5.41
WT. OF WET SOIL + CONTAINER, g	18.56
WT. OF DRY SOIL + CONTAINER, g	16.36
WT. OF MOISTURE, g	2.2
WT. OF DRY SOIL, g	10.95
MOISTURE CONTENT, %	20

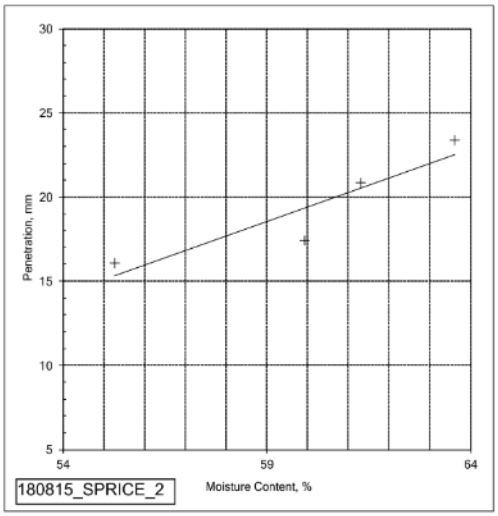

		Liquid Limits				Plastic Limits	
		1	2	3	4	I	II
PENETRATION, mm		12.95	17.05	20.25	21.50		
(or other M.C. test if stated)							
WT. OF CONTAINER, g		4.58	4.63	5.27	4.52	0.99	1.00
WT. OF WET SOIL + CONTAINER, g		21.69	22.84	29.18	26.22	16.88	15.37
WT. OF DRY SOIL + CONTAINER, g		15.45	15.78	19.44	17.28	13.43	12.25
WT. OF MOISTURE, g		6.24	7.06	9.74	8.94	3.46	3.12
WT. OF DRY SOIL, g		10.87	11.15	14.17	12.76	12.44	11.25
MOISTURE CONTENT, %		**57.4**	**63.3**	**68.7**	**70.1**	27.8	27.7
Preparation method 1 (Head, 2006)							

MC	From 1D consolidation test
WT. OF CONTAINER, g	4.58
WT. OF WET SOIL + CONTAINER, g	24.63
WT. OF DRY SOIL + CONTAINER, g	18.56
WT. OF MOISTURE, g	6.07
WT. OF DRY SOIL, g	13.98
MOISTURE CONTENT, %	43

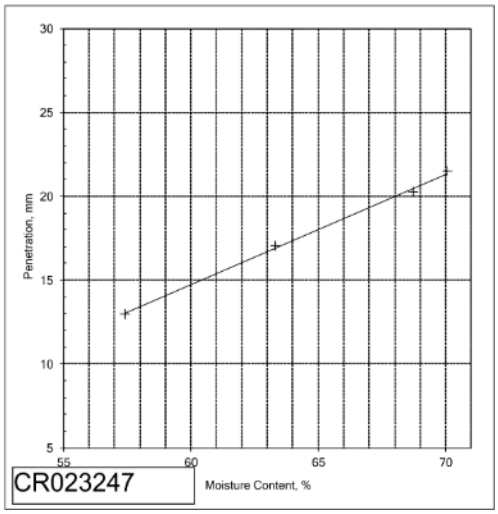

	Liquid Limits				Plastic Limits	
	1	2	3	4	I	II
PENETRATION, mm	15.07	18.00	20.65	22.25		
WT. OF CONTAINER, g	4.52	5.55	16.37	6.33	3.89	4.85
WT. OF WET SOIL + CONTAINER, g	24.11	26.98	37.96	27.07	13.74	14.57
WT. OF DRY SOIL + CONTAINER, g	16.01	17.70	28.32	17.66	11.58	12.41
WT. OF MOISTURE, g	8.10	9.28	9.64	9.41	2.16	2.16
WT. OF DRY SOIL, g	11.49	12.15	11.95	11.33	7.69	7.56
MOISTURE CONTENT, %	**70.5**	**76.4**	**80.7**	**83.1**	28.1	28.6
Preparation method 1 (Head, 2006)						

MC	
WT. OF CONTAINER, g	5.23
WT. OF WET SOIL + CONTAINER, g	25.57
WT. OF DRY SOIL + CONTAINER, g	20.44
WT. OF MOISTURE, g	5.13
WT. OF DRY SOIL, g	15.21
MOISTURE CONTENT, %	34

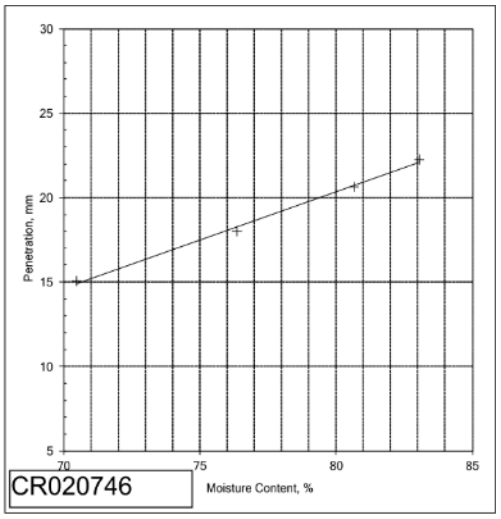

	Liquid Limits				Plastic Limits	
	1	2	3	4	I	II
PENETRATION, mm	14.80	18.45	20.55	22.55		
WT. OF CONTAINER, g	12.99	12.62	12.72	12.60	4.67	19.35
WT. OF WET SOIL + CONTAINER, g	33.39	35.85	32.90	34.66	13.28	28.56
WT. OF DRY SOIL + CONTAINER, g	27.79	29.12	26.81	27.88	12.02	27.20
WT. OF MOISTURE, g	5.60	6.73	6.09	6.78	1.26	1.36
WT. OF DRY SOIL, g	14.80	16.50	14.09	15.28	7.35	7.85
MOISTURE CONTENT, %	**37.8**	**40.8**	**43.2**	**44.4**	17.1	17.3
Preparation method 2 (Head, 2006)						

MC			DRY_MASS	
WT. OF CONTAINER, g	4.64		**WT. CONTAINER, g**	526.78
WT. OF WET SOIL + CONTAINER, g	16.72		**WT. WET SOIL + CONTAINER, g**	987.5
WT. OF DRY SOIL + CONTAINER, g	15.24		**WT. WET SOIL, g**	460.72
WT. OF MOISTURE, g	1.48		**WT. DRY SOIL >425 microns, g**	17.01
WT. OF DRY SOIL, g	10.6		**DRY MASS, g**	404.27
MOISTURE CONTENT, %	14			

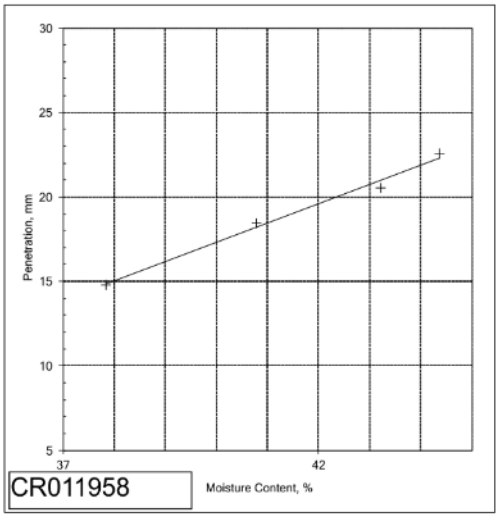

	Liquid Limits				Plastic Limits	
	1	2	3	4	I	II
PENETRATION, mm	14.45	18.95	21.43	27.65		
WT. OF CONTAINER, g	19.35	4.83	5.79	3.89	4.52	5.55
WT. OF WET SOIL + CONTAINER, g	36.02	25.42	30.71	28.94	18.05	18.58
WT. OF DRY SOIL + CONTAINER, g	31.59	19.48	23.33	20.85	16.01	16.62
WT. OF MOISTURE, g	4.43	5.94	7.38	8.09	2.04	1.96
WT. OF DRY SOIL, g	12.24	14.65	17.54	16.96	11.49	11.07
MOISTURE CONTENT, %	**36.2**	**40.5**	**42.1**	**47.7**	17.8	17.7
Preparation method 2 (Head, 2006)						

MC			DRY_MASS	
WT. OF CONTAINER, g	5.55		**WT. CONTAINER, g**	509.86
WT. OF WET SOIL + CONTAINER, g	28.33		**WT. WET SOIL + CONTAINER, g**	1036.06
WT. OF DRY SOIL + CONTAINER, g	25.69		**WT. WET SOIL, g**	526.2
WT. OF MOISTURE, g	2.64		**WT. DRY SOIL >425 microns, g**	33.76
WT. OF DRY SOIL, g	20.14		**DRY MASS, g**	465.22
MOISTURE CONTENT, %	13			

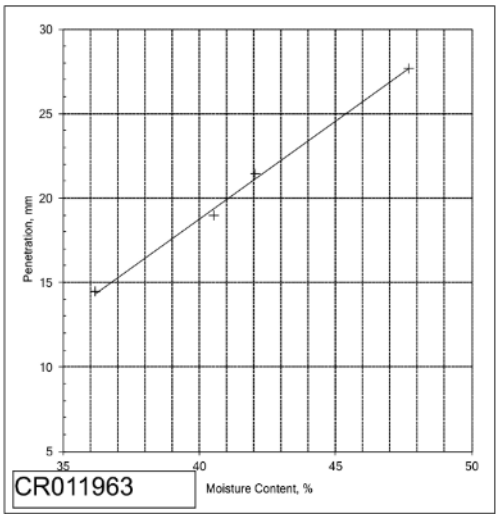

	Liquid Limits				Plastic Limits	
	1	**2**	**3**	**4**	**I**	**II**
PENETRATION, mm	14.40	19.55	22.05	24.35		
WT. OF CONTAINER, g	19.36	5.81	4.82	5.27	5.56	5.24
WT. OF WET SOIL + CONTAINER, g	42.74	30.97	23.01	25.00	15.78	12.89
WT. OF DRY SOIL + CONTAINER, g	36.50	23.69	17.51	18.80	14.25	11.76
WT. OF MOISTURE, g	6.24	7.28	5.50	6.20	1.53	1.13
WT. OF DRY SOIL, g	17.14	17.88	12.69	13.53	8.69	6.52
MOISTURE CONTENT, %	**36.4**	**40.7**	**43.3**	**45.8**	17.6	17.3
Preparation method 2 (Head, 2006)						

MC			DRY MASS	
WT. OF CONTAINER, g	5.27			
WT. OF WET SOIL + CONTAINER, g	25.65		**WT. CONTAINER, g**	452.22
WT. OF DRY SOIL + CONTAINER, g	23.04		**WT. WET SOIL + CONTAINER, g**	847.13
WT. OF MOISTURE, g	2.61		**WT. WET SOIL, g**	394.91
WT. OF DRY SOIL, g	17.77		**WT. DRY SOIL >425 microns, g**	21.73
MOISTURE CONTENT, %	14.7		**DRY MASS, g**	335.32

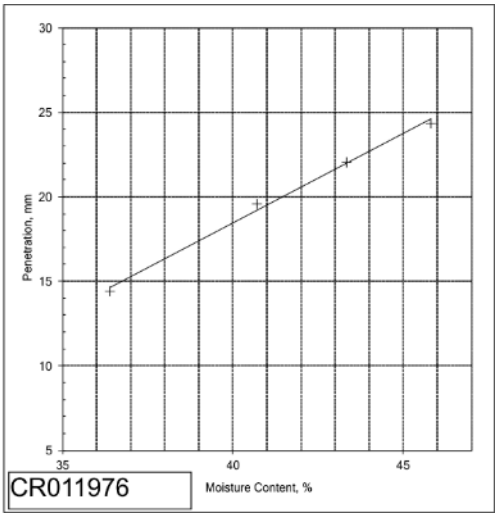

13.3 Particle density calculations

Sample	Bottle+ Stopper (m_1)	Bottle+ Stopper+Soil (m_2)	Bottle+Stopper+ Soil+Water (m_3)	Bottle+Water (m_4)	Particle density (ρ_s) M_g/m^3	Mean (ρ_s) M_g/m^3	In tolerance?[1] (y/n)
CR005904	31.180	40.599	89.946	84.053	2.67	2.65	Y
CR005904	25.280	34.678	81.602	75.944	2.62		
CR005864	25.322	33.706	79.844	74.825	2.49	2.62	n
CR005864	29.268	38.352	84.811	79.051	2.73		
CR005864	29.588	37.671	83.594	78.683	2.55		
CR005864	30.922	39.639	85.859	80.352	2.72		
CR005942	30.923	40.433	86.141	80.350	2.56	2.52	y
CR005942	28.649	38.460	86.064	80.194	2.49		
CR023761	31.367	38.510	83.935	79.650	2.50	2.56	n
CR023761	30.503	37.867	86.314	81.762	2.62		
CR022794	29.266	36.157	83.065	79.054	2.39	2.44	n
CR022794	28.471	35.095	83.033	79.062	2.50		

Particle density (small pyknometer method), Oxford Clay, Quaternary Domain 1.3. [1] tolerance of 0.03g between the measured value and the mean of each sample.

Sample	Bottle+ Stopper (m_1)	Bottle+ Stopper+Soil (m_2)	Bottle+Stopper+ Soil+Water (m_3)	Bottle+Water (m_4)	Particle density (ρ_s) M_g/m^3	Mean (ρ_s) M_g/m^3	In tolerance?[1] (y/n)
CR021545	23.357	34.348	81.351	74.568	2.61	2.63	Y
CR021545	29.770	38.708	84.291	78.721	2.65		

Particle density (small pyknometer method), Oxford Clay, Quaternary Domain 1.3.1. [1] tolerance of 0.03g between the measured value and the mean of each sample.

Sample	Bottle+ Stopper (m_1)	Bottle+ Stopper+Soil (m_2)	Bottle+Stopper+ Soil+Water (m_3)	Bottle+Water (m_4)	Particle density (ρ_s) M_g/m^3	Mean (ρ_s) M_g/m^3	In tolerance?[1] (y/n)
CR023247	31.179	38.572	88.795	84.050	2.79	2.78	y
CR023247	30.822	40.501	88.778	82.595	2.77		

Particle density (small pyknometer method), Oxford Clay, Quaternary Domain 2.3. [1] tolerance of 0.03g between the measured value and the mean of each sample.

Sample	Bottle+ Stopper (m_1)	Bottle+ Stopper+Soil (m_2)	Bottle+Stopper+ Soil+Water (m_3)	Bottle+Water (m_4)	Particle density (ρ_s) M_g/m^3	Mean (ρ_s) M_g/m^3	In tolerance?[1] (y/n)
CR011953	30.172	38.463	88.459	83.403	2.56	2.58	n
CR011953	29.588	38.532	84.162	78.718	2.64		
CR011953	25.321	32.444	79.066	74.594	2.69		
CR011953	30.503	35.500	84.697	81.750	2.44		
CR011971	30.503	39.000	87.118	81.753	2.71	2.62	n
CR011971	33.117	40.978	86.725	81.957	2.54		
CR011971	25.529	30.658	78.810	75.601	2.67		
CR011971	31.179	39.031	88.836	84.064	2.55		
CR011973	31.367	40.537	85.386	79.649	2.67	2.64	y
CR011973	28.647	37.719	85.786	80.198	2.60		
CR011973	28.647	36.024	84.783	80.203	2.64		
CR011973	25.527	34.62	81.377	75.694	2.67		
CR011958	30.823	40.332	88.569	82.584	2.70	2.69	y
CR011958	28.472	36.947	84.500	79.189	2.68		
CR011963	27.855	38.178	84.101	77.624	2.68	2.65	n
CR011963	31.368	40.257	85.110	79.628	2.61		

Particle density (small pyknometer method), till, Quaternary Domain 1.4.1. [1] tolerance of 0.03g between the measured value and the mean of each sample.

13.4 1D consolidation initial and final conditions

Initial conditions	Symbol	Value
Initial Height (mm)	H_o	19.86
Initial Diameter (mm)	D_o	63.47
Sample volume (cm^3)		62.84
Ring mass (g)	m_R	108.37
Sample + ring (g)	m_1	234.7
Initial mass (g)	m_o	126.33
Initial moisture content	ω_i	0.2
Initial dry mass (g)	m_{di}	105.28
Calculated initial moisture conten	ω_i	0.2
Bulk density (Mg/m^3)	ρ	2.01
Particle density (Mg/m^3)	ρ_s	2.65
Dry density (Mg/m^3)	ρ_D	1.68
Initial void ratio	e_o	0.58
Equivalent height of solids (mm)	H_s	12.56
Initial degree of saturation (%)	S_r	0.96

Final conditions	Symbol	Value
Sample + ring +tray (wet) (g)	m_3	246.76
Sample + ring + tray (dry) (g)		221.05
Ring + tray (g)	$m_{R+}m_T$	121.09
Tray mass, drying (g)	m_T	12.72
Wet sample (g)	m_f	125.67
Dry sample (g)	m_d	99.96
Weight of moisture (g)		25.71
Final moisture content	ω_f	0.3
Sample lost during test (g)		5.31
Final degree of saturation (%)	S_{rf}	1.35
Overall settlement (mm)		0.944
Volume change (mm^3)		3.62
Final volume (cm^3)		59.85
Final bulk density	ρ	2.10
Final dry density (Mg/m^3)	ρ_D	1.67
Final void ratio	e_f	0.51

Initial and final conditions for specimen CR005864, Oxford Clay, Quaternary Domain 1.3.

Masses and dimensions	Symbol	Value
Initial Height (mm)	H_o	19.97
Initial Diameter (mm)	D_o	63.62
Sample volume (cm^3)		63.48
Ring mass (g)	m_R	108.37
Sample + ring (g)	m_1	240.76
Initial mass (g)	m_o	132.39
Initial moisture content	ω_i	0.2
Initial dry mass (g)	m_{di}	110.325
Sample + ring + tray (wet) (g)	m_2	246.46
Tray mass, drying (g)	m_T	6.39
Sample + ring + tray (dry)	m_3	223.73
Calculated initial moisture content	ω_i	0.2
Bulk density (Mg/m^3)	ρ	2.09
Particle density (Mg/m^3)	ρ_s	2.65
Dry density (Mg/m^3)	ρ_D	1.74
Initial void ratio	e_o	0.52
Equivalent height of solids (mm)	Hs	13.10
Initial degree of saturation (%)	S_r	1.00

Final conditions	Symbol	Value
Sample + ring + tray (wet) (g)	m_3	246.46
Sample + ring + tray (dry) (g)		223.73
Ring + tray (g)	$m_R + m_T$	114.76
Tray mass, drying (g)	m_T	6.39
Wet sample (g)	m_f	131.70
Dry sample (g)	m_d	108.97
Weight of moisture (g)		22.73
Final moisture content	ω_f	0.2
Sample lost during test (g)		1.36
Final degree of saturation (%)	S_{rf}	1.19
Overall settlement (mm)		0.768
Volume change (mm^3)		2.58
Final volume (cm^3)		61.04
Final bulk density	ρ	2.16
Final dry density (Mg/m^3)	ρ_D	1.79
Final void ratio	e_f	0.47

Initial and final conditions for specimen CR005904, Oxford Clay, Quaternary Domain 1.3.

Initial conditions	Symbol	Value
Initial Height (mm)	H_o	19.04
Initial Diameter (mm)	D_o	63.23
Sample volume (cm^3)		59.79
Ring mass (g)	m_R	76.38
Sample + ring (g)	m_1	190.82
Initial mass (g)	m_o	114.44
Initial moisture content	ω_i	0.3
Initial dry mass (g)	m_{di}	88.03
Sample + ring + tray (wet) (g)	m_2	204.23
Calculated initial moisture content	ω_i	0.3
Bulk density (Mg/m^3)	ρ	1.91
Particle density (Mg/m^3)	ρ_s	2.53
Dry density (Mg/m^3)	ρ_D	1.47
Initial void ratio	e_o	0.72
Equivalent height of solids (mm)	Hs	11.08
Initial degree of saturation (%)	S_r	1.04

Final conditions	Symbol	Value
Sample + ring + tray (wet) (g)	m_3	204.23
Sample + ring + tray (dry) (g)		180
Ring + tray (g)	$m_R + m_T$	88.98
Tray mass, drying (g)	m_T	12.6
Wet sample (g)	m_f	115.25
Dry sample (g)	m_d	91.02
Weight of moisture (g)		24.23
Final moisture content	ω_f	0.3
Sample lost during test (g)		-2.99
Final degree of saturation (%)	S_{rf}	1.15
Overall settlement (mm)		0.873
Volume change (mm^3)		2.74
Final volume (cm^3)		57.05
Final bulk density	ρ	2.02
Final dry density (Mg/m^3)	ρD	1.60
Final void ratio	e_f	0.586

Initial and final conditions for specimen CR005942, Oxford Clay, Quaternary Domain 1.3.

Initial conditions	Symbol	Value
Initial Height (mm)	H_o	20.17
Initial Diameter (mm)	D_o	63.35
Sample volume (cm^3)		63.58
Ring mass (g)	m_R	108.37
Sample + ring (g)	m_1	223.16
Initial mass (g)	m_o	114.79
Initial moisture content	ω_i	0.3
Initial dry mass (g)	m_{di}	86.96
Calculated initial moisture content	ω_i	0.3
Bulk density (Mg/m^3)	ρ	1.81
Particle density (Mg/m^3)	ρ_s	2.65
Dry density (Mg/m^3)	ρ_D	1.37
Initial void ratio	e_o	0.94
Equivalent height of solids (mm)	Hs	10.41
Initial degree of saturation (%)	S_r	0.90

Final conditions	Symbol	Value
Sample + ring + tray (wet) (g)	m_3	236.72
Sample + ring + tray (dry) (g)		211.2
Ring + tray (g)	$m_R + m_T$	120.99
Tray mass, drying (g)	m_T	12.62
Wet sample (g)	m_f	115.73
Dry sample (g)	m_d	90.21
Weight of moisture (g)		25.52
Final moisture content	ω_f	0.3
Sample lost during test (g)		-3.25
Final degree of saturation (%)	S_{rf}	1.02
Overall settlement (mm)		1.455
Volume change (mm^3)		4.59
Final volume (cm^3)		58.99
Final bulk density	ρ	1.96
Final dry density (Mg/m^3)	ρD	1.53
Final void ratio	e_f	0.733

Initial and final conditions for specimen CR022794, Oxford Clay, Quaternary Domain 1.3.

Initial conditions	Symbol	Value
Initial Height (mm)	H_o	19.11
Initial Diameter (mm)	D_o	63.31
Sample volume (cm^3)		60.16
Ring mass (g)	m_R	76.36
Sample + ring (g)	m_1	194.9
Initial mass (g)	m_o	118.54
Initial moisture content	ω_i	0.22
Initial dry mass (g)	m_{di}	89.80
Calculated initial moisture content	ω_i	0.2
Bulk density (Mg/m^3)	ρ	1.97
Particle density (Mg/m^3)	ρ_s	2.65
Dry density (Mg/m^3)	ρ_D	1.49
Initial void ratio	e_o	0.78
Equivalent height of solids (mm)	Hs	10.76
Initial degree of saturation (%)	S_r	0.75

Final conditions	Symbol	Value
Sample + ring + tray (wet) (g)	m_3	207.17
Sample + ring + tray (dry) (g)		183.96
Ring + tray (g)	$m_R + m_T$	88.91
Tray mass, drying (g)	m_T	12.55
Wet sample (g)	m_f	118.26
Dry sample (g)	m_d	95.05
Weight of moisture (g)		23.21
Final moisture content	ω_f	0.2
Sample lost during test (g)		-5.25
Final degree of saturation (%)	S_{rf}	1.16
Overall settlement (mm)		1.369
Volume change (mm^3)		4.31
Final volume (cm^3)		55.85
Final bulk density	ρ	2.12
Final dry density (Mg/m^3)	ρD	1.70
Final void ratio	e_f	0.557

Initial and final conditions for specimen CR023761, Oxford Clay, Quaternary Domain 1.3.

Initial conditions	Symbol	Value
Initial Height (mm)	H_o	19.87
Initial Diameter (mm)	D_o	63.33
Sample volume (cm^3)		62.59
Ring mass (g)	m_R	108.37
Sample + ring (g)	m_1	234.71
Initial mass (g)	m_o	126.34
Initial moisture content	ω_i	0.23
Initial dry mass (g)	m_{di}	102.72
Calculated initial moisture content	ω_i	0.23
Bulk density (Mg/m^3)	ρ	2.02
Particle density (Mg/m^3)	ρ_s	2.63
Dry density (Mg/m^3)	ρ_D	1.64
Initial void ratio	e_o	0.60
Equivalent height of solids (mm)	Hs	12.40
Initial degree of saturation (%)	S_r	1.02

Final conditions	Symbol	Value
Sample + ring + tray (wet) (g)	m_3	286.03
Sample + ring + tray (dry) (g)		264.24
Ring + tray (g)	$m_R + m_T$	161.52
Tray mass, drying (g)	m_T	53.15
Wet sample (g)	m_f	124.51
Dry sample (g)	m_d	102.72
Weight of moisture (g)		21.79
Final moisture content	ω_f	0.2
Sample lost during test (g)		0.00
Final degree of saturation (%)	S_{rf}	1.12
Overall settlement (mm)		1.276
Volume change (mm^3)		4.76
Final volume (cm^3)		58.57
Final bulk density	ρ	2.13
Final dry density (Mg/m^3)	ρD	1.75
Final void ratio	e_f	0.500

Initial and final conditions for specimen CR021545, Oxford Clay, Quaternary Domain 1.3.1.

Initial conditions	Symbol	Value
Initial Height (mm)	H_o	19.99
Initial Diameter (mm)	D_o	63.44
Sample volume (cm^3)		63.19
Ring mass (g)	m_R	108.36
Sample + ring (g)	m_1	239.91
Initial mass (g)	m_o	131.55
Initial moisture content	ω_i	0.16
Initial dry mass (g)	m_{di}	113.41
Calculated initial moisture content	ω_i	0.16
Bulk density (Mg/m^3)	ρ	2.08
Particle density (Mg/m^3)	ρ_s	2.69
Dry density (Mg/m^3)	ρ_D	1.79
Initial void ratio	e_o	0.50
Equivalent height of solids (mm)	Hs	13.34
Initial degree of saturation (%)	S_r	0.85

Final conditions	Symbol	Value
Sample + ring + tray (wet) (g)	m_3	288.91
Sample + ring + tray (dry) (g)		270.98
Ring + tray (g)	$m_R + m_T$	158.48
Tray mass, drying (g)	m_T	50.12
Wet sample (g)	m_f	130.43
Dry sample (g)	m_d	112.50
Weight of moisture (g)		17.93
Final moisture content	ω_f	0.2
Sample lost during test (g)		0.91
Final degree of saturation (%)	S_{rf}	1.18
Overall settlement (mm)		1.954
Volume change (mm^3)		6.43
Final volume (cm^3)		57.01
Final bulk density	ρ	2.29
Final dry density (Mg/m^3)	ρD	1.97
Final void ratio	e_f	0.363

Initial and final conditions for specimen CR011958, till, Quaternary Domain 1.4.1.

PARAMETER	SYMBOL	VALUE
Initial Height (mm)	H_o	19.04
Initial Diameter (mm)	D_o	63.21
Sample volume (cm^3)		59.75
Ring mass (g)	m_R	76.36
Sample + ring (g)	m_1	182.57
Initial mass (g)	m_o	106.21
Initial moisture content	ω_i	0.4
Initial dry mass (g)	m_{di}	75.86
Sample + ring + tray (wet) (g)	m_2	246.46
Calculated initial moisture content	ω_i	0.4
Bulk density (Mg/m^3)	ρ	1.78
Particle density (Mg/m^3)	ρ_s	2.78
Dry density (Mg/m^3)	ρ_D	1.27
Initial void ratio	e_o	1.19
Equivalent height of solids (mm)	Hs	8.70
Initial degree of saturation (%)	S_r	1.01

FINAL_CONDITIONS	Symbol	Value
Sample + ring (wet) (g)	m_3	174.10
Sample + ring (dry) (g)		149.61
Ring (g)	m_R	76.36
Tray mass, drying (g)	m_T	
Wet sample (g)	m_f	97.74
Dry sample (g)	m_d	73.25
Weight of moisture (g)		24.49
Final moisture content	ω_f	0.3
Sample lost during test (g)		2.61
Final degree of saturation (%)	S_{rf}	1.03
Overall settlement (mm)		3.828
Volume change (mm^3)		15.47
Final volume (cm^3)		47.74
Final bulk density	ρ	2.05
Final dry density (Mg/m^3)	ρ_D	1.53
Final void ratio	e_f	0.81

Initial and final conditions for specimen CR023247, Oxford Clay, Quaternary Domain 2.3.

13.5 Triaxial initial and final conditions, experimental conditions

CR005864, Oxford Clay Formation, Peterborough Member	Isotropically consolidated, undrained, multistage with measurement of small-strain stiffness. BGS SPTTS configuration

Initial conditions

Initial conditions		
Parameter	Symbol	Value
Height (mm)	H_o	191.76
Diameter (mm)	D_o	99.43
Mass (g)	M_o	2999.01
Volume	cm^3	1489
Axial 1 Hall effect spacing (mm)		86
Axial 2 Hall effect spacing (mm)		85
Bulk density (Mg/m^3)	ρ_B	2.01
Dry density (Mg/m^3)	ρ_D	1.66
Moisture content (%)	M_o	21
Particle density (Mg/m^3)	ρ_s	2.62
Initial void ratio	e_o	0.574
Initial degree of saturation (%)	S_r	0.96

Final conditions

Final conditions		
Parameter	Symbol	Value
Moisture content (%)	MC_F	18
Final mass (g)	M_F	3067.46
Final bulk density (Mg/m^3)	ρ_{Bfinal}	2.06
Dry density (Mg/m^3)	ρ_{DF}	1.74
Final void ratio	e_F	0.506
Final degree of saturation (%)	S_{rF}	0.95

MC, initial (from 1D consolidation sample preparation)	
Tray (g)	6.38
Tray + sample (g) (wet)	21.35
Tray + sample (g) (dry)	18.75
Moisture content	0.21

MC, final	MC WHOLE SAMPLE
Tray (g)	179.71
Tray + sample (g) (wet)	3975.29
Tray + sample (g) (dry)	3358.25
Moisture content	0.18

Experimental conditions

Test conditions	Cell Pressure (kPa)	Back Pressure (kPa)	Effective stress (kPa)
Consolidation stage 1	980	880	100
Shear stage 1	980	880	100
Consolidation stage 2	1080	880	200
Shear stage 2	1080	880	200
Consolidation stage 3	1180	880	300
Shear stage 3	1180	880	300

Saturation	Value
Cell Pressure Incr. (kPa)	48.50
Back Pressure Incr. (kPa)	44.90
Differential Pressure (kPa)	25.00
Final Cell Pressure (kPa)	949.00
Final Pore Pressure (kPa)	920.50
Final B Value	0.93

Initial and final conditions and experimental conditions, specimen CR005864, Oxford Clay, Quaternary Domain 1.3.

CR005904, Oxford Clay Formation, Stewartby Member	Isotropically consolidated, undrained, multistage with measurement of small-strain stiffness. BGS SPTTS configuration

Initial conditions

Initial conditions		
Parameter	Symbol	Value
Height (mm)	H_o	195.27
Diameter (mm)	D_o	99.45
Mass (g)	M_o	3274.4
Volume	cm^3	1517
Axial 1 Hall effect spacing (mm)		86
Axial 2 Hall effect spacing (mm)		85
Bulk density (Mg/m^3)	ρ_B	2.16
Dry density (Mg/m^3)	ρ_D	1.80
Moisture content (%)	M_o	20
Particle density (Mg/m^3)	ρ_s	2.65
Initial void ratio	e_o	0.471
Initial degree of saturation (%)	S_r	1.12

(Hall effect separation taken from sample CR005864)

Final conditions

Final conditions		
Parameter	Symbol	Value
Moisture content (%)	MC_F	14
Final mass (g)	M_F	2901.81
Final bulk density (Mg/m^3)	ρ_{Bfinal}	1.91
Dry density (Mg/m^3)	ρ_{DF}	1.67
Final void ratio	e_F	0.585
Final degree of saturation (%)	S_{rF}	0.65

MC, initial (taken from 1D consolidation preparation)	
Tray (g)	5.5
Tray + sample (g) (wet)	22.96
Tray + sample (g) (dry)	20.07
Moisture content	0.2

MC, final	MC WHOLE SAMPLE
Tray (g)	914.8
Tray + sample (g) (wet)	4234.33
Tray + sample (g) (dry)	3700.26
Moisture content	0.14

Experimental conditions

Test conditions	Cell Pressure (kPa)	Back Pressure (kPa)	Effective stress (kPa)
Consolidation stage 1	440	370	70
Shear stage 1	440	370	70
Consolidation stage 2	510	370	140
Shear stage 2	510	370	140
Consolidation stage 3	570	370	200
Shear stage 3	570	370	200

Saturation	Value
Cell Pressure Incr. (kPa)	47.50
Back Pressure Incr. (kPa)	24.10
Differential Pressure (kPa)	53.40
Final Cell Pressure (kPa)	369.00
Final Pore Pressure (kPa)	312.70
Final B Value	0.90

Initial and final conditions and experimental conditions, specimen CR005904, Oxford Clay, Quaternary Domain 1.3.

CR005942, Oxford Clay Formation, Peterborough Member

Isotropically consolidated, undrained, multistage with measurement of small-strain stiffness. BGS SPTTS configuration

Initial conditions

Initial conditions		
Parameter	Symbol	Value
Height (mm)	H_o	192.15
Diameter (mm)	D_o	99.34
Mass (g)	M_o	2841.04
Volume	cm^3	1489
Axial 1 Hall effect spacing (mm)		87
Axial 2 Hall effect spacing (mm)		83
Bulk density (Mg/m^3)	ρ_B	1.91
Dry density (Mg/m^3)	ρ_D	1.54
Moisture content (%)	M_o	24
Particle density (Mg/m^3)	ρ_s	2.52
Initial void ratio	e_o	0.632
Initial degree of saturation (%)	S_r	0.94

Final conditions

Final conditions		
Parameter	Symbol	Value
Moisture content (%)	MC_F	23
Final mass (g)	M_F	2901.81
Final bulk density (Mg/m^3)	ρ_{Bfinal}	1.95
Dry density (Mg/m^3)	ρ_{DF}	1.58
Final void ratio	e_F	0.592
Final degree of saturation (%)	S_{rF}	0.98

MC, initial	
Tray (g)	15.96
Tray + sample (g) (wet)	45.37
Tray + sample (g) (dry)	39.76
Moisture content	0.24

MC, final		MC WHOLE SAMPLE
Tray (g)	15.97	1507.47
Tray + sample (g) (wet)	43.54	4409.28
Tray + sample (g) (dry)	38.36	3828.59
Moisture content	0.23	0.15

Experimental conditions

Test conditions	Cell Pressure (kPa)	Back Pressure (kPa)	Effective stress (kPa)
Consolidation stage 1	950	600	350
Shear stage 1	950	600	350
Consolidation stage 2	1125	600	525
Shear stage 2	1125	600	525
Consolidation stage 3	1300	600	700
Shear stage 3	1300	600	700

Saturation	Value
Cell Pressure Incr. (kPa)	48.00
Back Pressure Incr. (kPa)	24.60
Differential Pressure (kPa)	175.40
Final Cell Pressure (kPa)	799.00
Final Pore Pressure (kPa)	609.20
Final B Value	0.92

Initial and final conditions and experimental conditions, specimen CR005942, Oxford Clay, Quaternary Domain 1.3.

CR023761, Oxford Clay Formation, Peterborough Member

Isotropically consolidated, undrained, multistage with measurement of small-strain stiffness. BGS SPTTS configuration

Initial conditions

Initial conditions		
Parameter	Symbol	Value
Height (mm)	H_o	195.80
Diameter (mm)	D_o	100.07
Mass (g)	M_o	3126.9
Volume	cm^3	1540
Axial 1 Hall effect spacing (mm)		87
Axial 2 Hall effect spacing (mm)		85
Bulk density (Mg/m^3)	ρ_B	2.03
Dry density (Mg/m^3)	ρ_D	1.66
Moisture content (%)	M_o	22
Particle density (Mg/m^3)	ρ_s	2.56
Initial void ratio	e_o	0.539
Initial degree of saturation (%)	S_r	1.05

Final conditions

Final conditions		
Parameter	Symbol	Value
Moisture content (%)	MC_F	15
Final mass (g)	M_F	3215.92
Final bulk density (Mg/m^3)	ρ_{Bfinal}	2.09
Dry density (Mg/m^3)	ρ_{Df}	1.82
Final void ratio	e_F	0.408
Final degree of saturation (%)	S_{rF}	0.93

MC, initial (taken from 1D consolidation preparation)	
Tray (g)	3.57
Tray + sample (g) (wet)	16.13
Tray + sample (g) (dry)	13.86
Moisture content	0.22

MC, final	MC WHOLE SAMPLE
Tray (g)	1507.44
Tray + sample (g) (wet)	4723.36
Tray + sample (g) (dry)	4112.63
Moisture content	0.15

Some sample lost on drying?

Experimental conditions

Test conditions	Cell Pressure (kPa)	Back Pressure (kPa)	Effective stress (kPa)
Consolidation stage 1	790	670	120
Shear stage 1	790	670	120
Consolidation stage 2	910	670	240
Shear stage 2	910	670	240
Consolidation stage 3	1030	670	360
Shear stage 3	1030	670	360

Saturation	Value
Cell Pressure Incr. (kPa)	50.00
Back Pressure Incr. (kPa)	45.00
Differential Pressure (kPa)	67.00
Final Cell Pressure (kPa)	799.00
Final Pore Pressure (kPa)	723.20
Final B Value	0.95

Initial and final conditions and experimental conditions, specimen CR023761, Oxford Clay, Quaternary Domain 1.3.

CR021545, Oxford Clay Formation, Weymouth Member	Isotropically consolidated, undrained, multistage with measurement of small-strain stiffness. BGS SPTTS configuration

Initial conditions

Initial conditions		
Parameter	**Symbol**	**Value**
Height (mm)	H_o	195.04
Diameter (mm)	D_o	99.05
Mass (g)	M_o	3065.34
Volume	cm^3	1503
Axial 1 Hall effect spacing (mm)		87
Axial 2 Hall effect spacing (mm)		84
Bulk density (Mg/m^3)	ρ_B	2.04
Dry density (Mg/m^3)	ρ_D	1.65
Moisture content (%)	M_o	23
Particle density (Mg/m^3)	ρ_s	2.63
Initial void ratio	e_o	0.592
Initial degree of saturation (%)	S_r	1.04

MC, initial		
Tray (g)		8.42
Tray + sample (g) (wet)		19.36
Tray + sample (g) (dry)		17.28
Moisture content		0.23

Final conditions

Final conditions		
Parameter	**Symbol**	**Value**
Moisture content (%)	MC_F	26
Final mass (g)	M_F	3128.27
Final bulk density (Mg/m^3)	ρ_{Bfinal}	2.08
Dry density (Mg/m^3)	ρ_{DF}	1.66
Final void ratio	e_F	0.586
Final degree of saturation (%)	S_{rF}	1.15

MC, final		MC WHOLE SAMPLE	
Tray (g)	5.23	868.37	
Tray + sample (g) (wet)	28.15	3996.64	
Tray + sample (g) (dry)	23.49		Dry weight of whole sample not recorded
Moisture content	0.26		

Experimental conditions

Test conditions	Cell Pressure (kPa)	Back Pressure (kPa)	Effective stress (kPa)
Consolidation stage 1	770	570	200
Shear stage 1	770	570	200
Consolidation stage 2	870	570	300
Shear stage 2	870	570	300
Consolidation stage 3	970	570	400
Shear stage 3	970	570	400

Saturation	Value
Cell Pressure Incr. (kPa)	19.40
Back Pressure Incr. (kPa)	-0.50
Differential Pressure (kPa)	150.50
Final Cell Pressure (kPa)	719.00
Final Pore Pressure (kPa)	522.50
Final B Value	0.99

Initial and final conditions and experimental conditions, specimen CR021545, Oxford Clay, Quaternary Domain 1.3.1.

CR023247, Oxford Clay Formation, Peterborough Member	Isotropically consolidated, undrained, multistage with measurement of small-strain stiffness. BGS SPTTS configuration

Initial conditions

Initial conditions		
Parameter	**Symbol**	**Value**
Height (mm)	H_o	193.87
Diameter (mm)	D_o	100.25
Mass (g)	M_o	2805.7
Volume	cm^3	1530
Axial 1 Hall effect spacing (mm)		87
Axial 2 Hall effect spacing (mm)		85
Bulk density (Mg/m^3)	ρ_B	1.83
Dry density (Mg/m^3)	ρ_D	1.28
Moisture content (%)	M_o	43
Particle density (Mg/m^3)	ρ_s	2.78
Initial void ratio	e_o	1.174
Initial degree of saturation (%)	S_r	1.03

Final conditions

Final conditions		
Parameter	**Symbol**	**Value**
Moisture content (%)	MC_F	33
Final mass (g)	M_F	2716.07
Final bulk density (Mg/m^3)	ρ_{Bfinal}	1.78
Dry density (Mg/m^3)	ρ_{DF}	1.33
Final void ratio	e_F	1.088
Final degree of saturation (%)	S_{rF}	0.85

MC, final		MC WHOLE SAMPLE
Tray (g)	4.58	1508.45
Tray + sample (g) (wet)	24.87	2716.07
Tray + sample (g) (dry)	19.8	1994.77
Moisture content	0.33	0.36

MC, initial (taken from 1D consolidation preparation)		
Tray (g)		4.58
Tray + sample (g) (wet)		24.63
Tray + sample (g) (dry)		18.56
Moisture content		0.43

Experimental conditions

Test conditions	Cell Pressure (kPa)	Back Pressure (kPa)	Effective stress (kPa)
Consolidation stage 1	540	470	70
Shear stage 1	540	470	70
Consolidation stage 2	690	550	140
Shear stage 2	690	550	140
Consolidation stage 3	760	550	210
Shear stage 3	760	550	210

Saturation	Value
Cell Pressure Incr. (kPa)	20.10
Back Pressure Incr. (kPa)	19.10
Differential Pressure (kPa)	21.50
Final Cell Pressure (kPa)	439.60
Final Pore Pressure (kPa)	410.10
Final B Value	0.97

Initial and final conditions and experimental conditions, specimen CR023247, Oxford Clay, Quaternary Domain 2.3.

CR020746, Oxford Clay Formation, Peterborough Member	Isotropically consolidated, undrained, single-stage. University of Cambridge DYNTTS configuration

Initial conditions

Initial conditions		
Parameter	**Symbol**	**Value**
Height (mm)	H_o	191.00
Diameter (mm)	D_o	100.72
Mass (g)	M_o	3000.2
Volume	cm^3	1522
Axial 1 Hall effect spacing (mm)		N/A
Axial 2 Hall effect spacing (mm)		N/A
Bulk density (Mg/m^3)	ρ_B	1.97
Dry density (Mg/m^3)	ρ_D	1.47
Moisture content (%)	M_o	34
Particle density (Mg/m^3)	ρ_s	2.78
Initial void ratio	e_o	0.894
Initial degree of saturation (%)	S_r	1.07

Particle density derived from specimen CR023247

Final conditions

Final conditions		
Parameter	**Symbol**	**Value**
Moisture content (%)	MC_F	35
Final mass (g)	M_F	2986.4
Final bulk density (Mg/m^3)	ρ_{Bfinal}	1.96
Dry density (Mg/m^3)	ρ_{DF}	1.45
Final void ratio	e_F	0.913
Final degree of saturation (%)	S_{rF}	1.07

MC, initial	
Tray (g)	32.6
Tray + sample (g) (wet)	60.8
Tray + sample (g) (dry)	53.6
Moisture content	0.34

MC, final	
Tray (g)	31.8
Tray + sample (g) (wet)	68
Tray + sample (g) (dry)	58.6
Moisture content	0.35

Experimental conditions

Test conditions	Cell Pressure (kPa)	Back Pressure (kPa)	Effective stress (kPa)
Consolidation stage 1	600	550	50
Shear stage 1	600	550	50

Saturation	Value
Cell Pressure Incr. (kPa)	50.00
Back Pressure Incr. (kPa)	42.00
Differential Pressure (kPa)	27.00
Final Cell Pressure (kPa)	569.00
Final Pore Pressure (kPa)	539.14
Final B Value	0.94

Initial and final conditions and experimental conditions, specimen CR020746, Oxford Clay, Quaternary Domain 2.3.

CR011958, till

Isotropically consolidated, undrained, multistage with measurement of small-strain stiffness. BGS SPTTS configuration

Initial conditions

Initial conditions		
Parameter	**Symbol**	**Value**
Height (mm)	H_o	195.22
Diameter (mm)	D_o	99.18
Mass (g)	M_o	3331.68
Volume	cm^3	1508
Axial 1 Hall effect spacing (mm)		87
Axial 2 Hall effect spacing (mm)		85
Bulk density (Mg/m^3)	ρ_B	2.21
Dry density (Mg/m^3)	ρ_D	1.94
Moisture content (%)	M_o	14
Particle density (Mg/m^3)	ρ_s	2.69
Initial void ratio	e_o	0.388
Initial degree of saturation (%)	S_r	0.97

MC, initial		
Tray (g)		4.64
Tray + sample (g) (wet)		16.72
Tray + sample (g) (dry)		15.24
Moisture content		0.14

Final conditions

Final conditions		
Parameter	**Symbol**	**Value**
Moisture content (%)	MC_F	15
Final mass (g)	M_F	3615
Final bulk density (Mg/m^3)	ρ_{Bfinal}	2.40
Dry density (Mg/m^3)	ρ_{DF}	1.92
Final void ratio	e_F	0.40
Final degree of saturation (%)	S_{rF}	1.01

MC, final	
Tray (g)	4.8
Tray + sample (g) (wet)	29.29
Tray + sample (g) (dry)	26.08
Moisture content	0.15

Experimental conditions

Test conditions	Cell Pressure (kPa)	Back Pressure (kPa)	Effective stress (kPa)
Consolidation stage 1	800	600	200
Shear stage 1	800	600	200
Consolidation stage 1	1000	600	400
Shear stage 1	1000	600	400
Consolidation stage 1	1200	600	600
Shear stage 1	1200	600	600

Saturation	Value
Cell Pressure Incr. (kPa)	49.90
Back Pressure Incr. (kPa)	46.10
Differential Pressure (kPa)	39.20
Final Cell Pressure (kPa)	649.30
Final Pore Pressure (kPa)	604.60
Final B Value	0.92

Initial and final conditions and experimental conditions, specimen CR011958, till, Quaternary Domain 1.4.1.

13.6 1D consolidation curve fitting methodology example

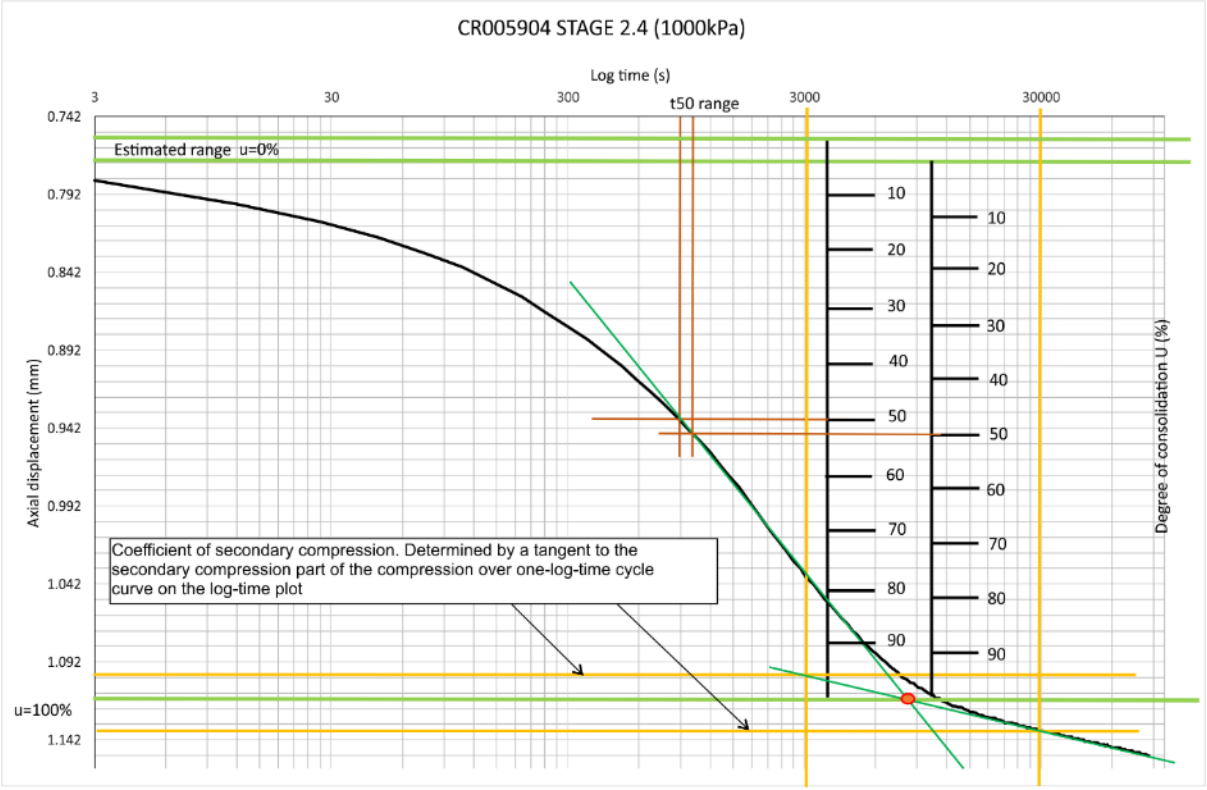

13.7 Preconsolidation pressure from 1D consolidation curve fitting methodology example

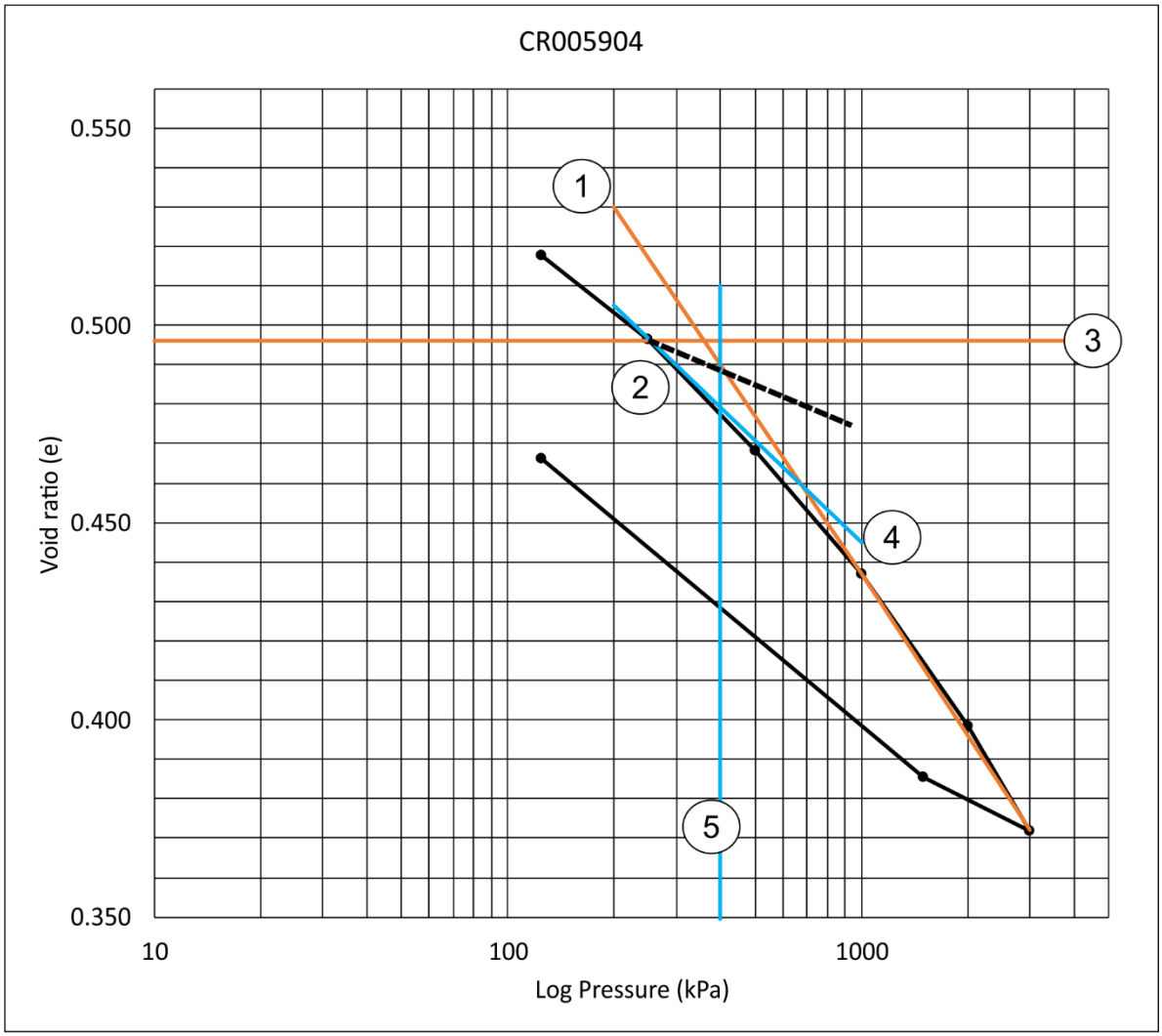

1. Back extension of the slope of the compression curve
2. Estimate point of maximum curvature on compression curve
3. Draw a horizontal line through the point estimated in 2
4. Draw a tangent to the curve at the point estimated in 2 and bisect the angle between this and the horizontal line plotted in 3
5. Draw a vertical line from the point of intersection of the line drawn in 1 and the bisector drawn in 4

Example methodology for the estimation of preconsolidation pressure from 1D compression curves for specimen CR005904, Oxford Clay